

**Study of the Impact of gut microbial butyrate on
RNA binding protein, AUF-1 on regulation of
gastrointestinal physiology**

**The thesis submitted for the Doctor of Philosophy
(Science) in Life Science and Biotechnology,
Jadavpur University
(2024)**

**By
OISHIKA DAS
(Index No.: 44/20/Life Sc./27)**

**Department of Life Science and Biotechnology
Jadavpur University
Kolkata, India
2024**



icmr
INDIAN COUNCIL OF
MEDICAL RESEARCH

NICED
NATIONAL INSTITUTE OF
CHOLERA AND ENTERIC DISEASES

आई. सी. एम. आर. - राष्ट्रीय कॉलरा और आंत्र रोग संस्थान
ICMR - NATIONAL INSTITUTE OF CHOLERA AND ENTERIC DISEASES
स्वास्थ्य अनुसंधान विभाग, स्वास्थ्य और परिवार कल्याण मंत्रालय, भारत सरकार
Department of Health Research, Ministry of Health and Family Welfare, Govt. of India

WHO COLLABORATING CENTRE FOR RESEARCH AND TRAINING ON DIARRHOEAL DISEASES

Date. 29/02/2024

CERTIFICATE FROM THE SUPERVISOR

This is to certify that the thesis entitled "Study of the Impact of gut microbial butyrate on RNA binding protein, AUF-1 on regulation of gastrointestinal physiology" submitted by **Oishika Das**, registered on 16.10.2020 for the award of Ph. D. (Science) Degree in Jadavpur University, is absolutely based upon her own work under my supervision. Neither this thesis nor any part of it has been submitted for any degree / diploma or any other academic award anywhere before.

Moumita Bhaumik

Moumita Bhaumik, PhD
Scientist D
Div of Immunology
ICMR-NICED

Dr. Moumita Bhaumik
Scientist - D
Division of Immunology
ICMR-National Institute of Cholera
and Enteric Diseases
Behaghat, Kolkata

ABSTRACT

The hepato-gastric metabolic function, immune function and the barrier function of a host body are regulated by the gut microbial metabolite, Short Chain Fatty Acids (SCFA), like propionate, butyrate, and acetate. In this thesis we aimed to dissect the "complex rules" by which gut microbial butyrate influences the cholesterol balance, barrier function and immune balance in hepato-gastrointestinal milieu in mice. Given butyrate causes anti- hypercholesterolemia, we have probed the mechanistic molecular details of butyrate action in maintaining cholesterol balance. Butyrate has the following consequences, as shown in the study: upregulation of RNA binding protein, AUF-1 isoforms, which resulted in Dicer-1 instability and reduced miR122 biosynthesis. The intracellular players placed in tandem establish a link as follows: butyrate-AUF-1-Dicer-1-miR122-cholesterol metabolic enzymes- serum cholesterol. To functionally validate decrease in cholesterol upon butyrate treatment we showed that butyrate increased membrane fluidity by disruption of cholesterol rich microdomains which resisted colonization of enteric pathogen.

We created a novel cell-penetrating morpholino-oligomer to selectively knock down AUF-1. Apart from hypercholesterolemia we showed AUF1 knockdown phenocopies colitis with increased barrier permeability, inflammation in the gut and reduced Th17 and Treg balance. We have shown AUF1 stabilizes occludin mRNA coding for Occludin, a tight junction protein and destabilizes claudin 2 mRNA which codes for a pore forming protein, Claudin 2 resulting into increase in barrier function. In a similar manner AUF1 regulates either positively or negatively the transcription factors, ROR γ t and FoxP3 respectively to influence Th17/Treg balance.

Together, these findings provide clear evidence that AUF1, upregulated by butyrate is an important protein which promotes gastrointestinal physiology by maintaining cholesterol balance, barrier function and immune function.

Oishika Das
29/2/2024

Moumita Bhaumik
29/02/2024
Dr. Moumita Bhaumik
Scientist - D
Division of Immunology
ICMR-National Institute of Cholera
and Enteric Diseases
Beleghata, Kolkata

DECLARATION

I do, hereby declare that the work embodied in this thesis entitled “**Study of the impact of gut microbial butyrate on RNA binding protein, AUF-1 on regulation of gastrointestinal physiology**” submitted for the award of Doctorate of Philosophy (Science) in Life Science and Biotechnology, is the completion of work carried put under the supervision of **Dr. Moumita Bhaumik, Scientist-D, at the Division of Immunology, ICMR-National Institute of Cholera and Enteric Diseases, Kolkata**. Neither this thesis nor any part of it has been submitted for either any equivalent degree/diploma or any other academic award elsewhere.

Date: 29/2/2024

Place: Kolkata

Oishika Das

Signature of the candidate

Oishika Das

This thesis is dedicated to
the memory of my beloved grandmother,
my diduma

Acknowledgements

I want to sincerely thank everyone for their innumerable contributions to the success of my thesis work and for making this experience one I will cherish forever.

To begin with, I want to sincerely thank Dr. Moumita Bhaumik for all of her guidance over the past five years. Her unwavering passion and encouragement as my mentor have enabled me to accomplish my objectives. I consider myself to be fortunate to have a practical, judicious, and efficient supervisor who is motivating and supportive like her. Her innumerable suggestions were crucial in determining the general course of my research.

I would also like to use this occasion to express my gratitude to the Department of Science and Technology-INSPIRE (DST-INSPIRE) for their financial support in the form of junior and senior research fellowships, which allowed me to be self-sufficient during my PhD studies.

I am grateful to the Director of ICMR-National Institute of Cholera and Enteric Diseases, Dr. Shanta Dutta for providing me the opportunity to work in this institute.

My deepest gratitude is extended to Dr. Syamal Roy (CSIR-IICB), Dr. Nabendu Sekhar Chatterjee (ICMR-Delhi), Dr. Amit Pal (Division of Pathophysiology, ICMR-NICED), and Dr. SantaSabuj Das (Division of Clinical Medicine, ICMR-NICED) for their wise counsel, insightful comments, and reagents that greatly aided in finishing this thesis work.

I also want to express my gratitude to Dr. Debmalya Mitra for his insightful advice, which enabled me to get over a lot of obstacles while completing my PhD. I also like to thank Animesh Gope for helping me with my experiments pertaining to confocal microscopy and Narayan Da for helping me with animal experiments.

My profound gratitude to my lab partners Mainak Da, Sohini and my juniors Aaheli, Ankita, and Diganta for making this trip unforgettable. Additionally, I appreciate the assistance and guidance I received from my seniors, Suparna Di, Rima Di, Niraj Da, and Saibal Da.

Last but not least, I would want to thank my husband Anubhab for being a continual source of encouragement and support for me. Furthermore, without the support of my parents and in-laws, I would not have gotten this far in life. I will be eternally grateful to them.

Table of content

<i>Topics</i>	<i>Page no.</i>
List of Figures	1-4
List of tables	5
Abbreviations	6-8
1.Introduction	9-14
Review of Literature	15-48
2. A brief background of Short Chain Fatty Acids (SCFA) and their interactions with cholesterol	16-48
2.1 SCFA	16
2.1.1 Formation and transportation of SCFA in the gut	16-17
2.1.2 Species of bacteria which generates SCFAs inside gut	17-18
2.1.3 Biochemical pathway of SCFA production	19
2.2 Receptors of Short chain fatty acids (SCFAs)	20-21
2.3 The routes for Cellular Signalling by SCFAs	21-22
2.4 Focusing on the SCFA-producing gut microbiota in diabetes along with obesity	22
2.5 Implications of SCFAs on Energy and Glucose Homeostasis	22-25
2.6 Butyrate among other SCFAs	25-34
2.6.1 Gastrointestinal Mechanisms of Butyrate Uptake	27
2.6.2 SCFAs' impact on the metabolism of cholesterol: Focus on Butyrate	28-29
2.6.3 MicroRNA modulation by butyrate reinforcing intestinal homeostasis	29
2.6.4 Butyrate in barrier function maintenance in gut	29-30
2.6.5 Butyrate's involvement as an immune modulator in combating bacterial infection	30-31
2.6.6 Role of Butyrate in combating IBDs and colorectal cancer	31-32
2.6.7 Mucosal immunity and Butyrate	32
2.6.7.1 Macrophage	32
2.6.7.2 Mast cells	33

2.6.7.3 Dendritic cell	33
2.6.7.4 Lymphocyte	33
2.7 Diet-related modifications on SCFA synthesis and cholesterol balance	34-35
2.8 Cholesterol and its metabolism in liver	35-40
2.8.1 The comprehension of the physiological purposes of Cholesterol	36-39
2.8.2 Progression of infectious navigation is tailored by cholesterol homeostasis interference	39-40
2.9 Impact of hepatic microRNAs in maintaining the cholesterol homeostasis	40-43
2.9.1 miR-122 in cholesterol homeostasis	40
2.9.2 miR-27a in cholesterol homeostasis	41
2.9.3 miR-33 in cholesterol homeostasis	41
2.9.4 miR-223 in cholesterol homeostasis	42
2.9.5 miR-96/182/183 in cholesterol homeostasis	42
2.9.6 miR-185 in cholesterol homeostasis	42
2.9.7 miR21 in cholesterol homeostasis	42
2.9.8 Modulation of Cholesterol by RNA binding proteins	43
2.10 The role of cholesterol efflux in preserving homeostasis	44
2.11 Role of RNA binding proteins in cholesterol metabolism	45-47
2.12 Role of RNA binding proteins in gut barrier maintenance	47
2.13 Role of RNA binding proteins in gut immunity	48
3. Materials and Methods	49-72
3.1 Chemicals and Reagents	50
3.2 Animals	51
3.3 Dietary supplementation of sodium butyrate	51
3.4 Food consumption	51
3.5 Collection of blood, preparation of serum samples, biochemical analysis estimation of cholesterol and lipoproteins and hepatic enzymes	51
3.6 Antibiotic treatment	52
3.7 Probiotic treatment	52
3.8 mir-122 overexpression in mice	52
3.9 Mice fecal sample collection	53
3.10 Fecal DNA extraction and determination of butyryl-coenzyme A (CoA): acetate CoA-transferase (ButCoAT) gene abundance by qPCR	53
3.11 Measurement of butyrate in feces by LC-MS	53
3.12 Cholesterol-liposome and cholesterol analogue-liposome synthesis	54
3.13 Administration of liposomal cholesterol in mice	54
3.14 Transmission Electron Microscopy	54
3.15 Propagation of Huh7 and RAW 264.7 cells and estimation of viability and toxicity after butyrate treatment	55

3.16 In silico analysis of global microarray data	56
3.17 Treatment of liposomal cholesterol on cells	57
3.18 Visualization of liposomes in transmission electron microscopy (TEM)	57
3.19 Fillipin staining	57-58
3.20 Membrane Anisotropy	58
3.21 Cholesterol efflux	58
3.22 Transfection	59
3.23 Fluorescence microscopy	59
3.24 Confocal Analysis and image processing	59
3.25 CD44 expression analysis by Flowcytometry	60
3.26 Bacterial strain	60
3.27 Pathogen invasion assay	60
3.28 Tissue homogenisation, preparation of RNA and Protein	61
3.29 RNA extraction and reversetranscription	61
3.30 Quantitative real-time PCR	61
3.31 Primers	62-65
3.32 Western blot	66
3.33 Synthesis of Guanidinium Morpholino Oligonucleotides-protected chlorophosphoramidate Morpholino Oligonucleotides (GMO-PMO)	66
3.33.1 Synthesis of Fmoc protected thiourea morpholino active monomer	66-67
3.33.2 Synthesis of Trityl protected chlorophosphoramidate morpholino active monomer	68
3.33.3 Functionalization of solid support with linker and loading monomer	68
3.33.4 Solid phase synthesis of GMO-PMO	68
3.34 GMO–PMO treatment to knock down AUF-1	69
3.35 Bacteria count (CFU) from colon tissue	69
3.36 Histopathological analysis	69
3.37 TEER Assay	69
3.38 Paracellular permeability assay	70
3.39 RNA immunoprecipitation assay	70
3.40 Gut permeability assay	71
3.41 Immunohistochemistry	71
3.42 ELISA	71
3.43 Bacterial translocation	72
3.44 FACS	72
3.45 Statistical Analysis	72
4. Chapter 1	73-103
4.1 Introduction	74-75
4.2 Result	76-97
4.3 Discussions	97-103

5. Chapter 2	104-120
5.1 Introduction	105-106
5.2 Results	107-117
5.3 Discussion	117-120
6. Chapter 3	121-128
6.1 Introduction	122-123
6.2 Results	123-127
6.3 Discussion	127-128
7. Chapter 4	129-144
7.1 Introduction	130-131
7.2 Results	132-142
7.3 Discussion	142-144
8. Summary	145-147
9. Future prospects	148-149
10. References	150-190
11. Publication and proceedings	191

List of figures

- Figure 2.1 SCFAs metabolism from dietary fibre to systemic flow
- Figure 2.2 The methods via which various SCFA are synthesized
- Figure 2.3 A diagram depicting the three mechanisms used by gut microorganisms to eliminate extra-reducing equivalents
- Figure 2.4 SCFA (short-chain fatty acid) receptor-mediated pathways
- Figure 2.5 Synopsis regarding the SCFA-mediated cellular signalling pathway
- Figure 2.6 Short chain fatty acids (SCFAs) govern human metabolic physiology
- Figure 2.7 The microbial manufacturing of butyrate in the intestinal lumen
- Figure 2.8 An overview of the significant impacts of butyrate and its potential mechanisms in the liver, adipose tissues, skeletal muscles, along with its effects in the colon and peripheral tissues
- Figure 2.9 Frameworks relating cholesterol transport and synthesis in the liver and gastrointestinal region to short-chain fatty acids (SCFAs)
- Figure 2.10 A Framework of gut immune function modification by Butyrate
- Figure 2.11 Route of Cholesterol synthesis via Mevalonate pathway
- Figure 2.12 Venn diagram illustrating the commonalities of the multiple facets of dyslipidaemia: high cholesterol, elevated triglycerides, and impaired HDL cholesterol
- Figure 2.13 Structural makeup of Lipid rafts
- Figure 2.14 The intricate involvement of caveolae and lipid rafts in bacterial pathogenicity
- Figure 2.15 hnRNPR lowers cholesterol levels by restricting the expression of HMGCR
- Figure 2.16 Mechanisms for removing unsterified cholesterol from peripheral cell
- Figure 3.0 GMO-PMO (MO) synthesis cycle and HPLC characterization of AUF1-MO and scramble-MO
- Figure 4.1 The effect of increasing SCFA concentration on cellular viability as well as cholesterol status indicated as μg cholesterol/mg cellular protein
- Figure 4.2 The possible targets of butyrate in the metabolism of cholesterol as revealed by STRING analysis of the protein-protein interaction network
- Figure 4.3 Effect of Butyrate on cholesterol metabolising genes observed via

microarray analysis

- Figure 4.4 Analysis of interaction between Butyrate and HMGCR
- Figure 4.5 Effect of Butyrate on weight gain, liver function and serum cholesterol
- Figure 4.6 Images taken with a TEM show lipid droplet in the liver sections
- Figure 4.7 Evaluation of cholesterol metabolic gene expression in the liver by using qPCR, the genes *hmgcs*, *hmgcr*, *dhcr7*, *acat-2*, and *cyp7A1* was examined in each group
- Figure 4.8 Western blot evaluation of ABCA1 as well as ABCA5 expression in relation to butyrate dosages in Huh7 cells and in animal experiment, β -actin was used as loading control
- Figure 4.9 Expression level of miR122 along with its precursor form pre-miR122 as assessed by qPCR in Huh7 cell line and animal model
- Figure 4.10 Butyrate's impact on Dicer1 and AUF-1 as demonstrated by qPCR and western blot evaluation
- Figure 4.11 Effect of Butyrate on four different isoforms of Auf-1
- Figure 4.12 Dicer1 expression, cellular cholesterol, and AUF1 silencing by siRNA -enhanced miR122 in Huh7 cells despite butyrate administration
- Figure 4.13 Effect of Butyrate on Sphk1 and Occludin
- Figure 4.14 Effect of butyrate on miR27a and miR27b
- Figure 4.15 Faecal butyrate, serum cholesterol and expression level of miR122, Dicer 1 along with AUF-1 in HFD, antibiotic treated and DSS induced colitis mice
- Figure 4.16 The impact of antibiotic treatment followed by probiotic administration on serum along with liver cholesterol levels, ButcoAT level, miR122, Dicer 1 and AUF1p40 production
- Figure 4.17 Reduced blood cholesterol brought on by butyrate is prevented by hepatic miR122 overexpression
- Figure 4.18 In vivo, AUF1 knockdown promotes cholesterol production by taking advantage of the AUF1, Dicer1 and miR122 mediated cholesterol route, regardless of butyrate administration
- Figure 5.1 Effect of Butyrate in membrane cholesterol, along with toxicity, proliferation and confluency level

- Figure 5.2 Filipin assay result showing the level of membrane cholesterol after administration of Butyrate
- Figure 5.3 Effect of Butyrate on membrane fluidity level after administrating liposomal cholesterol
- Figure 5.4 Effect of Butyrate on CD71 and CTX-B expression level in RAW 264.7 cell
- Figure 5.5 Effect of Butyrate on reducing cellular infection level and cholesterol content
- Figure 5.6 Effect of Butyrate on CD 44 expression level
- Figure 5.7 Effect of Butyrate on cholesterol content and the number of countable colonies obtained from colon tissue of mice
- Figure 5.8 Effect of Butyrate on the colon histology of mice
- Figure 5.9 Effect of Butyrate on the mucin 2 expression level and infiltration of neutrophil level on the colon tissue of mice
- Figure 5.10 Effect of Butyrate on the expression level of pro and anti-inflammatory cytokine and anti-microbial gene
- Figure 6.1 Effect of AUF-1 knockdown on serum and hepatic cholesterol level
- Figure 6.2 Effect of AUF-1 knockdown in the expression of transcription factors determining the fate of naïve T cells
- Figure 6.3 Effect of AUF-1 KD in maintaining the mRNA stability of T cell specific transcriptional factors
- Figure 6.4 Effect of AUF-1 knock down in the frequencies of CD8+ and CD4+ T cells
- Figure 6.4 Effect of AUF-1 Knockdown on IL-10 producing regulatory T cell Expression
- Figure 7.1 Effect of AUF-1 GMO-PMO in cell viability and reduction in AUF-1 protein expression
- Figure 7.2 Effect of AUF-1 GMO-PMO on transcellular electrical resistance and paracellular permeability
- Figure 7.3 Effect of AUF-1 KD in maintaining the mRNA stability of junctional Protein
- Figure 7.4 Pull down assay result showing the presence of possible direct targets of AUF-1
- Figure 7.5 Pull down assay result showing the possible target of phosphorylated

p37AUF1

Figure 7.6 Effect of AUF-1 knock down on tissue sample

Figure 7.7 Effect of AUF-1 knockdown on morphological changes

Figure 7.8 Effect of AUF-1 knockdown on colon histopathology

Figure 7.9 Effect of AUF-1 Knockdown in neutrophil infiltration and chemokine

Production

Figure 7.10 Effect of AUF-1 knock down in bacterial translocation

Figure 7.11 Effect of AUF-1 KD on junctional protein expression

Figure 7.12 AUF-1 Knockdown showing differential expression of junctional protein

Figure 7.13 Effect of knockdown of AUF-1 on the level of pro and anti-inflammatory cytokines

List of tables

Table 1.1 A collection of SCFAs with one to five carbon atoms.....	10
Table 2.1 Important short chain fatty acids, their types, common and synthetic namesand sources	11
Table 3.1 List of primers.....	62-64
Table 3.2 Antibodies for western blot.....	64-65

Abbreviations

Ab	Antibody
ABCA1	ATP-binding cassette transporter 1
ABCG5	ATP-binding cassette sub-family G member 5
ACAT2	Acetyl-CoA acetyltransferase
ALT	Alanine transaminase
AMPK	AMP-activated protein kinase
APC	Allophycocyanin
ARE	AU-rich elements
AST	Aspartate aminotransferase
AUF-1	AU binding factor 1
BSA	Bovine serum albumin
butCoAT	Butyryl-CoA: acetate CoA transferase
cDNA	Complementary DNA
CES1	Carboxylesterase 1
CFU	Colony forming unit
CYP7A1	Cytochrome P450 7A1
DMEM	Dulbecco's Modified Eagle Medium
DMSO	Dimethyl sulfoxide
DNase	Deoxyribonuclease
DSS	Dextran sulfate sodium
DTT	Dithiothreitol
DHCR7	7-dehydrocholesterol reductase
DHCR24	24-Dehydrocholesterol reductase
EGFP	Enhanced green fluorescent protein
ELISA	Enzyme-linked immunosorbent assay
FACS	Fluorescence-activated cell sorting
FBS	Fetal bovine serum
FFAR	Free fatty acid receptor
FITC	Fluorescein isothiocyanate

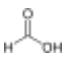
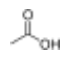
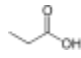
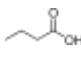
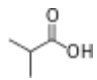
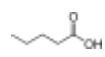
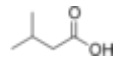
GAPDH	Glyceraldehyde 3-phosphate dehydrogenase
GLP-1	Glucagon-like peptide-1
GLUT-1	Glucose transporter 1
GMO	Guanidinium-linked morpholino
GPCR	G-protein-coupled receptors
HBSS	Hanks' Balanced Salt Solution
HDL	High-density lipoprotein
HFD	High fat diet
HMGCR	3-Hydroxy-3-Methylglutaryl-CoA Reductase
HMGCS	3-Hydroxy-3-methylglutaryl coenzyme A (CoA) synthase
HMGCoA	3-hydroxy-3-methylglutaryl coenzyme A
HRP	Horseradish Peroxidase
IFN	Interferons
IL	Interleukin
i.p.,	Intraperitoneal
LCFA	Long chain fatty acids
LC-MS	Liquid chromatography–mass spectrometry
LDH	Lactate dehydrogenase
LDL	Low-density lipoproteins
MCFA	Medium-chain fatty acid
mg	Milligram
min	Minutes
ml	Millilitre
MO	Morpholino oligo
mRNA	Messenger RNA
MTT	3-(4,5-Dimethylthiazol-2-yl)-2,5-diphenyltetrazolium bromide
µg	Microgram
µl	Microliter
NS	Non-significant
OD	Optical density
PAGE	Polyacrylamide Gel Electrophoresis
PPARγ	Peroxisome proliferator activated receptor gamma

PBS	Phosphate buffered saline
PCR	Polymerase chain reaction
PE	Phycoerythrin
PMSF	Phenylmethylsulfonyl fluoride
RIP	RNA immune pull-down assay
ROR	RAR-related orphan receptor
rpm	Revolutions per minute
RPMI 1640	Roswell Park Memorial Institute (RPMI) 1640
RT-PCR	Reverse transcription polymerase chain reaction
SCFA	Short chain fatty acid
SREBP	Sterol regulatory element binding proteins
Sphk1	Sphingosine Kinase 1
SEM	Scanning electron microscope
T2D	Type 2 diabetes
TG	Triglycerides
TEM	Transmission electron microscopy
TNF	Tumor necrosis factor
Tris	Trisaminomethane
TBS	Trisaminomethane buffered saline
TBST	Trisaminomethane buffered saline with Tween 20
TNBS	2,4,6-trinitrobenzene sulfonic acid
UV	Ultraviolet
U	Unit (only with numbers)
VLDL	Very-low-density lipoprotein
v/v	Volume to volume ratio
v/w	Volume to weight ratio
wk	Week (Only with numbers)

INTRODUCTION

Unsaturated or saturated aliphatic hydrocarbon chains are joined with carboxylic acids to form fatty acids. Short chain fatty acids (SCFAs), medium chain fatty acids (MCFAs), and long chain fatty acids (LCFAs) are different categories of fatty acids based on the number of carbon atoms they contain (Schönfeld and Wojtczak, 2016). SCFAs are fatty acids, lesser than 6-Catoms, MCFAs are fatty acids with seven to twelve carbon atoms, and LCFAs are fatty acids with more than twelve carbon atoms. The gut microbiota in the colon produces SCFAs, which are free fatty acids from the undigested meal. Straight and branched chain SCFAs with less than 6 carbons are created by the fermentation of resistant starch and dietary fibre from undigested meals by the gut flora. The primary sources of all SCFA fermentation are resistant starch, β -glucan from oat bran, and α -galactosides from kidney beans (Kaur et al., 2021). Acetate (C2), propionate (C3), and butyrate (C4) are the primary SCFAs obtained through the fermentation of carbohydrate, accounting for 90-95% of total SCFAs (Parada Venegas et al., 2019). The caecum and proximal colon are the sites of gut microbiota fermentation and SCFA synthesis, with a ratio of the molar concentration of propionate: butyrate: acetate as 20:20:60 (Chambers et al., 2018). Because the caecum contains the majority of the gut microbiota fermentation process, the concentrations of SCFAs are observed to be ten times higher than in the ileum (Procházková et al., 2023). The amino acids leucine, valine and isoleucine produce SCFAs having branching chains, for instance isovalerate, isobutyrate as well as 2-methyl butyrate, which account for 5% of total SCFAs (Rios-Covian et al., 2020). Table 1.1 shows the chemical formula along with structural configuration of SCFAs.

Table 1.1: A collection of SCFAs with one to five carbon atoms

SCFA along with carbon number	Structural Formula	IUPAC	Molecular Structure
Formic acid (C1)	HCOOH	Methanoic acid	
Acetic acid (C2)	CH ₃ COOH	Ethanoic acid	
Propionic acid (C3)	CH ₃ CH ₂ COOH	Propanoic acid	
Butyric acid (C4)	CH ₃ (CH ₂) ₂ COOH	Butanoic acid	
Isobutyric acid (C4)	(CH ₃) ₂ CHCOOH	2-Methylpropanoic acid	
Valeric acid (C5)	CH ₃ (CH ₂) ₃ COOH	Pentanoic acid	
Isovaleric acid (C5)	(CH ₃) ₂ CHCH ₂ COOH	3-Methylbutanoic acid	

Due to its effects on a number of tissue-specific processes, including immunological control and metabolism, SCFAs have both direct and indirect effects on human being. SCFAs, for instance, are helpful in regulating hunger and maintaining homeostasis of energy. SCFAs influence lipid and glucose metabolism once they have reached diverse tissues. On the host cells engaged in inflammatory and immunological pathways, SCFAs have a significant impact. The concentration of SCFAs in the circulation, other tissues in which SCFAs are carried, and the stomach can all have an impact on how an effect is felt. In the distal colon, the levels of SCFAs drop to 20 to 70 mM from the proximal colon's 70 to 140 mM concentration (Cong et al., 2022; den besten et al., 2013; Wong et al., 2006). SCFA concentrations can have a significant impact on the microbial population and fluctuate based on what kind of food is eaten and dietary consumption (Conlon and Bird 2015). Variations in the history of colonizations, physiological situations, food, antibiotics, the amount of alcohol intake, stress level, environment, and genetic variables can all affect the compositional alteration of gut microbiome, which ultimately leads to the variation in SCFA concentrations (Jandhyala et al., 2015; Odumaki et al., 2016).

Propionate, butyrate and acetate typically have peripheral blood concentrations of 4-5 μ M, and 1-3 μ M and 100-150 μ M accordingly, and are quickly transported from the gut to the bloodstream. The ratio of butyrate to propionate to acetate in the hepatic portal vein was shown to be 8:69:23, while that in the large intestine was found to be 21:57:22, indicating that butyrate is used as the main reservoir of energy by the colonocytes (Cummings et al., 1987). Propionate is mostly absorbed by the liver, with 50% of it being used in hepatic gluconeogenesis and the remaining 20% being used by peripheral organs, as seen by the proportions of propionate in hepatic venous along with portal blood (Rui 2014). The majority of the acetate is used by the liver as a co-substrate for the synthesis of glutamate and glutamine as well as a substrate for the production of long-chain fatty acids and cholesterol (Moffett et al., 2020). The remaining amount of acetate is degraded by other tissues in the periphery. When administered orally, intravenously, or by colonic infusion, the microbiota-produced SCFAs are said to have positive effects on the host. Increasing secretion of peptide YY (PYY) and oxidation of fat while decreasing lipogenesis and regulating energy expenditure in obese men were the effects of colonic infusion of acetate (Canfora et al., 2017). Another study demonstrating how SCFA regulates lipid metabolism revealed that colonic perfusion of SCFA also lowers the abundance of circulatory free fatty acids. The expression of peroxisome proliferator-activated receptor-gamma coactivator-1 (PGC-1) and the phosphorylation of adenosine-monophosphate-activated kinase (AMPK) are both increased by butyrate, which also increases fatty acid oxidation and thermogenesis in muscle and liver (den Besten et al., 2015a).

The increase in gut hormones caused by the stimulation of FFAR 2 and 3 receptors by SCFAs directly affects plasma glucose levels (Morrison and Preston 2016). Additionally, it has been demonstrated that

SCFAs can lower plasma levels of FFAs by triggering FAO, preventing adipose tissue lipolysis, and stimulating hepatic de novo synthesis (Ohira, Tsutsui, and Fujioka 2017). Studies emphasized that major SCFAs like acetate, propionate, and butyrate shielded mice from the weight gain and insulin resistance caused by HFD. By triggering gut hormones, butyrate and propionate but not acetate lowered food consumption. Rats fed soluble fibres produced propionate and butyrate, which stimulated intestinal gluconeogenesis and induced body weight loss (De Vadder et al. 2014).

Cholesterol is a crucial family of lipids that also serves as a precursor of bile acids, in addition to preserving the structural integrity of the plasma membrane synthesis of vitamin D steroid hormones. It activates intracellular signalling pathways because it is a vital component of lipid rafts. The "cholesterol homeostasis" process, which is used to describe how tightly controlled cholesterol levels are in mammalian cells, is a phenomenon. The creation of cholesterol from scratch, its absorption from the bloodstream, and the outflow of cholesterol from cells are all fine-tuned in this way (Hu et al., 2010). Blood lipid (triglyceride and cholesterol) levels that are abnormally elevated are signs of the disorder known as hypercholesterolemia (Soran et al., 2018). Additionally, it is a significant contributor to the development and progression of atherosclerotic lesions. Evidence suggests that lowering the increased serum levels of atherogenic lipoprotein and triglycerides can decrease the progression and prevent coronary heart disease (Feher 2003). Since statins significantly lower the risk of developing atherosclerosis and related cardiovascular diseases, they are most frequently prescribed to treat hypercholesterolemia and lower cholesterol levels (Zhou and Liao, 2009). Statins are a class of drugs that lower cholesterol by inhibiting the synthesis of cholesterol.

SREBPs, transcription factors, also known as sterol receptor element binding proteins, modulate the expression of genes involved in lipid metabolism, including cholesterol production and uptake (DeBose-Boyd and Ye, 2018). SREBF2 controls the expression of the genes HMGCR and LDLR to mediate cholesterol homeostasis. By changing the cellular metabolism, it has been shown that SREBP2 knockdown reduces tumour initiation and growth in cancer cells. Furthermore, it has been noted that SREBP2 is abundantly expressed in tumour cells, promoting metastasis and medication resistance. SREBP2's significance in the development of cancer is supported by existing literature, but only in studies using cell lines and animal models (Jie et al. 2019). Recent research suggests that miR-122 and SREBPs have a functional relationship in the control of cholesterol levels. SREBP-1 and SREBP-2 have been identified to interact with miR-122, which then regulates cholesterol metabolism (Menon et al., 2015; Shibata et al., 2013). In the liver, miR-122 is widely expressed and makes up roughly 70% of all hepatic miRNAs. It has been demonstrated that it controls the secretion along with the formation and absorption of cholesterol as well as other aspects of cholesterol metabolism (Moore et al., 2011). miR-

122 is crucial for preserving cholesterol homeostasis, as shown by studies utilising rodent models that show its blockage lowers plasma cholesterol levels (Rotllan and Fernández-Hernando, 2012).

Apart from maintaining the pivotal function of cell, cholesterol also function as one of the major components in the construction of cell membrane. It is known that membrane cholesterol aids in the creation and maintenance of lipid rafts—microdomains throughout the cell membrane that are rich in sphingolipids and cholesterol (Simons et al., 2002). Cellular functions like endocytosis and signal transmission are made easier by the clustering of different signalling molecules and receptors on lipid rafts. To enter host cells, enteric pathogens take advantage of these lipid rafts (Kulkarni et al., 2022). Cholesterol-rich lipid rafts are used by a number of bacterial pathogens, including *Escherichia coli*, *Salmonella*, *Campylobacter*, *Shigella* etc for host cell attachment and internalization (Toledo and Benach, 2015). Intracellular infections that strategically use lipid rafts to penetrate the host cell are the most frequent users. *Salmonella* and *Shigella* both need a type III secretion system or T3SS, a multi-component molecule-level instrument like feature that enables the passage of effector proteins via the cytoplasm through the membrane of bacteria (Both inner as well as outer) along with the host plasma membrane, and into cytoplasm (Coburn et al., 2007). These pathogens have particular virulence factors that interact with the cholesterol and related proteins on the membrane of the host cell, such as invasins or adhesins. The contacts set off a series of processes that promote the internalisation of the bacteria into the host cells by causing the development of membrane protrusions like ruffles or filopodia (van der Meer-Janssen et al., 2009).

1.1 Rationale and objectives of the study

The conventional Statin mediated modulation of cholesterol level is effective, but not free of side effects (Golomb and Evans, 2008). Till now individual studies have been conducted on the role of SCFA on regulating the level of cholesterol by several mode of operation, such as suppressing the activity of HMGCR as well as influencing the expression of several miRNAs associated with cholesterol metabolism (Dong et al., 2021; Hara et al., 1994). But the actual molecular mechanism is yet to be discovered. To stop or cure metabolic diseases brought on by interference with lipid and glucose metabolism, there are many pharmacological therapies available. The expense of these modern pharmaceuticals is one of their key disadvantages because many of them are out of reach for people from all socioeconomic strata. Establishing SCFAs' positive effects may point to them as a less expensive therapeutic approach for long-term treatment-required chronic disorders.

Since SCFA is already been produced inside the body, it can be beneficial to utilise this SCFA in the permissible range to prevent infectious diseases without fearing the toxicity. During the conceptualisation of the undertaking study, several questions come into the scenario, such as if SCFA can directly modulate the activity of small molecules like miRNA to prevent hypercholesterolemia and if yes then what could be possible molecular mechanism; if SCFA mediated lowering of cholesterol is similar in all kind of cell- be it hepatocytes or macrophages; if SCFA can influence the lowering of membrane cholesterol in a similar manner like that of depletion of overall cellular cholesterol and if it does then how SCFA mediated depletion of cholesterol in membrane can alter the intestinal colonisation resistance. In order to comprehend how and which one of the three major SCFA can mainly influence the homeostasis of cholesterol on the basis of the above-mentioned queries, the undertaking study has been divided under three major objectives, which are as follows:

Objective 1: To evaluate how Butyrate among other SCFA mediated regulation of microRNA can alter cholesterol content

Hypothesis: Butyrate corrects HFD diet induced hypercholesterolemia by exploiting AUF1 - Dicer-miR122 axis

Objective 2: To study the effect of Butyrate on cholesterol content in cell membrane and dynamicity of cell membrane as well as to study how Butyrate mediated decrease in cholesterol, if any, contributes towards impact on pathogen invasion

Hypothesis: Butyrate disrupts lipid rafts and prevents the entry of pathogen inside cell

Objective 3: To evaluate how Butyrate can influence the immunological parameters in gut dysbiosis

LITERATURE REVIEW

2. A brief background of Short Chain Fatty Acids (SCFA), RNA binding proteins and their interactions with cholesterol and role in gut barrier maintenance

2.1 SCFA

Short-chain fatty acids (SCFAs) are a type of fatty acid that contains less than six carbon atoms. They are produced through the fermentation of undigestible meals by gut microbes. SCFAs play a crucial role in maintaining gastrointestinal health as they serve as the primary source of energy for colonocytes (Canfora et al., 2015). Unlike longer chain fatty acids, SCFAs have different levels of water solubility, which means they are not able to mix or dissolve easily.

2.1.1 Formation and transportation of SCFA in the gut

Saturated fatty acids, or SCFAs, are the primary by products of the fermentation of dietary fibre in the colon (Miller, T.L. & Wolin, 1996). The lengths of the chain range from 1-6C atoms. Depending on the amount of fibre in the diet, the stomach produces 500–600 mmol of SCFAs everyday (Bergman 1990). The most prevalent SCFAs found inside intestinal portion of human body are acetate (C2), propionate (C3), and butyrate (C4) (Macfarlane S & Macfarlane, G.T., 2003). Examples of different types of SCFAs are elaborated in table 1. SCFAs are in charge of the pH decrease that occurs as one moves from the terminal ileum to the proximal colon. There is decreased production of SCFAs, specifically formate, valerate, and caproate (Cummings et al., 1987).

The molar ratios of intestinal acetate, propionate, along with butyrate are roughly 60: 20: 20 each, although the exact amounts and according to the substrate, microbiota mix, and gut transit time, each SCFA's relative fraction varies. SCFAs are rapidly absorbed by colonocytes when they are produced in the colon, primarily via active transport mediated by monocarboxylate transporters (MCTs). SCFA anion transport is carried out by the electrogenic, sodium-dependent monocarboxylate transporter 1 (SMCT1; also known as SLC5A8), whereas SCFA cation transport is carried out by MCT1. In comparison to substituting for HCO₃ by SLC26A3 (also known as downregulated-in-adenoma (DRA)), passive diffusion absorption of not dissociated SCFAs from the colon is likely to be of lesser importance. How SCFAs are metabolised from dietary fibre to the systemic circulation have been explained in Figure 2.1.

Table 2.1: Important short chain fatty acids, their types, common and synthetic names, and sources (Akhtar et al., 2022)

	General name	Derived name	Source	References
C1	Formic acid	Methanoic acid	<i>Clostridium difficile</i> <i>Eubacterium hallii</i>	Gregory et al., 2021 Pham et al., 2020
C2	Acetic acid	Ethanoic acid	<i>Bifidobacterium</i> sp., <i>Clostridium</i> sp., <i>Akkermansia muciniphila</i> ,	Krautkramer et al. 2020; Xu et al. 2020
C3	Propionic acid	Propanoic acid	<i>Megasphaera elsdenii</i> , <i>Ruminococcus obeum</i> , <i>Bacteroides</i> sp., <i>Veillonella</i> sp.,	den Besten et al., 2013; Xu et al. 2020
C4	Butyric acid	Butanoic acid	<i>Faecalibacterium prausnitzii</i> , <i>Eubacterium rectale</i> , <i>Eubacterium hallii</i> ,	Xu et al. 2020;Morrison and Preston 2016
C5	Valeric acid	Pentanoic acid	<i>Clostridium</i> sp. <i>Megasphaera massiliensis</i> MRx0029	Yuille et al. 2018
C6	Caproic Acid	Hexanoic acid	<i>Caproiciproducens galactitolivorans</i> BS-1T	Conteras-Davila et al., 2020; Bengelsdorf et al.,2019

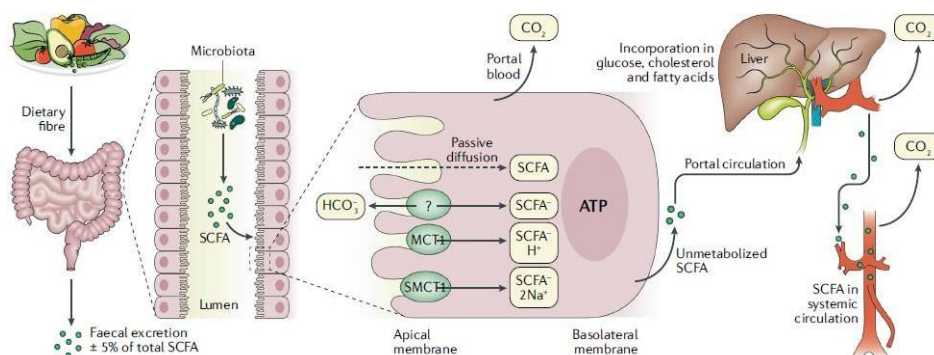


Figure 2.1: SCFAs metabolism from dietary fiber to systemic flow (Dalile et al., 2019)

2.1.2 Species of bacteria which generates SCFAs inside gut

The creation of SCFA is reliant on the gut bacteria, which creates these bioactive substances by fermentation of indigestible carbohydrates and producing the main end products, including and propionate, butyrate, acetate. For instance, the bacterium *Akkermansia muciniphila* is considered as a crucial bacterium for the production of propionate, a catalyst in the degradation of mucin. Similar to this, *Ruminococcus bromii* greatly contributes to butyrate production in the colon by digesting resistant starch. Bacteria like *Eubacterium hallii*, *Eubacterium rectal*, *Faecalibacterium prausnitzii*, etc are additionally perceived to be the principal producers of Butyrate (Morrison & Preston, 2016).

According to numerous studies, the production of a wide range of SCFA is linked to the presence of a diverse array of other gut bacteria. For instance, the Woode Ljungdahl pathway and the pyruvate decarboxylation to Acetyl CoA pathways are used by *Prevotella* sp., *Streptococcus* sp., *Bacteroides* sp., *Bifidobacterium* sp., *Clostridium* sp., *Blautia hydrogenotrophica*, and *Ruminococcus* sp to produce Acetate as a metabolite. Furthermore, *Megasphaera elsdenii*, *Veillonella* sp., *Phascolarctobacterium succinatutens*, *Ruminococcus obeum*, *Bacteroides*. sp., *Dialister* sp., *Salmonella* sp., *Coprococcus catus* and *Roseburia inulinivorans* are understood to effectively create propionate through the propanediol, succinate and acrylate pathways. Apart from that, the exogenous acetate and butyrate kinase pathways used by *Roseburia* sp., *Anaerostipes* sp., *Coprococcus comes* and *Coprococcus eutactus* enable the production of butyrate (Krautkramer et al., 2020, Besten et al., 2013; Macfarlane & Macfarlane, 2003; Cummings et al., 1987).

Additionally, it has been claimed that *Prevotella copri* along with *Prevotella stercorea* produce valerate using the enzymes thioesterase, aminotransferase, transacylase, dehydrogenase, to convert leucine, valine, isoleucine into valerate. Thiolase is used by *Megasphaera* sp., *Escherichia coli* and *Zoogloea ramigera* to break down ++ propionyl-, butyryl-, and acetyl-CoA into caproate and valerate. Similarly, *Megasphaera massiliensis* MRx0029 and *Acidobacteria* sp., also make valerate (Liu et al., 2019; Yuille et al., 2018). As seen in **Figure 2.2**, several SCFA's various synthesis pathways are also depicted.

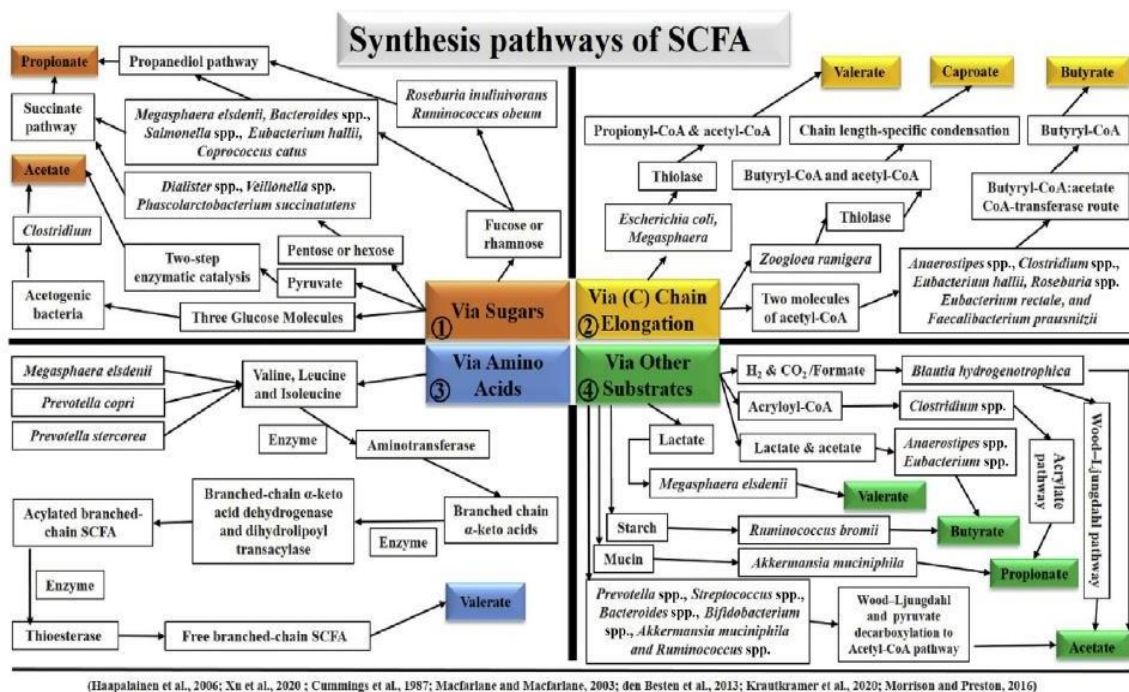


Figure 2.2: The methods via which various SCFA are synthesized. (Akhtar et al., 2022)

2.1.3 Biochemical pathway of SCFA production:

Within the oxygen-deprived environment of the gut, the microbiota breaks down indigestible carbohydrates into oligosaccharides and eventually monosaccharides. Bacteria utilize two significant metabolic pathways, namely the PEP (pentose-phosphate) pathway for 5-C sugars and EMF (Embden-Meyerhof-Parnas's) pathway (glycolysis) for 6-C sugars to modify the monosaccharides into phosphoenolpyruvate (Miller & Wolin, 1996). Subsequently, by products such as alcohols and organic acids are obtained through PEP fermentation (Figure 2.3).

The process begins with the procedure of carboxylation of PEP, resulting in the formation of oxaloacetate. Subsequently, oxaloacetate is converted to fumarate. In the next step, fumarate participates in an electron transfer chain with NADH. This chain involves fumarate reductase and NADH dehydrogenase, enabling the electrons flow which occurs to fumarate from NADH. NADH dehydrogenase facilitates the movement of protons across the cell membrane, which is crucial for the production of ATP through chemiosmosis. As a byproduct of fumarate reductase, succinate is formed. Under conditions of low CO₂ partial pressure, succinate is transformed into methylmalonate. Methylmalonate is then cleaved into CO₂ along with propionate. The latter can be carboxylated to create oxaloacetate, which can then be recycled into PEP. The SCFAs are the main byproducts of the fermentation pathways that have been described.

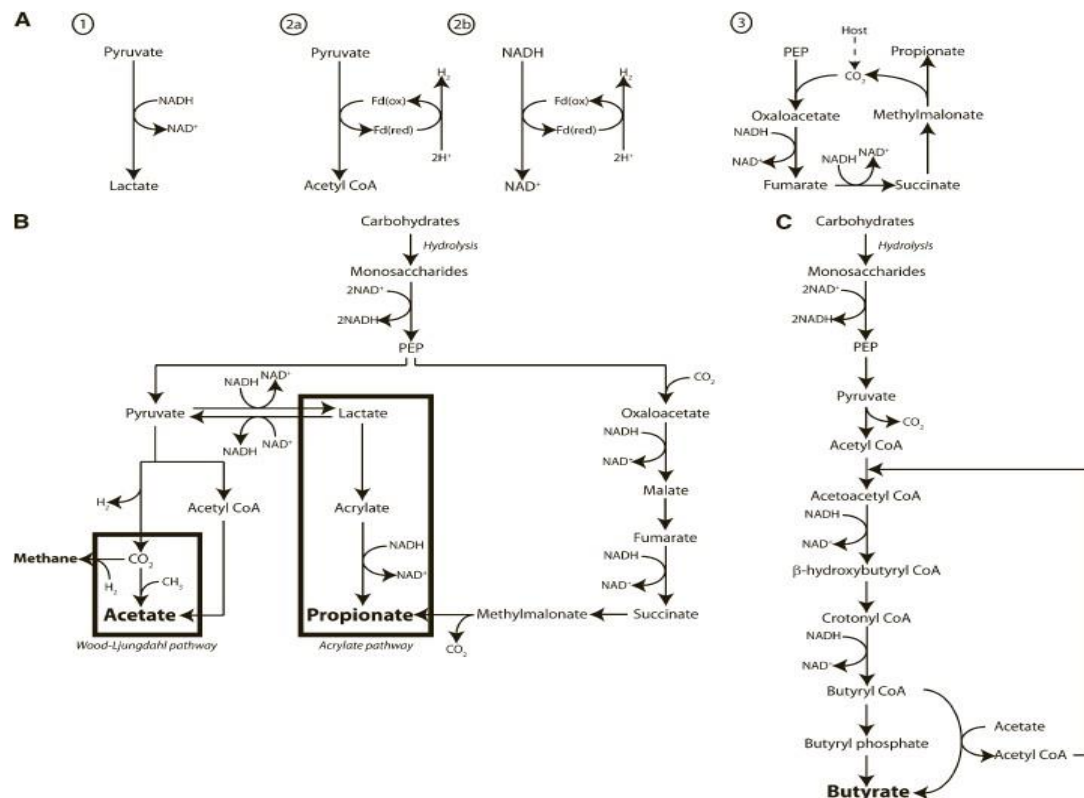


Figure 2.3: A diagram depicting the three mechanisms used by gut microorganisms to eliminate extra-reducing equivalents. (den besten at al., 2013)

2.2 Receptors of Short chain fatty acids (SCFAs):

Four receptors are involved, which are GPR43, GPR41, GPR109a, and OR51E2, are stimulated by SCFAs in human cell membranes (M Priyadarshini, 2018). GPR43 is normally triggered by propionic, acetic, and butyrate. Notably, the ability of butyrate and propionate to stimulate GPR41 is quite strong (Brown et al., 2003). Acetate and propionate are regarded as the Olfr-78 receptor's stimulators, while butyrate and β -hydroxybutyrate can activate the GPR109a receptor. Overall summary of SCFA receptors and their function in host energy metabolism in peripheral tissue is illustrated in figure 2.4.

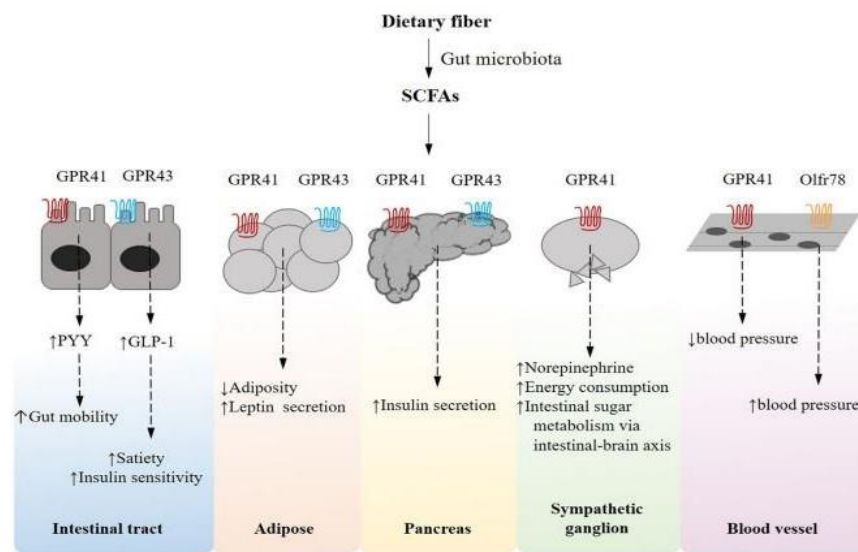


Figure 2.4: SCFA (short-chain fatty acid) receptor-mediated pathways (Li X, Watanabe K and Kimura I, 2017).

There is the documentation for FFA2 and GPR109a, two SCFA receptors, that goes beyond the conventional G-protein signalling and outlines arrestin-dependent pathways. In vitro transcriptional regulation of the expression of pro-inflammatory cytokines is orchestrated by human FFA2, as demonstrated by the use of -arrestin-dependent signalling (Lee et al., 2013). Physiological ligand accumulations could also have a bearing on the expression and activation of SCFA receptors. The gastrointestinal tract, where butyrate is utilized as an energy source and the remaining pool SCFAs is transported into the portal vein, exhibits the highest concentration of these SCFA compounds. Propionate undergoes breakdown in the liver, resulting in acetate being the SCFA with the highest systemic levels (Cummings et al., 1987). Studies conducted on FFAR2 knockout (KO) mice demonstrated that these mice experienced increased or unaltered inflammation in colitis models induced by trinitrobenzenesulfonic acid (TNBS) or dextran sulphate sodium (DSS). This led to the conclusion that the SCFAs directed activation of FFAR2, that was crucial for the proper cessation of some inflammatory reactions.

The scientists also shown that supplementing with acetate streamlined experimental colitis in germ-free animals and reversed it. According to these findings, FFAR2 has an anti-inflammatory function (Maslowski et al., 2009).

In 2013, Masui et al. provided evidence supporting the anti-inflammatory function of FFAR2 by showcasing that colitis (DSS mediated) was aggravated in FFAR2 KO mice by enhancement of the level of certain proinflammatory cytokines such as IL-17 and TNF- α along with the reduction of IL-10 level, (Considered to be anti-inflammatory) in the mucosa region of colon. Furthermore, mice were administered with water containing 150mM of acetate, which prompted the disease indices in the WT mice to vastly enhance even though it had no impact on the FFAR2 KO mice. (Mishra et al., 2020; Masui et al., 2013).

Other writers who treated WT mice with an FFAR2 agonist to treat DSS-induced colitis saw a diminution in symptoms relative to controls, corroborating the previous findings. The avoidance of intestinal inflammation is greatly aided by FFAR2 activation (Agus et al., 2016).

On intestinal epithelial cells, by interacting with HCAR2 and FFAR2, SCFAs were able to promote K⁺ efflux and hyperpolarization, which increased NLRP3 mediated inflammasome activation and accumulation of IL-18 (Macia et al., 2015).

Butyrate's activation of the HCAR2 receptor has been linked to advancement in colon wellness, in particular through its ability to soothe inflammation. In mice, this receptor's deletion heightened the development of colonic inflammation and resulted in altered gene expression in intestinal colonic cells that were linked to a variety of inflammatory signalling pathways (Zimmerman et al., 2012).

2.3 The routes for Cellular Signaling by SCFAs

SCFAs are employed as signaling molecules as well as energy sources since they induce orphan G protein-coupled receptors (GPRs) and impede histone deacetylases (HDACs). As a result, they have an array of outcomes designed to boost metabolic and energy homeostasis. G protein-coupled receptors (like GPR41 and GPR43) are capable of being bound to by SCFAs and being activated by them, as shown in figure 2.5. These receptors accumulate on the surfaces of many different types of cells, including immune cells, adipocytes, and enteroendocrine cells. SCFA activation of GPCRs may culminate in downstream signalling cascades leading to gene expression, cytokine production, and insulin release (Flock et al., 2017). HDACs are spontaneously obstructed by SCFAs. By infiltrating cells through transporters, SCFAs can either influence HDACs or passively via GPR activation. Butyrate has been highlighted to hinder HDAC3, oppress PPAR- expression, and speed up Fgf21 (a type of fibroblast growth enhancer) transcription, all of which encourage oxidation of lipids, clearance of TG, and ketogenesis inside liver (Sun et al., 2017). Additionally, the coactivator

P300 at the Nrf2 promoter strengthens the expression of Nrf2, a nuclear factor, for which evidence exists to raise its downstream targets and safeguard against the oxidative damage and inflammation brought on by diabetes in diabetic mice (Li et al., 2012; Wu et al., 2019).

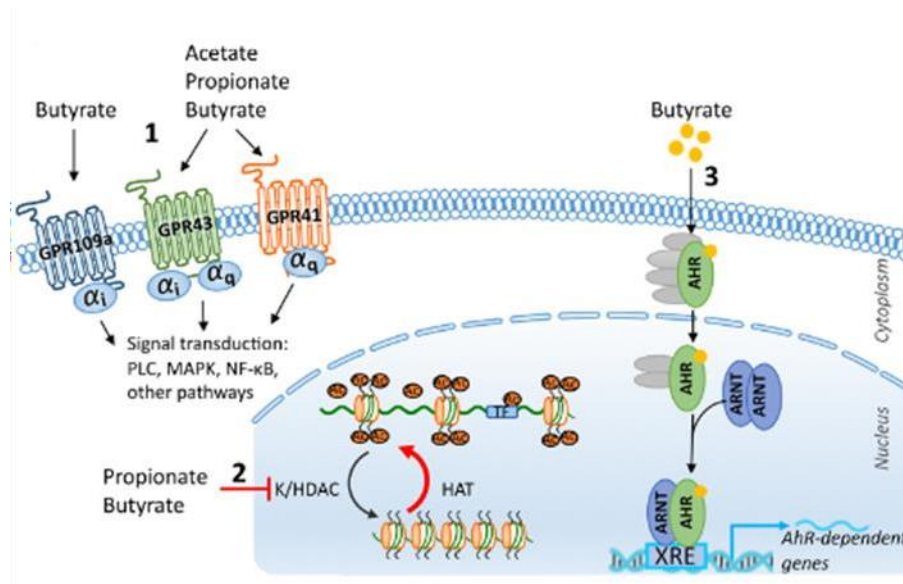


Figure 2.5: Synopsis regarding the SCFA-mediated cellular signalling pathway (Martin-Gallausiaux et al., 2021).

2.4 Focusing on the SCFA-producing gut microbiota in diabetes along with obesity

How the gut microbiome affects obesity and metabolic illnesses is a topic of substantial research. In accordance with a number of investigations, changing the gut microbiota through a variety of methods has been suggested to improve the course of the disease. As an outcome, multiple approaches to changing gut microbiota are being developed as potential cures for metabolic illnesses like obesity and diabetes. Alteration in eating habits may prove to be the most effective technique compared to other treatment options for overcoming obesity and diabetes because, as was previously noted, diet may have a role in influencing healthy gut flora. Additionally confirmed to affect gut flora are prebiotics and probiotics (Collado et al., 2009, Wang et al., 2020). The current strategy of employing paraprobiotics (nonviable/inactivated probiotics) and postbiotics, i.e., metabolic products of probiotics or nonviable bacterial products, for regulating gut microbiota is being intensively researched (Nataraj et al., 2020).

2.5 Implications of SCFAs on Energy and Glucose Homeostasis

SCFA insufficiency is a key factor in the onset of T2DM. Chinese T2DM patients' IM showed metagenome-wide correlations in the survey, whereby a modest level of intestinal dysbiosis showed

a reduced ratio of butyrate-generating bacteria (Qin et al., 2012). Fecal metagenome tests of European women with T2DM consistently demonstrated a large decrease in butyrate-producing microbiota, which somewhat correlated negatively with blood insulin, C-peptide, and TG levels (Karlsson et al., 2013).

In humans, dietary fibre and resistant starch can increase the buildup of SCFAs, which may aid with glucose homeostasis and insulin sensitivity. Supplements of superior quality including starch (resistant to amylase) has been demonstrated to lessen fat content, diminish the overall levels of early-phase insulin, acetate along with glucagon-like peptide-1, and upsurge the amount of gut microorganisms that made acetate in participants with average body weight, depicted in figure 2.6 (Zhang et al., 2019). In healthy middle-aged people, a particular type of bread (rye based) infused with resistant starch type 2 ameliorated fasting levels of GLP-2, peptide YY (PYY), insulin sensitivity, along with total SCFAs (Sandberg et al., 2018). On top of that, delivery of dietary fibre to T2DM patients dropped glycated haemoglobin levels and refined a group of SCFA producers, possibly due to increased GLP-1 production, which alleviated T2DM (Zhao et al., 2018).

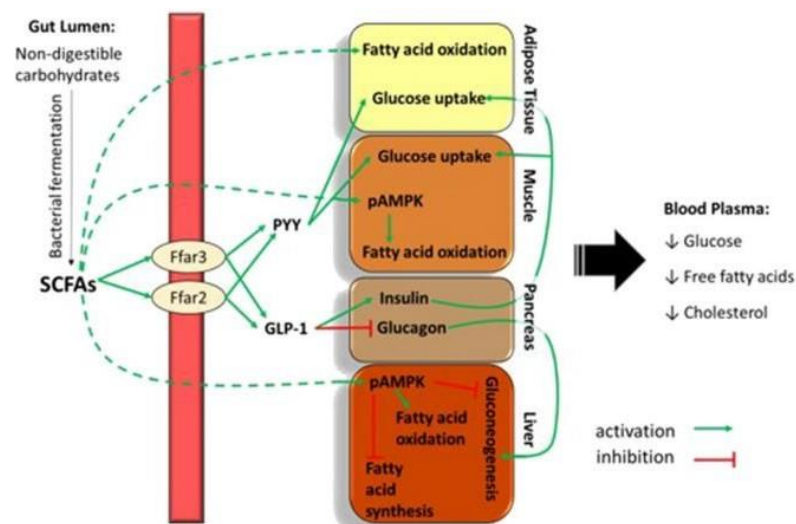


Figure 2.6: Short chain fatty acids (SCFAs) govern human metabolic physiology (Kagle 2020)

The outcomes from in-vivo models imply that the gut microbiota's makeup can affect metabolic ailments like insulin resistance, T2DM, obesity. This idea states that compared to healthy persons, prediabetic or T2DM patients frequently have intestinal dysbiosis. albeit precise microbial clusters are yet available (Krexnar et al., 2017) Maintaining the sturdiness of the intestinal barrier is one of the measures in treating T2DM, which also depends heavily on the microbial makeup of the gut (Federici et al., 2019). This step implies a lower likelihood of bacterium translocation and

endotoxemia-dependent systemic inflammation, both of which are likely to occur during the early stages of illness. T2DM patients have a lower prevalence of butyrate synthesizing bacteria (Qin et al., 2012). In T2DM patients, SCFA therapy increased the amount of GLP-1, butyrate producing bacteria and hemoglobin A1c levels. (Zhao et al., 2018).

The examination of the faecal microbiota allowed for more precise characterization of women with decreased glucose tolerance, potentially giving a tool for identifying those at a high risk of getting type 2 diabetes. Owing to research, alterations in the intestinal milieu of those with type 2 diabetes exist and are prone to alteration in many geographic locations, even if the core remains the same. This result was obtained in T2DM patients due to comparable conclusions about gene involvement, but from several actors, as revealed for the species of Lactobacilli and Clostridial species in the following research. (Karlsson et al., 2013; Qin et al., 2012).

The most recent investigations have concentrated on butyrate since it appears to be a crucial component in the onset of diabetes and obesity among SCFAs. It's interesting to take into account that oral sodium butyrate delivery to mice drastically raised plasma insulin levels, which is in accordance with incretins' stimulation of pancreatic beta-cells (Lin et al., 2012). Recently published findings from Mediators of Inflammation on obese versus lean participants disclosed that the count of bacteria that produce butyrate decreased drastically in the obese subjects, reinforcing the notion that butyrate may be liable for a healthy metabolism (Qin et al., 2012).

Two large studies were planned by Wu et al. and Zhang et al. using three subgroups of people: those with pre-diabetes, those with normal glucose tolerance, and those with T2DM. The study addressed the composition of faecal microbiota and found that it increased with an unhealthy state. Based on microbiota profiles, the scientists hypothesized that normal glucose tolerance patients had a higher presence of butyrate-producing bacteria than people with pre-diabetes or T2DM. The largest abundances of *Roseburia* (OTU1900), *Akkermansia muciniphila* ATCCBAA-835 and *Fecalibacterium prausnitzii* L2-6 isolated from individuals having glucose tolerance affirmed this.

In accordance with newly released research, the HCT116 CRC cell line verified heightened levels of glucose transporter 1 (GLUT1) and an upsurge in glucose absorption when FFAR2 and FFAR3 expression was lowered (Al Mahri et al., 2020).

After ingesting a high-fat diet for an extended period of time frame, FFAR2 knockout mice have been found to have lower insulin levels as opposed to wild-type controls. Furthermore, in a test of oral glucose tolerance the FFAR2 knockout mice showed lower insulin concentrations and poor glucose tolerance. Being able to determine that FFAR2 appears in pancreatic beta-cells, however, prompted researchers to hypothesize that FFAR2 might play a direct regulatory action on the effects of SCFA on islet cell function (Regard et al., 2007). This notion is supported by research on the effects of butyrate exposure on pancreatic beta-cell growth and function. By weakening the gut

barrier, increasing the tumour bacterial load, shifting the phenotypes and CD8⁺ T cell activities in tumours, and pertaining to the dendritic cell synthesis of IL-27, a loss of FFAR2 has been shown to promote colon carcinogenesis in mice. As siRNA-mediated gene suppression of FFAR2 decreased *C. butyricum*'s non-proliferative activity, the stimulation of FFAR2 may be connected to the defensive activity of this bacterium (Carretta et al., 2021; Chen et al., 2020b).

Leptin and ghrelin are two other metabolic hormones whose release may be susceptible to SCFAs. These hormones' effects on the brain are thought to be transmitted through the vagus nerve and -e BBB. By governing metabolic hormones like GLP-1, PYY, leptin, and ghrelin, SCFAs may have advantageous implications for curbing cravings and lower energy intake. SCFAs primarily preserve insulin sensitivity and hepatic metabolic activity via an AMPK-dependent framework (Zhang et al., 2019).

Direct delivery of SCFAs may modify the glucose metabolism's balance as well as boost insulin sensitivity. In fasting healthy volunteers, acute oral sodium propionate treatment enhanced resting-energy expenditure and was correlated with a spike oxidation of lipid from entire body (Chambers et al., 2018). Over a period of four days, the rectal administration of combinations of short-chain fatty acids (SCFAs) in normoglycemic overweight males resulted in enhanced fat oxidation during fasting, increased energy utilization, raised plasma levels of PYY, and reduced concentrations of fasting free glycerol (Canfora et al., 2017).

Overall, the clinical information reported above supports the notion that SCFA amendment may be able to prevent or treat T2DM. However, those are only starting points from studies using a limited sample size to examine how SCFAs impact the host's physiology. Additional prospective studies with substantially larger and more diversified sample sets are required due to the effects of long-term SCFA administration (through multiple modalities of delivery) on T2DM.

2.6 Butyrate among other SCFAs

Butyrate is the principal energy source of colonocytes (Riviere et al., 2016), as evidenced by the fact that in the human ascending and descending colon, butyrate oxidation enables primary colonocytes to take up more than 70% of oxygen (Roediger, 1980).

The Firmicute family includes two relevant gram-positive anaerobic bacteria, *Eubacterium rectale*/Roseburia sp and *Faecalibacterium prausnitzii* (Clostridial cluster IV) and (Clostridial cluster XIVa), are assumed to have the ability to yield butyrate (Louis et al., 2009). Butyrate-producing bacteria have the appearance of a functional unit than a particular phylogenetic family because numerous different strains that synthesis butyrate have been found in a broad spectrum of clostridial clusters (Liu et al., 2018).

Through the fusion of two molecules of acetyl coenzyme A, butyrate can be generated in the stomach from hexose carbohydrates (Blaak et al., 2020). The conclusion step, which converts butyryl-CoA to butyrate, can be accomplished by a pair of metabolic routes and standalone Endogenous enzymes: either butyrate-kinase, butyryl-CoA: acetate CoA-transferase or butyryl-CoA, which appears in figure 2.7. An investigation contrasting two in vitro gut models, one having luminal and mucosal microbial habitats and the other without—also disclosed that the presence of a mucosal environment prompted a shift in production from acetate to butyrate (Van den Abbeele et al., 2012).

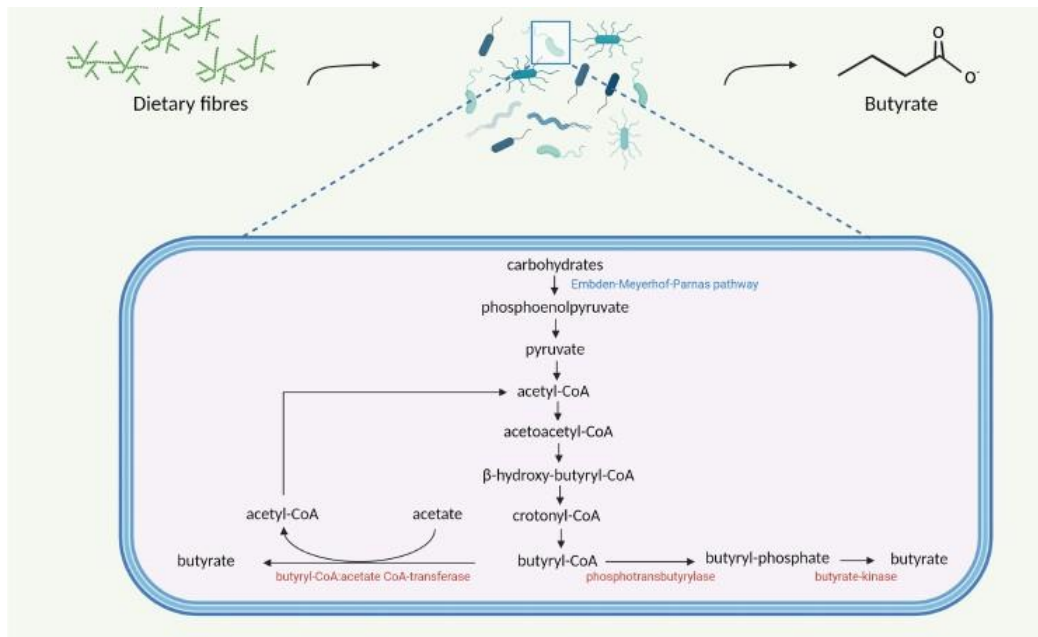


Figure 2.7: The microbial manufacturing of butyrate in the intestinal lumen (van Deuren et al., 2022)

It's interesting to note that in germ-free mouse colonocytes, a lack of energy (reflected by a decline in tricarboxylic acid cycle enzymes) results in reduced ATP levels and, eventually, autophagy. Recolonizing germ-free animals with bacteria producing butyrate and treating ex vivo germ free colonocytes with butyrate causes an upsurge in oxidative phosphorylation and a decrease in autophagy to baseline levels (Donohoe, 2011), suggesting the significance of host-microbe interaction in colonic epithelium's energy metabolism.

The advantages of butyrate as a treatment for inflammatory diseases, neurological disorders, and other conditions have received extensive research (Canani et al., 2018). Additionally, butyrate is said to influence the metabolic landscape of the host cell's energy, depicted in figure 2.8 (Liu et al., 2018).

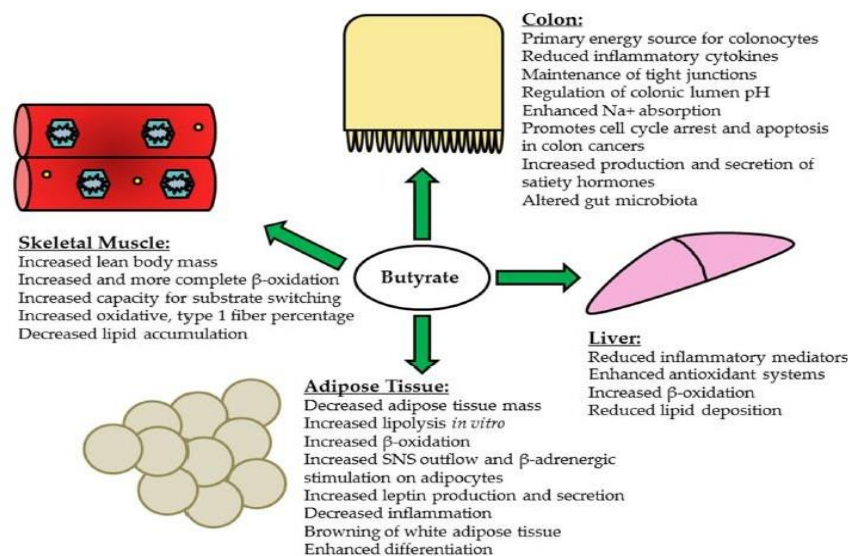


Figure 2.8: An overview of the significant impacts of butyrate and its potential mechanisms in the liver, adipose tissues, skeletal muscles, along with its effects in the colon and peripheral tissues. (McNabney & Henagan, 2017).

2.6.1 Gastrointestinal Mechanisms of Butyrate Uptake

Propionate, acetate and butyrate are quickly incorporated by colonocytes via non-ionic diffusion because of the SCFAs' general low molecular weight in their protonated states and hydrophobicity (Ganapathy et al., 2013; Charney et al., 1998). However, the finding that 10% of SCFAs are found in the faeces raises the possibility of additional absorption pathways (Wong et al., 2006). In fact, a mechanism of SCFA uptake known as sodium-coupled monocarboxylate transporters (SCMTs) that effectively uses the gradient in colonic Na⁺ concentration to trap SCFAs within colonocytes has been discovered (Bergman, 1990).

Butyrate binds to metabolite-sensing G-protein coupled receptors (GPCRs) on intestinal epithelial cells, such as GPR43, GPR41, and GPR109A, at the cell surface (Macia et al., 2015; Bindels et al., 2015; Kim et al., 2013; Brown et al., 2003). Another significant GPCR that is activated by butyrate is GPR109A (Thangaraju et al., 2009). GPR109A signalling stimulates dendritic cells and colonic macrophages' inflammasome pathways, causing IL-10 producing regulatory T cells, to differentiate as well as an enhanced production of IL-18 in intestinal epithelia. It is acknowledged that butyrate-induced GPCR signalling through FFAR2 and FFAR3 regulates downstream activation of a specific signalling pathway, i.e., MAPK pathway, which plays a crucial part for determining the health of the gut (Kim et al., 2013).

2.6.2 SCFAs' impact on the metabolism of cholesterol: Focus on Butyrate

Cholesterol is received through diet or is synthesised de novo mostly in the liver and gut. 3-hydroxy-3-methylglutaryl-CoA reductase (HMGCR), which turns 3-hydroxy-3-methylglutaryl-CoA into mevalonate, is the enzyme that restricts the rate at which cholesterol becomes manufactured. (Field et al., 1990; Feingold and Grunfeld 2015).

Propionate decreases the rate of cholesterol synthesis via inhibiting the activity of HMGCR in the liver, according to in vitro research (Hara et al., 1999). Butyrate has been demonstrated to suppress HMGCR activity, hence halting the production of cholesterol (Korcz et al., 2018). Butyrate's localized impact on Caco-2 cells (an intestinal permeability model) were examined because SCFAs levels are often low in the circulation. By reducing NPC1L1 and boosting expression of ABCG5/8, butyrate was found to decrease a dose-related absorption of cholesterol, as explained in figure 2.9 (Chen et al., 2018). By increasing ABCA1 in ApoE⁻ mice, it was also demonstrated to offer protection along with prevention of atherosclerosis caused by increased fat intake (Du et al., 2020).

The utilization of topical butyrate as a supplement is common, but the predominance of anaerobic bacteria responsible for its production leads to its limited bioavailability. This restricts the potential for generating significant amounts of this metabolite. To develop oral formulations that maintain pharmacologically active levels of butyrate, researchers are investigating its concentration in the small intestine through ongoing studies.

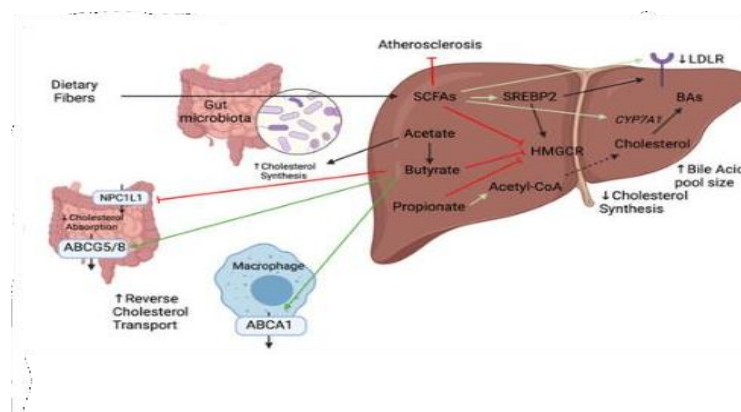


Figure 2.9: Frameworks relating cholesterol transport and synthesis in the liver and gastrointestinal region to short-chain fatty acids (SCFAs) (Vourakis et al., 2021)

2.6.3 MicroRNA modulation by butyrate reinforcing intestinal homeostasis

Single-stranded, brief microRNAs (miRs) are non-coding RNA molecules. with an estimated length of 22 nucleotides that are found in every living species (Londin et al., 2015; Lee et al., 1993;

Wrightman et al., 1993). MiRs are created through a number of metabolic processes. Following ribonuclease III Drosophila's nuclear cleavage of the primary miRs, precursor miRs (pre-miRs) emerge and drift to the cytoplasm. With the aid of another protein designated as argonaute (Ago), ribonuclease III Dicer continues to cleave them, resulting in stable single-stranded miRs (Denli et al., 2004; Hutvagner et al., 2001).

Each miR possesses the potential to attach to its complementing sequence in the 3'-UTR (untranslated region at 3' end) of a particular mRNA, causing the mRNA to degrade and preventing the information from being translated into its associated protein. Depending on whether they're exposed to harmful or beneficial signals, miRs can do this to stop the process of anti- or pro-apoptotic proteins being translated from their corresponding mRNAs. Additionally, treatment alongside sodium butyrate increased miR-203 expression, which hindered the NEDD9 gene's translation, set off proliferation, induced apoptosis, and prevented the development of colonies and invasion of healthy cells by cancerous ones. (Han et al., 2016).

Tissues containing irregular human colon cancer cells showed multiple times higher quantities of miR-92a compared to surrounding normal colon tissue. The levels of pri-miR-17-92a, a precursor of miR-92a, and its target protein c-myc, however, were reduced by butyrate therapy in human colon cancer cells. (Macfarlane & Murphy, 2010).

It was discovered that miR-106b, one of these miRNAs, targets p21 (Hinnebusch et al., 2002). By inhibiting HDAC, butyrate regulates p21 expression in a manner independent of miRNAs, as demonstrated by this partial suppression by miR-106b, thereby preventing colorectal cancer.

Sodium butyrate usage to treat breast cancer cells increased miR-31 expression, which decreased the abundance of the polycomb group (PcG) protein BMI1 and triggered cellular degeneration. Thus, butyrate can successfully stop the spread of colon cancer by boosting or reducing the manifestation of particular miRs.

2.6.4 Butyrate in barrier function maintenance in gut

Studies have demonstrated that butyrate can impact the differentiation of cells, apoptosis along with proliferation of the epithelium of intestinal region (Miao et al., 2016). By increasing transepithelial electrical resistance, butyrate has the ability to restore the barrier function in Cdx2-IEC and Caco-2 cells by promoting the expression of Claudin-1, ZO-1 as well as occluding (Wang et al., 2012; Peng et al., 2009; Miao et al., 2016). Furthermore, butyrate's effect on the barrier region of epithelial layer may also be attributed to the uprise of tight junction proteins through the stimulation of AMP-activated protein kinase (Yan & Ajuwon, 2017). Butyrate preserves intestinal barrier function in Caco-2 cell monolayers, according to an assessment recently published by Elamin et al., 2013. The

intestine mucosal surface's dominant mucin is MUC2, and butyrate is able to augment its expression (Willemssen et al., 2003). Strengthening the mucous layer increases safeguards against luminal pathogens. Additionally, butyrate can promote the development of trefoil factors (TFFs), classified as mucin-associated peptides which assist keep and restore the intestinal mucosa. Butyrate strengthens barrier functioning via a number of procedures; one of which is AMP-activated protein kinase activation in monolayers. Butyrate is associated with both cell division and apoptosis. Butyrate triggers growth halts while on the cell cycle's G1 phase and expands DNA synthesis in (Meijer et al., 2010). Excessive amounts of butyrate elicit apoptosis, whereas low concentrations of butyrate promote cell growth (Canani et al., 2012). Butyrate can affect immune cell adhesion, migration, and cellular events like proliferation and death, which cumulatively can have a consequence on the immunological response.

The critical role of HIF-1 in maintaining barrier integrity is highlighted by the fact that butyrate enhances barrier function (as demonstrated by FITC-dextran flow) in T84 cells, but this effect is absent in the absence of HIF-1 (Kelly et al., 2015). Furthermore, butyrate promotes the expression of genes involved in tight junction (TJ) formation and protein assembly by activating additional transcription factors, notably STAT3 and SP1. Consequently, butyrate sustains or even enhances the TEER value (transepithelial electrical resistance) in small intestinal porcine IPEC-J2 cells, human colonic T84, rat small intestinal cdx2-IEC cells, Caco-2 cells and even under inflamed conditions (Wang et al., 2012; Zheng et al., 2017).

Butyrate and propionate negate the activity of histone deacetylases, provoking anti-inflammatory effects in dendritic cells, macrophages intestinal cells (Li et al., 2018; Sun et al., 2017). Another benefit is that butyrate advocates the proper colonic epithelium-specific inflammasome activation and operation, enabling quick identification of invasive bacteria and minimizing any continuous degeneration of the barrier comprises of epithelial cells (Macia et al., 2015; Singh et al., 2021).

2.6.5 Butyrate's involvement as an immune modulator in combating bacterial infection

To keep the host's intestinal homeostasis in check, the host and commensal bacteria must interact. However, disruption of this procedure due to bacterial dysbiosis and human defense against alien bacterial species may result in persistent inflammation. It has recently been discovered that macrophages that are differentiating in the aftermath of butyrate treatment, derived from the microbiota, demonstrate higher antimicrobial activity. Such action can change macrophage metabolism, boost LC3-associated host defence, reduce mTOR kinase activity, and aid in the synthesis of anti-microbial peptides in the lack of pro-inflammatory cytokines (Schulthess et al., 2019).

According to reports, administering butyrate increases the host's intestinal macrophages' capacity to fight off harmful bacteria and activates their anti-microbial capability. SCFAs from the microbiota increase the function of intestinal epithelial barriers and control host immune strategies in mucosal layers. In this approach, butyrate acts as the first source of energy for epithelial cells, which serve as the initial line of defense for the host against invading bacterial infections (Vinolo et al., 2011). Microbiota-derived butyrate appears to have been shown to exert immunomodulatory benefits in in vivo models of intestinal inflammation (Furusawa et al., 2013). Listed below are additional details on the part butyrate plays in several immunological processes:

2.6.6 Role of Butyrate in combating IBDs and colorectal cancer

In Colorectal cancer (CRC) patients and inflammatory bowel disease (IBD), decreased frequencies of butyrate-forming bacterial species were seen in the stomach as well as in faecal samples. It has been proven that intestinal and tissue-resident phagocytes serve as barriers in the intestine against bacterial invasion. Deficient microbicidal reactions have been documented in monogenic and polygenic forms of IBD, which has led researchers to believe that this process' pathophysiology is dysfunctional (Frank et al., 2007; Wang et al., 2012).

Butyrate hinders oxidative damages by lowering cyclooxygenase-2 (COX-2) levels and improves hydrogen peroxide (H₂O₂) detoxification by inducing catalase. These are just a few of the multi-stage modulating effects butyrate has on intestinal defence mechanisms (Sauer et al., 2007).

The prophylactic and therapeutic effects of butyrate for colitis have been investigated in animal models either by modifying butyrate levels in the diet by adding butyrate-producing prebiotics, sodium salt of butyrate, or a butyrate analogue like tributyrin, or by administering sodium butyrate directly via rectal enemas. The addition of a bean snack and baked maize (20-40 g/kg body weight) to the meal led to the highest yield of butyrate in the cecum and stools, as well as promoting an inflammation resulting in reduction of IL-1 receptor, TNF-alpha and TLR receptors, in a male outbred-CD-1 colitis model (Luzardo-Ocampo et al., 2020). According to Smith et al., adding 150mM of butyrate to drinking water accelerated the frequency and summation of regulatory T cells from colon (cTregs) in germ-free mice. Similar to this, Zhang et al. investigated the outcomes of butyrate feeding in a rat model of colitis and found that it had a significant impact on the balance of Treg and Th17 cells as well as a protective effect against the onset of IBD. One of the primary processes beneath the emergence of IBD is speculated to be impaired intestinal barrier function and elevated permeability, and butyrate feeding has been demonstrated to alleviate this outcome in numerous in-vitro as well as animal models (Cresci et al., 2017; Venkatraman et al., 2000).

In human colonic cancer cell lines, sodium butyrate has been demonstrated to trigger apoptosis via a p-53-independent mechanism (Hague et al., 1993). Furthermore, butyrate offers a defence against DNA deterioration and oxidative stress (Rosignoli et al., 2001). The restrictive effects of butyrate on Neuropilin-1 (NRP-1) have also been reported, as have the impairment of the signalling pathway of MAPK (Zuo et al., 2013), differential regulation of the Wnt- β catenin signalling pathway, upsurge of microRNA miR-203, and promoting the apoptosis of cell (Han et al., 2016).

2.6.7 Mucosal immunity and Butyrate

Plenty of studies on both humans and animals appear to demonstrate that butyrate stimulates the intestine to suppress the expression of proinflammatory cytokines like IFN- γ , TNF- α , IL-8 and IL-6, while inducing cytokines having anti-inflammatory effects like TGF- β along with IL-10 (Mowat et al., 2014). Countless in vitro and in in-depth analysis have shown the results that butyrate inhibits NF-B, which is why it has a long history of being anti-inflammatory (Elec et al., 2017; Andoh et al., 1999).

The interaction of butyrate with GPR43, the triggering of the JNK and MEK/ERK pathways, and its effects on cell proliferation have all been shown to support the generation of AMPs by intestinal epithelial cells. Butyrate elevated bactericidal function in vitro and in vivo by guiding differentiation from monocytes to macrophages and compelling the procurement of S100A8, and S100A9 genes, several AMPs, and calprotectin, all without broadening the responses of proinflammatory cytokine (Schulthess et al., 2019).

In addition to being used to treat colitis, butyrate has been shown to be effective in reversing intestinal ulcers and lifting mucosal permeability associated with dextran sodium sulphate colitis. Mice are more vulnerable to experimentally induced intestinal inflammation when one of the host receptors for SCFAs, G-proteincoupled receptor is missing (Maslowski et al., 2009). Butyrate can also directly affect leucocytes, reducing co-stimulatory expression of molecules, blocking nuclear factor- κ B translocation in human dendritic cells, monocyte marrow-derived macrophages, and inhibiting IL-12 production (Millard et al., 2002).

2.6.7.1 Macrophage

Butyrate lowered IL-12p40, IL-6 and nitric oxide secretion to a larger amount than that of acetate or propionate in a dose-mediated way in bone marrow-derived macrophages challenged with LPS, reflecting butyrate has anti-inflammatory effects on macrophages. Conversely, butyrate had no effect on TNF or MCP-1 (Chang et al., 2014). Butyrate administration decreased IL-6 secretion and mRNA expression. IL-12 and inducible nitric oxide synthase expression were found in phages isolated from the intestinal lamina propria and driven with LPS.

2.6.7.2 Mast cells

Prebiotics that heightened faecal SCFA levels in animal models of colitis were tied to intestinal barrier protection, a decrease in inflammation, and inflammatory cytokines. When administered to rats in an experimental colitis model, barley that is germinated, a prebiotic that undergoes fermentation into SCFA, decreased recruitment of colon specific mast cells (Araki et al., 2007; Kanauchi et al., 2003). When butyrate's direct effects on mast cells were examined, the jejunal mucosa of pigs given the compound showed decreased mast cell degranulation and proinflammatory cytokine gene expression (Wang et al., 2018).

2.6.7.3 Dendritic cells

DC are in close contact with the derived metabolites and intestinal microbiome (Steinman 2006). Human monocyte-derived DC's ability to differentiate, mature, and exert all T lymphocyte-stimulating actions in the gut is said to be significantly impacted by butyrate therapy. Low non-toxic dosages of butyrate administration decreased the expression of adult surface markers dendritic cells (CD83, CD80, CD45, CD40, and MHC class II molecules) (Liu et al., 2012; Millard et al., 2002). In accordance with Liu et al., butyrate administration enabled DC to release IL-12 reduced by three times, IFN- decreased by five times, and IL-10 increased by eleven times. By activating Type-1 regulatory T cells (Tr1), butyrate-stimulated DC dramatically increased the production of IL-10 (Kaisar et al., 2017). By dramatically inhibiting the rate of extracellular acidification caused by LPS and by significantly lowering the mitochondrial oxygen intake rate in butyrate-treated DC at base level, butyrate rendered DC metabolically less active (Kaisar et al., 2017).

2.6.7.4 Lymphocytes

Through a comprehensive approach encompassing both the experiments of in-vivo as well as in-vitro, Arpaia et al. determined that butyrate has the ability to enhance the generation of extrathymic Treg cells by directly impacting T cells. Notably, in lack of dendritic cells (DC), this effect was facilitated by an upregulation in the extrathymic differentiation of Treg cells dependent on the Conserved Noncoding Sequence-1 (CNS1) (Arpaia et al., 2013). The formation of iNOS is likewise inhibited by butyrate, as seen in Figure 2.10.

Kespohl et al. marveled at how varied butyrate concentrations (0.1 mM to 1 mM for in-vitro and 50 mM to 200 mM for in-vivo via oral route) affected the CD4⁺ T cells oriented immunological response. They found that butyrate could differentiate Tregs both in vitro and in vivo at low concentrations (0.1 to 0.5 mM), but at elevated concentrations (1 mM), butyrate could activate the expression of T-bet, resulting in Tregs or normal T cells that could produce IFN (Kespohl et al., 2017). Through altering cellular mitochondrial metabolic flux, butyrate also boosted CD8⁺ Tmemory cells' (Tmem) recall ability and memory potential (Bachem et al., 2019; Ji et al., 2019). As the literature reports, butyrate inhibits the autoimmune response by having an inhibitory impact on HDAC and promoting class-switch DNA recombination, provoking B-cell intrinsic epigenetic modulation of antibody response (Sancez et al., 2020).

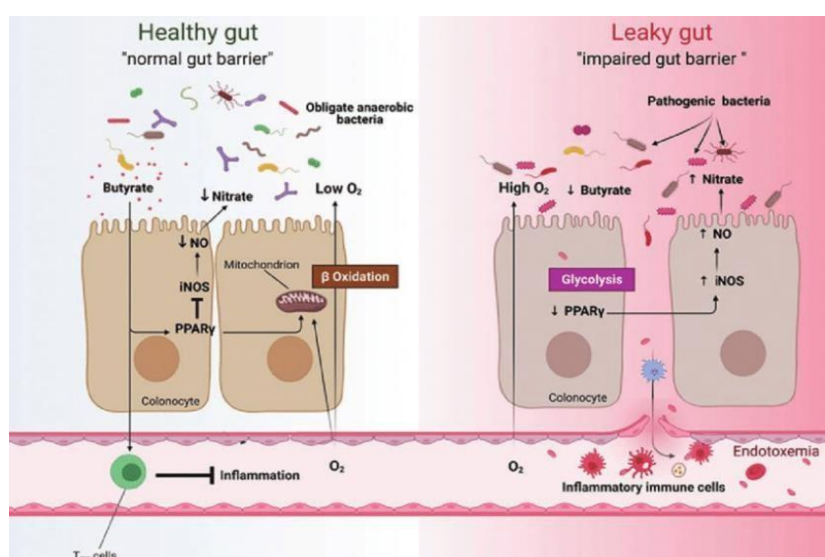


Figure 2.10: A Framework of gut immune function modification by Butyrate (Abot et al., 2021)

2.7 Diet-related modifications on SCFA synthesis and cholesterol balance

Diet shapes gut microbiota composition and SCFA production, and thus host metabolism and inflammation. In rats, inflammation of the liver and adipose tissue caused by a high-sugar, high-fat diet has been linked to insulin resistance and diabetes (Musso et al., 2010). High fibre diets pertain to SCFA profiles that assist control of host metabolism and inflammation, which in turn contributes to insulin sensitivity, in contrast to high fat and sugar diets.

Numerous studies indicate that the gut microbiota, through its function in the metabolism of bile acids and the production of microbial metabolites, has the ability to change the blood lipid composition, namely cholesterol (Kiraa et al., 2019; Rabo et al., 2019; Schoeler et al., 2019). Though the precise effects of these relationships on human health have just lately been considered

metabolism of cholesterol by gut microbes has been known for decades. A disruption in the creation of cholesterol has numerous negative effects on one's health given that it is a crucial signalling molecule in the body that governs many bodily functions, including the fabrication of BA and the regulation of hormones

2.8 Cholesterol and its metabolism in liver

Cholesterol refers to a class of chemical compounds known as lipids. It is a sterol, which is a category of lipid. The biosynthetic pathway of cholesterol formation is depicted in figure 2.2. All animal cells produce cholesterol, which is a crucial building block of cell membranes. It is a type of crystalline solid that turns yellow when isolated chemically.

Additionally, bile acid, vitamin D, and steroid hormones are all biosynthesized employing cholesterol as a precursor. The principal sterol that all mammals sum up is cholesterol. Hepatic cells normally generate the most in vertebrates. Prokaryotes (bacteria and archaea) do not have it, however, there are notable exceptions, such *Mycoplasma*, which necessitates cholesterol to flourish (Razin & Tully, 2007).

Mammalian cell membrane is made up of cholesterol and is necessary for maintenance of optimal fluidity of membrane, permeability along with organelle identity, and protein activity. Multiple feedback loops running through transcriptional and posttranscriptional pathways assist cells maintain sterol homeostasis (Maxfield & Van Meer, 2010).

Cellular activity and dietary intake result in the production of cholesterol. The liver serves as the main repository to sustain cholesterol homeostasis through an assortment of mechanisms, the process of cholesterol metabolism involves several steps, including biosynthesis via the activity of 3-hydroxy-3-methylglutaryl coenzyme A reductase (HMGR; E.C. 1.1.1.34), adoption by means of low-density lipoprotein receptors (LDLr), liberate into the bloodstream as lipoproteins, storage through esterification and degradation, and transformation into bile acids (Weber et al., 2004). Acetyl-CoA serves as a crucial precursor for the production of cholesterol, leading to the formation of hydroxyl methylglutaryl-CoA (HMG-CoA). The process of conversion of HMG-CoA to mevalonic acid (MVA) by HMGR, which transpires in the cholesterol biosynthesis pathway, is the rate-limiting step as shown in figure 2.11 ((Espenshade & Hughes, 2007).

The group of transcription factors known to be sterol regulatory element binding proteins (SREBPs) oversee the transcription of LDLr and various other proteins that play a role in regulating cholesterol metabolism, including HMGR. These regulatory actions are influenced by the cellular sterol levels. SREBPs are linked with the endoplasmic reticulum (ER) membrane shortly after being synthesised,

where they continue to be transcriptionally inactive. The cargo protein SCAP (SREBP cleavage activating protein), which serves as a sterol sensor, interacts with the SREBP C-terminus in the ER (Espenshade & Hughes, 2007).

Acyl-CoA-cholesterol Acyl transferase can enzymatically esterify the cholesterol pool created through hepatocytes' de novo synthesis and incorporate it into very low-density lipoproteins (VLDL) featuring apoprotein B (apoB)-100 for delivery to peripheral tissues (Bays et al., 2008). By transferring cholesterol to the liver through a process guided by high density lipoprotein (HDL) particles a process termed as reverse cholesterol transport), cholesterol generated in peripheral tissues ultimately contributes to the pool of liver cholesterol. Beyond that, HDL transports dietary cholesterol from the intestine to the liver, whereupon all HDL particles internalise and interact with the hepatic scavenger receptor (Bays et al., 2008). Once supplied by HDL particles to the hepatocyte, the cholesterol may be used up to satisfy hepatic cholesterol requirements, turned into bile acids, or driven out in bile and released by feces (Ikonen 2006).

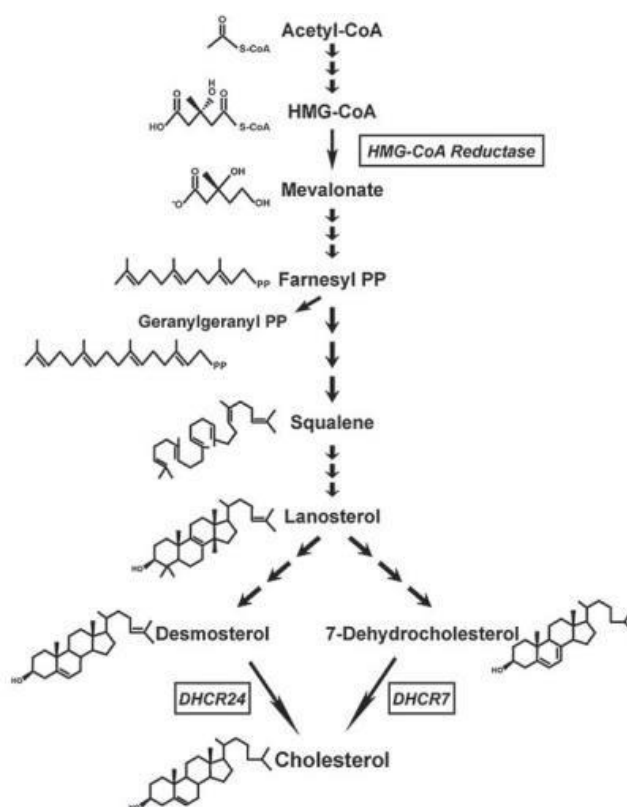


Figure 2.11: Route of Cholesterol synthesis via Mevalonate pathway

2.8.1 The comprehension of the physiological purposes of Cholesterol

Oestrogen, progesterone, testosterone, and vitamin D are all steroid hormones whose precursor is the cholesterol ring. Cholesterol, a hydrophobic substance, is circulated in the blood by spherical

plasma lipoproteins such as VLDL, HDL, chylomicrons and LDL. The amphipathic apoproteins, phospholipids, and non-esterified cholesterol that surround the neutral lipid core of the lipoproteins, which contains cholesteryl ester and triacylglycerol, are known as lipoproteins. Due to the fact that LDL particles carry cholesterol to peripheral tissues, high levels of LDL cholesterol can cause lipids to accumulate in the artery lumen, causing plaque to develop and atherosclerosis is characterized by the thickening or constriction of blood vessels. In contrast, from peripheral tissues to the liver for the production of bile acids and steroid hormones, as well as the elimination of cholesterol rings via bile HDL is in charge of reverse cholesterol transport. As was already established, to preserve cholesterol homeostasis, there is balancing and negative feedback. Dietary cholesterol obtained from outside of the body and de novo synthesized cholesterol (endogenous) are the two constituents of blood cholesterol. All cells and tissues synthesise endogenous cholesterol, but primarily the liver, intestine, and reproductive organs do so (Harvey et al., 2011).

High dietary cholesterol intake was once thought to be a contributory factor for cardiovascular disease (CVD), but new research hints at it has little to no effect on blood levels of low-density lipoprotein cholesterol (LDL-C). Analysis, nevertheless, are still debatable, perhaps as a byproduct of the connection to the consumption of saturated fat.

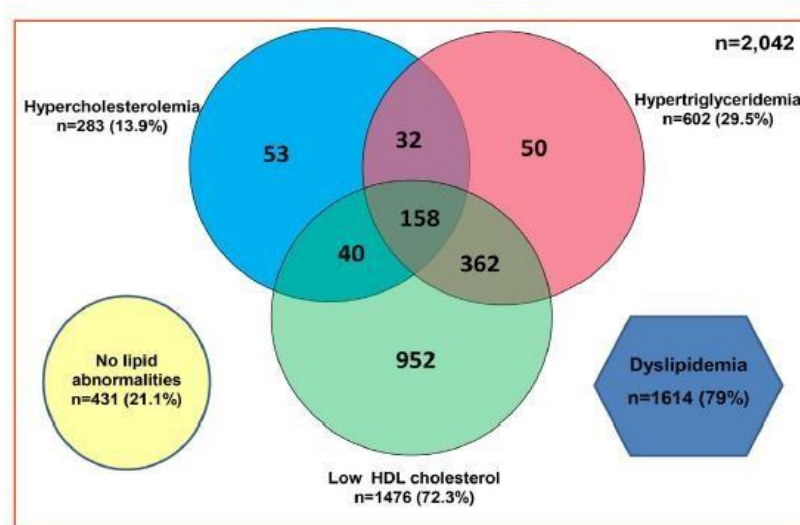


Figure 2.12: Venn diagram illustrating the commonalities of the multiple facets of dyslipidaemia: high cholesterol, elevated triglycerides, and impaired HDL cholesterol (Joshi et al., 2014)

The findings of a very intriguing study suggested that calorie restriction and aerobic exercise could produce an acute negative energy balance that ought to lower triglyceride levels by bringing down circulating large and medium very low-density lipoprotein (VLDL) particles, thus mitigating the risk of CVD (Chooi et al., 2018).

Despite the fact that blood cholesterol levels should be kept low to reduce the likelihood of developing chronic diseases, some organs in the body, like the eye, place a high value on cholesterol. The human lens fibre cell's plasma membranes possess an abundance of cholesterol, which causes the phospholipid enriched bilayer of these membranes to degrade and the creation of unadulterated cholesterol bilayer domains. The good and negative effects of cholesterol on the eye lens were the subject of a very intriguing review, with a special emphasis on excessive cholesterol, which serves another intent in the eye lens than it does in other organs and tissues (Widomska et al., 2019).

Through regulating the emergence and activity of osteoblasts and osteoclasts, cholesterol and its derivatives have a mark on bone homeostasis. In addition, the bulk of the bone cavity's volume is covered by hematopoietic cells and bone marrow adipocytes, and cholesterol's implications for hematopoietic stem cells proliferation, migration, and differentiation are well established and related to atherosclerotic lesions. Inferring a close connection between hyperlipidaemia or hypercholesterolemia and bone metabolism is the suggestion that there is an undeviating association between the risk of CVD and osteoporosis (Yin et al., 2019). Aside from its traditional function in determining the proper composition, fluidity, and performance of eukaryotic cell membranes, cholesterol also plays a key role in the organization of certain plasma membrane microdomains called lipid rafts. Figure 2.13 showcases the lipid raft's structural organization. Indeed, sphingolipids and cholesterol interact to produce lipid rafts in a specific location of the membrane where cholesterol accumulates (Pike 2006). Membrane lipid rafts are an assortment of lipid-based structure that control the assembling and operation of many cells signalling processes, in association with those tied to cancer such as cancerous cell proliferation, adhesion, migration, invasion, and apoptosis (Donatello et al., 2012; Yang et al., 2018).

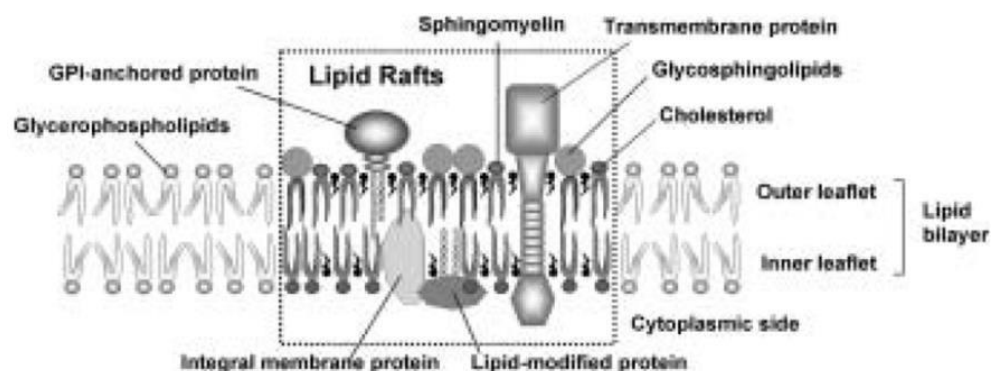


Figure 2.13: Structural makeup of Lipid rafts (Tachibana et. al.,2004)

2.8.2 Progression of infectious navigation is tailored by cholesterol homeostasis interference

Membrane cholesterol can be used by bacteria in a number of ways to infiltrate host cells. One technique includes the utilization of proteins on the surface of the bacteria that bind cholesterol and interact with areas of the host cell membrane that are high in cholesterol, resulting in the production of membrane invaginations or "caveolae" that engulf the bacteria (Shin et al., 2001).

Once inside these caveolae, the bacteria can control the machinery of the host cell to enter the cytoplasm and start an infection (Duncan et al., 2002). To enter the cytoplasm and escape the caveolae, some bacteria, for instance, can employ specialized proteins called "effector proteins" to sabotage host cell signalling networks. As shown in figure 2.14, a further method is the development of "raft-like domains" in the host cell membrane that are rich in lipids and cholesterol (Manes et al., 2003). To connect with these domains and encourage their own internalization within the host cell, bacteria can use cholesterol-binding proteins.

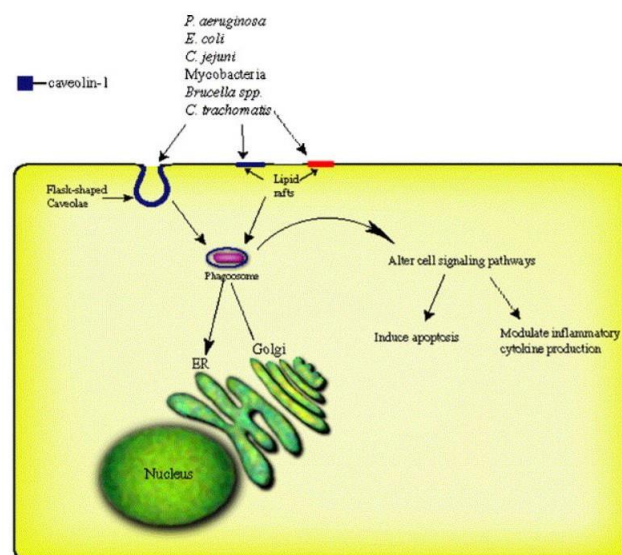


Figure 2.14: The intricate involvement of caveolae and lipid rafts in bacterial pathogenicity (Zaas et al., 2005).

An abundance of bacteria, including *Shigella flexneri*, *Salmonella sp.*, *Mycobacterium tuberculosis*, *Helicobacter pylori*, and *Listeria monocytogenes*, take advantage of the lipid raft's high cholesterol content to either access receptors like CD44, N-WASP, SopB, or E-cadherin to produce membrane ruffles or invaginations that facilitate bacteria's seamless entry into the host (Sanyal et al., 2011; LaRock et al., 2015; Suzuki et al., 2018). Apart from the precise components in lipid rafts that the microbes are targeting, the mechanism of entry seems to be dependent on cholesterol. Internalisation is greatly reduced when plasma membrane cholesterol is pharmacologically depleted or sequestered (Samuel et al., 2001). Cholesterol depletion hinders raft building and disables the development of new vacuoles, firmly demonstrating that rafts are essential for the establishment of a parasite vacuole.

It has been discovered that the class of medications known as statins, which inhibit HMGCoA reductase in the pathway of cholesterol manufacture, reduce intracellular bacterial multiplication. It is yet unknown what causes statins to have antimicrobial activity. The modulation of small GTPases, frequently used by pathogens, might have been affected by statins, according to a theory. The antibacterial impact might possibly be connected to the infection-induced cells' development of apoptosis. Patients taking statins had significantly lower total and attributable mortality when compared to patients not taking statins for bacteremic infections caused by gram-negative pathogens and *Staphylococcus aureus* (Carton et al., 2004; Liappis et al., 2001).

2.9 Impact of hepatic microRNAs in maintaining the cholesterol homeostasis

Data collected from in-vivo and in-vitro investigations have recently revealed that a number of miRNAs, including miR-370, miR122 and miR-27a/b, as well as miR 33a/b, play critical roles in lipid metabolism. Other microRNAs have also been identified, notably miR-378/378, miR 370, miR-27, miR-143, miR-302a miR-335, and miR-29a to control the equilibrium of lipids (Iliopoulos et al., 2010). It was discovered that miR-122 controls a number of crucial genes engaged with the synthesis and oxidation of fatty acids, and that miR-122 silencing reduced plasma levels of both complete triglyceride (TG) and cholesterol (TC). MiR-370 was discovered to have comparable effects on lipid metabolism as miR-122. Additionally, miR-370 has the ability to directly suppress the expression of the gene for carnitine palmitoyl transferase 1, which regulates fatty acid oxidation.

2.9.1 miR-122 in cholesterol homeostasis

miR-122 is expressed selectively and abundantly in hepatocytes, where it targets numerous genes involved in lipid and cholesterol metabolism. Not only is miR-122 well recognized for being the pathfinder miRNA to modulate metabolism of lipid to be uncovered, but it is also the site specific such as liver-enriched and liver-specific miRNA. Total serum cholesterol and triglyceride (TG) levels significantly decreased after liver-specific or whole-body ablation of the miR-122 gene. miR-122 intimidation reduced plasma cholesterol levels and rates of cholesterol synthesis in the livers of chow-fed mice, as shown by a more than two-fold downregulation of phosphomevalonate kinase (PMVK) (Esau et al., 2006). HMGCR, SQLE, FDFT1, 3-hydroxy-3-methylglutaryl-CoA synthase 1 (HMGCS1), and 7-dehydrocholesterol reductase (DHCR7) were amongst the additional genes whose expression dropped as a consequence of miR-122 inhibition (Krutdzfelt et al., 2005). miR-122's effect on metastasis and a poor prognosis appeared to be unrelated to their function in fat metabolism (Wen & Friedman, 2012).

Circulating cholesterol levels were significantly reduced (25%–30%) by anti-miR-122 treatment. The discovery of Smarcd1/Baf60a as an intriguing miR-122 target is consistent with the tight control of these genes. Smarcd1/Baf60a is a member of the SWI/SNF-related matrix associated actin reliant regulator of chromatin subfamily d. It's interesting to take into account that the nuclear receptor subfamily 1 group D member 1 (NR1D1/REV-ERB) transcriptional repressor is involved in the circadian transcription of the miR-122 locus. Most metabolic processes in the liver are regulated by the circadian rhythm. Metabolism of lipids and cholesterol are renowned for their daytime-dependent regulation, just like several hepatic processes requiring integrating food intake with a processing of nutrient and energy balance. The circadian rhythm and hepatic metabolism may be newly regulated by miR-122's molecular mechanism (Gatfield et al., 2019). Additionally, translation and replication of the hepatitis C virus (HCV) are accelerated by miR-122, which has been found to be linked with HCV genome. Down-regulation of miR-122 has a tendency linked to hepatocellular carcinoma (HCC), and miR-122 is involved in a number of hepatic illnesses (Jopling et al., 2005; Thomas & Deiters, 2013).

2.9.2 miR 27a in cholesterol homeostasis

miR-27a is known to control multiple genes engaged in lipid metabolism as well as adipogenesis. These include ATP-binding cassette transporter (ABCA1), Retinoid X receptor alpha (RXR), fatty acid synthase (FASN), also known as the cholesterol efflux regulatory protein, SREBP-1 and -2, PPAR- α and - γ , Apolipoprotein A-1, Apolipoprotein E-3 and Apolipoprotein B-100 (Yang et al., 2015). Furthermore, a comprehensive investigation into miR-27a targets revealed 21 pathways, encompassing biosynthesis of steroids, metabolism of fatty acids among others (Khan et al., 2020).

2.9.3 miR 33 in cholesterol homeostasis

MiR-33 is a miRNA that has been extensively researched in relation to cholesterol homeostasis. While similar miRNA mir-33b is encoded in the SREBF1 locus, highly conserved miR-33a is located in the intronic area of SREBF2 (Rayner et al., 2011). According to reports, miR-33 co-expresses with SREBP2 and targets ABCA1 for minimizing cholesterol efflux (Rayner et al., 2011; Gerin et al., 2010; Horie et al., 2010). ABCG1 was likewise suppressed by miR-33, but only in mouse macrophages (Marquart et al., 2011). As a result, miR-33 is crucial for maintaining acceptable levels of cholesterol and becomes malfunctioning during the development of cancer. Reduced miR-33a expression in prostate cancer boosted invasion and metastasis, highlighting that it has tumour suppressor elements. Furthermore, the tumour disrupted the normal scenario's beneficial partnership between miR-33 and SREBF2, which was ordinarily positive.

2.9.4 miR 223 in cholesterol homeostasis

It has been verified that miR-223 either directly or indirectly governs the three essential aspects of cholesterol homeostasis. Two genes linked in the metabolic activity of cholesterol, HMGCS1 and methylsterol monooxygenase 1 (SC4MOL), are believed to be objectives of miR-223. Additionally, SCARB1 was repressed by miR-223 to limit cholesterol uptake. On top of that, miR-223 increased the expression of ABCA1 via the transcription factor Specificity Protein 2(Sp3), so indirectly promoting cholesterol efflux

2.9.5 miR-96/182/183 in cholesterol homeostasis

On human chromosome 7, the conserved miRNA locus miR-96/182/183 exists by the identical transcription unit. It has been revealed whether SREBP2 interacts directly with the conserved binding pocket in the promoter section of these miRNAs and triggers them. This finding offered implications for a positive feedback loop controlling SREBP2 activity. Pre-miR-183 treatment boosted SREBP-1 levels as well, although the research did not identify its direct target gene (Jeon et al., 2013).

2.9.6 miR 185 in cholesterol homeostasis

By suppressing the expression level of SREBF2 and its target genes that are engaged with the de novo synthesis and absorption of cholesterol, miR-185 has been illustrated to control cholesterol homeostasis (Wang et al., 2014). In addition, by means of diminishing SCARB1 expression, miR-185, miR-96, and miR-223 modified the absorption of cholesterol (Wang et al., 2013). In prostate cancer, miR-185 inhibited SREBF1 and SREBF2 and their downstream targets (FASN and HMGCR) (Li et al., 2013).

2.9.7 miR21 in cholesterol homeostasis

The predicted target gene of miR-21 for HMGCR was discovered using prediction software (<http://www.microrna.org/>). HMGCR is an amplifier of miR-21's effects on metabolism of cholesterol and TG in NAFLD (Sun et al., 2015). Human patients with NAFLD have higher amounts of miR-21 in their blood, which may possess affect the manner in which adipose tissue features (Yamada et al., 2013). In fact, recent investigations have shown that miR-21 is involved in the development of adipocytes (Chartiumpekis 2018, Kang et al., 2013). There are four main cholesterol efflux routes known 1) Passive diffusion of cholesterol entering mature HDL particles, 2) Facilitated diffusion via SR-B1, 3) Efflux to apo A1 (pre-HDL) with low levels of lipid via

ABCA1, and 4) ABCG1-mediated efflux to mature HDL with high levels of lipid (Sankaranarayanan et al., 2009). The respective contributions of these pathways in mouse peritoneal macrophages were as follows: SR-BI 9%, aqueous diffusion 35%, ABCA1 35%, ABCG1 21%. Aqueous diffusion was the main efflux route in cholesterol-free murine macrophages, whilst ABCA1 played a major role in cholesterol-loaded macrophages (Adorni et al., 2007). ABCA1 acted as the main mediator of efflux in cholesterol-loaded human macrophages, without interference from ABCG1. The SR-BI pathway was also involved in the procedure (Larrede et al., 2009).

2.9.8 Modulation of Cholesterol by RNA binding proteins

RNA binding proteins (RBPs) are crucial for post-transcriptional control of gene expression, which entails controlling how considerably cholesterol is metabolized. Numerous RNA-binding proteins have recently been linked to cardiovascular diseases, abnormalities in the metabolism of lipids, and neuronal cholesterol. AUF-1 or hnRNPD, hnRNPA1, HuR, and other essential RBPs are a few of these. In cultured N2a and MN1 cells, hnRNPR collaborates in the neural metabolism and mitigates cholesterol by blocking HMGCR, as depicted in Figure 2.15 (Agbo et al., 2021).

The modulation of HMGCR expression by HNRNPA1, an mRNA splicing regulator, leads to decreased enzyme activity of HMGCR and increased uptake of LDL-C. This is achieved through the regulation of an alternatively spliced transcript of the HMGCR gene. It, therefore, appears that HNRNPA1 also participates in cellular cholesterol metabolism (Yu et al., 2013).

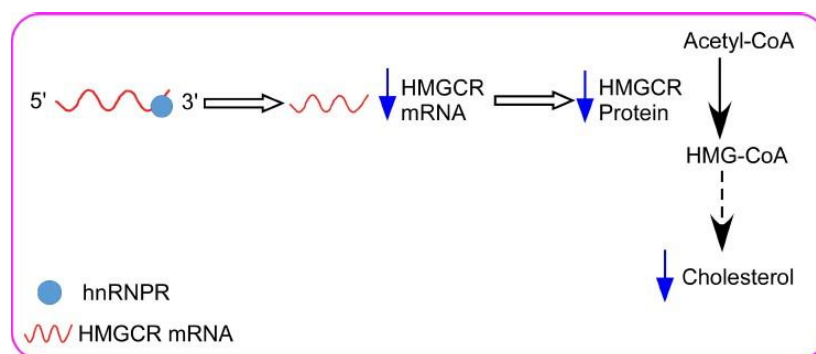


Figure 2.15: hnRNPR lowers cholesterol levels by restricting the expression of HMGCR (Agbo et al., 2021)

HuR has a direct interaction with the ABCA1 mRNA, which maximizes the expression of the ABCA1 protein and encourages cellular cholesterol efflux. HuR may play an indispensable role in regulating macrophage lipid homeostasis in vivo as evidenced by the fact that it is significantly expressed in macrophages accruing in both mice and human atherosclerotic plaques (Ramiez et al., 2014).

2.10 The role of cholesterol efflux in preserving homeostasis

Dietary cholesterol is the major avenues of gaining cholesterol in human beings and its absorption is mediated by NPC1L1 protein present in enterocytes (Altmann et al., 2011). NPC1L1 has transmembrane helices (total 13 in number), five of which encompass the SSD, which controls NPC1L1 mobility across the plasma membrane and the recycling compartment of endocytic nature in response to intracellular cholesterol levels (Wang et al., 2009; Yu et al., 2006). The structure of NPC1L1 was completely revealed by cryo-electron microscopy in 2020, making it simpler to comprehend the process of NPC1L1-mediated cholesterol uptake. Cholesterol causes NPC1L1 to modify its conformation after binding to the sterol-binding pocket, creating a route for delivery tube for uptake of cholesterol by cells (Huang et al., 2010).

Chylomicrons are created when triglycerides (TG) are loaded into ApoB-48 and NPC1L1 uptakes cellular cholesterol, which is subsequently undergoes the process of esterification with the help of ACAT 2 (acyl-CoA: cholesterol acyltransferase) in the ER. Once in circulation, hydrolysis of mature chylomicrons utilized in peripheral tissues and most of the cholesterol undergoes hepatic absorption. ABCG5/8 can transport FC back into the intestinal lumen, whereas ABCA1 can convert it to produce HDL-C and release it directly into circulation (Jia et al., 2011).

The majority of peripheral cells and tissues are unable to break down cholesterol, thus they mostly rely on efflux routes to keep their cellular homeostasis in check. Reverse cholesterol transport (RCT) is the procedure of the removal of extra cholesterol from cells and transferring it to the hepatic region for release into bile. An adequate acceptor, which HDL plays, is an indispensable need for efflux. The amount of cholesterol in the cell, the size, composition and concentration of HDL, as well as the expression of various efflux transporters, all affect how quickly cholesterol escapes the body (Rader et al., 2009). Oxysterols and desmosterol, which serve as intermediary precursors in cholesterol production, cause the activation of their corresponding receptors, or LXRs, as the level of cellular cholesterol rises. Likewise, LXRs result in increased transcription of genes that transport extra cholesterol to high-density lipoproteins (HDL) particles, such as ABCG1 as well as ABCA1 (Figure 2.16). The HDL particle transports its payload to the liver upon surveillance by the hepatic Scavenger receptor type B, class-I (SRB1), which is principally in charge of removing extra cholesterol into the bile (Lintol et al., 2017).

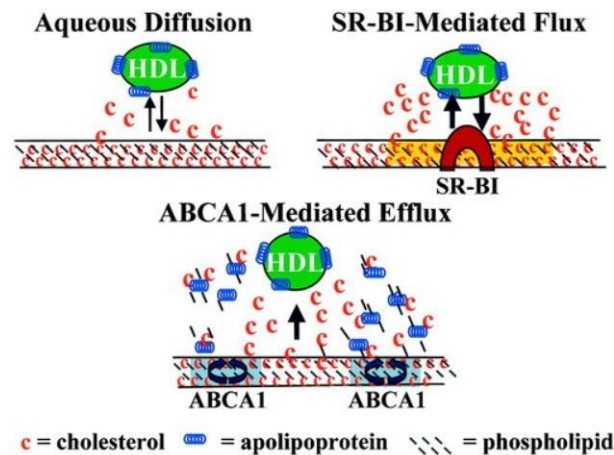


Figure 2.16: Mechanisms for removing unsterified cholesterol from peripheral cells. (Yancy et al., 2003)

There are four distinct cholesterol efflux routes known: 1) Cholesterol diffuses to advance HDL particles passively; 2) SR-B1 accelerates diffusion; 3) ABCA1-mediated efflux to lipid-poor apo A1 (pre-HDL), 4) ABCG1-mediated outflow to lipid-rich, seasoned HDL (Favari et al., 2009; Sankaranarayanan et al., 2009). In cholesterol-free murine macrophages, aqueous diffusion was the main driving force, but ABCA1 was crucial to the efflux in cholesterol-loaded macrophages (Adorni et al., 2007). ABCA1 emerged as the main mediator of efflux in cholesterol-loaded human macrophages, independent of ABCG1.

2.11 Role of RNA binding proteins in cholesterol metabolism

Along with lncRNAs and miRNAs, RNA binding proteins (RBPs), particularly those that regulate turnover and translation, are known to control every facet of mRNA metabolism, including synthesis, delivery, translation, and turnover. They achieve this by interacting with various RNA interaction motifs that are typically found in the 3'UTR of the target mRNA (Keene, 2007).

Numerous RBPs have been linked in recent research to lipid and cholesterol metabolism as well as cardiovascular diseases.

HuR or Human antigen R, commonly referred to as aberrant vision and embryonic fatal The Hu/Elav family of RBPs, Drosophila-like 1 (ELAVL1), is widely expressed and affects the stability and translational efficiency of mRNAs through interactions with uridylyte (U)-rich or adenylate-uridylyte (AU)-rich regions in the 3'UTR of target genes (Hinmal & Lou, 2008). HuR directly interacts with ABCA1 mRNA, as Ramirez and colleagues have shown, enhancing protein expression of ABCA1 and encouraging cellular cholesterol efflux. It's interesting to note that cellular cholesterol, which raised HuR's mRNA and protein levels, improved this relationship. On

the other hand, statins reduce the rate at which HuR translocates through the nucleus onto the cytoplasm and hinder the establishment of ABCA1 mRNA by HuR. Notably, HuR is extremely prevalent in macrophages gathered in atherosclerotic plaques in mice and humans, indicating a crucial function for HuR in regulating macrophage lipid equilibrium in vivo (Ramírez et al., 2014).

A family of RNA-binding proteins known as heterogeneous nuclear ribonucleoproteins (hnRNPs) binds to newly formed transcripts and plays critical roles in all stages of (pre)mRNA processing, including translational control, subcellular transport, the transcription process, wrapping, splicing, equilibrium, and depletion. A family of RNA-binding proteins known as heterogeneous nuclear ribonucleoproteins (hnRNPs) binds to newly formed transcripts and plays critical roles in all stages of (pre)mRNA processing, including translational control, subcellular transport, transcription, presentation, splicing, stability, and degeneration (Dreyfuss, 2002). Several subsets of hnRNP have been identified, which is also known as AUF-1 in mouse and numerous hnRNPs have also been connected, in addition to cancer, to several neurological illnesses, including AD, ALS, and frontotemporal lobar dementia (FTLD). Biologically, hnRNPR controls transcription, immune factors, and c-fos mRNA degradation (Bampton et al., 2020; Neumann et al., 2006; Huang et al., 2008). The functions that RBPs play in lipid and cerebral cholesterol metabolism, as numerous experts in the field have eloquently proven (Li et al., 2009; Grünler et al., 1994). It has been demonstrated that hnRNPR expression in vitro in neural cell lines can suppress HMGCR expression. In neuronal and non-neuronal cells, precise preservation of cholesterol equilibrium is essential because dysregulation or disturbance of cholesterol homeostasis can result in a wide range of clinical diseases. Given the important function cholesterol plays, it makes sense to develop a complex and comprehensive system to regulate cholesterol synthesis, metabolism, and excretion (Agbo et al., 2021).

The human AUF1 gene, which maps to 4q21, is home to an assortment of proteins called p37, p40, p42, and p45, each of which has a distinct molecular mass. Different tissues exhibit preferential expression of AUF1 isoforms, each with unique biological characteristics. AUF1 interacts with ARE-bearing mRNAs to affect the processes of growth, cancer and apoptosis (Moore et al., 2014; Abdelmohsen et al., 2012). Several cancer types may be encouraged to develop and spread by changes in AUF1 expression patterns. It was discovered that the stability of ARE-containing mRNAs was significantly impacted by AUF1 overexpression. According to research by Kumar et al, oral squamous cell carcinomas expressed nuclear AUF1 at a level that was noticeably greater than in normal cells. Reducing AUF1 with RNA interference (RNAi) also reduced the rate of cell proliferation (Kumar et al., 2012). It has been demonstrated that AUF1 promotes the degradation of some target mRNAs, but it can also occasionally affect the translation and stability of several target mRNAs. Numerous investigations have demonstrated the anti-tumorigenic function of AUF1

in controlling apoptosis and the cell cycle. As an instance, raising AUF1 by UVC may encourage apoptosis by lowering ARE-containing Bcl-2 mRNA (Lapucci et al., 2002).

Apart from HuR and AUF-1, another remarkable RNA binding protein is ZFP36. ZFP36 or Zinc finger protein-36, is expressed at low levels in the healthy aorta yet at high levels in foam cells and the endothelial cells that cover plaques. It is expressed in response to inflammation, acting as a defense mechanism by hindering a transcriptional stimulation of NF- κ B, connecting to AU-rich elements of cytokine mRNAs, and reducing transcript stability. This reduces the production of inflammatory cytokines, such as IL-6 and MCP-1. However, more research is needed to understand ZFP36's physiological function as atherosclerosis advances (Ramírez et al., 2014).

2.12 Role of RNA binding proteins in gut barrier maintenance

Normal TJ protein expression is required for integrity of intestinal barrier, as reduced levels of TJs or poor TJ assemblies led to the barrier failure and increased paracellular permeability of epithelium of intestine (Turner, 2009; Paris et al., 2007). Abundant expression of RBPs including AUF1, CUGBP1, HuR in IECs, and their functions are promptly and significantly altered in exchange for diverse medical conditions such as hypoxia, inflammation, injury along with malignancy (Burd & Dreyfuss, 1994; Yu et al., 2011).

IECs establish and sustain a barrier between the submucosa and the intestinal lumen. The junction complex, which includes the adherent junction (AJ) along with the tight junctions (TJs) regulates epithelial integrity (Peterson & Artis, 2014). The TJ complex is the primary regulator of intestinal permeability and trans-epithelial transit. Intestinal inflammation may result from disrupted TJ and increased intestinal permeability. Occludin is a crucial TJ protein that helps to maintain the integrity of the intestinal epithelium. Additionally, Occludin and claudin mRNAs are transient and are regulated post-transcriptionally (Yu et al., 2012). Occludin deletion mice had slower development and chronically irritated GI tracts while upregulated Claudin-2 makes the gut porous (Odenwald & Turner, 2016). According to several reports, RBPs like HuR, IGF2BP1 regulate occludin and thereby protect intestinal epithelial barrier function (Yu et al., 2012; Singh et al., 2020). mRNA stability of Occludin, Claudin-2 and other junctional proteins are likely to be regulated by these RBPs in a context dependent manner, either individually or cumulatively, but the exact molecular mechanism is yet to be discovered (Morrow et al., 2010).

2.13 Role of RNA binding proteins in gut immunity

The induction of inflammation is largely regulated by strong transcriptional regulation, although immune cells like T cells and macrophages also produce inflammatory cytokines and messengers at different rates, which is controlled by post-transcriptional mechanisms (Kafasla et al., 2014; Turner & Díaz-Muñoz, 2018; Hoefig & Heissmeyer, 2018). A form of mRNA-level gene expression control known as post-transcriptional manipulation governs the equilibrium, translation, alterations, localization, and alternative splicing of mRNA. These mechanisms, which are regulated by several RNA binding proteins (RBPs), effectively suppress immune responses as the inflammation resolves by coordinating the regulation of inflammatory gene activity in immune cells. Furthermore, recent research has demonstrated that post-transcriptional programs also control the various roles played by non-immune cells, controlling the interaction between immune cells and non-immune cells to aid in the removal of pathogens from the surrounding tissue.

Nutrients and microbes are among the many exogenous items that the gut mucosa comes into contact with. In order to prevent undesirable immune responses that lead to inflammatory bowel illnesses, it is necessary to correctly create immunological tolerance against nonharmful elements. It is well known that rolquin regulates the development of colitis (Essig et al., 2017). Since many inflammatory mRNAs (mRNAs encoding inflammatory mediators) have been demonstrated to be somewhat unpredictable, transcription and responses to inflammation can be precisely controlled (Hao & Baltimore, 2009). In unstable inflammatory mRNAs, a number of cis-elements are typically detected. The most well-characterized motifs among them are stem-loop structures and AU-rich elements (AREs). Adenine and uridine sequences usually consist of a stretch that is represented by the repeating AUUUA motif in AREs (Barreau et al., 2006). Proinflammatory genes such as IL-6, TNF, IL-2, cyclooxygenase 2 (COX2), IFN- γ , and GM-CSF have these motifs in their 3' UTRs. Human antigen R (HuR), AU-rich binding factor 1 (AUF1) ARE-binding proteins TTP (tristetraprolin, also known as ZFP36), ZFP36L1, ZFP36L2, and KH-type splicing regulatory protein (KHSRP) bind and recognize AREs. The majority of these ARE-binding proteins encourage target mRNAs to degrade, although HuR is known to stabilize mRNAs that include AREs (Wang et al., 2013).

MATERIALS AND METHODS

3.1 Chemicals and reagents

High Fat Diet (HFD) (Harlan Teklad TD93075), Chow diet (Harlan Teklad LM-486) was procured from ICMR-National Institute of Nutrition, Hyderabad, India. DMEM (Dulbecco's modified Eagle's medium), RPMI (Roswell Park Memorial Institute medium), HBSS (Hanks Balanced Salt solution) and foetal calf serum (FCS) were purchased from GIBCO (Waltham, MA, USA). kit used for estimation of protein was procured from Thermofisher. Gentamycin, apoptosis kit, BCIP-NBT kit, CFSE kit, LDH kit, were purchased from Thermofisher (Waltham, MA, USA). HEPES, Collagenase IV, EDTA, ampicillin, Penicillin, streptomycin, metronidazole, vancomycin, MTT (3-(4,5-dimethylthiazol-2-yl)-2,5-diphenyl tetrazolium bromide), leupeptin, Triton X100, acrylamide, PMSF, bis-acrylamide, glycine, para-formaldehyde, sodium propionate, sodium butyrate, sodium acetate, glutaraldehyde, Hoechst 33342, watersoluble cholesterol (MBCD-cholesterol), cholesterol estimation kit were purchased from Sigma (St. Louis, MO, USA). ALT and AST determination kit was purchased from Transasia Biomedicals (Mumbai, India). Phosphatidyl choline, Cholesterol, Cholesterol analogue (4-cholesten-3-one), 22-NBD-[22-(N-(7-Nitrobenz-2-Oxa-1,3-Diazol-4-yl) Amino)-23,24-Bisnor-5-Cholen-3 β -Ol]-cholesterol, were purchased from Avanti-polar lipids (Birmingham, USA). Probiotic capsules were obtained from Bifilac (Tablets India, Chennai, India). HDL was purchased from Beacon Diagnostics Pvt Ltd (Navsari, Gujrat, India). Poly ethylene glycol (PEG) solution was purchased from Jhaver Centre (Chennai, India). QIAamp stool mini kit was purchased from Qiagen (Hilden, Germany). PVDFmembrane, Opti-MeM, Lipofectamine 2000, Trizol, Amplex red cholesterol assay kit, Fillipin were purchased from Invitrogen (Carlsbad, CA, USA). (Ripa lysis buffer, Anti-AUF1 antibody (rabbit polyclonal), siAUF1, anti-ABCA1 antibody (rabbit monoclonal), anti- β -actin antibody (polyclonal), anti-HMGCR antibody (polyclonal), were purchased from Cell Signalling Technology (Danvers, MA, USA). Prime script first strand cDNA synthesis kit, qPCR kit Fiwas, TB Green Premix ex-Taq purchased from Takara (Shiga, Japan). All primers were purchased from IDT (Lowa, USA). Anti CD71-biotin was purchased from elabscience, Invitrogen (Massachusetts, Boston, USA). Secondary Steptavidin PE was purchased from ebioscience (USA). Anti-AUF1 antibody (mouse monoclonal IgG1), Anti-Dicer1 antibody (mouse monoclonal IgG2a) was purchased from Santa-cruz Biotechnology (Dallas, Texas, USA). Anti-ABCA-5 antibody (rabbit, polyclonal) was purchased from Abcam (Cambridge, UK). Anti-GAPDH antibody (rabbit polyclonal) was purchased from Bio-Bharati (Kolkata, India). RAW264.7 cell line was purchased from ATCC (USA). pEGFP-AUF1 isoforms were also gifted by Prof. Andrea Pautz, University of Mainz, Gutenberg. pEGFP and pEGFP-3'UTRDicer1 were a kind gift from Dr. Myriam Goropse, NIH, USA. pmiR122 and Human hepato-carcinoma cell line Huh7 were a kind gift from Dr. Suvendranath Bhattacharya (CSIR-IICB, India).

3.2 Animals

Six-week-old C57BL/6 mice free of pathogens were obtained from the Indian Council of Medical Research-NICED, an institutional animal facility in Kolkata, India. ICMR-NICED's (Indian Council of Medical Research-NICED, Kolkata, India) Animal Ethics Committee authorized entire study procedures (NICED/BS/MB-001/2019). A 12-hour light/dark cycle and a regulated temperature were applied to each mouse's housing. Research has been conducted in compliance with the protocols established by the Ministry of Environment and Forests, Government of India, New Delhi, India's Committee for Control and Supervision of Experiments on Animals (CPCSEA).

3.3 Dietary supplementation of sodium butyrate

Minor modifications were made to the originally described protocol of the food supplementation experiments, as reported by Xu et al. in 2018. To put it briefly, ten reproductively mature C57BL/6 mice, five in each group, were given a high-fat diet (carbohydrate, protein (both of them are 20% Kcal), 60% kcal fat), and a minute quantity of cholesterol (0.007% w/w). Animals (5 in number) were chosen at random and given an additional 15 days of 5% sodium butyrate (w/w) after receiving HFD for four weeks (HFD butyrate mice). The solid sodium butyrate was fully blended into the HFD. HFD mice were given to the remaining mice for a duration of 15 days. Every other day, a new diet was added. The control group consisted of age-matched chow mice that were fed a typical diet.

3.4 Food consumption

Food was given (put in the food container at time zero) and leftover (left in the food container 24 hours later) were weighed each day to record the amount of food consumed by the mice. We measured the total amount of food consumed daily by each group of five mice.

3.5 Collection of blood, preparation of serum samples, biochemical analysis, estimation of cholesterol and lipoproteins and hepatic enzymes

Serum was made by centrifuging the extracted blood at 1800 rpm for three hours at room temperature, and the Assay Kit was used to measure the serum cholesterol levels. Transasia Biomedicals' (India) kit was used to assess the serum levels of the aminotransferases aspartate (AST) and alanine (ALT).

3.6 Antibiotic treatment

After seven days of gavage with broad-spectrum antibiotics, the naturally occurring intestinal microbiota of mice (4 weeks) raised on chow diet was diminished (Reikvam et al., 2011). Vancomycin, metronidazole, and ampicillin were diluted in sterile water to create the antibiotic solution. Metronidazole and Ampicillin (200 mg/kg) along with Vancomycin at a dose of 100mg/kg were administered to mice once daily. The mice that were given antibiotics are now referred to as Abx mice.

3.7 Probiotic treatment

Probiotic treatment was carried out with slight adjustments to the previously published protocol (each of which comprising lactic acid bacteria (50 million), *S. faecalis* (30 million), *C. butyricum* (2 million) and *B. mesentericus* (1 million) (Le Roy et al., 2018). In short, five mice per cage received a 1.2 cc solution of polyethylene glycol (PEG) to cleanse their intestines before receiving probiotics. The group of twenty mice, four mice per cage, were fed a cocktail antibiotic for seven days. Since mice are coprophagous, their cages were kept clean and equipped with a wired net to prevent the ingestion of excrement. Before colon cleaning, urine and blood (from the tail vein) were taken.

Following a 2-hour fast (with free access to water), the PEG solution was distributed into equivalent 5 doses (200 µl/mouse/dose) and gavage was given at 30-minute time intervals. The PEG solution contained PEG 3350 (77.5 g/L), potassium chloride (0.98 g/L), sodium sulfate (7.4 g/L), sodium chloride (1.9 g/L) as well as sodium bicarbonate (2.2 g/L) diluted in sterile tap water. After the final antibiotic gavage, 24 hours later, the PEG solution and the inoculum were administered. Two probiotic inoculations (200 µl) were given orally to Abx mice every other day for two weeks, with each probiotic capsule suspended in one milliliter of water. Straw and a sterile cage were provided for the mice. Over the next fourteen days, all animals were fed an ad libitum chow diet and autoclaved deionized water. For a duration of 14 days, a set of five Abx mice were given antibiotics in addition to a chow diet supplemented with 5% sodium butyrate (Abx butyrate mice). For a further fourteen days, five Abx mice in that group received the same antibiotic regimen. A control group of five age-matched mice was given a regular chow diet for 21 days without receiving any antibiotic treatment.

3.8 mir-122 overexpression in mice

As previously mentioned, (Ghosh et al., 2013 Chang et al., 2004), mir-122 was overexpressed in mouse liver. To introduce 25 µg of DNA dissolved in 100 µl of saline per animal treated with butyrate, the empty plasmid (mock) or the mir-122 expressing plasmid was given into the tail vein. On day 4

following injection, mice were slaughtered, and liver expression of mir-122 and serum cholesterol were assessed.

3.9 Mice fecal sample collection

To reduce any circadian effects, fresh fecal samples from every mouse were taken at a set time each day. After being collected into sterile, empty microtubes on ice, the samples were immediately stored at -80°C for further use.

3.10 Extraction of fecal DNA and calculation of butyryl-coenzyme A (CoA): acetate CoA-transferase (ButCoAT) gene abundance by qPCR

40 mg of each mouse's fecal pellet was used for DNA extraction by using the QIAamp DNA stool minikit (Qiagen). With a QIAxpert spectrophotometer (Qiagen), the DNA was quantified. With the use of 16S rRNA-bacterial primers, the results of qPCR analysis were normalized to the overall bacterial abundance to assess the relative abundance of bacteria carrying the butCoAT gene in the fecal DNA of mice (Jian et al., 2020; Berding and Donovan, 2018). Table 1 contains a listing of the primer sequences used.

3.11 Measurement of butyrate in feces by LC-MS

A Dounce homogenizer was used to dissolve each mouse's feces (50 mg wet weight) in distilled water at a ratio of 1:10 (w/v). A 0.45- μ m syringe filter was used to filter the supernatant after the sample was centrifuged for 10 minutes at 10,000g. After being further dissolved in LC-MS quality distilled water to an end volume of 1 ml, the supernatant was tested by LC-MS for SCFA, following Cheng et al.'s (2020) protocol. Essentially, different internal parameters of butyrate ranging in calibration from 2 to 50 μ mol were used to create a calibration curve. The Agilent 1290 Infinity LC system was used for the LCMS separation. It was connected to an Agilent 6545 Accurate-Mass Quadrupole Time-of-Flight (QTOF) system using an Agilent Jet Stream Thermal Gradient Technology with an electrospray ionization (ESI) source.

Through the use of negative ionization mode during the analysis, the appropriate MS parameters were tuned and (HR) mass spectra were obtained. Using an Agilent ZORBAX SB-C18 column (2.1 \times 100 mm, 1.8 μ m) as the stationary phase, the chromatographic separation was accomplished. 1.0–1.0 min, 0% B (v/v); 1.0–3.0 min, 0%–30% B (v/v); 3.0–6.0 min, 30%–100% B (v/v); 6.0–12.0 min, 100% B (v/v); 12.50–15.0 min, 0% B. This was the linear gradient that made up the mobile phase. Before the subsequent injection, the tube was restored for five minutes. For analysis, a variable injection volume

and an average flow speed of 0.2 ml/min were employed. An autosampler and a diode array detector (DAD) were included in the assembly of the UPLC system. The quantity of SCFA available was determined by calculating the peak region of each SCFA, and the injection volume was utilized to further standardize the result. The information was shown as the quantity of butyrate found in each gram of excrement.

3.12 Cholesterol-liposome and cholesterol analogue-liposome synthesis

Liposomes were created by combining cholesterol, NBD-cholesterol, also known as 22-(N-(7-nitrobenz-2-oxa-1,3-diazol-4-yl)amino)-23,24-bisnor-5-cholesterol-3 β -ol], phosphatidylcholine, 4-cholesten-3-one by the methodology (Kheirloom and Ferrara, 2007). In a nutshell, PC, cholesterol, and cholesterol analogue (4-cholesten-3-one) were combined in a round-bottom flask at a ratio of 1:1.5 and stored overnight in a vacuum desiccator. A very fine layer of lipid was produced, which was subsequently solubilized in one milliliter of DMEM and passed through a 0.22 μ m membrane filter (Banerjee et al., 2009). Differential light scattering (DLS) was utilized to quantify the liposomes' size. NBD chol-lipo, ana-lipo, and cholesterol-liposome will now be referred to as chol-lipo, chol-lipo, and ana-lipo, respectively.

3.13 Administration of liposomal cholesterol in mice

The food supplementation studies were carried out for the pathogen invasion analysis test with minimal modifications from the previously reported results (Aartsma-Rus et al., 2017). In summary, ten adult C57BL/6 mice were split into five groups and given a chow diet along with autoclaved drinking water mixed with 150 mM sodium butyrate for a duration of thirty days. After 28 days of butyrate therapy, 5 animals were randomly chosen from the group and given an intracardiac injection of 200 μ L of suspension of liposome (chol-lipo mice). A control group of 5 mice was fed standard chow and had access to normal drinking water. On the 30th day, these animals received an infection intraperitoneally with 10⁸ cfu/mice *Shigella flexneri*. The animals were slaughtered on the second post-infection day, and samples were obtained for additional studies. An uninfected control group consisted of age-matched normal mice.

3.14 Transmission Electron Microscopy

The liver tissue has been preserved in 0.1M sodium cacodylate buffer with 3% glutaraldehyde. Following that, a second time preservation with 1% Osmium tetroxide was performed, afterwards

dehydration with escalating grades of acetone, and at the end embedding in Agar 100 resin as well as polymerization at 60°C. The tissue was cut into ultrathin sections (40-50 nm) utilizing a Leica Ultracut UCT ultramicrotome (Leica Microsystems, Germany), scooped up on nickel grids, and dual-stained with 0.2% lead citrate and 2% aqueous uranyl acetate. The slices were examined using an FEI Tecnai 12 Biotwin transmission electron microscope (FEI, Hillsboro, OR, USA) at 100 kV (Eid et al., 2016).

3.15 Propagation of Huh7 and RAW 264.7 cells and estimation of viability and toxicity after butyrate treatment along with cellular protein and cholesterol

Huh7 cells were grown at 37°C with 5% CO₂ in DMEM supplemented with 10% FCS and 50 g/ml gentamycin. MTT was used to determine cellular viability. The Amplex Red Cholesterol Assay kit was used to estimate cholesterol levels. Concentration of protein from the lysate was calculated by using PierceTM BCA Protein Assay Kit.

Murine macrophage cell line RAW264.7 was grown in DMEM (Dulbecco's modified Eagle's medium) with 10% FBS (Fetal bovine serum) supplemented with 1% Streptomycin and Penicillin in a humidified incubator (Heracell 150i, ThermoFisher Scientific) at 37° C with 5% CO₂. Cells were then cultured in six well culture plates (10⁶ cells/well) and given overnight time to adhere until reaching a confluency of 75-80%. The cells were subsequently treated for 18 hours with various amounts (5 mM or 10 mM) of sodium butyrate (butyrate), with 2 mL media in each well. Annexin/PI staining was used to determine cell viability. The LDH assay kit was used to measure the cellular toxicity following butyrate therapy. As previously mentioned, total crude cell membranes were isolated 24. The cells were homogenized in a 1 mL buffer containing a protease inhibitor mix (Roche Diagnostics, Mannheim, Germany) and 1 mM EDTA, 200 mM sucrose and 10 mM Tris-HCl (pH 7.4). Centrifugation was used to remove the nuclei and cellular debris for 10 minutes at 4°C at 900 x g. To get the crude membrane pellet, the resultant supernatant was centrifuged at 100,000 x g for 75 min at 4°C. The pellet was resuspended in PBS by the manufacturer's instructions, and an aliquot was utilized to quantify protein employing the PierceTM BCA Protein Assay Kit. 2:1 methanol/chloroform was used to extract the remaining portion of the pellet, which was then mixed with 0.5 mL of water and 0.5 mL of chloroform. In a vacuum desiccator, the methanol/chloroform (lipid phase) layer was vacuum-dried. The membrane cholesterol assay kit came with 200 µL of 1x Reaction buffer, which was used to suspend the dry lipid. The manufacturer's instructions for membrane cholesterol measurement were followed.

3.16 Isolation for Murine Hepatocytes:

With a few minor adjustments, hepatocytes from mice were extracted using the Percoll method (Goncalves et al., 2007). In short, an incision was made to adequately open the abdomen of deceased C57BL/6 mice, and the animals were positioned on top of a tissue paper pillow. A tiny cut was made to place a cannula into the portal vein, and 10 milliliters of perfusion buffer—25 millimoles of HEPES and half a milliliter of EDTA in HBSS—without Ca^{2+} and Mg^{2+} —were used to perfuse the liver. The vena cava was used to pass the digestion buffer, which included 25 $\mu\text{g}/\text{ml}$ Collagenase IV in HBSS with Ca^{2+} and Mg^{2+} and 25 mM HEPES. The liver was gently taken out and placed in a petridish with digestion buffer before being carefully dissociated. The cells underwent filtration using a BD 100 μm cell strainer, and centrifugation at 50g for 5 minutes was done. 10 milliliters of DMEM+10%FBS plating media were added following the removal of the supernatant and collection of the pellet. This solution was then covered with 90% Percoll, and the mixture was centrifuged for 10 minutes at 300g at 4°C. After discarding the supernatant, cells were washed and submerged in 10 milliliters of DMEM.

3.17 In silico analysis of global microarray data

Using the GEOquery software (DOI: 10.18129/B9.bioc.GEOquery), raw microarray expression data from the GSE4410 (mice) and GSE45220 (human) datasets was acquired in a CEL file format. Other R packages can use the GEOquery R package, which parses GEO data into R data structures. The Robust Multichip Average (RMA) algorithm in the oligo package was used to normalize and correct the background of the Gene Expression Measurements. This algorithm aims to eliminate local biases across samples so that pertinent differential expression testing can be conducted.

Through the use of basic component analysis and the hierarchical clustering method, variations are scanned throughout the samples. Next, using the Limma tool, distinction gene analysis was carried out. Using Limma-based adjusted P-value, the The R package limma (Linear Models for Microarray Analysis) has emerged as a commonly used statistical test for determining gene expression variations. P-values less than 0.05 are chosen. Huex10sttranscriptcluster.db for GSE4410 and hugene10sttranscriptcluster.db for GSE45220 and libraries are used to annotate the results. Only the most significant probes were selected when two or more were aligned or mapped, and the list of downregulated and upregulated genes was created as a result. The most significant genes are those with the highest logFC values and the least adjusted P-value. Using the KEGG pathway, BioGPS, and Reactome databases, genes that may be involved in cholesterol metabolism were chosen from among them and arranged in a certain order. The expression of every gene related to cholesterol was downregulated. Volcano plots were used to illustrate the data.

3.18 Treatment of liposomal cholesterol on cells

Huh7 cells were plated at a density of 105 cells per well in a 96-well plate. Overnight, 22-NBD-cholesterol-liposome was used to equilibrate the cells. Following liposome incubation, cells were treated with or without butyrate after being rinsed with 1× PBS.

A 24 well plate was plated with 106 cells/well of RAW 264.7 cells. After being treated with sodium butyrate, freshly generated 10 µL of liposomes (containing about 4.8×10^{14} lipoparticles) / 106 cells were cultured for 18 hours at 37 °C in an incubator with 5% CO₂. The following equation was used to calculate the liposome concentration. (doi.org/10.3390/scipharm89020015)

$$N(\text{lipo}) = [M(\text{ing}) \times N(\text{Avo})] / [N(\text{tot}) \times 1000]$$

where:

N(lipo) is the number of vesicles per mL

M(ing) is the molar concentration of ingredients of vesicles;

N(Avo) is the Avogadro Number (6.02×10^{23});

N(tot) is the total number of ingredients per vesicle.

N(tot) is calculated using the following equation:

$$N(\text{tot}) = 17.69 \times [(d/2)100 + (d/2 - 5)100] \text{ where, } d \text{ is the diameter of your vesicle}$$

3.19 Visualization of liposomes in transmission electron microscopy (TEM)

After negative staining samples with uranyl acetate, the morphologies of liposomes were examined using TEM (FEI Tecnai F20 (200kV) FEG TEM) to get a visual impression. Liposomes dissolved in PBS were combined with a same amount of 3% agar and stored at -20°C for the night in order to gather data regarding lamellation. Using a cryo ultramicrotome (Leica), the solidified agar containing vesicles was divided into 60 nm thick pieces for TEM observation.

3.20 Fillipin staining

After twice washing the cells in PBS, they were fixed for 30 minutes at room temperature using 2% cold paraformaldehyde. To quench paraformaldehyde, the cells were treated with 1 mL of 1.5 mg glycine/mL PBS for 10 min at room temperature after three PBS washes. Following that, the cells were stained for two hours at room temperature with 1 mL of Fillipin at a concentration of 0.05 mg/mL in PBS containing 10% FBS. The cells were subjected to three PBS washes before the fluorescence images

were examined under a Carl Zeiss microscope fitted with a CCD camera and analyzed using FACSDiva software in a FACS Aria II machine (both made by Becton Dickinson, San Jose, CA). At least 10,000 events were recorded in each sample. FloJo was used to evaluate the data.

3.21 Membrane Anisotropy:

Fluorescence and membrane fluidity were assessed in accordance with the methods mentioned (Chakraborty et al., 2005; Shinitzky and Barenholz, 1978). To put it briefly, 2 mM of stock solution was created by dissolving the fluorescent probe, Laurdan, in HPLC-grade water. To 10 mL of quickly swirling PBS (pH 7.2), 1 mL of the stock solution was added. 1 mL of Laurdan (Cf 1 μ M) was added to 2×10^6 cells in 1 mL PBS, and the mixture was incubated at 37°C for two hours. The cells were triple-washed and resuspended in PBS after incubation. A spectrofluorometer (Cary Eclipse Instrument (MY13130004)) was used to measure the intensity of emission at 435 nm after the Laurdan probe attached to the cell's membrane was excited at 350 nm. The equation $FA = [(I_{\parallel} - I_{\perp}) / (I_{\parallel} + 2I_{\perp})]$ was used to determine the fluorescence anisotropy (FA) value, where I_{\parallel} and I_{\perp} represent the fluorescent intensities oriented parallel and perpendicular to the direction of polarization of the stimulating light, respectively.

3.22 Cholesterol efflux assay

As previously mentioned, (Low et al., 2012), the cholesterol efflux assay was carried out. In short, $1 \times$ PBS was used to wash the cells loaded with cholesterol, then butyrate was added for the next 24 hours. In presence or absence of Butyrate, the cells were removed using $1 \times$ PBS and then allowed to rest for the following 18 hours in DMEM that was free of serum. To promote efflux, cells were given HDL at a dose of 1, 5, and 20 μ g/ml for 4 hours after the designated incubation period. After that, methanol was used to lyse the cells and collect the cell supernatant. Using 469-nm excitation and 537-nm emission filters in a black polystyrene 96-well plate (Costar, Corning Incorporated, USA), a microplate reader (MT-600F fluorescence, Corona Electric, Hitachinaka, Japan) was used to measure the fluorescence intensity (FI) of 22-NBD-cholesterol in the medium and cell lysate. This is how the percentage of cholesterol efflux was computed: $(FI_{\text{medium}} \times 100) / (FI_{\text{medium}} + FI_{\text{lysate}})$ equals the percentage of cholesterol efflux.

3.23 Transfection

At a density of 1×10^6 cells/well, cells were plated on 6-well culture plates and grown for 24 hours to 80% confluence in 2 ml of serum-free media. The manufacturer's recommended protocol was followed while using Lipofectamine 2000 for transfection. In summary, equal volumes of plasmid or siRNA and lipofectamine were combined at room temperature for 15 minutes after 1.0 μ l lipofectamine and 0.27 μ g siRNA or 0.5 μ g plasmid were diluted with 25 μ l Opti-MEM solution. Following a 6-hour incubation period at 37°C with 100 μ l of the lipofectamine-containing Opti-MEM solution containing plasmid or siRNA, cells were transfected and subsequently cultured in DMEM supplemented with 10% FCS (Wu et al., 2018).

3.24 Fluorescence microscopy

According to Pautz et al. (2009) and Abdelmohsen et al. (2012), cells cultured on glass cover slips were transfected for 24 hours with either the pEGFP-AUF1p40 plasmid, pEGFP-Dicer-1-3'UTR, or p-EGFP. Following a PBS wash, the cells were exposed to 1 μ g/ml Hoechst 33342 for five minutes at room temperature, and then they were repeatedly washed with PBS. ZEN software was utilized to control a CCD camera attached to a Carl Zeiss microscope located in Gottingen, Germany, to take fluorescence images.

3.25 Confocal Analysis and image processing:

The cells were grown onto a 1.5H coverslip with a thickness of 0.16–0.19 mm, and they were then treated with liposomal cholesterol and either 10 mM or 10 mM sodium butyrate. Following treatment, the coverslips were cleaned with PBS after 18 hours, and the cells were preserved by letting them sit at room temperature for 10 minutes in 4% paraformaldehyde. After three PBS washes, CTXB-FITC, anti-CD71-biotin, or anti-CD44-FITC antibody were used for cell staining and let to sit for half an hour at a 1:200 dilution. Streptavidin-PE antibody (1:200 dilution) was used for cell treatment with the objective of CD71 identification following three PBS washes. Three PBS washes of the cells were used to stop the response. The cells were counter stained by subjecting them to 1 μ g/mL Hoechst 33342 for five minutes at room temperature. Following this, they were triple-washed with PBS and mounted using 90% glycerol. Using a confocal microscope (Carl Zeiss, Germany), fluorescence pictures were taken at a magnification of 63X. ImageJ software was used to perform the analysis. To compute total cell fluorescence (corrected), use the formula:

Corrected Total cell fluorescence = (Integrated density) – (Area of selected cells x mean fluorescence of background).

3.26 CD44 expression analysis by Flowcytometry

To determine the overall expression of CD44 in RAW 267.4 cells treated with butyrate as well as control, the cells were fixed for 30 minutes at room temperature with 2% cooled paraformaldehyde after being permeabilized/unpermeabilized for 15 minutes using 0.1% Tween 20. After that, cells were gathered in FACS buffer (PBS+10%FBS). Aliquots of 10⁶ cells in FACS buffer were stained with FITC-conjugated anti-CD44 antibody at 1:500 dilutions for 30 minutes. The cells were subsequently analyzed using a FACS Aria II device (both from Becton Dickinson, San Jose, CA) using FACSDiva software. Minimum events of 10,000 were observed in each sample. FloJo was used to evaluate the data.

3.27 Bacterial strain:

Salmonella serovar typhimurium wild-type strain SL1344 and *Shigella flexneri* serotype 2a strain 2457T were cultivated in Luria broth (LB) at 37°C for an entire night before being re-inoculated with precultured bacteria (1%) in fresh media in the incubator at 37°C with gentle shaking. To conduct more studies, the culture dilution was made to 2 x 10⁹ CFU/mL in PBS once the Spectrophotometer's reading of OD600 reached 0.6.

3.28 Pathogen invasion assay:

To prevent serum cholesterol interference, the pathogen invasion assay was carried out in cells cultivated in serum-free media (Koestler et al., 2018). In a nutshell, cells (5 x 10⁵ cells/well in 500 µL media in a culture plate of 24 well) were inoculated with *Salmonella typhimurium* or *Shigella flexneri* at 100 multiplicity of infection (MOI) and allowed to incubate for one hour. After aspirating the media and rinsing the cells three times with PBS, DMEM with 50 µg/mL of Gentamycin was added, and the cells were then incubated for one hour at 37°C with 5% CO₂. Removal of incubated media followed by washing of cells 3 times with PBS was done. Preparation of cell lysate was done by adding 100 µL of 0.1% Triton X-100 to the cells. The lysate was then plated on either LB agar for *Salmonella typhimurium* or in XLD plates for *Shigella flexneri* and incubated at 37°C overnight. On the following day, the numbers of colonies were counted and the data is represented as percent control.

Percent control= Treated/Control × 100

3.29 Tissue homogenisation, preparation of RNA and Protein

Dissected liver and colon samples were combined with isolated cell samples and resuspended in either RIPA Lysis buffer (150 mM NaCl, 1 mM EDTA, 20 mM Tris-HCl pH 7.5, 1 mM EGTA, 1% NP-40, 1% Sodium deoxycholate, 1 mM β -glycophosphate, 2.5 mM Sodium Pyrophosphate, 1 mM Na₃VO₄, 1 μ g/ml leupeptin with 1 mM PMSF immediately before use) for protein isolation or for RNA isolation (in Trizol, Invitrogen, US). After utilizing a micropestle to homogenize the tissue, it was centrifuged for 15 minutes at 4°C at 13,000 g. The protein lysate from the clear supernatant was either kept at -80°C or used in a conventional procedure to isolate RNA (Wu et al., 2018).

3.30 RNA extraction and reverse transcription

In 24-well plates, cells were grown to 80% confluence. Trizol was used to extract total RNA from cells or tissue in accordance with the manufacturer's recommended technique. The isolated RNA was kept at -80° C after its concentration was measured using a Thermo Nanodrop spectrophotometer. Using the Super Reverse Transcriptase MuLV Kit and reverse specific primers, cDNA was created from whole RNA. Table 1 contains a list of primers for the reverse transcription. The expressions of miRNAs and other relevant genes were standardized for U6 and GAPDH, respectively. The reverse transcription process contained 20 μ l total volume, 5 ng of RNA template, 1 μ M of reverse primer, 1 μ l dNTP mix, 12 μ l DEPC treated water, 4 μ l 5X first strand buffer, 1 μ l 0.1 M DTT, 1 μ l RNase inhibitor, and 1 μ l Super RT MuLV. The protocol for reverse transcription was as follows: 5 minutes at 65°C, 1 hour of incubation at 55°C, and 15 minutes of heat inactivation at 70°C. (Abdelmohsen et al., 2012)

3.31 Quantitative real-time PCR

The RNA concentration was measured using a nanodrop after the total RNA was isolated from the snap-frozen liver using Trizol reagent. By using the manufacturer's instructions, Takara SYBR® Green qPCR Mastermix along with Applied Biosystems™ StepOne™ Real Time PCR, the genes and GAPDH levels were measured. Ten microliters of RT2 SYBR® Green qPCR Mastermix, forward and reverse primer (1 μ l each), nuclease-free water, and 5 ng of total RNA of cDNA were added to each 20 μ L qPCR experiment. The following circumstances were used for real-time PCR: 60°C for one minute, 72°C for one minute, 40 cycles of 95°C for 30 seconds, and 95°C for ten minutes. The $2^{-\Delta\Delta C_t}$ method previously reported (Abdelmohsen et al., 2012) was utilized to calculate the PCR product.

100 μ l of molecular biology grade mineral oil (Sigma) was applied on top of the stem loop primer stock. After being heated to 95°C, the mixture was maintained at 75°C, 68°C, 65°C, 62°C, and 60°C for one

hour at a time. Following that, a working stock of 10 μ M was created and kept at -20°C until needed (Varkonyi-Gasic et al., 2007).

3.32 Primers

Applying NCBI Primer BLAST (<https://www.ncbi.nlm.nih.gov/tools/primer-blast/>), primer sequences were created. The following factors were taken into account when choosing the primers: 40–60% G/C content, 18 to 24 bases long with 1-2 G/C pairings at the start and finish, 50–60°C melting temperature (Tm), and primer with Tms that were within 5 °C of one other without any complementary sections. Table 1 lists the primers that are used for PCR amplification.

Table 3.1: List of primers

Gene (References or Accession number of the gene)	Primer Sequence	
	Forward Primer	Reverse Primer
Dicer 1 (Human) (NM_001395690.1)	5`-GAACGCTTTTGTGCTGCTGA3` (Tm =59.97)	5`CACAGGGCTCTAAAGTGGGG3` (Tm= 60.04)
GAPDH (Human) (NM_001357943.2)	5`-GAGAAGGCTGGGGCTCATTT3` (Tm =60.03)	5`AGTGATGGCATGGACTGTGG3` (Tm=60.03)
U6SnRNA (Human) (NCBI's sra archive under bioproject accession number PRJNA616703)	5`-CTCGCTTCGGCAGCACATATACT3`	5`ACGCTTCACGAATTTGCGTGTC3`
miRNA122 (Human) (NR_029667.1)	5` TAGCAGAGCTGTGGAGTGTG 3` (Tm =59.39)	5` GCCTAGCAGTAGCTATTTAGTGTG 3` (Tm = 59.01)
PremiRNA122 (Human) (NR_029667.1)	5`-CCTTAGCAGAGCTGTGGAG-3` (Tm =57.24)	5`GCCTAGCAGTAGCTATTTAG-3` (Tm =52.71)
HMGCR (Human) (NM_000859.3)	5` - GTTAACTGGAGCCAGGCTGA-3` (Tm =59.68)	5`GTGAGTTGGAAGTGAAGGCA -3` (Tm =59.89)
HMGCS (Mouse) (NM_008255.2)	5`GTGCGTAAGCGCAGTTCCTT3` (Tm =61.57)	5`CACAGTCCTTGGATCCTCCG3` (Tm =59.82)
ACAT 2 (Mouse) (NM_009338.3)	5`-TTTGCTCTATGCCTGCTTC-3` (Tm =60.18)	5`-GTAGAACATCCTGTCTCC-3` (Tm =60.82)

DHCR7 (Mouse) (NM_001412322.1)	5' ATGGCTTCGAAATCCCAGCA -3' (Tm =60.03)	5' AGCTGTACTGGTCACATGCC 3' (Tm =60.04)
CYP7A1 (Mouse) (NM_007824.3)	5'-GGGCAGGCTTGGGAATTTTG -3' (Tm =60.04)	5' ACAGCTACTAGGGGGCTTCA-3' (Tm =59.96)
U6 snRNA (Mouse) (NR_004394)	5-CTCGCTTCGGCAGCACATATACT-3'	5'ACGCTTCACGAATTTGCGTGTC-3'
Dicer 1 (Mouse) (NM_001411829.1)	5'- GCCATGGCAACAAGAAGCAA -3' (Tm =59.97)	5' AGTTGACGAGGAACACGGTC -3' (Tm =59.97)
Auf-1p40 (Mouse) (XM_036164755.1)	5'-AGAACGAGGAGGATGAAGGGA-3' (Tm =59.99)	5'TGTGTCTGGAGAAAGGCCAC-3' (Tm =59.89)
GAPDH (Mouse) (NM_001411840.1)	5' - GAAGGTCGGTGTGAACGGAT -3' (Tm =60.04)	5' ACTGTGCCGTGAATTTGCC -3' (Tm =59.97)
Occludin (human) (NM_001205254.2)	5'-TGGAGGAGGACTGGATCAGG -3' (Tm =60.03)	5'- TTGTGATGCTCACAGAGGTT-3' (Tm =57.07)
miRNA122(Mouse) (NR_031864)	5' -GCTCGACCTCTCATGGGC-3' (Tm =60.01)	5' TTAAGCCCTGCGTGTCTCTCC-3' (Tm =59.99)
PremiRNA122 (Mouse) (Ghosh et al., 2013)	5'-CCTTAGCAGAGCTGTGGAG-3' (Tm =60.00)	5' GCCTAGCAGTAGCTATTTAG-3' (Tm =59.89)
miRNA27a (Mouse) (Khan et al., 2020)	5-`ACACTTTCACAGTGGCTAA-3`	5-`GTGCAGGGTCCGAGGT-3`
miRNA27a SL (Khan et al., 2020)	5-`GTCGTATCCAGTGCAGGGTCCGAGGTATTCGCACTGGATACGACGCGGAAC-3`	
ButCoAT (Louis et al., 2007)	5' GCIGAICATTTACITGGAAYWSITGGCA Y 3'	5' CCTGCCTTTGCAATRTCIACRAANGC 3'
16S rRNA (NCBI's sra archive under bioproject accession number PRJNA616703)	5' AGAGTTTGATCCTGGCTCAG 3'	5'AAGGAGGTGWTCCARCC 3'
MUC-2 (Mouse) (NM_023566.4)	5'-GCTGACGAGTGGTTGGTGAATG-3' (Tm=60.0)	5'- GATGAGGTGGCAGACAGGAGAC-3' (Tm=59.9)

IFN- γ (Mouse) (NM_008337.4)	5'- TCAAGTGGCATAGATGTGGAAGAA-3' (Tm=59.9)	5'-TGGCTCTGCAGGATTTTCATG-3' (Tm=59.9)
IL-10 (Mouse) (XM_036162094.1)	5'-GGTTGCCAAGCCTTATCGGA-3' (Tm=60.0)	5'-ACCTGCTCCACTGCCTTGCT-3' (Tm=59.9)
TNF- α (Mouse) (NM_001278601.1)	5'- CATCTTCTCAAAATTCGAGTGACAA- 3' (Tm=60.1)	5'- TGGGAGTAGACAAGGTACAACCC- 3' (Tm=60.2)
IL-6 (Mouse) (NM_001314054.1)	5'-GATAAGCTGGAGTCACAGAAGG-3' (Tm= 59.3)	5'-TTGCCGAGTAGATCTCAAAGTG- 3' (Tm=60.0)
IL-12 (Mouse) (NM_001303244.1)	5'-GGAAGCACGGCAGCAGAATA-3' (Tm=59.8)	5'- AACTTGAGGGAGAAGTAGGAATG G-3' (Tm=60.1)
Cathelicidin (Mouse) (NM_009921.2)	5'- GGCAGCTACCTGAGCAATGT-3' (Tm=59.6)	5'-CTGTGCACCAGGCTCGTTA-3' (Tm=59.8)
Occludin (Mouse) (NM_001360536.1)	5'-GTGAATGGGTCACCGAGGG-3' (Tm=60.08)	5'-AGATAAGCGAACCTGCCGAG-3' (Tm=55)
Claudin-2 (Mouse) (NM_001410421.1)	5'-TCCGTGAGTATCTGGTCGTT-3' (Tm=58.17)	5'-TCCTTTGCTTGTGACCCTGG-3' (Tm=60.18)
Claudin-1 (Mouse) (NM_016674.4)	5'-CAACCCGAGCCTTGATGGTA-3' (Tm=59.75)	5'-TCATGCCAATGGTGGACACA-3' (Tm=59.89)
ZO-1	5'-GTTTGCATGGCTTCCAATGGT-3'	5'-TCAAGGTCTCTGCTGGCTTG-3'

(Mouse) (NM_001417370.1)	(Tm=60)	(Tm=59.96)
RORγt (Mouse) (NM_001293734.1)	5'-GAC TTTCCTCTGGCACACA-3' (Tm=59.89)	5'-ATCCGGTCCTCTGCTTCTCT-3' (Tm=60.03)
Fox P3 (Mouse) (NM_054039.2)	5'-ATTGAGGGTGGGTGTCAGGA-3' (Tm=60.48)	5'-GTTCTTGTCAGAGGCAGGCT-3' (Tm=59.96)

3.33 Western blot

RIPA Lysis buffer was used to extract cell lysate or liver tissue protein. The protein concentration was calculated by the Pierce TM BCA Protein Assay Kit. Proteins (50 µg/lane) were electrotransferred by using a transferred buffer (150 mM Glycine, 20% Methanol, 25 mM Tris-HCl) PVDF membrane, after being separated using SDS-PAGE on 10% gel under reducing conditions. After blocking the membranes for two hours at room temperature with 5% non-fat skim milk in TBS, the primary antibody against a particular protein was then incubated. Alkaline phosphatase (AP) or horseradish peroxidase (HRP) conjugated secondary antibodies were incubated on the membranes for one hour at 37° C. The blotting findings were seen using the SuperSignal West Pico chemiluminescent substrate kit (Thermo) for HRP-conjugated antibody treatment. Using the Fluor Chem R system (ProteinSimple, San Jose, CA, USA), the blots were photographed (5). The blotting findings were seen using the BCIP-NBT substrate kit (Thermo) for AP-conjugated antibody treatment. (Abdelmohsen et al., 2012).

Table 3.2: Antibodies for western blot

Name of Antigen	Raised in	Source	Dilutions used
HMGCR	Rabbit	Cell Signalling Technology	1:1000
ABCA1	Rabbit	Cell Signalling Technology	1:1000
ABCA5	Rabbit	Abcam	1:1000
AUF-1 (p37 specific)	Rabbit	Cell Signalling Technology	1:1000

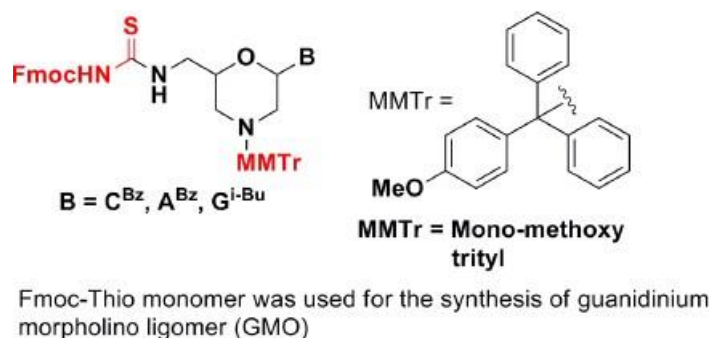
AUF-1/ HNRNP	Mouse	Santa Cruz	1:100
Dicer 1	Mouse	Santa Cruz technology	1:1000
Occludin	Mouse	Abcam	1:2000
Claudin-2	Mouse	Abcam	1:2000
β Actin	Rabbit	Cell Signalling Technology	1:1000
GAPDH	Rabbit	BioBharati	1:1000
Anti-mouse-HRP conjugated secondary antibody	Horse	Cell Signalling Technology	1:5000
Anti-rabbit- HRP conjugated secondary antibody	Goat	Cell Signalling Technology	1:5000
Anti-mouse-AP	Goat	Abcam	1:5000

3.34 Production of GMO-PMO (Guanidinium Morpholino Oligonucleotides- Protected chlorophosphoramidate Morpholino Oligonucleotides)

Reagents, unless indicated, were obtained from commercial sources and were used instead of added purification. Every reaction was conducted in glassware that had been oven-dried in an argon environment. As directed, solvents were dried and purified. Using strips of silica gel layer thickness of 0.25 mm (Merck) and 60 F254 on aluminum, thin-layer chromatography (TLC) was performed. With the use of CAM (ceric ammonium molybdate), UV rays or ninhydrin stains, the produced chromatogram may be seen. Silica gels with the mesh of 100-200 or 230-400 and Column chromatography was used to achieve chromatographic purification of goods. The Agilent Cary 3500 UV-visible spectrometer was used to record the UV/Vis spectra. Using the BrukerultrafleXtreme MALDI-TOF/TOF system, mass spectra of matrix-assisted laser desorption ionization (MALDI) were captured.

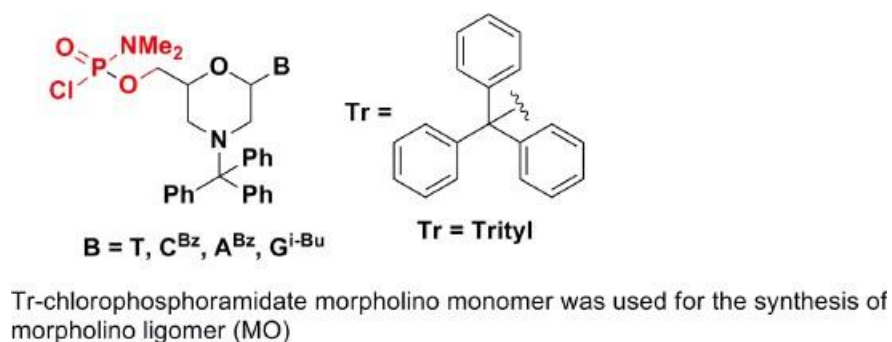
3.34.1 Production of Thiourea morpholino active monomer protected by Fmoc

G, A, and C nucleosides monomers that are Fmoc protected and thiourea MMTr-morpholino active were needed to synthesize the GMO portion of the chimera of GMO-PMO. The modified methodology, previously mentioned, was utilized to synthesize them. (Bhadra et al., 2015).



3.34.2 Production of chlorophosphoramidate morpholino active monomer trityl protected

Chlorophosphoramidate monomers of A, T, G, and C were employed in the synthesis of PMO, and they were created in accordance with a previous manuscript. (Bhadra et al., 2015).



3.34.3 Operationalization of solid support with loading as well as linker monomer

Before the synthesis of solid phase GMO-PMO sequences, polystyrene solid support was operationalized with loading monomer as well as aminocaproic acid linker as per earlier report (Kundu et al., 2023).

3.34.4 Solid phase synthesis of GMO-PMO

Implementation of GMO synthesis began with the effective loading of monomer and linker onto a firm polystyrene substrate. Five equivalents of HgCl_2 , five equivalents of NEM, and five equivalents of Fmoc-protected thiourea were added to NMP solvent for the GMO synthesis. In two hours, the same process was carried out twice more. Six hours were spent connecting each GMO unit. 20% Thiophenol-NMP and NMP were used to wash any leftover chemicals. 10% Ac_2O -NMP and 10% DIPEA-NMP were combined in a 1:1 ratio to cap the unreacted amine. Using the deblocking cocktail (CYPTFA), the MMTr group was made unprotected (Bhadra et al., 2015). To obtain the GMO unit, the synthetic cycle (cleaning, union, capping, and deblocking) was carried out once more for three additional GMO monomers (refer to the structures above). Chlorophosphoramidate monomer was used to further react with the GMO pentamer (refer to the structure above). The morpholino portion was produced using the methodology we have described (Bhadra et al., 2015). The full-length GMO-PMO was extracted by acetone precipitation after being split from solid support for 16 hours at 55°C using 33% aqueous ammonia. The synthetic GMO-PMOs' purity was examined using HPLC, and MALDI-TOF was used to describe them. GMO-PMO will henceforth be referred to as MO.

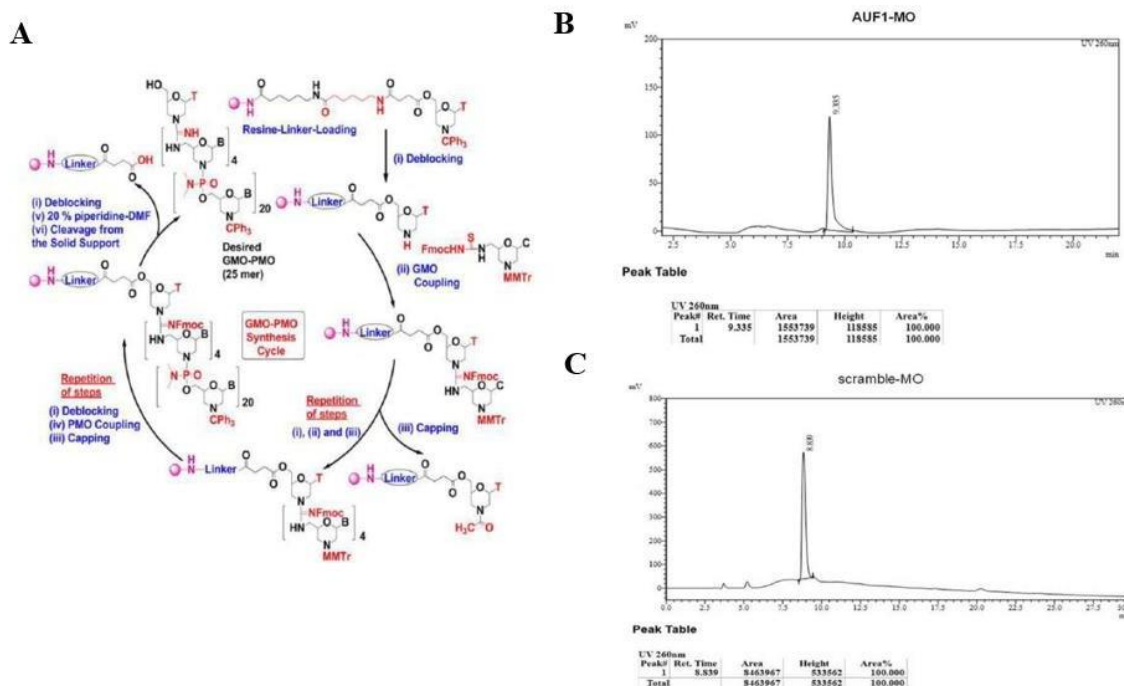


Figure 3.1: GMO-PMO (MO) synthesis cycle and HPLC characterization of AUF1-MO and scramble- MO.

Sequence of AUF1-MO

5'-TCCGAACTGCTCCTCCGACATAGTG-3' targets the following AUF1 mRNA region
[Red letter represents GMO part]

MALDI-TOF [M + H]⁺: Mass calculated for C₂₈₅H₄₃₇N₁₄₂O₉₂P₂₀ was 7943.8907, found 7945.703.

CDS: [314:1382](+)

**TACTTTGCTGCTAGTTTCGGTTCGCGGCGGGCGGCGGCGTTCGGCGGGTGTCGTC
TTCGGCGGCGGCAGTAG[CACT(ATG)TCGGAGGAGCAGTTCGGA]GGGG**

Sequence of scramble-MO

5'-**TCGCA**ACTCGTCCTCCAGCATAGTG-3' [Red letter represents GMO part]

MALDI-TOF [M + H]⁺: Mass calculated for C₂₈₅H₄₃₇N₁₄₂O₉₂P₂₀ was 7943.8907, found 7942.554.

3.35 Administration of GMO–PMO to block AUF-1 by knock down

After dissolving the GMO–PMO in saline, the concentration reached 1 mM, or 8.2 mg/ml. Mice were used for the in vivo knockdown of AUF-1 by administering AUF-1 GMO–PMO (AUF-1-MO) at a concentration of 3 mg/kg body weight through the tail vein on days 1 and 7. A pilot study has already established the effective dose based on the expression of AUF-1 in the liver. From day 1 to day 14, a different group of mice that had received an injection of AUF-1-MO were given a chow meal enriched with 5% butyrate. Days 7 and 14 saw the collection of blood from the tail vein in order to estimate cholesterol. Scramble-MO controls are animals who have received mock GMO-PMO treatment. After the initial dose injection, butyrate was given to a second group of scramble-MO for a period of 14 days. On day 14, the animals were slaughtered and their tissue was taken for additional examination.

3.36 Bacteria count (CFU) from colon tissue

40-50 mg of mice colon tissue was removed, thoroughly cleaned in PBS, and submerged in 1 mL PBS, and homogenized with a homogenizer. After being diluted ten times, the homogenate was spread in XLD agar plates and incubation was done at 37°C for the entire night. The next day, colonies were counted. The tissue's cfu/gm was computed as

Cfu/ gm tissue = (number of colonies x dilution factor) / gm of tissue

3.37 Histopathological analysis

Colon samples were completely cleaned in PBS, preserved for 48 hours at 4 °C in 4% paraformaldehyde, and then dehydrated with immersion in xylene, graded alcohol, and paraffin. Using a standard microtome, 5µm slices were cut from the paraffin block, stained with H&E, and examined with a Carl Zeiss Axiovert 40 CFL microscope. The amount of neutrophils in the colon at a high power field (X100) was counted to determine the extent of interstitial infiltration by inflammatory cells in response to *Shigella* infection, as previously described. (Nemmar et al., 2015).

3.38 TEER assay

Collagen-coated 12-well chamber inserts were used to cultivate HT-29 cells. The culture medium contained 1% nonessential amino acids, 4 mM glutamine, 10% FBS, 110 mg/L sodium pyruvate, 4.5 g/L D-glucose, and 1% antibiotic cocktail. For three weeks, cells were left to differentiate. Every two days, new media were added. The creation of monolayers was confirmed by measuring the TEER value via Millicell ERS-2 epithelial cell volt-ohm meter (Merck Millipore). whenever the trans-epithelial resistance plateaued, the cells were deemed differentiated and to have formed a tight monolayer. Scrambled morpholino oligo, or 0.75 μ M dose of AUF-1 morpholino oligo, was applied to HT-29 monolayers. As controls, untreated and LPS-treated cells were utilized. (PMID: 10555261, PMID: 10767597).

3.39 Paracellular permeability assay

The passage of FITC-dextran was observed through the apical-basal junction in a HT-29 monolayer cell culture, in-vitro permeability was ascertained. Collagen-covered 12-well chamber inserts were used to cultivate HT-29 cells. The medium consists of 1% nonessential amino acids, 4 mM glutamine, 10% FBS, 110 mg/L sodium pyruvate, 4.5 g/L D-glucose, and 1% antibiotic cocktail. For three weeks, cells were left to differentiate. Every two days, new media were added. Introduction of 1mg/ml of FITC-dextran at the apical chamber (0-hour time point) was done, following 24 hours of washing with HBSS solution. Following a 6-hour incubation period, 100 microliters of media were extracted from the basal chamber. Using a spectrofluorometer, the intensity of fluorescence of each sample was observed at 490 nm for excitation and 530 nm for emission. Using a FITC-dextran standard curve, the amount of FITC-dextran in the sample was determined. (PMID: 30394372).

3.40 RNA immunoprecipitation assay

To assess the association of endogenous AUF-1 with endogenous occludin and Claudin-2 mRNA, immunoprecipitation (IP) of ribonucleoprotein (RNP) complexes were performed as described (Martindale et al., 2020). In the presence of excess (30 mg) IP antibody (IgG, or anti-AUF-1 or anti-HuR), 20 million cells were obtained from each sample, and lysates were utilized for IP for 4 h at room temperature. Isolation of RNA from the entire IP materials was used in RT followed by qPCR analysis to find out the presence of occluding, Claudin-2 and housekeeping mRNAs (GAPDH, UBC).

3.41 Gut permeability assay

The in-vivo intestinal permeability was measured using the FITC-dextran assay as previously described. Mice, administered with AUF-1 morpholino oligo, scrambled oligo and 2% DSS for 6 days, and starvation was done for 4 hours before the procedures; FITC-dextran (at a dose of 44 mg/kg) was administered by oral gavage. Serum was obtained via retro-orbital bleeding minimum after 4 hours of FITC-dextran gavage, and calculated by using emission wavelength of 530 nm and excitation wavelength of 490 nm of spectrofluorometer (Cary Eclipse Fluorescence Spectrophotometer, Varian). A standard curve was built using FITC-dextran that had been diluted in phosphate buffered saline (PBS), and the serum concentration of FITC-dextran was determined. At least three runs of the process were made, with five participants in each group (Corr et al., 2014; Wang et al., 1999; Brandl et al., 2009).

3.42 Immunohistochemistry

Tissue sections that were embedded in paraffin and treated in paraformaldehyde were stained with a Vectastain kit. Following the dehydration and paraffin removal, the tissue slices were rinsed in PBS and 0.3% H₂O₂ was used to quench the endogenous peroxidase activity. After blocking the sections with 5% fetal bovine serum (FBS), diluted in PBST (0.02% Tween 20 in PBS), the sections were incubated at 4 °C for an entire night with the primary antibody against occludin. Following a PBST wash, sections were incubated for two hours at 25 °C with the biotinylated secondary antibody. After adding an avidin-biotinylated enzyme complex, slices were stained with hematoxylin and 3,3'-diaminobenzidine (DAB)-H₂O₂ to visualize them. For fluorescence staining, a secondary antibody that was fluorescently labeled was employed. DAPI was used for nuclear staining, and a Leica DM750 light microscope (Carl Zeiss Axiovert 40 CFL) was used to see the results.

3.43 ELISA

Colon tissue lysate was prepared by homogenizing the colon tissue in PBS and centrifuge for 10,000g at 5 minutes. As directed by the manufacturer, ELISA kits were used to detect CXCL1 and CXCL2 levels in the supernatant. Following that, absorption coefficients were applied to calculate TNF- α and IFN- γ concentrations.

3.44 Bacterial translocation

Following the sacrifice of the mice, aseptic procedures were used to obtain the liver, spleen, and mesenteric lymph nodes (MLN). After being cleaned in 5 milliliters of gentamicin (50 mg/mL) containing PBS, tissue samples were mashed in ice-cold PBS. For twenty-four hours, tissue homogenates were seeded in Luria-Bertani plates at 37°C. The dilution ratio was used to count the colonies, and the result was presented as colony-forming units (CFU). The number of bacteria per gram (CFU/g) was used to measure bacterial translocation. (Liu et al., 2021).

3.45 FACS

Immune cell populations in the spleen and MLN were investigated after mice were executed. The following mAbs were used to stain single-cell suspensions for 30 minutes at 4°C in PBS: anti-CD4 and -CD25. PMA (30 ng/ml; Sigma Aldrich) and ionomycin (1 mg/ml; Sigma Aldrich) were used to activate spleen and MLN (1×10^6 cells/ml) cells for intracellular cytokine measurement of IL-17A, IL-22, and Foxp3. After an hour, monensin (5 mg/ml; Sigma Aldrich) was added for 4 hours to disrupt the Golgi Complex/Endoplasmic Reticulum transport pathways, which would have otherwise allowed the intracellular proteins to accumulate. Every experiment had controls that were matched to the isotype. A BD FACS Aria was used for the flow cytometry, and Flowjo software was used for the analysis. (Jansen et al., 2015).

3.46 Statistical Analysis

Every data point is expressed as the means \pm Standard Error Mean (SEM). The significance among two groups was ascertained using the unpaired Student's t-test, and by using one-way analysis of variance (ANOVA) and Tukey's post hoc test, statistical significance level of more than two groups were determined. All data were analyzed using GraphPad Prism Version 8.01 software. Statistical significance was established for p-values less than 0.05. The Western blot experiment's figures are from a minimum of three separate trials that were conducted on various days.

CHAPTER-1

**Butyrate corrects HFD diet induced hypercholesterolemia by
exploiting AUF1- Dicer-miR122 axis**

4.1 Introduction

The gut microbiota has the unrivalled ability to regulate host metabolic activity in ways that the host cannot. The gut microbiota uses non-digestible carbohydrates as fuel to make SCFA (Short chain fatty acids) like butyrate, acetate, and propionate in a 1:1:3 ratio. Numerous studies have demonstrated the wide variety of beneficial effects that SCFAs produced in the gut have on both health and disease (Silva YP et al., 2020). Butyrate's benefits have been well studied as a treatment for inflammatory illnesses, neurological disorders, and other problems (Bourassa MW et al., 2016).

It is known that butyrate influences the metabolic scenery of the host cell's energy (Liu et al., 2018). In accordance with rodent research, the dietary polysaccharide pectin, which forms butyrate following fermentation in the intestine, reduces uptake of cholesterol and enhances efflux of cholesterol from enterocytes obtained from Apo E^{-/-} mice. Butyrate safeguards against high-fat diet (HFD) mediated obesity by decreasing PPAR activity and expression (den Besten et al., 2015). The ratios of phospholipids, protein, triglycerides, and cholesterol in different lipoproteins (HDL, LDL, VLDL, and chylomicron) vary.

As a precursor to vitamin D, 7-dehydrocholesterol, the intermediate metabolic precursor of cholesterol, controls a number of crucial cellular processes including production of steroid hormones, membrane fluidity, and the synthesis of bile acids (Warren T et al., 2021; Zampelas and Magriplis, 2019). Cholesterol metabolism dysregulation has been proven to cause neurological disorders, cardiovascular disease, cancer and diabetes (Natesan V et al., 2021; Vallejo-Vaz et al., 2017; Kuzu et al., 2016).

The efflux route, which governs cholesterol equilibrium at the cellular level, is pumped out by ABCA1 (ATP-binding cassette transporter A1) (He P et al., 2020). Catabolism, biosynthesis and efflux are a trio of processes governing the homeostasis of cholesterol. When butyrate is accessible, a single framework for host cholesterol homeostasis has been developed from these distinctly separate but connected notions.

At the cellular level, microRNAs regulate cholesterol efflux along with synthesis, with mir-122 and miR27 being two of the most significant ones (Canani et al., 2011; Krutzfeldt et al., 2005). Micro RNA, which accounts for up to 70% of all hepatic micro-RNA is miR122, plays a role in maintaining the mature liver phenotype (Girard et al., 2008). Administration of antagomir-122 in mice triggered an alteration of cholesterol metabolic genes, in accordance with the study conducted by Krutzfeldt et al, 2005.

mir-122, comparable to most miRNAs, is derived from the predecessor molecule, pre-mir-122 which gets processed by Dicer-1, one more RNase III nuclease which converts the precursor microRNA into a double-stranded RNA of 22 bp (O'Brien et al., 2018; Wu et al., 2018; Rakheja et al., 2014).

Progression of miR-122 through Dicer-1 is a vital phase in the biosynthesis of microRNA 122 in the cytoplasm. The existence of AU-rich elements (AREs) in the 3'-untranslated regions of the Dicer-1 mRNA in mammals renders it destabilizing. In conjunction with tying to several ARE-mRNAs, AUF-1 protein also brings together the remainder required for enlisting the mRNA degradation apparatus (Gratacos and Brewer, 2010). AUF-1p45, AUF-1p42, AUF-1p40 and AUF-1p37, are the four splice variants of the family of AUF-1 RNA binding proteins (Abdelmohsen et al., 2012). Its half-life diminishes as a consequence of the AUF-1's interaction with the Dicer-1's 3' UTR region of mRNA. Recurrent dermatitis and septicemic shock and can affect mice harbouring the AUF-1 KO gene (Yoon JH et al., 2014 Sadri and Schneider, 2009). Importantly, it has been found that AUF-1 degrades the mRNA of sphingosine kinase 1, and results in Sphingosine-1-phosphate (S1P), a biomarker inflammation and sepsis (Fettel J et al., 2019; Suh and Saba, 2015). Inflammatory signals drastically propagate by employing raising S1P in the absence of AUF-1 (Graler, 2012).

In this study we aim to demonstrate how cholesterol metabolic enzymes, AUF-1, Dicer-1, miRNAs, work together to govern metabolic phenotypes and modulate cholesterol homeostasis. We looked at the expression of the butyrate- and butyrate-independent genes for cholesterol synthesis, efflux proteins, and catabolism. We explored how butyrate modifies several RNA-binding proteins AUF-1 isoforms by downregulating Dicer-1 and mir-122 as well as cellular cholesterol. To deepen our understanding, we created an original self-transfecting antisense reagent to deactivate AUF-1 in mice using guanidinium morpholino oligos linked phosphorodiamidate morpholino oligos (GMO-PMO). We provided important proof that butyrate does in fact use AUF-1 to achieve its cellular action using AUF-1 knockdown mice. Our perception of the function of AUF-1 in cholesterol regulation has expanded as a result of the discussion above.

4.2 Results

4.2.1 The state of cellular viability and cholesterol content in mouse primary hepatocytes and mouse hepatoma cell line Huh7 before and after treatment with the major SCFAs

Mouse derived primary hepatocytes and mouse hepatoma cell line Huh7 were incubated with varying concentration (0, 5, 15, and 45 μ M and 5, 10, 20mM) of acetate, propionate and butyrate. Unlike propionate and acetate, 5, 15, and 45 μ M butyrate application suppressed cellular cholesterol by a great extent. Because primary hepatocytes degrade after a few days in the culture and their extreme susceptibility to dedifferentiate (Hu and Li, 2015), we expanded in vitro evaluation to hepatoma cell line Huh7, which are mostly employed to study hepatic processes. Butyrate administration at lower dosages did not result in a significant down regulation of cholesterol in Huh7 cells, whereas butyrate treatment at higher levels (5-20 mM) resulted in a considerable reduction in cellular cholesterol.

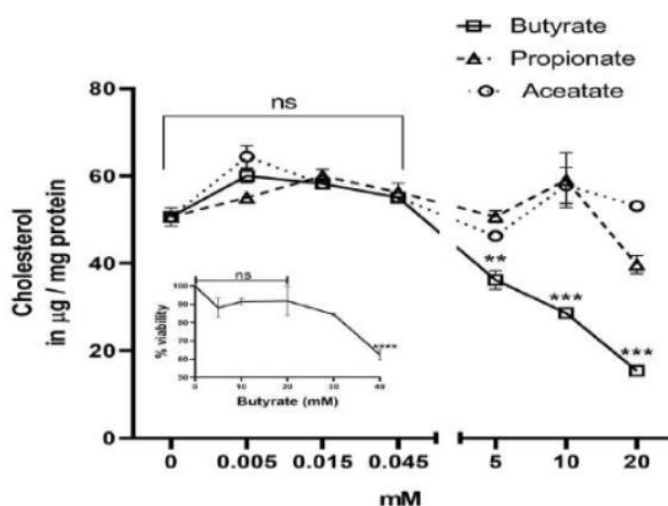


Figure 4.1: The effect of increasing SCFA concentration on cellular viability as well as cholesterol status indicated as μ g cholesterol/mg cellular protein. Each treatment, as well as the entire experiment, was carried out in replicates. Values are mean \pm SEM. Values considerably deviate from control at $p<0.001$

4.2.2 System Biology approach to study the targets of Butyrate in cholesterol biogenesis

A series of potential target of butyrate in cholesterol biogenesis were derived from Similarity Ensemble Approach (SEA) and the analysis was performed by using STRING 3.0 mediated protein-protein interaction. Among the number of targets, two important enzymes of cholesterol metabolism were identified: HMG CoA reductase (HMGCR) and Carboxyl esterase 1 (CES1). Since HMGCR is the main rate limiting enzyme in the route of cholesterol biosynthesis, in silico docking studies were performed to determine the binding affinity of butyrate with HMGCR.

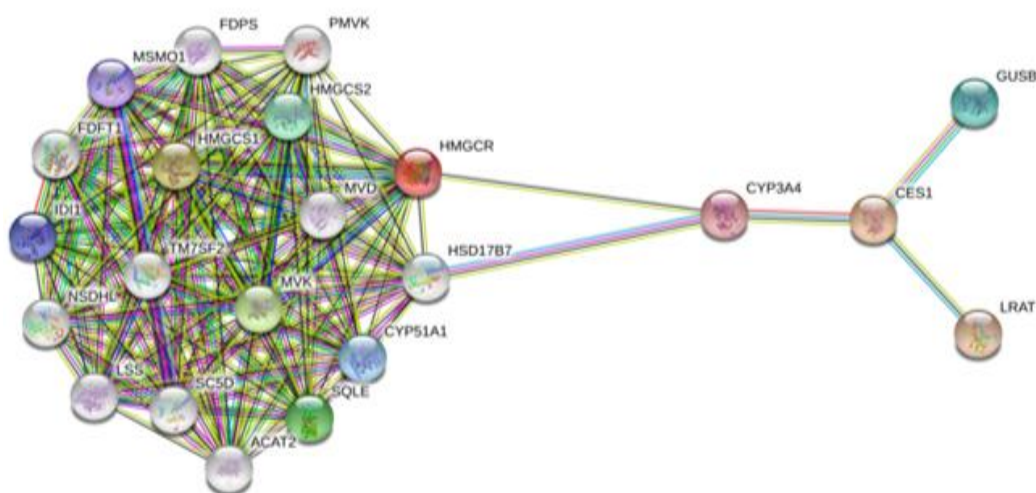


Figure 4.2: The possible targets of butyrate in the metabolism of cholesterol as revealed by STRING analysis of the protein-protein interaction network

4.2.3 In silico analysis of global microarray data

The microarray datasets that compare butyrate-treated HeLa cells to the corresponding untreated control (GSE45220) and colonic epithelial cells to the untreated control (MCE301) are both available in the public domain. These microarray data were evaluated to assess the functioning of the genes that govern cholesterol metabolism. The butyrate therapy led to an overall decrease in the expression of the genes involved in metabolizing cholesterol, in accordance with differential expression analysis. Some of these genes are directly and some indirectly implicated. The genes *hmgcs1*, *hmgcr*, 7-dehydrocholesterol reductase (*dhcr-7*), and 24-dehydrocholesterol reductase (*dhcr-24*), Acetyl CoA acetyltransferase-2 (*acat-2*), that were shared by the two data sets were taken into consideration for further research.

The data was visualised using a volcano graphic.

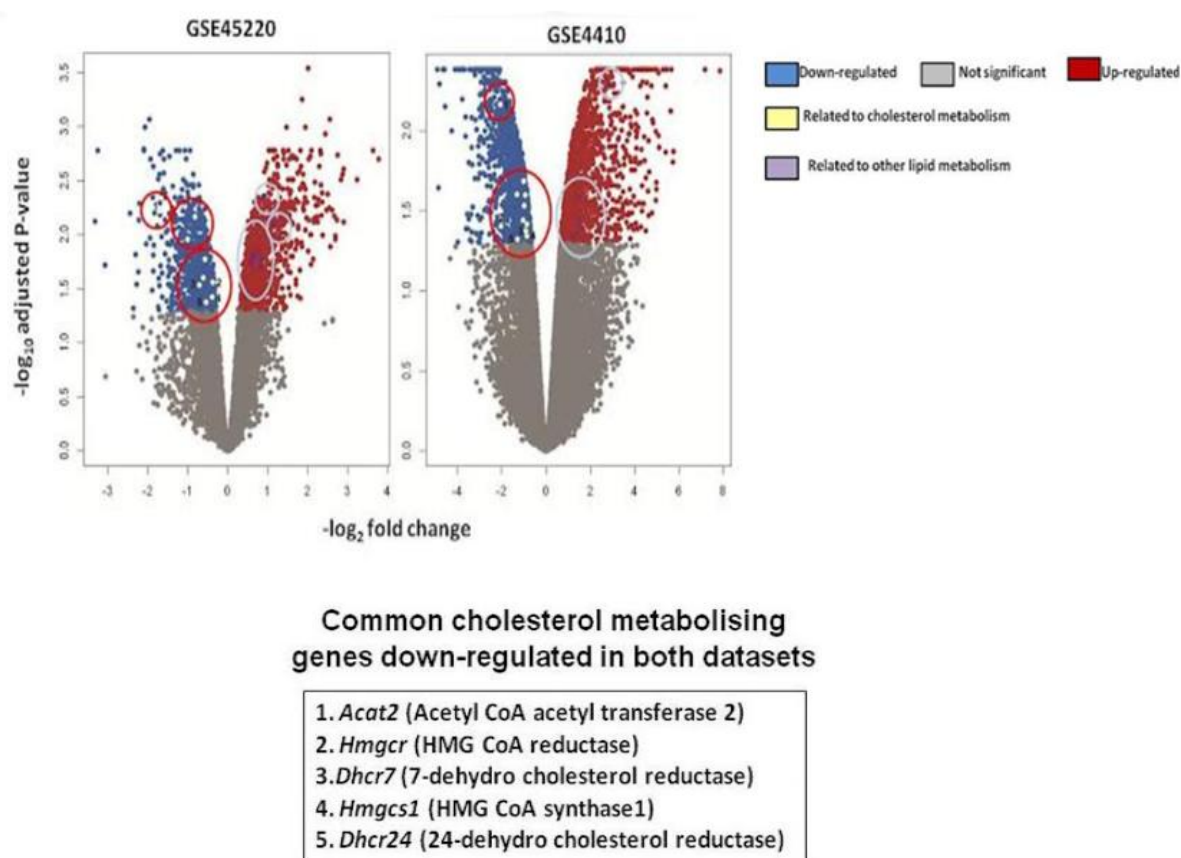


Figure 4.3: Effect of Butyrate on cholesterol metabolising genes observed via microarray analysis. Volcano map displaying microarray analysis when control vs butyrate-treated HeLa cells (GSE45220) and epithelial cell from colon MCE301 (GSE4410) were plotted. The plot encircles a cluster of down-regulated genes relevant to cholesterol biosynthesis. Down-regulated cholesterol metabolism genes in both datasets include *hmgcr*, *hmgcs*, *acat-2*, *dhcr-7*, and *dhcr-24*.

4.2.4 Molecular docking to assess the energy of binding

The docking investigation of butyrate with the active site of HMGCR produced a binding energy of -3.5 kcal/mol. All of the ligand association correspondence at the active site of the enzyme exhibits robust conventional hydrogen bonding. Butyrate interacts at the same active site of the HMGCR via three hydrogen bonds with two residues, notably Thr 558 and Glu559, with bond lengths of 2.94 (Thr 558), 1.96 (Thr 558), and 2.77 (Glu559). Simulation study was conducted and the result suggested that up to 5ns, butyrate remains intimately attached to the active sites of HMGCR and after 5ns, it becomes

dissociated. Butyrate happens to prevent the activity of HMGCR when given at a dose of 0.5 μ m, the effect was almost comparable to that of Statin, the most well-known commercially available inhibitor of HMGCR, use to prescribe in hypercholesterolemia.

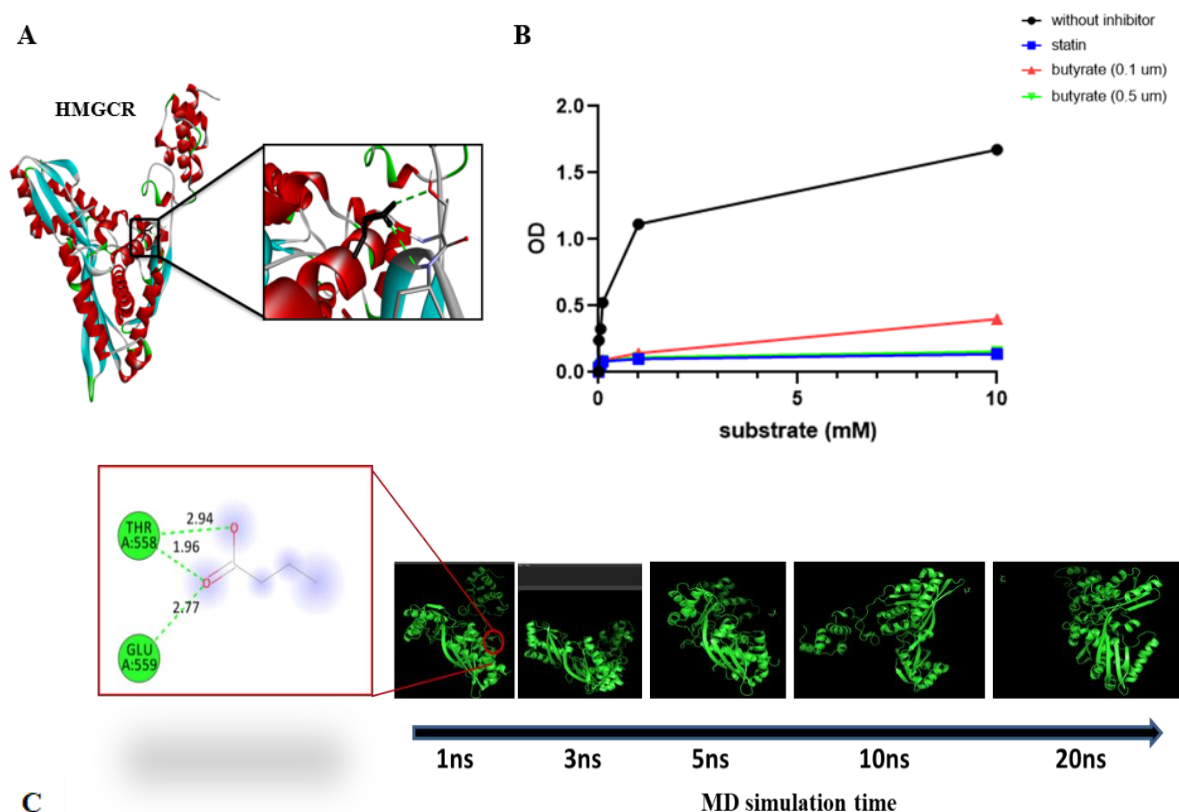


Figure 4.4: Analysis of interaction between Butyrate and HMGCR. Model displaying the complex formed following docking between butyrate and HMGCR (butyrate is shown by brownish-crimson sticks) (A). HMGC α A assay result indicating the comparable mode of action of Butyrate with that of Statin (B). Two amino acids in the active site, Glu559 and Thr558 with bond lengths of 2.94 (Thr 558), 1.96 (Thr 558), and 2.77 (Glu 559) are depicted in the inset as hydrogen bond interactions between butyrate and HMGCR. Simulation study displaying the alignment of butyrate at HMGCR active pocket along with the time of interaction (C).

4.2.5 Butyrate treatment corrects high fat diet induced hypercholesterolemia

Mice were given HFD for a month before being split under two groups. In first group, HFD was resumed (HFD-mice), whereas in second group, HFD was supplemented with sodium butyrate (butyrate) for an additional 15 days (HFD and butyrate treated mice). Another group of mice was retained to be the control group and was fed standard chow (control mice). On day 46, sacrifices of animals were made. Percentage of the body weight of these three groups were observed, where sharp rise of weight was found in HFD treated group and in case of second group, after introducing Butyrate,

the body weight began to decrease and almost became comparable to the chow fed diet control group. Results observed from the liver functioning test showed uprise of ALT and AST level in HFD fed group and Butyrate treatment lowered the level of ALT and AST, similar to the control one. Serum cholesterol levels in HFD-butyrates-mice reverted to the condition similar to the control group after being significantly higher in comparison to the control mice.

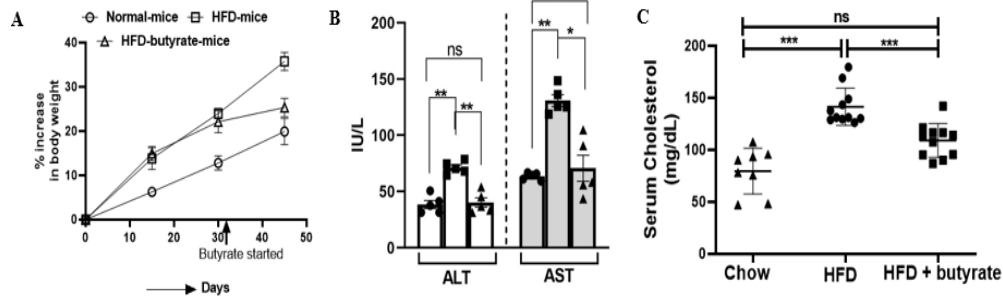


Figure 4.5: Effect of Butyrate on weight gain, liver function and serum cholesterol. Body weight gain as a function of days, expressed as a percentage (A), In all three groups of mice, the hepatic enzymes (ALT & AST) expressed in U/ml were measured (B). Levels of cholesterol in serum from chow fed mice, HFD fed mice, and HFD along with butyrate given mice were measured and denoted as mg/dl on day 46. N = 5 per group (c); the experimental analysis was performed three times. Data is shown as mean \pm SE with N = 5 for each group. The experiment was carried out thrice. ** stands for $p < 0.01$, * stands for $p < 0.05$, *** stands for $p < 0.001$. "ns" stands for "not significant".

4.2.6 Butyrate administration reduces the formation of hepatic lipid droplets

The state of hepatic droplets was determined using TEM on liver segments. The predominance of lipid droplets was highlighted in sample photographs of liver sections. HFD-mice had an abundance of lipid droplets with a diameter of 1.9 μ m, but HFD-butyrates-mice had a considerable decrease in both number and diameter to 0.6 μ m.

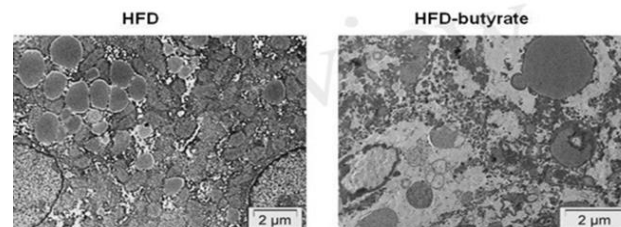


Figure 4.6: Images taken with a TEM show lipid droplet in the liver sections. In a transmission electron microscope equipped with an FEI Tecnai 12 Biotwin and an accelerating voltage of 100 kV, the sections were seen. The image has a 2 μ m scale bar.

4.2.7 Butyrate administration modifies the activity of cholesterol metabolising genes in hypercholesterolemia

We used qPCR to investigate hepatic expression of *hmgcr*, *hmgcs*, *acat2*, and *dhcr7* obtained from cell line data mentioned in the volcano plot. The level of hepatic *hmgcr* increased almost threefold in HFD fed mice in contrast with chow fed mice, but recovered to the level similar to normal condition in HFD and butyrate treated mice. The result was even verified in western blot analysis. There was a considerable uprise in the expression of hepatic *hmgcs*, *acat2*, and *dhcr7* in HFD mice in contrast with chow fed mice, but only *acat2* and *hmgcs* recovered to normal level in HFD butyrate animals. The level of *dhcr7* reduced considerably in the group of HFD and butyrate given mice when compared to HFD animals, but remained much greater in chow mice. Additionally, we chose to research the expression of the cytochrome P450 family member 7A1 (*cyp7a1*), a specific enzyme responsible for catabolism of cholesterol, that did not show in the volcano plot. In HFD butyrate mice, *cyp7a1* expression was dramatically restored to normal levels after being significantly decreased in HFD mice compared to chow mice.

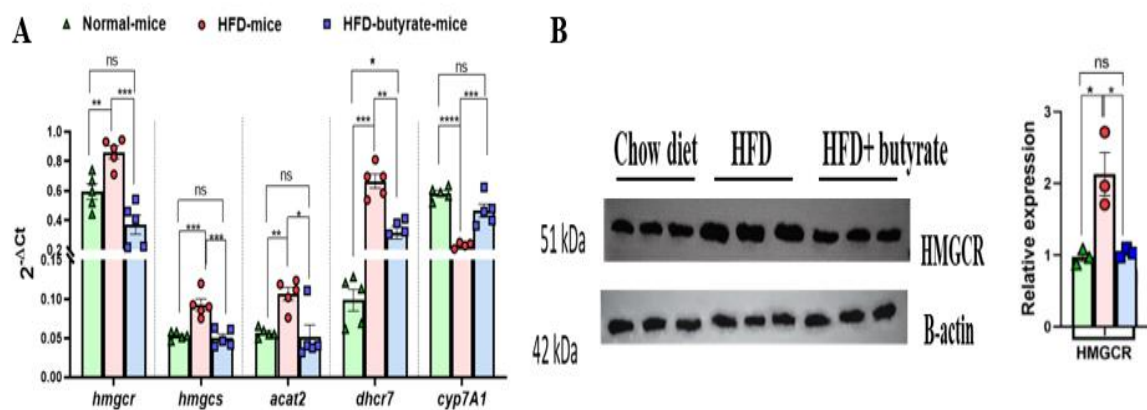


Figure 4.7: Evaluation of cholesterol metabolic gene expression in the liver by using qPCR, the genes *hmgcs*, *hmgcr*, *dhcr7*, *acat-2*, and *cyp7A1* was examined in each group. (A) Western blot evaluation of HMGR hepatic expression. Using ImageJ, densitometry was performed to reveal relative expression in comparison to the β -actin control (B). Data are presented as mean \pm SE; N = 5 per group. Three times the experiment was conducted. ** stands for $p < 0.0001$, *** for $p < 0.001$, ** for $p < 0.01$, and * for $p < 0.05$, and "ns" stands for "not significant."**

4.2.8 Examining the functionality and expression of transporter proteins after Butyrate treatment in relation to cholesterol efflux

Aside from manufacturing, cholesterol may also be modulated by a process known as efflux, in which cholesterol is pumped out of the cell and into the extracellular space via numerous transporter proteins such as ABCA1, ABCG5, ABCA8, and transporter-related accessory proteins such as ABCA5. The Western blot demonstrated that butyrate administration of Huh7 cells led to a gradual uprise in the level of ABCA1 as a function of the concentration of butyrate. This finding was verified in the in-vivo mouse model (chow, HFD, HFD+Butyrate).

Using Huh7 cells that had been loaded with 22-NBD-cholesterol and either butyrate or no butyrate treatment, we examined efflux. Before butyrate treatment, the cells that had been loaded with 22-NBD cholesterol were allowed to aqueously diffuse for 18 hours in the medium. No substantial amount of cholesterol was found to be ejected in the absence of HDL, regardless of butyrate therapy. Intriguingly, cholesterol efflux from Huh7 cells loaded with 22-NBD-cholesterol increased significantly with HDL levels and was markedly improved when cells were pretreated with butyrate.

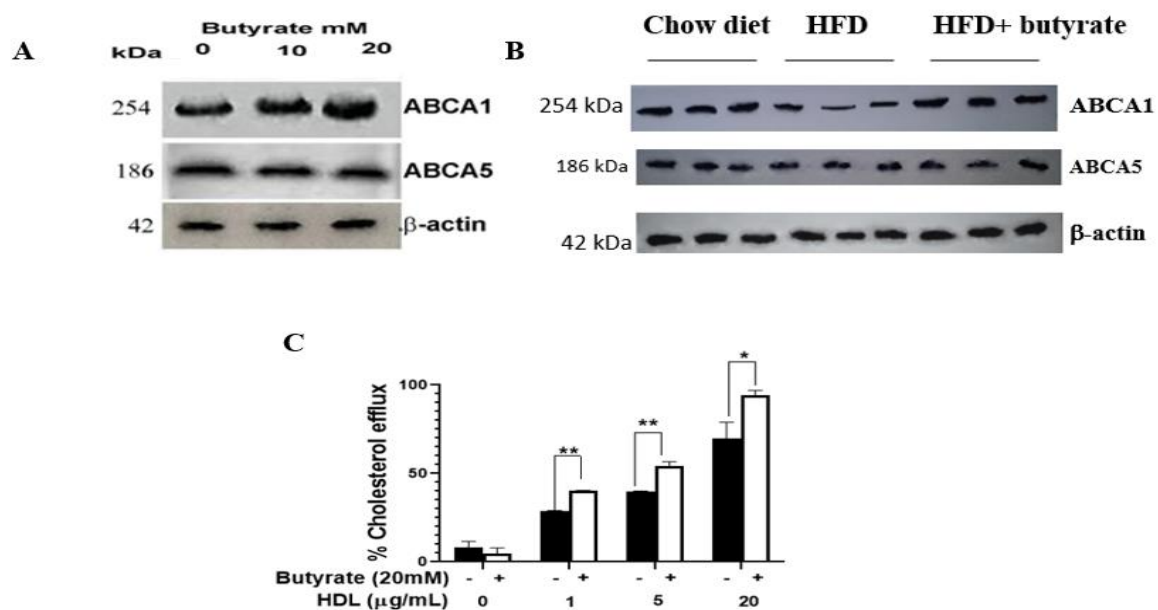


Figure 4.8: Western blot evaluation of ABCA1 as well as ABCA5 expression in relation to butyrate dosages in Huh7 cells and in animal experiment, β-actin was used as loading control (A, B). 22-NBD fluorescence was measured to track the percentage of cholesterol efflux as a function of butyrate concentration. Huh7 cells were washed and allowed to acclimatize for 18 hours, followed by HDL (1 g/ml, 5 g/ml, and 20 g/ml). A black polystyrene 96-well plate was used to detect the intensity of fluorescence (FI) of 22-NBD-cholesterol in the medium along with lysate of cells using the fluorescence microplate reader (MT-600F).

4.2.9 Butyrate treatment inhibits miR122 biogenesis with concurrent increase in pre-miR122

To find out if Butyrate mediated cholesterol catabolism, metabolism of cholesterol and efflux are intertwined together or not, we look into the expression of microRNA 122, which is reported to be associated with regulation of cholesterol. In Huh7 cells treated and untreated with butyrate, we used qPCR to track the maturation of miRNA122 from pre-miRNA. As a function of butyrate concentration, it was noticed that there was an increase in pre-miR122 and a contemporaneous decrease in miR122 expression. The above-mentioned result was also verified in our in-vivo study.

Additionally, we noticed that premir-122 and mir-122 showed no differences at 20 mM for propionate and acetate compared to control.

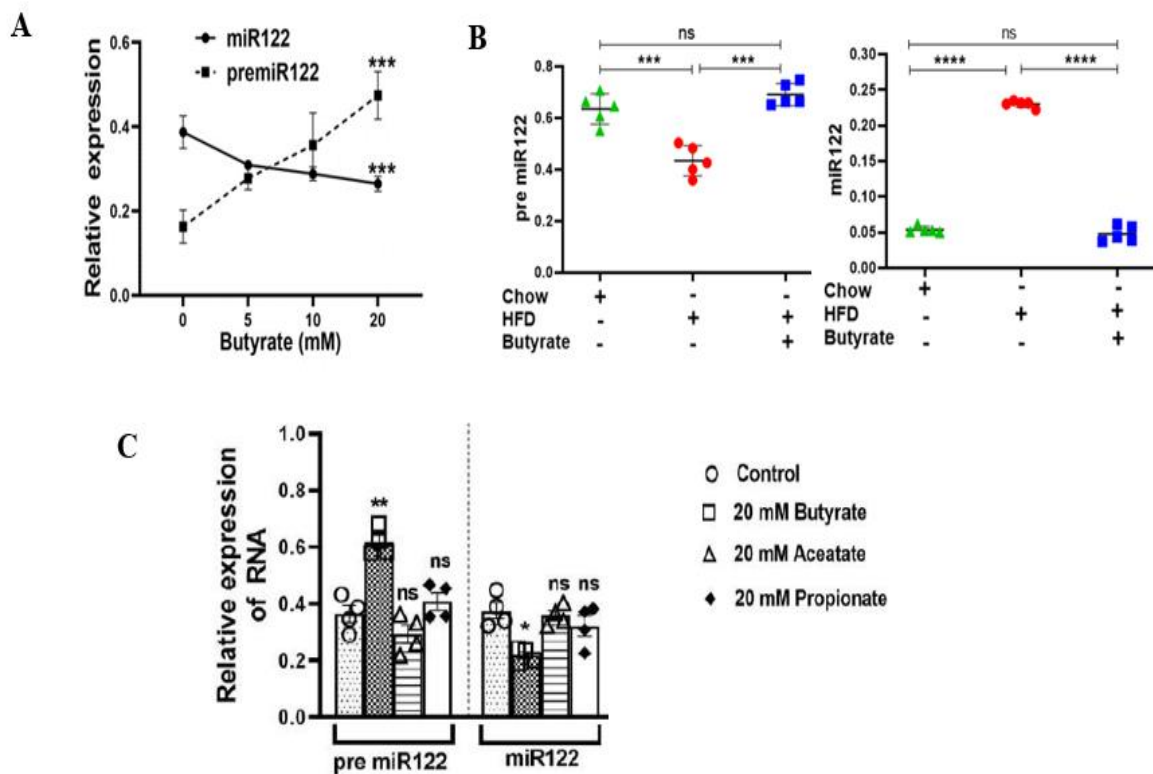


Figure 4.9: Expression level of miR122 along with its precursor form pre-miR122 as assessed by qPCR in Huh7 cell line and animal model (A, B). qPCR analysis revealed 20 mM of each after butyrate, propionate, or acetate treatment (C). For all N=3 data sets, the data is shown as mean \pm SE. *** stands for $p < 0.001$, ** for $p < 0.01$, * for $p < 0.05$, and "ns" stands for not significant.

4.2.10 Butyrate triggers the expression level of RNA binding protein AUF-1, causing Dicer1 mRNA to destabilize

In butyrate-treated Huh7 cells, we used qPCR experiment and western blot analysis to examine the expression of Dicer-1, the major endoribonuclease responsible for the synthesis of mature miRNA from its precursor form, along with its post-transcriptional regulator, AUF-1 which interacts with 3'UTR of target RNA. The four isoforms of AUF-1 are AUF-1p37, AUF-1p40, AUF-1p42, and AUF-1p45. At 10 mM and 20 mM butyrate, the AUF-1p40 fold increase over the untreated control was 7.36 and 8.7, respectively. A decrease in the expression of AUF-1p42 was accompanied by an increase in the expression of AUF-1p40, demonstrating a reciprocal relationship between the two. AUF-1p37 expression, on the contrary, increased marginally after 10 mM butyrate addition and significantly after supplementation of 20 mM butyrate. Furthermore, there was a gradual reduction in Dicer-1 level as a functional concentration of butyrate, which was four-fold in Huh7 cells treated with 20 mM butyrate.

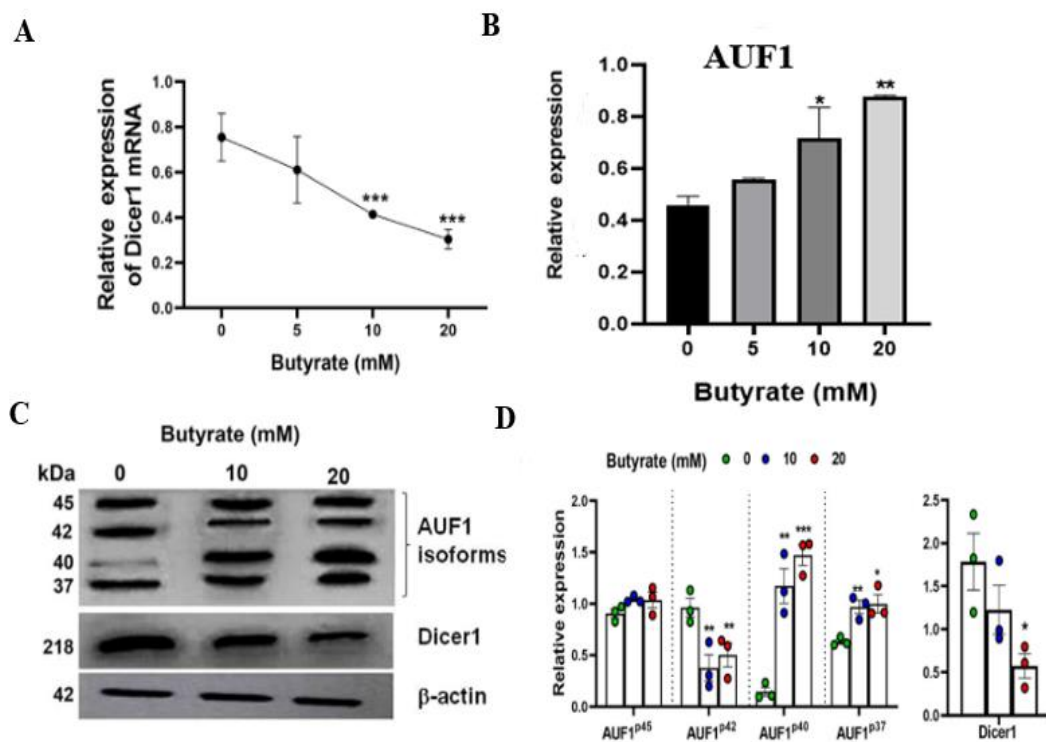


Figure 4.10: Butyrate's impact on Dicer1 and AUF-1 as demonstrated by qPCR and western blot evaluation (A,B,C). ImageJ was used to calculate the densitometry of AUF1 isoforms (AUF1p45/AUF1p42/AUF1p40/AUF1p37) and Dicer1 in relation to β -actin control (D).

4.2.11 Confocal investigation to confirm the crucial role of butyrate in governing the expression of various isoforms of AUF-1

In order to find out how Butyrate influences different isoforms of AUF-1, Huh7 cell line was transfected with four isoforms individually and then 20mM of Butyrate treatment was given for 24 hours. After 24 hours of treatment, apotome images were taken to check which of the isoforms become upraised. When Huh7 cells were treated with butyrate, the basal expression of AUF-1 isoforms changed to p40>p45>p37>p42 from p45>p42>p37>p40. AUF-1p42's expression dramatically decreased compared to the untreated control, but AUF-1p45's expression remained unchanged.

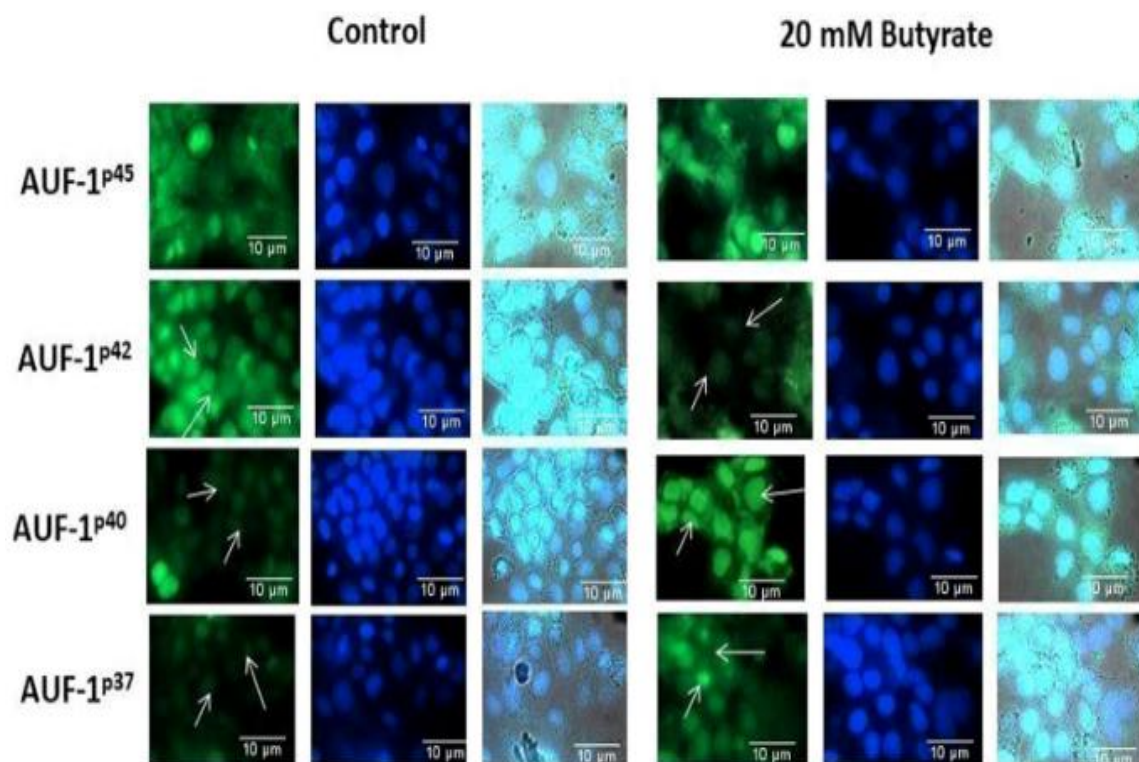


Figure 4.11: Effect of Butyrate on four different isoforms of AUF-1. The subsequent fluorescence images are captured at 60X in an Apotome Zeiss microscope using a CCD camera and ZEN software (Carl Zeiss, Gottingen, Germany).

4.2.12 Silencing AUF-1 boosted the expression of Dicer-1 and mir-122 in Huh7 cells

The expression of Dicer-1, mir-122, and the state of cellular cholesterol were two other effects of AUF-1 silencing that were investigated. However, it was not evident when transfection with only scramble siRNA was performed. Instead, silencing with si-AUF-1 caused a large rise in cellular cholesterol, Dicer-1, mir-122, and regardless of the butyrate treatment. The remaining tests were conducted using the AUF-1p40 isoform because it was relatively prominent among all the AUF-1 isoforms that were upregulated in response to butyrate therapy. Additional cellular effects of AUF-1 suppression were investigated, including cellular cholesterol state, Dicer-1 along with mir-122 expression, and. Regardless of butyrate treatment, si-AUF-1 silencing led to a large rise in cellular cholesterol, Dicer-1 and mir-122 but this was not obvious when the transfection was performed with scramble siRNA only. Because the overexpression of AUF-1p40 was the most significant of all the isoforms of AUF-1, as a result of butyrate therapy, the remaining research focused on AUF-1p40. A co-transfection experiment was carried out to demonstrate that AUF-1 suppressed Dicer-1 by interacting with mRNA's 3'-UTR region. Huh7 cells had been transfected with pEGFP, pEGFP-AUF-140, p-EGFP-3TRDicer-1, and the fluorescence was examined using fluorescence microscopy. The cells were treated with or without butyrate after another round of transfection with scramble or siAUF-1, giving sets of four experimental groups (i) scramble (only) (ii) scramble along with butyrate, (iii) siAUF-1 (only) and (iv) siAUF-1 along with butyrate, from left to right. Transfection was conducted from top to bottom using pEGFP-AUF-140, p-EGFP-3TRDicer-1, or pEGFP.

Co-transfecting scramble with pEGFP-AUF-1p40 in the first panel resulted in fluorescence, which grew after being exposed to butyrate. However, siAUF-1 did not have any influence on the fluorescence of EGFP-AUF-1p40, and the effect persisted even after butyrate treatment. A baseline amount of fluorescence from scramble siRNA was present in the next column for the p-EGFP-3TR Dicer-1 probe, but this level dropped down after butyrate treatment. With siAUF-1, EGFP-3TRDicer-1's fluorescence was enhanced; however, after butyrate treatment, it virtually stayed constant. The third panel demonstrated that over the period of the aforementioned treatments, there was no change in the EGFP expression. Until now, Huh7 cells were used to investigate the relationship between butyrate, AUF-1, Dicer-1, and mir-122. We used a mouse model to further interpret these results.

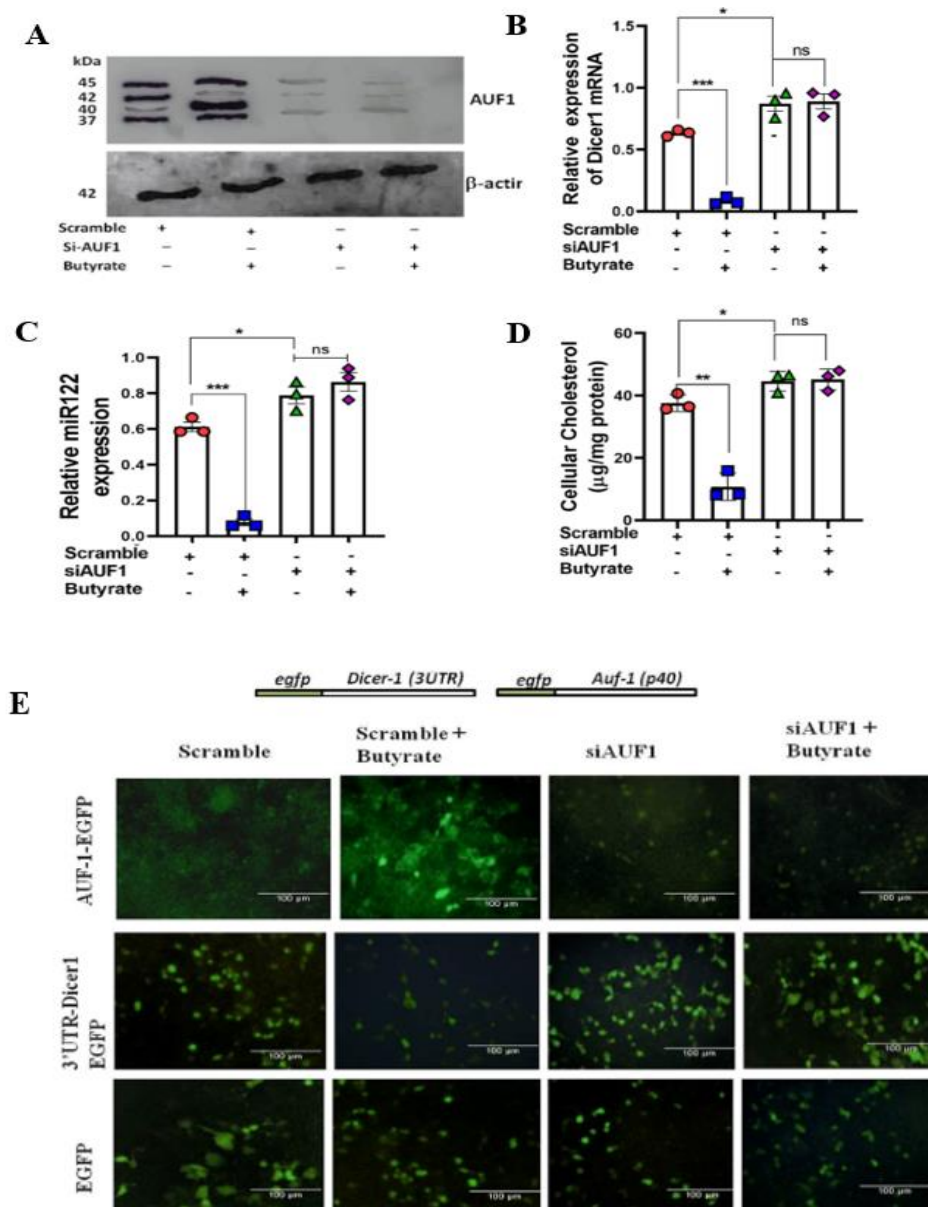


Figure 4.12: Dicer1 expression, cellular cholesterol, and AUF1 silencing by siRNA-enhanced miR122 in Huh7 cells despite butyrate administration. Following co-transfection with either scramble-RNA or siAUF1, Western blot of the AUF1 isoforms was performed, with β -actin serving as the control. qPCR analysis of Dicer1 and miR122 expression, as well as cellular cholesterol derived from cell lysate (B, C, D). Assessment of EGFP levels following transfection with EGFP-AUF1p40, EGFP-3TR-Dicer1, and only EGFP (ranging from the top to the bottom) in a study of co transfection under the subsequent circumstances: (I) scramble (only) (II) scramble along with 20 mM butyrate, (III) siAUF1 (only) and (iv) siAUF1 in addition to 20 mM butyrate (left to right) (E). A Carl Zeiss microscope with a CCD camera and ZEN software (Carl Zeiss, Gottingen, Germany) was used to capture the co-transfected cells' resulting fluorescent images at a magnification of 20 times. The experiment was repeated thrice and the data are shown as mean SE. The symbols ***, **, *, and ns stand for significance levels of $p < 0.001$, $p < 0.01$, and $p < 0.05$, respectively.

4.2.13 Butyrate uprises Sphingosine kinase 1 (AUF-1's typical target) and junctional protein Occludin (a well-known target of miR122) in Huh7 cell

We also investigated the expression of sphingosine kinase (Sphk1) because AUF-1 promotes mRNA degradation and may have crucial targets other than Dicer-1. Sphingosine kinase 1 (Sphk1) mRNA expression was likewise lowered in response to butyrate therapy. AUF-1 also targets the protein Sphk1 (Sobue et al., 2008). We also noticed that after Huh7 cells were treated with butyrate, Sphk1 expression significantly decreased. The relationship between Sphk1 and AUF-1 expression after butyrate administration provided support for the idea that butyrate targets AUF-1.

One of the classical targets of miR122 is occluding (Chakraborty et al., 2023). In vitro study in Huh7 cell line suggested that Occludin becomes upregulated in a dose dependent manner when Butyrate mediated reduction of miR122 was observed, and the observation indeed supported the notion that Butyrate acts on miR122.

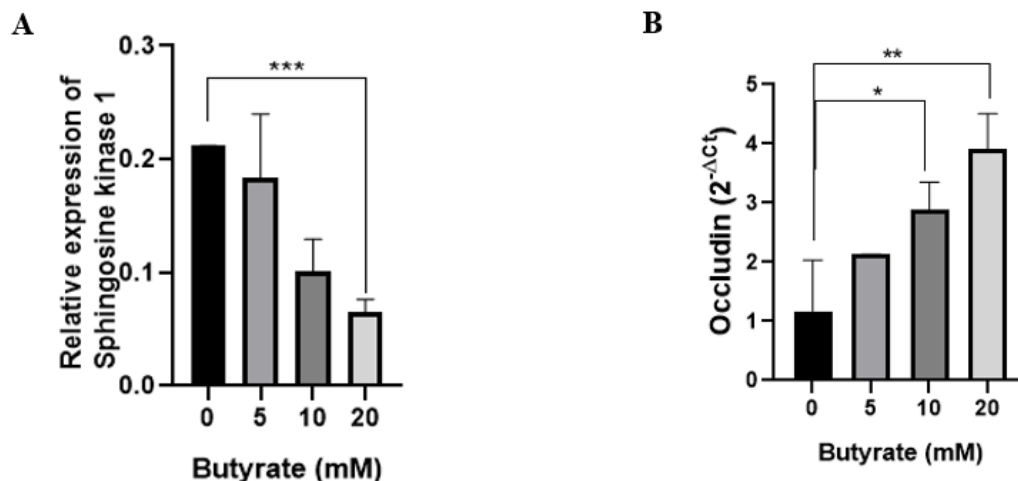


Figure 4.13: Effect of Butyrate on Sphk1 and Occludin. The expression analysis of Sphk1 (Sphingosine kinase1) and Occludin as a function of different dose of butyrate in Huh7 cells as obtained by qPCR N=3. The data is shown as mean \pm SE, where *** denotes $p < 0.001$, ** denotes $p < 0.01$, * denotes $p < 0.05$.

4.2.14 Butyrate administration additionally lowers microRNAs aside from miR122

There are indications that mir27 performs an essential part in lipid metabolism. To see if butyrate impacts microRNAs besides miR122, we looked at the hepatic level of miR27a and miR27b in control, HFD fed, and HFD along with butyrate given mice. We found that HFD-mice had a 6-fold rise in

hepatic level of miR27a activity relative to control mice, which recovered to the level similar to that of control one, in HFD and butyrate fed mice. Surprisingly, miR27b remains unaffected in all three groups.

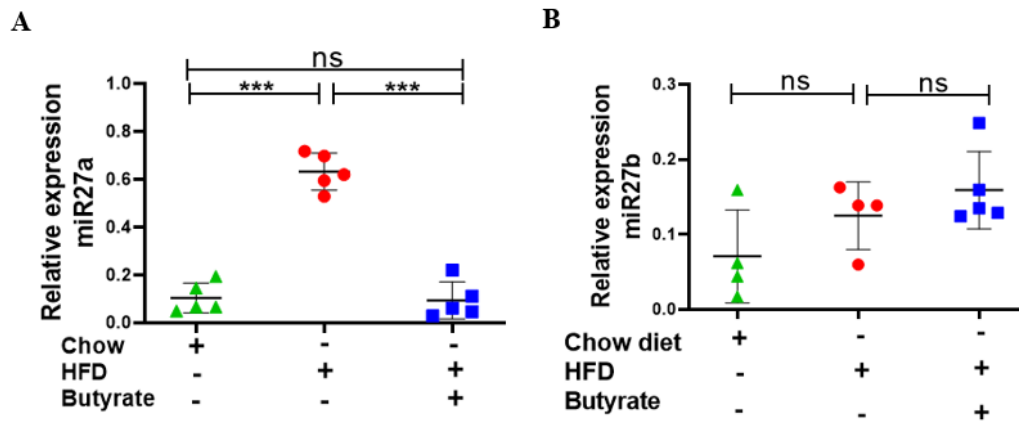


Figure 4.14: Effect of butyrate on miR27a and miR27b. Control mice, HFD fed mice, and HFD along with butyrate fed mice have the hepatocellular levels of miR27a and miR27b. qPCR analyses of the hepatic activity of miR27a along with miR27b in control mice, HFD fed mice, and HFD and butyrate treated mice. Data are shown as mean±SE with N=4 per group. P values are represented by the symbols *** (p <0.001), ** (p <0.01), and * (p <0.05)

4.2.15 Interactions between cholesterol, AUF-1, Dicer-1, and miR122 in animal models of intestinal dysbiosis

Three major animal models were used to assess the interaction between AUF-1-Dicer-1 miR122 with cholesterol, which are: 1) HFD-induced obese mouse to study the phenomenon of hypercholesterolemia, 2) long-term antibiotic-treated mice which served as a germ-free surrogate mice model, and 3) colitis caused by DSS mice to replicate a diseased condition.

a) HFD mice model

In the obese mice model, the hepatic production of miR122, Dicer-1, and AUF-1 along with serum cholesterol was investigated. In HFD-mice, there was a notable drop in pre-miRNA with an uprise in miR122 in contrast to normal. In HFD-butyrates mice, their expression was restored to control ones. It also turned out that in HFD-mice, Dicer-1 increased while AUF-1 decreased and that these values returned to the level similar to the control ones in HFD-butyrates-mice. In HFD mice, faeces butyrate levels were 9.5 times lower than in normal mice.

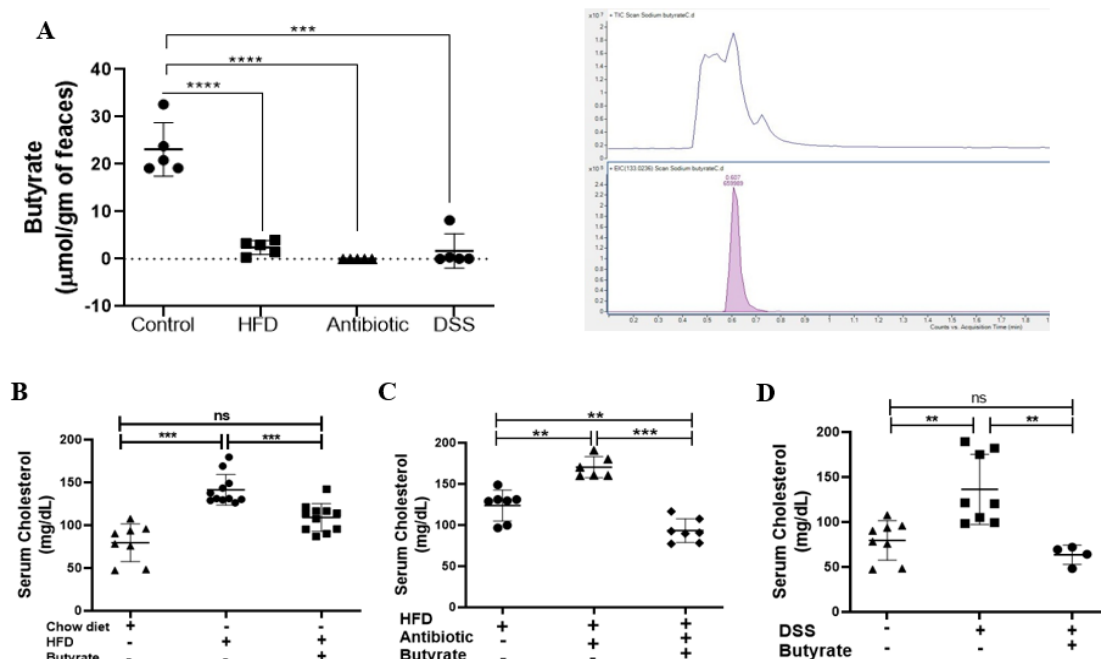
b) Antibiotic treated mice model

In this study, chow fed mice were given a range of antibiotic treatments for 21 days in an effort to diminish the amount of symbiotic gut bacteria. We measured the amounts of faecal butyrate in each group. The amount of faecal butyrate in chow given meal was 23.13 mol/g of faeces. Faecal butyrate in HFD-mice was 2.42 mol/g of faeces, while it was just 0.0075 mol/g in antibiotic-mice. Serum cholesterol also exhibited uprise in antibiotic treated group. Following butyrate treatment, blood cholesterol in antibiotic given group was dropped almost to control levels.

As anticipated, antibiotic-mice displayed decreased hepatic expression of AUF-1, along with enhanced expression of Dicer-1 and miR122. Butyrate therapy reversed these effects.

c) DSS mediated colitis

We found that DSS-treated mice (DSS-mice) had shorter colons, lower body weight, and loss of colonic epithelium, confirming colitis pathology in mice. Butyrate treatment restored both colon length and body weight to near-normal levels. We then investigated the status of faecal butyrate in colitis mice. Normal mice had a faecal butyrate content of 23.13 mol/g faeces, whereas colitis animals had a concentration of 1.73 mol/g faeces. When colitis mice were compared to normal mice, their serum cholesterol levels were considerably higher, but they reverted to normal after butyrate treatment. In colitis mice, hepatic AUF-1p40 expression was considerably lower, while Dicer-1 and miR122 expression increased.



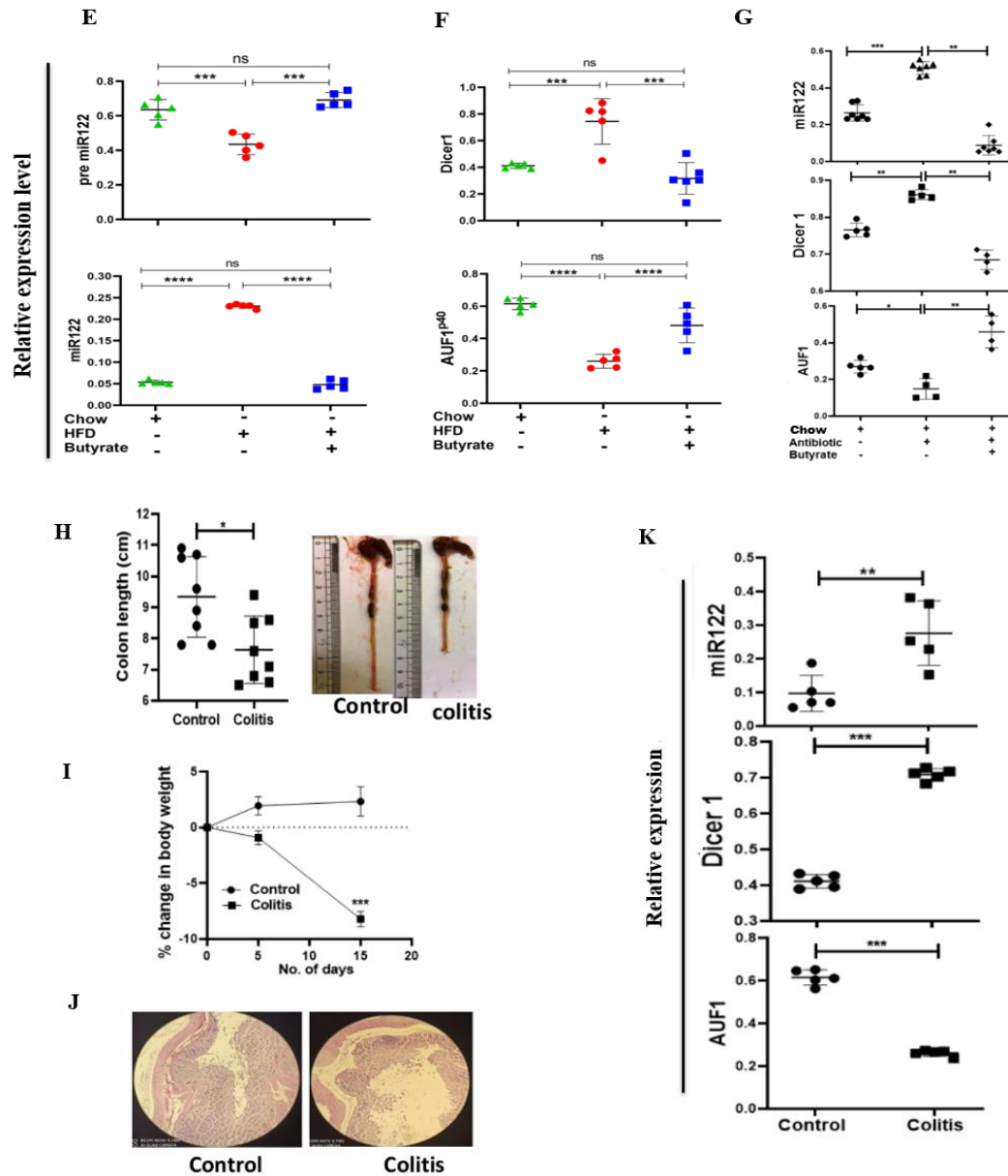


Figure 4.15: Faecal butyrate, serum cholesterol and expression level of miR122, Dicer 1 along with AUF-1 in HFD, antibiotic treated and DSS induced colitis mice. LC-MS measurement of faecal butyrate in control, HFD, antibiotic treated and DSS treated group, characteristic peak of Butyrate in LCMS (A) serum cholesterol of HFD, antibiotic and DSS expressed in mg/dl (C, D, E). Pre-miR122 and miR122 along with Dicer1 and AUF1p40, as detected by qPCR, are expressed in the livers of chow, HFD, and HFD butyrate mice (E, F, G). (B). Length of colon (in cm) in control, DSS- and DSS-butyratemic mice (H). Percent change in body weight in control, DSS and DSS-butyratemic mice (I). Histological section of colon tissue of control and DSS mice. The images were captured in 20X magnification under Carl Zeiss microscope with a CCD camera controlled with ZEN software (Carl Zeiss, Gottingen, Germany) (J). Relative expression of miR122, Dicer 1 and AUF-1 as determined from q PCR(K). $N \geq 4/\text{group}$. **** denotes $p < 0.0001$ *** denotes $p < 0.001$, **denotes $p < 0.01$, * denotes $p < 0.05$.

4.2.16 Insufficiency of gut microbial butyrate causes hypercholesterolemia by using miR122, Dicer1 and AUF-1 axis

To demonstrate that gut obtained butyrate is intricately associated with cholesterol modulation in mice, we used a same type of technique (Han et al., 2022; Wang et al., 2021) and diminished the murine intestinal microbial composition through regular gavage which was given the supplementation of the mixture of different antibiotics and this model acted as a germ-free surrogate mice model.

Figure 4.16 shows a schematic representation of the treatment protocol for each group of mice. Four groups of mice were formed: Group I was fed only chow diet (considered to be untreated mice), Group II was given a cocktail mixture of antibiotic (Abx mice), and Group III was given the cocktail mixture of antibiotic for 7 days then received probiotic therapy on an alternate day over 21 days (Abx probiotic mice), and the Group IV was given butyrate through day 8 to day 21 (Abx butyrate mice).

As an indirect measure of the relative number of bacteria producing butyrate, we evaluated the quantitative amount of the final enzyme of the butyrate biosynthesis route i.e., butCoAT or butyryl-CoA: acetate CoA-transferase through DNA samples from faeces. When compared to untreated mice, Abx mice had a 100-fold drop in the proportional abundance of the butCoAT gene, which was restored to virtually normal levels in Abx probiotic mice.

We assessed faecal butyrate using LC-MS to demonstrate that a decline in the proportion of the butCoAT gene was reliably reflected in butyrate synthesis. In Abx mice, the drop in faecal butyrate was more dramatic than uprise of butCoAT gene expression level. When contrasted with untreated mice, Abx animals had a 9,000-fold decrease in faecal butyrate, but probiotic treatment boosted faecal butyrate 70,000-fold and 7-fold greater than untreated mice.

We evaluated blood along with hepatic cholesterol and found that total cholesterol in the blood surged 2.5-fold level on 7th day and stayed unchanged even on 21st day in Abx animals versus untreated mice. Hepatic and blood cholesterol levels in Abx probiotic and Abx butyrate animals reduced dramatically when compared with Abx mice and restored to normal levels.

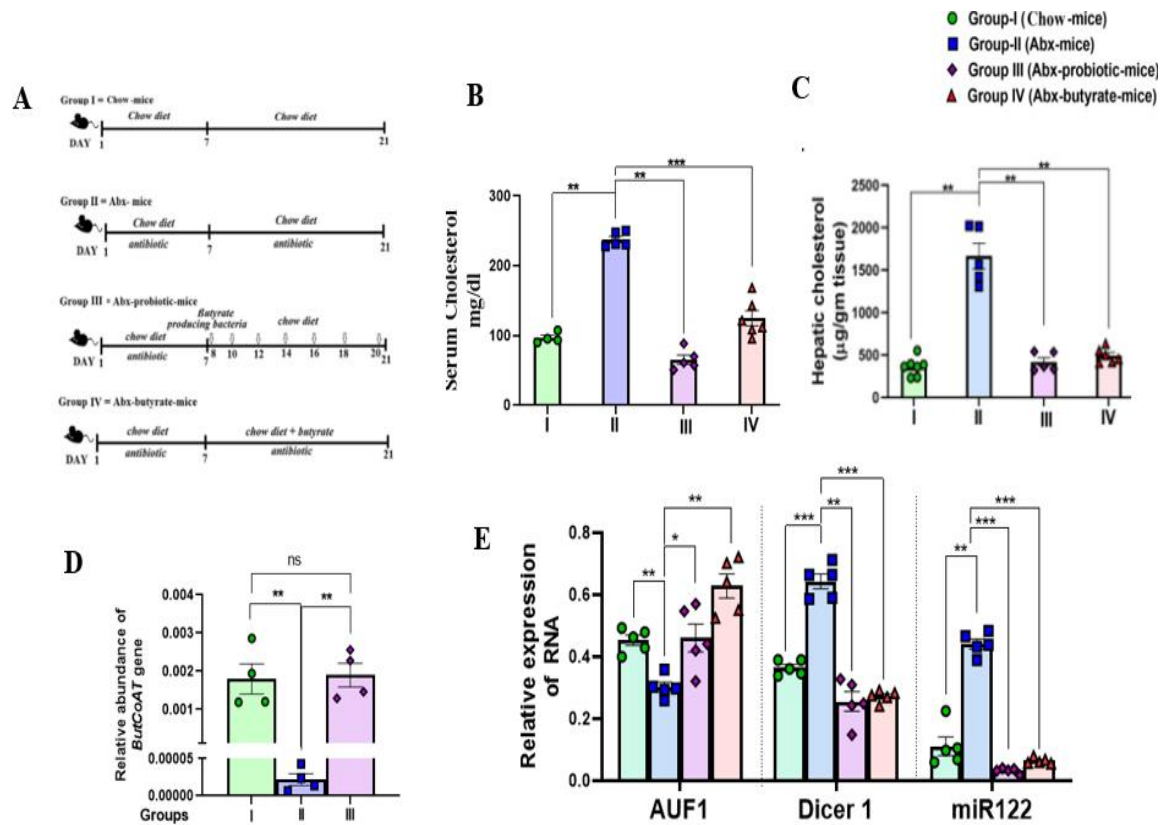


Figure 4.16: The impact of antibiotic treatment followed by probiotic administration on serum along with liver cholesterol levels, ButCoAT level, miR122, Dicer 1 and AUF1p40 production. The study employed female mice. The study's experimental design: Group I consist of untreated chow-fed mice. Group II mice (Abx mice) received a combination of antibiotic and a chow diet for 21 days. Group III mice were treated with an amalgam of antibiotic for initial 7 days, following the colon cleansing with PEG and treatment with probiotics (10^7 cfu in 200 μ l) by oral gavage every alternate day for the next 2 weeks (Abx probiotic mice). Between day 7 to 21 (Abx and butyrate treated mice), Abx treated mice were fed a supplement of 5% butyrate along with the chow diet (w/w) (A). On 21st day, blood, liver tissue, and faecal samples were obtained. serum and hepatic cholesterol level expressed in mg/dl and μ g/g subsequently (B, C) The apparent quantity of the level of butCoAT gene in faeces was determined via qPCR and standardised to the abundance of the 16S rRNA bacterial gene (D) qPCR was used to evaluate the expression of liver AUF1p40, Dicer1, and miR122 (E). N = 5 per group; results reported as mean \pm SE. The experimental analysis was carried out twice. **** denotes $p < 0.0001$, *** denotes $p < 0.001$, ** denotes $p < 0.01$, * denotes $p < 0.05$, "ns" stands for "not significant".

4.2.17 Impact of Butyrate driven hypocholesterolaemia in mice is reversed by excess expression of mir-122

It was clear from the prior studies that butyrate controls cholesterol biosynthesis by taking advantage of mir-122. By increasing mir-122 in mice treated with butyrate, a plasmid harbouring microRNA 122 was delivered by means of the tail vein of mice given only chow diet along with butyrate, and we were able to corroborate our observation. On day 4 after receiving a mock plasmid injection, a different group of mice were euthanized, and serum cholesterol were then examined. When compared to butyrate-fed mock-injected mice, we saw a 25-fold spike in liver mir-122 production and a four-time rise in serum cholesterol.

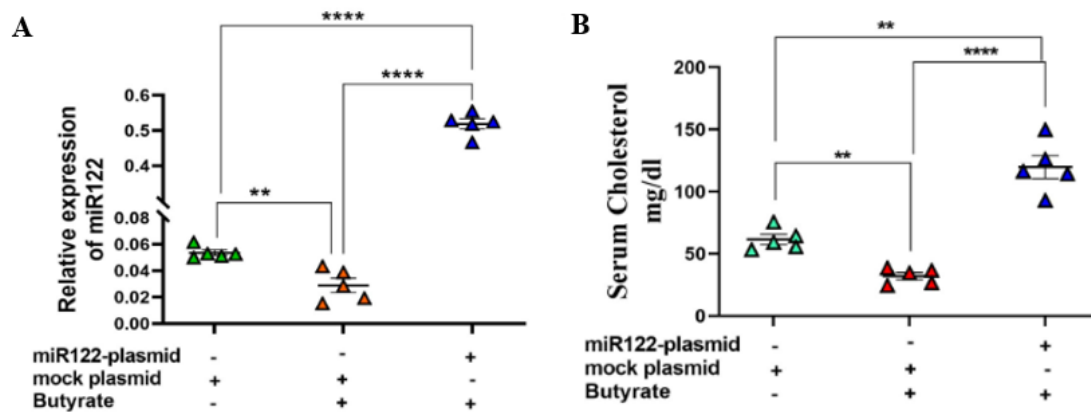
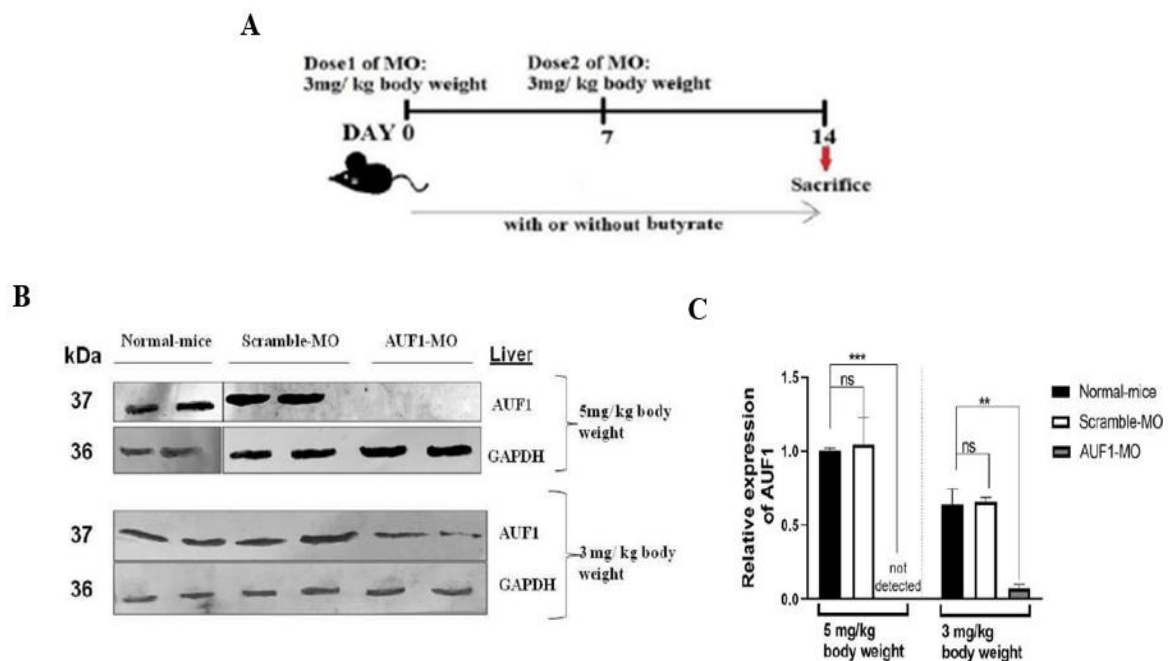


Figure 4.17: Reduced blood cholesterol brought on by butyrate is prevented by hepatic miR122 overexpression. Female mice treated with butyrate received an injection of either 25 ng/100 μ l of microRNA122-expressing plasmid or 25 ng/100 μ l of sham plasmid in the tail vein. Four days after the injection, the mice were killed. miR122 expression in the liver and serum cholesterol levels were assessed. Data are provided as mean \pm SE; N = 5. Two times the experiment was conducted. **** denotes $p < 0.0001$, ** denotes $p < 0.01$.

4.2.18 Effect of cholesterol-metabolizing enzyme level, Dicer-1, Mir-122, and sera cholesterol following knockdown of AUF-1 via morpholino oligomer (GMO-PMO)

We chose to use AUF-1-KD (AUF-1 mediated knockdown in mice) utilizing an innovative morpholino oligomer having cell penetrating ability (GMO-PMO) to prove the fundamental hypothesis that AUF-1 is a crucial component in the butyrate regulated cholesterol homeostasis. In this work, the scramble-specific GMO-PMO was designated as scramble-MO and the AUF-1-specific one was designated as

AUF-1-MO. On day 14, as shown in the illustration, mice that were administered morpholino upon days 0 and 7 were sacrificed. We demonstrated the role of AUF-1 and scramble GMO-PMOs which were pattern specific, as there was not any disparity in AUF-1 levels among control and only scramble-MO-treated mice, demonstrating the fact that the scramble-MO had no impact on AUF-1 expressing themselves through the AUF-1-MO did. The outcomes demonstrated that not solely in the liver itself but also in other organs including the heart and kidneys, AUF-1-MO dramatically diminished the AUF-1 isoform. Additionally, butyrate therapy had no effect on the AUF-1 condition in the liver of either scramble-MO or AUF-1 MO animals. When butyrate was combined with scramble-MO, mir-122 and Dicer-1 production in the liver was shown to be significantly downregulated in AUF-1-KD when compared to scramble-MO alone. As anticipated, AUF-1-MO treatment in mice increased mir-122 and Dicer-1 levels, while remaining unaffected when paired with butyrate administration. We also looked at the effects of mir-122 overexpression in AUF-1 knockdown mice, where two genes for cholesterol-metabolizing enzymes, CYP7A1 and HMGCR, are known mir-122 targets and are thought to be part of the cholesterol homeostatic system. As anticipated, there was an increase in *cyp7A1* and a decrease in *hmgcr* in the scramble-MO group that received butyrate. Regardless of butyrate administration, *hmgcr* was significantly upregulated and *cyp7A1* was significantly downregulated in AUF-1 knockout mice. *Hmgcr* and *cyp7A1* exhibit a reciprocal relationship, as seen by mir-122 and Dicer-1. As anticipated, scramble-MO mice treated with butyrate had much lower blood and cholesterol levels in liver than AUF-1-MO mediated KD mice, whose cholesterol levels were adequately increased but did not change in response to butyrate administration.



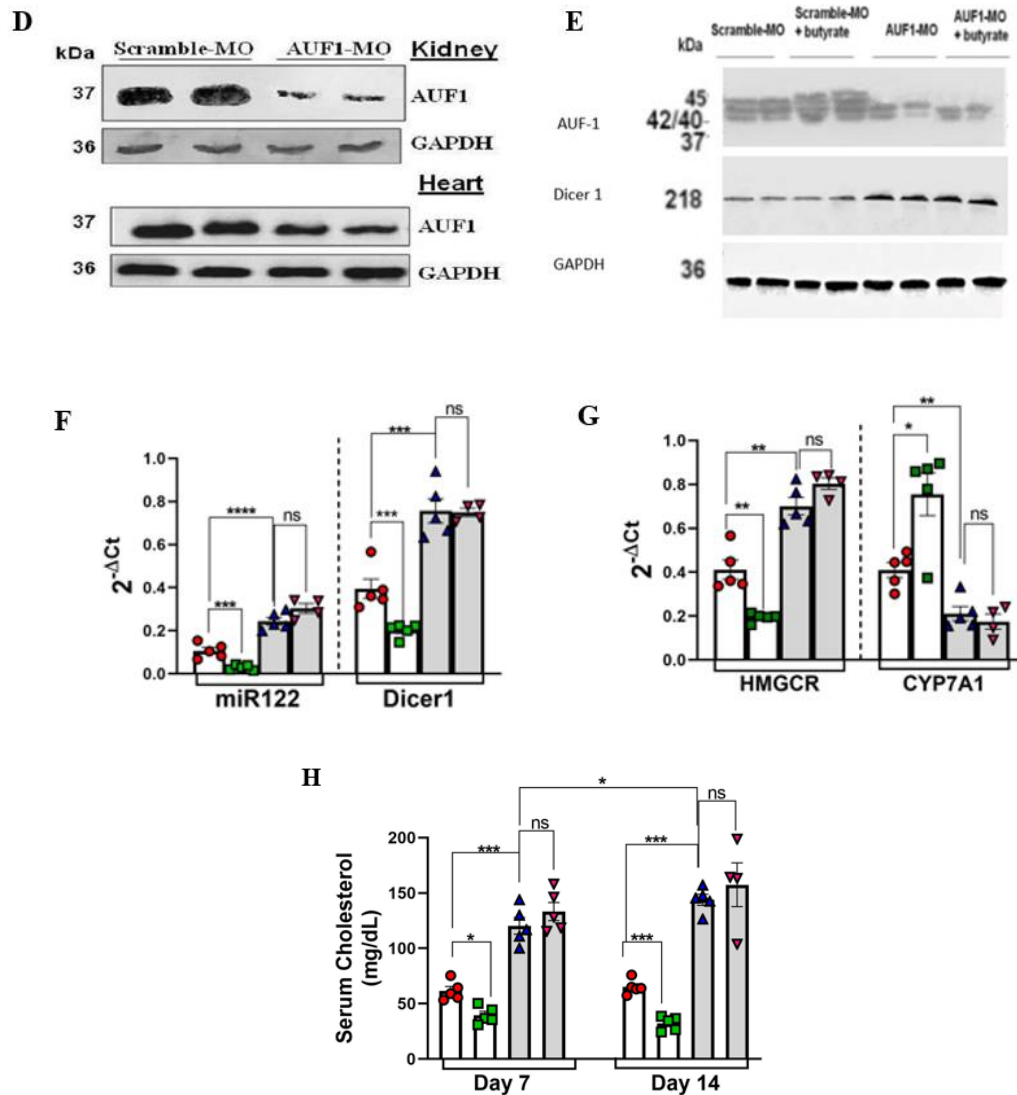


Figure 4.18: In vivo, AUF1 knockdown promotes cholesterol production by taking advantage of the AUF1, Dicer1 and miR122 mediated cholesterol route, regardless of butyrate administration. 20 mice (female) were allocated under four divisions at random: AUF1-MO mice (only AUF1-MO-injected mice), AUF1-MO-injected mice fed with supplementation of butyrate (AUF1 MO along with butyrate-treated mice), scramble MO mice (only scramble-MO-injected mice) and butyrate scramble MO mice (scramble MO mice given butyrate supplement); the layout was depicted graphically (A). Mice received either the dose of 5 mg/kg of body weight or as 3 mg/kg of body weight AUF1-MO/scramble-MO injections in the tail vein. The hepatic samples were taken 7 days after injection, and the expression of AUF1 was determined using western blot analysis (B) and ImageJ densitometric assessment (C). AUF1 Western blot in the heart and kidney of mouse administered AUF1-MO (D). AUF1 as well as Dicer1 hepatic expression was determined using Western blots (E). GAPDH served as a control. In Western blot, AP-conjugated secondary antibodies were utilised. qPCR was used to evaluate the levels of miR122 and Dicer1, along with HMGCR and CYP7A1 in the liver (F, G). Serum

and hepatic cholesterol levels were tested and reported respectively as mg/dl or $\mu\text{g/g}$ tissue). $N = 5$ in each group; results reported as $\text{mean} \pm \text{SE}$. The experimental analysis was carried out twice. **** denotes $p < 0.0001$, *** denotes $p < 0.001$, ** denotes $p < 0.01$, * denotes $p < 0.05$, and "ns" stands for "not significant".

4.3 Discussion

In order to better understand the part butyrate plays in maintaining host cholesterol homeostasis, a number of questions were posed: (a) Which intracellular actors and target genes are involved in the relationship between butyrate's impact on cholesterol metabolism? (b) Does endogenous butyrate from the gut use the same molecular mechanism as exogenously supplied butyrate? In order to strengthen our hypothesis, what cell line and mice abnormalities were observed when overexpression of specific key actors were done like microRNA 122, or diminished expression of AUF-1 by knock down?

The goal of this work is to establish a relationship between gut butyrate, one of the SCFAs, and cholesterol homeostasis in a range of gut pathologies. A rising number of investigations have shown that this adaptable small molecule has a variety of advantageous effects on peripheral tissues and the intestinal tract. In this study, we concentrated on butyrate since, in comparison with propionate and acetate, butyrate was detected as a hypocholesterolemic short-chain fatty acid in cell line, both in primary hepatocytes and secondary hepatoma cell line Huh7, and HFD fed mice. This has called for a mechanistic examination to find out how butyrate affects a wide range of purposes.

We used the publicly available microarray data sources (GSE4410 and GSE45220) to address the first issue, and we demonstrated that butyrate therapy decreased the expression of the important cholesterol-metabolizing genes *hmgcr*, *hmgcs1*, *acat2*, *dhcr7*, and *dhcr24*.

The network of variables involved in maintaining cholesterol homeostasis is complicated. To examine the effects of butyrate, the following in vivo and in vitro methods were taken into consideration: genes that are (a) associated with biosynthesis and (b) catabolism, (c) discovered intracellular players to maintain the impact in HFD-mice. As anticipated, therapy with butyrate decreased the serum hypercholesterolemia caused by the HFD. Identifying the target genes for butyrate in cholesterol biosynthesis and catabolism was an obvious choice as a result, and for this purpose, we investigated the "Similarity Ensemble Approach (SEA)," which predicts the targets of small compounds based on their resemblance to ligand sets of a reference database (Mathai et al., 2020). One of the most significant enzymes that promotes rate limiting step in cholesterol production pathway, HMGCR, was identified

as one of the other targets of butyrate via SEA research. We investigated the nature of the interaction between butyrate and HMGCR by molecular docking because there have been reports that butyrate inhibits HMGCR in enzymatic assays and that -OH-butyrates and its analogue, aceto-acetate, inhibit class II HMGCR to a different degree despite lacking -OH function (Marcil et al., 2003; Hedl and Rodwell, 2004). Our study showed binding energy of -3.5kcal/mol, indicating a moderate level interaction between the two without imposing specific orientation. At the enzyme's active site, it was discovered that Thr558 and Glu559 formed a potent conventional H-bond. Out of the four amino acids that HMG-CoA combines with HMGCR via (Lys691, Glu559, Asp767, and His866), Glu559 is a crucial catalytic component (Istvan and Deisenhofer, 2001). The phenolic derivative 2-(2-methoxyphenoxy)-2-oxoethyl 3-hydroxybenzoate interacts with Thr558 and Glu559 at the active site of HMGCR, according to a previous study screening for anti-hyperlipidaemic drugs. Thus, it is plausible that butyrate will interact with the HMGCR's active site, inhibiting it. This would be one of the many ways that butyrate influences cholesterol biosynthesis (Aqeel et al., 2018). We used publically accessible microarray datasets (GSE4410 and GSE45220) for *in silico* research to investigate any other butyrate-regulated cholesterol-regulating genes that may exist. The results are shown in the Volcano plot as log₂ (fold change) vs t-statistic (-log₁₀p-value). Crucial genes including *hmgcr*, *hmgcs1*, *acat-2*, *dhcr7*, and *dhcr-24* were shown to be down-regulated in both datasets' results. By using qPCR, we verified the following genes' expression in normal, HFD, and HFD-butyrates-mice. HMGCR, HMGCS, and DHCR7 are all directly involved in the production of cholesterol, with HMGCR and HMGCS serving as rate-limiting enzymes and DHCR7 serving as the pathway's last enzyme (Vock et al., 2008; Luu et al., 2015). ACAT2, on the other hand, contributes to the production of cholesterol esters (Anderson et al., 1998).

In contrast to normal and varying degrees of downregulation in HFD-butyrates-mice, we observed hepatic transcriptional overexpression of all the aforementioned genes in HFD-mice. In contrast to the previously mentioned genes, *cyp7A1*, a monooxygenase cytochrome P450 superfamily member which catalyses the conversion of bile acid from cholesterol, was significantly downregulated in HFD-mice as compared to normal, while it was significantly upregulated in response to butyrate treatment, which is consistent with earlier findings by others. According to our research, butyrate had an impact on a number of genes involved in the biosynthesis of cholesterol (Kharkwal et al., 2017; Zhao et al., 2017). HFD supplies an abundance of free cholesterol for esterification, which is then deposited as 'lipid droplets' in hepatic tissues (Alves-Bezerra and Cohen, 2017). Indeed, we observed enhanced hepatic 'lipid droplet' formation in HFD-mice, which was substantially decreased in size and number in HFD-butyrates-mice. Given their outward appearance, it is tempting to believe that these 'lipid droplets' have a larger electron density due to the presence of a higher cholesterol ester in HFD-mice. Cholesterol homeostatic routes are regulated not only by *de novo* synthesis but also by efflux pathways. There are at least two routes for cholesterol efflux from the cell: (a) passive diffusion of cholesterol, and (b) active

efflux through ABCA1 (Yancey et al., 2003). We found that HFD-mice had significantly lower levels of hepatic ABCA1 but not ABCA5, which was increased by butyrate therapy. Our findings are consistent with recent findings that butyrate increased the levels of ABCA1 in ApoE mice (Du et al., 2020). Butyrate thus not only controls cholesterol biosynthesis enzymes but also promotes cholesterol efflux transporters. Naturally, the issue arises as to how butyrate is scrutinizing these activities intracellularly. Cholesterol homeostatic routes are influenced not only by de novo synthesis but also by efflux pathways. There are at least two routes for cholesterol efflux from the cell: (a) passive diffusion of cholesterol, and (b) active efflux through ABCA1.

We found that HFD-mice had significantly lower levels of hepatic ABCA1 but not ABCA5, which was increased by butyrate therapy. Our findings are consistent with recent findings that butyrate increased the levels of ABCA1 in ApoE mice. Butyrate thus not only controls cholesterol biosynthesis enzymes but also promotes cholesterol efflux transporters. Naturally, the issue arises as to how butyrate is scrutinizing these activities intracellularly.

Butyrate has been shown to cause significant alterations in the levels of miRNA in MDCK cell line (Bishop et al., 2017). Our discovery showed that a few key miRNAs, specifically those linked with the metabolic regulation of cholesterol, including miR27a, miR27b and mir-122 (Goedeke et al., 2015; Krutzfeldt et al., 2005). An elegant investigation by other researchers found that when mice were treated with antagomir-mir-122, it led to the suppression of numerous gene expression level, with the cholesterol-manufacturing genes *hmgcs1*, *hmgcr* and *dhcr7* ranking first (Thakral et al., 2015; Krutzfeldt et al., 2005). *cyp7A1*mRNA was also destabilized by miR122 when it adhered to its 3'-UTR region. According to research, blocking of miR122 in chimps and African green monkeys' results in a significant decrease in total level of plasma cholesterol, while it restores excess lipid accumulation in the Huh7 cell line (Zhou et al., 2019; Long et al., 2019; Song et al., 2010).

We conducted research with the hepatoma cell line Huh7, which has been shown to have increased mir-122 level (Fukuhara et al., 2012), to observe butyrate's impact on the cholesterol regulation scenario. Since it is widely known that isolated primary hepatocyte function is difficult to maintain, when these cells are grown in vitro, they easily suffer dedifferentiation and lose their hepatocyte function. Therefore, Huh7 cells that simulate liver activity were applied. It was necessary to use a substantially greater dose of butyrate for gene expression studies in vitro research on cancer cells like Huh7. Butyrate may be used differently in normal and malignant cells as an epigenetic modulator (Donohoe et al., 2012). Consequently, it is appealing to assume that Huh7 requires an elevated amount of butyrate to be affected. The amount of butyrate utilized was consistent with results from a previous investigation (Zhao et al., 2021). The effects of butyrate administration included an uprise of expressional level of ABCA1, which was supported by data demonstrating an elevation in efflux of cholesterol and a decline

in miR27a, that induced ABCA1 mRNA to decay (Goedeke et al., 2015). Huh7 cells treated with butyrate displayed decreased Dicer-1 level, that prevented the formation of mir-122 from the precursor, establishing a connection between butyrate and mir-122 biogenesis. Because both propionate and acetate showed no effect, the effect was indeed butyrate-specific.

Dicer-1 is a crucial protein for the canonical biogenesis of miRNA; hence it is reasonable to wonder if butyrate's downregulation of Dicer-1 results in a reduction in overall microRNA synthesis. We demonstrate that butyrate treatment inhibited the level of miRNAs that degrade ABCA1 mRNA by interacting with 3'-UTR region, such as miR27a but not miR27b, indicating that not all miRNAs were equally affected by butyrate treatment (Kim et al., 2016; Goedeke et al., 2015). This is consistent with reports of Dicer-1-independent miRNA biogenesis, in which of Argonaute2's (Ago2) slicer activity serves a crucial role in the breakdown of pre-miRNA (Cheloufi et al., 2010).

Most miRNAs require Dicer, although 5p miRNAs appear to be synthesized at least partially in a Dicer independent manner (Kim et al., 2016). As a result, it will be fascinating to see if Dicer independent boosting ability of Butyrate for miRNA production further. Our early finding of enhanced Ago2 level in butyrate administrated cells suggests such a phenomenon. Because miR27b has been tightly associated with Ago2 it is tempting to infer that miR27b, which continues to be unaffected even after butyrate administration, may be synthesised in an Ago2-dependent manner (Miao et al., 2018).

The outcome of two opposing mechanisms, namely transcription and decay, is the maintenance of cellular stable state mRNA levels. According to a report, the RNA interacting protein AUF-1 binds to the 3'-UTR of Dicer-1 to decrease the stability of the mRNA (Abdelmohsen et al., 2012). Another example of RNA control that uses posttranscriptional regulation to coordinate many physiological processes is the degradation of transcripts with AU-rich elements (AREs) (Schoenberg and Maquat, 2012). AUF-1 performs a wide range of tasks, including RNA turnover, mRNA translation efficiency and DNA binding (Enokizono et al., 2005). The net mRNA stability of transcripts containing ARE is determined by the relative levels of the four isoforms of the AUF-1 family, AUF-1p37, AUF-1p40, AUF-1p42 and AUF-1p45 rather than the absolute amounts of each isoform (Kishor et al., 2013). Despite the fact that distinct isoforms of AUF-1 have varying binding affinities to particular 3'-UTR region of mRNA (Wagner et al., 1998; Kajita et al., 1995), it is unclear how exactly AUF-1 isoforms govern Dicer-1-mRNA turnover in a specific manner.

In Huh7 cells, we demonstrated that butyrate causes overexpression of AUF-1p40 and AUF-1p37 whereas not AUF-1p42 and AUF-1p45. The remaining experiments solely used the AUF-1p40 isoform as AUF-1p40 production was more prominent compared to the other isoforms. AUF-1p37's potential involvement in the procedures for regulation is not, however, completely ruled out. A prior study found

that butyrate affects the alternative splicing of numerous proteins, including the Defensin -1 gene, IL-18, and vascular endothelial growth factor (VEGF) (Wu et al., 2012). Hence, it is possible to hypothesize that butyrate may control gene expression by affecting the alternative splicing of AUF-1. We investigated the hepatic expression of sphingosine kinase 1 (sphk1), a known classic target of AUF-1 and an indicator of prognosis for several carcinoma like HCC (Cai et al., 2017), in order to functionally validate the upregulation of AUF-1 caused by butyrate. The anticancer effects of butyrate on HCC may also be due to Sphk1 degradation mediated by butyrate (Wang et al., 2013). Uncertainty exists regarding Butyrate's actual method that triggers AUF-1. According to a prior study by Sobolewski et al. (2015), HDAC inhibitors activate the transcription factors of initial growth response protein, which in turn stimulates the of RNA binding protein's (RBP) transcription. Because butyrate is an inhibitor of HDAC it might boost AUF-1 via these transcription factors (Davie, 2003). We demonstrated that independent of the presence or absence of butyrate, siRNA mediated shutting down of AUF-1 resulted in the downregulation of all AUF-1 isoforms, together with an enhancement of cellular cholesterol, Dicer-1, mir-122, and. As a result, butyrate may act as a primary modulator of the stability of Dicer-1 via AUF-1. The readily accessible siRNA seems to suppress all isoforms of AUF-1, making it difficult to determine the significance of each particular isoform in the procedure. The aforementioned discoveries depict the step wise interplay of numerous intracellular identities that work in unison as "butyrate regulating AUF-1-Dicer-1-miRNA122-cholesterol biosynthesizing enzymes-cholesterol level", whose sophistication was again confirmed utilizing the model of HFD mediated dysbiosis of the gut. Current research has shown that butyrate lowers lipid profiles and specifically cholesterol, mostly through the signalling pathway of LKB1-AMK-Insig (Zhao et al., 2021). Curiously, the LKB1-AMK pathway was activated in mice with knockdown of mir-122. According to this research, the "AUF-1-Dicer-1-miRNA122" axis downstream of the convergence of butyrate and cholesterol is connected by the LKB1-AMK-Insig route.

The discoveries mentioned above encapsulate the key characteristics of the sequential interactions between many participants in butyrate-mediated cholesterol homeostasis, such as "butyrate-AUF-1-Dicer-1-miRNA122-cholesterol," which can be loosely characterized as an axis. Now, in addition to the HFD model that causes obesity, the exquisite nature of this axis has also been confirmed in two other models, including (a) gut dysbiosis caused by antibiotics and (b) colitis caused by DSS. There has been a lot of research that particularly assessed the potential contribution of the microbiota to the control of cholesterol homeostasis using standard methods like antibiotic therapy as a substitute for germ-free animals (Kennedy et al., 2018). According to reports, HFD-mice receiving sub-therapeutic antibiotic treatment develop hepatic steatosis by becoming more obese (Mahana et al., 2016). Here, we demonstrate how HFD treatment alone considerably reduced faecal butyrate, which then nearly disappeared after receiving further antimicrobial therapy. We further demonstrate that liver hypercholesterolemia was associated with a considerable rise in miR122 and Dicer-1, a decrease in

AUF1p40, and these changes were caused by combined HFD plus antibiotic treatment. The above parameters then recovered to normal following butyrate treatment. Our findings are in line with other studies that found that antibiotic therapy increased adiposity in HFD-mice (Mahana et al., 2016). Firmicutes and Bifidobacterium are depleted in mice with DSS-induced colitis, which reduces butyrate synthesis and their ratio is also reported to be significantly reduced in inflammatory bowel disease (IBD) (Eichele and Kharbanda, 2017; Dou et al., 2020). We demonstrate that there was a large decrease in faecal butyrate in colitis animals when compared to controls, which is similar to a report from another group and with an accompanying rise in serum cholesterol (Zhang et al., 2016). The epidemiological results of the incidence of dyslipidaemia in IBD patients are supported by our data on the colitis model (Sappati Biyyani et al., 2010). In DSS-mice, we once more demonstrate the butyrate-AUF-1-Dicer-1-miRNA122-cholesterol axis by demonstrating that AUF-1 is down-regulated in colitis mice while miR122 and Dicer-1 are up-regulated.

To answer the second question and demonstrate that intestinal-derived butyrate is the primary mediator of cholesterol homeostasis as a proxy for germ-free animals, we decreased gut flora through antibiotic treatment, which we subsequently replenished using probiotics (Kennedy et al., 2018). The probiotic included LAB (Lactic acid-producing bacteria), *Streptococcus faecalis*, *Bacillus mesentericus*, *Clostridium butyricum*, which directly or indirectly procures SCFA (Isono et al., 2007; Mishra et al., 2019).

Butyrate kinase (buk) and butCoAT typically catalyse the final stage of butyrate synthesis (Louis and Flint, 2007). According to a metagenome-based analysis, the butCoAT influenced pathway is anticipated to be ten times more common than the buk-mediated route (Louis et al., 2004). As part of our investigation, we assessed the quantitative abundance of the butCoAT gene in the faecal samples and directly assessed the concentration of butyrate from the faeces, using LC-MS. Interestingly, we found that in the probiotic-treated group, the abundance of the butCoAT gene was substantially higher than the faecal butyrate content; the reason for this apparent temporal mismatch is unknown. Normally, 79.7% of the butyrate produced by gut microorganisms comes through the acetyl-CoA pathway (Vital et al., 2014). Butyrate is also produced through additional routes, such as those involving glutamate, lysine, and 4-aminobutyrate. These routes are common in the phyla Firmicutes and a few others, including Bacteroidetes and Fusobacteria (Barker et al., 1982. Buckel and Barker, 1974). The possibility that additional butyrate-producing pathways could be active and add to the total butyrate pool is alluring to consider. Similar to our findings of elevated blood and hepatic cholesterol in Abx animals, a previous study found that antibiotic-induced intestinal microbiota depletion increased bile acid absorption and the synthesis of HMGCS and HMGCR in the liver, leading to a 55% serum cholesterol rise (Le Roy et al., 2019).

Another report suggested that mice in germ free condition have 1.5 times the liver cholesterol of regular mice (Le et al., 2022; Mistry et al., 2017). In order to find answer of the third concern, we established that mir-122 is in fact involved in the restoration of blood cholesterol. Next, we excessively expressed mir-122 in butyrate administered mice, which resulted in a notable restoration of serum cholesterol. We used morpholino oligomers, which are brief single-stranded DNA analogues with a morpholine ring's backbone and are tolerant to host enzymes present, making them specifically suited for in vivo applications, to knock down AUF-1 in order to further set up the connection in cholesterol homeostasis and AUF-1. In MO, the guanidinium residues linked to the antisense are stiffer, which aids in obtaining a favourable conformation to connect with the mRNA with complementary sequence (Corey and Abrams, 2001).

MO's reduced molecular weight increases endosomal escape effectiveness (Abes et al., 2008). Notably, morpholino-based treatment for Duchenne muscular dystrophy (DMD) has received FDA approval, which has become a landmark of morpholino-based antisense treatment (Bertoni, 2014). The chimera of GMO-PMO-producing MO employed in this experiment carries unique proof of self-transfection and delivery without the usage of a vehicle, avoiding the danger of toxicity influenced by vector (doi: <https://doi.org/10.1101/2021.06.04.447039>). A unique opportunity to test our theory in vivo was provided by the targeted AUF-1 knockdown by MO since septicaemia developed due to knockout of AUF-1 in mice exhibit high death rates. AUF-1 is the principal regulator of cholesterol biosynthesis, according to the uprise in hmgcr, decrease in cyp7A1 expression, and rise in serum cholesterol in AUF-1 KD mice in contrast to scrambled mice. Additionally, it was found that exogenous butyrate does not reverse hypercholesterolemia in AUF-1 KD mice. In contrast to scrambling, AUF-1 KD significantly increased Dicer-1 and mir-122 expression. Since mir-122 directly interacts with cyp7A1 mRNA and causes its degradation (Song et al., 2010), the difference between the two proteins in AUF-1-MO mice is significant.

The overall results of the study show that butyrate is an effective controller of the stability of cholesterol at various levels. We describe how gastrointestinal microbiome derived butyrate governs cholesterol equilibrium by including intercellular individuals in conjunction as follows: "butyrate-AUF-1-Dicer-1-mir-122-cholesterol metabolic enzymes-cholesterol level" where each member contributes individually through enhancement or downregulation.

CHAPTER-2

**Butyrate disrupts lipid rafts and prevents the entry of pathogen
inside cell**

5.1 Introduction

A prime example of symbiotic relationships with the host is the population of bacteria that lines the intestinal system (Zheng et al., 2020; Chow et al., 2010). A tremendous diversity and richness of beneficial microorganisms adorn the mammalian gut (Rinninella et al., 2019; Sorbara et al., 2019). Through a variety of methods, including ecological competitiveness for nutrition, active resistance via secreting antimicrobial substances like bactericidins and peptides, and metabolite dependent prohibition, the commensal gut bacteria prevent pathogen colonization (Garcia-Gutierrez et al., 2019; Rooks et al., 2016). The restoration of host biological processes like metabolism, gut barrier function, and immunological development has been related to the gut microbiota (Gasaly et al., 2021). Additionally, "colonization resistance" refers to the ability of commensal microbes to inhibit the development of opportunistic bacteria while shielding the host from infection (Khan et al., 2021). The ground breaking research that showed how antibiotic-mediated disturbance of the gut microbiota in mice dramatically increased susceptibility to *Salmonella enteritidis* infection provided a crucial opening for solving the issue with centrality (Grzymajlo 2022). Short chain fatty acids (SCFA), which mostly consist of acetate, propionate, and butyrate, are one type of metabolite produced by gut microorganisms that is particularly crucial in preventing pathogen colonisation (Ducarmon et al., 2019). Pigs on a high-fibre diet were shown to be less vulnerable to *C. difficile* infection, establishing the initial connection among SCFAs and *Clostridium difficile* infection (Grześkowiak et al., 2019; May et al., 1994). Later studies showed that a decrease in SCFA synthesis was associated with an increased risk of enteric infection (Rios-Covian et al., 2016). Even in the absence of an inflammatory cytokine response, it has been demonstrated that SCFA influences antimicrobial characteristics in macrophages (Schulthess et al., 2019). Since it was shown in vitro that the non-ionization of these acids caused toxicity, which are prevalent at low level of pH, SCFA also acts as an essential pathogen defence mechanism by exerting detrimental acid stress (Sun and O'Riordan, 2013; Hentges et al., 1967). Additionally, SCFA is essential to preserve the low levels of nitrate and oxygen that reduce *Salmonella* infection (Rivera-Chavez et al., 2016). It is necessary to assess the role of SCFA-mediated resistance in the host's ability to impede colonization given that SCFAs control a variety of the host's metabolic processes (Mirzaei et al., 2022; He et al., 2020).

Cholesterol is an indispensable part of the cell membrane, influencing an extensive spectrum of biophysical properties. When cholesterol appears on the membranes with designated membrane dynamics in general, a segment enriched with cholesterol in the membrane region determined to be lipid raft is developed (Simons and Ehehalt, 2002). Numerous pathogens are intended to enter the body through these lipid rafts. Pathogens can use membrane microdomains to avoid detection by immune

defences in a novel way. Several pathogens have learned to evade immune defences (both innate as well as adaptive) by exploiting raft-associated routes. In order to penetrate the host cell, the majority of intracellular infections exploits the lipid enriched membrane rafts (Kulkarni et al., 2021). *Shigella* and *Salmonella* both need a type III secretion system (T3SS), a multicomponent molecular syringe that enables the passage of effector molecules from cytoplasm to the bacterial membrane (inner as well as outer) along with the host plasma membrane, and into cytoplasm (Lou et al., 2019; Coburn et al., 2007). Its effector proteins, identified as IpaB and IpaC for *Shigella* and SipB and SipC for *Salmonella* respectively, must interact with a direct contact with that of the host cell in order to start the system (Lafont et al., 2002; Myeni et al., 2013; Cardenal-Muñoz et al., 2014; Muthuramalingam et al., 2021). In the membranes on the downstream side of T3SS activation, cholesterol is necessary for SipB/IpaB binding to that of the host cells (Hotinger et al., 2021; Guignot and Tran Van Nhieu, 2016). The host cell membrane's cholesterol-rich region is where the pathogenic compartments of enterotoxigenic *E. coli* merge (Caruana and Walper, 2020; Dubreuil et al., 2016). The internalization of *Helicobacter pylori* in the epithelial cells of gut is decreased by cholesterol-depleting substances (Hsu et al., 2021; Qaria et al., 2021; Lai et al., 2008). Hole-forming bacteria, such as *Vibrio cholerae*, prefer to perforate in lipid enriched microdomains because these structures can support the holes for a longer period of time (Li et al., 2021; Day and Kenworthy, 2015).

Using reliable studies as our foundation, we seek to determine whether butyrate, which decreases cholesterol biosynthesis, may perturb lipid rafts and stop pathogen invasion. By connecting the dots between the stories from our experimental research, we were able to demonstrate that intestinal microbiota derived butyrate reduces cholesterol from membrane and impedes lipid rafts, which in turn results in a decrease in the invasion of several pathogens—a "critical" component of resistance against pathogens. Our research adds new, distinct factors that contribute to gut pathogen resistance.

5.2 Results

5.2.1 Butyrate treated RAW 264.7 cell exhibited reduction in membrane cholesterol

RAW264.7 cells were exposed to sodium butyrate in higher concentrations of 5 and 10 mM for 18 hours in order to examine the effects of butyrate on membrane cholesterol. The cholesterol content was then assessed from the prepared membrane. Even at the highest dose utilized, sodium butyrate exposure to RAW 264.7 did not cause toxicity in the cells or reduce cell survival or confluency along with the rate of cellular proliferation. Images taken under a microscope showed that butyrate therapy altered the morphology of the cell at the highest dose (10 mM). Administration with 5 mM and 10 mM of butyrate caused membrane cholesterol to drop by 1.5-fold and 2.4-fold, respectively, which is 36% and 52% less than the control.

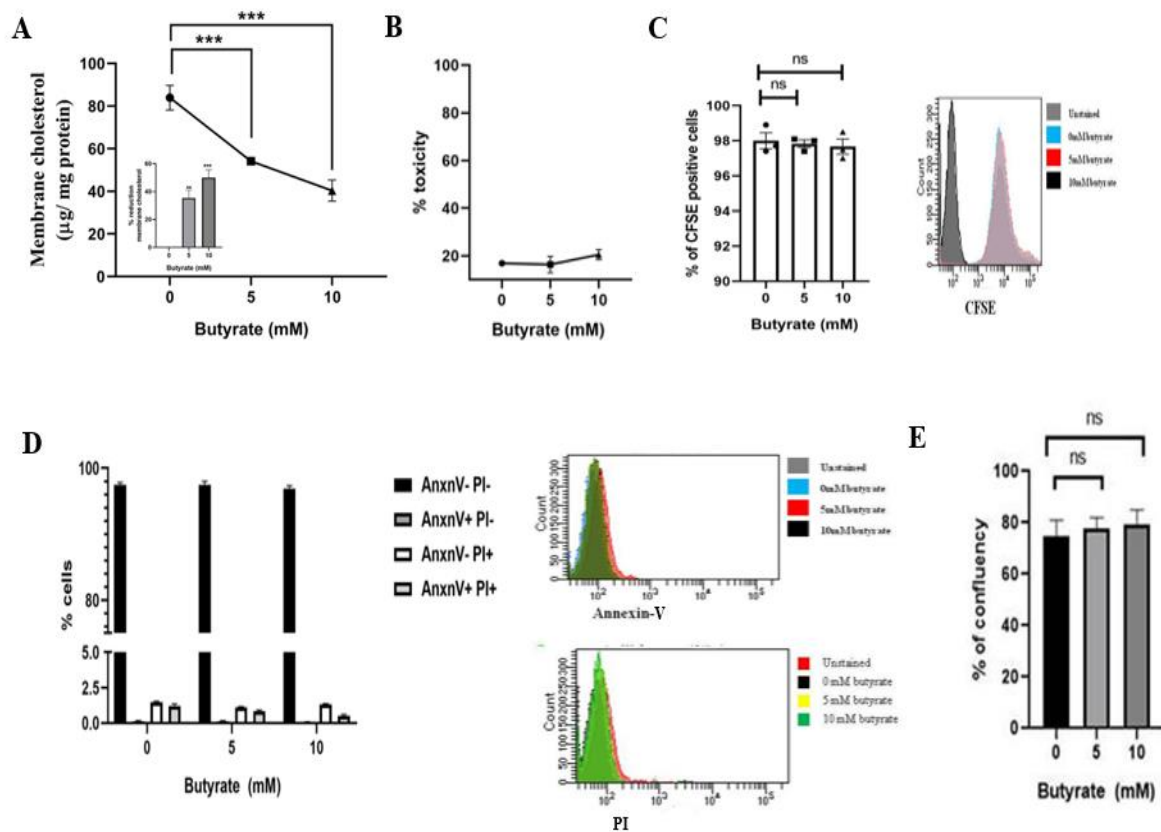


Figure 5.1: Effect of Butyrate in membrane cholesterol, along with toxicity, proliferation and confluency level. 0 mM, 5 mM, 10 mM of sodium butyrate were applied to RAW 264.7 cells for an 18-hour treatment period. The membrane was procured after washing the cells. With the aid of cholesterol test kit (Amplex red, Invitrogen), the membrane cholesterol was determined and represented

as μg of cholesterol isolated from membrane per mg of protein, or as a percentage of the total amount of protein (Inset) (A). By using the LDH assay (B), CFSE staining in flowcytometry (C), and Apoptosis/PI staining in flowcytometry (D), respectively, the toxicity, proliferation, and viability of cells in present or absent of butyrate administration were assessed. Under a phase contrast microscope with a 20X magnification, the confluency of cells treated or untreated with butyrate was seen. The information is presented as the mean \pm SEM of three independent experiments (E). * Stands for $p<0.05$, ** stands for $p<0.01$

Filipin staining for determining membrane cholesterol level revealed an overall reduction in fluorescence intensity after butyrate administration compared to the control group.

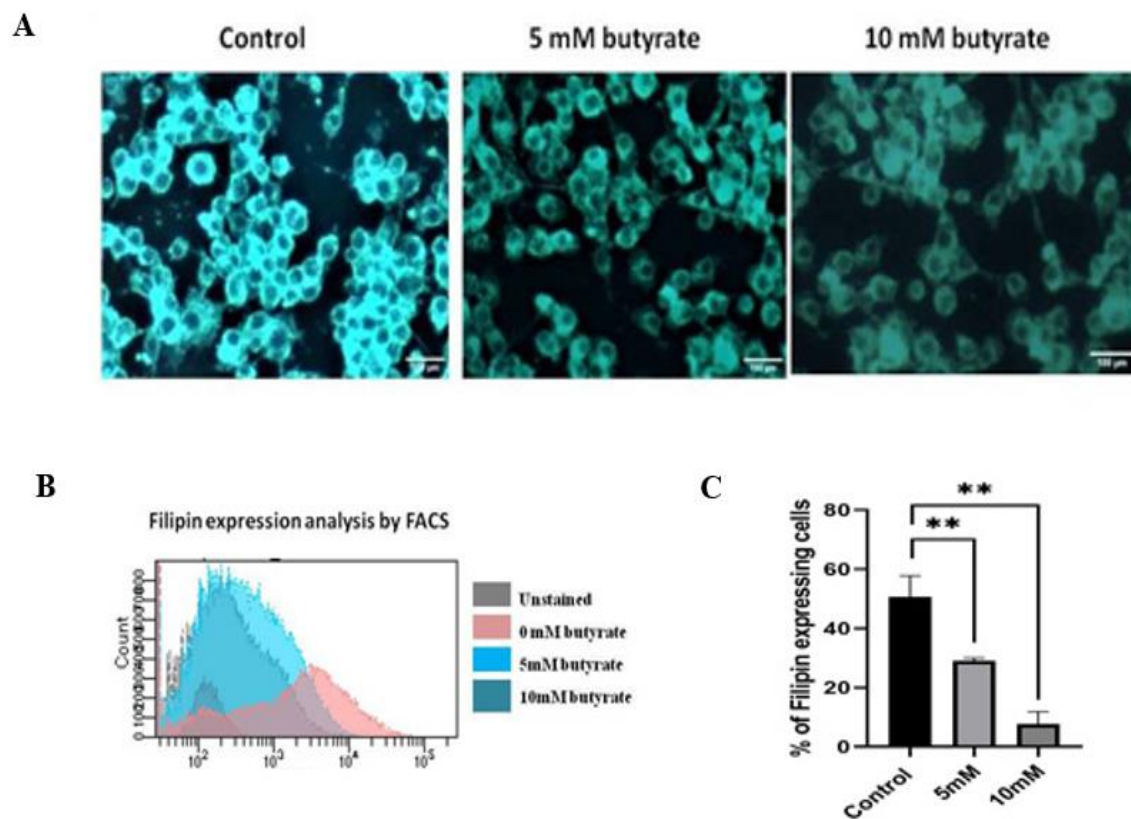


Figure 5.2: Filipin assay result showing the level of membrane cholesterol after administration of Butyrate. The cells had been stained with Filipin and difference in fluorescence intensity among control and butyrate treated groups (5 and 10mM) were inspected both by visually (via fluorescence microscope) (A) and by means of flowcytometry analysis (B, C). Each experiment was repeated thrice. ** stands for $p<0.01$

5.2.2 The administration of butyrate alters the fluidity of membranes and disturbs cholesterol enriched microdomains or lipid raft

In order to assess the fluidity of the cells in presence or absence of butyrate administration by FA or fluorescence anisotropy, Laurdan probe was used. Following butyrate administration, dose dependent reduction of FA was noticed. The lowering of FA was to 1.4 and 2.4-fold, accordingly, after treatments using 5- and 10-mM butyrate. Cholesterol replacement into the membrane of cells of butyrate administered group via distribution of cholesterol via liposomes (chol-lipo), to ensure that the alteration in the fluidity of membrane was caused by cholesterol depletion. Phosphatidyl choline (PC) and cholesterol were used to make liposomes. The formation of liposomes after sonication was verified by TEM. The manufactured liposomes have a similar size distribution, according to the Differential Light Scattering (DLS) investigation. The FA was essentially restored to normal level when cholesterol was reintroduced in the butyrate administered cells by liposomal cholesterol. We calculated the cholesterol level from the membrane of the liposomal cholesterol treated cells using medium lacking in cholesterol (serum-free circumstances) to support the rise in membrane cholesterol with liposomal cholesterol treatment. In cells treated with 5 mM and 10 mM butyrate, respectively, it was shown that 16% and 40% of the original cholesterol had been recovered in the membranes after liposomal cholesterol treatment.

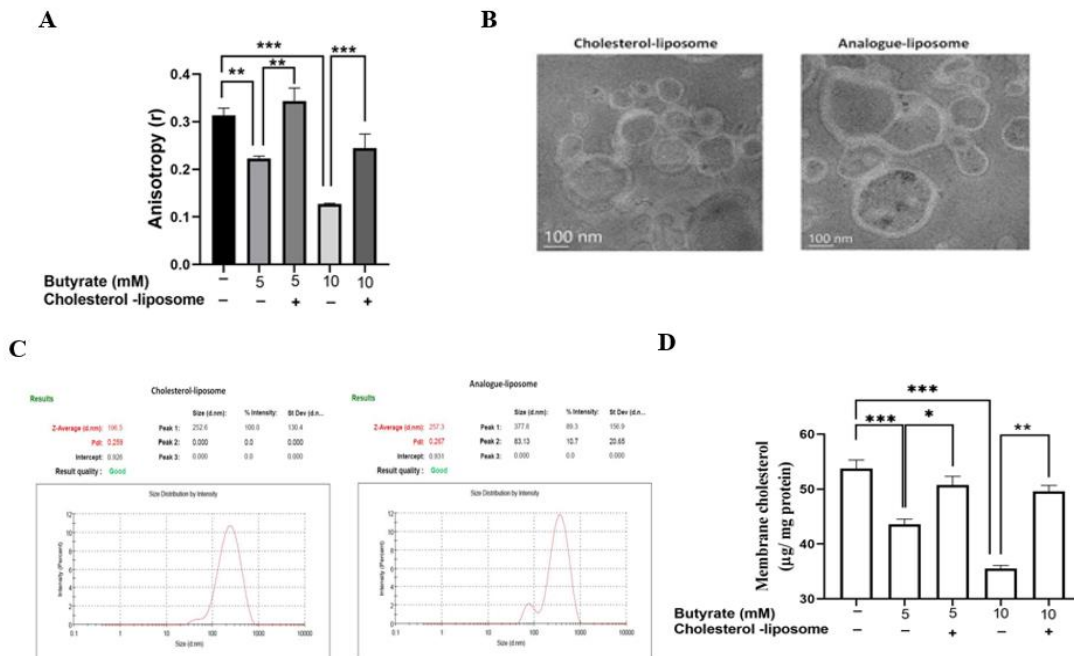


Figure 5.3: Effect of Butyrate on membrane fluidity level after administrating liposomal cholesterol. 0 mM, 5 mM, 10 mM of sodium butyrate were applied to RAW 264.7 cells for an 18-hour treatment period. The cells were subjected to another 18-hour treatment of either with or without liposomal cholesterol after the butyrate administration. Employing a Laurdan probe, the anisotropy of

cell membrane was quantified and represented as 'r'. The cholesterol liposome and analogue of cholesterol-liposome, as determined by TEM and DLS, accordingly, in terms of shape (A) and size (B). Amplex red kit (Invitrogen) was used to analyse the amount of cholesterol in the membranes of the cells in presence or absence of butyrate, then with or without the liposomal cholesterol treatment.

To investigate the relationship between butyrate and decreased fluidity of cell membrane, we examined the existence of lipid raft in untreated control as well as treated (Butyrate administered) cells. CTX-B or cholera toxin beta interacts with the GM1 ganglioside found in microdomains enriched with membrane cholesterol and is termed as a biomarker for these domains. The initial row displays the control untreated cells, the second row displays the butyrate-treated cells at a concentration of 10 mM, the third row displays the butyrate-treated cells after chol-lipolysis, and the fourth row displays the butyrate-treated cells after ana-lipolysis in Fig. 5.4 A. The first column exhibits anti-CD71 binding, the second CTX-B binding, the third represents the nucleus stain, and the fourth represents the merging image. The results were obtained using ImageJ, that revealed reduced binding of CTX-B-FITC after administration of butyrate at a dose of 10mM in contrast to control, which was restored back after administration with liposomal cholesterol but not analogue liposome. However, the interaction of CD 71 binding anti-CD71 antibody, in the non-raft area of the membrane, was unaffected by butyrate, liposomal cholesterol, or analogue liposome treatment.

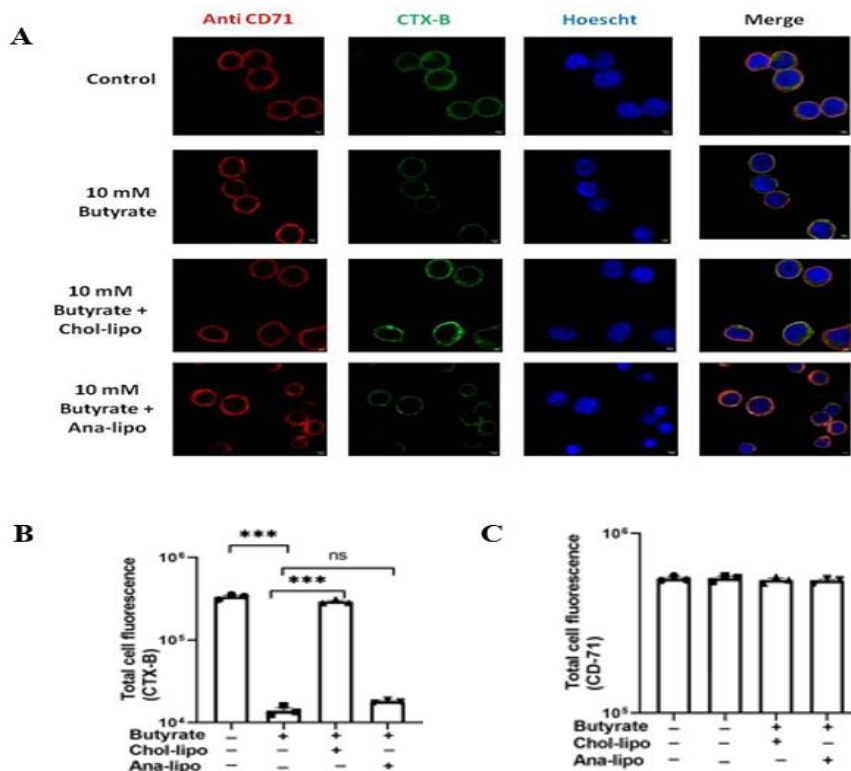


Figure 5.4: Effect of Butyrate on CD71 and CTX-B expression level in RAW 264.7 cell.

The cells were counterstained with Hoechst 33342 after having been stained using either CTX-B-FITC or an anti-CD71 antibody. Using a Zeiss confocal microscope, the cells were seen. the quantitative evaluation of ImageJ-measured CTX-B and anti-CD71 antibody total fluorescence. Corrected total fluorescence (CTCF) = (Integrated density) - (Area of selected cells x mean fluorescence of background) is the formula for calculating the corrected total cell fluorescence. The data from three trials are plotted as Mean \pm SEM. Each experiment was set up in triplicate. * Stands for $p < 0.05$, ** stands for $p < 0.01$, *** stands for $p < 0.001$.

5.2.3 Butyrate administration reduces the invasion of enteric pathogen

After determining that butyrate disrupts the architecture of cholesterol-rich microdomains in cellular membranes, we investigated its effect on the entry of enteric pathogen, which uses these domains as portal or point of entry to penetrate the host cells. To investigate the influence of butyrate on the invasion of enteric pathogen, we employed *Shigella flexneri* and *Salmonella typhimurium* as model enteric pathogens that enter cells via lipid rafts. Butyrate therapy was studied for its influence on *Shigella* and *Salmonella* invasion in macrophages.

Butyrate was found to reduce *Shigella* and *Salmonella* invasion in a dose-dependent manner when compared to infected controls. Butyrate treatments at 5 and 10mM reduced invasion of *Salmonella* by 60% and 75% and invasion of *Shigella* by 60% and 85% accordingly (Fig 5.5 A and 5.5 B). Subsequently, the administration of butyrate-treated cells with liposomal cholesterol exhibited enhanced bacterial invasion compared to only butyrate treatment and was virtually comparable to *Shigella* infected control group.

To make sure that the impact of reversion was only for incorporated cholesterol in the membranes rather than increased phagocytosis resulting from treatment with liposome, instead of cholesterol, we prepared liposomes with ana-lipo, which is cholesterol analogue (4-cholesten-3-one) and applied them to butyrate-treated cells. Ana-lipo therapy, as anticipated, did not promote invasion of pathogen, and the percentage of intracellular *Salmonella* and *Shigella* was comparable to macrophages after butyrate administration.

Similar results were obtained in subsequent investigations using cholesterol that is water soluble or M β CD-Chol or methyl cyclodextrin cholesterol to transport cholesterol to cell membrane from medium. *Salmonella* and *Shigella* invasion of butyrate-treated cells was boosted in a dose-related way by MBCD-cholesterol replenishing membrane cholesterol (Fig. 5.5 C).

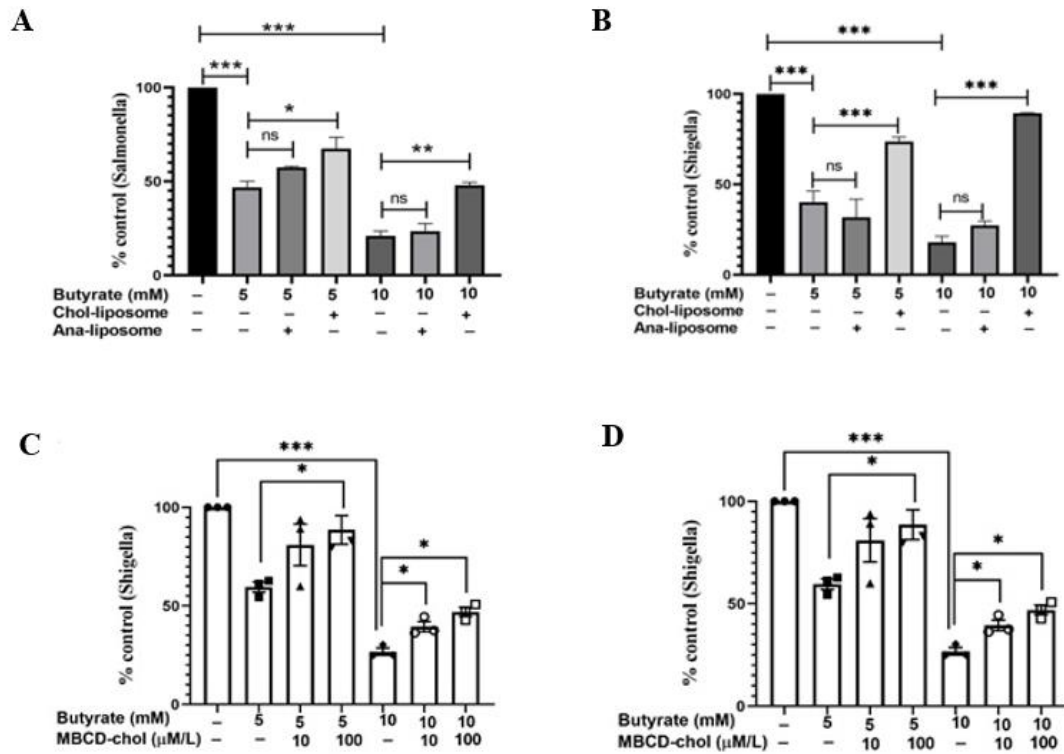


Figure 5.5: Effect of Butyrate on reducing cellular infection level and cholesterol content. *Salmonella typhimurium* (A) and *Shigella flexneri* (B) were infected into Butyrate treated (0, 5, 10 mM) RAW264.7 cells followed with MBCD-cholesterol at the appropriate concentrations (C and D), at a MOI of 1:100 each. The results are shown as a percent control (Percent control= Treated/Control X 100). The result is presented as the mean \pm SEM of three individual experiments (E). * Stands for $p < 0.05$, ** stands for $p < 0.01$, *** stands for $p < 0.001$, where “ns” is non-significant.

5.2.4. Butyrate therapy reduces anti-CD44 antibody interaction on the surface of cell while having no effect on the total population of CD44 in the cell

IpaB from *Shigella flexneri* interacts to the CD44 marker that is expressed on the surface of macrophages. As a result, we examined the expression of CD44 using butyrate therapy. Butyrate administration causes a reduction in anti-CD44-FITC antibody interaction, which is reversed by additional treatment with liposomal cholesterol. To demonstrate that the reduction in fluorescence was

caused by CD44 displacement from lipid rafts rather than a decline in total expression of CD44, we assessed CD44 expression in non-permeabilized as well as permeabilized cells using flow cytometry.

The permeabilized cells allows the antibody to penetrate them and interact with intracellular CD44, while non-permeabilization allows only bind to CD44 on the cell surface. Flow cytometry measurement of CD44 expression on permeabilized cells clearly indicates that overall CD44 expression remains constant regardless of butyrate or liposomal cholesterol administration (Fig 5.6 B). Flowcytometry study of unpermeabilized cells, however, revealed that butyrate treatment diminished intensity of fluorescence, which was restored by liposomal cholesterol treatment (Fig 5.6 C). This finding supports the notion that the binding receptor CD44 of *Shigella* is found in lipid rafts that are replaced with butyrate therapy.

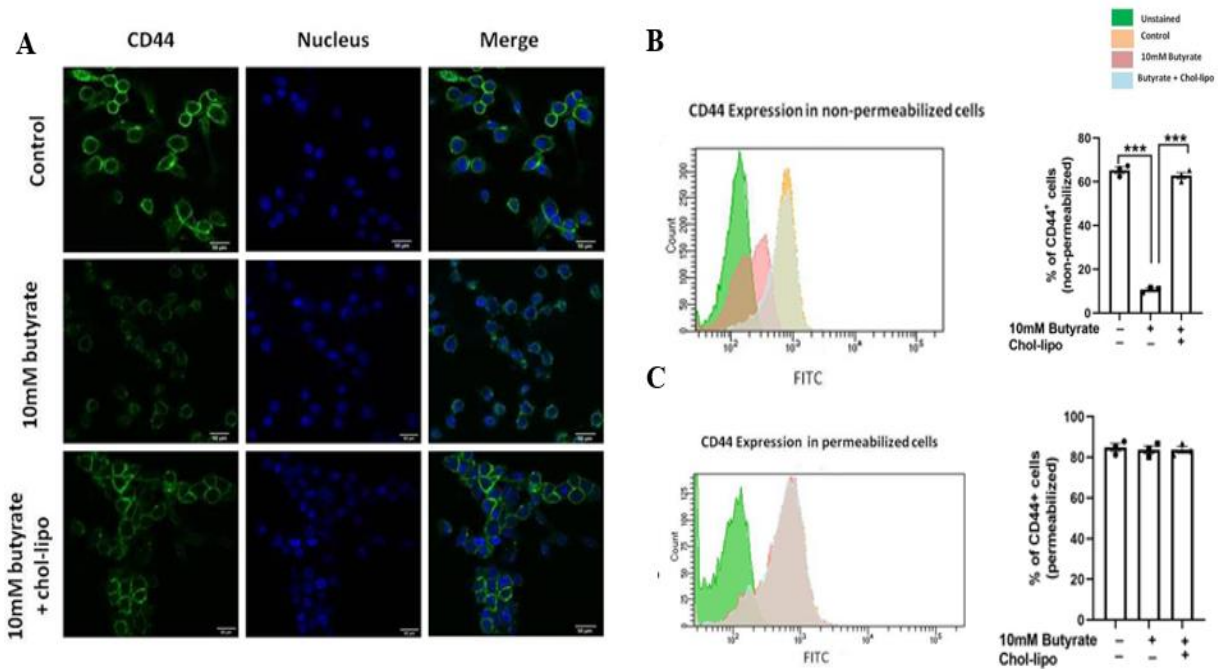


Figure 5.6: Effect of Butyrate on CD 44 expression level. The cells were labelled with either FITC conjugated anti-CD44 antibody or nucleus stain Hoechst 33342. A Zeiss confocal microscope was used to image the cells at a magnification of 63X (A). To determine the total amount of FITC conjugated anti-CD44-FITC antibody fluorescence on the cell surface, flowcytometry was used to compare permeabilized (B) and non-permeabilized cells (C) that had received the same treatment.

5.2.5 Administration of Butyrate lowers *Shigella flexneri* infection in mice but can be restored by the treatment with liposomal cholesterol

We investigated the impact of butyrate on *Shigella*-infected mice to comprehend its implications. *Shigella flexneri* was administered intraperitoneally to mice after 30 days of butyrate treatment at a concentration of 10^8 cfu/animal for the purpose of studying pathogen load and immunological parameters. Mice were then euthanized 24 hours after infection. The mice that were uninfected, infected with *Shigella*, and *Shigella*-infected after treatment with butyrate will now be referred to as control-mice, infected-mice, and butyrate-mice, accordingly. Two days ahead of the infection, cholesterol liposomes were also given intracardially to a group of butyrate-mice (butyrate-cholesterol liposomal treated mice). To verify gut directed optimal cholesterol delivery, the total content of the cholesterol from the intestinal tissue was evaluated (Fig 5.7 A). The level of cholesterol from infected mice's gastrointestinal tissue was found to be substantially higher than that of control mice. Butyrate-mice had lower level of gut tissue cholesterol than infected mice, but it was much higher in butyrate-chol-mice. When compared to infected mice, butyrate- animals had a roughly 12-fold reduction in bacterial burden in colon tissue. When butyrate-mice were given liposomal cholesterol, the bacterial load in the colon was essentially restored (Fig 5.7 B).

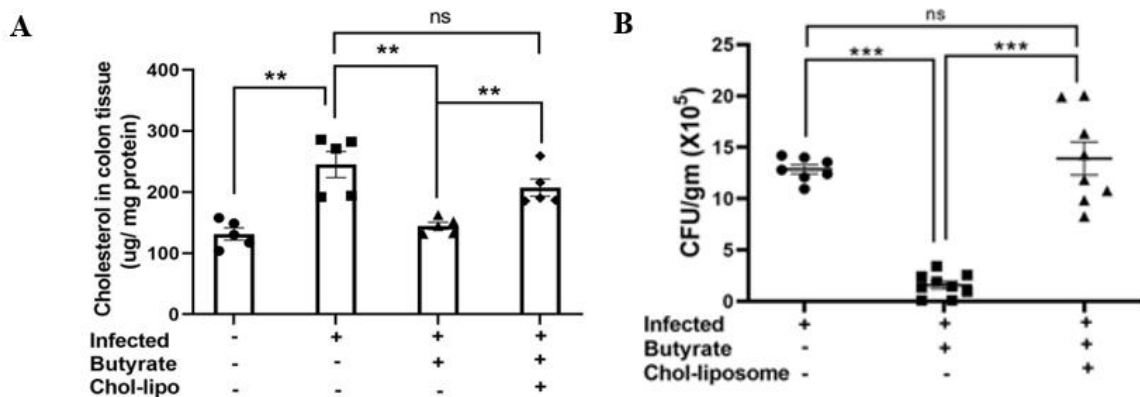


Figure 5.7: Effect of Butyrate on cholesterol content and the number of contable colonies obtained from colon tissue of mice. Amplex red test kit (Invitrogen) was used to evaluate the concentration of cholesterol in the colons of uninfected control, infected mice, butyrate treated mice, and butyrate-liposomal cholesterol -mice (A). For 30 days, chow diet fed C57BL/6 mice were given 150 mM sodium butyrate dissolved in drinking water. After 28 days of treatment with butyrate, 200 μ L solution of liposomal cholesterol was administered intracardially into half of the animals (known as chol-lipo mice). On the 30th day, all animals were intraperitoneally infected with 10^8 cfu/mice *Shigella flexneri*. The animals were euthanized on the second post-infection day, and faeces were collected for study. By

mounting diluted faecal samples on XLD plates, the bacterial burden was measured and expressed in terms of cfu/gm faeces.

5.2.6 Treatment with butyrate lessens *Shigella* mediated intestinal pathogenesis, which was reversed by liposomal cholesterol administration

In the colons of *Shigella* infected mice, histological sections revealed cell death in the crypt and villi, shedding of the cells from epithelial region, hyperplasia of goblet cells, and infiltration of several inflammatory cells. A small number of neutrophils were found in the colons of butyrate-mice.

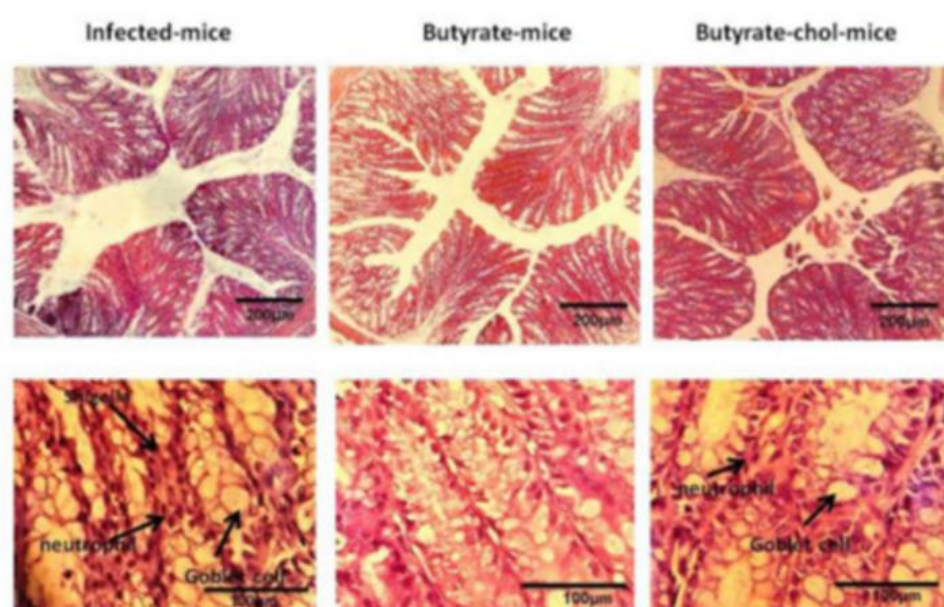


Figure 5.8: Effect of Butyrate on the colon histology of mice. For 30 days, chow fed C57BL/6 mice were given 150 mM sodium butyrate dissolved in drinking water. After 28 days of treatment with butyrate, 200 µL solution of liposomal cholesterol was administered intracardially into half of the animals (known as chol-lipo mice). On the 30th day, inoculum of *Shigella flexneri* at a dose of 10^8 cfu/mice (Intraperitoneally) was given. The animals were euthanized on the second post-infection day, and colon tissues were obtained for the study. A microscopic examination of colonic histological of a representative animal from each group. 10X and 100X magnifications are shown in Panels 1 and 2, respectively.

Shigella-infected animals displayed clinical signs such as increased level of mucin 2 secretion in the colon, which could be caused by inflamed goblet cells. Butyrate-mice had lower level of mucin 2 expression than infected animals, whereas butyrate along with liposomal cholesterol treated mice had expression level of mucin-2, that was virtually equal to that of infected mice (Fig 5.9A) In comparison to butyrate-mice, liposomal cholesterol therapy dramatically boosted neutrophil infiltration (Fig 5.9 B).

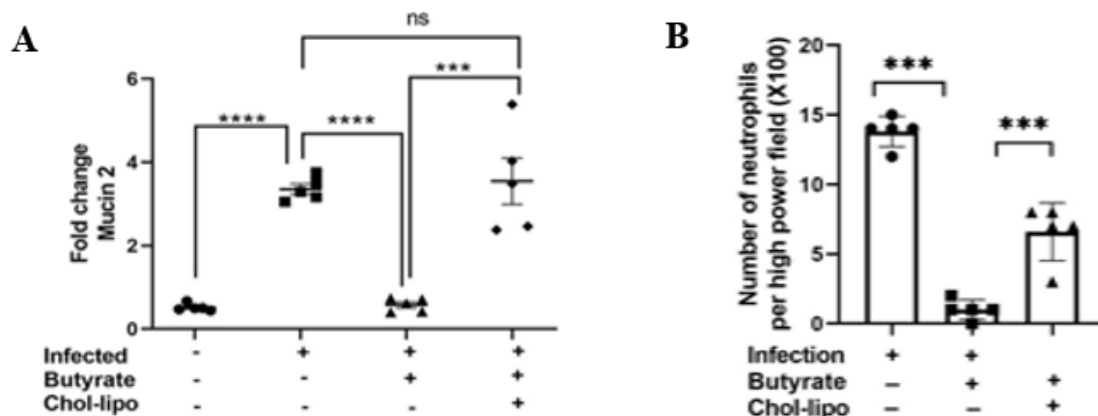


Figure 5.9: Effect of Butyrate on the mucin 2 expression level and infiltration of neutrophil level on the colon tissue of mice. qPCR was used to assess the expression level of mucin 2 (A). Neutrophil number at high level of magnification (100X) in the colon of *Shigella flexneri* infected mice, butyrate treated along with *Shigella* infected mice, and butyrate liposomal cholesterol treated mice (B).

Proinflammatory cytokines such IFN γ , IL-6 and TNF α were discovered to be considerably greater in infected animals compared to control mice (Fig. 5.10 A). Proinflammatory cytokines were markedly reduced by butyrate therapy and then returned to levels comparable to those of infected mice in butyrate-liposomal cholesterol treated-mice. When compared to infected mice, butyrate-mice have a 3.7 times higher expression of the host defensive cytokine IL-10. As anticipated, butyrate-chol-mice had lower levels of IL-10 expression than infected-mice.

Additional research on the expression of antimicrobial genes, such as cathelicidin, revealed a considerable rise in butyrate administered infected mice when in comparison with the infected control mice and a return to the initial level of infection in butyrate treated liposomal cholesterol administered mice (Fig. 5.10 B).

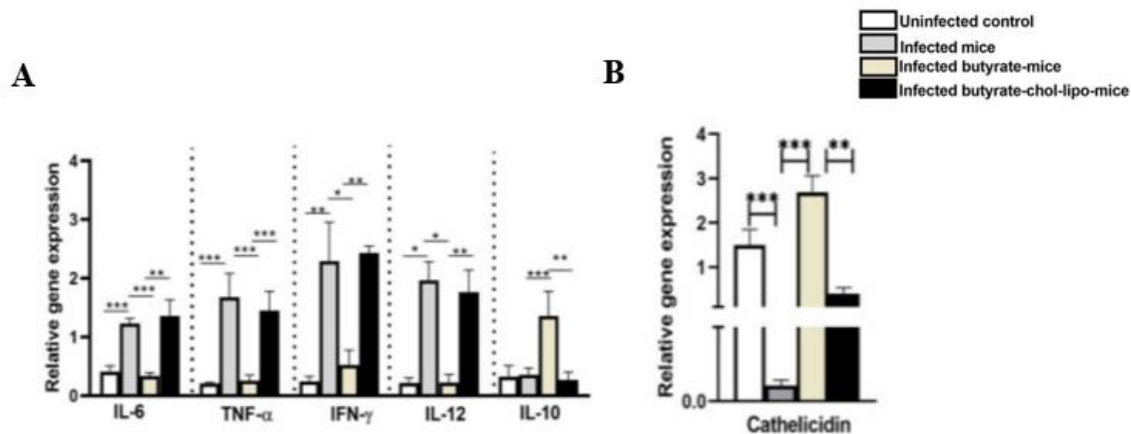


Figure 5.10: Effect of Butyrate on the expression level of pro and antiinflammatory cytokine and anti-microbial gene. qPCR was used to determine expression level of the cytokine mRNA and cathelicidin genes in colon tissue (A and B). The result is presented as the mean±SEM of three independent experiments (E). * Stands for $p<0.05$, ** stands for $p<0.01$, *** represents $p<0.001$, where “ns” is non-significant

5.3 Discussion

In this section, discussion on the possible mechanism which is dependent on the host cell, through which gut microbiota derived butyrate to thwart pathogen invasion was done. Since for the purpose of the studies on macrophages and pathogens, RAW 264.7 is considered to be a suitable model, we conducted experiments in RAW 264.7 since it is a sentinel cell of immunological homeostasis in the gut (Bain and Schridde; 2018; Marathe et al., 2012; Shi et al., 2009). The amount of butyrate employed in the study was comparable to the physiological amount that has been discovered in the intestine, and it had no effect on cell confluency, viability, or proliferation (den Besten et al., 2013). With the use of butyrate, we noticed a considerable drop in cholesterol level of membrane. Despite not causing apoptosis in the cells, butyrate led to the alteration in the morphology of the cells. It is tempting to surmise that administration of butyrate, which was responsible for depletion of membrane cholesterol, altered the cytoskeletal structure, which in turn affected cellular morphology, as cholesterol influences a cell's mechanical characteristics through the cytoskeleton underneath (Sun et al., 2007). Due to the fact that it controls membrane fluidity, cholesterol is a key factor in determining the characteristics of cell membranes (Subczynski et al., 2017). Using a Laurdan probe, we looked at the fluidity with respect to the obtained ‘r’ value of FA, of the macrophage membrane (Harris et al., 2002). In order to quantify changes in the emission spectrum of Laurdan probe, brought on by alterations in the content of membrane water, the generalised polarisation was calculated. The increase in cell membrane fluidity, which is suggestive of a drop in membrane cholesterol, is indicated by a decrease in FA after butyrate

therapy. The fluidity of the membranes, which is similarly connected with the reversion of the cholesterol in membrane, was reversed by additional administration of liposomal cholesterol to the butyrate-treated cells. Unilamellar vesicles called Chol-lipo are utilised for effective cholesterol distribution in cells. They are made of phosphatidyl choline along with cholesterol where the ratio is 1.5:1 (Kheirloom and Ferrara, 2007). Reversal of FA with liposomal cholesterol administration is a sign that butyrate is removing cholesterol from the membrane of the cell.

We checked for the presence of lipid rafts or microdomains to connect butyrate with a reduction in membrane fluidity. In cholesterol-rich microdomains on rafts, CTX-B, (cholera toxin B) binds to the GM1 ganglioside (Aman et al., 2001). Reduced fluorescence intensity of CTX-B-FITC indicated that lipid raft disruption decreased CTX-B binding (Petrov et al., 2017). Butyrate's CTX-B binding significantly decreased when compared to the control, however treatment with chol-lipo but not ana-lipo effectively restored things to normal. Anti-CD71 antibody interaction, however, was unaffected in all four instances. As an indicator protein for the non-raft region, transferrin receptors or CD71 were found to located in the cell membrane's non-raft region (Boesze-Battaglia, 2006).

Lipid rafts on the host are used by pathogens to spread the infection (Bukrinsky et al., 2020). The first physiological interface of a host cell with a bacterium is a crucial first step that frequently determines what follows because initial contact with the lipid rafts is the only route to enter the host cell. In our research, we have taken into account the spread of gastrointestinal infections mediated by *Salmonella* and *Shigella*. Pathogen invasion that had been inhibited by butyrate treatment was recovered by adding cholesterol via liposomal cholesterol administration or MBCD-chol to butyrate-treated cells. *Shigella flexneri*'s invasin IpaB needs domains enriched with sphingolipid/cholesterol to interact with the CD44 on the surface of cell membrane of host during the earliest stages of the invasion process (Lafont et al., 2002). In cholesterol-rich vacuoles, *Salmonella* attaches to CD55 that is linked with lipid rafts (Knodler et al., 2003; Catron et al., 2002). We demonstrate that in the presence of butyrate, CD44, which had previously been demonstrated to be concentrated in membrane rafts, relocates to a different region of the membrane or internalised in the cell without altering its total expression (Donatello et al., 2012; Sun et al., 2020). Along with this, we showed that butyrate-treated cells greatly reduced *Salmonella* and *Shigella* invasion, but that invasion of pathogens returned to normal after liposomal cholesterol treatment. Further support for our hypothesis comes from research on a natural chemical called capsaicin, which is found in chillies and reduces the infection of intestinal cells with *Shigella flexneri*. Capsaicin makes biomembranes fluid (Sharma et al., 2019; Basak et al., 2022).

Shigella infection was selected in order to confirm our ex vivo findings from the mouse model. because infection with *Salmonella* in mice requires treatment with antibiotics that is likely to affect the composition of gut microbiome and intestinal butyrate production (Ramirez et al., 2020; Barthel et al., 2003). For the examination of the in vivo processes of pathogenesis mediated by *Shigella* infection, there is currently no adequate animal model that can take the place of human-based investigations (Kim et al., 2013; Yang et al., 2014); however, a more contemporary murine model in accordance with peritoneal infection with highly pathogenic *Shigella flexneri* 2a has been recognised. In line with the earlier findings, compared to infected animals, butyrate treatment resulted in a significant decrease in the bacterial quantity in the colons. In comparison to butyrate mice, the pathogen load increased when liposomal cholesterol was supplemented. In bodily fluid, the half-life of liposomes (Unilamellar) containing more cholesterol is longer than that of liposomes containing less cholesterol (Kirby et al., 1980). A large variety of plasma proteins are readily absorbed by liposomes while they are in circulation (Gabizon and Papahadjopoulos, 1988). Some of these proteins may serve as opsonins, guiding liposomes to the receptors present on the surface of cells and making it easier for cells to absorb them. The liver is assumed to be the target of liposomes, which might theoretically allow passage via its wide fenestrations, including sinusoidal capillaries. (Fielding et al., 1999). To ensure the effective transport of cholesterol into the gut, we assessed the cholesterol in the intestinal tissue. Notably, infected mice also displayed a rise in cholesterol in colon tissue. It is tempting to hypothesize that because *Shigella* infection reduces the amount of butyrate-producing bacteria in the gut, the amount of cholesterol in the guts of infected mice will also increase (Yang et al., 2020). Infection with *Salmonella* also caused a similar rise in lipid levels, which returned to normal after recovery (Khosla et al., 1991). We also noticed that enhancement in the relative gene expression level of mucin 2, pro inflammatory cytokines, Infiltration of inflammatory cells, and damage of the gut lining of epithelial cells in addition to the decreasing bacterial load in the gut. According to earlier research, colon mucin may be directly harmed by inflammation and infection (Bergstrom et al., 2008; Bergstrom et al., 2010). For instance, when infected with *Citrobacter rodentium*, *Muc2*^{-/-} mice showed high rate of loss of body weight, higher mortality, and heavy bacterial load. The expression of mucin 2 was also upregulated in infected mice, but it was considerably reduced by butyrate therapy and again enhanced in liposomal cholesterol treated mice. As a result, it appears probable that *Shigella* colonisation along with invasion of the colon can result in a variety of histological alterations that are brought on by the host's natural immune response to infection. Secreted cytokines attracted immune cells to the infection site, activating the host defence mechanisms against invasion of *Shigella* (Ashida et al., 2015).

We identified the host variables in the protection mechanism after establishing that butyrate therapy lowers invasion of enteric pathogens, that can be reverted by treatment with liposome cholesterol. We measured the levels of expressed cytokines in colon tissue to further investigate whether butyrate therapy lessens the inflammatory reactions brought on by infection with *Shigella*. We discovered that

infected mice had levels of proinflammatory cytokines such as IFN γ , IL-6, and TNF α that were considerably greater than in the control group. The proinflammatory cytokines were dramatically reduced by butyrate therapy and returned to the same level as the infection group in butyrate-cholesterol liposomal treated-mice. Together, our findings show that *Shigella* organisms are unable to stimulate the major cytokines that lead to a reduction in the recruitment of polymononuclear cells into the resident colon of butyrate-mice. In colonic macrophages' defence mechanisms against bacterial infection, the cathelicidin, an antimicrobial peptide, is thought to be crucial. Our findings support past publications that indicated butyrate increases the promoter activity of the cathelicidin gene, causing it to function (Kida et al., 2006).

Lipid rafts or microdomains on the membrane have an important part in a number of vital cellular functions, such as cellular signalling, endo and exocytosis, in addition to their significance in pathogen invasion. The issue of whether butyrate administration can stop any such process therefore arises. It is clear that deficiency of cholesterol obtained from membrane results in exocytosis spontaneously (Petrov et al., 2014). In light of this, butyrate also exhibits enhanced mucin secretion through exocytosis in the intestine (Barcelo et al., 2000). IFN- γ signalling requires membrane cholesterol (Morana et al., 2022). Butyrate, which we show to be a cholesterol-lowering substance, is also known to block IFN- γ signalling (Klampfer et al., 2003). As a result, butyrate through a membrane-oriented endeavour demonstrates homeostasis of intestine, by building the mucosal system resistant to pathogen invasion.

In general, this study introduces a novel approach to intestinal colonisation resistance. We find that butyrate decreases the level of cholesterol procured from the membrane, which is responsible for the enhancement of the fluidity and rupture of lipid microdomains. This effect might be altered by restoring cholesterol in the cell membrane. We have demonstrated that butyrate's breakdown of lipid rafts reduces enteric pathogen invasion using in vitro and in vivo investigations. By restoring cholesterol to the membranes, we confirm that butyrate therapy prevents enteric pathogen colonization by lipid microdomain disruption.

CHAPTER-3

Role of RNA Binding proteins in the modulation of gut immunity

6.1 Introduction

Bioactive lipids such as cholesterol and its metabolites interact with and affect the activity of different proteins as well as signalling networks that regulate a wide range of pathological as well as physiological processes. Recent research appears to indicate that the retinoic acid-related orphan receptors, RORs, which are components of the ligand-mediated nuclear receptor superfamily, have a broad interaction selectivity for a range of different types of sterols (Kallen et al., 2002). Several cholesterol metabolites as well as intermediates operate as the natural ligands of ROR γ and ROR α , acting as agonists or inverse agonists (Kallen et al., 2004). Alterations in the homeostasis level of cholesterol, affecting the type of cholesterol metabolites in cells, may promote or block ROR γ transcriptional activity, resulting in alterations of the physiological processes regulated by RORs, such as diverse immunological responses and metabolic pathways. Transcriptional activation and Th17 cell differentiation rely on ROR γ . Genes involved in cholesterol breakdown and efflux are downregulated during Th17 differentiation, but genes involved in cholesterol biosynthesis are upregulated (Cai et al., 2019). In skin biopsies, there was a positive connection observed between IL-17 levels and genes involved in cholesterol production (Varshney et al., 2016). Elevated gene expression related to cholesterol biosynthesis amplifies the effects of ROR γ agonists, promoting Th17 differentiation, IL-17 synthesis, and inflammatory illnesses.

Numerous investigations have indicated that interference with the cholesterol production pathway negatively impacts Th17 differentiation and ROR γ activation. The initial stage in the manufacture of cholesterol is the conversion of HMG-CoA to mevalonic acid, which is catalyzed by 3-hydroxy-3-methylglutaryl coenzyme A (HMG-CoA) reductase (HMGCR), of which the cholesterol-lowering medications known as statins bind. It has been demonstrated that statins prevent Th17 differentiation and inflammatory cytokine production (Ulivieri & Baldari, 2014).

Several RNA binding proteins are seemed to regulate the activation of ROR γ transcription factor during hypercholesterolemia and tumour genesis, which determines the fate of IL-17 producing Th17 cells, however the mechanism is yet to be discovered (Cai et al., 2019; Zou et al., 2022). Many immunological activities, including the secretion of cytokines, the transmission of signals, and immediate-early transcriptional response, are governed post-transcriptionally by AU-rich elements (AREs) in mRNA 3'-untranslated regions (3'-UTR) (Vlasova-St Louis & Bohjanen, 2014). Frequently, AUF-1 destabilizes mRNAs of interest by binding 3'-UTR AREs and enlisting the aid of degradation and deadenylation proteins (Wilson et al., 1999; Sirenko et al., 1997; Sarkar et al., 2003). Even though there are still many unanswered questions, AUF-1 is essential for immune function because losing it results in spontaneous septicemia in mice (Wang et al., 2022; Lu et al., 2006). Among the four isoforms of AUF-1, the p40 isoform triggers an anti-inflammatory response by enhancing the stability and translation of IL10 mRNA, whereas the p37 isoform is crucial in suppressing the production of cytokine genes (Sarkar et

al., 2011). AUF1 is crucial in controlling the cellularity of splenic lymphocytes and the maintenance of follicular B cells (Sadri et al., 2010).

In this chapter, our findings shed light on new roles for AUF1 in ROR γ t-mediated Th17 differentiation and provide a foundation for comprehending and regulating its activity in hypercholesterolemia.

6.2 Results

6.2.1 AUF-1 morpholino oligo administration shows decrease in overall serum and liver cholesterol

Serum cholesterol was measured before and after administration of morpholino oligo, which revealed clear reduction in overall serum cholesterol after 14 days of morpholino administration, when compared with their untreated condition on day '0'. Clear difference between the hepatic serum level was also observed between untreated control and morpholino treated group.

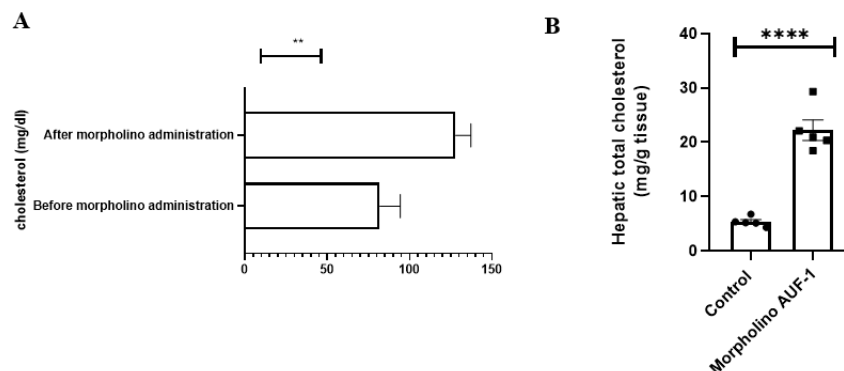


Figure 6.1: Effect of AUF-1 knockdown on serum and hepatic cholesterol level. serum cholesterol of mice before and after administrating of AUF-1 morpholino oligo was measured and expressed in mg/dl (A). Hepatic cholesterol level was analysed from untreated control and morpholino treated group and expressed as mg/g tissue (B). N = 5 in each group; results reported as mean \pm SE. The experimental analysis was carried out twice. **** denotes p < 0.0001, ** denotes p < 0.01.

6.2.2 AUF-1 knockdown promotes the upregulation of ROR γ t and decrease in the expression of FOX P3 mRNA

Real time PCR data obtained from splenocytes showed that transcription factor of regulatory T cells, FOX P3, was downregulated while transcription factor that determines the fate of Th17 cells, that is ROR γ t, was upregulated in the cells of morpholino mediated AUF-1 knockdown mice. GATA3, which

is responsible for the development of naïve T cells to Th2 cells, remained unchanged between AUF-1 and untreated control mice.

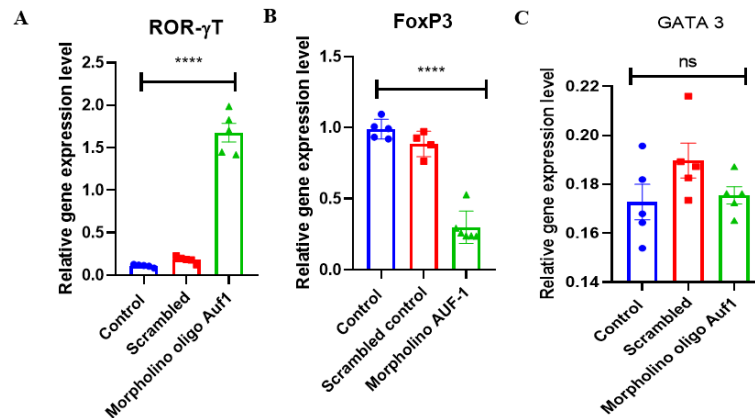


Figure 6.2: Effect of AUF-1 knockdown in the expression of transcription factors determining the fate of naïve T cells. Real time PCR results revealed the upregulation of ROR γ t, and decrease in the expression of FOXP3 mRNA (A, B). The expression of GATA 3 remained unaltered in all the three groups (C). The data from three trials are plotted as Mean \pm SEM. **** stands for $p < 0.0001$, ‘ns’ denotes non-significant.

6.2.3 AUF-1 alters the half-life of T cell specific transcription factor ROR γ t and FOX P3

In order to find out how AUF-1 regulate the stability of T cell specific transcription factors in inverse way, we look into the half-life of these transcription factors. After isolating splenocytes from AUF-1 morpholino oligo as well as scrambled control treated group, cells were administered with Actinomycin D and DRB to block the synthesis of RNA at differential time points (0, 30, 60, 90, 120 minutes). RNA and cDNA were obtained and real time PCR was performed. Exponential graph obtained from concentration derived from the Ct value when plotted against different time points, suggested that morpholino mediated blocking of AUF-1 decreased the half-life of the mRNA of transcriptional factor FOXP3 (Half-life of untreated control group is 60 ± 1.27 minutes and morpholino treated group is 31.5 ± 2.23 minutes), while enhancing the half-life of the mRNA of ROR γ t (Half-life of untreated control group is 18.22 ± 2.68 minutes and morpholino treated group is 48.17 ± 3.4 minutes). Since TNF α is a direct target of AUF-1, it was used as a negative control (Wilson et al., 2003) Half-life of housekeeping gene GAPDH remained unchanged even after morpholino treatment, indicating that it might not be the direct target of AUF-1.

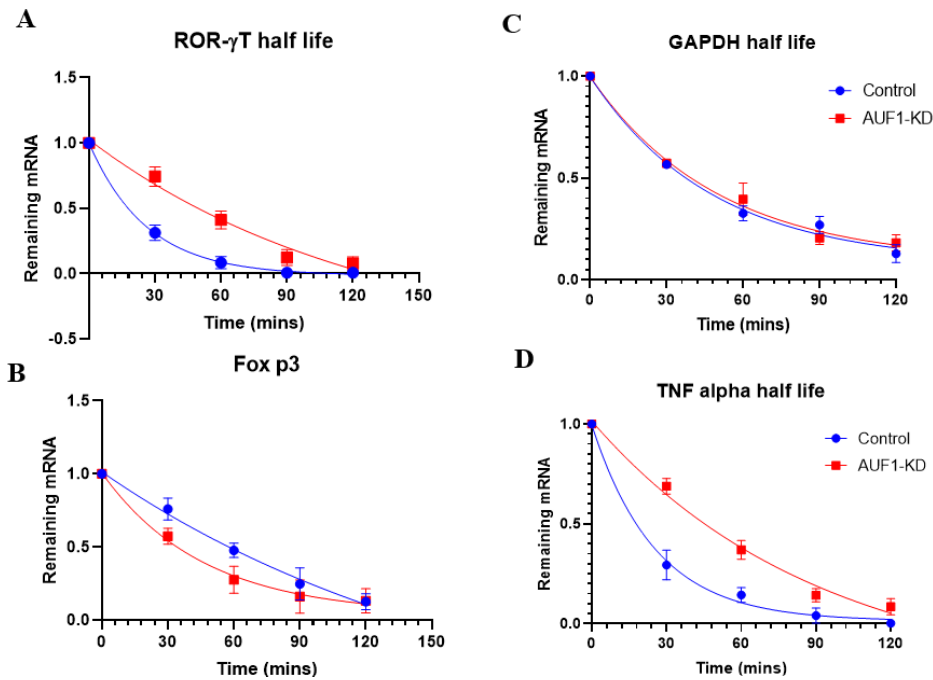


Figure 6.3: Effect of AUF-1 KD in maintaining the mRNA stability of T cell specific transcriptional factors. Splenocytes obtained from AUF-1 knockdown and scramble control was plated and actinomycin-D was administered to block the synthesis of mRNA in a time dependent manner. Remaining mRNA was plotted against time in an exponential curve to determine the half-life of mRNA. ROR γ t, FOXP3, GAPDH and TNF- α half-lives were plotted (A-D). The data from three trials are plotted as Mean \pm SEM.

6.2.4 FACS results revealed the alteration in the expression of CD4⁺ cells in AUF-1 knockdown mice

The mice were examined for the frequency of splenic CD4⁺ and CD8⁺ T-cells. The data exhibited that the absolute number of CD8⁺ cells remain unaltered in the mice of control, scrambled as well as AUF-1 knockdown group, whereas, almost 20% uprise of CD4⁺ cells were observed in AUF-1 knockdown mice.

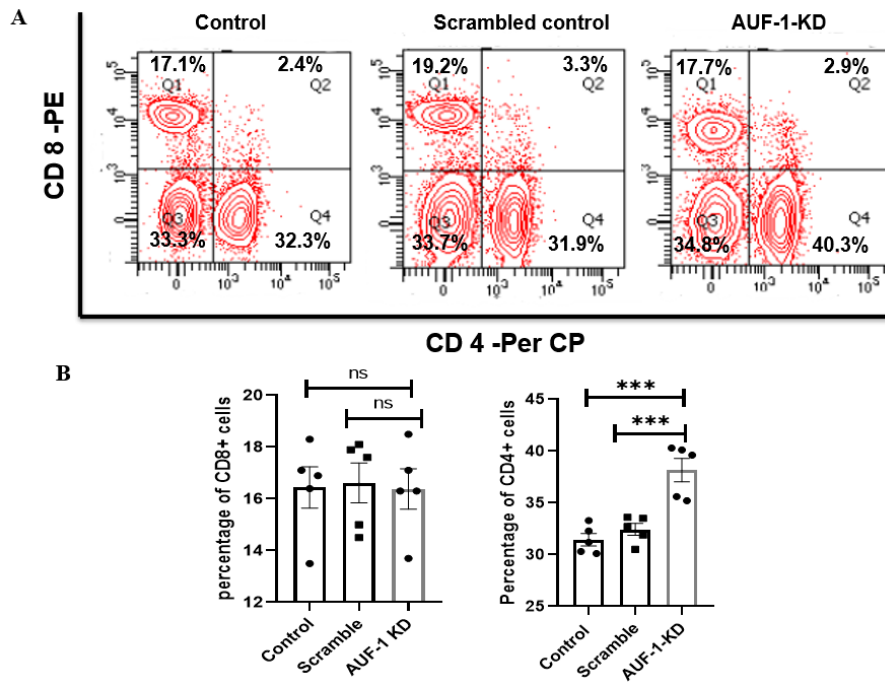


Figure 6.4: Effect of AUF-1 knock down in the frequencies of CD8+ and CD4+ T cells. Following a 14-day morpholino delivery period, splenocytes were obtained from individual mice, as well as from the scrambled control group and the control group. The CD8+ and CD4+ populations were then assessed using flow cytometry. Exemplary dot-plots displaying CD8+ and CD4+ T-cells in the three groups of mice (A). CD4+ and CD8+ T-cell percentages (n = 5/group). the value differs substantially from the control (B). The data from three trials are plotted as Mean \pm SEM. *** stands for $p < 0.001$, 'ns' denotes non-significant.

6.2.5 FACS analysis suggesting reduction of IL-10 producing regulatory T cells

As detailed in the "Materials and Methods" section, CD4+CD25+ populations were isolated from the spleen and MLN from three groups (Control, scrambled control and AUF-1 KD). FOXP3 expression was labelled with immunofluorescence, and the number of FOXP3+ cells in each sample were counted. The data obtained from spleen sample showed that $7.2 \pm 0.9\%$ FOXP3+ cells in control group and $6.6 \pm 1.2\%$ FOXP3+ cells in scrambled group, suggesting no significant difference. In contrast, $1.9 \pm 0.2\%$ cells expressed FOXP3 in AUF-1 KD group, indicating depletion of regulatory T cells

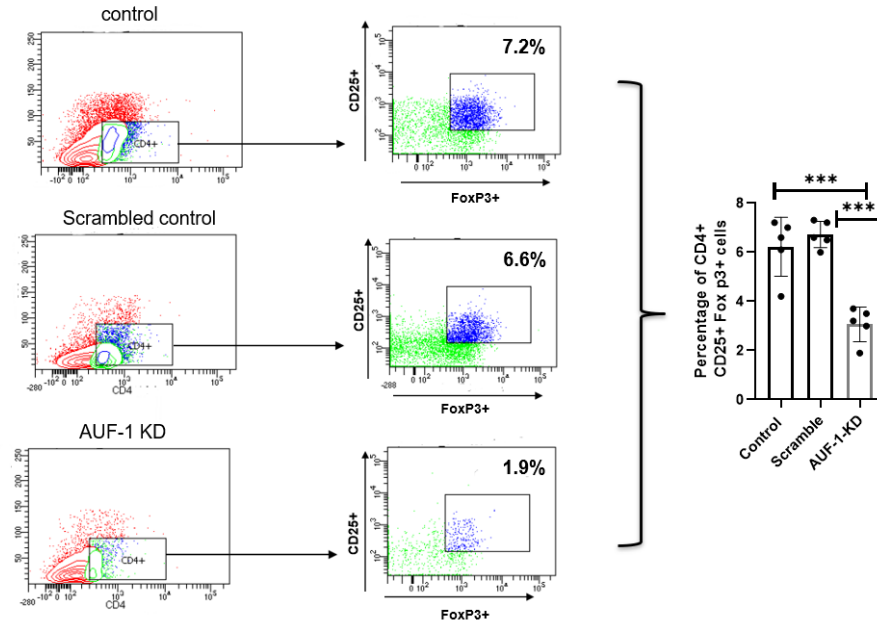


Figure 6.4: Effect of AUF-1 Knockdown on IL-10 producing regulatory T cell expression. FACS data revealed that the percentage of CD25+FOXP3+ IL-10 producing T cells, where untreated control showed 7.2%, scrambled control showed 6.6% and AUF-1 knockdown showed 1.9% of IL-10 producing cells. The result is presented as the mean±SEM of three independent experiments (E). *** stands for $p < 0.001$

6.3 Discussion

Research on ROR γ t has revealed that this transcription factor is essential for several aspects of immunological control, cellular development as well as metabolism related disorders. Here, we demonstrated that RNA binding protein AUF-1 mediated modulation of ROR γ t has a noteworthy role in encouraging metabolic dysregulation leading to hypercholesterolemia in mice model. The balance between FOXP3 and ROR γ t is essential to maintain immune homeostasis and it is possible that FOXP3 inhibits Th17 cell transcription in vivo. By opposing ROR γ t activity, for example, FOXP3 can inhibit Th17 cell development (Ivanov et al., 2017). The complex molecular pathway of the reciprocal interaction between ROR γ t and FOXP3 is highly context specific (Ziegler & Buckner, 2009). Our study revealed that during the time of hypercholesterolemia, the delicate balance between FOXP3 and ROR γ t is regulated by RNA binding protein AUF-1. Earlier study revealed that loss of AUF-1 causes septicaemia, that led to a disruption in the balance of Th17 and Treg cell formation, skewing the developmental paths toward the Th17 lineage (Lu et al., 2006; Dey & Bishayi, 2017). We have previously shown that AUF-1 is decreased in hypercholesterolemia (Das et al., 2022) and the current study revealed that in absence of AUF-1 in hypercholesterolemia, ROR γ t mRNA is up regulated, where

FOXP3 mRNA is decreased, which verified previous finding, suggesting that decrease in the expression of FOXP3 may lead to the development of hypercholesterolemia (Klingenberg et al., 2013).

Studies revealed that through direct association with ROR γ t, Foxp3 blocks ROR γ t-mediated IL-17A mRNA Transcription (Ichiyama et al., 2008). By morpholino oligo directed blocking of AUF-1, we found that mRNA stability of ROR γ t has been increased up to 50%, while half-life of FOXP3 mRNA has been reduced drastically. FACS results also demonstrated the overall reduction of IL-10 producing CD4⁺CD25⁺FOXP3⁺ T cells, which validated the previous notion of the presence of lesser amount of IL-10 in hypercholesterolemia like situations and ROR γ t being a contextually specific exemplary regulator of cholesterol biosynthesis (Caligiuri et al., 2003; Zou et al., 2022).

Our study showed uprise of IL-22 production in the MLN of AUF-1 knockdown mice. The interaction between Th17 cells and IL-22 indicates a positive feedback loop that enhances immune responses. Th17 cells boost the generation of IL-22, which in turn promotes Th17 cell development and maintenance. This tightly controlled reciprocal regulation adds to immune system resilience (Zheng et al., 2020; Keir et al., 2020).

Based on our findings of how AUF-1 mediated modulation of ROR γ t and FOXP3 transcription factor playing pivotal role in the fate determination of naïve T cells to regulatory T cells or IL-17 producing Th17 cells in the context of hypercholesterolemia, we can uphold the role of AUF-1 as a potential therapeutic target to treat IL-17 mediated inflammation related to imbalanced homeostasis of cholesterol.

CHAPTER-4

Role of RNA binding proteins in the regulation of junctional protein, leading to the maintenance of gut barrier integrity

7.1 Introduction

mRNA stability and translation are important aspects of post-transcriptional gene expression. mRNA stability accounts for almost half of all physiologically driven gene expression. (Nouaille et al., 2014; O'Brien et al., 2017). The decay rate of mRNA is controlled by post-transcriptional processes, with mRNA cis-acting regulatory elements located in the 3' UTR of certain mRNAs. (McKay, 2014). RNA-binding proteins, such as AUF-1, recognize and interact with AU-rich regions (AREs) in the 3' UTR of mRNA, altering its stability. It also regulates mRNA translation by interacting with the 5' UTR and inhibiting translation initiation (White et al., 2013). Variations in exon splicing from a common mRNA precursor produced the four related isoforms of the AUF1 family of proteins, known as p^{45AUF1}, p^{42AUF1}, p^{40AUF1} and p^{37AUF1}, based on their molecular weights. (Wagner, 1998). The presence of differently spliced exons gives different protein isoforms overlapping and separate functions, vastly different subcellular localization, expression levels, and post-translational modifications. (Zucconi et al., 2010; Moore et al., 2014).

AUF1 members are now recognized to have a dual influence on mRNA stability, translational initiation, editing, and transcription. (White et al., 2017). Comprehensive studies of the interactions of AUF1s revealed that they tended to be less rigorous for both GU-rich and AU- to U-rich sequences. Additionally, these studies showed that AUF1 members bind to non-coding RNAs to facilitate these RNAs' maturation, target loading, and function. (Meyer et al., 2019; Zucconi et al., 2010).

The intestinal lumen and the submucosa are separated by a barrier that has been generated and maintained by intestinal epithelial cells (IECs) (Peterson and Artis, 2014). The paracellular route between cells needs to be sealed in order to form an unbroken epithelial cell layer. This is mediated via the junction complex, which is made up of the tight junction (TJs) along with the adjacent adherens junction. TJs are made up of a variety of transmembrane and intracellular proteins (Furuse, 2010). The trans-epithelial transport (TEJ) complex is the primary factor influencing intestinal permeability. Internal inflammation might be caused by altered TJ and enhancement of the intestinal permeability (Turner, 2009; Marchiando et al., 2010). Occludin was the earliest TJ protein discovered, and it aids in TJ stabilization and barrier function (Furuse, 1993). Claudins are the structural framework of the TJ strand and govern junctional permeability (Tsukita et al., 2019). Representatives belonging to the Claudin family are categorized as channel-creating or sealing proteins based on their permeability. Claudin-2 is a TJ protein that forms cation-selective channels and appears in leaky epithelia (Venugopal et al., 2019). It is noteworthy that Occludin and the sub sets of Claudin mRNAs exhibits instability and is subject to post-transcriptional regulation (Yu et al., 2013; Günzel & Yu, 2013).

With significant pathophysiology and few effective treatments, IBD or inflammatory bowel disease is considered to be a chronic inflammatory disorder. Ulcerative colitis (UC) and Crohn's disease are the

two main IBD subtypes (Hendrickson et al., 2002). There is a lack of knowledge on the pathogenesis of IBD. The depletion of barrier function of intestinal epithelial layer is a characteristic of IBD that frequently results in an inflammatory response and barrier disruption. TJ act as a determining factor of intestinal permeability and bowel inflammation could be caused by heightened intestinal permeability and a disturbed TJ (Vanuytsel et al., 2021).

According to recent research, inflammation can be influenced by the absence of AUF-1 (Lu et al., 2006; Sadri & Schneider, 2009). The specific role that AUF-1 plays in the onset of IBD is still unclear, despite the fact that it has been discovered to be associated with inflammation (Dai et al., 2019; Zucconi & Wilson, 2011). In this study, we reported the role of AUF-1 in regulating junctional protein. To do this, we used a mouse paradigm in which the expression of all AUF1 isoforms was specifically inhibited by administering morpholino oligo against AUF-1. We show that ablation of AUF-1 in colon tissue causes acute colitis like symptoms in mice, and that AUF-1 deficit in colon reduces occludin levels along with the enhancement of pore forming Claudin-2, resulting in a deficient barrier function. These findings reveal an essential role for AUF-1 in regulating the processing of junctional proteins in an antagonistic way, providing protection against colitis.

7.2 Results

7.2.1 Selection of effective concentration of GMO-PMO for conducting in-vitro study

To assess the working concentration as well as cytotoxic effect of novel, cell penetrating GMO-PMO in case of in-vitro analysis, HT-29 cells were treated with different dose (0-20 μ M) of AUF-1 GMO-PMO for 24 hours, where scrambled GMO-PMO with several mismatches were used as negative control. The results obtained from MTT assay suggested that up to the dose of 5 μ M of GMO-PMO, 90% of cells remain viable. The cytotoxic effect of GMO-PMO was observed via LDH assay. The protein expression analysis with various dose of morpholino oligo (0, 0.1, 0.2, 0.25, 0.5, 0.75 μ M) revealed that almost 0%, 25 %, 27 %, 50 %, 60 %, 75% reduction in the expression of AUF-1. This finding directed us to conduct further in-vitro research using 0.75 μ M dose of GMO-PMO.

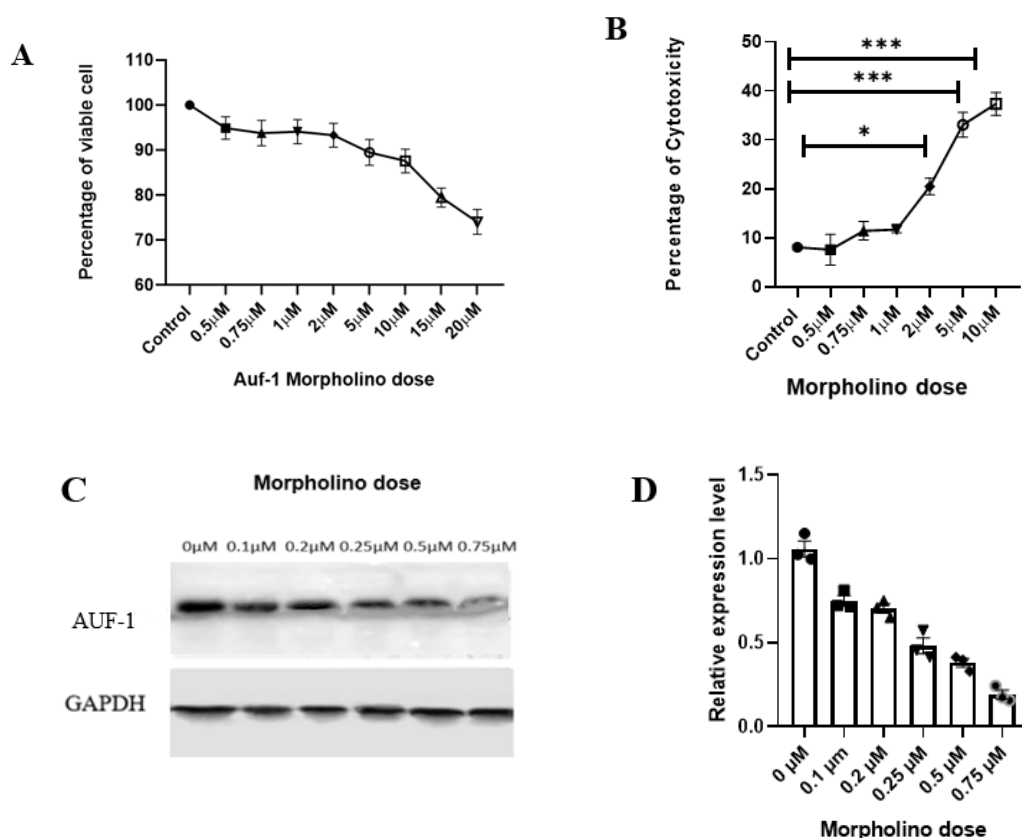


Figure 7.1: Effect of AUF-1 GMO-PMO in cell viability and reduction in AUF-1 protein expression. 0 μ M, 0.5 μ M, 0.75 μ M, 1 μ M, 2 μ M, 5 μ M, 10 μ M, 15 μ M and 20 μ M of AUF-1 GMO-PMO were applied to HT-29 cells for 24-hour treatment period. MTT assay result revealed that up to 5 μ M dose, almost 90% of cells remained viable and then viability dropped (A). Cytotoxicity result revealed that up to 1 μ M dose is nontoxic to the cellular health (B). Western blot analysis suggested that the optimal dose of morpholino oligo for blocking the expression of AUF-1 is 0.75 μ M, which was

verified by the corresponding densitometric analysis (C, D). The information is presented as the mean \pm SEM of three independent experiments (E). * Stands for $p<0.05$, ** stands for $p<0.01$

7.2.2 Morpholino mediated repression of AUF-1 lessens the barrier integrity in HT-29 cell

To examine the effect of AUF-1 on the integrity of intestinal epithelial barrier, HT-29 cells were treated with 0.75 μ M dose of AUF-1 morpholino oligo to block the expression of AUF-1. Transepithelial electrical resistance (TEER) was evaluated at differential time points (0, 2, 4, 8, 10, 12, 20, 24 hours) following AUF-1 morpholino administration. TEER value of the AUF-1 morpholino treated cells decreased steeply up to 8 hours of culturing and reduced gradually afterwards, similar to the LPS treated group, which served as a positive control, even though the TEER of untreated control cells as well as scrambled control group remained largely steady. In order to complement the TEER result and establish the functional impact of AUF-1 on the integrity of epithelial barrier, in-vitro paracellular permeability assay was performed using FITC dextran. Inhibiting the expression of AUF-1 on HT-29 by using morpholino oligo showed the quantified amount of FITC leakage into the bottom chamber of the trans well, similar to that of LPS mediated lack of integrity of epithelial layer.

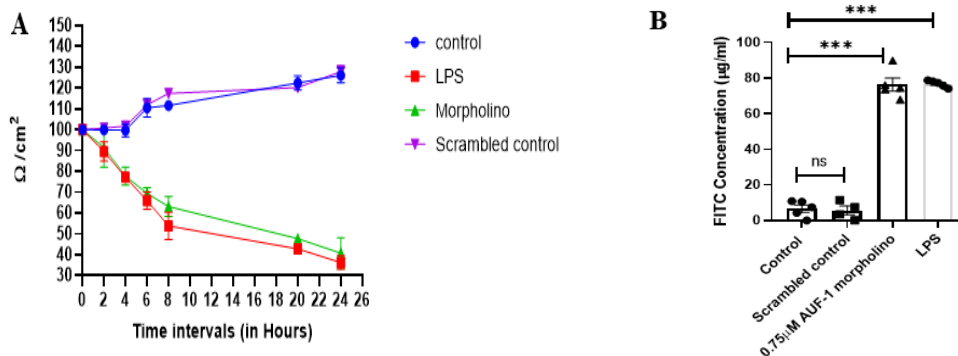
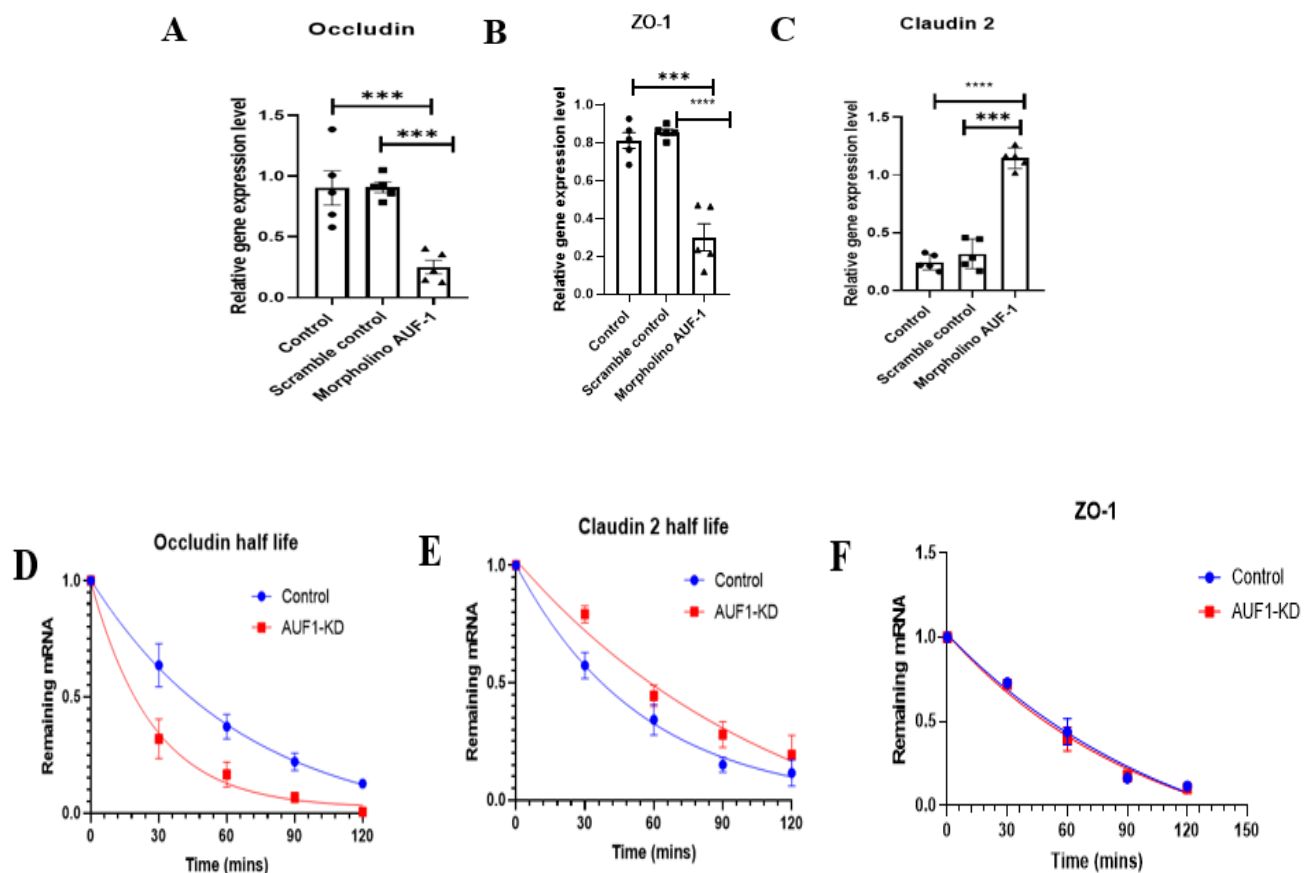


Figure 7.2: Effect of AUF-1 GMO-PMO on transcellular electrical resistance and paracellular permeability. HT-29 cells were treated with 0.75 μ M of AUF-1 GMO-PMO (considered to be treated group) and LPS (Positive control) for 24 hours and time dependent TEER values were measured to check transcellular permeability (A), along with Paracellular permeability, where cells were treated with FITC- Dextran and media was collected from the basal chamber of the transwell to measure the fluorescence level and the overall FITC concentration was plotted (B).

7.2.3 AUF-1 alters the half-life of junctional protein Occludin and Claudin 2 to maintain barrier integrity

Real time PCR data also showed that Occludin and ZO-1 were downregulated in morpholino mediated AUF-1 knockdown cells, while Claudin-2 was upregulated. In order to find out how AUF-1 regulate the stability of junctional proteins in inverse way, we look into the half-life of these junctional proteins. After treating HT-29 cells with 0.75 μ M dose of AUF-1 morpholino oligo, cells were administered with Actinomycin D and DRB to block the synthesis of RNA at differential time points (0, 30, 60, 90, 120 minutes). RNA and cDNA were obtained and real time PCR was performed. Exponential graph obtained from concentration derived from the C_t value when plotted against different time points, suggested that morpholino mediated blocking of AUF-1 decreased the half-life of the mRNA of junctional protein Occludin (Half-life of untreated control group is 42.5 \pm 5.51 minutes and morpholino treated group is 19 \pm 2.34 minutes), while enhancing the half-life of the mRNA of pore forming protein Claudin-2 (Half-life of untreated control group is 38.5 \pm 6.27minutes and morpholino treated group is 60 \pm 7.11minutes). No alteration in the expression of ZO-1 was observed. Since Dicer-1 is a direct target of AUF-1, it was used as a positive control (Abdelmohsen et al., 2012) Half-life of housekeeping gene GAPDH remained unchanged even after morpholino treatment, indicating that it might not be the direct target of AUF-1.



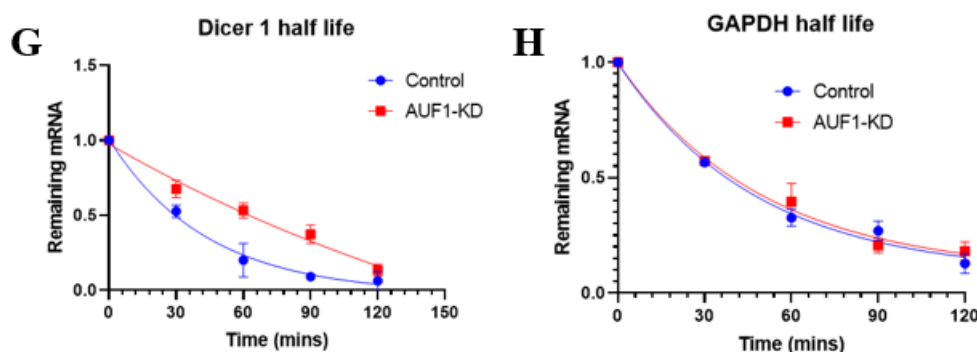


Figure 7.3: Effect of AUF-1 KD in maintaining the mRNA stability of junctional protein. HT-29 cells were treated with AUF-1 GMO-PMO and relative m RNA expression was observed (A, B, C). actinomycin-D was administered to block the synthesis of mRNA in a time dependent manner after morpholino treatment. Remaining mRNA was plotted against time in an exponential curve to determine the half-life of m RNA. Occludin, Claudin-2, ZO-1, Dicer 1 and GAPDH half-lives were plotted (D-H). The data from three trials are plotted as Mean \pm SEM.

7.2.4 Occludin and Claudin-2 are the direct targets of AUF-1

We initially tested whether AUF-1 directly interacts with the occludin mRNA by utilizing anti-AUF-1 antibody in RNP-IP experiments under circumstances that protected RNP integrity. Figure (6.4 B, C) illustrates how AUF-1 samples were significantly more enriched in Occludin and Claudin-2 PCR products than control IgG samples. Since Dicer-1 mRNA is a target of AUF-1, the enrichment of this PCR product was also investigated and used as a positive control (Das et al., 2022); however, as previously reported, the amplification of GAPDH PCR products, which have been detected in all samples as low-level contaminants in housekeeping transcripts but are not AUF-1 targets, had served to monitor the uniformity of sample input. Apart from Claudin-2, other sub types of Claudin like Claudin-1, Claudin-4 showed low level of enrichment, indicating that they may not be the direct target of AUF-1 We also checked the interactions of AUF-1 with other RBPs like HuR and TTP by performing co immunoprecipitation assay, where the result revealed that AUF-1 is not directly associating itself with HuR or TTP (Figure 7.4A).

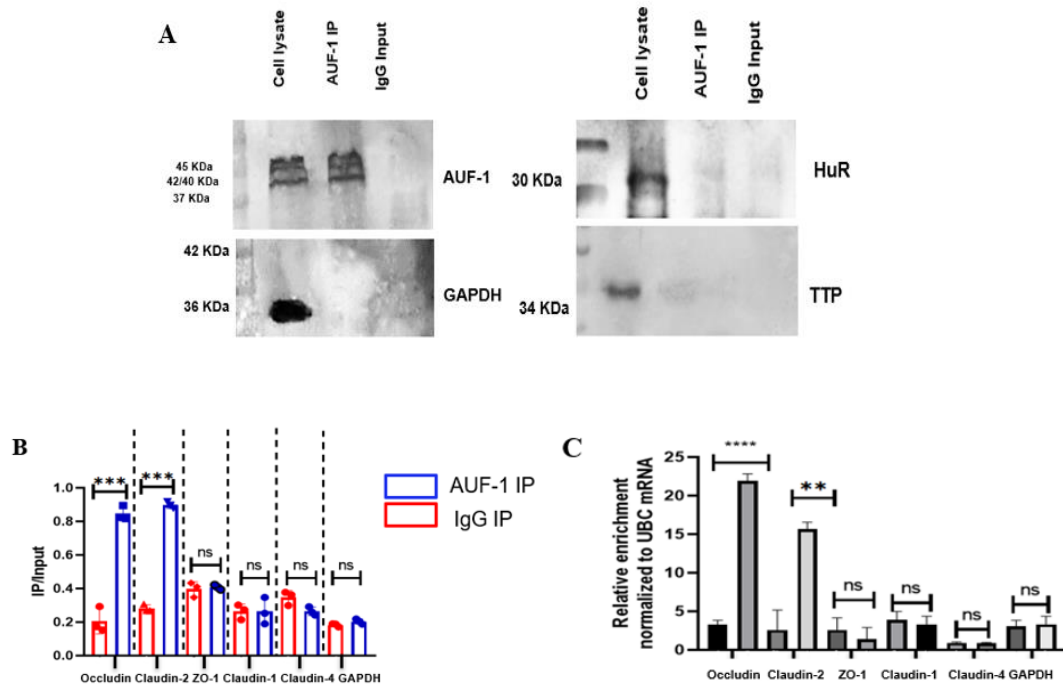


Figure 7.4: Pull down assay result showing the presence of possible direct targets of AUF-1. Western blot result revealed the presence of AUF-1 in whole cell lysate and AUF-1 immunoprecipitated sample, but HuR and TTP was not detected in the sample (A). Presence of possible target and non-target m RNAs in the pull-down samples were plotted in terms of IP/Input and relative enrichment level (B, C). The data from three trials are plotted as Mean \pm SEM. Each experiment was set up in triplicate.

7.2.5 Phosphorylation of AUF-1 determines its ability to regulate stabilisation and destabilisation of target m RNAs

Post-Translational modifications (PTMs), including the phosphorylation of RBPs, significantly impact the function and/or affinity of these proteins toward their targets, which in turn affects the translation efficiency, turnover, and stability of mRNA. The phosphorylation of p37^{AUF1} shown to stabilise the expression of junctional protein Occludin mRNA, while it did not show any effect on other junctional proteins like Claudin-2, Claudin-1.

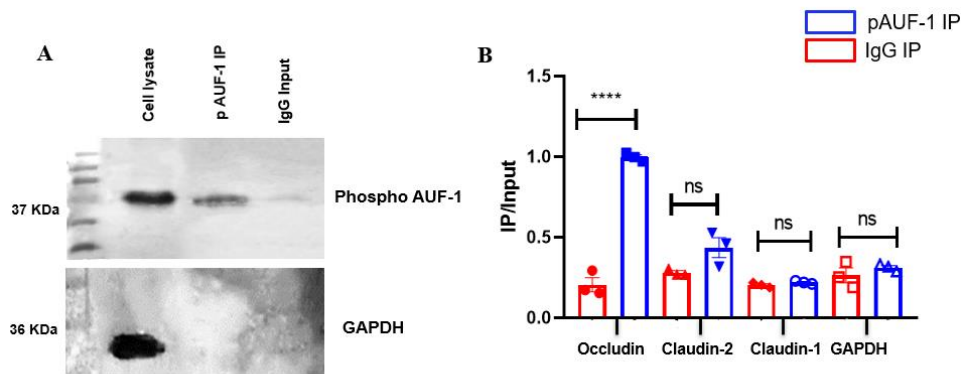


Figure 7.5: Pull down assay result showing the possible target of phosphorylated p37^{AUF1}. Western blot analysis was done to confirm the presence of p37^{AUF1} in the pull-down sample by using AUF-1 37KDa specific antibody (A). Presence of possible target and non-target m RNAs in the pull-down samples were plotted in terms of IP/Input (B). The data from three trials are plotted as Mean ± SEM. Each experiment was set up in triplicate.

7.2.6 Morpholino mediated knockdown of AUF-1 in animal model

To establish the fundamental notion that AUF-1 plays a crucial role in the preservation of intestinal barrier integrity, we employed knockdown of AUF-1 (AUF-1-KD) in mice utilizing the cell-penetrating morpholino oligomer (GMO-PMO) used in the in-vitro analysis. Toxicity level was evaluated by liver functioning test, suggesting that GMO-PMO did not hamper the normal body functioning. We found no disparity in the expression level of AUF-1 among control along with scramble-MO-treated mice, indicating that the scramble-MO failed to impact the expression level of AUF-1, while the AUF-1-MO did, demonstrating the sequence specific effects of the AUF-1 and scramble GMO-PMOs. The results showed that AUF-1-MO significantly decreased the AUF-1 isoform in the colon as well as in other organs such as the heart and kidney.

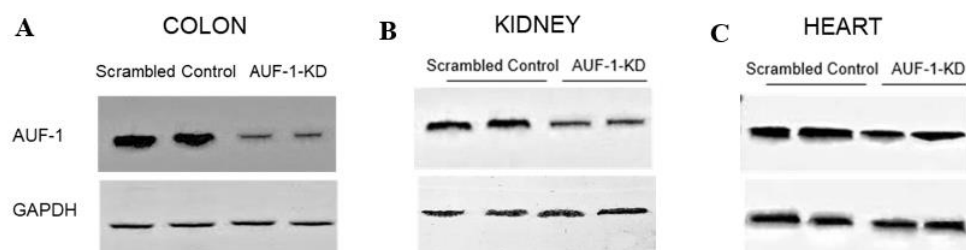


Figure 7.5: Effect of AUF-1 knock down on tissue sample. Western blot in the colon, kidney and heart of mouse administered AUF1-MO showing significance reduction in the expression of AUF-1 in

the colon sample compared to kidney and heart tissue, GAPDH served as control (A, B, C). Experiments were repeated thrice.

7.2.7 Colon permeability and colon histopathological score in AUF-1-KD mice is similar to that of DSS induced colitis mice

While there was no observable significant alteration in the body weight of AUF-KD mice group, the overall length of the colon was decreased along with observable splenomegaly. Food consumption among four experimental groups remain unaltered but water intake was drastically reduced in DSS treated and AUF-1 KD group, indicating obvious shrinkage in colon length. The dramatic upsurge of FITC dextran value in AUF-KD mice indicated the enhancement of colon permeability in AUF-KD mice which was comparable to the DSS-colitis group.

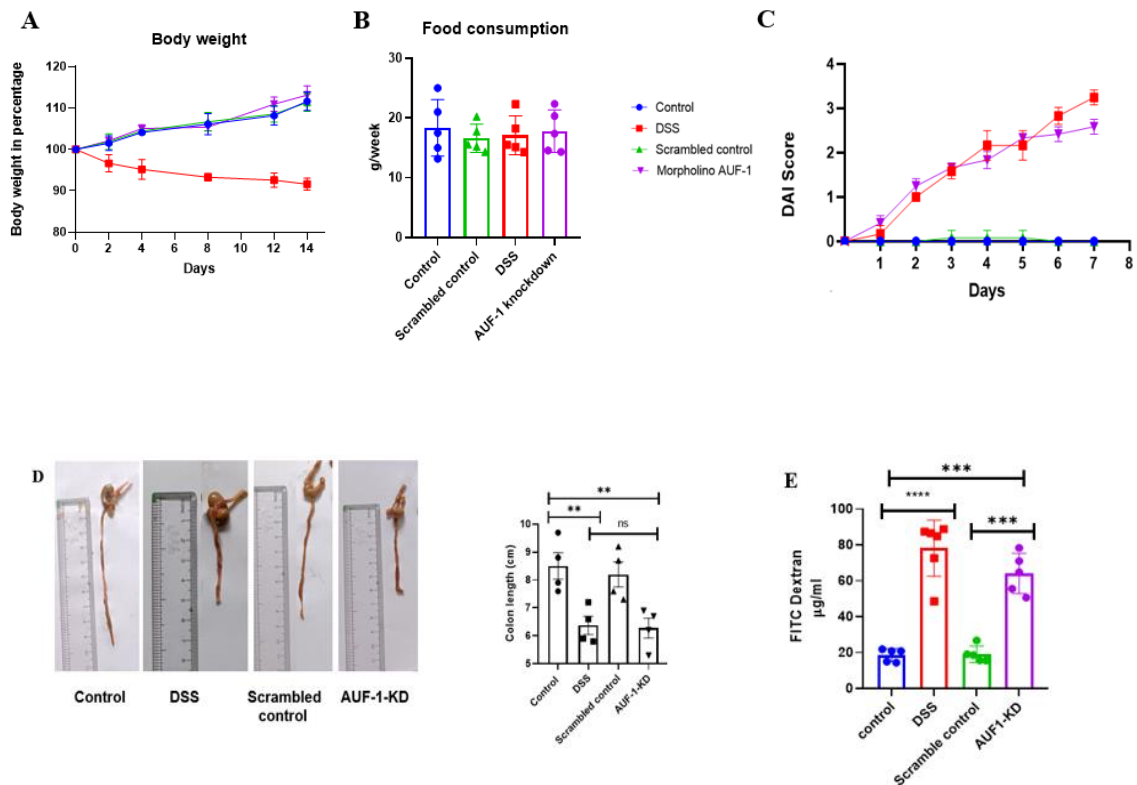


Figure 7.6: Effect of AUF-1 knockdown on morphological changes. Knockdown of AUF-1 did not show any alteration in body weight as well as food consumption (A, B). DAI index revealed that the score of AUF-1 KD group is in between 2-3, indicating severe gut inflammation (C). Characteristic shortening of colon length was observed in knockdown group (D). Gut barrier permeability of knockdown group was observed and comparable to DSS treated group. (E).

Histopathological analysis revealed from the scoring data suggested severe damage in epithelial layer, leading to impaired histological architecture along with moderate infiltration of neutrophils as well as the presence of the inflammation of goblet cells in DSS treated and AUF-1 KD group. Figure (?) revealed that the DAI score in AUF-KD mice increased considerably, and it was nearly equivalent to the DAI score in the 2% DSS mediated colitis group.

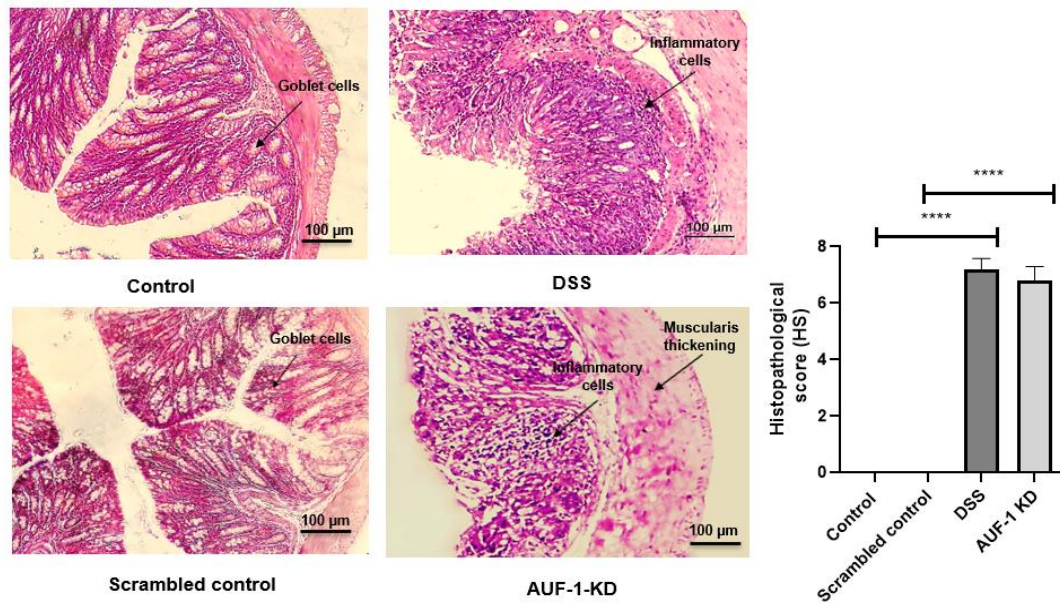


Figure 7.7: Effect of AUF-1 knockdown on colon histopathology. A microscopic examination of colonic histological of a representative animal from each group. 20X magnification is shown in Panels. Knockdown of AUF-1 revealed the thickening of muscularis layer, distortion of crypt and inflammation of inflammatory cells, similar to DSS treated colitis group. Based on these findings, histopathological score was plotted.

7.2.8 Infiltration of neutrophils as inflammatory marker in AUF-1 KD mice colon

During an inflammatory response, activated neutrophils create lysosomal proteins known as myeloperoxidases (MPOs). Accumulation of MPO is directly related to neutrophil infiltration. MPO expression has been determined as the average number of positive cells per optical field (cells/OF). A quantitative score was utilized to determine the quantity of MPO-positive cells expressed in the colon section, measuring the number of cells that have been stained by immunohistochemistry under a light microscope. The evaluation of at least 5 microscopic fields (magnification 100X) on two slides per sample (about three samples for group) resulted in scores, and analysis of inflammatory marker by observing the total number of neutrophils in high power field (under 100X magnification) revealed the high level of inflammatory cell infiltration in DSS treated and AUF-1 KD group compared to the control one. This finding further strengthens by evaluating the elevated level of CXCL1 and CXCL2 in AUF-

1 KD mice colon as CXCL1 and CXCL2 operated precisely, non-redundantly, and sequentially to direct neutrophils through venular walls as dictated by their separate cellular origins.

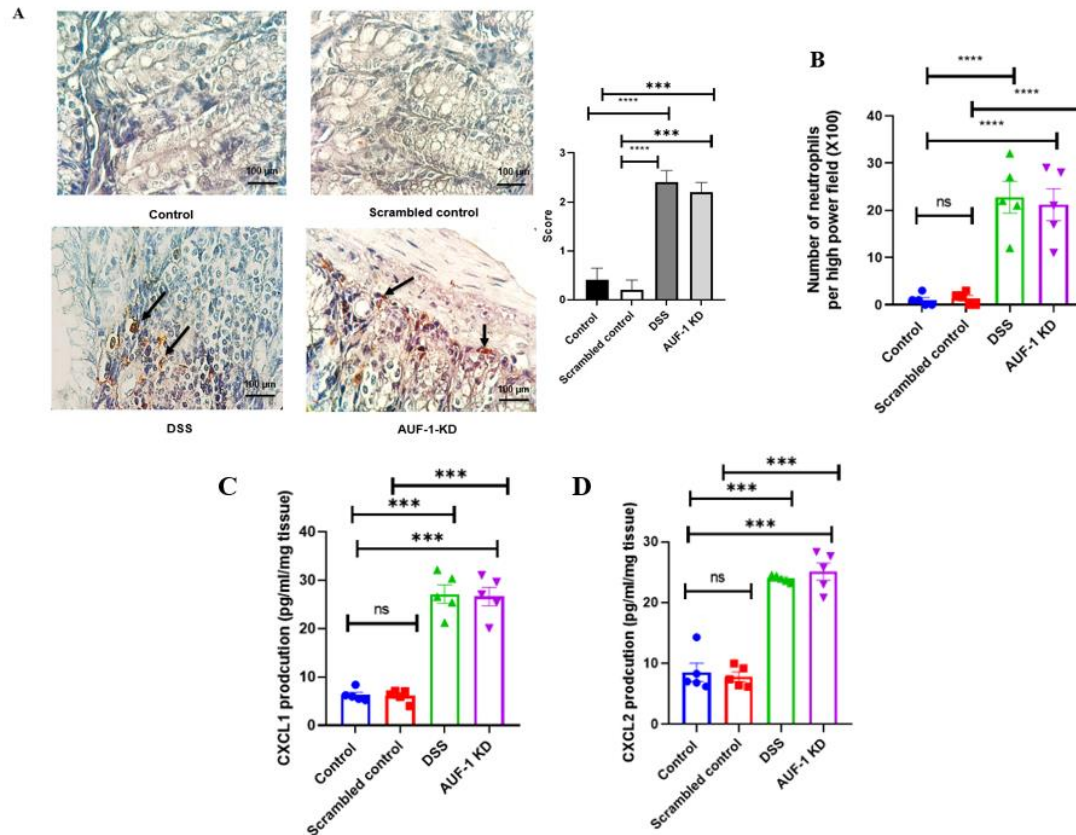


Figure 7.8: Effect of AUF-1 Knockdown in neutrophil infiltration and chemokine production. Myeloperoxidase antibody was used to stain paraffin-embedded, 10% normal buffer formalin fixed colon sections. Neutrophils and nuclei were dyed in brown and blue, respectively (magnification = 100X), and counted under high power field (A, B). CXCL1 and CXCL2 were estimated in colon sample by ELISA, which indicated the uprise of both of these two chemokines in knockdown group (C, D). The information is presented as the mean±SEM of three independent experiments (E). *** Stands for $p < 0.001$, **** stands for $p < 0.0001$

7.2.9 Evaluation of bacterial translocation determined the presence of leaky gut in AUF-KD mice

To assess the development of leaky gut, bacterial translocation was evaluated from liver, Spleen and MLN homogenate of AUF-KD mice, while the liver, Spleen, MLN homogenate obtained from DSS induced colitis group served as a positive control as this model is known to prompt the bacterial translocation. Following bacterial cultivation from the liver, Spleen as well as MLN homogenate, we discovered that the number of CFU/gm showed greater frequency in AUF 1-KD mice, specifically in liver sample, which was almost similar to the result obtained from colitis group. In summary, this result

suggested that indeed AUF-KD mice developed leaky gut, which forced the bacteria to translocate to the other organs.

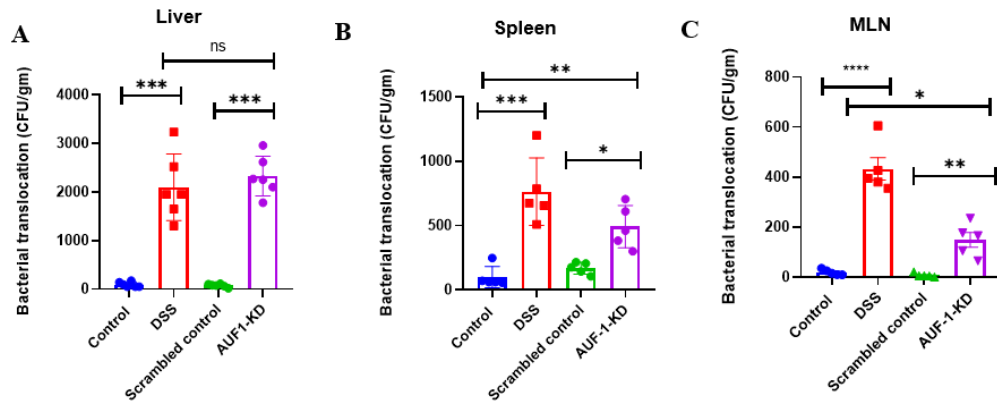


Figure 7.9: Effect of AUF-1 knock down in bacterial translocation. A quantitative investigation of translocation of bacteria to liver, spleen and MLN were demonstrated (A, B, C).

7.2.10 Expression analysis of junctional protein from colon tissue in AUF-KD mice

Occludin, claudin-1, and ZO-1 are tightly connected proteins that play key role in the maintenance of the integrity of intestinal epithelial barrier as well as permeability, while Claudin-2 is pore forming protein, which becomes upregulated when the intestinal permeability is compromised leading to the development of leaky gut. Our in vitro finding revealed that blocking of AUF-1 in HT-29 lessens the relative expression level of the tight junction proteins. In order to verify these findings, the gene as well as protein expression levels of these tight junction proteins in the colon were measured in order to assess the gut barrier function. The data revealed that relative gene expression level as well as protein profile of Occludin, Claudin-1, ZO were downregulated while uprise of Claudin-2 was observed in AUF-1-KD mice. Since DSS colitis serves as a well-developed model for leaky gut analysis, junctional proteins were also observed from the colon samples from this group. The reduction in the expression of junctional protein showed similar pattern to that of colitis mice.

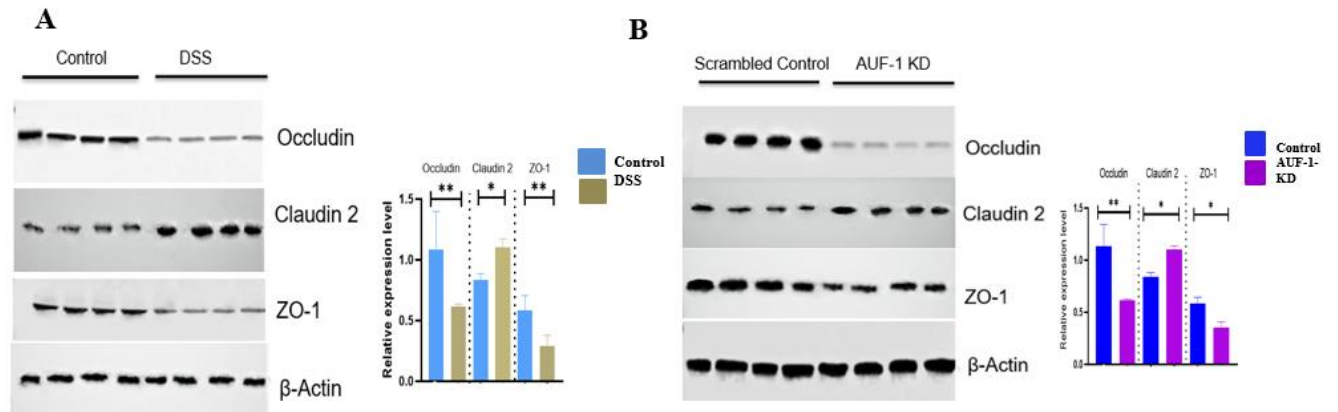


Figure 7.10: Effect of AUF-1 KD on junctional protein expression. Western blot analysis revealed decreased expression of Occludin and ZO-1 in knockdown group, similar to DSS treated group, where β -actin was used as loading control. Corresponding densitometry were also shown here. (A, B).

Results obtained from immunofluorescence study by staining of colon sections from control and AUF-1 KD group revealed that AUF-1 KD mice had low fluorescence intensity of Occludin but stronger staining of Claudin-2.

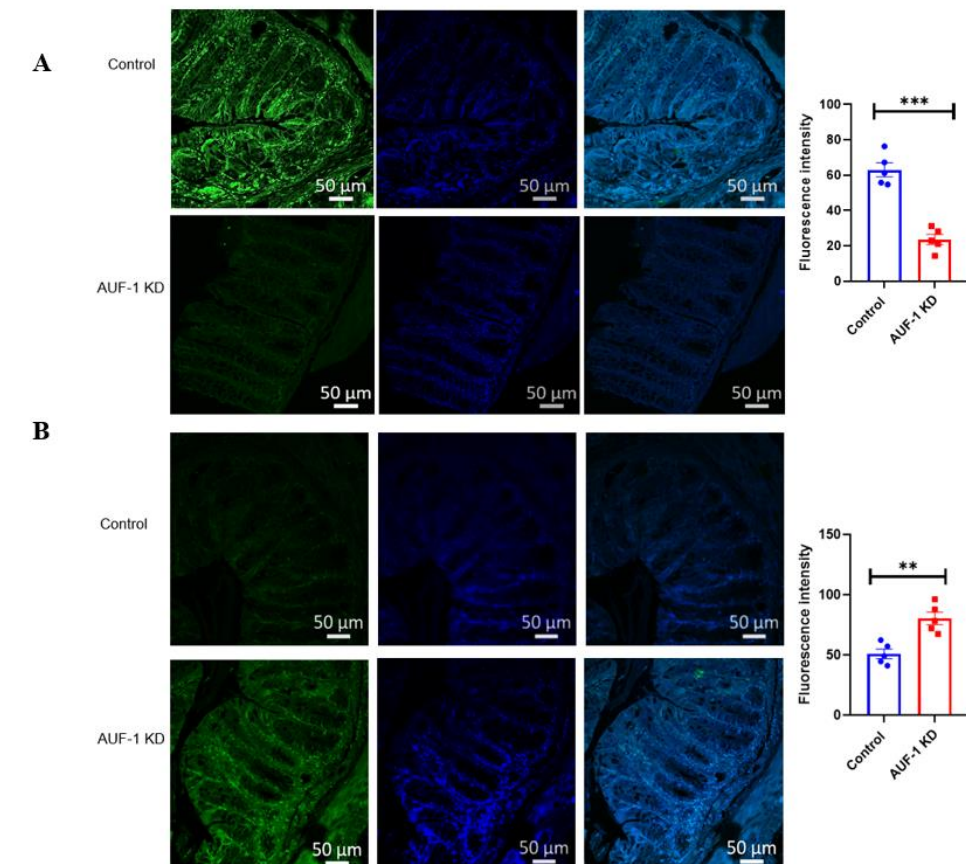


Figure 7.11: AUF-1 Knockdown showing differential expression of junctional protein. The subsequent fluorescence images are captured at 20X in a Zeiss Confocal microscope using a CCD

camera and ZEN software (Carl Zeiss, Gottingen, Germany). Immunofluorescence intensity revealed that in AUF-1 knock down group, junctional protein Occludin showed decrease in expression where Claudin-2 was increased. Corresponding fluorescence intensity was also plotted. (A, B).

7.2.11 Knockdown of AUF-1 led to alteration in pro and anti-inflammatory cytokine levels

To examine the impact of the knockdown of AUF-1 in the cytokine level of colon tissues, we determined the mRNA expression level of pro inflammatory cytokines IL-6, IL-1 β , TNF- α , IFN- γ along with anti-inflammatory cytokines TFG- β and IL-10.

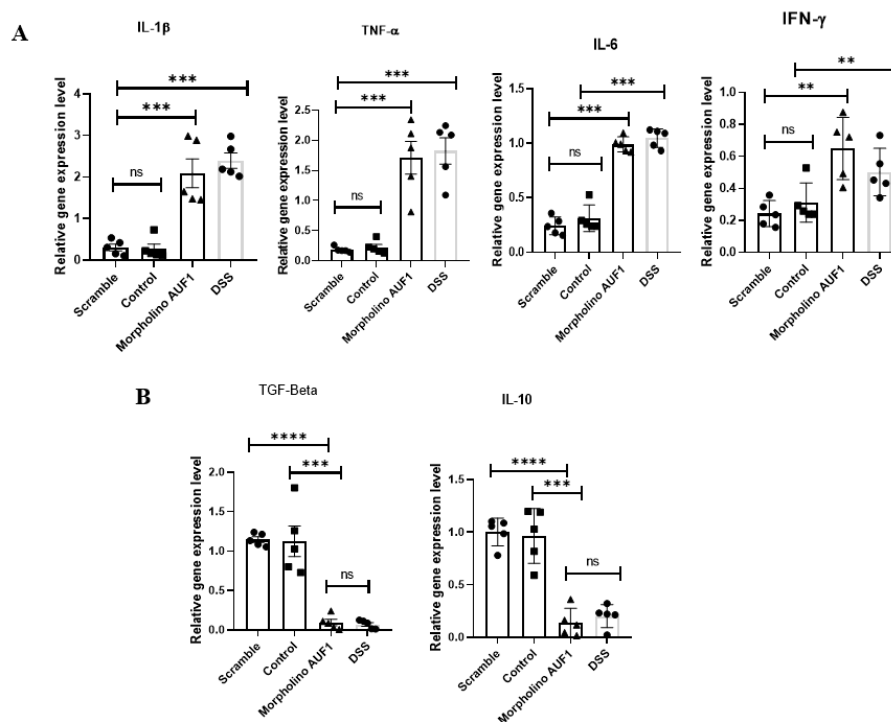


Figure 7.12: Effect of knockdown of AUF-1 on the level of pro and anti-inflammatory cytokines. qPCR was used to determine expression level of the cytokine mRNA in colon tissue (A and B). The result is presented as the mean \pm SEM of three independent experiments (E). * Stands for $p < 0.05$, ** stands for $p < 0.01$, *** represents $p < 0.001$, **** represents $p < 0.0001$, where “ns” is non-significant

7.3 Discussion

Our research has shown that AUF-1 knockdown in mice causes severe gut barrier damage and intensifies experimental colitis like symptoms. AUF-1 ensures the intestinal epithelial barrier's functionality by stabilising occluding and de stabilising Claudin-2 mRNA. Preserving the intestinal epithelial membrane along with the tight junction integrity depend on the level of sealing tight junction

proteins (Cummins, 2012; Suzuki, 2013). Changes in tight junction proteins can have serious consequences for patient care. Changes in occludin levels are linked to intestinal permeability. Occludin is a key tight junction protein that regulates paracellular permeability, which shows contrast in their function to that of Claudin-2, that act as leaky protein (Al-Sadi et al., 2011). Gut epithelium of AUF-1 knockdown mice exhibited inverse relation between Occludin and Claudin-2. Several mechanisms have been documented regarding junctional protein regulation; RBP mediated modulation is one of them (Feldman et al., 2005). Our results demonstrated that AUF-1 blockage promote the stabilisation of pore forming protein Claudin-2 by increasing its half-life, while destabilising the tight junction protein Occludin. We also found that modulation of the stability of Occludin in our experiment was dependent on the phosphorylation of p37 isoform of AUF-1, which is one of the uniqueness in this study as it determines the role of phosphorylation state in AUF-1, that drives its nature in destabilising target mRNAs. The development of diarrhea and the maintenance of inflammation in IBD are both facilitated by changes in tight junction proteins (Camilleri et al., 2012). Our AUF-1 knockdown model revealed the characteristic shortening of colon length, occult bleeding and development of leaky gut that led to bacterial translocation in other organs, as well as neutrophil infiltration at the site of severe inflammation which indicates spontaneous colitis development and the pathological features showing similarity to DSS mediated colitis mice (Yan et al., 2009; Kotla et al., 2022; Fournier & Parkos, 2012). The results revealed the importance of AUF-1 in regulating the healthy gut barrier function and on the basis of our findings, it's also important to assess if such events happen to people as their diseases worsen, which may firmly establish the role of AUF-1 in protecting the gut barrier and maintaining a healthy equilibrium between Occludin and Claudin-2.

SUMMARY

Summary

SCFA or short chain fatty acids are obtained in the gut when bacterial species metabolize resistant starches and fibers present in the diet. In the physiology of the host, SCFA is involved in energy production, lipid metabolism, gut barrier maintenance, immunomodulation, and anti-inflammatory processes. It has been well-documented that butyrate, one of the SCFA can reduce hypercholesterolemia, barrier function and reduce inflammation. In most of these processes, key enzymes or proteins are rapidly stimulated through increased activity of a number of RNA binding proteins (RBPs). Numerous investigations have demonstrated that RBPs can interact with the cis-elements found in the 3' untranslated regions (3' UTRs) of mRNAs, such as uridylate- and adenylylate-rich elements (ARE), to quickly control their levels and adjust to shifting physiological situations. Some of these proteins—such as hnRNP A1, AUF1 (hnRNP D), HuR/ELAVL1, tristetraprolin (TTP), CUGBP2, TIAR and TIA-1—promote mRNA stabilization or destabilization, which results in enhanced or decreased protein expression, accordingly. In this thesis we showed that gut microbial butyrate increases the expression of such an RBP, AUF1 (AU-rich RNA-binding factor 1). We showed that butyrate production was significantly decreased compared to control in obese mice, antibiotic treated surrogate of germ-free mice and DSS induced colitis mice. Additionally, treatment with Butyrate led to the upregulated AUF-1 which further cause instable Dicer-1, RNase-III nuclease, and notable reduction of miR122. In AUF-1-knock-down mice, we revealed the crucial role of AUF-1 and successive downstream actors. To demonstrate that butyrate acts through AUF-1, we created a special self-transfecting GMO (guanidinium-morpholino-oligonucleotides) connected PMO (phosphorodiamidate-morpholino oligonucleotides) antisense reagent. When introduced into mice, this reagent nearly eliminated AUF-1 in the liver and increased Dicer-1 and miR122. It also decreased serum cholesterol regardless of butyrate treatment. The intracellular players' roster looked like this: AUF-1-Dicer-1-miR122 for activating butyrate-induced hypocholesterolemia. As an impact of decrease in cholesterol we showed, butyrate significantly downregulates membrane cholesterol and increases the membrane fluidity by disrupting the lipid rafts. Butyrate induced lipid raft disruption inhibits enteric pathogen invasion. The association of gut microbial butyrate and raft disruption is of prime importance to explain colonization resistance to pathogenic bacteria.

AUF1 having multiple targets its knockdown in mice model caused multiple physiological changes. Having a morpholino based unique model of AUF1 knockdown in mice, we explored the effect of AUF1 in barrier function and immune function of the gut. We studied the role of AUF-1 in regulating gut inflammation in hypercholesterolemia induced by obese mice. We showed AUF-1 knockdown inhibits ROR γ t-mediated decrease in Th17 cells by destabilising ROR γ t mRNA and stabilizing FOXP3 mRNA resulting to increase in Tregcells. We also showed that AUF1 targets the tight junction proteins: occludin and claudin2 and increases the gut permeability. Interestingly we have shown p37 isoform of AUF1 targets occludin mRNA and increases its half-life. On the other hand, p40 isoform of AUF1 sits

on claudin2 mRNA, destabilizing the mRNA. Decrease in occludin and increase in claudin2 results in the increase in gut permeability in AUF1 knockdown mice. The loss of barrier function, gut inflammation, neutrophil infiltration in gut results into colitis like phenotype in AUF1 knockdown in mice.

Overall, the study deciphers the molecular events by which gut microbial-derived butyrate induced AUF-1 regulate gastrointestinal physiology by influencing cholesterol modulation, maintaining junctional protein stability, and immune functions in the gut. The thesis emphasizes on the importance of AUF1 in maintaining normal gastro intestinal physiology.

FUTURE PROSPECT

FUTURE PROSPECTS

Future commercialization potential of gut-derived butyrate presents a novel dual-purpose solution in the rapidly developing fields of metabolic health and gastrointestinal resilience. Gut-derived butyrate is a versatile substance that could be used to prevent enteric pathogen invasion in addition to its potential use as a substitute for commercially available Statin for controlling hypercholesterolemia. In addition to having cholesterol-lowering properties, this short-chain fatty acid strengthens the intestinal barrier by being produced in the intestine through the microbial fermentation of undigested fibres. By strengthening the intestinal lining, butyrate provides a strong barrier against enteric pathogen invasion, which may lower the incidence of gastrointestinal illnesses. The application of gut-derived butyrate to preventive cardiovascular and gastrointestinal concerns represents a visionary approach, providing a comprehensive strategy for health maintenance and disease prevention, as research advances and biotechnological innovations streamline the commercialization process.

The potential integration of morpholino-based therapeutics holds considerable promise in the evolving landscape of gastroenterology for tackling the multifaceted issues of leaky gut syndrome and enhancing gut immunity. Morphinos, with their unique capacity to modify gene expression, offer a tailored strategy to repairing the weakened intestinal barrier associated with leaky gut as precision medicine evolves. Morphinos have the potential to restore the barrier integrity of gut by fine-tuning the tight junction protein's expression and reducing inflammatory responses. Furthermore, by precisely modulating genes essential in immune cell function and the delicate balance of host-microbiota interactions, these synthetic compounds may play a critical role in bolstering gut immunity. While difficulties such as methods of administration remain, the future promise of morpholino-based medicines represents a significant step toward individualized treatments for individuals suffering from gut health conditions. The convergence of molecular precision with gastroenterological knowledge may pave the way for revolutionary therapies, ushering in an era where the delicate interplay between morpholinos and the gut bacteria holds the key to a healthier, more robust gastrointestinal milieu.

REFERENCE

Reference:

- Aartsma-Rus A, Krieg AM. FDA Approves Eteplirsen for Duchenne Muscular Dystrophy: The Next Chapter in the Eteplirsen Saga. *Nucleic Acid Ther.* 2017;27(1):1-3. doi:10.1089/nat.2016.0657
- Abdelmohsen K, Gorospe M. RNA-binding protein nucleolin in disease. *RNA Biol.* 2012;9(6):799-808. doi:10.4161/rna.19718
- Abdelmohsen K, Gorospe M. RNA-binding protein nucleolin in disease. *RNA Biol.* 2012;9(6):799-808. doi:10.4161/rna.19718
- Abdelmohsen K, Tominaga-Yamanaka K, Srikantan S, Yoon JH, Kang MJ, Gorospe M. RNA-binding protein AUF1 represses Dicer expression. *Nucleic Acids Res.* 2012;40(22):11531-11544. doi:10.1093/nar/gks930
- Abd-Rabo F, Elshagabee MF, Sakr SS, El-Arabi NI, Dietary fats impact on biochemical and histological parameters and gene expression of lipogenesis-related genes in rats, *Food Bioscience.* 2020; 34: 2212-4292. doi: 10.1016/j.fbio.2020.100540.
- Abes R, Moulton HM, Clair P, et al. Delivery of steric block morpholino oligomers by (R-X-R)₄ peptides: structure-activity studies. *Nucleic Acids Res.* 2008;36(20):6343-6354. doi:10.1093/nar/gkn541
- Adorni MP, Zimetti F, Billheimer JT, et al. The roles of different pathways in the release of cholesterol from macrophages. *J Lipid Res.* 2007;48(11):2453-2462. doi:10.1194/jlr.M700274- JLR200
- Agbo J, Akinyemi AR, Li D, et al. RNA-binding protein hnRNPR reduces neuronal cholesterol levels by binding to and suppressing HMGCR. *J Integr Neurosci.* 2021;20(2):265-276. doi:10.31083/j.jin2002026
- Agus A, Denizot J, Thévenot J, et al. Western diet induces a shift in microbiota composition enhancing susceptibility to Adherent-Invasive E. coli infection and intestinal inflammation. *Sci Rep.* 2016; 6:19032. Published 2016 Jan 8. doi:10.1038/srep190
- Akhtar M, Chen Y, Ma Z, et al. Gut microbiota-derived short chain fatty acids are potential mediators in gut inflammation. *Anim Nutr.* 2021; 8:350-360. Published 2021 Dec 29. doi: 10.1016/j.aninu.2021.11.005
- Al Mahri S, Malik SS, Al Ibrahim M, Haji E, Dairi G, Mohammad S. Free Fatty Acid Receptors (FFARs) in Adipose: Physiological Role and Therapeutic Outlook. *Cells.* 2022;11(4):750. Published 2022 Feb 21. doi:10.3390/cells11040750

- Al-Sadi R, Khatib K, Guo S, Ye D, Youssef M, Ma T. Occludin regulates macromolecule flux across the intestinal epithelial tight junction barrier. *Am J Physiol Gastrointest Liver Physiol*. 2011;300(6):G1054-G1064. doi:10.1152/ajpgi.00055.2011
- Altmann SW, Davis HR Jr, Zhu LJ, et al. Niemann-Pick C1 Like 1 protein is critical for intestinal cholesterol absorption. *Science*. 2004;303(5661):1201-1204. doi:10.1126/science.1093131
- Alves-Bezerra M, Cohen DE. Triglyceride Metabolism in the Liver. *Compr Physiol*. 2017;8(1):1-8. Published 2017 Dec 12. doi:10.1002/cphy.c170012
- Aman AT, Fraser S, Merritt EA, et al. A mutant cholera toxin B subunit that binds GM1- ganglioside but lacks immunomodulatory or toxic activity. *Proc Natl Acad Sci U S A*. 2001;98(15):8536-8541. doi:10.1073/pnas.161273098
- Anderson RA, Joyce C, Davis M, et al. Identification of a form of acyl-CoA:cholesterol acyltransferase specific to liver and intestine in nonhuman primates. *J Biol Chem*. 1998;273(41):26747-26754. doi:10.1074/jbc.273.41.26747
- Andoh A, Fujiyama Y, Hata K, et al. Counter-regulatory effect of sodium butyrate on tumour necrosis factor- α (TNF- α)-induced complement C3 and factor B biosynthesis in human intestinal epithelial cells. *Clin Exp Immunol*. 1999;118(1):23-29. doi:10.1046/j.1365- 2249.1999.01038.x
- Aqeel MT, Ur-Rahman N, Khan AU, et al. Antihyperlipidemic studies of newly synthesized phenolic derivatives: in silico and in vivo approaches. *Drug Des Devel Ther*. 2018; 12:2443-2453. Published 2018 Aug 9. doi:10.2147/DDDT.S158554
- Araki H, Cooper B, Blouin MS. Genetic effects of captive breeding cause a rapid, cumulative fitness decline in the wild. *Science*. 2007;318(5847):100-103. doi:10.1126/science.1145621
- Arpaia N, Campbell C, Fan X, et al. Metabolites produced by commensal bacteria promote peripheral regulatory T-cell generation. *Nature*. 2013;504(7480):451-455. doi:10.1038/nature12726
- Bachem A, Makhoulouf C, Binger KJ, et al. Microbiota-Derived Short-Chain Fatty Acids Promote the Memory Potential of Antigen-Activated CD8⁺ T Cells. *Immunity*. 2019;51(2):285-297.e5. doi:10.1016/j.immuni.2019.06.002
- Bain CC, Schridde A. Origin, Differentiation, and Function of Intestinal Macrophages. *Front Immunol*. 2018; 9:2733. Published 2018 Nov 27. doi:10.3389/fimmu.2018.02733
- Banerjee S, Ghosh J, Sen S, et al. Designing therapies against experimental visceral leishmaniasis by modulating the membrane fluidity of antigen-presenting cells. *Infect Immun*. 2009;77(6):2330-2342. doi:10.1128/IAI.00057-09

Barcelo A, Claustre J, Moro F, Chayvialle JA, Cuber JC, Plaisancié P. Mucin secretion is modulated by luminal factors in the isolated vascularly perfused rat colon. *Gut*. 2000;46(2):218-224. doi:10.1136/gut.46.2.218

Barker HA, Kahn JM, Hedrick L. Pathway of lysine degradation in *Fusobacterium nucleatum*. *J Bacteriol*. 1982;152(1):201-207. doi:10.1128/jb.152.1.201-207.1982

Barthel M, Hapfelmeier S, Quintanilla-Martínez L, et al. Pretreatment of mice with streptomycin provides a *Salmonella enterica* serovar Typhimurium colitis model that allows analysis of both pathogen and host. *Infect Immun*. 2003;71(5):2839-2858. doi:10.1128/IAI.71.5.2839-2858.2003

Basak P, Maitra P, Khan U, et al. Capsaicin Inhibits *Shigella flexneri* Intracellular Growth by Inducing Autophagy. *Front Pharmacol*. 2022; 13:903438. Published 2022 Jul 6. doi:10.3389/fphar.2022.903438

Bays HE, Tighe AP, Sadovsky R, Davidson MH. Prescription omega-3 fatty acids and their lipid effects: physiologic mechanisms of action and clinical implications. *Expert Rev Cardiovasc Ther*. 2008;6(3):391-409. doi:10.1586/14779072.6.3.391

Berding K, Donovan SM. Diet Can Impact Microbiota Composition in Children with Autism Spectrum Disorder. *Front Neurosci*. 2018; 12:515. Published 2018 Jul 31. doi:10.3389/fnins.2018.00515

Bergman EN. Energy contributions of volatile fatty acids from the gastrointestinal tract in various species. *Physiol Rev*. 1990;70(2):567-590. doi:10.1152/physrev.1990.70.2.567

Bergman EN. Energy contributions of volatile fatty acids from the gastrointestinal tract in various species. *Physiol Rev*. 1990;70(2):567-590. doi:10.1152/physrev.1990.70.2.567

Berni Canani R, Nocerino R, Terrin G, et al. Effect of *Lactobacillus GG* on tolerance acquisition in infants with cow's milk allergy: a randomized trial. *J Allergy Clin Immunol*. 2012;129(2):580-582.e5825. doi: 10.1016/j.jaci.2011.10.004

Bertoni C. Emerging gene editing strategies for Duchenne muscular dystrophy targeting stem cells. *Front Physiol*. 2014; 5:148. Published 2014 Apr 21. doi:10.3389/fphys.2014.00148

Bhadra J, Pattanayak S, Sinha S. Synthesis of Morpholino Monomers, Chlorophosphoramidate Monomers, and Solid-Phase Synthesis of Short Morpholino Oligomers. *Curr Protoc Nucleic Acid Chem*. 2015; 62:4.65.1-4.65.26. Published 2015 Sep 1. doi:10.1002/0471142700.nc0465s62

Bindels LB, Neyrinck AM, Salazar N, et al. Non-Digestible Oligosaccharides Modulate the Gut Microbiota to Control the Development of Leukemia and Associated Cachexia in Mice. *PLoS One*. 2015;10(6): e0131009. Published 2015 Jun 22. doi: 10.1371/journal.pone.0131009

Bishop KS, Xu H, Marlow G. Epigenetic Regulation of Gene Expression Induced by Butyrate in

Colorectal Cancer: Involvement of MicroRNA. *Genet Epigenet.* 2017; 9:1179237X17729900. Published 2017 Sep 25. doi:10.1177/1179237X17729900

Blaak EE, Canfora EE, Theis S, et al. short chain fatty acids in human gut and metabolic health. *Benef Microbes.* 2020;11(5):411-455. doi:10.3920/BM2020.0057

Boesze-Battaglia K. Isolation of membrane rafts and signaling complexes. *Methods Mol Biol.* 2006; 332:169-179. doi:10.1385/1-59745-048-0:167

Bourassa MW, Alim I, Bultman SJ, Ratan RR. Butyrate, neuroepigenetics and the gut microbiome: Can a high fiber diet improve brain health? *Neurosci Lett.* 2016; 625:56-63. doi:10.1016/j.neulet.2016.02.009

Brown AJ, Goldsworthy SM, Barnes AA, et al. The Orphan G protein-coupled receptors GPR41 and GPR43 are activated by propionate and other short chain carboxylic acids. *J Biol Chem.* 2003;278(13):11312-11319. doi:10.1074/jbc.M211609200

Buckel W, Barker HA. Two pathways of glutamate fermentation by anaerobic bacteria. *J Bacteriol.* 1974;117(3):1248-1260. doi:10.1128/jb.117.3.1248-1260.1974

Bukrinsky MI, Mukhamedova N, Sviridov D. Lipid rafts and pathogens: the art of deception and exploitation. *J Lipid Res.* 2020;61(5):601-610. doi:10.1194/jlr.TR119000391

Cai D, Wang J, Gao B, et al. ROR γ is a targetable master regulator of cholesterol biosynthesis in a cancer subtype. *Nat Commun.* 2019;10(1):4621. Published 2019 Oct 11. doi:10.1038/s41467-019-12529-3

Cai H, Xie X, Ji L, Ruan X, Zheng Z. Sphingosine kinase 1: A novel independent prognosis biomarker in hepatocellular carcinoma. *Oncol Lett.* 2017;13(4):2316-2322. doi:10.3892/ol.2017.5732

Caligiuri G, Rudling M, Ollivier V, et al. Interleukin-10 deficiency increases atherosclerosis, thrombosis, and low-density lipoproteins in apolipoprotein E knockout mice. *Mol Med.* 2003;9(1-2):10-17.

Camilleri M, Madsen K, Spiller R, Greenwood-Van Meerveld B, Verne GN. Intestinal barrier function in health and gastrointestinal disease [published correction appears in *Neurogastroenterol Motil.* 2012 Oct;24(10):976. Van Meerveld, B G [corrected to Greenwood-Van Meerveld, B]]. *Neurogastroenterol Motil.* 2012;24(6):503-512. doi:10.1111/j.1365-2982.2012.01921.x

Canani RB, Costanzo MD, Leone L, Pedata M, Meli R, Calignano A. Potential beneficial effects of butyrate in intestinal and extraintestinal diseases. *World J Gastroenterol.* 2011;17(12):1519-1528. doi:10.3748/wjg.v17.i12.1519

Canani RB, Costanzo MD, Leone L, Pedata M, Meli R, Calignano A. Potential beneficial effects of butyrate in intestinal and extraintestinal diseases. *World J Gastroenterol.* 2011;17(12):1519-1528. doi:10.3748/wjg.v17.i12.1519

Canfora EE, Jocken JW, Blaak EE. Short-chain fatty acids in control of body weight and insulin sensitivity. *Nat Rev Endocrinol.* 2015;11(10):577-591. doi:10.1038/nrendo.2015.128

Canfora EE, van der Beek CM, Hermes GDA, et al. Supplementation of Diet with Galactooligosaccharides Increases Bifidobacteria, but Not Insulin Sensitivity, in Obese Prediabetic Individuals. *Gastroenterology.* 2017;153(1):87-97. e3. doi: 10.1053/j.gastro.2017.03.051

Canfora EE, van der Beek CM, Hermes GDA, et al. Supplementation of Diet with Galactooligosaccharides Increases Bifidobacteria, but Not Insulin Sensitivity, in Obese Prediabetic Individuals. *Gastroenterology.* 2017;153(1):87-97. e3. doi: 10.1053/j.gastro.2017.03.051

Cardenal-Muñoz E, Gutiérrez G, Ramos-Morales F. Global impact of Salmonella type III secretion effector SteA on host cells. *Biochem Biophys Res Commun.* 2014;449(4):419-424. doi: 10.1016/j.bbrc.2014.05.056

Carretta MD, Quiroga J, López R, Hidalgo MA, Burgos RA. Participation of Short-Chain Fatty Acids and Their Receptors in Gut Inflammation and Colon Cancer. *Front Physiol.* 2021; 12:662739. Published 2021 Apr 8. doi:10.3389/fphys.2021.662739

Caruana JC, Walper SA. Bacterial Membrane Vesicles as Mediators of Microbe - Microbe and Microbe - Host Community Interactions. *Front Microbiol.* 2020; 11:432. Published 2020 Mar 24. doi:10.3389/fmicb.2020.00432

Catron DM, Lange Y, Borensztajn J, Sylvester MD, Jones BD, Haldar K. Salmonella enterica serovar Typhimurium requires nonsterol precursors of the cholesterol biosynthetic pathway for intracellular proliferation. *Infect Immun.* 2004;72(2):1036-1042. doi:10.1128/IAI.72.2.1036-1042.2004

Catron DM, Sylvester MD, Lange Y, et al. The Salmonella-containing vacuole is a major site of intracellular cholesterol accumulation and recruits the GPI-anchored protein CD55. *Cell Microbiol.* 2002;4(6):315-328. doi:10.1046/j.1462-5822.2002.00198.x

Chakraborty D, Banerjee S, Sen A, Banerjee KK, Das P, Roy S. Leishmania donovani affects antigen presentation of macrophage by disrupting lipid rafts. *J Immunol.* 2005;175(5):3214-3224. doi:10.4049/jimmunol.175.5.3214

Chakraborty M, Gautam A, Das O, Masid A, Bhaumik M. Prenatal arsenic exposure stymies gut butyrate production and enhances gut permeability in post-natal life even in absence of arsenic dectly through miR122-Occludin pathway. *Toxicol Lett.* 2023; 374:19-30. doi: 10.1016/j.toxlet.2022.11.011

Chambers ES, Byrne CS, Aspey K, et al. Acute oral sodium propionate supplementation raises resting

energy expenditure and lipid oxidation in fasted humans. *Diabetes Obes Metab.* 2018;20(4):1034-1039. doi:10.1111/dom.13159

Chambers ES, Preston T, Frost G, Morrison DJ. Role of Gut Microbiota-Generated Short-Chain Fatty Acids in Metabolic and Cardiovascular Health. *Curr Nutr Rep.* 2018;7(4):198-206. doi:10.1007/s13668-018-0248-8

Chang J, Nicolas E, Marks D, et al. miR-122, a mammalian liver-specific microRNA, is processed from hcr mRNA and may downregulate the high affinity cationic amino acid transporter CAT-1. *RNA Biol.* 2004;1(2):106-113. doi:10.4161/rna.1.2.1066

Chang MH, Chou JW, Chen SM, et al. Faecal calprotectin as a novel biomarker for differentiating between inflammatory bowel disease and irritable bowel syndrome. *Mol Med Rep.* 2014;10(1):522-526. doi:10.3892/mmr.2014.2180

Charney AN, Micic L, Egnor RW. Nonionic diffusion of short-chain fatty acids across rat colon. *Am J Physiol.* 1998;274(3): G518-G524. doi:10.1152/ajpgi.1998.274.3. G518

Chartoumpekis DV, Palliyaguru DL, Wakabayashi N, et al. Nrf2 deletion from adipocytes, but not hepatocytes, potentiates systemic metabolic dysfunction after long-term high-fat diet-induced obesity in mice. *Am J Physiol Endocrinol Metab.* 2018;315(2):E180-E195. doi:10.1152/ajpendo.00311.2017

Cheloufi S, Dos Santos CO, Chong MM, Hannon GJ. A dicer-independent miRNA biogenesis pathway that requires Ago catalysis. *Nature.* 2010;465(7298):584-589. doi:10.1038/nature09092

Chen D, Jin D, Huang S, et al. *Clostridium butyricum*, a butyrate-producing probiotic, inhibits intestinal tumor development through modulating Wnt signaling and gut microbiota. *Cancer Lett.* 2020; 469:456-467. doi: 10.1016/j.canlet.2019.11.019

Chen KJ, Jin RM, Shi CC, et al. The prognostic value of Niemann-Pick C1-like protein 1 and Niemann-Pick disease type C2 in hepatocellular carcinoma. *J Cancer.* 2018;9(3):556-563. Published 2018 Jan 1. doi:10.7150/jca.19996

Cheng K, Brunius C, Fristedt R, Landberg R. An LC-QToF MS based method for untargeted metabolomics of human fecal samples. *Metabolomics.* 2020;16(4):46. Published 2020 Apr 3. doi:10.1007/s11306-020-01669-z

Chooi YC, Ding C, Magkos F. The epidemiology of obesity. *Metabolism.* 2019; 92:6-10. doi: 10.1016/j.metabol.2018.09.005

Chow J, Tang H, Mazmanian SK. Pathobionts of the gastrointestinal microbiota and inflammatory disease. *Curr Opin Immunol.* 2011;23(4):473-480. doi: 10.1016/j.coi.2011.07.010

Coburn B, Sekirov I, Finlay BB. Type III secretion systems and disease. *Clin Microbiol Rev.*

- 2007;20(4):535-549. doi:10.1128/CMR.00013-07
- Coburn B, Sekirov I, Finlay BB. Type III secretion systems and disease. *Clin Microbiol Rev.* 2007;20(4):535-549. doi:10.1128/CMR.00013-07
- Collado MC, Isolauri E, Salminen S, Sanz Y. The impact of probiotic on gut health. *Curr Drug Metab.* 2009;10(1):68-78. doi:10.2174/138920009787048437
- Cong J, Zhou P, Zhang R. Intestinal Microbiota-Derived Short Chain Fatty Acids in Host Health and Disease. *Nutrients.* 2022;14(9):1977. Published 2022 May 9. doi:10.3390/nu14091977
- Conlon MA, Bird AR. The impact of diet and lifestyle on gut microbiota and human health. *Nutrients.* 2014;7(1):17-44. Published 2014 Dec 24. doi:10.3390/nu7010017
- Contreras-Dávila CA, Carrión VJ, Vonk VR, Buisman CNJ, Strik DPBTB. Consecutive lactate formation and chain elongation to reduce exogenous chemicals input in repeated-batch food waste fermentation. *Water Res.* 2020; 169:115215. doi: 10.1016/j.watres.2019.115215
- Corey DR, Abrams JM. Morpholino antisense oligonucleotides: tools for investigating vertebrate development. *Genome Biol.* 2001;2(5): REVIEWS1015. doi:10.1186/gb-2001-2-5-reviews1015
- Cummings JH, Pomare EW, Branch WJ, Naylor CP, Macfarlane GT. Short chain fatty acids in human large intestine, portal, hepatic and venous blood. *Gut.* 1987;28(10):1221-1227. doi:10.1136/gut.28.10.1221
- Cummings JH, Pomare EW, Branch WJ, Naylor CP, Macfarlane GT. Short chain fatty acids in human large intestine, portal, hepatic and venous blood. *Gut.* 1987;28(10):1221-1227. doi:10.1136/gut.28.10.1221
- Cummins PM. Occludin: one protein, many forms. *Mol Cell Biol.* 2012;32(2):242-250. doi:10.1128/MCB.06029-11
- Dai W, Mu L, Cui Y, et al. Berberine Promotes Apoptosis of Colorectal Cancer via Regulation of the Long Non-Coding RNA (lncRNA) Cancer Susceptibility Candidate 2 (CASC2)/AU-Binding Factor 1 (AUF1)/B-Cell CLL/Lymphoma 2 (Bcl-2) Axis. *Med Sci Monit.* 2019; 25:730-738. Published 2019 Jan 25. doi:10.12659/MSM.912082
- Dai W, Mu L, Cui Y, et al. Berberine Promotes Apoptosis of Colorectal Cancer via Regulation of the Long Non-Coding RNA (lncRNA) Cancer Susceptibility Candidate 2 (CASC2)/AU-Binding Factor 1 (AUF1)/B-Cell CLL/Lymphoma 2 (Bcl-2) Axis. *Med Sci Monit.* 2019; 25:730-738. Published 2019 Jan 25. doi:10.12659/MSM.912082
- Dalile B, Van Oudenhove L, Vervliet B, Verbeke K. The role of short-chain fatty acids in microbiota-gut-brain communication. *Nat Rev Gastroenterol Hepatol.* 2019;16(8):461-478. doi:10.1038/s41575-019-0157-3

Das O, Kundu J, Ghosh A, et al. AUF-1 knockdown in mice undermines gut microbial butyrate-driven hypocholesterolemia through AUF-1-Dicer-1-mir-122 hierarchy. *Front Cell Infect Microbiol.* 2022; 12:1011386. Published 2022 Dec 19. doi:10.3389/fcimb.2022.1011386

Davie JR. Inhibition of histone deacetylase activity by butyrate. *J Nutr.* 2003;133(7 Suppl):2485S-2493S. doi:10.1093/jn/133.7.2485S

Day CA, Kenworthy AK. Functions of cholera toxin B-subunit as a raft cross-linker. *Essays Biochem.* 2015; 57:135-145. doi:10.1042/bse0570135

De Vadder F, Kovatcheva-Datchary P, Goncalves D, et al. Microbiota-generated metabolites promote metabolic benefits via gut-brain neural circuits. *Cell.* 2014;156(1-2):84-96. doi: 10.1016/j.cell.2013.12.016

DeBose-Boyd RA, Ye J. SREBPs in Lipid Metabolism, Insulin Signaling, and Beyond. *Trends Biochem Sci.* 2018;43(5):358-368. doi: 10.1016/j.tibs.2018.01.005

den Besten G, Bleeker A, Gerding A, et al. Short-Chain Fatty Acids Protect Against High-Fat Diet-Induced Obesity via a PPAR γ -Dependent Switch from Lipogenesis to Fat Oxidation. *Diabetes.* 2015;64(7):2398-2408. doi:10.2337/db14-1213

den Besten G, Bleeker A, Gerding A, et al. Short-Chain Fatty Acids Protect Against High-Fat Diet-Induced Obesity via a PPAR γ -Dependent Switch from Lipogenesis to Fat Oxidation. *Diabetes.* 2015;64(7):2398-2408. doi:10.2337/db14-1213

den Besten G, van Eunen K, Groen AK, Venema K, Reijngoud DJ, Bakker BM. The role of short-chain fatty acids in the interplay between diet, gut microbiota, and host energy metabolism. *J Lipid Res.* 2013;54(9):2325-2340. doi:10.1194/jlr.R036012

den Besten G, van Eunen K, Groen AK, Venema K, Reijngoud DJ, Bakker BM. The role of short-chain fatty acids in the interplay between diet, gut microbiota, and host energy metabolism. *J Lipid Res.* 2013;54(9):2325-2340. doi:10.1194/jlr.R036012

den Besten G, van Eunen K, Groen AK, Venema K, Reijngoud DJ, Bakker BM. The role of short-chain fatty acids in the interplay between diet, gut microbiota, and host energy metabolism. *J Lipid Res.* 2013;54(9):2325-2340. doi:10.1194/jlr.R036012

Denli AM, Tops BB, Plasterk RH, Ketting RF, Hannon GJ. Processing of primary microRNAs by the Microprocessor complex. *Nature.* 2004;432(7014):231-235. doi:10.1038/nature03049

Dey I, Bishayi B. Role of Th17 and Treg cells in septic arthritis and the impact of the Th17/Treg - derived cytokines in the pathogenesis of *S. aureus* induced septic arthritis in mice. *Microb Pathog.* 2017; 113:248-264. doi: 10.1016/j.micpath.2017.10.033

Donatello S, Babina IS, Hazelwood LD, Hill AD, Nabi IR, Hopkins AM. Lipid raft association

restricts CD44-ezrin interaction and promotion of breast cancer cell migration. *Am J Pathol.* 2012;181(6):2172-2187. doi: 10.1016/j.ajpath.2012.08.025

Donatello S, Babina IS, Hazelwood LD, Hill AD, Nabi IR, Hopkins AM. Lipid raft association restricts CD44-ezrin interaction and promotion of breast cancer cell migration. *Am J Pathol.* 2012;181(6):2172-2187. doi: 10.1016/j.ajpath.2012.08.025

Dong Y, Li X, Liu Y, Gao J, Tao J. The molecular targets of taurine confer anti-hyperlipidemic effects. *Life Sci.* 2021; 278:119579. doi: 10.1016/j.lfs.2021.119579

Donohoe DR, Collins LB, Wali A, Bigler R, Sun W, Bultman SJ. The Warburg effect dictates the mechanism of butyrate-mediated histone acetylation and cell proliferation. *Mol Cell.* 2012;48(4):612-626. doi: 10.1016/j.molcel.2012.08.033

Donohoe DR, Garge N, Zhang X, et al. The microbiome and butyrate regulate energy metabolism and autophagy in the mammalian colon. *Cell Metab.* 2011;13(5):517-526. doi: 10.1016/j.cmet.2011.02.018

Dou X, Gao N, Yan D, Shan A. Sodium Butyrate Alleviates Mouse Colitis by Regulating Gut Microbiota Dysbiosis. *Animals (Basel).* 2020;10(7):1154. Published 2020 Jul 7. doi:10.3390/ani10071154

Du Y, Li X, Su C, et al. Butyrate protects against high-fat diet-induced atherosclerosis via up-regulating ABCA1 expression in apolipoprotein E-deficiency mice. *Br J Pharmacol.* 2020;177(8):1754-1772. doi:10.1111/bph.14933

Du Y, Li X, Su C, et al. Butyrate protects against high-fat diet-induced atherosclerosis via up-regulating ABCA1 expression in apolipoprotein E-deficiency mice. *Br J Pharmacol.* 2020;177(8):1754-1772. doi:10.1111/bph.14933

Dubreuil JD, Isaacson RE, Schifferli DM. Animal Enterotoxigenic *Escherichia coli*. *EcoSal Plus.* 2016;7(1): 10.1128/ecosalplus.ESP-0006-2016. doi: 10.1128/ecosalplus.ESP-0006-2016

Ducarmon QR, Zwartink RD, Hornung BVH, van Schaik W, Young VB, Kuijper EJ. Gut Microbiota and Colonization Resistance against Bacterial Enteric Infection. *Microbiol Mol Biol Rev.* 2019;83(3): e00007-19. Published 2019 Jun 5. doi:10.1128/MMBR.00007-19

Duncan MJ, Shin JS, Abraham SN. Microbial entry through caveolae: variations on a theme. *Cell Microbiol.* 2002;4(12):783-791. doi:10.1046/j.1462-5822.2002.00230.x

Eichele DD, Kharbanda KK. Dextran sodium sulfate colitis murine model: An indispensable tool for advancing our understanding of inflammatory bowel diseases pathogenesis. *World J Gastroenterol.* 2017;23(33):6016-6029. doi:10.3748/wjg.v23.i33.6016

- Eid N, Ito Y, Maemura K, Otsuki Y. Elevated autophagic sequestration of mitochondria and lipid droplets in steatotic hepatocytes of chronic ethanol-treated rats: an immunohistochemical and electron microscopic study. *J Mol Histol.* 2013;44(3):311-326. doi:10.1007/s10735-013-9483-x
- Elamin EE, Masclee AA, Dekker J, Pieters HJ, Jonkers DM. Short-chain fatty acids activate AMP-activated protein kinase and ameliorate ethanol-induced intestinal barrier dysfunction in Caco-2 cell monolayers. *J Nutr.* 2013;143(12):1872-1881. doi:10.3945/jn.113.179549
- Elce A, Amato F, Zarrilli F, et al. Butyrate modulating effects on pro-inflammatory pathways in human intestinal epithelial cells. *Benef Microbes.* 2017;8(5):841-847. doi:10.3920/BM2016.0197
- Enokizono Y, Konishi Y, Nagata K, et al. Structure of hnRNP D complexed with single-stranded telomere DNA and unfolding of the quadruplex by heterogeneous nuclear ribonucleoprotein D. *J Biol Chem.* 2005;280(19):18862-18870. doi:10.1074/jbc.M411822200
- Esau C, Davis S, Murray SF, et al. miR-122 regulation of lipid metabolism revealed by in vivo antisense targeting. *Cell Metab.* 2006;3(2):87-98. doi: 10.1016/j.cmet.2006.01.005
- Espenshade PJ, Hughes AL. Regulation of sterol synthesis in eukaryotes. *Annu Rev Genet.* 2007;41:401-427. doi:10.1146/annurev.genet.41.110306.130315
- Espenshade PJ, Hughes AL. Regulation of sterol synthesis in eukaryotes. *Annu Rev Genet.* 2007; 41:401-427. doi: 10.1146/annurev.genet.41.110306.130315
- Favari E, Calabresi L, Adorni MP, et al. Small discoidal pre-beta1 HDL particles are efficient acceptors of cell cholesterol via ABCA1 and ABCG1. *Biochemistry.* 2009;48(46):11067-11074. doi:10.1021/bi901564g
- Federici C, Detzel P, Petracca F, Dainelli L, Fattore G. The impact of food reformulation on nutrient intakes and health, a systematic review of modelling studies [published correction appears in *BMC Nutr.* 2019 Feb 4; 5:9]. *BMC Nutr.* 2019; 5:2. Published 2019 Jan 7. doi:10.1186/s40795-018-0263-6
- Feher MD. Lipid lowering to delay the progression of coronary artery disease. *Heart.* 2003;89(4):451-458. doi:10.1136/heart.89.4.451
- Feldman GJ, Mullin JM, Ryan MP. Occludin: structure, function and regulation. *Adv Drug Deliv Rev.* 2005;57(6):883-917. doi: 10.1016/j.addr.2005.01.009
- Fettel J, Kühn B, Guillen NA, et al. Sphingosine-1-phosphate (S1P) induces potent anti-inflammatory effects in vitro and in vivo by S1P receptor 4-mediated suppression of 5-lipoxygenase activity. *FASEB J.* 2019;33(2):1711-1726. doi:10.1096/fj.201800221R
- Field FJ, Kam NT, Mathur SN. Regulation of cholesterol metabolism in the intestine. *Gastroenterology.* 1990;99(2):539-551. doi:10.1016/0016-5085(90)91040-d Feingold KR, & Grunfeld

C.Introduction to Lipids and Lipoproteins 2015.

Fielding RM, Moon-McDermott L, Lewis RO, Horner MJ. Pharmacokinetics and urinary excretion of amikacin in low-clearance unilamellar liposomes after a single or repeated intravenous administration in the rhesus monkey. *Antimicrob Agents Chemother.* 1999;43(3):503-509. doi:10.1128/AAC.43.3.503

Flock T, Hauser AS, Lund N, Gloriam DE, Balaji S, Babu MM. Selectivity determinants of GPCR-G-protein binding. *Nature.* 2017;545(7654):317-322. doi:10.1038/nature22070

Fournier BM, Parkos CA. The role of neutrophils during intestinal inflammation. *Mucosal Immunol.* 2012;5(4):354-366. doi:10.1038/mi.2012.24

Frank DN, St Amand AL, Feldman RA, Boedeker EC, Harpaz N, Pace NR. Molecular-phylogenetic characterization of microbial community imbalances in human inflammatory bowel diseases. *Proc Natl Acad Sci U S A.* 2007;104(34):13780-13785. doi:10.1073/pnas.0706625104

Fukuhara T, Kambara H, Shiokawa M, et al. Expression of microRNA miR-122 facilitates an efficient replication in nonhepatic cells upon infection with hepatitis C virus. *J Virol.* 2012;86(15):7918-7933. doi:10.1128/JVI.00567-12

Furusawa Y, Obata Y, Fukuda S, et al. Commensal microbe-derived butyrate induces the differentiation of colonic regulatory T cells [published correction appears in *Nature.* 2014 Feb 13;506(7487):254]. *Nature.* 2013;504(7480):446-450. doi:10.1038/nature12721

Furuse M, Hirase T, Itoh M, et al. Occludin: a novel integral membrane protein localizing at tight junctions. *J Cell Biol.* 1993;123(6 Pt 2):1777-1788. doi:10.1083/jcb.123.6.1777

Furuse M. Molecular basis of the core structure of tight junctions. *Cold Spring Harb Perspect Biol.* 2010;2(1):a002907. doi:10.1101/cshperspect. a002907

Gabizon A, Papahadjopoulos D. Liposome formulations with prolonged circulation time in blood and enhanced uptake by tumors. *Proc Natl Acad Sci U S A.* 1988;85(18):6949-6953. doi:10.1073/pnas.85.18.6949

Ganapathy V, Thangaraju M, Prasad PD, Martin PM, Singh N. Transporters and receptors for short-chain fatty acids as the molecular link between colonic bacteria and the host. *Curr Opin Pharmacol.* 2013;13(6):869-874. doi: 10.1016/j.coph.2013.08.006

Garcia-Gutierrez E, Mayer MJ, Cotter PD, Narbad A. Gut microbiota as a source of novel antimicrobials. *Gut Microbes.* 2019;10(1):1-21. doi:10.1080/19490976.2018.1455790

Gasaly N, de Vos P, Hermoso MA. Impact of Bacterial Metabolites on Gut Barrier Function and Host

Immunity: A Focus on Bacterial Metabolism and Its Relevance for Intestinal Inflammation. *Front Immunol.* 2021; 12:658354. Published 2021 May 26. doi:10.3389/fimmu.2021.658354

Gatfield D, Le Martelot G, Vejnar CE, et al. Integration of microRNA miR-122 in hepatic circadian gene expression. *Genes Dev.* 2009;23(11):1313-1326. doi:10.1101/gad.1781009

Gerin I, Clerbaux LA, Haumont O, et al. Expression of miR-33 from an SREBP2 intron inhibits cholesterol export and fatty acid oxidation. *J Biol Chem.* 2010;285(44):33652-33661. doi:10.1074/jbc.M110.152090

Gerin I, Clerbaux LA, Haumont O, et al. Expression of miR-33 from an SREBP2 intron inhibits cholesterol export and fatty acid oxidation. *J Biol Chem.* 2010;285(44):33652-33661. doi:10.1074/jbc.M110.152090

Ghosh J, Bose M, Roy S, Bhattacharyya SN. Leishmania donovani targets Dicer1 to downregulate miR-122, lower serum cholesterol, and facilitate murine liver infection. *Cell Host Microbe.* 2013;13(3):277-288. doi: 10.1016/j.chom.2013.02.005

Ghosh J, Bose M, Roy S, Bhattacharyya SN. Leishmania donovani targets Dicer1 to downregulate miR-122, lower serum cholesterol, and facilitate murine liver infection. *Cell Host Microbe.* 2013;13(3):277-288. doi: 10.1016/j.chom.2013.02.005

Girard M, Jacquemin E, Munnich A, Lyonnet S, Henrion-Caude A. miR-122, a paradigm for the role of microRNAs in the liver. *J Hepatol.* 2008;48(4):648-656. doi: 10.1016/j.jhep.2008.01.019

Goedeke L, Rotllan N, Canfrán-Duque A, et al. MicroRNA-148a regulates LDL receptor and ABCA1 expression to control circulating lipoprotein levels. *Nat Med.* 2015;21(11):1280-1289. doi:10.1038/nm.3949

Golomb BA, Evans MA. Statin adverse effects: a review of the literature and evidence for a mitochondrial mechanism. *Am J Cardiovasc Drugs.* 2008;8(6):373-418. doi:10.2165/0129784-200808060-00004

Gonçalves LA, Vigário AM, Penha-Gonçalves C. Improved isolation of murine hepatocytes for in vitro malaria liver stage studies. *Malar J.* 2007; 6:169. Published 2007 Dec 20. doi:10.1186/1475-2875-6-169

Gräler MH. The role of sphingosine 1-phosphate in immunity and sepsis. *Am J Clin Exp Immunol.* 2012;1(2):90-100. Published 2012 Sep 27

Gratacós FM, Brewer G. The role of AUF1 in regulated mRNA decay. *Wiley Interdiscip Rev RNA.* 2010;1(3):457-473. doi:10.1002/wrna.26

Gregory AL, Pensinger DA, Hryckowian AJ. A short chain fatty acid-centric view of Clostridioides

difficile pathogenesis. *PLoS Pathog.* 2021;17(10):e1009959. Published 2021 Oct 21. doi:10.1371/journal.ppat.1009959

Grześkowiak ŁM, Pieper R, Huynh HA, Cutting SM, Vahjen W, Zentek J. Impact of early-life events on the susceptibility to *Clostridium difficile* colonisation and infection in the offspring of the pig. *Gut Microbes.* 2019;10(2):251-259. doi:10.1080/19490976.2018.1518554

Grzymajlo K. The Game for Three: Salmonella-Host-Microbiota Interaction Models. *Front Microbiol.* 2022; 13:854112. Published 2022 Apr 18. doi:10.3389/fmicb.2022.854112

Guignot J, Tran Van Nhieu G. Bacterial Control of Pores Induced by the Type III Secretion System: Mind the Gap. *Front Immunol.* 2016; 7:84. Published 2016 Mar 9. doi:10.3389/fimmu.2016.00084

Günzel D, Yu AS. Claudins and the modulation of tight junction permeability. *Physiol Rev.* 2013;93(2):525-569. doi:10.1152/physrev.00019.2012

Hague A, Manning AM, Hanlon KA, Huschtscha LI, Hart D, Paraskeva C. Sodium butyrate induces apoptosis in human colonic tumour cell lines in a p53-independent pathway: implications for the possible role of dietary fibre in the prevention of large-bowel cancer. *Int J Cancer.* 1993;55(3):498-505. doi:10.1002/ijc.2910550329

Han D, Gao X, Wang M, et al. Long noncoding RNA H19 indicates a poor prognosis of colorectal cancer and promotes tumor growth by recruiting and binding to eIF4A3. *Oncotarget.* 2016;7(16):22159-22173. doi:10.18632/oncotarget.8063

Han H, Chen Y, Cheng L, Prochownik EV, Li Y. microRNA-206 impairs c-Myc-driven cancer in a synthetic lethal manner by directly inhibiting MAP3K13. *Oncotarget.* 2016;7(13):16409-16419. doi:10.18632/oncotarget.7653

Han W, Huang C, Zhang Q, et al. Alterations in gut microbiota and elevated serum bilirubin in primary biliary cholangitis patients treated with ursodeoxycholic acid. *Eur J Clin Invest.* 2022;52(2):e13714. doi:10.1111/eci.13714

Hara H, Haga S, Aoyama Y, Kiriya S. Short-chain fatty acids suppress cholesterol synthesis in rat liver and intestine. *J Nutr.* 1999;129(5):942-948. doi:10.1093/jn/129.5.942

Hara H, Haga S, Aoyama Y, Kiriya S. Short-chain fatty acids suppress cholesterol synthesis in rat liver and intestine. *J Nutr.* 1999;129(5):942-948. doi:10.1093/jn/129.5.942

Harris FM, Best KB, Bell JD. Use of laurdan fluorescence intensity and polarization to distinguish between changes in membrane fluidity and phospholipid order. *Biochim Biophys Acta.* 2002;1565(1):123-128. doi:10.1016/s0005-2736(02)00514-x

He J, Zhang P, Shen L, et al. Short-Chain Fatty Acids and Their Association with Signalling Pathways

in Inflammation, Glucose and Lipid Metabolism. *Int J Mol Sci.* 2020;21(17):6356. Published 2020 Sep 2. doi:10.3390/ijms21176356

He P, Gelissen IC, Ammit AJ. Regulation of ATP binding cassette transporter A1 (ABCA1) expression: cholesterol-dependent and - independent signaling pathways with relevance to inflammatory lung disease. *Respir Res.* 2020;21(1):250. Published 2020 Sep 25. doi:10.1186/s12931-020-01515-9

He Q, Shi Y, Xing H, et al. Modulating effect of Xuanfei Baidu granule on host metabolism and gut microbiome in rats. *Front Pharmacol.* 2022; 13:922642. Published 2022 Sep 6. doi:10.3389/fphar.2022.922642

Hedl M, Tabernero L, Stauffacher CV, Rodwell VW. Class II 3-hydroxy-3-methylglutaryl coenzyme A reductases. *J Bacteriol.* 2004;186(7):1927-1932. doi:10.1128/JB.186.7.1927-1932.2004

Hendrickson BA, Gokhale R, Cho JH. Clinical aspects and pathophysiology of inflammatory bowel disease. *Clin Microbiol Rev.* 2002;15(1):79-94. doi:10.1128/CMR.15.1.79-94.2002

Hendrickson BA, Gokhale R, Cho JH. Clinical aspects and pathophysiology of inflammatory bowel disease. *Clin Microbiol Rev.* 2002;15(1):79-94. doi:10.1128/CMR.15.1.79-94.2002

Hentges DJ, Maier BR. Inhibition of *Shigella flexneri* by the Normal Intestinal Flora III. Interactions with *Bacteroides fragilis* Strains in Vitro. *Infect Immun.* 1970;2(4):364-370. doi:10.1128/iai.2.4.364-370.1970

Hinnebusch BF, Meng S, Wu JT, Archer SY, Hodin RA. The effects of short-chain fatty acids on human colon cancer cell phenotype are associated with histone hyperacetylation. *J Nutr.* 2002;132(5):1012-1017. doi:10.1093/jn/132.5.1012

Horie M, Honda T, Suzuki Y, et al. Endogenous non-retroviral RNA virus elements in mammalian genomes. *Nature.* 2010;463(7277):84-87. doi:10.1038/nature08695

Hsu CY, Yeh JY, Chen CY, et al. *Helicobacter pylori* cholesterol- α -glucosyltransferase manipulates cholesterol for bacterial adherence to gastric epithelial cells. *Virulence.* 2021;12(1):2341-2351. doi:10.1080/21505594.2021.1969171

Hu X, Wang T, Liang S, Li W, Wu X, Jin F. Antibiotic-induced imbalances in gut microbiota aggravates cholesterol accumulation and liver injuries in rats fed a high-cholesterol diet. *Appl Microbiol Biotechnol.* 2015;99(21):9111-9122. doi:10.1007/s00253-015-6753-4

Hu Z, Chen X, Zhao Y, et al. Serum microRNA signatures identified in a genome-wide serum microRNA expression profiling predict survival of non-small-cell lung cancer. *J Clin Oncol.* 2010;28(10):1721-1726. doi:10.1200/JCO.2009.24.9342

- Huang B, Song BL, Xu C. Cholesterol metabolism in cancer: mechanisms and therapeutic opportunities. *Nat Metab.* 2020;2(2):132-141. doi:10.1038/s42255-020-0174-0
- Hutvagner G, McLachlan J, Pasquinelli AE, Bálint E, Tuschl T, Zamore PD. A cellular function for the RNA-interference enzyme Dicer in the maturation of the let-7 small temporal RNA. *Science.* 2001;293(5531):834-838. doi:10.1126/science.1062961
- Ichiyama K, Yoshida H, Wakabayashi Y, et al. Foxp3 inhibits RORgammat-mediated IL-17A mRNA transcription through direct interaction with RORgammat. *J Biol Chem.* 2008;283(25):17003-17008. doi:10.1074/jbc.M801286200
- Ikonen E. Mechanisms for cellular cholesterol transport: defects and human disease. *Physiol Rev.* 2006;86(4):1237-1261. doi:10.1152/physrev.00022.2005
- Iliopoulos D, Jaeger SA, Hirsch HA, Bulyk ML, Struhl K. STAT3 activation of miR-21 and miR-181b-1 via PTEN and CYLD are part of the epigenetic switch linking inflammation to cancer. *Mol Cell.* 2010;39(4):493-506. doi: 10.1016/j.molcel.2010.07.023
- Isono A, Katsuno T, Sato T, et al. Clostridium butyricum TO-A culture supernatant downregulates TLR4 in human colonic epithelial cells. *Dig Dis Sci.* 2007;52(11):2963-2971. doi:10.1007/s10620-006-9593-3
- Istvan ES, Deisenhofer J. Structural mechanism for statin inhibition of HMG-CoA reductase. *Science.* 2001;292(5519):1160-1164. doi:10.1126/science.1059344
- Ivanov II, Zhou L, Littman DR. Transcriptional regulation of Th17 cell differentiation. *Semin Immunol.* 2007;19(6):409-417. doi: 10.1016/j.smim.2007.10.011
- Jandhyala SM, Talukdar R, Subramanyam C, Vuyyuru H, Sasikala M, Nageshwar Reddy D. Role of the normal gut microbiota. *World J Gastroenterol.* 2015;21(29):8787-8803. doi:10.3748/wjg.v21.i29.8787
- Jeon TI, Osborne TF. SREBPs: metabolic integrators in physiology and metabolism. *Trends Endocrinol Metab.* 2012;23(2):65-72. doi: 10.1016/j.tem.2011.10.004
- Jia L, Betters JL, Yu L. Niemann-pick C1-like 1 (NPC1L1) protein in intestinal and hepatic cholesterol transport. *Annu Rev Physiol.* 2011; 73:239-259. doi:10.1146/annurev-physiol-012110-142233
- Jian C, Luukkonen P, Yki-Järvinen H, Salonen A, Korpela K. Quantitative PCR provides a simple and accessible method for quantitative microbiota profiling. *PLoS One.* 2020;15(1):e0227285. Published 2020 Jan 15. doi: 10.1371/journal.pone.0227285
- Jie Z, Xie Z, Xu W, et al. SREBP-2 aggravates breast cancer associated osteolysis by promoting osteoclastogenesis and breast cancer metastasis. *Biochim Biophys Acta Mol Basis Dis.*

2019;1865(1):115-125. doi: 10.1016/j.bbadis.2018.10.026

Jopling CL, Yi M, Lancaster AM, Lemon SM, Sarnow P. Modulation of hepatitis C virus RNA abundance by a liver-specific MicroRNA. *Science*. 2005;309(5740):1577-1581. doi:10.1126/science.1113329

Joshi SR, Anjana RM, Deepa M, et al. Prevalence of dyslipidemia in urban and rural India: the ICMR-INDIAB study. *PLoS One*. 2014;9(5):e96808. Published 2014 May 9. doi: 10.1371/journal.pone.0096808

Jun CH, Kim KR, Yoon JH, et al. Clinical outcomes of gastric variceal obliteration using N-butyl-2-cyanoacrylate in patients with acute gastric variceal hemorrhage. *Korean J Intern Med*. 2014;29(4):437-444. doi:10.3904/kjim.2014.29.4.437

Kaiser S, Lyne J, Agartz I, Clarke M, Mørch-Johnsen L, Faerden A. Individual negative symptoms and domains - Relevance for assessment, pathomechanisms and treatment. *Schizophr Res*. 2017; 186:39-45. doi: 10.1016/j.schres.2016.07.013

Kajita Y, Nakayama J, Aizawa M, Ishikawa F. The UUAG-specific RNA binding protein, heterogeneous nuclear ribonucleoprotein D0. Common modular structure and binding properties of the 2xRBD-Gly family. *J Biol Chem*. 1995;270(38):22167-22175. doi:10.1074/jbc.270.38.22167

Kallen J, Schlaeppli JM, Bitsch F, Delhon I, Fournier B. Crystal structure of the human RORalpha Ligand binding domain in complex with cholesterol sulfate at 2.2 Å. *J Biol Chem*. 2004;279(14):14033-14038. doi:10.1074/jbc.M400302200

Kallen JA, Schlaeppli JM, Bitsch F, et al. X-ray structure of the hRORalpha LBD at 1.63 Å: structural and functional data that cholesterol or a cholesterol derivative is the natural ligand of RORalpha. *Structure*. 2002;10(12):1697-1707. doi:10.1016/s0969-2126(02)00912-7

Kanauchi O, Mitsuyama K, Homma T, et al. Treatment of ulcerative colitis patients by long-term administration of germinated barley foodstuff: multi-center open trial. *Int J Mol Med*. 2003;12(5):701-704.

Kang SW, Kang SI, Shin HS, et al. Sasa quelpaertensis Nakai extract and its constituent p-coumaric acid inhibit adipogenesis in 3T3-L1 cells through activation of the AMPK pathway. *Food Chem Toxicol*. 2013; 59:380-385. doi: 10.1016/j.fct.2013.06.033

Karlsson FH, Tremaroli V, Nookaew I, et al. Gut metagenome in European women with normal, impaired and diabetic glucose control. *Nature*. 2013;498(7452):99-103. doi:10.1038/nature12198

Kaur AP, Bhardwaj S, Dhanjal DS, et al. Plant Prebiotics and Their Role in the Amelioration of Diseases. *Biomolecules*. 2021;11(3):440. Published 2021 Mar 16. doi:10.3390/biom11030440

- Keir M, Yi Y, Lu T, Ghilardi N. The role of IL-22 in intestinal health and disease. *J Exp Med*. 2020;217(3):e20192195. Published 2020 Feb 13. doi:10.1084/jem.20192195
- Kelly JR, Kennedy PJ, Cryan JF, Dinan TG, Clarke G, Hyland NP. Breaking down the barriers: the gut microbiome, intestinal permeability and stress-related psychiatric disorders. *Front Cell Neurosci*. 2015; 9:392. Published 2015 Oct 14. doi:10.3389/fncel.2015.00392
- Kennedy EA, King KY, Baldrige MT. Mouse Microbiota Models: Comparing Germ-Free Mice and Antibiotics Treatment as Tools for Modifying Gut Bacteria. *Front Physiol*. 2018; 9:1534. Published 2018 Oct 31. doi:10.3389/fphys.2018.01534
- Kespohl M, Vachharajani N, Luu M, et al. The Microbial Metabolite Butyrate Induces Expression of Th1-Associated Factors in CD4+ T Cells. *Front Immunol*. 2017; 8:1036. Published 2017 Aug 28. doi:10.3389/fimmu.2017.01036
- Khan AA, Agarwal H, Reddy SS, et al. MicroRNA 27a Is a Key Modulator of Cholesterol Biosynthesis. *Mol Cell Biol*. 2020;40(9):e00470-19. Published 2020 Apr 13. doi:10.1128/MCB.00470-19
- Khan I, Bai Y, Zha L, et al. Mechanism of the Gut Microbiota Colonization Resistance and Enteric Pathogen Infection. *Front Cell Infect Microbiol*. 2021; 11:716299. Published 2021 Dec 23. doi:10.3389/fcimb.2021.716299
- Khan MJ, Singh P, Dohare R, et al. Inhibition of miRNA-34a Promotes M2 Macrophage Polarization and Improves LPS-Induced Lung Injury by Targeting Klf4. *Genes (Basel)*. 2020;11(9):966. Published 2020 Aug 20. doi:10.3390/genes11090966
- Kharkwal H, Batool F, Koentgen F, et al. Generation and phenotypic characterisation of a cytochrome P450 4x1 knockout mouse. *PLoS One*. 2017;12(12):e0187959. Published 2017 Dec 11. doi: 10.1371/journal.pone.0187959
- Kheirilomoom A, Ferrara KW. Cholesterol transport from liposomal delivery vehicles. *Biomaterials*. 2007;28(29):4311-4320. doi: 10.1016/j.biomaterials.2007.06.008
- Kheirilomoom A, Ferrara KW. Cholesterol transport from liposomal delivery vehicles. *Biomaterials*. 2007;28(29):4311-4320. doi: 10.1016/j.biomaterials.2007.06.008
- Kim MH, Kang SG, Park JH, Yanagisawa M, Kim CH. Short-chain fatty acids activate GPR41 and GPR43 on intestinal epithelial cells to promote inflammatory responses in mice. *Gastroenterology*. 2013;145(2):. doi: 10.1053/j.gastro.2013.04.056
- Kim YJ, Yeo SG, Park JH, Ko HJ. Shigella vaccine development: prospective animal models and current status. *Curr Pharm Biotechnol*. 2013;14(10):903-912.

doi:10.2174/1389201014666131226123900

Kim YK, Kim B, Kim VN. Re-evaluation of the roles of DROSHA, Exportin 5, and DICER in microRNA biogenesis. *Proc Natl Acad Sci U S A*. 2016;113(13):E1881-E1889. doi:10.1073/pnas.1602532113

Kirby C, Clarke J, Gregoriadis G. Effect of the cholesterol content of small unilamellar liposomes on their stability in vivo and in vitro. *Biochem J*. 1980;186(2):591-598. doi:10.1042/bj1860591

Kishor A, Tandukar B, Ly YV, et al. Hsp70 is a novel posttranscriptional regulator of gene expression that binds and stabilizes selected mRNAs containing AU-rich elements. *Mol Cell Biol*. 2013;33(1):71-84. doi:10.1128/MCB.01275-12

Klampfer L, Huang J, Sasazuki T, Shirasawa S, Augenlicht L. Inhibition of interferon gamma signaling by the short chain fatty acid butyrate. *Mol Cancer Res*. 2003;1(11):855-862.

Klingenberg R, Gerdes N, Badeau RM, et al. Depletion of FOXP3⁺ regulatory T cells promotes hypercholesterolemia and atherosclerosis. *J Clin Invest*. 2013;123(3):1323-1334. doi:10.1172/JCI63891

Knodler LA, Vallance BA, Hensel M, Jäckel D, Finlay BB, Steele-Mortimer O. Salmonella type III effectors PipB and PipB2 are targeted to detergent-resistant microdomains on internal host cell membranes. *Mol Microbiol*. 2003;49(3):685-704. doi:10.1046/j.1365-2958.2003.03598.x

Koestler BJ, Ward CM, Payne SM. Shigella Pathogenesis Modeling with Tissue Culture Assays. *Curr Protoc Microbiol*. 2018;50(1):e57. doi:10.1002/cpmc.57

Korcz E, Kerényi Z, Varga L. Dietary fibers, prebiotics, and exopolysaccharides produced by lactic acid bacteria: potential health benefits with special regard to cholesterol-lowering effects. *Food Funct*. 2018;9(6):3057-3068. doi:10.1039/c8fo00118a

Kotla NG, Isa ILM, Rasala S, et al. Modulation of Gut Barrier Functions in Ulcerative Colitis by Hyaluronic Acid System. *Adv Sci (Weinh)*. 2022;9(4):e2103189. doi:10.1002/advs.202103189

Krautkramer KA, Fan J, Bäckhed F. Gut microbial metabolites as multi-kingdom intermediates. *Nat Rev Microbiol*. 2021;19(2):77-94. doi:10.1038/s41579-020-0438-4

Kreznar JH, Keller MP, Traeger LL, et al. Host Genotype and Gut Microbiome Modulate Insulin Secretion and Diet-Induced Metabolic Phenotypes. *Cell Rep*. 2017;18(7):1739-1750. doi:10.1016/j.celrep.2017.01.062

Kriaa A, Bourgin M, Potiron A, et al. Microbial impact on cholesterol and bile acid metabolism: current status and future prospects. *J Lipid Res*. 2019;60(2):323-332. doi:10.1194/jlr.R088989

- Krützfeldt J, Rajewsky N, Braich R, et al. Silencing of microRNAs in vivo with 'antagomirs'. *Nature*. 2005;438(7068):685-689. doi:10.1038/nature04303
- Krützfeldt J, Rajewsky N, Braich R, et al. Silencing of microRNAs in vivo with 'antagomirs'. *Nature*. 2005;438(7068):685-689. doi:10.1038/nature04303
- Kulkarni R, Wiemer EAC, Chang W. Role of Lipid Rafts in Pathogen-Host Interaction - A Mini Review. *Front Immunol*. 2022; 12:815020. Published 2022 Jan 20. doi:10.3389/fimmu.2021.815020
- Kulkarni VV, Anand A, Herr JB, Miranda C, Vogel MC, Maday S. Synaptic activity controls autophagic vacuole motility and function in dendrites. *J Cell Biol*. 2021;220(6):e202002084. doi:10.1083/jcb.202002084
- Kundu J, Banerjee P, Bose C, Das U, Ghosh U, Sinha S. Internal Oligoguanidinium Transporter: Mercury-Free Scalable Synthesis, Improvement of Cellular Localization, Endosomal Escape, Mitochondrial Localization, and Conjugation with Antisense Morpholino for NANOG Inhibition to Induce Chemosensitization of Taxol in MCF-7 Cells. *Bioconjug Chem*. 2020;31(10):2367-2382. doi:10.1021/acs.bioconjchem.0c00444
- Kuzu OF, Noory MA, Robertson GP. The Role of Cholesterol in Cancer. *Cancer Res*. 2016;76(8):2063-2070. doi: 10.1158/0008-5472.CAN-15-2613
- Lafont F, Tran Van Nhieu G, Hanada K, Sansonetti P, van der Goot FG. Initial steps of *Shigella* infection depend on the cholesterol/sphingolipid raft-mediated CD44-IpaB interaction. *EMBO J*. 2002;21(17):4449-4457. doi:10.1093/emboj/cdf457
- Lai CH, Chang YC, Du SY, et al. Cholesterol depletion reduces *Helicobacter pylori* CagA translocation and CagA-induced responses in AGS cells. *Infect Immun*. 2008;76(7):3293-3303. doi:10.1128/IAI.00365-08
- LaRock DL, Chaudhary A, Miller SI. *Salmonellae* interactions with host processes. *Nat Rev Microbiol*. 2015;13(4):191-205. doi:10.1038/nrmicro3420
- Larrede S, Quinn CM, Jessup W, et al. Stimulation of cholesterol efflux by LXR agonists in cholesterol-loaded human macrophages is ABCA1-dependent but ABCG1-independent. *Arterioscler Thromb Vasc Biol*. 2009;29(11):1930-1936. doi:10.1161/ATVBAHA.109.194548
- Le HH, Lee MT, Besler KR, Comrie JMC, Johnson EL. Characterization of interactions of dietary cholesterol with the murine and human gut microbiome. *Nat Microbiol*. 2022;7(9):1390-1403. doi:10.1038/s41564-022-01195-9
- Le Roy T, Debédât J, Marquet F, et al. Comparative Evaluation of Microbiota Engraftment Following

Fecal Microbiota Transfer in Mice Models: Age, Kinetic and Microbial Status Matter. *Front Microbiol.* 2019; 9:3289. Published 2019 Jan 14. doi:10.3389/fmicb.2018.03289

Le Roy T, Lécuyer E, Chassaing B, et al. The intestinal microbiota regulates host cholesterol homeostasis. *BMC Biol.* 2019;17(1):94. Published 2019 Nov 27. doi:10.1186/s12915-019-0715-8

Lee RC, Feinbaum RL, Ambros V. The *C. elegans* heterochronic gene *lin-4* encodes small RNAs with antisense complementarity to *lin-14*. *Cell.* 1993;75(5):843-854. doi:10.1016/0092-8674(93)90529-y

Lee SU, In HJ, Kwon MS, et al. β -Arrestin 2 mediates G protein-coupled receptor 43 signals to nuclear factor- κ B. *Biol Pharm Bull.* 2013;36(11):1754-1759. doi:10.1248/bpb. b13-00312

Leonel AJ, Alvarez-Leite JJ. Butyrate: implications for intestinal function. *Curr Opin Clin Nutr Metab Care.* 2012;15(5):474-479. doi:10.1097/MCO.0b013e32835665fa

Li B, Liu S, Miao L, Cai L. Prevention of diabetic complications by activation of Nrf2: diabetic cardiomyopathy and nephropathy. *Exp Diabetes Res.* 2012; 2012:216512. doi:10.1155/2012/216512

Li Q, Barres BA. Microglia and macrophages in brain homeostasis and disease. *Nat Rev Immunol.* 2018;18(4):225-242. doi:10.1038/nri.2017.125

Li Q, Zhang H, Zou J, Feng X, Feng D. Bisphenol A induces cholesterol biosynthesis in HepG2 cells via SREBP-2/HMGCR signaling pathway. *J Toxicol Sci.* 2019;44(7):481-491. doi:10.2131/jts.44.481

Li X, Watanabe K, Kimura I. Gut Microbiota Dysbiosis Drives and Implies Novel Therapeutic Strategies for Diabetes Mellitus and Related Metabolic Diseases. *Front Immunol.* 2017; 8:1882. Published 2017 Dec 20. doi:10.3389/fimmu.2017.01882

Liappis AP, Kan VL, Rochester CG, Simon GL. The effect of statins on mortality in patients with bacteremia. *Clin Infect Dis.* 2001;33(8):1352-1357. doi:10.1086/323334

Lin HV, Frassetto A, Kowalik EJ Jr, et al. Butyrate and propionate protect against diet-induced obesity and regulate gut hormones via free fatty acid receptor 3-independent mechanisms. *PLoS One.* 2012;7(4):e35240. doi: 10.1371/journal.pone.0035240

Lin Z, Murtaza I, Wang K, Jiao J, Gao J, Li PF. miR-23a functions downstream of NFATc3 to regulate cardiac hypertrophy. *Proc Natl Acad Sci USA.* 2009;106(29):12103-12108. doi:10.1073/pnas.0811371106

Linton MF, Yancey PG, Davies SS, et al. The Role of Lipids and Lipoproteins in Atherosclerosis. In: Feingold KR, Anawalt B, Blackman MR, et al., eds. *Endotext*. South Dartmouth (MA): MDText.com, Inc.; January 3, 2019.

Liu H, Wang J, He T, et al. Butyrate: A Double-Edged Sword for Health? *Adv Nutr*. 2018;9(1):21-29. doi:10.1093/advances/nmx009

Liu Y, Ho RC, Mak A. Interleukin (IL)-6, tumour necrosis factor alpha (TNF- α) and soluble interleukin-2 receptors (sIL-2R) are elevated in patients with major depressive disorder: a meta-analysis and meta-regression. *J Affect Disord*. 2012;139(3):230-239. doi: 10.1016/j.jad.2011.08.003

Londin E, Loher P, Telonis AG, et al. Analysis of 13 cell types reveals evidence for the expression of numerous novel primate- and tissue-specific microRNAs. *Proc Natl Acad Sci U S A*. 2015;112(10):E1106-E1115. doi:10.1073/pnas.1420955112

Long T, Hassan A, Thompson BM, McDonald JG, Wang J, Li X. Structural basis for human sterol isomerase in cholesterol biosynthesis and multidrug recognition. *Nat Commun*. 2019;10(1):2452. Published 2019 Jun 5. doi:10.1038/s41467-019-10279-w

Lou L, Zhang P, Piao R, Wang Y. Salmonella Pathogenicity Island 1 (SPI-1) and Its Complex Regulatory Network. *Front Cell Infect Microbiol*. 2019; 9:270. Published 2019 Jul 31. doi:10.3389/fcimb.2019.00270

Louis P, Flint HJ. Development of a semiquantitative degenerate real-time pcr-based assay for estimation of numbers of butyryl-coenzyme A (CoA) CoA transferase genes in complex bacterial samples. *Appl Environ Microbiol*. 2007;73(6):2009-2012. doi:10.1128/AEM.02561-06

Louis P, Flint HJ. Development of a semiquantitative degenerate real-time pcr-based assay for estimation of numbers of butyryl-coenzyme A (CoA) CoA transferase genes in complex bacterial samples. *Appl Environ Microbiol*. 2007;73(6):2009-2012. doi:10.1128/AEM.02561-06

Louis P, Flint HJ. Diversity, metabolism and microbial ecology of butyrate-producing bacteria from the human large intestine. *FEMS Microbiol Lett*. 2009;294(1):1-8. doi:10.1111/j.1574-6968.2009.01514.x

Low H, Hoang A, Sviridov D. Cholesterol efflux assay. *J Vis Exp*. 2012;(61):e3810. Published 2012 Mar 6. doi:10.3791/3810

Lu JY, Sadri N, Schneider RJ. Endotoxic shock in AUF1 knockout mice mediated by failure to degrade proinflammatory cytokine mRNAs. *Genes Dev*. 2006;20(22):3174-3184. doi:10.1101/gad.1467606

Lu JY, Sadri N, Schneider RJ. Endotoxic shock in AUF1 knockout mice mediated by failure to degrade proinflammatory cytokine mRNAs. *Genes Dev*. 2006;20(22):3174-3184. doi:10.1101/gad.1467606

Lu JY, Sadri N, Schneider RJ. Endotoxic shock in AUF1 knockout mice mediated by failure to degrade proinflammatory cytokine mRNAs. *Genes Dev*. 2006;20(22):3174-3184. doi:10.1101/gad.1467606

- Luu W, Hart-Smith G, Sharpe LJ, Brown AJ. The terminal enzymes of cholesterol synthesis, DHCR24 and DHCR7, interact physically and functionally [published correction appears in J Lipid Res. 2015 May;56(5):1079]. J Lipid Res. 2015;56(4):888-897. doi:10.1194/jlr.M056986
- Luzardo-Ocampo I, Ramírez-Jiménez AK, Yañez J, Mojica L, Luna-Vital DA. Technological Applications of Natural Colorants in Food Systems: A Review. Foods. 2021;10(3):634. Published 2021 Mar 17. doi:10.3390/foods10030634
- Macfarlane LA, Murphy PR. MicroRNA: Biogenesis, Function and Role in Cancer. Curr Genomics. 2010;11(7):537-561. doi:10.2174/138920210793175895
- Macfarlane S, Macfarlane GT. Regulation of short-chain fatty acid production. *Proc Nutr Soc.* 2003;62(1):67-72. doi:10.1079/PNS2002207
- Macia L, Tan J, Vieira AT, et al. Metabolite-sensing receptors GPR43 and GPR109A facilitate dietary fibre-induced gut homeostasis through regulation of the inflammasome. Nat Commun. 2015; 6:6734. Published 2015 Apr 1. doi:10.1038/ncomms7734
- Mahana D, Trent CM, Kurtz ZD, et al. Antibiotic perturbation of the murine gut microbiome enhances the adiposity, insulin resistance, and liver disease associated with high-fat diet. Genome Med. 2016;8(1):48. Published 2016 Apr 27. doi:10.1186/s13073-016-0297-9
- Mañes S, del Real G, Martínez-A C. Pathogens: raft hijackers. Nat Rev Immunol. 2003;3(7):557- 568. doi:10.1038/nri1129
- Marathe SA, Sen M, Dasgupta I, Chakravorty D. Differential modulation of intracellular survival of cytosolic and vacuolar pathogens by curcumin. Antimicrob Agents Chemother. 2012;56(11):5555-5567. doi:10.1128/AAC.00496-12
- Marchiando AM, Graham WV, Turner JR. Epithelial barriers in homeostasis and disease. Annu Rev Pathol. 2010; 5:119-144. doi: 10.1146/annurev.pathol.4.110807.092135
- Marcil V, Delvin E, Garofalo C, Levy E. Butyrate impairs lipid transport by inhibiting microsomal triglyceride transfer protein in Caco-2 cells. J Nutr. 2003;133(7):2180-2183. doi:10.1093/jn/133.7.2180
- Marquart TJ, Allen RM, Ory DS, Baldán A. miR-33 links SREBP-2 induction to repression of sterol transporters. Proc Natl Acad Sci U S A. 2010;107(27):12228-12232. doi:10.1073/pnas.1005191107
- Martin-Gallausiaux C, Marinelli L, Blottière HM, Larraufie P, Lapaque N. SCFA: mechanisms and functional importance in the gut. Proc Nutr Soc. 2021;80(1):37-49. doi:10.1017/S0029665120006916
- Maslowski KM, Vieira AT, Ng A, et al. Regulation of inflammatory responses by gut microbiota and

- chemoattractant receptor GPR43. *Nature*. 2009;461(7268):1282-1286.
doi:10.1038/nature08530
- Maslowski KM, Vieira AT, Ng A, et al. Regulation of inflammatory responses by gut microbiota and chemoattractant receptor GPR43. *Nature*. 2009;461(7268):1282-1286.
doi:10.1038/nature08530
- Masui R, Sasaki M, Funaki Y, et al. G protein-coupled receptor 43 moderates gut inflammation through cytokine regulation from mononuclear cells. *Inflamm Bowel Dis*. 2013;19(13):2848-2856.
doi: 10.1097/01.MIB.0000435444.14860.ea
- Mathai N, Kirchmair J. Similarity-Based Methods and Machine Learning Approaches for Target Prediction in Early Drug Discovery: Performance and Scope. *Int J Mol Sci*. 2020;21(10):3585. Published 2020 May 19. doi:10.3390/ijms21103585
- Maxfield FR, van Meer G. Cholesterol, the central lipid of mammalian cells. *Curr Opin Cell Biol*. 2010;22(4): 422-429.doi: 10.1016/j.ceb.2010.05.004
- May T, Mackie RI, Fahey GC Jr, Cremin JC, Garleb KA. Effect of fiber source on short-chain fatty acid production and on the growth and toxin production by *Clostridium difficile*. *Scand J Gastroenterol*. 1994;29(10):916-922. doi:10.3109/00365529409094863
- McKay BC. Post-transcriptional regulation of DNA damage-responsive gene expression. *Antioxid Redox Signal*. 2014;20(4):640-654. doi:10.1089/ars.2013.5523
- McKay BC. Post-transcriptional regulation of DNA damage-responsive gene expression. *Antioxid Redox Signal*. 2014;20(4):640-654. doi:10.1089/ars.2013.5523
- McNabney SM, Henagan TM. Short Chain Fatty Acids in the Colon and Peripheral Tissues: A Focus on Butyrate, Colon Cancer, Obesity and Insulin Resistance. *Nutrients*. 2017;9(12):1348. Published 2017 Dec 12. doi:10.3390/nu9121348
- Menon B, Gulappa T, Menon KM. miR-122 Regulates LH Receptor Expression by Activating Sterol Response Element Binding Protein in Rat Ovaries. *Endocrinology*. 2015;156(9):3370-3380. doi:10.1210/en.2015-1121
- Meyer A, Golbik RP, Sanger L, Schmidt T, Behrens SE, Friedrich S. The RGG/RG motif of AUF1 isoform p45 is a key modulator of the protein's RNA chaperone and RNA annealing activities. *RNA Biol*. 2019;16(7):960-971. doi:10.1080/15476286.2019.1602438
- Meyer A, Golbik RP, Sanger L, Schmidt T, Behrens SE, Friedrich S. The RGG/RG motif of AUF1 isoform p45 is a key modulator of the protein's RNA chaperone and RNA annealing activities. *RNA Biol*. 2019;16(7):960-971. doi:10.1080/15476286.2019.1602438

Miao H, Zeng H, Gong H. microRNA-212 promotes lipid accumulation and attenuates cholesterol efflux in THP-1 human macrophages by targeting SIRT1. *Gene*. 2018; 643:55-60. doi:10.1016/j.gene.2017.11.058

Miao W, Wu X, Wang K, et al. Sodium Butyrate Promotes Reassembly of Tight Junctions in Caco-2 Monolayers Involving Inhibition of MLCK/MLC2 Pathway and Phosphorylation of PKC β 2. *Int J Mol Sci*. 2016;17(10):1696. Published 2016 Oct 10. doi:10.3390/ijms17101696

Millard AL, Mertes PM, Ittelet D, Villard F, Jeannesson P, Bernard J. Butyrate affects differentiation, maturation and function of human monocyte-derived dendritic cells and macrophages. *Clin Exp Immunol*. 2002;130(2):245-255. doi:10.1046/j.0009-9104.2002.01977.x

Miller TL, Wolin MJ. Pathways of acetate, propionate, and butyrate formation by the human fecal microbial flora. *Appl Environ Microbiol*. 1996;62(5):1589-1592. doi:10.1128/aem.62.5.1589-1592.1996

Miller TL, Wolin MJ. Pathways of acetate, propionate, and butyrate formation by the human fecal microbial flora. *Appl Environ Microbiol*. 1996;62(5):1589-1592. doi:10.1128/aem.62.5.1589-1592.1996

Mirzaei R, Dehkhodaie E, Bouzari B, et al. Dual role of microbiota-derived short-chain fatty acids on host and pathogen. *Biomed Pharmacother*. 2022; 145:112352. doi: 10.1016/j.biopha.2021.112352

Mishra SP, Karunakar P, Taraphder S, Yadav H. Free Fatty Acid Receptors 2 and 3 as Microbial Metabolite Sensors to Shape Host Health: Pharmacophysiological View. *Biomedicines*. 2020;8(6):154. Published 2020 Jun 8. doi:10.3390/biomedicines8060154

Mishra SP, Karunakar P, Taraphder S, Yadav H. Free Fatty Acid Receptors 2 and 3 as Microbial Metabolite Sensors to Shape Host Health: Pharmacophysiological View. *Biomedicines*. 2020;8(6):154. Published 2020 Jun 8. doi:10.3390/biomedicines8060154

Mistry HD, Kurlak LO, Mansour YT, Zurkinden L, Mohaupt MG, Escher G. Increased maternal and fetal cholesterol efflux capacity and placental CYP27A1 expression in preeclampsia. *J Lipid Res*. 2017;58(6):1186-1195. doi:10.1194/jlr.M071985

Moffett JR, Puthillathu N, Vengilote R, Jaworski DM, Namboodiri AM. Acetate Revisited: A Key Biomolecule at the Nexus of Metabolism, Epigenetics and Oncogenesis-Part 1: Acetyl-CoA, Acetogenesis and Acyl-CoA Short-Chain Synthetases. *Front Physiol*. 2020; 11:580167. Published 2020 Nov 12. doi:10.3389/fphys.2020.580167

Moore AE, Chenette DM, Larkin LC, Schneider RJ. Physiological networks and disease functions of RNA-binding protein AUF1. *Wiley Interdiscip Rev RNA*. 2014;5(4):549-564. doi:10.1002/wrna.1230

- Moore AE, Chenette DM, Larkin LC, Schneider RJ. Physiological networks and disease functions of RNA-binding protein AUF1. *Wiley Interdiscip Rev RNA*. 2014;5(4):549-564. doi:10.1002/wrna.1230
- Moore KJ, Rayner KJ, Suárez Y, Fernández-Hernando C. The role of microRNAs in cholesterol efflux and hepatic lipid metabolism. *Annu Rev Nutr*. 2011; 31:49-63. doi:10.1146/annurev-nutr-081810-160756
- Morana O, Nieto-Garai JA, Björkholm P, et al. Identification of a New Cholesterol-Binding Site within the IFN- γ Receptor that is Required for Signal Transduction. *Adv Sci (Weinh)*. 2022;9(11):e2105170. doi:10.1002/advs.202105170
- Morrison DJ, Preston T. Formation of short chain fatty acids by the gut microbiota and their impact on human metabolism. *Gut Microbes*. 2016;7(3):189-200. doi:10.1080/19490976.2015.1134082
- Morrison DJ, Preston T. Formation of short chain fatty acids by the gut microbiota and their impact on human metabolism. *Gut Microbes*. 2016;7(3):189-200. doi:10.1080/19490976.2015.1134082
- Mowat AM, Agace WW. Regional specialization within the intestinal immune system. *Nat Rev Immunol*. 2014;14(10):667-685. doi:10.1038/nri3738
- Musso G, Gambino R, Cassader M. Obesity, diabetes, and gut microbiota: the hygiene hypothesis expanded? *Diabetes Care*. 2010;33(10):2277-2284. doi:10.2337/dc10-0556
- Muthuramalingam M, Whittier SK, Picking WL, Picking WD. The Shigella Type III Secretion System: An Overview from Top to Bottom. *Microorganisms*. 2021;9(2):451. Published 2021 Feb 22. doi:10.3390/microorganisms9020451
- Myeni S, Child R, Ng TW, et al. Brucella modulates secretory trafficking via multiple type IV secretion effector proteins. *PLoS Pathog*. 2013;9(8):e1003556. doi: 10.1371/journal.ppat.1003556
- Nakanishi N, Nakagawa Y, Tokushige N, et al. The up-regulation of microRNA-335 is associated with lipid metabolism in liver and white adipose tissue of genetically obese mice. *Biochem Biophys Res Commun*. 2009;385(4):492-496. doi: 10.1016/j.bbrc.2009.05.058
- Nataraj BH, Ali SA, Behare PV, Yadav H. Postbiotics-parabiotics: the new horizons in microbial biotherapy and functional foods. *Microb Cell Fact*. 2020;19(1):168. Published 2020 Aug 20. doi:10.1186/s12934-020-01426-w
- Natesan V, Kim SJ. Lipid Metabolism, Disorders and Therapeutic Drugs - Review. *Biomol Ther (Seoul)*. 2021 Nov 1;29(6):596-604. doi: 10.4062/biomolther.2021.122. PMID: 34697272; PMCID: PMC8551734.
- Nemmar A, Al Hemeiri A, Al Hammadi N, Yuvaraju P, Beegam S, Yasin J, et al. Early pulmonary events of nose-only water pipe (shisha) smoking exposure in mice. *Physiol Rep* 2015; 3.

Nouaille S, Mondeil S, Finoux AL, Moulis C, Girbal L, Cocaign-Bousquet M. The stability of an mRNA is influenced by its concentration: a potential physical mechanism to regulate gene expression. *Nucleic Acids Res.* 2017;45(20):11711-11724. doi:10.1093/nar/gkx781

Nouaille S, Mondeil S, Finoux AL, Moulis C, Girbal L, Cocaign-Bousquet M. The stability of an mRNA is influenced by its concentration: a potential physical mechanism to regulate gene expression. *Nucleic Acids Res.* 2017;45(20):11711-11724. doi:10.1093/nar/gkx781

O'Brien J, Hayder H, Zayed Y, Peng C. Overview of MicroRNA Biogenesis, Mechanisms of Actions, and Circulation. *Front Endocrinol (Lausanne).* 2018; 9:402. Published 2018 Aug 3. doi:10.3389/fendo.2018.00402

O'Brien J, Hayder H, Zayed Y, Peng C. Overview of MicroRNA Biogenesis, Mechanisms of Actions, and Circulation. *Front Endocrinol (Lausanne).* 2018; 9:402. Published 2018 Aug 3. doi:10.3389/fendo.2018.00402

O'Brien J, Hayder H, Zayed Y, Peng C. Overview of MicroRNA Biogenesis, Mechanisms of Actions, and Circulation. *Front Endocrinol (Lausanne).* 2018; 9:402. Published 2018 Aug 3. doi:10.3389/fendo.2018.00402

Odamaki T, Kato K, Sugahara H, et al. Age-related changes in gut microbiota composition from newborn to centenarian: a cross-sectional study. *BMC Microbiol.* 2016; 16:90. Published 2016 May 25. doi:10.1186/s12866-016-0708-5

Ohira H, Tsutsui W, Fujioka Y. Are Short Chain Fatty Acids in Gut Microbiota Defensive Players for Inflammation and Atherosclerosis. *J Atheroscler Thromb.* 2017;24(7):660-672. doi:10.5551/jat.RV17006

Parada Venegas D, De la Fuente MK, Landskron G, et al. Short Chain Fatty Acids (SCFAs)-Mediated Gut Epithelial and Immune Regulation and Its Relevance for Inflammatory Bowel Diseases [published correction appears in *Front Immunol.* 2019 Jun 28; 10:1486]. *Front Immunol.* 2019; 10:277. Published 2019 Mar 11. doi:10.3389/fimmu.2019.00277

Pautz A, Linker K, Altenhöfer S, et al. Similar regulation of human inducible nitric-oxide synthase expression by different isoforms of the RNA-binding protein AUF1. *J Biol Chem.* 2009;284(5):2755-2766. doi:10.1074/jbc.M809314200

Peng L, Li ZR, Green RS, Holzman IR, Lin J. Butyrate enhances the intestinal barrier by facilitating tight junction assembly via activation of AMP-activated protein kinase in Caco-2 cell monolayers. *J Nutr.* 2009;139(9):1619-1625. doi:10.3945/jn.109.104638

Peterson LW, Artis D. Intestinal epithelial cells: regulators of barrier function and immune homeostasis. *Nat Rev Immunol.* 2014;14(3):141-153. doi:10.1038/nri3608

- Petrov AM, Kravtsova VV, Matchkov VV, et al. Membrane lipid rafts are disturbed in the response of rat skeletal muscle to short-term disuse. *Am J Physiol Cell Physiol*. 2017;312(5):C627-C637. doi:10.1152/ajpcell.00365.2016
- Pham VT, Lacroix C, Braegger CP, Chassard C. Lactate-utilizing community is associated with gut microbiota dysbiosis in colicky infants. *Sci Rep*. 2017;7(1):11176. Published 2017 Sep 11. doi:10.1038/s41598-017-11509-1
- Pike LJ. Rafts defined: a report on the Keystone Symposium on Lipid Rafts and Cell Function. *J Lipid Res*. 2006;47(7):1597-1598. doi:10.1194/jlr.E600002-JLR200
- Priyadarshini M, Kotlo KU, Dudeja PK, Layden BT. Role of Short Chain Fatty Acid Receptors in Intestinal Physiology and Pathophysiology. *Compr Physiol*. 2018;8(3):1091-1115. Published 2018 Jun 18. doi:10.1002/cphy.c170050
- Procházková N, Falony G, Dragsted LO, Licht TR, Raes J, Roager HM. Advancing human gut microbiota research by considering gut transit time. *Gut*. 2023;72(1):180-191. doi:10.1136/gutjnl-2022-328166
- Qaria MA, Kumar S, Sepe LP, Ahmed N. Cholesterol glucosylation-based survival strategy in *Helicobacter pylori*. *Helicobacter*. 2021;26(2):e12777. doi:10.1111/hel.12777
- Qin J, Li Y, Cai Z, et al. A metagenome-wide association study of gut microbiota in type 2 diabetes. *Nature*. 2012;490(7418):55-60. doi:10.1038/nature11450
- Rader DJ, Alexander ET, Weibel GL, Billheimer J, Rothblat GH. The role of reverse cholesterol transport in animals and humans and relationship to atherosclerosis. *J Lipid Res*. 2009;50 Suppl (Suppl):S189-S194. doi:10.1194/jlr.R800088-JLR200
- Rakheja D, Chen KS, Liu Y, et al. Somatic mutations in DROSHA and DICER1 impair microRNA biogenesis through distinct mechanisms in Wilms tumours [published correction appears in *Nat Commun*. 2017 Nov 29; 8:16177]. *Nat Commun*. 2014; 2:4802. Published 2014 Sep 5. doi:10.1038/ncomms5802
- Ramírez CM, Lin CS, Abdelmohsen K, et al. RNA binding protein HuR regulates the expression of ABCA1. *J Lipid Res*. 2014;55(6):1066-1076. doi:10.1194/jlr.M044925
- Ramirez J, Guarner F, Bustos Fernandez L, Maruy A, Sdepanian VL, Cohen H. Antibiotics as Major Disruptors of Gut Microbiota. *Front Cell Infect Microbiol*. 2020; 10:572912. Published 2020 Nov 24. doi:10.3389/fcimb.2020.572912
- Rayner KJ, Esau CC, Hussain FN, et al. Inhibition of miR-33a/b in non-human primates raises plasma HDL and lowers VLDL triglycerides. *Nature*. 2011;478(7369):404-407. Published 2011 Oct 19.

doi:10.1038/nature10486

Razin S, Tully JG. Cholesterol requirement of mycoplasmas. *J Bacteriol.* 1970;102(2):306-310. doi:10.1128/jb.102.2.306-310.1970

Regard JB, Kataoka H, Cano DA, et al. Probing cell type-specific functions of Gi in vivo identifies GPCR regulators of insulin secretion. *J Clin Invest.* 2007;117(12):4034-4043. doi:10.1172/JCI32994

Reikvam DH, Erofeev A, Sandvik A, et al. Depletion of murine intestinal microbiota: effects on gut mucosa and epithelial gene expression. *PLoS One.* 2011;6(3):e17996. Published 2011 Mar 21. doi:10.1371/journal.pone.0017996

Rinninella E, Raoul P, Cintoni M, et al. What is the Healthy Gut Microbiota Composition? A Changing Ecosystem across Age, Environment, Diet, and Diseases. *Microorganisms.* 2019;7(1):14. Published 2019 Jan 10. doi:10.3390/microorganisms7010014

Rios-Covian D, González S, Nogacka AM, et al. An Overview on Fecal Branched Short-Chain Fatty Acids Along Human Life and as Related with Body Mass Index: Associated Dietary and Anthropometric Factors. *Front Microbiol.* 2020; 11:973. Published 2020 May 27. doi:10.3389/fmicb.2020.00973

Ríos-Covián D, Ruas-Madiedo P, Margolles A, Gueimonde M, de Los Reyes-Gavilán CG, Salazar N. Intestinal Short Chain Fatty Acids and their Link with Diet and Human Health. *Front Microbiol.* 2016; 7:185. Published 2016 Feb 17. doi:10.3389/fmicb.2016.00185

Rivera-Chávez F, Zhang LF, Faber F, et al. Depletion of Butyrate-Producing Clostridia from the Gut Microbiota Drives an Aerobic Luminal Expansion of Salmonella. *Cell Host Microbe.* 2016;19(4):443-454. doi: 10.1016/j.chom.2016.03.004

Rivière A, Selak M, Lantin D, Leroy F, De Vuyst L. Bifidobacteria and Butyrate-Producing Colon Bacteria: Importance and Strategies for Their Stimulation in the Human Gut. *Front Microbiol.* 2016; 7:979. Published 2016 Jun 28. doi:10.3389/fmicb.2016.00979

Roediger WE. The colonic epithelium in ulcerative colitis: an energy-deficiency disease? *Lancet.* 1980;2(8197):712-715. doi:10.1016/s0140-6736(80)91934-0

Rooks MG, Garrett WS. Gut microbiota, metabolites and host immunity. *Nat Rev Immunol.* 2016;16(6):341-352. doi:10.1038/nri.2016.42

Rosignoli P, Fabiani R, De Bartolomeo A, et al. Protective activity of butyrate on hydrogen peroxide-induced DNA damage in isolated human colonocytes and HT29 tumour cells. *Carcinogenesis.* 2001;22(10):1675-1680. doi:10.1093/carcin/22.10.1675

Rotllan N, Fernández-Hernando C. MicroRNA Regulation of Cholesterol Metabolism. *Cholesterol.*

- 2012; 2012:847849. doi:10.1155/2012/847849
- Rui L. Energy metabolism in the liver. *Compr Physiol*. 2014;4(1):177-197. doi:10.1002/cphy.c130024
- Sadri N, Lu JY, Badura ML, Schneider RJ. AUF1 is involved in splenic follicular B cell maintenance. *BMC Immunol*. 2010; 11:1. Published 2010 Jan 11. doi:10.1186/1471-2172-1
- Sadri N, Schneider RJ. Auf1/Hnrnpd-deficient mice develop pruritic inflammatory skin disease. *J Invest Dermatol*. 2009;129(3):657-670. doi:10.1038/jid.2008.298
- Sadri N, Schneider RJ. Auf1/Hnrnpd-deficient mice develop pruritic inflammatory skin disease. *J Invest Dermatol*. 2009;129(3):657-670. doi:10.1038/jid.2008.298
- Sadri N, Schneider RJ. Auf1/Hnrnpd-deficient mice develop pruritic inflammatory skin disease. *J Invest Dermatol*. 2009;129(3):657-670. doi:10.1038/jid.2008.298
- Samuel CE. Antiviral actions of interferons. *Clin Microbiol Rev*. 2001;14(4):778-809. doi:10.1128/CMR.14.4.778-809.2001
- Sandberg JC, Björck IME, Nilsson AC. Impact of rye-based evening meals on cognitive functions, mood and cardiometabolic risk factors: a randomized controlled study in healthy middle-aged subjects. *Nutr J*. 2018;17(1):102. Published 2018 Nov 6. doi:10.1186/s12937-018-0412-4
- Sankaranarayanan S, Oram JF, Asztalos BF, et al. Effects of acceptor composition and mechanism of ABCG1-mediated cellular free cholesterol efflux. *J Lipid Res*. 2009;50(2):275-284. doi:10.1194/jlr.M800362-JLR200
- Sanyal A, Antony R, Samui G, Thampan M. Microbial communities and their potential for degradation of dissolved organic carbon in cryoconite hole environments of Himalaya and Antarctica. *Microbiol Res*. 2018; 208:32-42. doi: 10.1016/j.micres.2018.01.004
- Sappati Biyyani RS, Putka BS, Mullen KD. Dyslipidemia and lipoprotein profiles in patients with inflammatory bowel disease. *J Clin Lipidol*. 2010;4(6):478-482. doi: 10.1016/j.jacl.2010.08.021
- Sarkar B, Lu JY, Schneider RJ. Nuclear import and export functions in the different isoforms of the AUF1/heterogeneous nuclear ribonucleoprotein protein family. *J Biol Chem*. 2003;278(23):20700-20707. doi:10.1074/jbc.M301176200
- Sarkar S, Han J, Sinsimer KS, et al. RNA-binding protein AUF1 regulates lipopolysaccharide-induced IL10 expression by activating IkappaB kinase complex in monocytes. *Mol Cell Biol*. 2011;31(4):602-615. doi:10.1128/MCB.00835-10
- Sauer AJ, Moss AJ, McNitt S, et al. Long QT syndrome in adults. *J Am Coll Cardiol*. 2007;49(3):329-337. doi: 10.1016/j.jacc.2006.08.057

- Schoeler M, Caesar R. Dietary lipids, gut microbiota and lipid metabolism. *Rev Endocr Metab Disord*. 2019;20(4):461-472. doi:10.1007/s11154-019-09512-0
- Schoenberg DR, Maquat LE. Regulation of cytoplasmic mRNA decay [published correction appears in *Nat Rev Genet*. 2012 Jun;13(6):448]. *Nat Rev Genet*. 2012;13(4):246-259. Published 2012 Mar 6. doi:10.1038/nrg3160
- Schönfeld P, Wojtczak L. Short- and medium-chain fatty acids in energy metabolism: the cellular perspective. *J Lipid Res*. 2016;57(6):943-954. doi:10.1194/jlr.R067629
- Schulthess J, Pandey S, Capitani M, et al. The Short Chain Fatty Acid Butyrate Imprints an Antimicrobial Program in Macrophages. *Immunity*. 2019;50(2):432-445.e7. doi: 10.1016/j.immuni.2018.12.018
- Schulthess J, Pandey S, Capitani M, et al. The Short Chain Fatty Acid Butyrate Imprints an Antimicrobial Program in Macrophages. *Immunity*. 2019;50(2):432-445.e7. doi: 10.1016/j.immuni.2018.12.018
- Sen S, Roy K, Mukherjee S, Mukhopadhyay R, Roy S. Restoration of IFN γ R subunit assembly, IFN γ signaling and parasite clearance in *Leishmania donovani* infected macrophages: role of membrane cholesterol. *PLoS Pathog*. 2011;7(9):e1002229. doi: 10.1371/journal.ppat.1002229
- Sharma N, Phan HTT, Yoda T, Shimokawa N, Vestergaard MC, Takagi M. Effects of Capsaicin on Biomimetic Membranes. *Biomimetics (Basel)*. 2019;4(1):17. Published 2019 Feb 13. doi:10.3390/biomimetics4010017
- Shi L, Chowdhury SM, Smallwood HS, Yoon H, Mottaz-Brewer HM, Norbeck AD, et al. Proteomic investigation of the time course responses of RAW 264.7 macrophages to infection with *Salmonella enterica*. *Infect Immun* 2009; 77:3227-33.
- Shibata C, Ohno M, Otsuka M, et al. The flavonoid apigenin inhibits hepatitis C virus replication by decreasing mature microRNA122 levels. *Virology*. 2014;462-463:42-48. doi: 10.1016/j.virol.2014.05.024
- Shin JS, Abraham SN. Caveolae as portals of entry for microbes. *Microbes Infect*. 2001;3(9):755-761. doi:10.1016/s1286-4579(01)01423-x
- Shinitzky M, Barenholz Y. Fluidity parameters of lipid regions determined by fluorescence polarization. *Biochim Biophys Acta*. 1978;515(4):367-394. doi:10.1016/0304-4157(78)90010-2
- Silva YP, Bernardi A, Frozza RL. The Role of Short-Chain Fatty Acids from Gut Microbiota in Gut-Brain Communication. *Front Endocrinol (Lausanne)*. 2020; 11:25. Published 2020 Jan 31. doi:10.3389/fendo.2020.00025

- Simons K, Ehehalt R. Cholesterol, lipid rafts, and disease. *J Clin Invest.* 2002;110(5):597-603. doi:10.1172/JCI16390
- Simons K, Ehehalt R. Cholesterol, lipid rafts, and disease. *J Clin Invest.* 2002;110(5):597-603. doi:10.1172/JCI16390
- Singh TP, Tehri N, Kaur G, Malik RK. Cell surface and extracellular proteins of potentially probiotic *Lactobacillus reuteri* as an effective mediator to regulate intestinal epithelial barrier function. *Arch Microbiol.* 2021;203(6):3219-3228. doi:10.1007/s00203-021-02318-2
- Sirenko OI, Lofquist AK, DeMaria CT, Morris JS, Brewer G, Haskill JS. Adhesion-dependent regulation of an A+U-rich element-binding activity associated with AUF1. *Mol Cell Biol.* 1997;17(7):3898-3906. doi:10.1128/MCB.17.7.3898
- Sobolewski C, Sanduja S, Blanco FF, Hu L, Dixon DA. Histone Deacetylase Inhibitors Activate Tristetraprolin Expression through Induction of Early Growth Response Protein 1 (EGR1) in Colorectal Cancer Cells. *Biomolecules.* 2015;5(3):2035-2055. Published 2015 Aug 28. doi:10.3390/biom5032035
- Sobue S, Nemoto S, Murakami M, et al. Implications of sphingosine kinase 1 expression level for the cellular sphingolipid rheostat: relevance as a marker for daunorubicin sensitivity of leukemia cells. *Int J Hematol.* 2008;87(3):266-275. doi:10.1007/s12185-008-0052-0
- Song K, Han C, Zhang J, et al. Epigenetic regulation of MicroRNA-122 by peroxisome proliferator activated receptor-gamma and hepatitis b virus X protein in hepatocellular carcinoma cells. *Hepatology.* 2013;58(5):1681-1692. doi:10.1002/hep.26514
- Soran H, Adam S, Mohammad JB, et al. Hypercholesterolaemia - practical information for non-specialists. *Arch Med Sci.* 2018;14(1):1-21. doi:10.5114/aoms.2018.72238
- Sorbara MT, Dubin K, Littmann ER, et al. Inhibiting antibiotic-resistant Enterobacteriaceae by microbiota-mediated intracellular acidification. *J Exp Med.* 2019;216(1):84-98. doi:10.1084/jem.20181639
- Steinman G. Mechanisms of twinning: VII. Effect of diet and heredity on the human twinning rate. *J Reprod Med.* 2006;51(5):405-410.
- Subczynski WK, Pasenkiewicz-Gierula M, Widomska J, Mainali L, Raguz M. High Cholesterol/Low Cholesterol: Effects in Biological Membranes: A Review. *Cell Biochem Biophys.* 2017;75(3-4):369-385. doi:10.1007/s12013-017-0792-7
- Suh JH, Saba JD. Sphingosine-1-phosphate in inflammatory bowel disease and colitis-associated colon cancer: the fat's in the fire. *Transl Cancer Res.* 2015;4(5):469-483. doi: 10.3978/j.issn.2218-

676X.2015.10.06

Sun C, Huang F, Liu X, et al. miR-21 regulates triglyceride and cholesterol metabolism in non-alcoholic fatty liver disease by targeting HMGCR. *Int J Mol Med*. 2015;35(3):847-853. doi:10.3892/ijmm.2015.2076

Sun F, Fan G, Hu Q, et al. The high-quality genome of *Brassica napus* cultivar 'ZS11' reveals the introgression history in semi-winter morphotype. *Plant J*. 2017;92(3):452-468. doi:10.1111/tpj.13669

Sun F, Schroer CFE, Palacios CR, Xu L, Luo SZ, Marrink SJ. Molecular mechanism for bidirectional regulation of CD44 for lipid raft affiliation by palmitoylations and PIP2. *PLoS Comput Biol*. 2020;16(4):e1007777. Published 2020 Apr 9. doi: 10.1371/journal.pcbi.1007777

Sun H, Sherrier M, Li H. Skeletal Muscle and Bone - Emerging Targets of Fibroblast Growth Factor-21. *Front Physiol*. 2021; 12:625287. Published 2021 Mar 8. doi:10.3389/fphys.2021.625287

Sun M, Northup N, Marga F, et al. The effect of cellular cholesterol on membrane-cytoskeleton adhesion. *J Cell Sci*. 2007;120(Pt 13):2223-2231. doi:10.1242/jcs.001370

Sun Y, O'Riordan MX. Regulation of bacterial pathogenesis by intestinal short-chain Fatty acids. *Adv Appl Microbiol*. 2013; 85:93-118. doi:10.1016/B978-0-12-407672-3.00003-4

Suzuki T. Regulation of intestinal epithelial permeability by tight junctions. *Cell Mol Life Sci*. 2013;70(4):631-659. doi:10.1007/s00018-012-1070-x

Tachibana H, Fujimura Y, Yamada K. Tea polyphenol epigallocatechin-3-gallate associates with plasma membrane lipid rafts: lipid rafts mediate anti-allergic action of the catechin. *Biofactors*. 2004;21(1-4):383-385. doi:10.1002/biof.552210174

Thakral S, Ghoshal K. miR-122 is a unique molecule with great potential in diagnosis, prognosis of liver disease, and therapy both as miRNA mimic and antimir. *Curr Gene Ther*. 2015;15(2):142-150. doi:10.2174/1566523214666141224095610

Thangaraju M, Cresci GA, Liu K, et al. GPR109A is a G-protein-coupled receptor for the bacterial fermentation product butyrate and functions as a tumor suppressor in colon. *Cancer Res*. 2009;69(7):2826-2832. doi: 10.1158/0008-5472.CAN-08-4466

Thomas M, Deiters A. MicroRNA miR-122 as a therapeutic target for oligonucleotides and small molecules. *Curr Med Chem*. 2013;20(29):3629-3640. doi:10.2174/0929867311320290009

Toledo A, Benach JL. Hijacking and Use of Host Lipids by Intracellular Pathogens. *Microbiol Spectr*. 2015;3(6): 10.1128/microbiolspec.VMBF-0001-2014. doi: 10.1128/microbiolspec.VMBF-0001-2014

Tsukita S, Tanaka H, Tamura A. The Claudins: From Tight Junctions to Biological Systems. *Trends Biochem Sci.* 2019;44(2):141-152. doi: 10.1016/j.tibs.2018.09.008

Turner JR. Intestinal mucosal barrier function in health and disease. *Nat Rev Immunol.* 2009;9(11):799-809. doi:10.1038/nri2653

Ulivieri C, Baldari CT. Statins: from cholesterol-lowering drugs to novel immunomodulators for the treatment of Th17-mediated autoimmune diseases. *Pharmacol Res.* 2014; 88:41-52. doi: 10.1016/j.phrs.2014.03.001

Vallejo-Vaz AJ, Robertson M, Catapano AL, et al. Low-Density Lipoprotein Cholesterol Lowering for the Primary Prevention of Cardiovascular Disease Among Men with Primary Elevations of Low-Density Lipoprotein Cholesterol Levels of 190 mg/dL or Above: Analyses from the WOSCOPS (West of Scotland Coronary Prevention Study) 5-Year Randomized Trial and 20-Year Observational Follow-Up. *Circulation.* 2017;136(20):1878-1891. doi:10.1161/CIRCULATIONAHA.117.027966

Van den Abbeele P, Belzer C, Goossens M, et al. Butyrate-producing *Clostridium* cluster XIVa species specifically colonize mucins in an in vitro gut model. *ISME J.* 2013;7(5):949-961. doi:10.1038/ismej.2012.158

van der Meer-Janssen YP, van Galen J, Batenburg JJ, Helms JB. Lipids in host-pathogen interactions: pathogens exploit the complexity of the host cell lipidome. *Prog Lipid Res.* 2010;49(1):1-26. doi: 10.1016/j.plipres.2009.07.003

Van Deuren T, Blaak EE, Canfora EE. Butyrate to combat obesity and obesity-associated metabolic disorders: Current status and future implications for therapeutic use. *Obes Rev.* 2022;23(10):e13498. doi:10.1111/obr.13498

Vanuytsel T, Tack J, Farre R. The Role of Intestinal Permeability in Gastrointestinal Disorders and Current Methods of Evaluation. *Front Nutr.* 2021; 8:717925. Published 2021 Aug 26. doi:10.3389/fnut.2021.717925

Vanuytsel T, Tack J, Farre R. The Role of Intestinal Permeability in Gastrointestinal Disorders and Current Methods of Evaluation. *Front Nutr.* 2021; 8:717925. Published 2021 Aug 26. doi:10.3389/fnut.2021.717925

Varkonyi-Gasic E, Wu R, Wood M, Walton EF, Hellens RP. Protocol: a highly sensitive RT-PCR method for detection and quantification of microRNAs. *Plant Methods.* 2007; 3:12. Published 2007 Oct 12. doi:10.1186/1746-4811-3-12

Varshney P, Narasimhan A, Mittal S, Malik G, Sardana K, Saini N. Transcriptome profiling unveils the role of cholesterol in IL-17A signaling in psoriasis. *Sci Rep.* 2016; 6:19295. Published 2016 Jan 19. doi:10.1038/srep19295

Venkatraman JT, Leddy J, Pendergast D. Dietary fats and immune status in athletes: clinical implications. *Med Sci Sports Exerc.* 2000;32(7 Suppl):S389-S395. doi:10.1097/00005768-200007001-00003

Venugopal S, Anwer S, Szászi K. Claudin-2: Roles beyond Permeability Functions. *Int J Mol Sci.* 2019;20(22):5655. Published 2019 Nov 12. doi:10.3390/ijms20225655

Venugopal S, Anwer S, Szászi K. Claudin-2: Roles beyond Permeability Functions. *Int J Mol Sci.* 2019;20(22):5655. Published 2019 Nov 12. doi:10.3390/ijms20225655

Vickers KC, Landstreet SR, Levin MG, et al. MicroRNA-223 coordinates cholesterol homeostasis. *Proc Natl Acad Sci U S A.* 2014;111(40):14518-14523. doi:10.1073/pnas.1215767111

Vinolo MA, Rodrigues HG, Nachbar RT, Curi R. Regulation of inflammation by short chain fatty acids. *Nutrients.* 2011;3(10):858-876. doi:10.3390/nu3100858

Vital M, Howe AC, Tiedje JM. Revealing the bacterial butyrate synthesis pathways by analyzing (meta)genomic data. *mBio.* 2014;5(2):e00889. Published 2014 Apr 22. doi:10.1128/mBio.00889-14

Vlasova-St Louis I, Bohjanen PR. Post-transcriptional regulation of cytokine signaling by AU-rich and GU-rich elements. *J Interferon Cytokine Res.* 2014;34(4):233-241. doi:10.1089/jir.2013.0108

Vock C, Döring F, Nitz I. Transcriptional regulation of HMG-CoA synthase and HMG-CoA reductase genes by human ACBP. *Cell Physiol Biochem.* 2008;22(5-6):515-524. doi:10.1159/000185525

Vourakis M, Mayer G, Rousseau G. The Role of Gut Microbiota on Cholesterol Metabolism in Atherosclerosis. *Int J Mol Sci.* 2021;22(15):8074. Published 2021 Jul 28. doi:10.3390/ijms22158074

Wagner AD, Schacter DL, Rotte M, et al. Building memories: remembering and forgetting of verbal experiences as predicted by brain activity. *Science.* 1998;281(5380):1188-1191. doi:10.1126/science.281.5380.1188

Wagner BJ, DeMaria CT, Sun Y, Wilson GM, Brewer G. Structure and genomic organization of the human AUF1 gene: alternative pre-mRNA splicing generates four protein isoforms. *Genomics.* 1998;48(2):195-202. doi:10.1006/geno.1997.5142

Wagner BJ, DeMaria CT, Sun Y, Wilson GM, Brewer G. Structure and genomic organization of the human AUF1 gene: alternative pre-mRNA splicing generates four protein isoforms. *Genomics.* 1998;48(2):195-202. doi:10.1006/geno.1997.5142

Wang HB, Wang PY, Wang X, Wan YL, Liu YC. Butyrate enhances intestinal epithelial barrier function via up-regulation of tight junction protein Claudin-1 transcription. *Dig Dis Sci.* 2012;57(12):3126-3135. doi:10.1007/s10620-012-2259-4

- Wang HB, Wang PY, Wang X, Wan YL, Liu YC. Butyrate enhances intestinal epithelial barrier function via up-regulation of tight junction protein Claudin-1 transcription. *Dig Dis Sci*. 2012;57(12):3126-3135. doi:10.1007/s10620-012-2259-4
- Wang J, Yang K, Zhou L, et al. MicroRNA-155 promotes autophagy to eliminate intracellular mycobacteria by targeting Rheb. *PLoS Pathog*. 2013;9(10):e1003697. doi:10.1371/journal.ppat.1003697
- Wang K, Li J, Zhao L, et al. Gut microbiota protects honey bees (*Apis mellifera* L.) against polystyrene microplastics exposure risks. *J Hazard Mater*. 2021; 402:123828. doi: 10.1016/j.jhazmat.2020.123828
- Wang T, He C. Pro-inflammatory cytokines: The link between obesity and osteoarthritis. *Cytokine Growth Factor Rev*. 2018; 44:38-50. doi: 10.1016/j.cytogfr.2018.10.002
- Wang XC, Zhan XR, Li XY, Yu JJ, Liu XM. MicroRNA-185 regulates expression of lipid metabolism genes and improves insulin sensitivity in mice with non-alcoholic fatty liver disease. *World J Gastroenterol*. 2014;20(47):17914-17923. doi:10.3748/wjg. v20.i47.17914
- Wang Y, Chen D, Xie H, et al. AUF1 protects against ferroptosis to alleviate sepsis-induced acute lung injury by regulating NRF2 and ATF3. *Cell Mol Life Sci*. 2022;79(5):228. Published 2022 Apr 7. doi:10.1007/s00018-022-04248-8
- Wang Y, Jiang Y, Deng Y, et al. Probiotic Supplements: Hope or Hype? *Front Microbiol*. 2020; 11:160. Published 2020 Feb 28. doi:10.3389/fmicb.2020.00160
- Wang Y, Xu N, Xi A, Ahmed Z, Zhang B, Bai X. Effects of *Lactobacillus plantarum* MA2 isolated from Tibet kefir on lipid metabolism and intestinal microflora of rats fed on high-cholesterol diet. *Appl Microbiol Biotechnol*. 2009;84(2):341-347. doi:10.1007/s00253-009-2012-x
- Wang Z, Min X, Xiao SH, et al. Molecular basis of sphingosine kinase 1 substrate recognition and catalysis. *Structure*. 2013;21(5):798-809. doi: 10.1016/j.str.2013.02.025
- Warren T, McAllister R, Morgan A, et al. The Interdependency and Co-Regulation of the Vitamin D and Cholesterol Metabolism. *Cells*. 2021;10(8):2007. Published 2021 Aug 6. doi:10.3390/cells10082007
- Weber C, Schober A, Zernecke A. Chemokines: key regulators of mononuclear cell recruitment in atherosclerotic vascular disease. *Arterioscler Thromb Vasc Biol*. 2004;24(11):1997-2008. doi:10.1161/01.ATV.0000142812.03840.6f
- Wen J, Friedman JR. miR-122 regulates hepatic lipid metabolism and tumor suppression. *J Clin Invest*. 2012;122(8):2773-2776. doi:10.1172/JCI63966

White EJ, Brewer G, Wilson GM. Post-transcriptional control of gene expression by AUF1: mechanisms, physiological targets, and regulation. *Biochim Biophys Acta*. 2013;1829(6-7):680-688. doi: 10.1016/j.bbagr.2012.12.002

White EJ, Matsangos AE, Wilson GM. AUF1 regulation of coding and noncoding RNA. *Wiley Interdiscip Rev RNA*. 2017;8(2):10.1002/wrna.1393. doi:10.1002/wrna.1393

White EJ, Matsangos AE, Wilson GM. AUF1 regulation of coding and noncoding RNA. *Wiley Interdiscip Rev RNA*. 2017;8(2):10.1002/wrna.1393. doi:10.1002/wrna.1393

Widomska J, Subczynski WK. Why Is Very High Cholesterol Content Beneficial for the Eye Lens but Negative for Other Organs? *Nutrients*. 2019;11(5):1083. Published 2019 May 15. doi:10.3390/nu11051083

Wightman B, Ha I, Ruvkun G. Posttranscriptional regulation of the heterochronic gene *lin-14* by *lin-4* mediates temporal pattern formation in *C. elegans*. *Cell*. 1993;75(5):855-862. doi:10.1016/0092-8674(93)90530-4

Willemsen LE, Koetsier MA, van Deventer SJ, van Tol EA. Short chain fatty acids stimulate epithelial mucin 2 expression through differential effects on prostaglandin E(1) and E(2) production by intestinal myofibroblasts. *Gut*. 2003;52(10):1442-1447. doi:10.1136/gut.52.10.1442

Wilson GM, Lu J, Sutphen K, et al. Phosphorylation of p40AUF1 regulates binding to A + U-rich mRNA-destabilizing elements and protein-induced changes in ribonucleoprotein structure. *J Biol Chem*. 2003;278(35):33039-33048. doi:10.1074/jbc.M305775200

Wilson GM, Sun Y, Lu H, Brewer G. Assembly of AUF1 oligomers on U-rich RNA targets by sequential dimer association. *J Biol Chem*. 1999;274(47):33374-33381. doi:10.1074/jbc.274.47.33374

Wong JM, de Souza R, Kendall CW, Emam A, Jenkins DJ. Colonic health: fermentation and short chain fatty acids. *J Clin Gastroenterol*. 2006;40(3):235-243. doi:10.1097/00004836-200603000-00015

Wong JM, de Souza R, Kendall CW, Emam A, Jenkins DJ. Colonic health: fermentation and short chain fatty acids. *J Clin Gastroenterol*. 2006;40(3):235-243. doi:10.1097/00004836-200603000-00015

Wu B, Zhang Z, Lui W, et al. Endocardial cells form the coronary arteries by angiogenesis through myocardial-endocardial VEGF signaling. *Cell*. 2012;151(5):1083-1096. doi: 10.1016/j.cell.2012.10.023

Wu S, Lu H, Bai Y. Nrf2 in cancers: A double-edged sword. *Cancer Med*. 2019;8(5):2252-2267. doi:10.1002/cam4.2101

- Wu X, Yang B, Udo-Inyang I, et al. Research Techniques Made Simple: Single-Cell RNA Sequencing and its Applications in Dermatology. *J Invest Dermatol*. 2018;138(5):1004-1009. doi: 10.1016/j.jid.2018.01.026
- Wu X, Yang Y, Huang Y, et al. RNA-binding protein AUF1 suppresses miR-122 biogenesis by down-regulating Dicer1 in hepatocellular carcinoma. *Oncotarget*. 2018;9(19):14815-14827. Published 2018 Jan 9. doi:10.18632/oncotarget.24079
- Xu YH, Gao CL, Guo HL, et al. Sodium butyrate supplementation ameliorates diabetic inflammation in db/db mice. *J Endocrinol*. 2018;238(3):231-244. doi:10.1530/JOE-18-0137
- Yamada H, Suzuki K, Ichino N, et al. Associations between circulating microRNAs (miR-21, miR-34a, miR-122 and miR-451) and non-alcoholic fatty liver. *Clin Chim Acta*. 2013; 424:99-103. doi: 10.1016/j.cca.2013.05.021
- Yan H, Ajuwon KM. Butyrate modifies intestinal barrier function in IPEC-J2 cells through a selective upregulation of tight junction proteins and activation of the Akt signaling pathway. *PLoS One*. 2017;12(6):e0179586. Published 2017 Jun 27. doi: 10.1371/journal.pone.0179586
- Yan Y, Kolachala V, Dalmaso G, et al. Temporal and spatial analysis of clinical and molecular parameters in dextran sodium sulfate induced colitis. *PLoS One*. 2009;4(6):e6073. Published 2009 Jun 29. doi: 10.1371/journal.pone.0006073
- Yancey PG, Bortnick AE, Kellner-Weibel G, de la Llera-Moya M, Phillips MC, Rothblat GH. Importance of different pathways of cellular cholesterol efflux. *Arterioscler Thromb Vasc Biol*. 2003;23(5):712-719. doi: 10.1161/01.ATV.0000057572.97137.DD
- Yang AN, Zhang HP, Sun Y, et al. High-methionine diets accelerate atherosclerosis by HHcy-mediated FABP4 gene demethylation pathway via DNMT1 in ApoE(-/-) mice. *FEBS Lett*. 2015;589(24 Pt B):3998-4009. doi: 10.1016/j.febslet.2015.11.010
- Yang H, Wang W, Romano KA, et al. A common antimicrobial additive increases colonic inflammation and colitis-associated colon tumorigenesis in mice. *Sci Transl Med*. 2018;10(443):eaan4116. doi:10.1126/scitranslmed. aan4116
- Yang J, Chen W, Xia P, Zhang W. Dynamic comparison of gut microbiota of mice infected with *Shigella flexneri* via two different infective routes. *Exp Ther Med*. 2020;19(3):2273-2281. doi:10.3892/etm.2020.8469
- Yang JY, Lee SN, Chang SY, Ko HJ, Ryu S, Kweon MN. A mouse model of shigellosis by intraperitoneal infection. *J Infect Dis*. 2014;209(2):203-215. doi:10.1093/infdis/jit399
- Yin J, Zhu Y, Malik V, et al. Intake of Sugar-Sweetened and Low-Calorie Sweetened Beverages and

Risk of Cardiovascular Disease: A Meta-Analysis and Systematic Review. *Adv Nutr.* 2021;12(1):89-101. doi:10.1093/advances/nmaa084

Yu TX, Rao JN, Zou T, et al. Competitive binding of CUGBP1 and HuR to occludin mRNA controls its translation and modulates epithelial barrier function. *Mol Biol Cell.* 2013;24(2):85-99. doi:10.1091/mbc.E12-07-0531

Yu Y, Chipot C, Cai W, Shao X. Molecular dynamics study of the inclusion of cholesterol into cyclodextrins. *J Phys Chem B.* 2006;110(12):6372-6378. doi:10.1021/jp056751a

Yuille S, Reichardt N, Panda S, Dunbar H, Mulder IE. Human gut bacteria as potent class I histone deacetylase inhibitors in vitro through production of butyric acid and valeric acid. *PLoS One.* 2018;13(7):e0201073. Published 2018 Jul 27. doi: 10.1371/journal.pone.0201073

Zaas AK, Chen M, Varkey J, et al. Gene expression signatures diagnose influenza and other symptomatic respiratory viral infections in humans. *Cell Host Microbe.* 2009;6(3):207-217. doi: 10.1016/j.chom.2009.07.006

Zampelas A, Magriplis E. New Insights into Cholesterol Functions: A Friend or an Enemy? *Nutrients.* 2019;11(7):1645. Published 2019 Jul 18. doi:10.3390/nu11071645

Zhang Y, Lanjuin A, Chowdhury SR, et al. Neuronal TORC1 modulates longevity via AMPK and cell nonautonomous regulation of mitochondrial dynamics in *C. elegans*. *Elife.* 2019;8: e49158. Published 2019 Aug 14. doi:10.7554/eLife.49158

Zhang Y, Parajuli KR, Fava GE, et al. GLP-1 Receptor in Pancreatic α -Cells Regulates Glucagon Secretion in a Glucose-Dependent Bidirectional Manner [published correction appears in *Diabetes.* 2020 Feb;69(2):267-268]. *Diabetes.* 2019;68(1):34-44. doi:10.2337/db18-0317

Zhao K, Ridgway ND. Oxysterol-Binding Protein-Related Protein 1L Regulates Cholesterol Egress from the Endo-Lysosomal System. *Cell Rep.* 2017;19(9):1807-1818. doi: 10.1016/j.celrep.2017.05.028

Zhao L, Zhang F, Ding X, et al. Gut bacteria selectively promoted by dietary fibers alleviate type 2 diabetes. *Science.* 2018;359(6380):1151-1156. doi:10.1126/science.aao5774

Zhao M, Luo Z, He H, et al. Decreased Low-Density Lipoprotein Cholesterol Level Indicates Poor Prognosis of Severe and Critical COVID-19 Patients: A Retrospective, Single-Center Study. *Front Med (Lausanne).* 2021; 8:585851. Published 2021 May 26. doi:10.3389/fmed.2021.585851

Zhao ZH, Wang ZX, Zhou D, et al. Sodium Butyrate Supplementation Inhibits Hepatic Steatosis by Stimulating Liver Kinase B1 and Insulin-Induced Gene. *Cell Mol Gastroenterol Hepatol.* 2021;12(3):857-871. doi: 10.1016/j.jcmgh.2021.05.006

- Zheng D, Liwinski T, Elinav E. Interaction between microbiota and immunity in health and disease. *Cell Res.* 2020;30(6):492-506. doi:10.1038/s41422-020-0332-7
- Zheng D, Liwinski T, Elinav E. Interaction between microbiota and immunity in health and disease. *Cell Res.* 2020;30(6):492-506. doi:10.1038/s41422-020-0332-7
- Zheng L, Kelly CJ, Battista KD, et al. Microbial-Derived Butyrate Promotes Epithelial Barrier Function through IL-10 Receptor-Dependent Repression of Claudin-2. *J Immunol.* 2017;199(8):2976-2984. doi:10.4049/jimmunol.1700105
- Zhou AL, Swaminathan SK, Curran GL, et al. Apolipoprotein A-I Crosses the Blood-Brain Barrier through Clathrin-Independent and Cholesterol-Mediated Endocytosis. *J Pharmacol Exp Ther.* 2019;369(3):481-488. doi:10.1124/jpet.118.254201
- Zhou Q, Liao JK. Statins and cardiovascular diseases: from cholesterol lowering to pleiotropy. *Curr Pharm Des.* 2009;15(5):467-478. doi:10.2174/138161209787315684
- Ziegler SF, Buckner JH. FOXP3 and the regulation of Treg/Th17 differentiation. *Microbes Infect.* 2009;11(5):594-598. doi: 10.1016/j.micinf.2009.04.002
- Zimmerman MA, Singh N, Martin PM, et al. Butyrate suppresses colonic inflammation through HDAC1-dependent Fas upregulation and Fas-mediated apoptosis of T cells. *Am J Physiol Gastrointest Liver Physiol.* 2012;302(12):G1405-G1415. doi:10.1152/ajpgi.00543.2011
- Zou H, Yang N, Zhang X, Chen HW. ROR γ is a context-specific master regulator of cholesterol biosynthesis and an emerging therapeutic target in cancer and autoimmune diseases. *Biochem Pharmacol.* 2022; 196:114725. doi: 10.1016/j.bcp.2021.114725
- Zucconi BE, Ballin JD, Brewer BY, et al. Alternatively expressed domains of AU-rich element RNA-binding protein 1 (AUF1) regulate RNA-binding affinity, RNA-induced protein oligomerization, and the local conformation of bound RNA ligands. *J Biol Chem.* 2010;285(50):39127-39139. doi:10.1074/jbc.M110.180182
- Zucconi BE, Ballin JD, Brewer BY, et al. Alternatively expressed domains of AU-rich element RNA-binding protein 1 (AUF1) regulate RNA-binding affinity, RNA-induced protein oligomerization, and the local conformation of bound RNA ligands. *J Biol Chem.* 2010;285(50):39127-39139. doi:10.1074/jbc.M110.180182
- Zucconi BE, Ballin JD, Brewer BY, et al. Alternatively expressed domains of AU-rich element RNA-binding protein 1 (AUF1) regulate RNA-binding affinity, RNA-induced protein oligomerization, and the local conformation of bound RNA ligands. *J Biol Chem.* 2010;285(50):39127-39139. doi:10.1074/jbc.M110.180182

Zucconi BE, Ballin JD, Brewer BY, et al. Alternatively expressed domains of AU-rich element RNA-binding protein 1 (AUF1) regulate RNA-binding affinity, RNA-induced protein oligomerization, and the local conformation of bound RNA ligands. *J Biol Chem*. 2010;285(50):39127-39139. doi:10.1074/jbc.M110.180182

Zucconi BE, Wilson GM. Modulation of neoplastic gene regulatory pathways by the RNA-binding factor AUF1. *Front Biosci (Landmark Ed)*. 2011;16(6):2307-2325. Published 2011 Jun 1. doi:10.2741/3855

Zucconi BE, Wilson GM. Modulation of neoplastic gene regulatory pathways by the RNA-binding factor AUF1. *Front Biosci (Landmark Ed)*. 2011;16(6):2307-2325. Published 2011 Jun 1. doi:10.2741/3855

Zuo L, Lu M, Zhou Q, Wei W, Wang Y. Butyrate suppresses proliferation and migration of RKO colon cancer cells through regulating endocan expression by MAPK signaling pathway. *Food Chem Toxicol*. 2013; 62:892-900.

Publications and Proceedings

AUF-1 knockdown in mice undermines gut microbial butyrate-driven hypocholesterolaemia through AUF-1-Dicer-1-mir-122 hierarchy

Das O, Kundu J, Ghosh A, et al. AUF-1 knockdown in mice undermines gut microbial butyrate-driven hypocholesterolaemia through AUF-1-Dicer-1-mir-122 hierarchy. *Front Cell Infect Microbiol.* 2022; 12:1011386. Published 2022 Dec 19. doi:10.3389/fcimb.2022.1011386

Butyrate driven raft disruption trots off enteric pathogen invasion: possible mechanism of colonization resistance

Das O, Masid A, Chakraborty M, Gope A, Dutta S, Bhaumik M. Butyrate driven raft disruption trots off enteric pathogen invasion: possible mechanism of colonization resistance. *Gut Pathog.* 2023;15(1):19. Published 2023 Apr 21. doi:10.1186/s13099-023-00545-0

Prenatal arsenic exposure stymies gut butyrate production and enhances gut permeability in post-natal life even in absence of arsenic deftly through miR122-Occludin pathway

Chakraborty M, Gautam A, **Das O**, Masid A, Bhaumik M. Prenatal arsenic exposure stymies gut butyrate production and enhances gut permeability in post-natal life even in absence of arsenic deftly through miR122-Occludin pathway. *Toxicol Lett.* 2023; 374:19-30. doi: 10.1016/j.toxlet.2022.11.011

Gum Odina prebiotic prevents experimental colitis in C57BL/6 mice model and its role in shaping gut microbial diversity

Mitra D, Sikdar S, Chakraborty M, **Das O**, Samanta A, Dutta S. Gum Odina prebiotic prevents experimental colitis in C57BL/6 mice model and its role in shaping gut microbial diversity. *Food Bioscience*, 2023; (53). Published 2023 June 12. doi:org/10.1016/j.fbio.2023.102509



OPEN ACCESS

EDITED BY

Tianying Wang,
Qingdao University Medical College,
China

REVIEWED BY

Nitish R. Mahapatra,
Indian Institute of Technology Madras,
India
Jon D. Moulton,
Gene Tools, LLC, United States

*CORRESPONDENCE

Moumita Bhaumik
drmmoumitabhaumik@gmail.com

SPECIALTY SECTION

This article was submitted to
Intestinal Microbiome,
a section of the journal
Frontiers in Cellular and
Infection Microbiology

RECEIVED 04 August 2022

ACCEPTED 28 November 2022

PUBLISHED 19 December 2022

CITATION

Das O, Kundu J, Ghosh A, Gautam A,
Ghosh S, Chakraborty M, Masid A,
Gauri SS, Mitra D, Dutta M,
Mukherjee B, Sinha S and Bhaumik M
(2022) AUF-1 knockdown in mice
undermines gut microbial butyrate-
driven hypocholesterolemia through
AUF-1–Dicer-1–mir-122 hierarchy.
Front. Cell. Infect. Microbiol.
12:1011386.
doi: 10.3389/fcimb.2022.1011386

COPYRIGHT

© 2022 Das, Kundu, Ghosh, Gautam,
Ghosh, Chakraborty, Masid, Gauri, Mitra,
Dutta, Mukherjee, Sinha and Bhaumik.
This is an open-access article
distributed under the terms of the
[Creative Commons Attribution License
\(CC BY\)](https://creativecommons.org/licenses/by/4.0/). The use, distribution or
reproduction in other forums is
permitted, provided the original
author(s) and the copyright owner(s)
are credited and that the original
publication in this journal is cited, in
accordance with accepted academic
practice. No use, distribution or
reproduction is permitted which does
not comply with these terms.

AUF-1 knockdown in mice undermines gut microbial butyrate-driven hypocholesterolemia through AUF-1–Dicer-1–mir-122 hierarchy

Oishika Das¹, Jayanta Kundu², Atanu Ghosh²,
Anupam Gautam^{3,4,5}, Souradeepa Ghosh⁶, Mainak
Chakraborty¹, Aaheli Masid¹, Samiran Sona Gauri⁶, Debmalya
Mitra¹, Moumita Dutta¹, Budhaditya Mukherjee⁶, Surajit Sinha²
and Moumita Bhaumik^{1*}

¹Department of Immunology, Indian Council of Medical Research–National Institute of Cholera and Enteric Diseases, Kolkata, India, ²School of Applied and Interdisciplinary Sciences, Indian Association for Cultivation of Science, Kolkata, India, ³Department of Algorithms in Bioinformatics, Institute for Bioinformatics and Medical Informatics, University of Tübingen, Tübingen, Germany, ⁴International Max Planck Research School “From Molecules to Organisms”, Max Planck Institute for Biology Tübingen, Tübingen, Germany, ⁵Cluster of Excellence: EXC 2124: Controlling Microbes to Fight Infection, University of Tübingen, Tübingen, Germany, ⁶School of Medical Science and Technology, Indian Institute of Technology, Kharagpur, India

Introduction and objective: Cholesterol homeostasis is a culmination of cellular synthesis, efflux, and catabolism to important physiological entities where short chain fatty acid, butyrate embodied as a key player. This discourse probes the mechanistic molecular details of butyrate action in maintaining host-cholesterol balance.

Methods: Hepatic mir-122 being the most indispensable regulator of cholesterol metabolic enzymes, we studied upstream players of mir-122 biogenesis in the presence and absence of butyrate in Huh7 cells and mice model. We synthesized unique self-transfecting GMO (guanidinium-morpholino-oligo) linked PMO (Phosphorodiamidate-Morpholino Oligo)-based antisense cell-penetrating reagent to selectively knock down the key player in butyrate mediated cholesterol regulation.

Results: We showed that butyrate treatment caused upregulation of RNA-binding protein, AUF1 resulting in RNase-III nuclease, Dicer1 instability, and significant diminution of mir-122. We proved the importance of AUF1 and sequential downstream players in AUF1-knock-down mice. Injection of GMO-PMO of AUF1 in mouse caused near absence of AUF1 coupled with increased

Dicer1 and mir-122, and reduced serum cholesterol regardless of butyrate treatment indicating that butyrate acts through AUF1.

Conclusion: The roster of intracellular players was as follows: AUF1-Dicer1-mir-122 for triggering butyrate driven hypocholesterolemia. To our knowledge this is the first report linking AUF-1 with cholesterol biogenesis.

KEYWORDS

AUF-1, butyrate, cholesterol metabolism, Dicer-1, GMO-PMO, microbiome, mir-122.

Introduction

The gut microbiome is endowed with the special ability to govern host metabolic function, which cannot be accomplished by the host itself. Gut microbiota on fermentation of non-digestible carbohydrates produce short-chain fatty acids (SCFAs) like acetate, propionate, and butyrate at a ratio of 3:1:1 (Chambers et al., 2018). There is colossal evidence that gut-derived SCFAs display overarching effects on health and diseases (Rios-Covian et al., 2016). The benefits of butyrate are particularly well-researched as a therapeutic agent against inflammatory diseases, neurological disorders, and others (Canani et al., 2011). Butyrate is also reported to mediate the host cellular energy metabolic landscape (Liu et al., 2018). Studies in mouse models have shown that a diet supplemented with butyrate prevents high-fat diet (HFD)-induced obesity, by downregulating the expression and activity of PPAR- γ (den Besten et al., 2015), while the intake of dietary polysaccharide pectin that produces butyrate after fermentation in gut inhibits cholesterol uptake and promotes cholesterol efflux from enterocytes in Apo E^{-/-} mice (Chen et al., 2018). There are different types of lipoproteins (HDL, LDL, VLDL, and chylomicron) consisting of different percentages of cholesterol, protein, triglyceride, and phospholipids.

Cholesterol orchestrates a number of important cellular functions like membrane fluidity, steroid hormone synthesis, and bile acid synthesis, while its intermediate metabolic precursor, 7-dehydrocholesterol, serves as a precursor of vitamin D (Zampelas and Magriplis, 2019). Dysregulation of cholesterol metabolism is associated with cardiovascular disease, neurodegenerative diseases, diabetes, and cancer (Merscher-Gomez et al., 2013; Kuzu et al., 2016; Vallejo-Vaz et al., 2017).

Cholesterol homeostasis at the cellular level is governed at multiple layers like biosynthesis, catabolism, and efflux; the latter pathway is accomplished by ATP-binding cassette transporter A1 (ABCA1) (Yancey et al., 2003). These distinctly different, linked paradigms are converged to a singular framework of host cholesterol homeostasis under the influence of butyrate.

At the cellular level, the regulation of cholesterol biogenesis and efflux is governed by microRNAs; the important ones include mir-122 and miR27 (Krutzfeldt et al., 2005; Canani et al., 2011). mir-122, making up 70% of the total hepatic miRNA (Lagos-Quintana et al., 2002), contributes to the maintenance of the adult liver phenotype (Girard et al., 2008). Mice treated with antagomir-122 were shown to modulate cholesterol metabolic genes (Krutzfeldt et al., 2005). Like most miRNAs, mir-122 is generated from the primary precursor, pri-mir-122, by nuclear RNaseIII Drosha; the resultant pre-mir-122 undergoes processing with the help of Dicer-1, another RNase III nuclease that processes the pre-miRNA into a 22-bp double-stranded RNA (O'Brien et al., 2018). Dicer-1-mediated mir-122 maturation is a critical step in mir-122 biogenesis, which occurs in the cytoplasm.

In mammals, the Dicer-1 mRNA is destabilized by the presence of AU-rich elements (AREs) in their 3'-untranslated regions (Abdelmohsen et al., 2012). The protein ARE/poly(U)-binding/degradation factor-1 (AUF-1) binds to many ARE-mRNAs and assembles other factors necessary to recruit the mRNA degradation machinery (Gratacos and Brewer, 2010). AUF-1 RNA binding proteins are a family with four splice variants: AUF-1^{P45}, AUF-1^{P42}, AUF-1^{P40}, and AUF-1^{P37} (Abdelmohsen et al., 2012). The AUF-1 interacts with the 3'-UTR of Dicer-1 mRNA and causes mRNA destabilization, reducing its half-life (Abdelmohsen et al., 2012). AUF-1 KO mice develop chronic dermatitis (Sadri and Schneider, 2009) and are prone to septicemic shock (Lu et al., 2006). Importantly, AUF-1 is found to decay mRNA of sphingosine kinase1 (Sobue et al., 2008), which produces Sphingosine-1-phosphate (S1P), a biomarker of sepsis (Hasan and Karst, 1989) and other inflammatory diseases (Suh and Saba, 2015). The absence of AUF-1 thus increases S1P, which causes rapid expansion of inflammatory signals (Graler, 2012).

This study determines that gut-derived butyrate flux affects metabolic phenotype through miRNAs, Dicer-1, AUF-1, and cholesterol metabolic enzymes and controls cholesterol homeostasis. We explored domains like expression of

cholesterol synthesis, catabolic genes, and efflux protein in the presence and absence of butyrate. We showed that butyrate modulates selective isoforms of RNA binding protein AUF-1, leading to downregulation of Dicer-1 and mir-122, resulting in decrease in cellular cholesterol. To provide further leverage in our understanding, we had synthesized a unique self-transfecting GMO (guanidinium morpholino oligos)-linked PMO (phosphorodiamidate morpholino oligos)-based antisense reagent, to knock down AUF-1 in mice. Using AUF-1 knockdown mice, we provided crucial evidence that butyrate indeed exploits AUF-1 to accomplish its cellular effect. The above discourse led to a new element of our understanding on the role of AUF-1 in cholesterol metabolism. Narratives from our experimental studies when considered in tandem culminated in the following trajectory of butyrate action “butyrate–AUF-1–Dicer-1–mir-122–cholesterol metabolic enzymes–cholesterol”, which is tentatively posited as “axis”.

Results

Butyrate effectively reduces cellular cholesterol at lower concentration than propionate and acetate in murine primary hepatocytes but requires higher concentration to reduce cholesterol and HMGCR expression in Huh7 cells

To witness which one of the SCFAs may interfere in cholesterol biogenesis with fidelity, we undertook an initial approach in the primary hepatocyte culture, although most of our obvious thrust is in the mouse model. To assess the effects of SCFAs on cellular cholesterol biogenesis, hepatocytes were treated with increasing concentration (0–0.045 mM) of either sodium butyrate (butyrate) or sodium propionate (propionate) or sodium acetate (acetate) for 24 h, following which cellular cholesterol was measured. The concentration of SCFAs used in the study was based on the concentration reaching the liver *via* portal vein (Cummings et al., 1987). It was observed that unlike propionate and acetate (Figure S1), 5, 15, and 45 μ M butyrate treatment caused 27%, 36%, and 40% decrease in cellular cholesterol, respectively (Figure S1A inset). As primary hepatocytes die in a couple of days in culture and highly prone to dedifferentiation (Hu and Li, 2015), we extended our *in vitro* study in Huh7 cells, which is considered essentially as a model for studying hepatic processes. Interestingly, butyrate treatment at lower doses did not show significant reduction in cholesterol in Huh7 cells, but higher doses (5–20 mM) of butyrate treatment caused a significant decrease in cellular cholesterol. The higher concentration of SCFAs used to treat Huh7 cells was based on an earlier report (Zhao et al., 2021). To ensure the viability of the cells at higher doses of butyrate, we performed an MTT assay where we show that more than 85% of Huh7 cells were viable at 20 mM butyrate (Figure S2 inset). Since butyrate but not the others reduced

cellular cholesterol, we studied the ability of butyrate on the rate-limiting enzyme of the cholesterol biogenesis pathway and opted to study the status of HMGCR (3-hydroxy-3-methylglutaryl-CoA reductase) by Western blot in butyrate-treated and untreated Huh7 cells. It was observed that there was a significant decrease in HMGCR in butyrate-treated cells as compared to untreated cells as a function of butyrate concentration (Figure S1B). The results were presented by densitometric analysis (Figure S1C). The percentage decrease in HMGCR in Huh7 cells upon the addition of 10 and 20 mM butyrate was 37% and 74%, respectively. Based on the cell line results, we asked the same question in the animal model.

Butyrate corrects hypercholesterolemia in mice receiving HFD (HFD mice) and reverses elevated hepatic enzymes

The mice were fed with HFD for 30 days and then divided into two groups. One group of mice continued to receive HFD (HFD mice) and another group received butyrate with HFD for another 15 days (HFD butyrate mice). A third group of mice kept as control received regular chow diet (chow mice). All three groups were sacrificed on day 45 to study a variety of parameters. To start with, body weight and food intake of all three groups of mice were recorded. It was observed that in HFD mice, the body weight continued to increase at a higher rate as compared to chow mice up to the 30-day treatment protocol. With the commencement of butyrate treatment on day 31 in HFD mice for another 15 days (HFD butyrate mice), there was a significant decrease in body weight as compared to HFD mice. In other words, on day 45, there was hardly any difference noticed in body weight between normal and HFD butyrate mice (Figure S2A, inset). It was observed that all three groups showed a similar magnitude of food intake (Figure S2B). Then, we went on to study the status of cholesterol and lipoproteins in all the three groups.

It was observed that compared to chow mice, HFD mice showed a 60% increase in serum cholesterol, which returned to normal in HFD butyrate mice (Figure 1). Two liver-specific enzymes, alanine transaminase (ALT) and aspartate aminotransferase (AST), were studied as markers of HFD-induced hepatic stress. It was observed that both ALT and AST were significantly increased in HFD mice, which returned to normal in HFD butyrate mice (Figure S2C).

Butyrate influences cholesterol metabolic genes

The microarray datasets comparing butyrate-treated colonic epithelial cells (MCE301) vs. untreated control (GSE4410) and HeLa cells treated with butyrate vs. corresponding untreated control (GSE45220) are available in public domain. The results were presented in volcano plots and gene expression showing that a statistically significant fold change revealed an array of

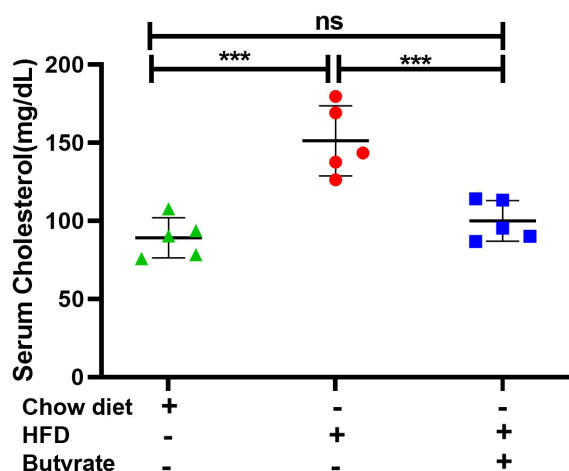


FIGURE 1

Effect of butyrate treatment on serum cholesterol level of HFD (high-fat diet) fed mice (HFD mice). Female mice (10 in number) were fed with HFD for 30 days and then divided randomly into two groups equally. One group continued receiving HFD (HFD mice) and another group received 5% sodium butyrate (butyrate) supplemented with HFD (w/w) for another 15 days (HFD butyrate mice). Another independent group of mice (five in number) were fed with normal chow diet for 45 days, which served as a control (chow mice). On day 45, serum cholesterol levels in chow mice, HFD mice, and HFD butyrate mice were determined and expressed in mg/dL. $N = 5/\text{group}$; the experiment was repeated thrice. The data are presented as mean \pm SE. ns represents not significant, *** represents $p < 0.001$.

information on cholesterol metabolic genes (Figure S3A). Differential expression analysis indicated that butyrate treatment resulted in an overall repression of cholesterol metabolizing genes, of which some are directly and some are indirectly involved. The common genes between two datasets that were considered for further studies included HMG CoA reductase (*hmgcr*), acetyl CoA acetyltransferase-2 (*acat2*), 7-dehydrocholesterol reductase (*dhcr7*), HMG CoA synthase 1 (*hmgcs1*), and 24-dehydrocholesterol reductase (*dhcr24*). A significant downregulation in *hmgcr*, *acat2*, *dhcr7*, *hmgcs1*, and *dhcr24* expression with butyrate treatment was observed (Figure S3B). By enriching our initial data derived from two independent cell lines, our study was expanded to chow mice, HFD mice, and HFD butyrate mice to study the expression of hepatic cholesterol metabolic genes by qPCR.

Butyrate treatment to HFD mice alters cholesterol metabolic gene expression and decreases lipid droplet formation in the liver

Based on the results from cell lines as described in the volcano plot, we studied hepatic expression of *hmgcr*, *hmgcs*, *acat2*, and *dhcr7*

by qPCR. There was about a twofold increase in hepatic *hmgcr* expression in HFD mice compared to chow mice, which was returned to normal level in HFD butyrate mice (Figure 2A). It was observed that in HFD mice, there was a significant increase in hepatic expression of *hmgcs*, *acat2*, and *dhcr7* as compared to chow mice, while the expression of only *hmgcs* and *acat2* returned to normal in HFD butyrate mice. The expression of *dhcr7* in HFD butyrate mice decreased significantly compared to HFD mice, but its expression remained significantly higher compared to chow mice. In addition, we opted to study the expression of the cholesterol catabolic enzyme, which did not surface in the volcano plot: 7A1 of the cytochrome P450 family (*cyp7a1*). *cyp7a1* expression was significantly reduced in HFD mice compared to chow mice and returned to the normal level in HFD butyrate mice (Figure 2A).

The liver sections from the mice were inspected by TEM and the representative images of sections were analyzed, highlighting the preponderance of lipid droplets. It was observed that there was an abundance of lipid droplets of an average diameter of $\sim 1.2 \mu\text{m}$ in HFD mice whereas in HFD butyrate mice, the droplets were significantly reduced not only in number but also by size with an average diameter of $\sim 0.7 \mu\text{m}$ (Figure 2B).

Since HMGCR is a key regulatory enzyme of cholesterol biogenesis, the results observed in the qPCR study were further validated by Western blot. It was observed that there was twofold increase in the expression of HMGCR in HFD mice compared to chow mice, while the expression returned to normal in HFD butyrate mice (Figures 2C, D).

The hepatic expression of proteins ABCA1 (ATP binding cassette subfamily A member 1) and ABCA5 (ATP binding cassette subfamily A member 5) was studied by Western blot (Figure 2C).

Densitometry analysis revealed that there was a significant decrease in ABCA1 expression in HFD mice compared to chow mice, and it returned to normal status in HFD butyrate mice (Figure 2D). Notably, the expression of ABCA5 remained unchanged in all the three groups (Figures 2C, D). For further functional analysis of efflux proteins, we used the Huh7 cell line.

Butyrate upregulates ABCA1 but not ABCA5 expression and increases cholesterol efflux in Huh7 cells

Butyrate treatment of Huh7 cells showed progressive increase in ABCA1 expression as a function of butyrate concentration as evident from the Western blot (Figure S4A) and its corresponding densitometry. On the other hand, expression of ABCA5 remained unaltered regardless of butyrate treatment (Figure S4B).

To study efflux, we used 22-NBD-cholesterol-loaded Huh7 cells treated with or without butyrate. The 22-NBD-cholesterol-loaded cells were kept for 18 h in medium before butyrate treatment to allow aqueous phase diffusion of cholesterol. It was

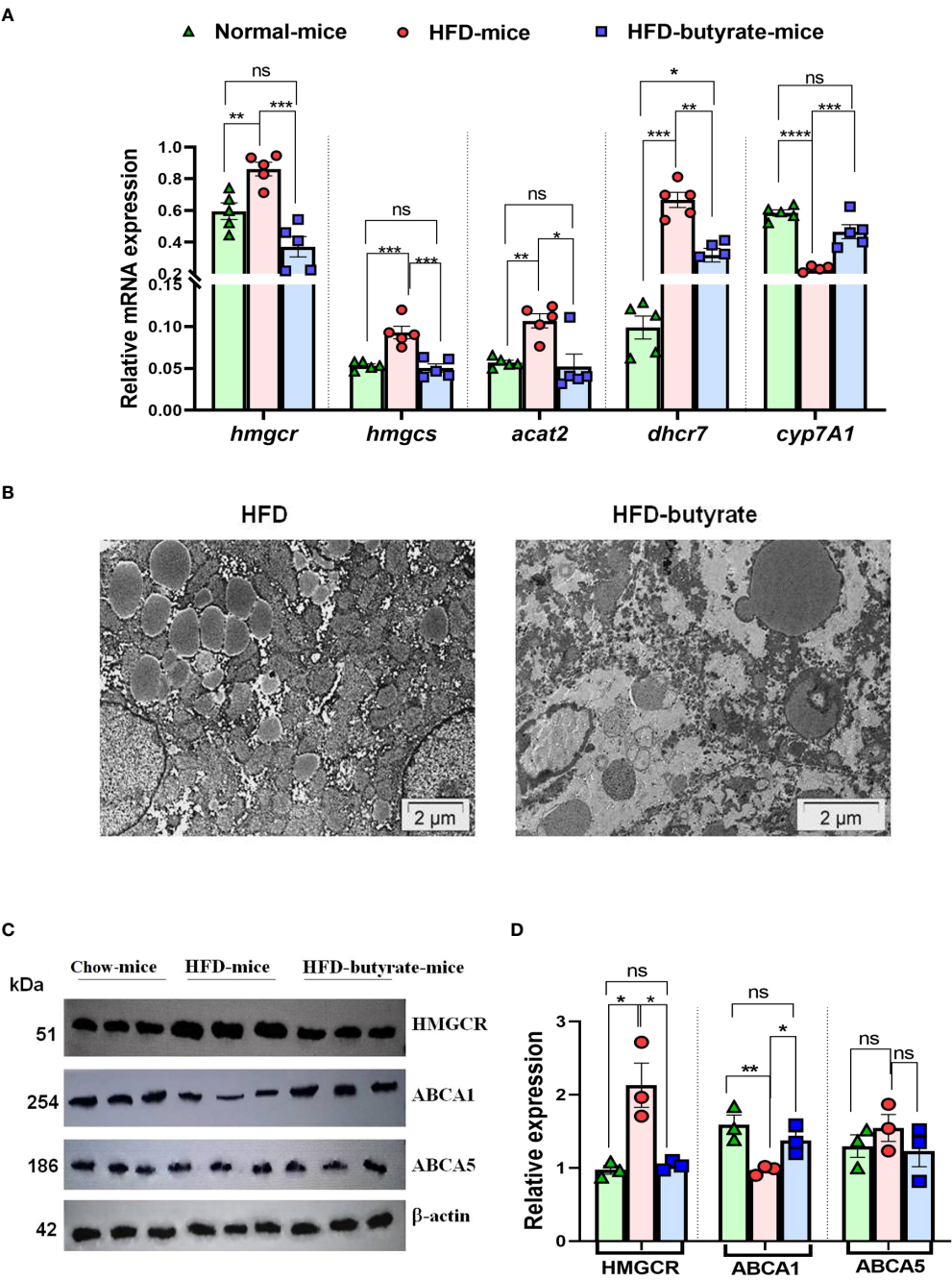


FIGURE 2
Analysis of hepatic expression of cholesterol metabolic genes by qPCR, lipid droplet status in the liver, and HMGCR, ABCA1, and ABCA5 expression by Western blot in chow mice, HFD mice, and HFD butyrate mice. Hepatic expression of cholesterol metabolic pathway: *hmgcr*, *hmgcs*, *dhcr7*, *acat-2*, and *cyp7A1* were studied in all the groups by qPCR (A). TEM images of the liver sections showing lipid droplets. The sections were visualized under a FEI Tecnai 12 Biotwin transmission electron microscope (FEI, Hillsboro, OR, USA) at an accelerating voltage of 100 kV. Scale bar in the image is 2 μm (B). Analysis of hepatic expression of HMGCR, ABCA1, and ABCA5 by Western blot (C). Densitometry was done using ImageJ showing relative expression with respect to β-actin control (D). *N* = 5/group; data are presented as mean ± SE. The experiment was repeated thrice. **** represents *p* < 0.0001, *** represents *p* < 0.001, ** represents *p* < 0.01, * represents *p* < 0.05, ns represents not significant.

observed that in the absence of HDL, regardless of butyrate treatment, there was negligible efflux of cholesterol. Interestingly, there was a significant increase in cholesterol efflux from 22-NBD-cholesterol-loaded Huh7 cells as a function of HDL concentration, which was significantly enhanced while cells were pretreated with butyrate (Figure S4C).

Butyrate downregulates mir-122 biogenesis in Huh7 cells

We then monitored the pre-mir-122, mir-122, and Dicer-1 status in Huh7 cells by qPCR. It was observed that there was a decrease in mir-122 (Figure 3A) and Dicer-1 (Figure 3B) with a concurrent increase in pre-mir-122 (Figure 3A) expression as a function of butyrate concentration. We also observed that propionate and acetate at 20 mM did not show any difference in pre-mir-122, mir-122, and Dicer-1 with respect to control (Figure S4D).

Butyrate upregulates AUF-1 and downregulates Dicer-1 and Sphingosine kinase 1 (a classical target of AUF-1) in Huh7 cells

We studied the expression of the posttranscriptional regulator of Dicer-1, AUF-1, in butyrate-treated Huh7 cells using Western blot (Figure 3C). The basal expression of AUF-1 isoforms in Huh7 cells was initially p45>p42>p37>p40 which altered to p40>p45>p37>p42 due to butyrate treatment. From the densitometry analyses, it was clear that the expression of AUF-1^{P45} remained unaltered whereas that of AUF-1^{P42} significantly decreased due to butyrate treatment with respect to the untreated control. On the other hand, there was an upregulation of the other two isoforms due to butyrate treatment. The fold increase for AUF-1^{P40} after the addition of 10 and 20 mM of butyrate was 7.36 and 8.7, respectively, with respect to the control. On the other hand, there was a marginal increase in AUF-1^{P37} expression after 10 mM butyrate addition and a low but significant increase after 20 mM of butyrate supplementation (Figure 3D). Furthermore, there was a progressive decrease in Dicer-1 as a function of butyrate concentration, which was fourfold in the case of 20 mM butyrate-treated Huh7 cells (Figure 3D).

We subsequently validated the results by transfection of Huh7 cells with EGFP constructs of each of the AUF-1 isoforms in the presence and absence of 20 mM butyrate (Figure 3E). We show that butyrate treatment of Huh7-transfected cells resulted in a decrease in EGFP-AUF-1^{P42} fluorescence and an increase in EGFP-AUF-1^{P40} and EGFP-AUF-1^{P37} fluorescence within transfected cells. Conversely, EGFP-AUF-1^{P45} fluorescence remained essentially unaltered with or without butyrate treatment. As the fluorescent-fused cDNAs were expressed

from plasmid promoters, differences in fluorescence would not be due to differences in transcription or splicing but rather due to differences in the stability of mRNA or protein. It is also worth mentioning that unlike butyrate, propionate and acetate did not show any significant increase in AUF-1^{P40} expression as studied by qPCR (Figure S4D).

Since AUF-1 is mRNA decay-promoting protein, for which there may be other important targets other than Dicer-1, we also studied the expression of sphingosine kinase (Sphk1). The expression of sphingosine kinase 1 (Sphk1) mRNA, which is another target of AUF-1 (Sobue et al., 2008), was also decreased upon butyrate treatment. We also observed a significant decrease in Sphk1 expression by butyrate treatment to Huh7 cells (Figure S5). The reciprocal relation of AUF-1 and Sphk1 expression upon butyrate treatment offered credence to the notion that butyrate acts by targeting AUF-1.

AUF-1 silencing increased Dicer-1 and mir-122 expression in Huh7 cells

The importance of AUF-1 on the expression of Dicer-1 and mir-122 was studied by silencing AUF-1 in Huh7 cells to which the following treatments were added: scramble siRNA (scramble), scramble plus butyrate, siAUF-1 alone, or siAUF-1 plus butyrate. The expression profile of AUF-1 was analyzed by Western blot (Figure 4A). Interestingly, silencing AUF-1 with siAUF-1 led to reduction in all the isoforms of AUF-1 regardless of the presence or absence of butyrate (Figure 4A). Other cellular consequences due to AUF-1 silencing like the expression of Dicer-1, mir-122, and cellular cholesterol status were also studied. It was observed that silencing with si-AUF-1 resulted in a significant increase in Dicer-1 (Figure 4B), mir-122 (Figure 4C), and cellular cholesterol (Figure 4D) regardless of butyrate treatment, but this was not seen when the cells were transfected with scramble siRNA. Since the upregulation of AUF-1^{P40} was quite prominent of all the AUF-1 isoforms due to butyrate treatment, the rest of the studies were carried out with the AUF-1^{P40} isoform.

To show that AUF-1 repressed Dicer-1 by binding to the 3'-UTR of its mRNA, a co-transfection experiment was performed. Huh7 cells were transfected with either pEGFP-AUF-1^{P40}, p-EGFP-3'UTRDicer-1, or pEGFP, and the resulting EGFP fluorescence was analyzed by fluorescence microscopy. Following the second round of transfection with either scramble or siAUF-1, the cells were treated with or without butyrate generating four experimental sets from left to right as follows: (i) scramble, (ii) scramble plus butyrate, (iii) siAUF-1, and (iv) siAUF-1 plus butyrate. From top to bottom, transfection was done with pEGFP-AUF-1^{P40}, p-EGFP-3'UTRDicer-1, or pEGFP, respectively.

In the first panel pEGFP-AUF-1^{P40}, fluorescence was observed when co-transfected with scramble, which increased after butyrate treatment. On the other hand, the fluorescence of EGFP-AUF-1^{P40}

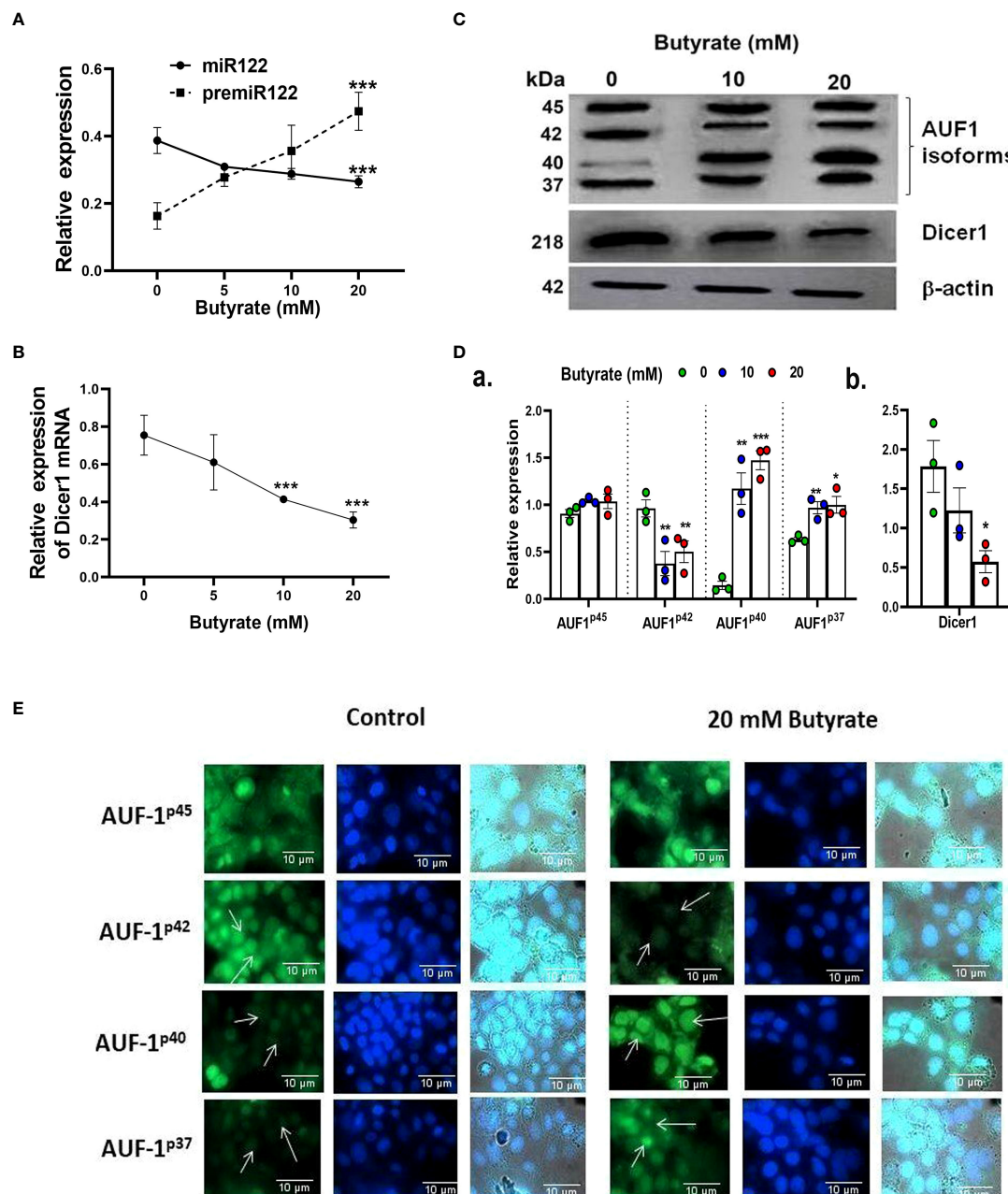


FIGURE 3

Effect of butyrate on miR122 maturation, Dicer1 expression, AUF1 isoform expression by Western blot, and EGFP reporter assays in Huh7 cells. Expression of pre-miR122 and miR122 (A) and Dicer1 (B) as determined by qPCR and Western blot of AUF1 isoforms (upper panel) and Dicer1 protein (middle panel) as a function of butyrate concentration (C) and corresponding densitometry of AUF1 isoforms (AUF1^{p45}/AUF1^{p42}/AUF1^{p40}/AUF1^{p37}) (D, a) and Dicer1 (D, b) with respect to β -actin control using ImageJ. Transfection of Huh7 cells with individual AUF1 isoforms of EGFP reporter construct (pEGFP-AUF1^{p45} or pEGFP-AUF1^{p42} or pEGFP-AUF1^{p40} or pEGFP-AUF1^{p37}) in the absence and presence of 20 mM butyrate for 24 h (E). The resulting fluorescence images are taken under 60 \times in Apotome Zeiss microscope with a CCD camera controlled with ZEN software (Carl Zeiss, Gottingen, Germany). $N = 3$. The data are presented as mean \pm SE. *** represents $p < 0.001$, ** represents $p < 0.01$, * represents $p < 0.05$.

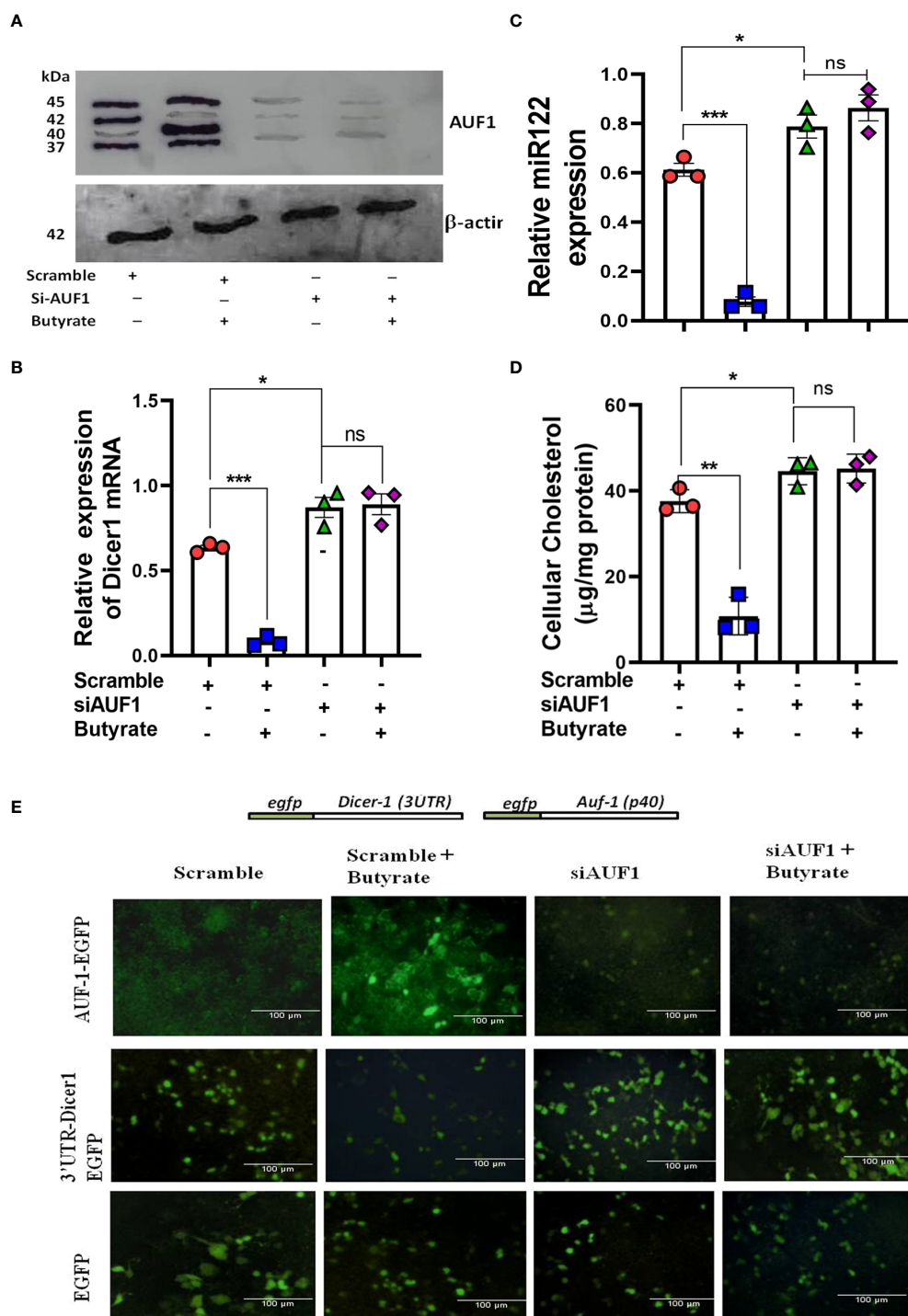


FIGURE 4

Silencing of AUF1 by siRNA-enhanced miR122, Dicer1 expression, and cellular cholesterol in Huh7 cells regardless of butyrate treatment. Western blot of AUF1 isoforms after co-transfecting with either siAUF1 or scramble-RNA (scramble) where β -actin is used as control (A). The corresponding expression of Dicer1 (B) and miR122 (C) as analyzed by qPCR and cellular cholesterol in cell lysate (D). Analysis of EGFP expression upon transfection with reporter construct of EGFP-AUF1^{p40}, EGFP-3'UTR-Dicer1, and EGFP (from top to bottom) in a co-transfection experiment under the following conditions: (i) scramble, (ii) scramble plus 20 mM butyrate, (iii) siAUF1 alone, and (iv) siAUF1 plus 20 mM butyrate (from left to right) (E). Resulting fluorescence images of co-transfected cells were captured in 20 \times magnification in a Carl Zeiss microscope equipped with a CCD camera controlled with ZEN software (Carl Zeiss, Gottingen, Germany). $N = 3$; the data are presented as mean \pm SE. *** represents $p < 0.001$, ** represents $p < 0.01$, * represents $p < 0.05$, and ns represents not significant.

was diminished with siAUF-1, and the effect remained the same even after butyrate treatment. In the second panel for the p-EGFP-3'UTR Dicer-1 probe, there was a basal level of fluorescence due to scramble siRNA, which diminished after butyrate treatment. The fluorescence of EGFP-3'UTR Dicer-1 was increased with siAUF-1, but remained essentially unchanged after butyrate treatment. The third panel showed that the EGFP expression remained the same during the course of the above treatments (Figure 4E). So far, the relation among butyrate–AUF-1–Dicer-1–mir-122 was studied in Huh7 cells. We further translated these findings in a mouse model.

Hepatic expression of mir-122, Dicer-1, and AUF-1^{p40} in chow mice, HFD mice, and HFD butyrate mice

It was observed that there was a significant decrease in pre-mir-122 with an increase in mir-122 in HFD mice as compared to chow mice. This expression returned to normal in HFD butyrate mice (Figures 5A, B). It was also observed that there was an increase in Dicer-1 (Figure 5C) with a concomitant decrease in AUF-1^{p40} (Figure 5D) in HFD mice and was restored to normal levels in HFD butyrate mice.

Butyrate downregulates other microRNAs

Since there are reports that mir27 plays an important role in lipid metabolism, we also studied hepatic expression of miR27a and miR27b in chow mice, HFD mice, and HFD butyrate mice. We showed that there was a sixfold increase in hepatic miR27a expression in HFD mice compared to chow mice, which returned to normal levels in HFD butyrate mice. Interestingly, miR27b remained unaltered in all the three groups (Figure S6).

Oral butyrate or probiotic treatment increases fecal butyrate and reduces serum cholesterol in antibiotic-treated mice following the AUF-1–Dicer-1–mir-122 pathway; probiotic treatment restores gut butyrate-producing bacteria

To show that the gut-derived butyrate is intimately linked with cholesterol metabolism in mice, we followed a similar approach (Wang et al., 2021) and depleted the gut microbiota of mice by daily gavage supplemented with a cocktail of antibiotics as a surrogate of

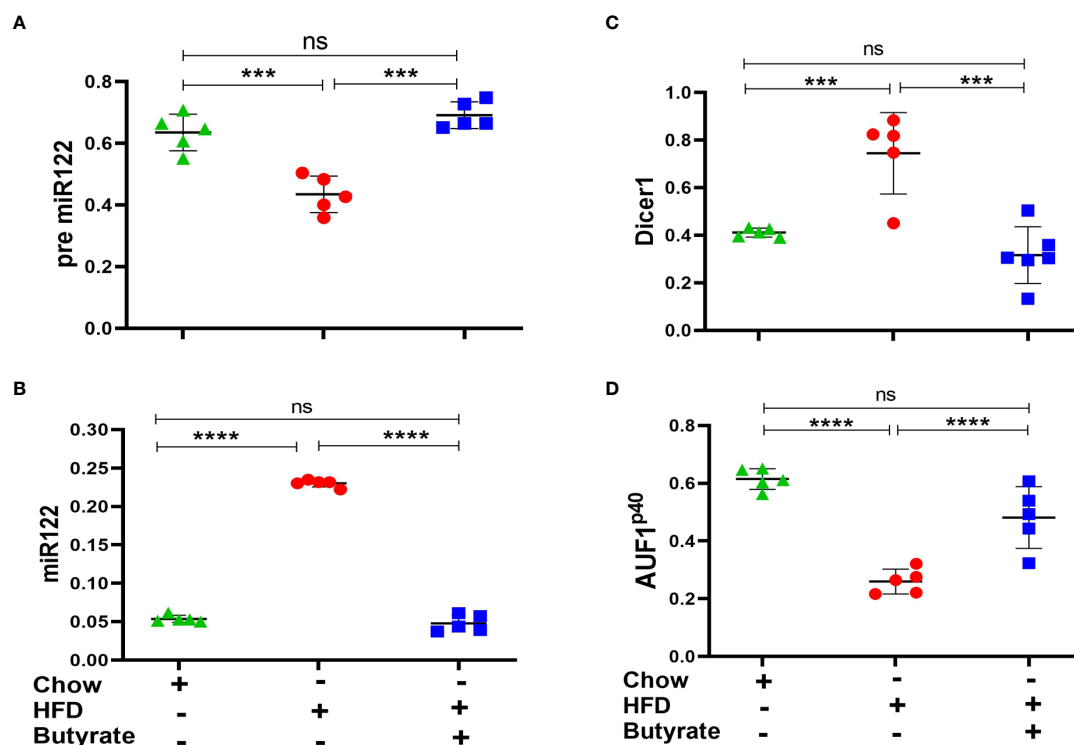


FIGURE 5

Hepatic miR122, Dicer1, and AUF1^{p40} in chow mice, HFD mice, and HFD butyrate mice. Hepatic expression of pre-miR122 (A), miR122 (B), Dicer1 (C), and AUF1^{p40} (D), in chow mice, HFD mice, and HFD butyrate mice by qPCR. $N = 5/\text{group}$; data are presented as mean \pm SE. The experiment was repeated thrice. **** represents $p < 0.0001$, *** represents $p < 0.001$, and ns represents not significant.

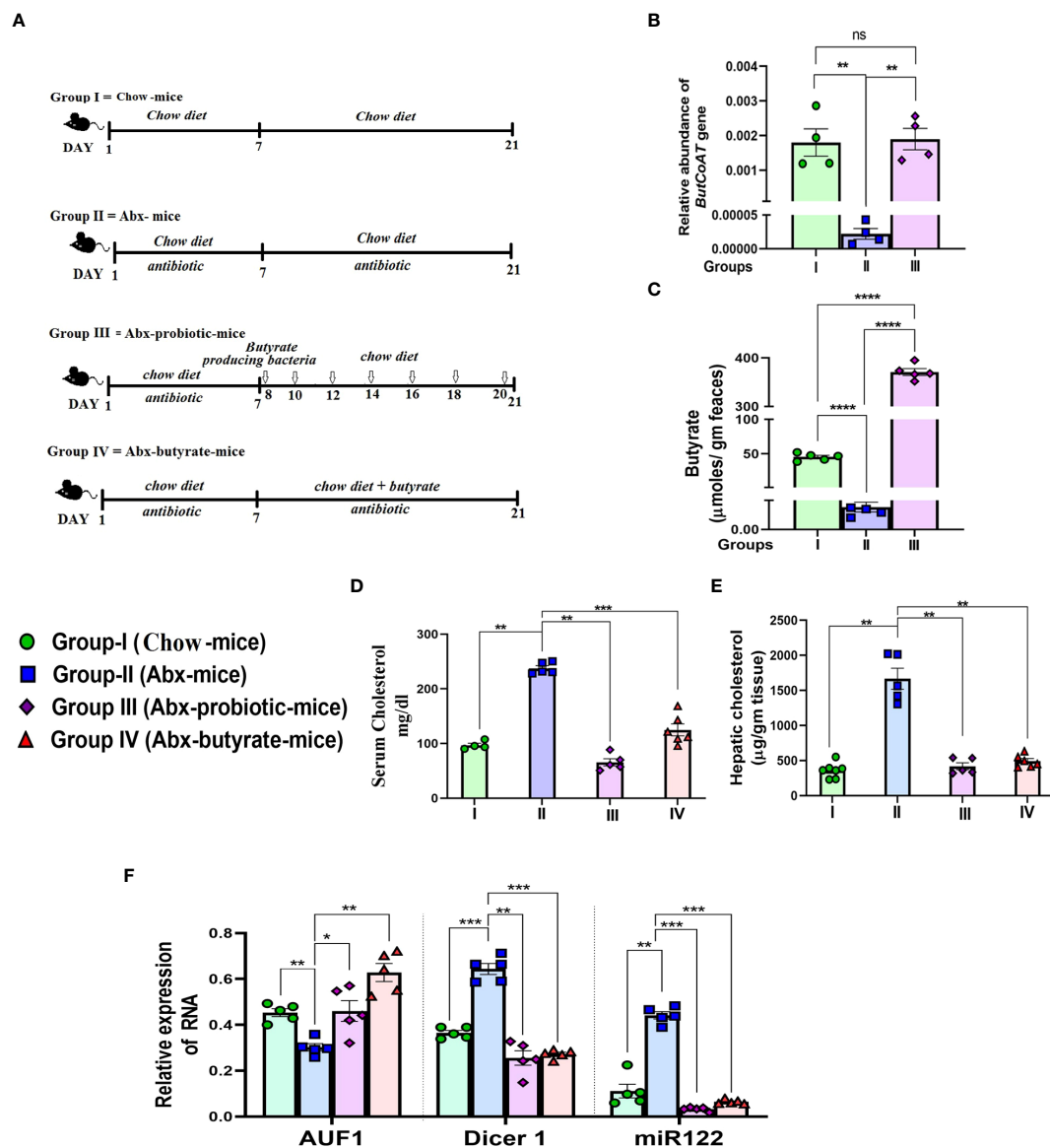


FIGURE 6

Effect of antibiotic treatment and subsequent probiotic treatment on fecal butyrate, serum and cholesterol, AUF1p40, Dicer1, and miR122 expression. Female mice were used for the study. Experimental design of the study: Group I = untreated chow-fed mice (untreated mice). Group II = mice receiving cocktail antibiotic and chow diet for 21 days (Abx mice). Group III = mice receiving cocktail antibiotic for the first 7 days followed by bowel cleansing by PEG and administration of probiotics (10^7 cfu in 200 μl) via oral gavage/day, on every alternate day till 2 weeks (Abx probiotic mice). Group IV = Abx mice fed with 5% butyrate fortified chow diet (w/w) from day 7 to day 21 (Abx butyrate mice) (A). Blood, liver tissue, and fecal samples were collected on day 21. The relative abundance of the *butCoAT* gene in the feces measured by qPCR and normalized to 16S rRNA bacterial gene abundance (B). Fecal butyrate (expressed in μg/g of feces) on day 21 estimated by LC-MS (C). The serum cholesterol in mg/dl (D) and hepatic 903 cholesterol expressed in μg/g liver tissue (E). Expression of hepatic AUF1^{p40}, Dicer1, and miR122 904 determined by qPCR (F). $N = 5$ /group; data are presented as mean \pm SE. The experiment was repeated twice. **** represents $p < 0.0001$, *** represents $p < 0.001$, ** represents $p < 0.01$, * represents $p < 0.05$, and ns represents not significant.

germ-free mice. The treatment protocol of each group of mice is schematically presented in Figure 6A. The mice were divided into four groups: Group I: fed with chow diet only (untreated mice), Group II: received cocktail antibiotic (Abx mice), Group III: treated with the cocktail antibiotic for 7 days followed by probiotic

treatment every other day for 21 days (Abx probiotic mice), and Group IV: Abx mice receiving butyrate from day 8 to 21 (Abx butyrate mice). We determined the relative abundance of the terminal enzyme [butyryl-CoA: acetate CoA-transferase (*butCoAT*)] of the butyrate synthesis pathway from fecal DNA

samples as an indirect indicator of the relative abundance of butyrate-producing bacteria. Abx mice showed a ~100-fold decrease in the relative abundance of *butCoAT* gene compared to untreated mice which was restored to essentially a normal level in Abx probiotic mice (Figure 6B). To show that a decrease in relative abundance of *butCoAT* gene was faithfully reflected in butyrate production, we estimated the fecal butyrate by LC-MS. The decrease in fecal butyrate was more pronounced than the *butCoAT* gene abundance in Abx mice. There was a ~9,000-fold reduction in fecal butyrate in Abx mice compared to untreated mice, whereas with probiotic treatment, the fecal butyrate increased 70,000-fold higher compared to Abx mice and ~7-fold higher than untreated mice (Figure 6C). We measured serum and liver cholesterol and showed that the serum cholesterol was increased 2.5-fold on day 7 and remained the same on day 21 in the Abx mice compared to untreated mice (Figure S8). In Abx probiotic mice and Abx butyrate mice, the hepatic and serum cholesterol decreased significantly compared to Abx mice and returned to normal levels (Figures 6D, E).

The rise in serum cholesterol and decrease in fecal butyrate production were correlated with a ~1.7-fold decrease in AUF-1 and a concomitant 2-fold and 4-fold increase in Dicer-1 and mir-122, respectively, in Abx mice, compared to untreated mice. As expected, there was a significant increase in AUF-1 and decrease in Dicer-1 and mir-122 in Abx probiotic mice and Abx butyrate mice, compared to Abx mice (Figure 6F).

mir-122 overexpression rescues hypocholesterolemic effect of butyrate in mice

From the previous experiments, it was apparent that butyrate regulates cholesterol biogenesis by exploiting mir-122. Therefore, we validated our observation by overexpressing mir-122 in butyrate-treated mice for which plasmid expressing mir-122 was injected through the tail vein of mice fed with chow diet supplemented with butyrate. Another group of mice were injected with mock plasmid, and on day 4 post-injection, the animals were sacrificed, following which serum and liver cholesterol were analyzed. We observed a 25-fold increase in mir-122 expression in the liver coupled with a 4-fold increase in serum cholesterol compared to butyrate-fed mock-injected mice (Figures 7A, B).

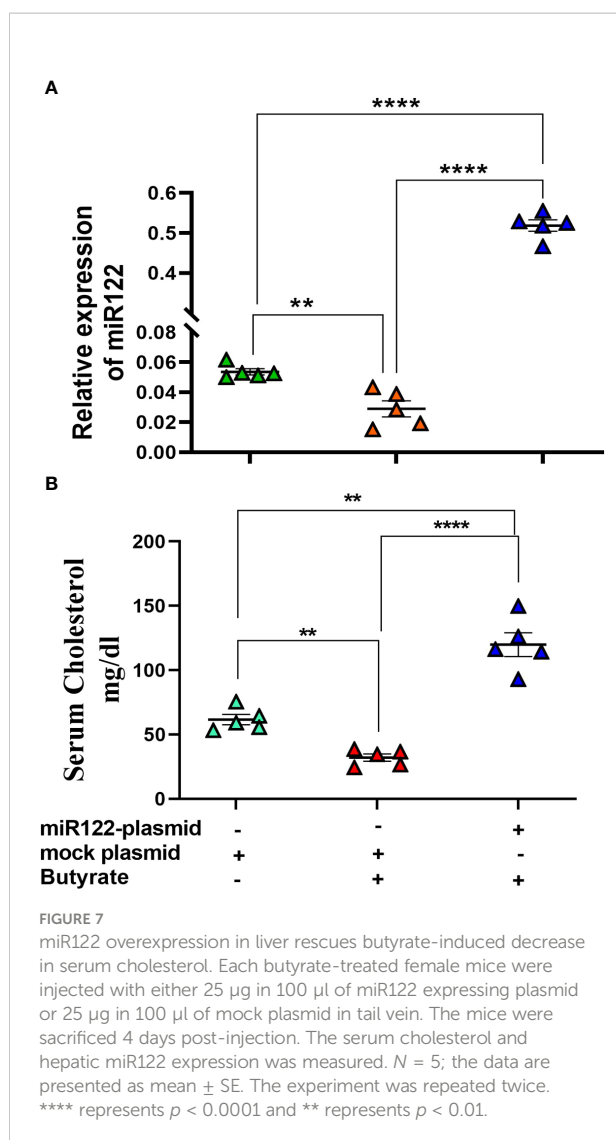
Effect of AUF-1 knockdown by morpholino oligomer (GMO-PMO) on the expression of Dicer-1, mir-122, and cholesterol metabolic enzymes and on serum cholesterol levels

To establish the basic tenet that AUF-1 is an important factor in the butyrate-mediated cholesterol homeostasis, we

opted for AUF-1 knockdown (AUF-1-KD) in mice using a novel cell-penetrating morpholino oligomer (GMO-PMO). In this study, GMO-PMO specific to AUF-1 was denoted as AUF-1-MO and the corresponding scramble one was denoted as scramble-MO. Mice that received morpholino on days 0 and 7 were sacrificed on day 14, as depicted pictorially (Figure 8A). We showed that there was no difference in AUF-1 expression between normal and scramble-MO-treated mice showing that the scramble-MO did not interfere in AUF-1 expression though the AUF-1-MO did, supporting that the effects of the AUF-1 and scramble GMO-PMOs were sequence specific (Figures S10A, B), and in subsequent experiments, normal mice were not included. The results showed that AUF-1-MO significantly downregulated the AUF-1 isoform not only in the liver (Figure S10A), but also in other organs such as the kidneys and heart (Figure S10C). Furthermore, butyrate treatment in the scramble-MO or AUF-1 MO mice did not change their respective AUF-1 status in liver (Figure 8B). AUF-1-KD in hepatic mir-122 and Dicer-1 expression was studied, and it was observed that compared to scramble-MO alone, the combination of butyrate with scramble-MO led to a significant downregulation of mir-122 and Dicer-1. As expected, AUF-1-MO treatment in mice led to upregulation of both mir-122 and Dicer-1 and remained unaltered when combined with butyrate treatment (Figure 8C). We also studied the impact of upregulation of mir-122 in AUF-1-KD mice for which two genes of cholesterol metabolic enzymes, HMGCR and CYP7A1, are considered of cholesterol homeostatic pathway and are the known targets of mir-122. As expected, in the scramble-MO group receiving butyrate, there was downregulation of *hmgcr* coupled with upregulation of *cyp7A1*. In AUF-1-KO mice, regardless of butyrate treatment, there was a significant upregulation of *hmgcr* coupled with downregulation of *cyp7A1* (Figure 8D). Both mir-122 and Dicer-1 capture a reciprocal relation between *hmgcr* and *cyp7A1* (Figure 8E). As expected, butyrate treatment of scramble-MO mice showed a significant decrease in serum and hepatic cholesterol, whereas AUF-1-MO-KD mice showed an amply surged cholesterol level, which remained unaltered regardless of butyrate treatment (Figure 8E).

Discussion

This discourse attempts to shed light on a deeper understanding of the role of butyrate in host cholesterol homeostasis for which the following questions were asked: (a) What are the target genes and the intracellular players to link the effect of butyrate on cholesterol metabolism? (b) Does endogenous gut-derived butyrate exploit a similar molecular pathway like exogenously fed butyrate? (c) What are the cell line and mouse phenotypes when selective important players were either overexpressed like mir-122 or knocked down like AUF-1 to bring strength to our notion?



We showed that unlike acetate and propionate, butyrate has emerged as a hypocholesterolemic short-chain fatty acid in primary hepatocytes, Huh7 cells, and HFD mice, which has warranted a mechanistic look to understand how butyrate influences a diverse repertoire of functions. To address the first point, we sought assistance of the published microarray datasets (GSE4410 and GSE45220) and showed that the key cholesterol-metabolic genes, *hmgcr*, *hmgcs1*, *acat2*, *dhcr7*, and *dhcr24*, were downregulated upon butyrate treatment, which we have also validated by qPCR in HFD mice and HFD butyrate mice except *dhcr24*, as it is involved in the later stages of cholesterol biosynthesis. The enzymes HMGCR and HMGCS are rate-limiting (Vock et al., 2008); DHCR7 is the terminal enzyme in the cholesterol synthesis pathway (Luu et al., 2015), whereas ACAT2 is involved in cholesterol ester formation (Anderson et al., 1998).

In addition, we also studied the expression of two other important entities: (a) *cyp7A1*, a member of the monooxygenase

cytochrome P450 superfamily that catalyzes cholesterol to bile acid (Li et al., 2013), and (b) ABCA1, involved in cholesterol efflux (Yancey et al., 2003). We report the downregulation of ABCA1 expression in HFD mice compared to chow mice, which is in contrast to a previously published result (Jeon et al., 2015). The diet composition and duration of treatment of HFD may possibly explain this disparity. The expression of *acat2* and *cyp7a1* appeared to be quite opposite in HFD mice as compared to HFD butyrate mice, which may have contributed to the “lipid droplet” formation, and butyrate treatment may have caused their dissolution. HFD mice showed elevated ALT and AST, indicating hepatic stress, which returned to normal levels in HFD butyrate mice. Our results are concordant with earlier reports on the beneficial effect of butyrate on liver damage and dyslipidemia (Endo et al., 2013; Zhao et al., 2021).

It has been reported that butyrate induces profound changes in miRNA in MDCK cells (Bishop et al., 2017). We identified few important miRNA, particularly those that are associated with cholesterol metabolism, such as mir-122, miR27a, and miR27b (Krutzfeldt et al., 2005; Goedeke et al., 2015). An elegant study by others shows that the treatment of mice with antagomir-mir-122 led to the downregulation of a large number of genes, of which the top-ranking functional category includes the cholesterol biosynthesis genes, namely, *hmgcr*, *hmgcs1*, and *dhcr7* (Krutzfeldt et al., 2005). Additionally, mir-122 destabilizes *cyp7A1* mRNA by binding to its 3'-UTR (Song et al., 2010). Reports show that silencing of mir-122 in African green monkeys and chimpanzees has resulted in substantial reduction in total plasma cholesterol (Zhou et al., 2019), while in the Huh7 cell line, it rescues excess lipid deposition (Long et al., 2019).

To witness the effect of butyrate on the cholesterol metabolic landscape, we undertook studies with the Huh7 cell line, which is known to have higher mir-122 expression (Fukuhara et al., 2012). As it is well known that the function of isolated primary hepatocytes is hard to maintain, when cultured *in vitro*, these cells readily undergo dedifferentiation, causing them to lose hepatocyte function (Hu and Li, 2015); thus, Huh7 cells that mimic the function of liver were used. For *in vitro* experiments on a cancer cell like Huh7, a relatively higher dose of butyrate was needed for gene expression study. As an epigenetic modifier, butyrate may be differentially utilized in normal and cancerous cells (Donohoe et al., 2012); therefore, it is tempting to speculate that a higher dose of butyrate is required to induce an effect in Huh7. The butyrate concentration used was in tune with an earlier study (Zhao et al., 2021). Butyrate treatment showed an increase in ABCA1 expression whose function was validated by showing an increase in cholesterol efflux and a decrease in miR27a, which caused decay of ABCA1 mRNA (Goedeke et al., 2015). To link butyrate with mir-122 biogenesis, butyrate-treated Huh7 cells showed reduced Dicer-1 expression, which halted maturation of mir-122 from its precursor. The effect was butyrate-specific, because neither propionate nor acetate caused any effect.

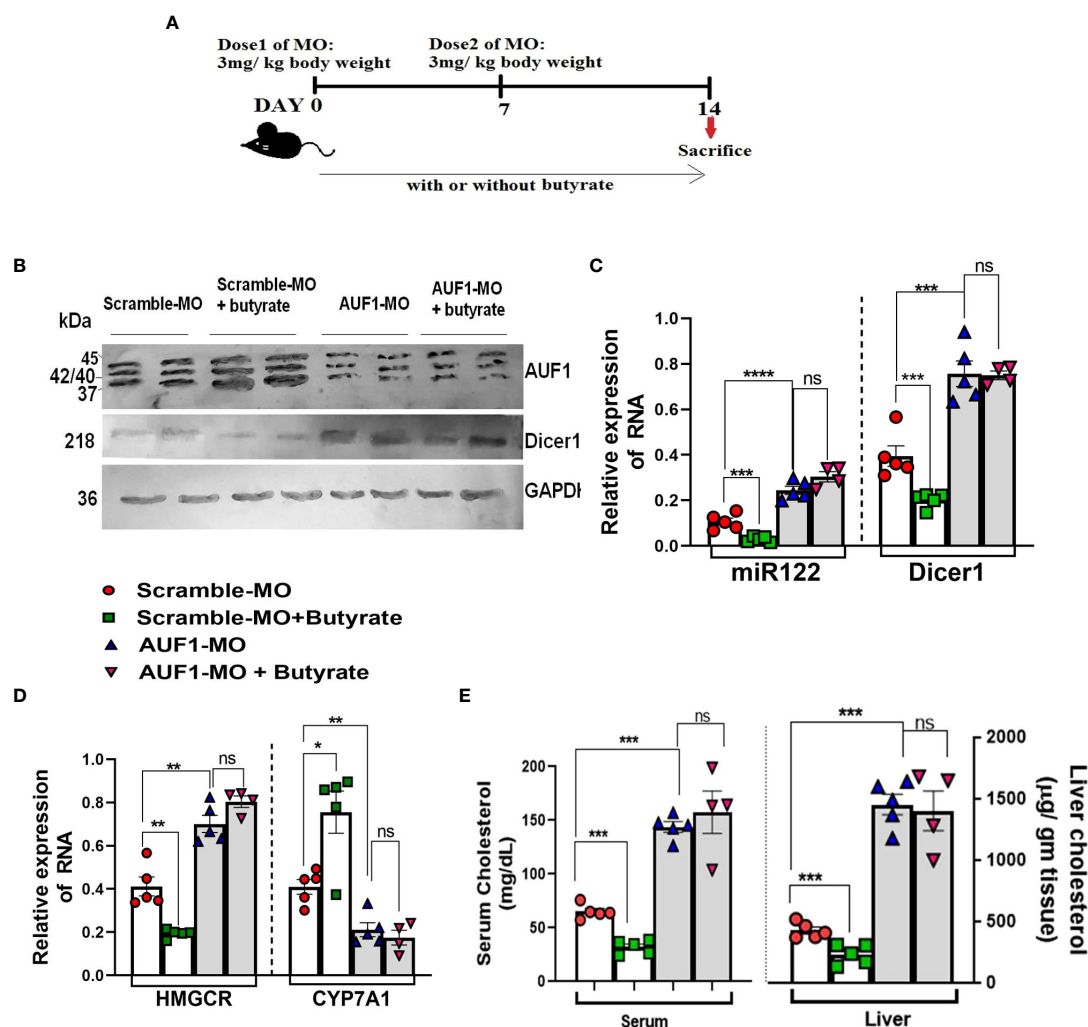


FIGURE 8

In vivo knockdown of AUF1 increases cholesterol synthesis by exploiting the AUF1–Dicer1–miR122–cholesterol pathway regardless of butyrate treatment. Female mice (20 in number) were divided randomly into four groups: AUF1-MO-injected mice (AUF1-MO mice), AUF1-MO-injected mice fed with butyrate supplement (butyrate AUF1 MO mice), scramble-MO-injected mice (scramble MO mice), and scramble-MO-injected mice fed with butyrate supplement (butyrate scramble MO mice); the scheme was shown schematically (A). Western blots to determine hepatic expression of AUF1 and Dicer1 (B). GAPDH was used as control. AP-conjugated secondary antibodies were used in Western blot. Expression of hepatic miR122 and Dicer1 determined by qPCR (C). Hepatic expression of cholesterol metabolizing enzymes: HMGCR and Cyp7A1 determined by qPCR (D). Serum and liver cholesterol were measured and expressed in mg/dl and μg/g tissue, respectively (E). $N = 5/\text{group}$; data are presented as mean \pm SE. The experiment was repeated twice. **** represents $p < 0.0001$, *** represents $p < 0.001$, ** represents $p < 0.01$, * represents $p < 0.05$, and ns represents not significant.

Since Dicer-1 is an important protein for the canonical miRNA biogenesis, the question arises whether all microRNA synthesis is reduced due to Dicer-1 downregulation by butyrate. We show that the expression of miRNAs that decay ABCA1 mRNA by binding to its 3'-UTR (Goedeke et al., 2015), like miR27a but not miR27b, was inhibited due to butyrate treatment, suggesting that all miRNAs were not equally affected by butyrate treatment as there are reports of Dicer-1-independent miRNA biogenesis (Cheloufi et al., 2010; Yang et al., 2012; Kim et al., 2016) where the slicer activity of

Argonaute2 (Ago2) plays a vital role in pre-miRNA cleavage (Cheloufi et al., 2010).

Dicer is critical for most miRNAs, but the 5p miRNAs appear to be produced to an extent without Dicer (Kim et al., 2016). Therefore, it will be interesting to investigate further if butyrate enhances the Dicer-independent pathway for miRNA biogenesis. Our preliminary observation of increased Ago2 expression in butyrate-treated cells (data not shown) is indicative of such phenomena. It is tempting to speculate that miR27b, which remains unaltered in butyrate treatment, may be

synthesized in an Ago2-dependent manner as miR27b is found to be closely associated with Ago2 (Miao et al., 2018).

Cellular steady-state mRNA levels are maintained by the result of two opposite mechanisms, i.e., transcription and decay. There is a report that AUF-1, an RNA binding protein, lowers the Dicer-1 mRNA stability by binding to its 3'-UTR (Abdelmohsen et al., 2012). The decay of transcripts containing AU-rich elements (AREs) is another example of RNA regulation that coordinates several physiological processes through posttranscriptional regulation (Schoenberg and Maquat, 2012). AUF-1 has a multitude of functions, such as DNA binding (Enokizono et al., 2005), RNA turnover (DeMaria and Brewer, 1996), and mRNA translation efficiency (Liao et al., 2007). The AUF-1 family contains four isoforms, AUF-1^{P45}, AUF-1^{P42}, AUF-1^{P40}, and AUF-1^{P37}, and their relative levels, rather than the absolute amount of individual AUF-1 isoforms, determine the net mRNA stability of ARE-containing transcripts (Kishor et al., 2013). Although different AUF-1 isoforms have different binding affinity to specific mRNA 3'-UTRs (Kajita et al., 1995; Wagner et al., 1998), the detailed mechanism by which AUF-1 isoforms selectively regulate Dicer-1-mRNA turnover is unclear.

We showed that butyrate induces upregulation of both AUF-1^{P40} and AUF-1^{P37}, but not AUF-1^{P42} and AUF-1^{P45}, in Huh7 cells. Since AUF-1^{P40} expression was quite prominent among all the isoforms, the rest of the studies were done with the AUF-1^{P40} isoform only. However, it does not exclude the possibility of the role of AUF-1^{P37} in the regulatory processes. There is a previous report stating that butyrate influences alternative splicing of many proteins like vascular endothelial growth factor (VEGF), IL-18, Defensin β -1 gene, and some others (Wu et al., 2012). Therefore, one may speculate that butyrate, by influencing alternative splicing of AUF-1, may regulate gene expression. For functional validation of butyrate-induced upregulation of AUF-1, we studied hepatic expression of a known classic target of AUF-1 sphingosine kinase1 (sphk1) (Sobue et al., 2008), responsible for cellular proliferation (Sobue et al., 2008) and a prognostic marker for hepatocellular carcinoma (HCC) (Cai et al., 2017). Butyrate-mediated decay of Sphk1 may also explain anticancer effects of butyrate on HCC (Wang et al., 2013). The precise mechanism by which butyrate activates AUF-1 is not clear. A previous study showed that HDAC inhibitor promotes transcription of RNA binding protein (RBP) through the activation of the transcription factors of early growth response protein (Sobolewski et al., 2015).

Butyrate being an HDAC inhibitor (Davie, 2003) may also activate AUF-1 through these transcription factors. We showed that silencing of AUF-1 by siRNA led to the downregulation of all the isoforms of AUF-1, coupled with an increase in Dicer-1, mir-122, and cellular cholesterol, regardless of absence or presence of butyrate. Thus, butyrate may serve as a master regulator of Dicer-1 stability through AUF-1. The limitation of our study is that the commercially available siRNA appears to

downregulate all the isoforms of AUF-1, which makes it difficult for one to ascertain the importance of any specific isoform in the process. The above findings portray the sequential interplay of several intracellular players that operate seamlessly as “butyrate–AUF-1–Dicer-1–miRNA122–cholesterol–metabolic enzymes–cholesterol level”, whose elegance was further verified using the HFD-induced gut dysbiosis model. A recent study demonstrated that butyrate decreases lipid profile including cholesterol largely by the LKB1–AMK–Insig signaling pathway (Zhao et al., 2021). Interestingly, mir-122 knockdown in mice showed activation of the LKB1–AMK pathway (Long et al., 2019). This study lends credence to the notion that the LKB1–AMK–Insig pathway connects butyrate and cholesterol convergence in the downstream of the “AUF-1–Dicer-1–miRNA122” axis.

To address the second query and to show that gut-derived butyrate is the prime regulator of cholesterol homeostasis, we depleted gut bacteria by antibiotic treatment as a surrogate of germ-free mice (Kennedy et al., 2018) and then reconstituted with probiotics. The probiotic consisted of *Clostridium butyricum*, lactic acid-producing bacteria (LAB), *Bacillus mesentericus*, and *Streptococcus faecalis*, which produces SCFA either directly or indirectly (He et al., 2005; Bourriaud et al., 2005; Isono et al., 2007; Mishra et al., 2019).

The final step of butyrate production is usually catalyzed by *butCoAT* and butyrate kinase (*buk*) (Louis and Flint, 2007). In a metagenome-based study, it was predicted that the *butCoAT*-mediated route is 10-fold more abundant than that mediated by *buk* (Louis et al., 2004). In our investigation, we have studied the butyrate production indirectly by measuring the relative abundance of *butCoAT* gene in the fecal samples and directly by measuring the fecal butyrate concentration by LC-MS. Oddly enough, we observed that the fecal butyrate concentration was much higher as compared to *butCoAT* gene abundance in the probiotic-treated group; the cause of such temporal mismatch is not clear. Usually, the acetyl–CoA pathway contributes to 79.7% of all butyrate production in gut microbes (Vital et al., 2014). However, other pathways like lysine, glutarate, and 4-aminobutyrate pathways also contribute to butyrate production (Vital et al., 2014). These pathways are prevalent in Firmicutes and some other phyla, such as Fusobacteria and Bacteroidetes (Barker et al., 1982; Buckel and Barker, 1974). It is tempting to speculate that other butyrate-producing pathways may operate to contribute to the total butyrate pool. Harmonious to our result of increased serum and liver cholesterol in Abx mice, an earlier report showed that depleting intestinal microbiota by antibiotics enhanced bile acid absorption and expression of HMGCR and HMGCS in liver, resulting in 55% increase in serum cholesterol (Le Roy et al., 2019).

Another study showed that germ-free mice display 1.5 times higher liver cholesterol than conventional mice (Mistry et al., 2017). To address the third point, we showed that mir-122 is

indeed involved in the recovery of serum cholesterol, and we overexpressed mir-122 in butyrate-treated mice, which showed appreciable recovery of serum cholesterol. To further establish the link between AUF-1 and cholesterol homeostasis, we knocked down AUF-1 by deploying morpholino oligomers (MO), which are short single-stranded DNA analogues that are built upon a backbone of morpholine rings and are resistant to host enzymes present, a characteristic that makes them highly suitable for *in vivo* applications. In MO, the guanidinium units that are tethered with the antisense are more rigid, which helps to get a favorable conformation to bind with the complementary mRNA (Corey and Abrams, 2001). The lower molecular weight of MO helps in endosomal escape efficiency (Abes et al., 2008). Notably, morpholino-based therapy for Duchenne muscular dystrophy (DMD) has been approved by the FDA, which is now a hallmark for morpholino-based antisense therapy (Bertoni, 2014). The chimera of GMO- and PMO-producing MO used in this investigation bears a unique proof of self-transfecting ability and nonuse of vehicle for delivery, eliminating the possibility of vehicle-induced toxicity (doi: <https://doi.org/10.1101/2021.06.04.447039>). Since AUF-1 knockout mice have high mortality due to high septicemia (Lu et al., 2006), the selective AUF-1 knockdown (KD) by MO offered a unique platform to test our hypothesis *in vivo*. The rise in serum cholesterol along with the increase in *hmgcr* and the decrease in *cyp7A1* expression in the liver of AUF-1 KD mice compared to scramble was noted, indicating that AUF-1 is the master regulator of cholesterol biogenesis. Furthermore, it was also observed that exogenous butyrate fails to correct hypercholesterolemia in AUF-1 KD mice. Importantly, AUF-1 KD showed high levels of Dicer-1 and mir-122 expression compared to scramble. The increase in mir-122 and the decrease in *cyp7A1* in AUF-1-MO mice is significant as mir-122 directly binds to *cyp7A1* mRNA (Song et al., 2010) leading to its decay.

Overall, the present study demonstrates the effectiveness of butyrate as a powerful regulator of cholesterol homeostasis at multiple layers. By aligning a series of *in vitro* and *in vivo* experiments, we report how the intestinal microbial butyrate regulates cholesterol balance by involving intercellular players in tandem as follows: “butyrate–AUF-1–Dicer-1–mir-122–cholesterol metabolic enzymes–cholesterol level” where the individual members contribute either *via* up- or downregulation.

Materials and methods

Propagation of Huh7 cells and estimation of cellular protein and cholesterol

Huh7 cells were cultured in DMEM supplemented with 10% FCS and 50 µg/ml gentamycin at 37°C with 5% CO₂. Cellular viability was assayed by MTT. Cholesterol estimation was

performed using Amplex Red Cholesterol Assay kit. An aliquot of cell lysate was used for protein estimation using the Pierce™ BCA Protein Assay Kit following manufacturer's protocol.

Mice and animal ethics

Pathogen-free C57BL/6 mice (6 weeks old) were procured from the institutional animal facility of Indian Council of Medical Research-NICED, Kolkata, India. All the study protocols were approved by the Institutional Animal Ethics Committee of Indian Council of Medical Research-NICED, Kolkata, India (NICED/BS/MB-001/2019). All mice were housed under a 12-h light/dark cycle at a controlled temperature. Experiments have been carried out in accordance with the guidelines laid down by the Committee for the Purpose of Control and Supervision of Experiments on Animals (CPCSEA), Ministry of Environment and Forests, Government of India, New Delhi, India.

Dietary supplementation of sodium butyrate

The dietary supplementation studies were performed as reported earlier with minor modifications (Xu et al., 2018). Briefly, a group of 10 adult C57BL/6 mice (with 5 in each group) were fed with HFD having 20% kcal protein, 20% kcal carbohydrate, 60% kcal fat, and trace amount of cholesterol (0.007% w/w). After 4 weeks of HFD feed, five animals from the group were selected randomly and was further fed with 5% sodium butyrate (w/w) (sodium butyrate in solid form was thoroughly blended into HFD) for 15 days (HFD butyrate mice). The remaining mice were continued with HFD for 15 days (HFD mice). Fresh diet was replenished in alternate days. Age-matched mice fed with regular chow diet served as the normal group (chow mice).

Antibiotic treatment

The endogenous intestinal microbiota of 4-week-old chow-fed mice was depleted by gavage with broad-spectrum antibiotics over 7 days (Reikvam et al., 2011). The antibiotics solution consisted of ampicillin, metronidazole, and vancomycin diluted in sterile water. Mice received 200 mg/kg of ampicillin and metronidazole and 100 mg/kg of vancomycin once a day. Henceforth, the antibiotic-treated mice are called Abx mice.

Probiotic treatment

Probiotic (each capsule containing 50 million lactic acid bacteria, 2 million *C. butyricum*, 30 million *S. faecalis*, and 1 million *B. mesentericus*) treatment was done as described

previously with minor modifications (Le Roy et al., 2018). Briefly, a group of 20 mice (4 mice in each cage) were fed with cocktail antibiotic for 7 days and 5 mice were subjected to bowel cleansing with 1.2 ml of polyethylene glycol (PEG) solution for each mouse prior to probiotic administration. Since mice are coprophagous, they were placed in clean cages having wired net at the bottom of the cage to prevent feeding of feces. Feces and blood (from tail vein) were collected before bowel cleansing.

The PEG solution contained PEG 3350 (77.5 g/L), sodium chloride (1.9 g/L), sodium sulfate (7.4 g/L), potassium chloride (0.98 g/L), and sodium bicarbonate (2.2 g/L) diluted in sterile tap water and was divided in five equal doses (200 µl/mouse/dose) that were administered by oral gavage at 30-min intervals after a 2-h fasting (free access to water). The PEG solution and the inoculum were provided 24 h after the last antibiotic gavage. Each capsule of probiotic was suspended in 1 ml of water and two inoculations of probiotics (200 µl) were administered *via* oral gavage to Abx mice, every other day till 2 weeks. The mice were transferred to a sterile cage and straw. All animals received autoclaved deionized water and chow diet *ad libitum* for the next 14 days. A group of five Abx mice were continued with antibiotic feeding along with 5% sodium butyrate supplemented with chow diet for next 14 days (Abx butyrate mice). Another group of five Abx mice were continued with antibiotic treatment for the next 14 days. Age-matched mice (five in number) fed with normal chow diet without antibiotic treatment throughout the period of 21 days served as a control (chow mice).

mir-122 overexpression in mice

mir-122 was overexpressed in mouse liver as described earlier (Chang et al., 2004; Ghosh et al., 2013). The mir-122 expression plasmid or empty plasmid (mock) was injected through the tail vein of butyrate-treated mice at a dose of 25 µg of DNA in 100 µl of saline/mouse. Mice were sacrificed on day 4 post-injection, and serum cholesterol and mir-122 expression in liver were measured.

Mice fecal sample collection

Fresh fecal samples of all mice were collected at a fixed time of a day to minimize possible circadian effects. Samples were collected into empty sterile microtubes on ice and stored at -80°C within 1 h for future use.

Fecal DNA extraction and determination of butyryl-coenzyme A (CoA):acetate CoA-transferase (ButCoAT) gene abundance by qPCR

The QIAamp DNA stool minikit (Qiagen) was used to extract DNA in QIAcube (Qiagen) from 40 mg of fecal pellet

from each mouse. The DNA was measured using a QIAxpert spectrophotometer (Qiagen). To compare the relative abundance of bacteria having the *butCoAT* gene in fecal DNA of mice, qPCR analysis was carried out and quantified by SYBR green and the data were normalized to total bacterial abundance using 16S rRNA-bacterial primers (Berding and Donovan, 2018; Jian et al., 2020). The sequence of the primers used is listed in Table S1.

Measurement of butyrate in feces by LC-MS

The fecal content of each mouse (50 mg wet weight) was dissolved in distilled water at 1:10 (w/v) and homogenized in a Dounce homogenizer. Then, the content was centrifuged at 10,000g for 10 min and the supernatant was filtered through a 0.45-µm syringe filter. The supernatant was further diluted in LC-MS grade distilled water up to a final volume of 1 ml and was subjected to LC-MS analysis for SCFA as described by Cheng et al. (2020). In brief, a calibration curve was generated by using varying calibrations of internal standards of butyrate from 2 to 50 µmol. The LCMS separation was performed on the Agilent 1290 Infinity LC system, which was coupled to Agilent 6545 Accurate-Mass Quadrupole Time-of-Flight (QTOF) with an Agilent Jet Stream Thermal Gradient Technology with electrospray ionization (ESI) source. The suitable MS parameters were optimized and the high-resolution mass spectra were obtained by performing the analysis in negative ionization mode. The chromatographic separation was achieved on an Agilent ZORBAX SB-C18 column (2.1 × 100 mm, 1.8 µm) as a stationary phase. The mobile phase consisted of a linear gradient of 0.1% (v/v) aqueous formic acid (A) and methanol (B): 0–1.0 min, 0% B (v/v); 1.0–3.0 min, 0%–30% B (v/v); 3.0–6.0 min, 30%–100% B (v/v); 6.0–12.0 min, 100% B (v/v); 12.50–15.0 min, 0% B. The column was reconditioned for 5 min before the next injection. A flow rate of 0.2 ml/min and a varying injection volume were used for analysis. The UPLC system was assembled with a diode array detector (DAD) and an auto sampler. The peak area of each SCFA was used to calculate the amount of SCFA present, which was further normalized by the injection volume. The data were represented as the amount of butyrate present per gram of feces.

Preparation of liposome and loading of cholesterol to Huh7 cells

Liposomes were prepared using 22-NBD-cholesterol [22-(N-(7-nitrobenz-2-oxa-1,3-diazol-4-yl)amino)-23,24-bisnor-5-cholesterol-3β-ol] as previously described (Kheirloom and Ferrara, 2007). Briefly, 22-NBD-cholesterol (1 mg), cholesterol (4.8 mg), and phosphatidylcholine (8 mg) were dissolved in 1 ml

of chloroform. The solvent was evaporated to obtain a homogeneous thin lipid film and put into a 100-ml round-bottom flask, followed by solvent removal by rotary evaporation under reduced pressure. The lipid film was then hydrated in serum-free DMEM and sonicated (Microson Ultrasonic cell disruptor with a Misonix 2-mm probe) at 4°C three times for 1 min each at maximum output and filtered with a 0.2-µm Millipore filter (Banerjee et al., 2009). Huh7 cells were plated in a 96-well plate at a cell density of 10^5 cells/well. Cells were equilibrated with 22-NBD-cholesterol-liposome overnight. After incubation with liposome, cells were washed with 1× PBS and were subjected to treatment with or without butyrate.

Cholesterol efflux assay

The cholesterol efflux assay was performed as previously described (Low et al., 2012). Briefly, cholesterol-loaded cells were washed with 1× PBS and then treated with butyrate for the next 24 h. Following treatment with or without butyrate, cells were washed with 1× PBS and incubated in serum-free DMEM for the next 18 h. After the specified time of incubation, cells were treated with 1, 5, and 20 µg/ml HDL, respectively, for 4 h to induce efflux. Thereafter, cell supernatant was collected and cells were lysed using methanol. The fluorescence intensity (FI) of 22-NBD-cholesterol in the medium and cell lysate was detected by an MT-600F fluorescence microplate reader (Corona Electric, Hitachinaka, Japan) using 469-nm excitation and 537-nm emission filters in a black polystyrene 96-well plate (Costar, Corning Incorporated, USA). The percent cholesterol efflux was calculated as follows: % cholesterol efflux = $(\text{FI medium} \times 100) / (\text{FI medium} + \text{FI lysate})$.

GMO-PMO treatment to knock down AUF-1

The GMO-PMO was dissolved in saline to make a concentration of 1 mM, which was equivalent to 8.2 mg/ml. *In vivo* knockdown of AUF-1 was carried out in mice by injecting AUF-1 GMO-PMO (AUF-1-MO) through the tail vein on day 1 and day 7 at a dose of 3 mg/kg body weight. The effective dose was previously determined based on AUF-1 expression in liver by a pilot study. Another group of AUF-1-MO-injected mice were fed with 5% butyrate-supplemented chow diet from day 1 and continued till day 14. Blood was collected from the tail vein on day 7 and day 14 for cholesterol estimation. Mock GMO-PMO-treated animals are called scramble-MO controls. Another group of scramble-MO were fed with butyrate for 14 days after

the first dose injection. Animals were sacrificed after day 14 and tissue was collected for further analysis.

Statistical analysis

All values in the figures and text are expressed as arithmetic mean ± SEM. Data were analyzed with GraphPad Prism Version 8.01 software and statistical significance between groups was determined using unpaired Student's *t*-test. *p* values <0.05 were considered statistically significant. In the experiment involving Western blot, the figures shown are representative of at least three experiments performed on different days.

Data availability statement

The original contributions presented in the study are included in the article/Supplementary Material. Further inquiries can be directed to the corresponding author.

Ethics statement

The animal study was reviewed and approved by Institutional Animal Ethics Committee of Indian Council of Medical Research-NICED, Kolkata, India, (NICED/BS/MB-001/2019).

Author contributions

OD performed majority of the experiments and analyzed data. JK and AGh designed and synthesized GMO-PMOs. AGa, SG, MC, AM, SSG, and DM performed experiments. MD performed TEM study. BM and SS prepared the manuscript and analyzed data. MB conceived, designed, supervised, arranged funding, and wrote the manuscript. All authors contributed to the article and approved the submitted version.

Funding

This work was supported by Indian Council of Medical Research-NICED intramural grant (IM/MB/17-18/09) and DST-SERB, New Delhi, Govt of India (TTR/2021/000044).

Acknowledgments

We acknowledge the support of the Director of Indian Council of Medical Research-NICED, Kolkata, for carrying out

the study. Our deepest gratitude to Prof. Syamal Roy (CSIR-IICB, Kolkata) for his support, helpful discussion, and suggestions for the manuscript. We thank Ms. Shatarupa Bhattacharya and Rahul Gajbiye for LC-MS analysis. We acknowledge Dr. Amit Ghosh and Dr. Santasabuj Das (Indian Council of Medical Research-NICED) for critically reviewing the manuscript. OD is recipient of a fellowship from the DST. MC and AM are recipients of a fellowship from CSIR.

Conflict of interest

The authors declare that the research was conducted in the absence of any commercial or financial relationships that could be construed as a potential conflict of interest.

References

- Abdelmohsen, K., Tominaga-Yamanaka, K., Srikantan, S., Yoon, J. H., Kang, M. J., and Gorospe, M. (2012). RNA-Binding protein AUF-1 represses dicer expression. *Nucleic Acids Res.* 40, 11531–11544. doi: 10.1093/nar/gks930
- Abes, R., Moulton, H. M., Clair, P., Yang, S. T., Abes, S., Melikov, K., et al. (2008). Delivery of steric block morpholino oligomers by (R-X-R)₄ peptides: structure-activity studies. *Nucleic Acids Res.* 36, 6343–6354. doi: 10.1093/nar/gkn541
- Anderson, R. A., Joyce, C., Davis, M., Reagan, J. W., Clark, M., Shelness, G. S., et al. (1998). Identification of a form of acyl-CoA:cholesterol acyltransferase specific to liver and intestine in nonhuman primates. *J. Biol. Chem.* 273, 26747–26754. doi: 10.1074/jbc.273.41.26747
- Banerjee, S., Ghosh, J., Sen, S., Guha, R., Dhar, R., Ghosh, M., et al. (2009). Designing therapies against experimental visceral leishmaniasis by modulating the membrane fluidity of antigen-presenting cells. *Infect. Immun.* 77, 2330–2342. doi: 10.1128/IAI.00057-09
- Barker, H. A., Kahn, J. M., and Hedrick, L. (1982). Pathway of lysine degradation in *fusobacterium nucleatum*. *J. Bacteriol.* 152, 201–207. doi: 10.1128/jb.152.1.201-207.1982
- Berding, K., and Donovan, S. M. (2018). Diet can impact microbiota composition in children with autism spectrum disorder. *Front. Neurosci.* 12, 515. doi: 10.3389/fnins.2018.00515
- Bertoni, C. (2014). Emerging gene editing strategies for duchenne muscular dystrophy targeting stem cells. *Front. Physiol.* 5, 148. doi: 10.3389/fphys.2014.00148
- Bishop, K. S., Xu, H., and Marlow, G. (2017). Epigenetic regulation of gene expression induced by butyrate in colorectal cancer: Involvement of MicroRNA. *Genet. Epigenet* 9, 1179237X17729900. doi: 10.1177/1179237X17729900
- Bourriaud, C., Robins, R. J., Martin, L., Kozlowski, F., Tenailleau, E., Cherbut, C., et al. (2005). Lactate is mainly fermented to butyrate by human intestinal microfloras but inter-individual variation is evident. *J. Appl. Microbiol.* 99, 201–212. doi: 10.1111/j.1365-2672.2005.02605.x
- Buckel, W., and Barker, H. A. (1974). Two pathways of glutamate fermentation by anaerobic bacteria. *J. Bacteriol.* 117, 1248–1260. doi: 10.1128/jb.117.3.1248-1260.1974
- Cai, H., Xie, X., Ji, L., Ruan, X., and Zheng, Z. (2017). Sphingosine kinase 1: A novel independent prognosis biomarker in hepatocellular carcinoma. *Oncol. Lett.* 13, 2316–2322. doi: 10.3892/ol.2017.5732
- Canani, R. B., Costanzo, M. D., Leone, L., Pedata, M., Meli, R., and Calignano, A. (2011). Potential beneficial effects of butyrate in intestinal and extraintestinal diseases. *World J. Gastroenterol.* 17, 1519–1528. doi: 10.3748/wjg.v17.i12.1519
- Chambers, E. S., Preston, T., Frost, G., and Morrison, D. J. (2018). Role of gut microbiota-generated short-chain fatty acids in metabolic and cardiovascular health. *Curr. Nutr. Rep.* 7, 198–206. doi: 10.1007/s13668-018-0248-8
- Chang, J., Nicolas, E., Marks, D., Sander, C., Lerro, A., Buendia, M. A., et al. (2004). miR-122, a mammalian liver-specific microRNA, is processed from hcr mRNA and may downregulate the high affinity cationic amino acid transporter CAT-1. *RNA Biol.* 1, 106–113. doi: 10.4161/rna.1.2.1066
- Cheloufi, S., Dos Santos, C. O., Chong, M. M., and Hannon, G. J. (2010). A dicer-independent miRNA biogenesis pathway that requires ago catalysis. *Nature* 465, 584–589. doi: 10.1038/nature09092
- Cheng, K., Brunius, C., Fristedt, R., and Landberg, R. (2020). An LC-QToF MS based method for untargeted metabolomics of human fecal samples. *Metabolomics* 16, 46. doi: 10.1007/s11306-020-01669-z
- Chen, Y., Xu, C., Huang, R., Song, J., Li, D., and Xia, M. (2018). Butyrate from pectin fermentation inhibits intestinal cholesterol absorption and attenuates atherosclerosis in apolipoprotein e-deficient mice. *J. Nutr. Biochem.* 56, 175–182. doi: 10.1016/j.jnutbio.2018.02.011
- Corey, D. R., and Abrams, J. M. (2001). Morpholino antisense oligonucleotides: tools for investigating vertebrate development. *Genome Biol.* 2, REVIEWS1015. doi: 10.1186/gb-2001-2-5-reviews1015
- Cummings, J. H., Pomare, E. W., Branch, W. J., Naylor, C. P., and Macfarlane, G. T. (1987). Short chain fatty acids in human large intestine, portal, hepatic and venous blood. *Gut* 28, 1221–1227. doi: 10.1136/gut.28.10.1221
- Davie, J. R. (2003). Inhibition of histone deacetylase activity by butyrate. *J. Nutr.* 133, 2485S–2493S. doi: 10.1093/jn/133.7.2485S
- DeMaria, C. T., and Brewer, G. (1996). AUF-1 binding affinity to A+U-rich elements correlates with rapid mRNA degradation. *J. Biol. Chem.* 271, 12179–12184. doi: 10.1074/jbc.271.21.12179
- den Besten, G., Bleeker, A., Gerding, A., van Eunen, K., Havinga, R., van Dijk, T. H., et al. (2015). Short-chain fatty acids protect against high-fat diet-induced obesity via a PPARgamma-dependent switch from lipogenesis to fat oxidation. *Diabetes* 64, 2398–2408. doi: 10.2337/db14-1213
- Donohoe, D. R., Collins, L. B., Wali, A., Bigler, R., Sun, W., and Bultman, S. J. (2012). The warburg effect dictates the mechanism of butyrate-mediated histone acetylation and cell proliferation. *Mol. Cell* 48, 612–626. doi: 10.1016/j.molcel.2012.08.033
- Endo, H., Niioka, M., Kobayashi, N., Tanaka, M., and Watanabe, T. (2013). Butyrate-producing probiotics reduce nonalcoholic fatty liver disease progression in rats: new insight into the probiotics for the gut-liver axis. *PLoS One* 8, e63388. doi: 10.1371/journal.pone.0063388
- Enokizono, Y., Konishi, Y., Nagata, K., Ouhashi, K., Uesugi, S., Ishikawa, F., et al. (2005). Structure of hnRNP d complexed with single-stranded telomere DNA and unfolding of the quadruplex by heterogeneous nuclear ribonucleoprotein d. *J. Biol. Chem.* 280, 18862–18870. doi: 10.1074/jbc.M411822200
- Fukuhara, T., Kambara, H., Shiokawa, M., Ono, C., Katoh, H., Morita, E., et al. (2012). Expression of microRNA miR-122 facilitates an efficient replication in nonhepatic cells upon infection with hepatitis c virus. *J. Virol.* 86, 7918–7933. doi: 10.1128/JVI.00567-12
- Ghosh, J., Bose, M., Roy, S., and Bhattacharyya, S. N. (2013). Leishmania donovani targets Dicer-1 to downregulate miR-122, lower serum cholesterol, and

Publisher's note

All claims expressed in this article are solely those of the authors and do not necessarily represent those of their affiliated organizations, or those of the publisher, the editors and the reviewers. Any product that may be evaluated in this article, or claim that may be made by its manufacturer, is not guaranteed or endorsed by the publisher.

Supplementary material

The Supplementary Material for this article can be found online at: <https://www.frontiersin.org/articles/10.3389/fcimb.2022.1011386/full#supplementary-material>

- facilitate murine liver infection. *Cell Host Microbe* 13, 277–288. doi: 10.1016/j.chom.2013.02.005
- Girard, M., Jacquemin, E., Munnich, A., Lyonnet, S., and Henrion-Caupe, A. (2008). miR-122, a paradigm for the role of microRNAs in the liver. *J. Hepatol.* 48, 648–656. doi: 10.1016/j.jhep.2008.01.019
- Goedeke, L., Rotllan, N., Ramirez, C. M., Aranda, J. F., Canfran-Duque, A., Araldi, E., et al. (2015). miR-27b inhibits LDLR and ABCA1 expression but does not influence plasma and hepatic lipid levels in mice. *Atherosclerosis* 243, 499–509. doi: 10.1016/j.atherosclerosis.2015.09.033
- Graler, M. H. (2012). The role of sphingosine 1-phosphate in immunity and sepsis. *Am. J. Clin. Exp. Immunol.* 1, 90–100.
- Gratcos, F. M., and Brewer, G. (2010). The role of AUF-1 in regulated mRNA decay. *Wiley Interdiscip. Rev. RNA* 1, 457–473. doi: 10.1002/wrna.26
- Hasan, Z., and Karst, G. M. (1989). Muscle activity for initiation of planar, two-joint arm movements in different directions. *Exp. Brain Res.* 76, 651–655. doi: 10.1007/BF00248921
- He, G. Q., Kong, Q., Chen, Q. H., and Ruan, H. (2005). Batch and fed-batch production of butyric acid by clostridium butyricum ZJUCB. *J. Zhejiang Univ. Sci. B* 6, 1076–1080. doi: 10.1631/jzus.2005.B1076
- Hu, C., and Li, L. (2015). *In vitro* culture of isolated primary hepatocytes and stem cell-derived hepatocyte-like cells for liver regeneration. *Protein Cell* 6, 562–574. doi: 10.1007/s13238-015-0180-2
- Isono, A., Katsuno, T., Sato, T., Nakagawa, T., Kato, Y., Sato, N., et al. (2007). Clostridium butyricum TO-a culture supernatant downregulates TLR4 in human colonic epithelial cells. *Dig. Dis. Sci.* 52, 2963–2971. doi: 10.1007/s10620-006-9593-3
- Jeon, B. H., Lee, Y. H., Yun, M. R., Kim, S. H., Lee, B. W., Kang, E. S., et al. (2015). Increased expression of ATP-binding cassette transporter A1 (ABCA1) as a possible mechanism for the protective effect of cilostazol against hepatic steatosis. *Metabolism* 64, 1444–1453. doi: 10.1016/j.metabol.2015.07.014
- Jian, C., Luukkainen, P., Yki-Jarvinen, H., Salonen, A., and Korpela, K. (2020). Quantitative PCR provides a simple and accessible method for quantitative microbiota profiling. *PLoS One* 15, e0227285. doi: 10.1371/journal.pone.0227285
- Kajita, Y., Nakayama, J., Aizawa, M., and Ishikawa, F. (1995). The UAG-specific RNA binding protein, heterogeneous nuclear ribonucleoprotein D0, common modular structure and binding properties of the 2xRBD-gly family. *J. Biol. Chem.* 270, 22167–22175. doi: 10.1074/jbc.270.38.22167
- Kennedy, E. A., King, K. Y., and Baldrige, M. T. (2018). Mouse microbiota models: Comparing germ-free mice and antibiotics treatment as tools for modifying gut bacteria. *Front. Physiol.* 9, 1534. doi: 10.3389/fphys.2018.01534
- Kheirloomoom, A., and Ferrara, K. W. (2007). Cholesterol transport from liposomal delivery vehicles. *Biomaterials* 28, 4311–4320. doi: 10.1016/j.biomaterials.2007.06.008
- Kim, Y. K., Kim, B., and Kim, V. N. (2016). Re-evaluation of the roles of DROSHA, export in 5, and DICER in microRNA biogenesis. *Proc. Natl. Acad. Sci. U.S.A.* 113, E1881–E1889. doi: 10.1073/pnas.160253211
- Kishor, A., Tandukar, B., Ly, Y. V., Toth, E. A., Suarez, Y., Brewer, G., et al. (2013). Hsp70 is a novel posttranscriptional regulator of gene expression that binds and stabilizes selected mRNAs containing AU-rich elements. *Mol. Cell Biol.* 33, 71–84. doi: 10.1128/MCB.01275-12
- Krutzfeldt, J., Rajewsky, N., Braich, R., Rajeev, K. G., Tuschl, T., Manoharan, M., et al. (2005). Silencing of microRNAs *in vivo* with a ntamir. *Nature* 438, 685–689. doi: 10.1038/nature04303
- Kuzu, O. F., Noory, M. A., and Robertson, G. P. (2016). The role of cholesterol in cancer. *Cancer Res.* 76, 2063–2070. doi: 10.1158/0008-5472.CAN-15-2613
- Lagos-Quintana, M., Rauhut, R., Yalcin, A., Meyer, J., Lendeckel, W., and Tuschl, T. (2002). Identification of tissue-specific microRNAs from mouse. *Curr. Biol.* 12, 735–739. doi: 10.1016/S0960-9822(02)00809-6
- Le Roy, T., Debedat, J., Marquet, F., Da-Cunha, C., Ichou, F., Guerre-Millo, M., et al. (2018). Comparative evaluation of microbiota engraftment following fecal microbiota transfer in mice models: Age, kinetic and microbial status matter. *Front. Microbiol.* 9, 3289. doi: 10.3389/fmicb.2018.03289
- Le Roy, T., Lecuyer, E., Chassaing, B., Rhimi, M., Lhomme, M., Boudebouze, S., et al. (2019). The intestinal microbiota regulates host cholesterol homeostasis. *BMC Biol.* 17, 94. doi: 10.1186/s12915-019-0715-8
- Liao, B., Hu, Y., and Brewer, G. (2007). Competitive binding of AUF-1 and TIAR to MYC mRNA controls its translation. *Nat. Struct. Mol. Biol.* 14, 511–518. doi: 10.1038/nsmb1249
- Li, T., Franc, J. M., Boehme, S., and Chiang, J. Y. (2013). Regulation of cholesterol and bile acid homeostasis by the cholesterol 7 α -hydroxylase/steroid response element-binding protein 2/microRNA-33a axis in mice. *Hepatology* 58, 1111–1121. doi: 10.1002/hep.26427
- Liu, H., Wang, J., He, T., Becker, S., Zhang, G., Li, D., et al. (2018). Butyrate: A double-edged sword for health? *Adv. Nutr.* 9, 21–29. doi: 10.1093/advances/nmx009
- Long, J. K., Dai, W., Zheng, Y. W., and Zhao, S. P. (2019). miR-122 promotes hepatic lipogenesis via inhibiting the LKB1/AMPK pathway by targeting Sirt1 in non-alcoholic fatty liver disease. *Mol. Med.* 25, 26. doi: 10.1186/s10020-019-0085-2
- Louis, P., Duncan, S. H., McCrae, S. I., Millar, J., Jackson, M. S., and Flint, H. J. (2004). Restricted distribution of the butyrate kinase pathway among butyrate-producing bacteria from the human colon. *J. Bacteriol.* 186, 2099–2106. doi: 10.1128/JB.186.7.2099-2106.2004
- Louis, P., and Flint, H. J. (2007). Development of a semiquantitative degenerate real-time PCR-based assay for estimation of numbers of butyryl-coenzyme A (CoA) CoA transferase genes in complex bacterial samples. *Appl. Environ. Microbiol.* 73, 2009–2012. doi: 10.1128/AEM.02561-06
- Low, H., Hoang, A., and Sviridov, D. (2012). Cholesterol efflux assay. *J. Vis. Exp.* 61, e3810. doi: 10.3791/3810
- Lu, J. Y., Sadri, N., and Schneider, R. J. (2006). Endotoxic shock in AUF-1 knockout mice mediated by failure to degrade proinflammatory cytokine mRNAs. *Genes Dev.* 20, 3174–3184. doi: 10.1101/gad.1467606
- Luu, W., Hart-Smith, G., Sharpe, L. J., and Brown, A. J. (2015). The terminal enzymes of cholesterol synthesis, DHCR24 and DHCR7, interact physically and functionally. *J. Lipid Res.* 56, 888–897. doi: 10.1194/jlr.M056986
- Merscher-Gomez, S., Guzman, J., Pedigo, C. E., Lehto, M., Aguilon-Prada, R., Mendez, A., et al. (2013). Cyclodextrin protects podocytes in diabetic kidney disease. *Diabetes* 62, 3817–3827. doi: 10.2337/db13-0399
- Miao, X., Rahman, M. F., Jiang, L., Min, Y., Tan, S., Xie, H., et al. (2018). Thrombin-reduced miR-27b attenuates platelet angiogenic activities *in vitro* via enhancing platelet synthesis of anti-angiogenic thrombospondin-1. *J. Thromb. Haemost.* 16, 791–801. doi: 10.1111/jth.13978
- Mishra, A. K., Kumar, S. S., and Ghosh, A. R. (2019). Probiotic enterococcus faecalis AG5 effectively assimilates cholesterol and produces fatty acids including propionate. *FEMS Microbiol. Lett.* 366(4), fnz039. doi: 10.1093/femsle/fnz039
- Mistry, R. H., Verkade, H. J., and Tietge, U. J. (2017). Reverse cholesterol transport is increased in germ-free mice—brief report. *Arterioscler. Thromb. Vasc. Biol.* 37, 419–422. doi: 10.1161/ATVBAHA.116.308306
- O'Brien, J., Hayder, H., Zayed, Y., and Peng, C. (2018). Overview of MicroRNA biogenesis, mechanisms of actions, and circulation. *Front. Endocrinol. (Lausanne)* 9, 402. doi: 10.3389/fendo.2018.00402
- Reikvam, D. H., Erofeev, A., Sandvik, A., Grdic, V., Jahnsen, F. L., Gaustad, P., et al. (2011). Depletion of murine intestinal microbiota: effects on gut mucosa and epithelial gene expression. *PLoS One* 6, e17996. doi: 10.1371/journal.pone.0017996
- Rios-Covian, D., Ruas-Madiedo, P., Margolles, A., Gueimonde, M., de Los Reyes-Gavilan, C. G., and Salazar, N. (2016). Intestinal short chain fatty acids and their link with diet and human health. *Front. Microbiol.* 7, 185. doi: 10.3389/fmicb.2016.00185
- Sadri, N., and Schneider, R. J. (2009). AUF-1/Hnnpd-deficient mice develop pruritic inflammatory skin disease. *J. Invest. Dermatol.* 129, 657–670. doi: 10.1038/jid.2008.298
- Schoenberg, D. R., and Maquat, L. E. (2012). Regulation of cytoplasmic mRNA decay. *Nat. Rev. Genet.* 13, 246–259. doi: 10.1038/nrg3160
- Sobolewski, C., Sanduja, S., Blanco, F. F., Hu, L., and Dixon, D. A. (2015). Histone deacetylase inhibitors activate tristetrin expression through induction of early growth response protein 1 (EGR1) in colorectal cancer cells. *Biomolecules* 5, 2035–2055. doi: 10.3390/biom5032035
- Sobue, S., Murakami, M., Banno, Y., Ito, H., Kimura, A., Gao, S., et al. (2008). V-src oncogene product increases sphingosine kinase 1 expression through mRNA stabilization: alteration of AU-rich element-binding proteins. *Oncogene* 27, 6023–6033. doi: 10.1038/onc.2008.198
- Song, K. H., Li, T., Owsley, E., and Chiang, J. Y. (2010). A putative role of micro RNA in regulation of cholesterol 7 α -hydroxylase expression in human hepatocytes. *J. Lipid Res.* 51, 2223–2233. doi: 10.1194/jlr.M004531
- Suh, J. H., and Saba, J. D. (2015). Sphingosine-1-phosphate in inflammatory bowel disease and colitis-associated colon cancer: the fat's in the fire. *Transl. Cancer Res.* 4, 469–483. doi: 10.3978/j.issn.2218-676X.2015.10.06
- Vallejo-Vaz, A. J., Robertson, M., Catapano, A. L., Watts, G. F., Kastelein, J. J., Packard, C. J., et al. (2017). Low-density lipoprotein cholesterol lowering for the primary prevention of cardiovascular disease among men with primary elevations of low-density lipoprotein cholesterol levels of 190 mg/dL or above: Analyses from the WOSCOPS (West of Scotland coronary prevention study) 5-year randomized trial and 20-year observational follow-up. *643 Circ.* 136, 1878–1891. doi: 10.1161/CIRCULATIONAHA.117.027966
- Vital, M., Howe, A. C., and Tiedje, J. M. (2014). Revealing the bacterial butyrate synthesis pathways by analyzing (meta)genomic data. *mBio* 5, e00889. doi: 10.1128/mBio.00889-14
- Vock, C., Doring, F., and Nitz, I. (2008). Transcriptional regulation of HMG-CoA synthase and HMG-CoA reductase genes by human ACBP. *Cell Physiol. Biochem.* 22, 515–524. doi: 10.1159/000185525

- Wagner, B. J., DeMaria, C. T., Sun, Y., Wilson, G. M., and Brewer, G. (1998). Structure and genomic organization of the human AUF-1 gene: alternative pre-mRNA splicing generates four protein isoforms. *Genomics* 48, 195–202. doi: 10.1006/geno.1997.5142
- Wang, R. X., Henen, M. A., Lee, J. S., Vogeli, B., and Colgan, S. P. (2021). Microbiota-derived butyrate is an endogenous HIF prolyl hydroxylase inhibitor. *Gut Microbes* 13, 1938380. doi: 10.1080/19490976.2021.1938380
- Wang, H. G., Huang, X. D., Shen, P., Li, L. R., Xue, H. T., and Ji, G. Z. (2013). Anticancer effects of sodium butyrate on hepatocellular carcinoma cells *in vitro*. *Int. J. Mol. Med.* 31, 967–974. doi: 10.3892/ijmm.2013.1285
- Wu, S., Li, C., Huang, W., Li, W., and Li, R. W. (2012). Alternative splicing regulated by butyrate in bovine epithelial cells. *PloS One* 7, e39182. doi: 10.1371/journal.pone.0039182
- Xu, Y. H., Gao, C. L., Guo, H. L., Zhang, W. Q., Huang, W., Tang, S. S., et al. (2018). Sodium butyrate supplementation ameliorates diabetic inflammation in db/db mice. *J. Endocrinol.* 238, 231–244. doi: 10.1530/JOE-18-0137
- Yancey, P. G., Bortnick, A. E., Kellner-Weibel, G., de la Llera-Moya, M., Phillips, M. C., and Rothblat, G. H. (2003). Importance of different pathways of cellular cholesterol efflux. *Arterioscler. Thromb. Vasc. Biol.* 23, 712–719. doi: 10.1161/01.ATV.0000057572.97137.DD
- Yang, J. S., Maurin, T., and Lai, E. C. (2012). Functional parameters of dicer-independent microRNA biogenesis. *RNA* 18, 945–957. doi: 10.1261/rna.032938.112
- Zampelas, A., and Magriplis, E. (2019). New insights into cholesterol functions: A friend or an enemy? *Nutrients* 11. doi: 10.3390/nu11071645
- Zhao, Z. H., Wang, Z. X., Zhou, D., Han, Y., Ma, F., Hu, Z., et al. (2021). Sodium butyrate supplementation inhibits hepatic steatosis by stimulating liver kinase B1 and insulin-induced gene. *Cell Mol. Gastroenterol. Hepatol.* 12, 857–871. doi: 10.1016/j.jcmgh.2021.05.006
- Zhou, X. J., Wang, J., Ye, H. H., and Fa, Y. Z. (2019). Signature MicroRNA expression profile is associated with lipid metabolism in African green monkey. *Lipids Health Dis.* 18, 55. doi: 10.1186/s12944-019-0999-2

BRIEF REPORT

Open Access



Butyrate driven raft disruption trots off enteric pathogen invasion: possible mechanism of colonization resistance

Oishika Das¹, Aaheli Masid¹, Mainak Chakraborty¹, Animesh Gope¹, Shanta Dutta¹ and Moumita Bhaumik^{1*}

Abstract

The gut microbiome derived short chain fatty acids perform multitude of functions to maintain gut homeostasis. Here we studied how butyrate stymie enteric bacterial invasion in cell using a simplistic binary model. The surface of the mammalian cells is enriched with microdomains rich in cholesterol that are known as rafts and act as entry points for pathogens. We showed that sodium butyrate treated RAW264.7 cells displayed reduced membrane cholesterol and less cholera-toxin B binding coupled with increased membrane fluidity compared to untreated cells indicating that reduced membrane cholesterol caused disruption of lipid rafts. The implication of such cellular biophysical changes on the invasion of enteric pathogenic bacteria was assessed. Our study showed, in comparison to untreated cells, butyrate-treated cells significantly reduced the invasion of *Shigella* and *Salmonella*, and these effects were found to be reversed by liposomal cholesterol treatment, increasing the likelihood that the rafts' function against bacterial invasion. The credence of ex vivo studies found to be in concordance in butyrate fed mouse model as evident from the significant drift towards a protective phenotype against virulent enteric pathogen invasion as compared to untreated mice. To produce a cytokine balance towards anti-inflammation, butyrate-treated mice produced more of the gut tissue anti-inflammatory cytokine IL-10 and less of the pro-inflammatory cytokines TNF- α , IL-6, and IFN- γ . In histological studies of *Shigella* infected gut revealed a startling observation where number of neutrophils infiltration was noted which was correlated with the pathology and was essentially reversed by butyrate treatment. Our results ratchet up a new dimension of our understanding how butyrate imparts resistance to pathogen invasion in the gut.

Keywords Butyrate, Cholesterol, Lipid raft, Pathogen invasion

Introduction

The community of bacteria that lines the intestinal tract is an epitome of symbiotic relation with the host [1]. The intestine of mammals is colonized by a complex group of bacteria. The commensal gut bacteria stymies pathogen colonization by exploiting array of mechanisms including ecological competition for nutrients, active antagonism

by secretion of antimicrobial peptides and bactericidins and metabolite mediated inhibition [2]. The gut microbiota has been linked to restoring biological functions of the host including metabolism, gut barrier function and immune development [3]. Furthermore, the commensal microbes resist growth of opportunistic bacteria protecting the host from pathogen infection, phenomena called "colonization resistance" [4]. The pioneering work demonstrating dramatic increase in susceptibility to *Salmonella enteritidis* infection in antibiotic mediated disruption of gut bacteria in mice opened critical window to address the problem with centrality [5]. Metabolites produced by the gut microbes especially short chain fatty

*Correspondence:

Moumita Bhaumik
drmmoumitabhaumik@gmail.com

¹ ICMR-National Institute of Cholera and Enteric Diseases, P-33 C.I. T Road, Belegata, Kolkata, West Bengal 700010, India



© The Author(s) 2023. **Open Access** This article is licensed under a Creative Commons Attribution 4.0 International License, which permits use, sharing, adaptation, distribution and reproduction in any medium or format, as long as you give appropriate credit to the original author(s) and the source, provide a link to the Creative Commons licence, and indicate if changes were made. The images or other third party material in this article are included in the article's Creative Commons licence, unless indicated otherwise in a credit line to the material. If material is not included in the article's Creative Commons licence and your intended use is not permitted by statutory regulation or exceeds the permitted use, you will need to obtain permission directly from the copyright holder. To view a copy of this licence, visit <http://creativecommons.org/licenses/by/4.0/>. The Creative Commons Public Domain Dedication waiver (<http://creativecommons.org/publicdomain/zero/1.0/>) applies to the data made available in this article, unless otherwise stated in a credit line to the data.

acids (SCFA) constituting mainly acetate, propionate and butyrate plays an important role in resisting pathogen from colonization [6]. A link between SCFAs and *Clostridium difficile* infection was first discovered in 1994 that found pigs fed a high-fiber diet were less susceptible to *C. difficile* infection [7]. Later, copious reports demonstrated that loss of SCFA production correlated with susceptibility to enteric infection [8], [9]. SCFA is shown to imprint antimicrobial properties in macrophages even in the absence of increased inflammatory cytokine response [10]. SCFA also provide an important resistance mechanism against pathogen by exerting toxic acid stress [8] as demonstrated in vitro that the toxicity was attributable to the non-ionized forms of these acids, which exist more prominently at low pH [8, 11]. SCFA also plays a critical role in maintaining the limited availability of oxygen and nitrate leading to decrease *Salmonella* infection [12]. Considering SCFAs regulate multiple metabolic pathways of the host [13], the contribution of SCFA mediated antagonism to resist colonization in light of host cell function needs to be evaluated.

Earlier we have shown that butyrate but not acetate or propionate regulates cholesterol homeostasis exploiting a probable axis “AUF-1-Dicer1-miR122-cholesterol” [14]. Cholesterol is an important component of the cell membrane, modulating a plethora of biophysical properties of the membrane. A cholesterol-rich station in the membrane known as a lipid raft is formed when cholesterol is present in membranes with pre-determined membrane dynamics [15]. These lipid rafts are intended to serve as a gateway for the entry of numerous pathogens [16]. Pathogens can elude the immune system in an innovative way by using membrane microdomains [16]. Some pathogens have acquired strategies to thwart innate and adaptive immune responses by co-opting raft-associated pathways. Most intracellular pathogens tactically exploit lipid rafts for entering the host cell. *Salmonella* and *Shigella* have a common requirement for a T3SS (type III secretion system), which is a multicomponent molecular syringe that allows the translocation of so called effector proteins from bacterial cytoplasm, through the inner and outer bacterial membrane, as well as the host plasma membrane, directly into cytoplasm [17]. It has effector proteins called SipB and SipC for *Salmonella* [18] and IpaB and IpaC for *Shigella* [19] that must come into contact with the host cell in order to activate the system. The binding of SipB/IpaB to host cells requires cholesterol in the membranes on the downstream of the T3SS activation [20]. The pathogenic vesicles of Enterotoxigenic *E. coli* fuses to the cell membrane in the cholesterol rich domain of the host cell membrane [21]. Cholesterol depleting agents reduces internalization

of *Helicobacter pylori* in gut epithelial cells [22]. Hole forming bacteria like *Vibrio cholerae* prefers to create holes in the lipid rafts as rafts can sustain the holes for longer time [23].

Armed with credible studies we aim to study if butyrate that reduces cholesterol biosynthesis can disrupt lipid rafts and prevents pathogen invasion. We studied butyrate treatment reduces the cholesterol content and alters the physical properties of cell membrane. Here we performed fluorescence polarization using Laurdan probe for measuring the fluidity in cell membranes with or without butyrate treatment. Employing gentamycin protection assay we have shown that butyrate prevents invasion of *Shigella* and *Salmonella* in macrophages. Further leverage on reduced pathogen invasion on butyrate treatment was due to lack of membrane cholesterol was stemmed from restoration of cholesterol in membranes by liposomal delivery which showed reversal of butyrate effect. Our observation in cell line also resonates in mice model. By harmonising narratives from our experimental studies, we showed that gut microbial butyrate decreases membrane cholesterol and disrupts lipid rafts resulted in decrease in pathogen invasion, a “critical” denominator for pathogen resistance. Our study provides additional unique forces of pathogen resistance in gut.

Materials and methods

Reagents and chemicals

Chow diet (Harlan Teklad LM-485) was purchased from ICMR-NIN, Hyderabad, India. Dulbecco's modified Eagle's medium (DMEM) and foetal calf serum (FCS) were purchased from GIBCO (Waltham, MA, USA). Gentamycin, BCA protein assay kit, apoptosis kit, LDH kit, CFSE kit was purchased from ThermoFisher (Waltham, MA, USA). Triton X100, sodium butyrate, sodium propionate, sodium acetate, Hoechst 33342, Laurdan, CTX-B-FITC, water soluble cholesterol (MBCD-cholesterol) was purchased from Sigma (St. Louis, MO, USA). Amplex red cholesterol assay kit, Trizol, Fillipin was purchased from Invitrogen (Carlsbad, CA, USA). Cholesterol, Cholesterol analogue (4-cholesten-3-one) and Phosphatidylcholine were obtained from Avanti polar lipids. Anti CD44-FITC antibody was purchased from BD Pharmingen™. Anti CD71-biotin was purchased from Bioss (Massachusetts, Boston, USA). Secondary Streptavidin PE was purchased from Biolegend (San Diego, CA, USA). Super Reverse Transcriptase MuLV Kit, RT [2] SYBR® Green qPCR Mastermix, were purchased from Qiagen (Hilden, Germany). Protease inhibitor was purchased from Takara. Primers were purchased from IDT (Germany). RAW264.7 cell line was purchased from ATCC (USA).

Propagation of RAW 264.7 cells, estimation of cellular protein and cholesterol

Murine macrophage cell line RAW264.7 were cultured in Dulbecco's modified Eagle's medium (DMEM) along with 10% Fetal Bovine Serum (FBS), supplemented with 1% Penicillin and Streptomycin at 37° C with 5% CO₂ in the humidified incubator (Heracell 150i, ThermoFisher Scientific). RAW 264.7 cells were seeded in 6 well tissue culture plates (10⁶ cells/ well) and allowed to adhere for overnight and reach confluency approximately 75–80%. Cells were then treated with different concentrations (5 mM or 10 mM) of sodium butyrate (butyrate) for 18 h having 2 mL media in each well. The viability and toxicity in the cells were assayed by Annexin/PI and LDH assay. Total crude cell membranes were isolated as described [24]. Cells were homogenized in 1 mL of buffer [10 mM Tris-HCl (pH 7.4), 1 mM EDTA, 200 mM sucrose] and protease inhibitor mix (Roche Diagnostics, Mannheim, Germany). The nuclei and cellular debris were removed by centrifugation at 900 × g for 10 min at 4 °C. The resulting supernatant was centrifuged at 100,000 × g for 75 min at 4 °C to obtain the crude membrane pellet. The pellet was resuspended in PBS and an aliquot of it was used for protein measurement using Pierce™ BCA Protein Assay Kit following manufacturer's protocol. The rest of the pellet was extracted with 2:1 methanol/chloroform, followed by 0.5 mL of chloroform and 0.5 mL of water. The methanol/chloroform (lipid phase) layer was dried under vacuum in a vacuum desiccator. The dry lipid was suspended in 200 µL of 1 × Reaction buffer supplied with Amplex Red Cholesterol Assay Kit and membrane cholesterol quantification was performed by following the manufacturer's instructions.

Fillipin staining

Cells were washed with PBS twice, fixed with 2% chilled paraformaldehyde for 30 min at room temperature. After washing with PBS thrice the cells were incubated with 1 mL of 1.5 mg glycine/mL PBS for 10 min at room temperature to quench paraformaldehyde. Thereafter the cells were stained with 1 mL of 0.05 mg/mL of Fillipin in PBS containing 10% FBS for 2 h at room temperature. After washing with PBS thrice, the fluorescence images of the cells were visualized under Carl Zeiss microscope equipped with a CCD camera controlled with ZEN software (Carl Zeiss, Gottingen, Germany) and also analyzed using FACSDiva software in FACS Aria II machine (both Becton Dickinson, San Jose, CA). Each sample had at least 10,000 occurrences

recorded in it. The data was analyzed using FloJo software.

Membrane anisotropy

Membrane fluidity and fluorescence were measured as described [26, 52]. Briefly, Laurdan, the fluorescent probe, was dissolved in HPLC grade water to make a stock solution of 2 mM. This 1 mL stock solution was added to 10 mL of rapidly stirring PBS (pH 7.2). To 2 × 10⁶ cells in 1 mL PBS, 1 mL of Laurdan (C_f 1 µM) was added and incubated for 2 h at 37 °C. Following incubation, the cells were washed thrice and resuspended in PBS. The Laurdan probe bound to the membrane of the cell was excited at 350 nm and the intensity of emission was recorded at 435 nm in a spectrofluorometer (Cary Eclipse Instrument (MY13130004)). The fluorescence anisotropy (FA) value was calculated using the equation: $FA = [(I_{\parallel} - I_{\perp}) / (I_{\parallel} + 2I_{\perp})]$, where I_{\parallel} and I_{\perp} are the fluorescent intensities oriented, respectively, parallel and perpendicular to the direction of polarization of the exciting light.

Cholesterol-liposome and cholesterol analogue-liposome synthesis and treatment of liposomal cholesterol on cells

Liposomes were prepared by mixing cholesterol/ cholesterol analogue (4-cholesten-3-one) and Phosphatidylcholine according to the protocol [27]. Briefly, cholesterol/ cholesterol analogue (4-cholesten-3-one) and PC were mixed at a ratio of 1:1.5 in a round bottom flask and kept inside a vacuum desiccator for overnight. A thin film of lipid layer was obtained which was then dissolved in 1 mL DMEM and filtered with 0.22 µm of membrane filter. The size of the liposomes was measured by Differential light Scattering (DLS). Henceforth, cholesterol-liposome and analogue-liposome will be denoted as chol-lipo and ana-lipo respectively.

Freshly prepared 10 µL (containing approx 4.8 × 10¹⁴ lipoparticles) of liposomes/10⁶ cells were treated to sodium butyrate treated cells and incubated 18 h at 37 °C in 5% CO₂ incubator. The concentration of liposome was determined by following equation (<https://doi.org/10.3390/scipharm89020015>).

$N_{(lipo)} = [M_{(ing)} \times N_{(Avo)}] / [N_{(tot)} \times 1000]$. where:
 $N_{(lipo)}$ is the number of vesicles per mL;
 $M_{(ing)}$ is the molar concentration of ingredients of vesicles;
 $N_{(Avo)}$ is the Avogadro Number (6.02 × 10²³);
 $N_{(tot)}$ is the total number of ingredients per vesicle.
 $N_{(tot)}$ is calculated using the following equation:
 $N_{(tot)} = 17.69 \times [(d/2)100 + (d/2-5)100]$ where, d is the diameter of the vesicle.

Visualization of liposomes in transmission electron microscopy (TEM)

To obtain a visual impression, the morphologies of liposomes were studied by performing TEM (200 kV FEG TEM) after negative staining of samples with uranyl acetate. To obtain information about lamellation, liposomes in PBS were mixed with an equal volume of 3% agar and kept at -20°C overnight. The solidified agar containing vesicles was cut into sections that were 60 nm thick with a cryo ultramicrotome. The sections were taken in a 300 mesh carbon coated Copper grid and dried overnight to observe in TEM.

Confocal analysis and image processing

The cells were seeded on a 1.5H coverslip (0.16–0.19 mm thick) and treated with 10 mM sodium butyrate or 10 mM sodium butyrate followed by liposomal cholesterol. After 18 h the coverslips were washed with PBS after treatment and fixed by incubating the cells with 4% paraformaldehyde for 10 min at room temperature. Cells were washed with PBS for thrice and stained with CTXB-FITC or anti-CD71-biotin or anti-CD44-FITC antibody by incubating them for 30 min at 1:200 dilution. For CD71 detection, after 3 times PBS washing, the cells were further stained with streptavidin-PE antibody (1:200 dilution). The reaction was terminated by washing the cells thrice with PBS. Counter stain was done by treating the cells with 1 $\mu\text{g}/\text{mL}$ Hoechst 33342 for 5 min at room temperature and washed again with PBS three times and mounted with 90% glycerol. Fluorescence images were captured in 63X magnification in confocal microscope (Carl Zeiss (Germany)). The analysis was done by ImageJ software. Corrected total cell fluorescence is calculated as:

Corrected Total cell fluorescence = (Integrated density) – (Area of selected cells \times mean fluorescence of background).

CD44 expression analysis by flowcytometry

To estimate the total expression of CD44 in both control and butyrate treated RAW 264.7 cells, the cells were permeabilized/ unpermeabilized using 0.1% Tween 20 for 15 min and then fixed with 2% chilled paraformaldehyde for 30 min at room temperature. Cells were then collected in FACS buffer (PBS + 10%FBS). Aliquots containing 10^6 cells in FACS buffer were stained for 30 min in room temperature using FITC conjugated anti-CD44 antibody in 1:500 dilutions. The cells were then examined using FACSDiva software in a FACS Aria II machine (both Becton Dickinson, San Jose, CA). Each sample had at least 10,000 occurrences recorded in it. The data was analyzed using FloJo software.

Bacterial strain

Shigella flexneri serotype 2a strain 2457 T and *Salmonella* serovar typhimurium wild-type strain SL1344 were grown in Luria broth (LB) at 37°C overnight and reinoculated with 1% precultured bacteria in fresh media in a shaking incubator at 37°C . OD_{600} was measured by Spectrophotometer for monitoring and when the OD reached the value of 0.6, the culture was diluted to 2×10^9 CFU/mL in PBS for further experiments.

Pathogen invasion assay

Pathogen invasion assay [28] was performed in the cells cultured in serum free medium to avoid interference of serum cholesterol. Briefly, *Shigella flexneri* or *Salmonella typhimurium* was added to the cells (5×10^5 cells/ well in 500 μL medium in a 24 well plate) at 100 multiplicity of infection (MOI) and incubated for 1 h. Media was aspirated and cells were washed thrice with PBS, followed by addition of DMEM containing 50 $\mu\text{g}/\text{mL}$ of Gentamycin and incubated for 1 h at 5% CO_2 at 37°C . After incubation, media was removed and cells were washed thrice with PBS. Cell lysate was prepared by adding 100 μL of 0.1% Triton X-100 to the cells. The lysate was then plated on either XLD plates for *Shigella flexneri* or LB agar for *Salmonella typhimurium* and incubated at 37°C overnight. The numbers of colonies were counted on the next day and the data is represented as percent control.

Percent control = Treated/Control \times 100.

Dietary supplementation of sodium butyrate and chol-lipo treatment in mice

The dietary supplementation studies were performed as reported earlier with minor modification [27]. Briefly, a group of 10 adult C57BL/6 mice (divided as 5 in each group) were fed with chow diet and 150 mM sodium butyrate in drinking water for 30 days. On 28th day of butyrate treatment, 5 animals from the group were selected randomly and was injected chol-lipo (200 μL of liposomal suspension) through intracardiac route (chol-lipo mice) [24]. Another set of 5 mice with regular chow diet and normal drinking water served as normal group.

These animals were infected intraperitoneally with 10^8 cfu/mice of *Shigella flexneri* on 30th day. On day 2 post infection the animals were sacrificed and biomaterials were collected for further analysis. A group of age matched normal mice served as uninfected control.

Bacteria count (CFU) from colon tissue

The colon tissue (40–50 mg) collected from mice were extensively washed with PBS, resuspended in 1 mL PBS and homogenised using Dounce Homogeniser. The ten-fold diluted homogenate was plated in XLD agar plates and subjected to overnight incubation at 37°C . Colonies

were counted on the following day. The cfu/ gm tissue was calculated as.

Cfu/ gm tissue = (number of colonies x dilution factor)/ gm of tissue.

Histopathological analysis

Colon samples were washed thoroughly with PBS and fixed in 4% paraformaldehyde at 4 °C for 48 h and then dehydrated by soaking then in graded alcohol, xylene, embedded in paraffin. 5 µm sections were obtained from paraffin block by routine microtome and stained with H&E and subjected to microscopic analysis (Carl Zeiss Axiovert 40 CFL). The degree of interstitial infiltration by inflammatory cells, in response to *Shigella* infection, was evaluated by counting the number of neutrophils in the colon at high power field (X100) as previously described [29].

RNA extraction and reverse transcription

The cytokine mRNA expression was studied from gut tissue as reported previously [30]. Total RNA from the tissue was extracted with Trizol according to the protocol recommended by the manufacturer. The concentration of the extracted RNA was analyzed by Nanodrop spectrophotometer (Thermo) and RNA was stored at −80 °C. cDNA was prepared from total RNA by reverse specific primers using Super Reverse Transcriptase MuLV Kit. The primers for the reverse transcription are listed in Table 1. GAPDH was normalized for the expressions of each gene. The total reaction volume for reverse transcription was 20 µl in which 1 µM of reverse primer, 5 ng of RNA template, 1 µl dNTP mix, 12 µl of DEPC treated water, 4 µl of 5 X first strand buffer, 1 µl of 0.1 M DTT, 1 µl of RNase inhibitor and 1 µl Super RT MuLV. Reverse transcription was carried out for 65 °C for 5 min, followed by incubation at 55 °C for 1 h and then heat inactivating the reaction at 70 °C for 15 min.

Quantitative real-time PCR

Total RNA was extracted with Trizol reagent from snap frozen liver and RNA concentration was determined using a nanodrop spectrophotometer. The genes and GAPDH levels were quantified with Applied Biosystems™ StepOne™ Real Time PCR System with RT² SYBR® Green qPCR Mastermix following the manufacturer's instructions. Each 20 µL qPCR reaction contained an amount of cDNA equivalent to 5 ng of total RNA, 10 µL of RT² SYBR® Green qPCR Mastermix, 1 µM of the forward and reverse primer (each) and nuclease free water. Real-time PCR was performed with the following conditions: 95 °C for 10 min, 40 cycles of 95 °C for 30 s, 60 °C for 1 min and 72 °C for 1 min PCR product was calculated according to the $2^{-\Delta C_t}$ method described previously [31].

Primers

The primer sequences have been designed by using NCBI Primer BLAST (<https://www.ncbi.nlm.nih.gov/tools/primer-blast/>). Following few things were considered for selecting the primers: 18–24 bases long, 40–60% G/C content, having 1–2 G/C pairs in beginning and end, 50–60 °C melting temperature (T_m) and primer did not have complimentary areas and their T_ms were within 5 °C of one another. The list of primers use for PCR amplification is as follows in Table 1.

Statistical analysis

All data are reported as means ± Standard Error Mean (SEM). All the data were reanalyzed with GraphPad Prism Version 8.01 software and statistical significance between more than two groups were determined by one way analysis of variance (ANOVA) followed by Tukey's post hoc test. The p values of <0.05 were considered statistically significant. The necessary changes were made under the section.

Table 1 List of Primers used in the study

Gene (Accession number of the gene)	Primer sequence	
	Forward primer	Reverse primer
GAPDH (NM_008084.4)	5'-AGAGAGGCCAGCTACTCG-3' (T _m = 59.8)	5'GGCACTGCACAAGAAGATGC-3' (T _m = 59.9)
MUC-2 (NM_023566.4)	5'-GCTGACGAGTGGTTGGTAATG-3' (T _m = 60.0)	5'-GATGAGGTGGCAGACAGGAGAC-3' (T _m = 59.9)
IFN-γ (NM_008337.4)	5'-TCAAGTGGCATAGATGTGAAGAA-3' (T _m = 59.9)	5'-TGGCTCTGCAGGATTTTCATG-3' (T _m = 59.9)
IL-10 (XM_036162094.1)	5'-GGTTGCCAAGCCTTATCGGA-3' (T _m = 60.0)	5'-ACCTGCTCCACTGCCTTGCT-3' (T _m = 59.9)
TNF-α (NM_001278601.1)	5'-CATCTTCTCAAATTCGAGTGACAA-3' (T _m = 60.1)	5'-TGGGAGTAGACAAGGTACAACCC-3' (T _m = 60.2)
IL-6 (NM_001314054.1)	5'-GATAAGCTGGAGTCACAGAAGG-3' (T _m = 59.3)	5'-TTGCCGAGTAGATCTCAAAGTG-3' (T _m = 60.0)
IL-12 (NM_001303244.1)	5'-GGAAGCACGGCAGCAGAATA-3' (T _m = 59.8)	5'-AACTTGAGGGAGAAGTAGGAATGG-3' (T _m = 60.1)
Cathelicidin (NM_009921.2)	5'-GGCAGCTACCTGAGCAATGT-3' (T _m = 59.6)	5'-CTGTGCCACAGGCTCGTTA-3' (T _m = 59.8)

Results

Butyrate treatment decreases membrane cholesterol in RAW 264.7 cells

To assess the effects of butyrate on membrane cholesterol, RAW264.7 cells were treated with increasing concentration (5 mM and 10 mM) of sodium butyrate (butyrate) for 18 h following which membrane was prepared and cholesterol content was measured. Treatment with 5 mM and 10 mM of butyrate showed 1.5 fold and 2.4 fold decrease in membrane cholesterol (Fig. 1A) which corresponds to 36% and 52% decrease (Fig. 1A inset) with respect to control respectively. Staining with filipin to detect cholesterol also showed decrease in fluorescence with butyrate treatment compared to control (Fig. 1B). Sodium butyrate treatment to RAW 264.7 neither decreased cell viability or confluency, proliferation nor did it induced toxicity in the cells even at the highest concentration that was used (Additional file 1: Fig S1). Butyrate treatment induced changes in the morphology of the cell which was evident from the microscopy images (Additional file 1: Fig S1D).

As membrane cholesterol consists of 60–80% of the total cellular cholesterol [32], its depletion is likely to change the physical properties of the membrane. To estimate the changes in the physical properties we next measured the membrane fluidity in butyrate treated and untreated cells.

Butyrate treatment increases membrane fluidity and disrupts cholesterol rich microdomains

Fluidity of the cells treated with or without butyrate was measured by fluorescence anisotropy (FA) using Laurdan probe. It was observed that there was a dose dependent decrease in the FA value following treatment with butyrate. With 5 mM and 10 mM butyrate treatment FA was reduced to 1.4 fold and 2.4 fold respectively (Fig. 1E). To ensure the change in membrane fluidity was due to depletion of cholesterol we replenished cholesterol into the cell membrane of butyrate treated cells using liposomal delivery of cholesterol (chol-lipo). Liposomes were prepared using phosphatidyl choline (PC) with cholesterol. TEM confirmed that liposomes were indeed formed upon sonication (Additional file 1: Fig S2A). The Differential Light Scattering (DLS) study showed the liposomes prepared are of similar size distribution (Additional file 1: Fig S2B). When cholesterol was restored in the cells treated with butyrate by chol-lipo, the FA was reversed essentially to normal level (Fig. 1E). To warrant the increase in the membrane cholesterol with chol-lipo treatment we estimated the membrane cholesterol of the chol-lipo treated cells (Additional file 1: Fig S2C) using medium deficient in cholesterol (serum free condition). It was observed that approximately 16% and

40% cholesterol was restored in membranes upon chol-lipo treatment in 5 mM and 10 mM butyrate treated cells respectively.

For linking butyrate with decrease in membrane fluidity, we tested the presence of lipid microdomains in butyrate treated and untreated cells. Cholera toxin B (CTX-B) binds to GM1 ganglioside present in the cholesterol rich microdomains in the membrane [33] and is known as biomarkers for these domains. In Fig. 1F the first row shows the control cells without any treatment, second row shows the cells treated with 10 mM butyrate, the third row shows the cells treated with 10 mM butyrate followed by chol-lipo and the fourth row shows the cells treated with 10 mM butyrate followed by ana-lipo treatment. Column one depicts anti-CD71 binding, column 2 indicates CTX-B binding, column 3 shows the nucleus stain and column four is the merge image. The fluorescence images were quantified using imageJ which showed reduced CTX-B-FITC binding in at 10 mM butyrate treatment compared to control and was reversed back upon further treatment with chol-lipo but not with ana-lipo (Fig. 1G). But the binding of anti-CD71 antibody that binds to CD71 which is located in the non-raft region of the membrane [34] remained unaltered irrespective of butyrate, chol-lipo or ana-lipo treatment (Fig. 1H).

Having established that butyrate disrupts cholesterol rich microdomains in the membranes, we next asked the question of its impact on the enteric pathogen invasion which exploits these domains for host cell entry.

Butyrate treatment decreases enteric pathogen invasion

To study the effect of butyrate on enteric pathogen invasion we used *Salmonella typhimurium* and *Shigella flexneri* as representative enteric pathogens which exploits lipid rafts to enter the cell. The effect of butyrate treatment on the *Shigella* and *Salmonella* invasion in macrophages were analysed. It was observed that butyrate decreased the invasion of *Shigella* and *Salmonella* compared to infected control in a dose dependent manner. With 5 mM and 10 mM treatment of butyrate there was 60% and 85% decrease in *Shigella* invasion respectively and 60% and 75% decrease in *Salmonella* invasion respectively (Fig. 2A, B). Further treatment with chol-lipo to butyrate treated cells showed increased invasion of bacteria compared to butyrate treatment and essentially near to infected control for *Shigella* infection. To ensure the effect of reversal was due to cholesterol incorporation into the membranes and not due to enhanced phagocytosis caused by liposome treatment, we prepared liposomes using cholesterol analogue (4-cholesten-3-one) (ana-lipo) instead of cholesterol and applied to butyrate treated cells. As expected, the treatment with ana-lipo

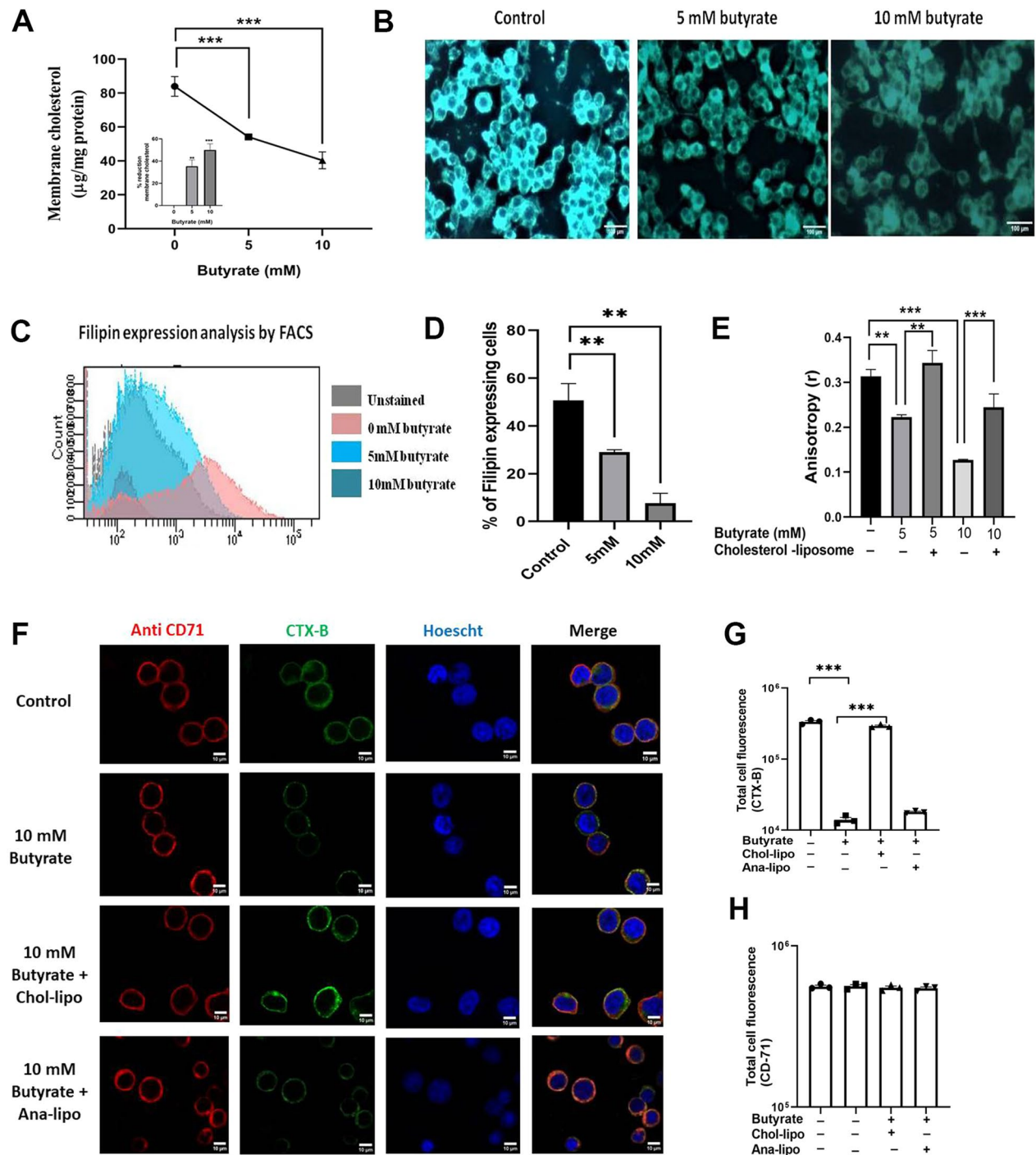


Fig. 1 Butyrate treatment decreases membrane cholesterol, increases fluidity and disrupts lipid rafts in RAW264.7 cells. RAW 264.7 cells were treated with 5 mM or 10 mM or without sodium butyrate for 18 h. The cells were washed and membrane was prepared. The membrane cholesterol was estimated by amplex red cholesterol assay kit (Invitrogen) and expressed as μg of membrane cholesterol/ mg protein **A**, the percent reduction of membrane cholesterol (Inset). The cells treated with/without butyrate were stained with Filipin and observed under fluorescence microscope **B** and measured in flow cytometry **C**, **D**. After 18 h of butyrate treatment the cells were further treated with or without chol-lipo for another 18 h. The membrane anisotropy was measured by using Laurdan probe and expressed as r **E**. The cells were stained with either CTX-B-FITC or anti-CD71 antibody and counterstained with Hoechst 33342. The cells were imaged in Zeiss confocal microscope **F**. The quantitative analysis of total fluorescence of CTX-B **G**, and anti-CD71 antibody **H**, as measured by ImageJ. The corrected total cell fluorescence is calculated as Corrected total fluorescence (CTCF) = (Integrated density) — (Area of selected cells \times mean fluorescence of background). Each experiment was set in triplicate and the data of three experiments are plotted as Mean \pm SEM. * represents $p < 0.05$, ** represents $p < 0.01$, *** represents $p < 0.001$

failed to increase the pathogen invasion and the percent of intracellular pathogens (*Shigella* and *Salmonella*) were near to butyrate treated macrophages.

Further studies with water soluble cholesterol or methyl β cyclodextrin (MBCD)-cholesterol (MBCD-chol) that transfer cholesterol from medium to cell membrane showed similar results. Replenishing membrane cholesterol by MBCD-chol in butyrate treated cells increased invasion of *Shigella* and *Salmonella* in a dose dependent manner (Additional file 1: Fig S3).

IpaB of *Shigella flexneri* binds to CD44 molecule [19] expressing on the surface of macrophage. Therefore, we checked the expression of CD44 with butyrate treatment.

Butyrate treatment decreases anti-CD44 antibody binding on cell surface but does not change the total pool of CD44 in cell

The cells treated with butyrate shows decrease in anti-CD44-FITC antibody binding which was restored with further treatment with chol-lipo (Fig. 2C). To prove that the decrease in fluorescence was due to dislocation of CD44 from lipid rafts but not due to the decrease in overall cellular expression of CD44, we measured the expression of CD44 in permeabilized and unpermeabilized cells by flow cytometry. Permeabilization of cells enables the antibody to enter into the cell and bind to intracellular CD44, whereas in an unpermeabilized cell, the binding of the antibody occurs only on the cell surface wherever CD44 is expressed. Expression analysis of CD44 by flow cytometry on permeabilized cells clearly shows that the total expression of CD44 remains same irrespective of butyrate or chol-lipo treatment (Fig. 2E). But flowcytometry analysis of unpermeabilized cells showed reduced fluorescence with butyrate treatment which is restored with chol-lipo (Fig. 2F). This observation confirms that *Shigella* binding receptor CD44 localizes in the lipid rafts which are displaced after butyrate treatment.

To understand its ramification, we studied the effect of butyrate in *Shigella* infected mice.

Butyrate treatment in mice reduces *Shigella flexneri* infection but reversed with liposomal delivery of cholesterol

Following 30 days of butyrate treatment, mice were infected with *Shigella flexneri* at a dose of 10^7 cfu/ animal intraperitoneally and were sacrificed 24 h post infection to study pathogen burden and immune parameters. Hereafter the uninfected mice, *Shigella* infected mice and butyrate treated plus infected mice will be denoted as control-mice, infected-mice and butyrate-mice respectively. A group of butyrate-mice were further administered cholesterol liposome through intracardiac route 2 days prior to infection (butyrate-chol-mice). To ensure proper delivery of cholesterol in the gut, the cholesterol content of the gut tissue was measured (Additional file 1: Fig S4). It was observed that the cholesterol content in the gut tissue of infected-mice was significantly more than control-mice. As expected, the gut tissue cholesterol of butyrate-mice were decreased compared to infected-mice but was increased significantly in butyrate-chol-mice. Butyrate- mice showed nearly 12 fold decrease in bacterial load in the colon tissue compared to infected-mice. Further treatment with chol-lipo to butyrate-mice essentially restored bacterial load in the colon as compared to butyrate-mice (Fig. 3A).

Butyrate treatment reduces *Shigella* induced pathogenesis in gut which was reversed by chol-lipo

The *Shigella* infected-mice showed pathological symptoms like excess secretion of mucin 2 in the colon that might originate from goblet cells. Butyrate-mice showed reduction in mucin 2 expression compared to infected-mice and in butyrate-chol-lipo-mice the mucin 2 expression was essentially equivalent to infected-mice (Fig. 3B). Of note, epithelial shedding, cell death in the crypt and villi, goblet cell hyperplasia and infiltration of inflammatory cells were found in the histological sections of the colon of infected-mice. Almost negligible number of neutrophils was infiltrated in the colon of butyrate-mice. Butyrate treatment did not change the gut pathology but in butyrate-chol-mice epithelial shedding, cell death was prominent (Fig. 3C). Chol-lipo treatment increased neutrophil infiltration significantly compared to butyrate-mice (Fig. 3D).

(See figure on next page.)

Fig. 2 Butyrate treatment decreases pathogen invasion in macrophage cells. RAW264.7 cells were treated with or without butyrate and followed by chol-lipo was infected with *Shigella flexneri* **A** and *Salmonella typhimurium* **B** at a MOI 1:100 and the data are represented as percent control (Percent control = Treated/Control \times 100). The cells were stained with either anti-CD44-FITC antibody and counterstained with Hoechst 33342. The cells were imaged in Zeiss confocal microscope at 63X magnification **C**. The cells with similar treatment were analyzed in flowcytometry in non-permeabilized **D** and permeabilized **E** to estimate the total fluorescence of anti-CD44-FITC antibody and on the cell surface respectively. The mean fluorescence was estimated and represented in F and G for non-permeabilized and permeabilized cells respectively. N = 3, the data is represented as Mean \pm SEM. * represents $p < 0.05$, ** represents $p < 0.01$, *** represents $p < 0.001$

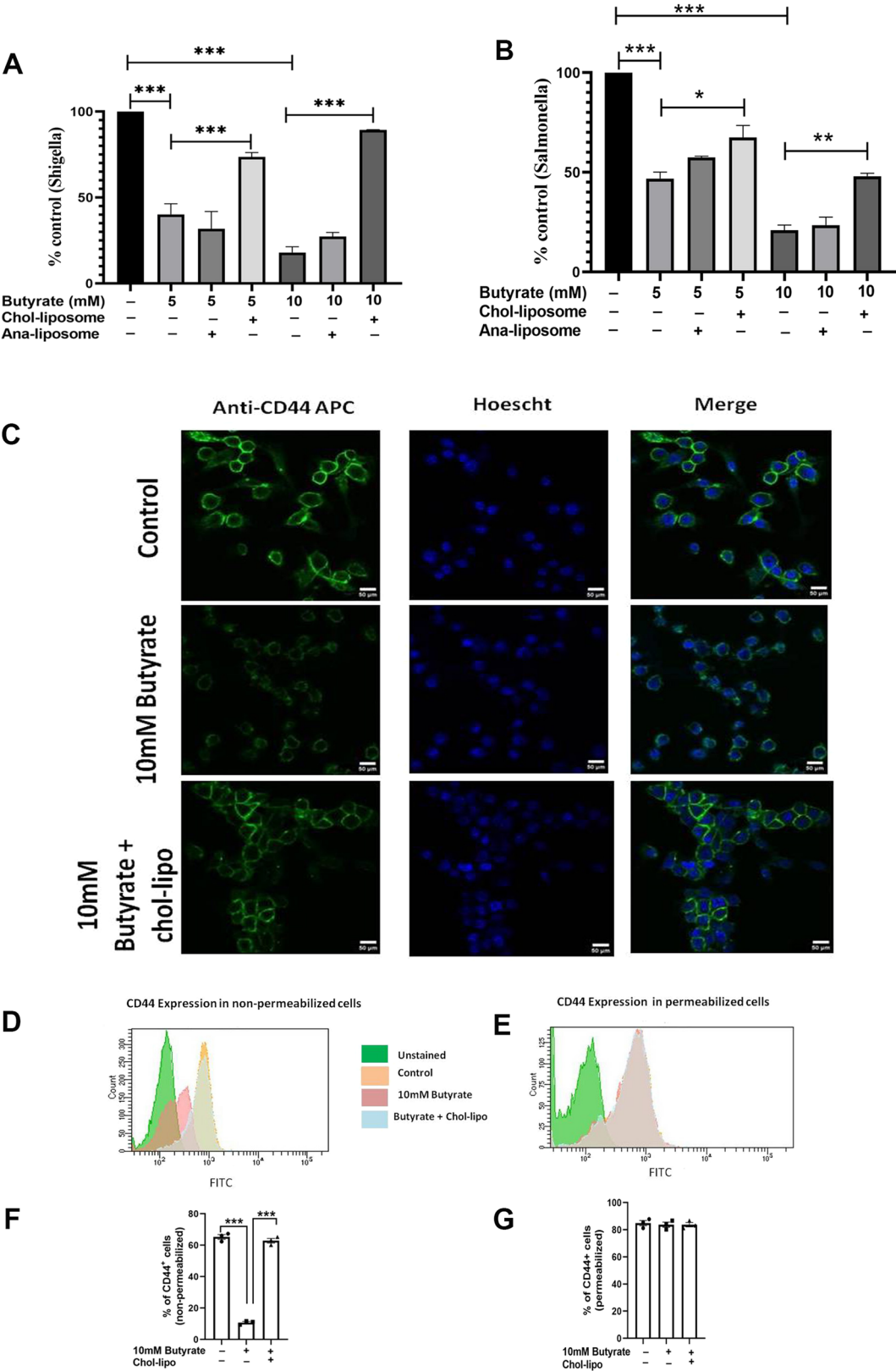


Fig. 2 (See legend on previous page.)

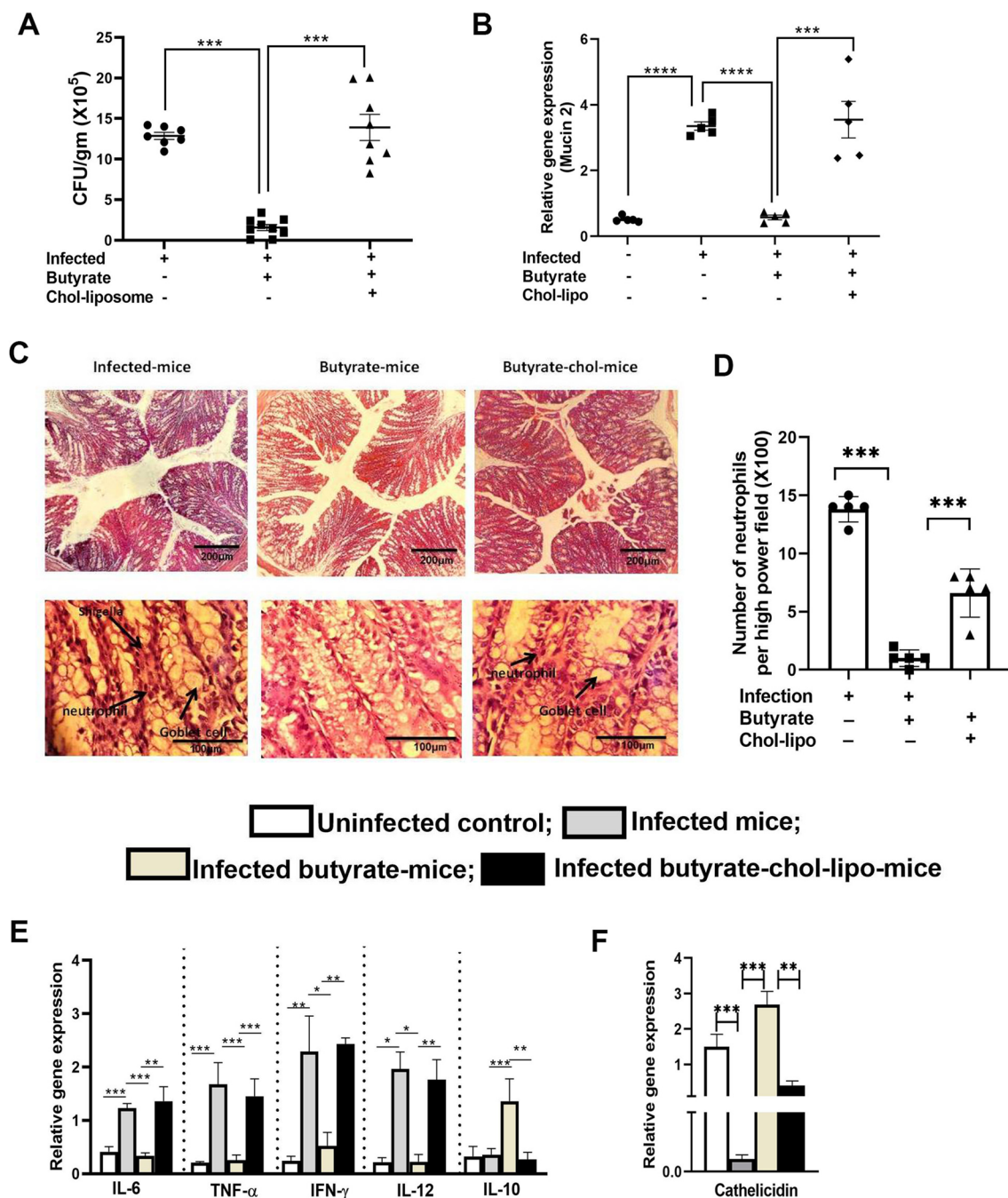


Fig. 3 Butyrate treatment decreases pathogen invasion in mice which was reversed upon chol-lipo treatment. A group of adult C57BL/6 mice were fed with chow diet and 150 mM sodium butyrate in drinking water for 30 days. On 28th day of butyrate treatment, half of the animals were selected randomly and was injected liposome-cholesterol (200 μ L of liposomal suspension) through intracardiac route (chol-lipo mice). All the animals were infected with 10^8 cfu/mice of *Shigella flexneri* on 30th day intraperitoneally. On day 2 of post infection the animals were sacrificed and feces and colon tissue were collected for analysis. The bacterial load was determined by plating diluted fecal samples on XLD plates. The bacterial load is determined as cfu/ gm feces **A**. The mucin 2 expression was measured by qPCR **B**. The microscopic view of histological sections of the colon of representative animal per group **C**, number of neutrophils in high power field (100X) in the colon section of infected-mice, butyrate-mice and chol-lipo-mice **D**, Panel1, 10X magnification, Panel2, 100X magnification. The mRNA expression of the cytokines **E** and antimicrobial gene cathelicidin **F** from colon tissue was measured by qPCR. N=3, 5 animals were taken per group, the data is represented as Mean \pm SEM. * represents $p < 0.05$, ** represents $p < 0.01$, *** represents $p < 0.001$

We found that proinflammatory cytokines such as IL-6, IFN- γ , and TNF- α were significantly higher in infected-mice than those of the control-mice (Fig. 3E). Butyrate treatment decreased the proinflammatory cytokines significantly which was restored to the equivalent level of infected-mice in butyrate-chol-mice. Further analysis of expression of host protective cytokine IL-10 shows 3.7 times increase in butyrate-mice compared to infected-mice. As expected, the expression of IL-10 decreased in butyrate-chol-mice and was essentially similar to infected-mice (Fig. 3E last column).

Further study on antimicrobial gene expression like cathelicidin showed significant increase in butyrate-mice compared to infected control and restored to infection level in butyrate-chol-mice (Fig. 3F).

Discussion

We previously reported that butyrate but not propionate or acetate reduces cholesterol synthesis following "AUF1-Dicer1-miR122" pathway [14]. In this discourse, we describe the host cell-dependent mechanism of gut microbial butyrate for resisting invasion of enteric pathogens. As macrophages are sentinel cells of immune homeostasis in gut [35] we undertook studies in RAW 264.7 as it is an appropriate model for macrophages [36] and the pathogens used in this study is reported to infect RAW 264.7 cells [37, 38]. The concentration of butyrate used in the study is in tune with the physiological concentration reported to be found in the intestine [39] and it did not show any change in cell proliferation, confluency and viability. We observed significant decrease in membrane cholesterol with butyrate treatment. Although butyrate treatment did not induce apoptosis in the cells, it altered the cell shape. Since cholesterol affects the mechanical properties of a cell through the underlying cytoskeleton [40], it is tempting to speculate that depletion of membrane cholesterol with butyrate treatment likely changes the cytoskeletal structure and therefore affects cellular morphology. Cholesterol plays a major role in determination of cell membrane properties as it regulates membrane fluidity [41]. We studied the macrophage membrane fluidity in terms of FA using Laurdan probe. By computing the generalised polarisation, alterations in the Laurdan emission spectrum caused by variations in membrane water content were quantified [42]. Employing this property Laurdan probe was shown to distinguish effects of perturbations on membrane fluidity by comparing the results of FA measurements [42]. The decrease in FA with butyrate treatment is an indicator of increase in the fluidity of the cell membrane which corresponds to the decrease in membrane cholesterol. Further treatment with chol-lipo to the butyrate treated cells reversed the fluidity of the membranes which is also

correlated with restoration of membrane cholesterol. Chol-lipo composed of phosphatidyl choline and cholesterol at a ratio of 1:1.5 are unilamellar vesicles used in efficient delivery of cholesterol in the cells [43]. Reversal of FA with chol-lipo is indicative of the cholesterol depleting effect of butyrate from the cell membrane.

To link butyrate with decrease in membrane fluidity, we tested the presence of lipid microdomains or lipid rafts. Cholera toxin B (CTX-B) binds to GM1 ganglioside present in cholesterol rich microdomains on rafts [33]. Disruption of lipid rafts reduces CTX-B binding [44] and can be determined by decrease in fluorescence of CTX-B-FITC. Butyrate showed significant decrease in CTX-B binding compared to control and was reversed essentially to normal with chol-lipo treatment but not with ana-lipo treatment. On the other hand, anti CD71 antibody binding remained unaltered in all four cases. CD71 or transferrin receptors are located in non-raft region of the cell membrane and serves as a marker protein for non-raft region [45].

Pathogens exploit host lipid rafts to advance the infection [46]. Initial physical interaction of bacteria with a host cell is a key first step often determining what happens next, and there is no better place to gain control of the host cell than through initial contact with the lipid rafts. We have considered the invasion of enteric pathogens like: *Shigella* and *Salmonella* in our study. Replenishment of cholesterol either by chol-lipo or MBCD-chol to butyrate treated cells restored pathogen invasion that was decreased with butyrate treatment. The initial steps of binding of the invasin IpaB of *Shigella flexneri* to CD44 present on the host cell membrane depends on the presence of cholesterol/shingolipid rich lipid domains [19]. *Salmonella* anchors to lipid raft associated CD55 [47] in cholesterol rich vacuoles [48]. We show that CD44 which was shown to be localized in membrane raft [49, 50] get internalized or relocate itself in non raft portion of the membrane in presence of butyrate without changing the overall expression. In conjunction to this, we provide evidence that butyrate treated cells significantly decreases invasion of both *Shigella* and *Salmonella* but with chol-lipo treatment the pathogen invasion reverts back to normal. Another report on a natural compound found in chillies called capsaicin which makes biomembranes fluid [51] is recently been shown to reduce *Shigella flexneri* infection in intestinal cells [52] adds further credence to our notion.

Since antibiotic treatment which is likely to disrupt gut microbiota and butyrate production in gut [53] is required prior to *Salmonella* infection in mice [54], we preferred to use *Shigella* infection (infected-mice) to validate our ex vivo results in mice model. Although there is no suitable animal model that can replace human-based

studies for the investigation of the in vivo mechanisms of *Shigella* pathogenesis [55], a recent murine model based on peritoneal infection with virulent *S. flexneri* 2a is currently accepted [56]. In tune to the previous results, we observed significant decrease in bacterial burden in the colon of butyrate-mice compared to infected-mice. Supplementation of chol-lipo to butyrate-mice increased the pathogen burden compared to butyrate-mice. The half-life of the cholesterol rich unilamellar liposomes is longer than that of cholesterol poor liposomes in the body fluid [57]; Liposomes are believed to be targeted to liver and theoretically allow passage through large fenestrations, such as those of sinusoidal capillaries [58]; and while in circulation, liposomes readily absorb a vast collection of plasma proteins, some of which may act as opsonins directing liposomes to cell surface receptors and promoting their uptake by the cells [59]. We estimated the gut tissue cholesterol to ensure successful delivery of cholesterol into the gut. Notably infected mice also showed increase in colon tissue cholesterol. As *Shigella* infection causes decrease in butyrate producing bacteria in the gut [60], it is tempting to speculate that decrease in butyrate production increases cholesterol content in the gut of infected-mice. Similar increase in lipid profile was also noted in *Salmonella* infection which reverted back to normal with recovery [61]. Along with decreased bacterial load in gut, we also observed increase in mucin 2 expression, inflammatory cytokines, inflammatory cell infiltration and destruction of gut tissue lining. Previous studies suggest that mucin in the colon can be subject to direct colonic infection and inflammation [62, 63]. For instance, *Muc2*^{-/-} mice exhibited rapid weight loss, high mortality, and greater bacterial burden when infected with *Citrobacter rodentium* [63]. Similarly, we find increase in mucin 2 expression in infected mice which was decreased significantly upon butyrate treatment and reversed in chol-lipo-mice. Thus, it seems likely that *Shigella* invasion and colonization of the colon can lead to multiple histological changes that are produced by the intrinsic host defense system in response to infection. The host defense systems against *Shigella* invasion were activated by secretion of cytokines and subsequent recruitment of immune cells to the site of infection [64].

Having established butyrate treatment reduces enteric pathogen invasion which can be reversed by liposome cholesterol we determined the host factors in the protection process. In order to further address whether butyrate treatment reduces the inflammatory responses in the colon elicited by *Shigella* infection, we determined secretion levels of cytokines expression in colon tissue. We found that proinflammatory cytokines such as IL-6, IFN- γ , and TNF- α were significantly higher in infected-mice than those of the control group. Butyrate treatment

decreased the proinflammatory cytokines significantly which was restored to the equivalent level of infection group in butyrate-chol-mice. Collectively, these data indicate that the decrease in bacterial burden in butyrate-mice resident colon, *Shigella* organisms cannot provoke predominant cytokines, which contribute to lesser recruitment of polymononuclear cells into the colon. In turn, these may be involved in secretion of reduced proinflammatory cytokines. The antimicrobial protein cathelicidin is considered to play an important role in the defense mechanisms against bacterial infection in colonic macrophages [65]. Our results are in conjunction to earlier reports showing butyrate induces cathelicidin gene expression by augmenting its promoter activity [65].

Other than playing a role in pathogen invasion, lipid microdomains on the membrane plays crucial role in various essential cellular processes, including endocytosis, exocytosis and cellular signalling. Therefore, question arises whether butyrate treatment can disrupt any such process. It is evident that cholesterol depletion in the membrane causes spontaneous exocytosis [66]. Bearing with this knowledge butyrate also shows increased mucin secretion in the gut by exocytosis [67]. Membrane cholesterol is required for IFN- γ signalling [68]. Butyrate which we demonstrate as cholesterol decreasing agent is also reported to inhibit IFN- γ signalling [69]. Therefore, butyrate through a membrane centric enterprise shows gut homeostasis by making mucosal system being protective against pathogen invasion.

Overall, this discourse adds a new mechanism of colonization resistance in gut. We report that butyrate decreases membrane cholesterol which leads to increased fluidity and disruption of lipid microdomains which can be reversed by restoration of cholesterol in the cell membrane. Employing in vitro and in vivo experiments we have shown lipid raft disruption by butyrate decreases enteric pathogen invasion. By rescuing cholesterol in the membranes, we validate that butyrate treatment resist colonization of enteric pathogen by disruption of lipid microdomains in the membrane.

Abbreviations

PBS	Phosphate buffered saline
IL	Interleukin
TNF	Tumour necrosis factor
IFN	Interferon
CD	Cluster of differentiation
qPCR	Quantitative polymerase chain reaction
Tm	Melting temperature
LDH	Lactate dehydrogenase
PI	Propidium iodide
GM1	Monosialotetrahexosylganglioside
Ipa	<i>Shigella</i> Virulence factor Invasion plasmid antigen
Sip	<i>Salmonella</i> Invasion protein
GAPDH	Glyceraldehyde-3-phosphate dehydrogenase
DEPC	Diethyl pyrocarbonate
DTT	Dithiothreitol

Supplementary Information

The online version contains supplementary material available at <https://doi.org/10.1186/s13099-023-00545-0>.

Additional file 1: Figure S1. The viability, toxicity and proliferation of cells with/without butyrate treatment were measured by Apoptosis/PI staining in flowcytometry (A), LDH assay (B) and CFSE staining in flowcytometry (C) respectively. The confluency of cells with/without butyrate treatment was observed under phase contrast microscope (magnification 20X) (D). The data is represented as Mean \pm SEM of 3 independent experiments. * represents $p < 0.05$, ** represents $p < 0.01$. **Figure S2.** The shape (A) and size (B) of the chol-lipo and ana-lipo measured by TEM and DLS respectively. The cholesterol content of the membranes of the cells treated with/without butyrate followed by with/without chol-lipo was measured by amplex red cholesterol assay kit (C). The data is represented as Mean \pm SEM of 3 independent experiments. * represents $p < 0.05$, ** represents $p < 0.01$, *** represents $p < 0.001$. **Figure S3.** The cells treated with/without butyrate and then followed by MBCD-chol at an indicated concentrations were infected with *Shigella flexneri* (A) and *Salmonella typhimurium* (B) at a MOI 1:100 and the data are represented as percent control (Percent control = Treated/Control \times 100). The data is represented as Mean \pm SEM of 3 independent experiments. * represents $p < 0.05$, ** represents $p < 0.01$, *** represents $p < 0.001$. **Figure S4.** The cholesterol content in the colon of normal, inf-mice, butyrate-mice and butyrate-chol-lipo-mice measured by Amplex red cholesterol assay kit. $N = 5/\text{group}$. The data is represented as Mean \pm SEM of 2 independent experiments. ** represents $p < 0.01$.

Acknowledgements

Our deepest gratitude to Prof Syamal Roy (CSIR-ICB, Kolkata) for his support, helpful discussion and suggestions for the manuscript. We thank Santasabuj Das (ICMR-NICED) and Ashish Mukherjee (ICMR-NICED) for providing the *Salmonella*, *Shigella* strain respectively. We also thank Dr. Subrata Majumder (Bose Institute) and Dr. Anjan Das for providing CTX-B-FITC and analysing the histology data respectively. OD is recipient of fellowship from the DST. MC and AM are recipient of fellowships from CSIR.

Author contributions

OD designed and performed most of the experiments. MC and AM performed animal treatment. AG performed all confocal experiments. MB conceptualised, supervised and arranged for funding. All authors contributed to manuscript writing and revision. All authors contributed to the article and approved the submitted version. All authors read and approved the final manuscript.

Funding

This work was supported by ICMR-NICED intramural grant (IM/MB/17-18/09).

Availability of data and materials

The original contributions presented in the study are included in the article/supplementary material. Further inquiries can be directed to the corresponding author.

Declarations

Ethics approval and consent to participate

All of the protocols for the study were approved by the Institutional Animal Ethics Committee of ICMR-NICED, Kolkata, India, (NICED/BS/MB-001/2019). Experiments have been carried out in accordance with the guidelines laid down by the committee for the purpose of control and supervision of experiments on animals (CPCSEA), Ministry of Environment and Forests, Government of India, New Delhi, India.

Consent for publication

All the authors and ICMR-NICED, Kolkata gave the consent for publication.

Competing interests

The authors declare no competing interest.

Received: 31 October 2022 Accepted: 9 April 2023

Published online: 21 April 2023

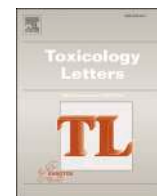
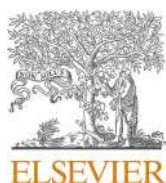
References

- Chow J, Lee SM, Shen Y, Khosravi A, Mazmanian SK. Host-bacterial symbiosis in health and disease. *Adv Immunol*. 2010;107:243–74.
- Sorbara MT, Pamer EG. Interbacterial mechanisms of colonization resistance and the strategies pathogens use to overcome them. *Mucosal Immunol*. 2019;12:1–9.
- Rooks MG, Garrett WS. Gut microbiota, metabolites and host immunity. *Nat Rev Immunol*. 2016;16:341–52.
- Khan I, Bai Y, Zha L, Ullah N, Ullah H, Shah SRH, et al. Mechanism of the gut microbiota colonization resistance and enteric pathogen infection. *Front Cell Infect Microbiol*. 2021;11:716299.
- Bohnhoff M, Drake BL, Miller CP. The effect of an antibiotic on the susceptibility of the mouse's intestinal tract to *Salmonella* infection. *Antibiot Annu*. 1955;3:453–5.
- Ducarmon QR, Zwiittink RD, Hornung BVH, van Schaik W, Young VB, Kuijper EJ. Gut microbiota and colonization resistance against bacterial enteric infection. *Microbiol Mol Biol Rev*. 2019. <https://doi.org/10.1128/MMBR.00007-19>.
- May T, Mackie RI, Fahey GC Jr, Cremin JC, Garleb KA. Effect of fiber source on short-chain fatty acid production and on the growth and toxin production by *Clostridium difficile*. *Scand J Gastroenterol*. 1994;29:916–22.
- Sun Y, O'Riordan MX. Regulation of bacterial pathogenesis by intestinal short-chain fatty acids. *Adv Appl Microbiol*. 2013;85:93–118.
- Rios-Covian D, Ruas-Madiedo P, Margolles A, Gueimonde M, de Los Reyes-Gavilan CG, Salazar N. Intestinal short chain fatty acids and their link with diet and human health. *Front Microbiol*. 2016;7:185.
- Schulthess J, Pandey S, Capitani M, Rue-Albrecht KC, Arnold I, Franchini F, et al. The short chain fatty acid butyrate imprints an antimicrobial program in macrophages. *Immunity*. 2019;50(432–45): e7.
- Hentges DJ. Influence of pH on the inhibitory activity of formic and acetic acids for *Shigella*. *J Bacteriol*. 1967;93:2029–30.
- Rivera-Chavez F, Zhang LF, Faber F, Lopez CA, Byndloss MX, Olsan EE, et al. Depletion of butyrate-producing clostridia from the gut microbiota drives an aerobic luminal expansion of salmonella. *Cell Host Microbe*. 2016;19:443–54.
- He J, Zhang P, Shen L, Niu L, Tan Y, Chen L, et al. Short-chain fatty acids and their association with signalling pathways in inflammation, glucose and lipid metabolism. *Int J Mol Sci*. 2020. <https://doi.org/10.3390/ijms21176356>.
- Das O, Kundu J, Ghosh A, Gautam A, Ghosh S, Chakraborty M, et al. AUF-1 knockdown in mice undermines gut microbial butyrate-driven hypocholesterolemia through AUF-1-Dicer-1-mir-122 hierarchy. *Front Cell Infect Microbiol*. 2022;12:1011386.
- Simons K, Ehehalt R. Cholesterol, lipid rafts, and disease. *J Clin Invest*. 2002;110:597–603.
- Kulkarni R, Wiemer EAC, Chang W. Role of lipid rafts in pathogen-host interaction—a mini review. *Front Immunol*. 2021;12:815020.
- Coburn B, Sekirov I, Finlay BB. Type III secretion systems and disease. *Clin Microbiol Rev*. 2007;20:535–49.
- Myeni SK, Wang L, Zhou D. SipB-SipC complex is essential for translocon formation. *PLoS ONE*. 2013;8:e60499.
- Lafont F, Tran Van Nhieu G, Hanada K, Sansonetti P, van der Goot FG. Initial steps of *Shigella* infection depend on the cholesterol/sphingolipid raft-mediated CD44-IpaB interaction. *EMBO J*. 2002;21:4449–57.
- Guignot J, Tran Van Nhieu G. Bacterial control of pores induced by the type III secretion system: mind the gap. *Front Immunol*. 2016;7:84.
- Caruana JC, Walper SA. bacterial membrane vesicles as mediators of microbe—microbe and microbe—host community interactions. *Front Microbiol*. 2020;11:432.
- Lai CH, Chang YC, Du SY, Wang HJ, Kuo CH, Fang SH, et al. Cholesterol depletion reduces *Helicobacter pylori* CagA translocation and CagA-induced responses in AGS cells. *Infect Immun*. 2008;76:3293–303.
- Day CA, Kenworthy AK. Functions of cholera toxin B-subunit as a raft cross-linker. *Essays Biochem*. 2015;57:135–45.
- Sen S, Roy K, Mukherjee S, Mukhopadhyay R, Roy S. Restoration of IFN γ mAR subunit assembly, IFN γ signaling and parasite clearance in

- Leishmania donovani infected macrophages: role of membrane cholesterol. *PLoS Pathog.* 2011;7:e1002229.
25. Shinitzky M, Barenholz Y. Fluidity parameters of lipid regions determined by fluorescence polarization. *Biochim Biophys Acta.* 1978;515:367–94.
 26. Chakraborty D, Banerjee S, Sen A, Banerjee KK, Das P, Roy S. Leishmania donovani affects antigen presentation of macrophage by disrupting lipid rafts. *J Immunol.* 2005;175:3214–24.
 27. Aartsma-Rus A, Krieg AM. FDA approves eteplirsen for duchenne muscular dystrophy: the next chapter in the Eteplirsen saga. *Nucleic Acid Ther.* 2017;27:1–3.
 28. Koestler BJ, Ward CM, Payne SM. Shigella pathogenesis modeling with tissue culture assays. *Curr Protoc Microbiol.* 2018;50:e57.
 29. Nemmar A, Al Hemeiri A, Al Hammadi N, Yuvaraju P, Beegam S, Yasin J, et al. Early pulmonary events of nose-only water pipe (shisha) smoking exposure in mice. *Physiol Rep.* 2015. <https://doi.org/10.7707/hmj.542>.
 30. Autenrieth IB, Bucheler N, Bohn E, Heinze G, Horak I. Cytokine mRNA expression in intestinal tissue of interleukin-2 deficient mice with bowel inflammation. *Gut.* 1997;41:793–800.
 31. Abdelmohsen K, Tominaga-Yamanaka K, Srikanth S, Yoon JH, Kang MJ, Gorospe M. RNA-binding protein AUF1 represses Dicer expression. *Nucleic Acids Res.* 2012;40:11531–44.
 32. Liscum L, Munn NJ. Intracellular cholesterol transport. *Biochim Biophys Acta.* 1999;1438:19–37.
 33. Aman AT, Fraser S, Merritt EA, Rodighiero C, Kenny M, Ahn M, et al. A mutant cholera toxin B subunit that binds GM1- ganglioside but lacks immunomodulatory or toxic activity. *Proc Natl Acad Sci U S A.* 2001;98:8536–41.
 34. Popik W, Alce TM, Au WC. Human immunodeficiency virus type 1 uses lipid raft-colocalized CD4 and chemokine receptors for productive entry into CD4(+) T cells. *J Virol.* 2002;76:4709–22.
 35. Bain CC, Schridde A. Origin, differentiation, and function of intestinal macrophages. *Front Immunol.* 2018;9:2733.
 36. Taciak B, Bialasek M, Braniewska A, Sas Z, Sawicka P, Kiraga L, et al. Evaluation of phenotypic and functional stability of RAW 264.7 cell line through serial passages. *PLoS ONE.* 2018;13:e0198943.
 37. Marathe SA, Sen M, Dasgupta I, Chakravorty D. Differential modulation of intracellular survival of cytosolic and vacuolar pathogens by curcumin. *Antimicrob Agents Chemother.* 2012;56:5555–67.
 38. Shi L, Chowdhury SM, Smallwood HS, Yoon H, Mottaz-Brewer HM, Norbeck AD, et al. Proteomic investigation of the time course responses of RAW 264.7 macrophages to infection with Salmonella enterica. *Infect Immun.* 2009;77:3227–33.
 39. den Besten G, van Eunen K, Groen AK, Venema K, Reijngoud DJ, Bakker BM. The role of short-chain fatty acids in the interplay between diet, gut microbiota, and host energy metabolism. *J Lipid Res.* 2013;54:2325–40.
 40. Sun M, Northup N, Marga F, Huber T, Byfield FJ, Levitan I, et al. The effect of cellular cholesterol on membrane-cytoskeleton adhesion. *J Cell Sci.* 2007;120:2223–31.
 41. Subczynski WK, Pasenkiewicz-Gierula M, Widomska J, Mainali L, Raguz M. High cholesterol/low cholesterol: effects in biological membranes: a review. *Cell Biochem Biophys.* 2017;75:369–85.
 42. Harris FM, Best KB, Bell JD. Use of laurdan fluorescence intensity and polarization to distinguish between changes in membrane fluidity and phospholipid order. *Biochim Biophys Acta.* 2002;1565:123–8.
 43. Kheirloomoom A, Ferrara KW. Cholesterol transport from liposomal delivery vehicles. *Biomaterials.* 2007;28:4311–20.
 44. Petrov AM, Kravtsova VV, Matchkov VV, Vasiliev AN, Zefirov AL, Chibalin AV, et al. Membrane lipid rafts are disturbed in the response of rat skeletal muscle to short-term disuse. *Am J Physiol Cell Physiol.* 2017;312:C627–37.
 45. Boesze-Battaglia K. Isolation of membrane rafts and signaling complexes. *Methods Mol Biol.* 2006;332:169–79.
 46. Bukrinsky MI, Mukhamedova N, Sviridov D. Lipid rafts and pathogens: the art of deception and exploitation. *J Lipid Res.* 2020;61:601–10.
 47. Knodler LA, Vallance BA, Hensel M, Jackel D, Finlay BB, Steele-Mortimer O. Salmonella type III effectors PipB and PipB2 are targeted to detergent-resistant microdomains on internal host cell membranes. *Mol Microbiol.* 2003;49:685–704.
 48. Catron DM, Sylvester MD, Lange Y, Kadekoppala M, Jones BD, Monack DM, et al. The Salmonella-containing vacuole is a major site of intracellular cholesterol accumulation and recruits the GPI-anchored protein CD55. *Cell Microbiol.* 2002;4:315–28.
 49. Donatello S, Babina IS, Hazelwood LD, Hill AD, Nabi IR, Hopkins AM. Lipid raft association restricts CD44-ezrin interaction and promotion of breast cancer cell migration. *Am J Pathol.* 2012;181:2172–87.
 50. Sun F, Schroer CFE, Palacios CR, Xu L, Luo SZ, Marrink SJ. Molecular mechanism for bidirectional regulation of CD44 for lipid raft affiliation by palmitoylations and PIP2. *PLoS Comput Biol.* 2020;16:e1007777.
 51. Sharma N, Phan HTT, Yoda T, Shimokawa N, Vestergaard MC, Takagi M. Effects of capsaicin on biomimetic membranes. *Biomimetics (Basel).* 2019. <https://doi.org/10.3390/biomimetics4010017>.
 52. Basak P, Maitra P, Khan U, Saha K, Bhattacharya SS, Dutta M, et al. Capsaicin inhibits Shigella Flexneri intracellular growth by inducing autophagy. *Front Pharmacol.* 2022;13:903438.
 53. Ramirez J, Guarner F, Bustos Fernandez L, Maruy A, Sdepanian VL, Cohen H. Antibiotics as major disruptors of gut microbiota. *Front Cell Infect Microbiol.* 2020;10:572912.
 54. Barthel M, Hapfelmeier S, Quintanilla-Martinez L, Kremer M, Rohde M, Hogardt M, et al. Pretreatment of mice with streptomycin provides a Salmonella enterica serovar Typhimurium colitis model that allows analysis of both pathogen and host. *Infect Immun.* 2003;71:2839–58.
 55. Kim YJ, Yeo SG, Park JH, Ko HJ. Shigella vaccine development: prospective animal models and current status. *Curr Pharm Biotechnol.* 2013;14:903–12.
 56. Yang JY, Lee SN, Chang SY, Ko HJ, Ryu S, Kweon MN. A mouse model of shigellosis by intraperitoneal infection. *J Infect Dis.* 2014;209:203–15.
 57. Kirby C, Clarke J, Gregoriadis G. Effect of the cholesterol content of small unilamellar liposomes on their stability in vivo and in vitro. *Biochem J.* 1980;186:591–8.
 58. Gabizon A, Papahadjopoulos D. Liposome formulations with prolonged circulation time in blood and enhanced uptake by tumors. *Proc Natl Acad Sci U S A.* 1988;85:6949–53.
 59. Fielding RM, Moon-McDermott L, Lewis RO, Horner MJ. Pharmacokinetics and urinary excretion of amikacin in low-clearance unilamellar liposomes after a single or repeated intravenous administration in the rhesus monkey. *Antimicrob Agents Chemother.* 1999;43:503–9.
 60. Yang J, Chen W, Xia P, Zhang W. Dynamic comparison of gut microbiota of mice infected with Shigella flexneri via two different infective routes. *Exp Ther Med.* 2020;19:2273–81.
 61. Khosla SN, Goyle N, Seth RK. Lipid profile in enteric fever. *J Assoc Physicians India.* 1991;39:260–2.
 62. Bergstrom KS, Guttman JA, Rumi M, Ma C, Bouzari S, Khan MA, et al. Modulation of intestinal goblet cell function during infection by an attaching and effacing bacterial pathogen. *Infect Immun.* 2008;76:796–811.
 63. Bergstrom KS, Kissoon-Singh V, Gibson DL, Ma C, Montero M, Sham HP, et al. Muc2 protects against lethal infectious colitis by disassociating pathogenic and commensal bacteria from the colonic mucosa. *PLoS Pathog.* 2010;6:e1000902.
 64. Ashida H, Mimuro H, Sasakawa C. Shigella manipulates host immune responses by delivering effector proteins with specific roles. *Front Immunol.* 2015;6:219.
 65. Kida Y, Shimizu T, Kuwano K. Sodium butyrate up-regulates cathelicidin gene expression via activator protein-1 and histone acetylation at the promoter region in a human lung epithelial cell line, EBC-1. *Mol Immunol.* 2006;43:1972–81.
 66. Petrov AM, Yakovleva AA, Zefirov AL. Role of membrane cholesterol in spontaneous exocytosis at frog neuromuscular synapses: reactive oxygen species-calcium interplay. *J Physiol.* 2014;592:4995–5009.
 67. Barcelo A, Claustre J, Moro F, Chayvialle JA, Cuber JC, Plaisancie P. Mucin secretion is modulated by luminal factors in the isolated vasculature perfused rat colon. *Gut.* 2000;46:218–24.
 68. Morana O, Nieto-Garai JA, Bjorkholm P, Bernardino de la Serna J, Terrones O, Arboleya A, et al. Identification of a new cholesterol-binding site within the IFN-gamma receptor that is required for signal transduction. *Adv Sci (Weinh).* 2022;9:e2105170.
 69. Klampfer L, Huang J, Sasazuki T, Shirasawa S, Augenlicht L. Inhibition of interferon gamma signaling by the short chain fatty acid butyrate. *Mol Cancer Res.* 2003;1:855–62.

Publisher's Note

Springer Nature remains neutral with regard to jurisdictional claims in published maps and institutional affiliations.



Prenatal arsenic exposure stymies gut butyrate production and enhances gut permeability in post natal life even in absence of arsenic deftly through miR122-Occludin pathway

Mainak Chakraborty^a, Anupam Gautam^{b,c}, Oishika Das^a, Aaheli Masid^a, Moumita Bhaumik^{a,*}

^a Division of Immunology, ICMR-National Institute of Cholera and Enteric Diseases, Belegata, Kolkata 700010, India

^b Department of Algorithms in Bioinformatics, Institute for Bioinformatics and Medical Informatics, University of Tübingen, Sand 14, 72076 Tübingen, Germany

^c International Max Planck Research School "From Molecules to Organisms", Max Planck Institute for Biology Tübingen, Max-Planck-Ring-5, 72076 Tübingen, Germany

ARTICLE INFO

Keywords:

Prenatal
Arsenic
Butyrate
Occludin
Tight junction
MiR122

ABSTRACT

This discourse attempts to capture a few important dimensions of gut physiology like microbial homeostasis, short chain fatty acid (SCFA) production, occludin expression, and gut permeability in post-natal life of mice those received arsenic only during pre-natal life. Adult Balb/c mice were fed with 4 ppm arsenic trioxide in drinking water during breeding and gestation. After the birth of the pups, the arsenic water was withdrawn and replaced with clean drinking water. The pups were allowed to grow for 28 days (pAs-mice) and age matched Balb/c mice which were never exposed to arsenic served as control. The pAs-mice showed a striking reduction in Firmicutes to Bacteroidetes (F/B) ratio coupled with a decrease in tight junction protein, occludin resulting in an increase in gut permeability, increased infiltration of inflammatory cells in the colon and decrease in common SCFAs in which butyrate reduction was quite prominent in fecal samples as compared to normal control. The above phenotypes of pAs-mice were mostly reversed by supplementing 5% sodium butyrate (w/w) with food from 21st to 28th day. The ability of butyrate in enhancing occludin expression, in particular, was dissected further. As miR122 causes degradation of Occludin mRNA, we transiently overexpressed miR122 by injecting appropriate plasmids and showed reversal of butyrate effects in pAs-mice. Thus, pre-natal arsenic exposure orchestrates variety of effects by decreasing butyrate in pAs-mice leading to increased permeability due to reduced occludin expression. Our research adds a new dimension to our understanding that pre-natal arsenic exposure imprints in post-natal life while there was no further arsenic exposure.

1. Introduction

Arsenic is a highly potent environmental toxin affecting more than 200 million people globally where south east Asian countries including India, Bangladesh, Pakistan, Nepal, and China are largely affected (Mukherjee et al., 2006). As arsenic is readily absorbed *in utero* the intake of arsenic by children (per unit body mass) is higher than that of adults increasing the risk of infant mortality, health risks and impaired intellectual development with associated impacts later in life (Donohoe et al., 2012; Cherry et al., 2010; Myers et al., 2010). Earlier we have shown that prenatal arsenic exposure causes compromised immune response in juvenile mice which leads to susceptibility to pathogen infection (Chakraborty and Bhaumik, 2020). Recent reports showed that

environmentally relevant level of arsenic exposure in mice causes gut microbial dysbiosis (Chi et al., 2017). Although the children in arsenic affected areas showed altered gut microbial composition (Dong et al., 2017), however there is no report on *in utero* arsenic exposure and effect on gut microbiome.

Maternal–offspring microbiota exchanges play a significant role in the development and maturation of the neonatal microbiome (Dong et al., 2015). Epidemiological studies also indicate antibiotic usage during pregnancy has also been linked to an increased incidence of juvenile obesity (Mor et al., 2015) and asthma (Stensballe et al., 2013). It has also been reported that the children born to mothers suffering from ulcerative colitis whose disease was active during pregnancy have a higher risk of developing childhood illnesses (Hashash and Kane, 2015).

* Correspondence to: Division of Immunology, ICMR-National Institute of Cholera and Enteric Diseases, P-33 C.I. T Road, Belegata, Kolkata 700010, West Bengal, India.

E-mail address: drmmoumitabhaumik@gmail.com (M. Bhaumik).

<https://doi.org/10.1016/j.toxlet.2022.11.011>

Received 25 May 2022; Received in revised form 15 November 2022; Accepted 21 November 2022

Available online 5 December 2022

0378-4274/© 2022 Elsevier B.V. All rights reserved.

Recent reports showed that arsenic exposure in early life alters the gut microbiome during the critical window of infant development (Hoen et al., 2018; Dong et al., 2017). These observations festoon an impending issue which nudge us to investigate the impact of prenatal arsenic exposure on the gut physiology in post-natal life. Germane with the idea that mother's microbiome plays a role in an infant's gut microbial establishment; it is plausible that subtle alterations in microbiota in early life may act as a vulnerability factor, impacting on disturbances in gut physiological functions which may lead to disorders in adult hood.

Short chain fatty acids (SCFA), an important metabolite produced by the gut microbes after fermentation of dietary fibres are significantly decreased in arsenic exposure (Chi et al., 2017). Butyrate, one of the important SCFA controls pleiotropic functions in the body including the development of the immune system (Yip et al., 2021; Schulthess et al., 2019). Butyrate can down-regulate inflammation by inhibiting the growth of pathobionts (Chen and Vitetta, 2020), increasing mucosal barrier integrity (Okumura et al., 2021), encouraging obligate anaerobic bacteria dominance (Chen and Vitetta, 2020) and decreasing oxygen availability in the gut (Kelly et al., 2015). In an in vitro model of the intestinal epithelial barrier employing Caco-2 cells, SCFA, particularly butyrate, has been demonstrated to enhance intestinal barrier function as measured by an increase in transepithelial electrical resistance (TEER) and a decrease in inulin permeability (Peng et al., 2007; Peng et al., 2009). Inflammatory bowel disease (IBD), obesity, non-alcoholic steatohepatitis (NASH), and non-alcoholic fatty liver disease (NAFLD) are all linked to a defective intestinal tight junction (TJ) barrier, which can be corrected by butyrate (Silva et al., 2018; Coppola et al., 2021; Endo et al., 2013). Reports showed that butyrate enhances the intestinal barrier by regulating the assembly of TJ proteins like occludin (Peng et al., 2009). Occludin, having four transmembrane domains is highly expressed at cell-cell contact sites and is important in the assembly and maintenance of TJ (Al-Sadi et al., 2011). Importantly, occludin knockout mice showed exhibited elevated inflammation, hyperplasia, and growth retardation (Saitou et al., 2000). Dysregulation of TJ has been implicated in various gut associated diseases including, IBD and colon cancer (Casalino et al., 2016). TJ protein expression at the cellular level is being governed by microRNAs, small regulatory RNAs (Ye et al., 2011). MiR122 is one of the microRNA that promotes occludin mRNA decay by binding to its 3'UTR (Jingushi et al., 2017; Yang et al., 2022). MiR122 is abundantly present in liver but also reported to be found in gut where it targets NOD2 and plays important role in colon cancer (Li et al., 2019).

The study is designed to investigate the effect of prenatal arsenic exposure on gut functional phenotype in the post natal life. We studied the microbial composition, metabolite production, and TJ protein expression and gut permeability in prenatally arsenic exposed mice and compared with normal control. Our results showed a decrease in Firmicutes to Bacteriodes ratio in gut microbiota coupled with a decrease in SCFA production of prenatally arsenic exposed mice. The lack of butyrate increased miR122 expression in gut, causing decrease in occludin and resulted in increased gut permeability. By replenishing butyrate, the prominently decreased SCFA due to pre-natal arsenic exposed (pAs-mice) we showed that butyrate renders a crucial base in the maintenance of gut physiology. Further leverage on the role of miRNA122 was stemmed from over-expressing miR122 to butyrate treated prenatally arsenic exposed mice which led to decrease in occludin. By harmonising narratives from our experimental studies, we showed that in prenatal arsenic exposure, imbalance of the gut microbiota resulted in decrease in gut butyrate, a "critical" denominator for maintaining general gut homeostasis. We showed a lasting imprint of prenatal arsenic exposure on post-natal gut physiology in adult life even in absence of butyrate.

2. Materials and methods

2.1. Reagents, chemicals, and buffers

Chow diet (Harlan Teklad LM-485), was purchased from ICMR-NIN,

Hyderabad, India. Dulbecco's modified Eagle's medium (DMEM) and foetal calf serum (FCS) were purchased from GIBCO (Waltham, MA, USA). BCA protein assay kit was purchased from Thermofisher (Waltham, MA, USA). Penicillin, streptomycin, Triton X100, PMSF, leupeptin, glycine, acrylamide, bis-acrylamide, para-formaldehyde, sodium butyrate, sodium propionate, sodium acetate, Hoechst 33342, and FITC-Dextran 4000 were purchased from Sigma (St. Louis, MO, USA). PVDF membrane, Trizol, were purchased from Invitrogen (Carlsbad, CA, USA). Super Reverse Transcriptase MuLV Kit, RT² SYBR® Green qPCR Mastermix were purchased from Qiagen (Hilden, Germany). Ripa lysis buffer, Occludin (rabbit, polyclonal) were purchased from Abcam (Cambridge, UK). Anti-GAPDH antibody (rabbit polyclonal) was purchased from Bio-Bharati (Kolkata, India). All primers were purchased from ID (Lowa, USA). Human colon carcinoma cell line HT-29 cells were a kind gift from Dr. Amit Pal (ICMR- NICED, India). miR122 expression plasmid was a kind gift from Dr. Suvendranath Bhattacharya (CSIR-IICB).

2.2. Mice and animal ethics

Balb/c mice (6 weeks old) were procured from ICMR-NICED animal facility of the institute. All the protocol for the study was approved by the Institutional Animal Ethics Committee of ICMR-NICED, Kolkata, India, (PRO/151/July 2018–June2021). Experiments have been carried out in accordance with the guidelines laid down by the committee for the purpose of control and supervision of experiments on animals (CPCSEA), Ministry of Environment and Forests, Government of India, New Delhi, India.

2.3. Arsenic treatment to dams

All Balb/c mice were housed in cages containing straw bedding held in pathogen-free facilities maintained at 24 °C with a 50% relative humidity and 12-h light:dark cycle. All mice had ad libitum access to standard rodent chow. After 2 weeks of acclimatization, the Balb/c mice were bred by housing two females with a male and given ad libitum access to drinking water containing with/ without 4 ppm Arsenic trioxide (As₂O₃) as described (Chakraborty and Bhaumik, 2020). The water was changed twice weekly. Each dam gave birth to average 4 litters. After birth, the mothers were then given ad libitum access to As-free water. For the experiments, when pups reached 4week-of-age, groups were randomly collected, and processed for biomaterials. Age-matched juvenile mice whose mothers were never exposed to Arsenic were processed in parallel as controls. For each experiment, 5–6 juvenile mice of same age were randomly chosen (without any sex bias) from 2 or more dams for evaluation. The experiments were set in duplicate at a time to increase the chances of pregnancy in mice and to get the pAs- mice of same age.

2.4. Dietary supplementation of sodium butyrate

The dietary supplementation studies were performed as reported earlier with minor modifications (Lin et al., 2012). Briefly, a group of 5 prenatally arsenic exposed mice pups (3 weeks old) were fed with 5% sodium butyrate (w/w) (Sodium butyrate in solid form were thoroughly blended into chow diet) for next 7 days (pAs-butyrate-mice) (Xu et al., 2018).

2.5. MiR122 overexpression in mice

MiR-122 was overexpressed in mouse gut in an identical procedure as described earlier (Ghosh et al., 2013). The miR-122 expression plasmid or empty plasmid (mock) was injected through the tail vein of pAs-butyrate-mice at a dose of 25 µg plasmid DNA dissolved in 100 µl saline. Following sacrifice of the mice after 4 days, the expression of occludin and miR122 in the colon was determined by qPCR.

2.6. Determination of *in vivo* gut permeability

The gut permeability assay was performed following previously reported protocol (Rangan et al., 2019). Briefly, mice were starved 16 h prior to FITC Dextran 4000 (FD-4) administration. FD-4 (44 mg/100 g body weight) was administered by oral gavage with a needle attached to a 1 ml syringe. A gap of 30 min between each mouse was kept for the FD-4 oral gavage. After 4 h, the blood was collected from tail vein. The blood was immediately transferred to a Microtainer SST tube and was mixed by inverting the tube 3–4 times and was stored at 4 °C in the dark. Once blood was collected from all the mice, SST tubes are processed to separate the serum following the manufacturer's instruction. The serum was then diluted with an equal amount of PBS. The concentration of FD-4 in sera was determined by spectrophotofluorometry with an excitation of 485 nm (20 nm band width) and an emission wavelength of 528 nm (20 nm band width) in Fluoroskan™ Microplate Fluorometer (Thermo Fisher Scientific).

2.7. Mice fecal samples collection

Fresh fecal samples of all mice pups were collected at 15:00–17:00 p.m. to minimize possible circadian effects. Samples were collected into empty sterile microtubes on ice and stored at – 80 °C within 1 h for future use.

2.8. 16 S rRNA gene sequencing and analysis

For extraction of fecal DNA, fecal pellets were incubated for 24 hr at 56 °C with proteinase K. DNA was then isolated using QIAamp DNA Mini Kits (Qiagen) using ~25 mg of feces.

2.9. Evaluation of changes in the gut microbiome

Faecal pellets were collected from juvenile mice (irrespective of sex) from both the control and prenatally Arsenic exposed group. Bacterial genomic DNA was extracted using QIAamp Fast DNA Stool Mini Kit (Qiagen, Valencia, CA, United States) by following the manufacturer's protocol. DNA concentration was evaluated by NanoDrop spectrophotometer from Thermo Fisher Scientific (Waltham, MA). Illumina standardized V3-V4 regions of 16 s rRNA library protocol were employed for the preparation of the library. The library which was generated contained V3-V4 amplicons were then sequenced on an Illumina MiSeq platform following the manufacturer's protocol. The generated reads (data) were processed by using QIIME2 (Bolyen et al., 2019) (version 2021.8.0). Filtering, merging and denoising was carried out by using DADA2 (Callahan et al., 2016) plugin within QIIME2. RESCRIPt (Robeson et al., 2021) plugin was used for processing and filtering of SILVA 138 (Quast et al., 2013) database to make it compatible with QIIME2 for carrying out taxonomy assignment. V3-V4 region primers were used for trimming SILVA sequences. and classify-sklearn (Pedregosa et al., 2011) was used for taxonomical classification. Further, the biome and taxonomy table was exported and diversity analyses were carried out by using phyloseq (McMurdie and Holmes, 2013) in R Data. Alpha diversity and rarefaction curve were studied on samples (biom table) rarely to a depth of 10,952 reads per sample. Samples generated during this experiment were submitted to Sequence Read Archives (SRA) of National Centre for Biotechnology Information (NCBI) under accession numbers (Control1 = SRR19309430, Control 2 = SRR19309429, pAs1 = SRR19309428 and pAs2 = SRR19309427). The raw data is available in bioproject accession PRJNA839617.

2.10. Estimation of faecal SCFA by GC/MS

The faecal concentrations of butyrate were measured by GC/MS as previously described (Li et al., 2020). Briefly, 50 mg of faecal samples from both groups were homogenized in 200 µl of distilled water. The

samples were then centrifuges at 4000 rpm for 5 min and the resulting supernatant was collected. 200 µl of a benzyl alcohol–pyridine mixture (3:2) and 100 µl DMSO was added to the supernatant and the mixture was vortexed for 5 s 100 µl of derivatizing agent benzyl chloroformate was added very carefully and the tube lids were kept open for 1 min to release the gas formed during the reaction. The tube lids were then closed and the resulting mixture was vortexed for 3 min. After the derivatization, 200 µl of cyclohexane was added and the resulting mixture was vortexed for 1 min which was then followed by centrifugation at 4000 rpm for 5 min. 100 µl of the resulting derivative extract (upper cyclohexane layer) was isolated and 1 µl was injected into GC-MS instrument for further analysis. The samples were analysed using Shimadzu GCMS-QP2020 (Shimadzu Corporation, Kyoto, Japan) with an AOC-20i auto injector. An InertCap WAX capillary column (30 m × 0.32 mm × 0.25 µm; GL Sciences Inc., Tokyo, Japan) was used for separation. Helium was used as a carrier gas with a flow rate of 1 ml/min. The temperature of the front inlet was set at 250 °C while the temperatures of the transfer line and the ion source were set to 280 °C and 230 °C respectively. The initial column temperature was held at 70 °C for 3 min and then was increased to 200 °C at a rate of 10 °C /min and was finally increased to 290 °C at a rate of 35 °C /min and then was held at this temperature for 7 min. A single run took 25.5 min. The solvent delay time was set to 6.7 min. The electron energy was – 70 eV and the gain factor was set to 2.0.

2.11. Immunofluorescence Staining and imaging

Colon samples were collected from all the groups during necroscopy examination and were fixed in 4% paraformaldehyde. The sections were then embedded in paraffin and 5 µm sections were generated. The paraffin embedded sections were then de-paraffinized in xylene and were rehydrated by passing through a graded series of ethanol followed by rinsing with distilled water. Antigen retrieval was performed by immersing the slides in 1 mM EDTA buffer pH 8.0 for 5 min. at sub boiling temperatures. The slides were then washed with distilled water. The sections were then permeabilized by 0.1% sodium citrate and 0.5% Triton-X in Tris Buffered Saline with 0.1% Tween 20 detergent (TBST) for 15 min. The sections were then blocked with 5% fetal bovine sera in TBST for 1 h at room temperature. The primary antibody to Occludin was then diluted (1:200) in the blocking solution and added to the sections which were then incubated overnight in a humidified chamber at 4°C. Following incubation, the sections were washed Tris Buffered Saline (TBS) and TBST alternatively for 5 min. The sections were then incubated with goat anti-mouse or goat-anti rabbit secondary antibody conjugated with Alexa Fluor 488 for 2 h at room temperature while being protected from light. Following incubation, the slides were again washed with TBS and TBST alternatively for 5 min. The sections were then mounted with 1 µg/ml Hoechst 33342 stain which acted as a nuclear counterstain. Fluorescence images were then captured using Carl Zeiss microscope equipped with a CCD camera and controlled by Zen software (Carl Zeiss, Gottingen, Germany) (Gumber et al., 2014).

2.12. Histopathologic examination of proximal colon

The proximal colon samples were fixed in 4% paraformaldehyde for 48 h at 4°C. The fixed tissues were then dehydrated through graded alcohols, embedded in paraffin, and routine microtomy then carried out to generate 5 µm sections. The sections, in turn, were stained with hematoxylin and eosin for later microscopic examination. (Chakraborty and Bhaumik, 2020).

2.13. Propagation of HT-29 cells and SCFA treatment

HT-29 cells were cultured in DMEM supplemented with 10% FCS and 50 µg/ml penicillin and streptomycin at 37°C with 5% CO₂. Cellular viability was assayed by MTT. Cells (10⁶ cells/ml) were treated with

either sodium butyrate (butyrate) or sodium propionate (propionate) or sodium acetate (acetate) at concentrations indicated in the figures for 24 h. Thereafter the cells were washed and processed for further analysis.

2.14. Tissue homogenisation and RNA and protein isolation

Colon samples (dissected into small pieces) or the cells were resuspended either in RIPA Lysis buffer (20 mM Tris-HCl pH 7.5, 150 mM NaCl, 1 mM EDTA, 1 mM EGTA, 1% NP-40, 1% Sodium deoxycholate, 2.5 mM Sodium Pyrophosphate, 1 mM β -glycophosphate, 1 mM Na_2VO_4 1 $\mu\text{g}/\text{m}^1$ leupeptin with 1 mM of phenylmethylsulfonyl fluoride (PMSF) immediately before use) for protein isolation or in Trizol (Invitrogen, US) for RNA isolation. The tissue was homogenized using a micropestle and centrifuged at 13,000 g for 15 min at 4 °C. The clear supernatant was collected and either stored as protein lysate in – 80 °C or further processed to isolate RNA using the standard protocol (Wu et al. 2018). The concentration of the extracted RNA was analyzed by Nanodrop and RNA was stored at –80 °C.

2.15. RNA extraction and reverse transcription

cDNA was prepared from total RNA by reverse specific primers using Super Reverse Transcriptase MuLV Kit. The primers for the reverse transcription are listed in Table 1. U6 and GAPDH were normalized for the expressions of miR122 and other genes of interest. The total reaction volume for reverse transcription was 20 μl in which 1 μM of reverse primer, 5 ng of RNA template, 1 μl dNTP mix, 12 μl of Diethyl pyrocarbonate (DEPC) treated water, 4 μl of 5X first strand buffer, 1 μl of 0.1 M Dithiothreitol (DTT), 1 μl of RNase inhibitor and 1 μl Super RT MuLV. Reverse transcription was carried out at 65 °C for 5 min, followed by incubation at 55 °C for 1 h and then heat inactivating the reaction at 70 °C for 15 min (Abdelmohsen et al., 2012).

2.16. Quantitative real-time PCR

Total RNA was extracted with Trizol reagent from snap frozen colon and RNA concentration was determined using a nanodrop. The miR-122, occludin, claudin1, claudin 2, claudin 4, ZO-1, GAPDH, and U6 levels

were quantified with Applied Biosystems™ StepOne™ Real Time PCR System with RT² SYBR® Green qPCR Mastermix following the manufacturer's instructions. Each 20 μl qPCR reaction contained an amount of cDNA equivalent to 5 ng of total RNA, 10 μl of RT² SYBR® Green qPCR Mastermix, 1 μM of the forward and reverse primer (each) and nuclease free water. Real-time PCR was performed with the following conditions: 95 °C for 10 min, 40 cycles of 95 °C for 30 s, 60 °C for 1 min and 72 °C for 1 min PCR product was calculated according to the $2^{-\Delta\Delta\text{Ct}}$ method described previously (Abdelmohsen et al., 2012).

2.17. Microbial analysis via PCR

To compare the relative abundances of various bacterial taxa in fecal DNA from female mice, we used qPCR analysis quantified by SYBR green and normalized the data to total bacterial abundance using pan-bacterial primers. The data is represented as $2^{-\Delta\Delta\text{Ct}}$ (Guo et al., 2008). The primer sequences use for PCR amplification are as follows:

2.18. Western blot

Colon tissue protein and cell lysate were extracted in RIPA Lysis buffer. Protein concentration was measured using Pierce™ BCA Protein Assay Kit. Proteins (50 $\mu\text{g}/\text{lane}$) were separated by using SDS-PAGE on 10% gel under reducing condition and electro transferred to polyvinylidene difluoride (PVDF) membrane in a transfer buffer (25 mM Tris-HCl, 150 mM Glycine, 20% Methanol). Membranes were blocked at room temperature with 5% non fat skim milk in TBS for 2 h, and then incubated with primary antibody against specific protein. The membranes were incubated with the horseradish peroxidase (HRP)-conjugated secondary antibodies at 37 °C for 1 h. SuperSignal West Pico chemiluminescent substrate kit (Thermo) was used to visualize the blotting results. The blots were imaged with Fluor Chem R system (ProteinSimple, San Jose, CA, USA) (Abdelmohsen et al., 2012). Antibody used for Western Blots:

Name of Antigen	Raised in	Source	Dilutions used
Anti-mouse-HRP	Horse	Cell Signalling Technology	1:5000

(continued on next page)

Table 1
Primers used for Real time PCR.

Gene	Primer Sequence	
	Forward Primer	Reverse Primer
GAPDH (Human)	5'-GAGAAGGCTGGGCTCATTT3'	5' AGTGATGGCATGGACTGTGG3'
U6snRNA (Human)	5'-CTCGCTTCGGCAGCACATATACT3'	5' ACGCTTCACGAATTTGCGTGTG3'
miRNA122 (Human)	5'TAGCAGAGCTGTGGAGTGTG3'	5' GCCTAGCAGTAGCTATTAGTG3'
U6snRNA(Mouse)	5-CTCGCTTCGGCAGCACATATACT-3'	5' ACGCTTCACGAATTTGCGTGTG-3'
GAPDH (Mouse)	5'-AGAGAGGCCAGCTACTCG-3'	5' GGCAGCTGCACAAGAAGATGC-3'
miRNA122(Mouse)	5'-GCTCGACCTCTCATGGGC-3'	5' TTAAGCCCTGCGTGTCTCC-3'
Occludin (human)	5'- AAGAGTTGACAGTCCATGGCATA C-3'	5' ATCCACAGGCGAAGTTAATGG AAG – 3'
Occludin (mice)	5'-TCACCTTTTCCTGGGTGACT-3'	5'- GGGAACGTGGCCGATATAATG-3'
Claudin1 (mouse)	5'- CTGGAAGATGATGAGGTGCAAG A-3'	5'- CCACATAATGTCGCCAGACCTGA A-3'
Claudin 2 (mouse)	5'-GGCTGTTAGGCACATCCAT – 3'	5'-TGGCACCAACATAGGAATC – 3'
JAM-A(mouse)	5'-ACCCTCCCTCCTTCCTTAC – 3'	5'-CTAGGACTCTTGCCCAATCC – 3'
ZO-1 (mouse)	5'- AGCTCATAGTTCAACACAGCCTCCA G-3'	5'- TTCTTCCACAGCTGAAGGACTCA CAG-3'
16 SrRNA panprimer	5'- AGAGTTTGATCCTGGCTCAG-3'	5'- AAGGAGGTGWTCCARCC-3'
Firmicutes	5'- GGAGAATGTGGTTTAATTCGAAGC A-3'	5'- AGCTGACGACAACCATGCAC-3'
Bacteroidetes	5'- GTTAAATTCGATGATACGCGAG-3'	5'- TTAACCCGACACCTCACGG-3'

(continued)

Name of Antigen	Raised in	Source	Dilutions used
conjugatedsecondary antibody			
Anti-rabbit-HRP conjugatedsecondary antibody	Goat	Cell Signalling Technology	1:5000
Occludin	Rabbit	Abcam	1:1000
GAPDH	Rabbit	Biobharati	1:1000

2.19. Statistical analysis

All values in the figures and text are expressed as arithmetic mean \pm SE. Data were analyzed with GraphPad Prism Version 8.01 software and statistical significance between groups was determined using unpaired student's t-test. Significance of more than two groups was determined by one way analysis of variance (ANOVA) followed by Tukey's post hoc test. The p values of < 0.05 were considered statistically significant. In the experiment involving Western blot, the figures shown are representative of at least 3 experiments performed on different days.

3. Results

3.1. Arsenic trioxide (arsenic) in drinking water decreases *Firmicutes* and increases *Bacteroidetes* in female mice

We investigated whether arsenic would perturb the abundance of *Firmicutes* (F) and *Bacteroidetes* (B) present in the gut microbiome of the dams. We observed 2.5 fold decrease ($p = 0.04$) in *Firmicutes* and 7 fold increase ($p = 0.0008$) in *Bacteroidetes* in As-exposed dams (Fig. S1 A and B) resulting in 18 fold decrease ($p = 0.005$) in F/B ratio compared to control (Fig. S1C). Next, we asked whether arsenic exposure during breeding and gestation would perturb the compositional profile of the gut microbiome of the offspring.

3.2. Prenatal arsenic exposure perturbs normal community composition of gut microbes

The pups from the As-exposed-dams were not exposed to arsenic any further after their birth and referred to as pAs-mice henceforth for convenience. The pups from the control-dams were referred as control-mice. The feces were collected from the pups on day 21 post birth as represented pictorially (Fig. 1 A). The total number of taxonomically classified ASVs (Amplicon Sequence Variants) identified upon analysis of sequenced 16S-rRNA dataset from the feces in both the groups is represented in a Venn diagram (Fig. 1 B). The identified genera are enlisted in Table S1. Around 13.2% ASV was found to be common in both the groups. But control-mice and pAs-mice showed the presence of 49.7% and 37% unique ASV respectively. Overall this observation indicates pAs-mice have lost about 12.7% of ASV compared to control-mice (Fig. 1 B). The predominant bacterial phyla in all the samples were *Firmicutes* and *Bacteroidetes* as assessed by 16S-rRNA sequencing (Fig. 1 C). Alpha diversity of the samples was measured by chao1 index. Following prenatal arsenic exposure, the microbial component of the gut microbiome was lowered significantly compared to control, along with a Species Rarefaction Curve (Fig. 1 D) showing reduction in the number of bacterial species in the pAs mice (line in red) with respect to control-mice (line in blue). There was also a decrease in diversity (chao1-values) in pAs exposed mice when compared with control (Fig. 1 E). At the phylum level, the prevalence of *Firmicutes* and *Bacteroidetes* as determined by metagenomic analysis were significantly decreased and increased respectively in the pAs-mice compared to control-mice (Fig. 1 F). Considering the decrease in *Firmicutes* (F) and increase in *Bacteroidetes* (B) in pAs-mice, the F/B ratio is also decreased ($p = 0.0254$) in

pAs-mice compared to control (Fig. 1 G). The abundance of these phyla were further validated by qPCR using phyla specific primers which also showed decrease and increase in *Firmicutes* and *Bacteroidetes* respectively in pAs-mice compared to control-mice (Fig. 1 H). We report 6.67 fold decreases ($p = 0.0013$) in F/B ratio in pAs-mice compared to control (Fig. 1 I).

3.3. pAs-mice showed reduced SCFA production compared to control-mice

The decrease in the abundance in *Firmicutes* in pAs mice faithfully reflected decrease in fecal SCFA compared to control as estimated by GC-MS. We observed 4 fold ($p = 0.0079$), 2 fold ($p = 0.0049$) and 1.7 fold ($p = 0.025$) decrease in butyrate, acetate and propionate respectively in the feces of pAs-mice compared to control-mice (Fig. 2). As SCFAs perform multiple functions including intestinal barrier integrity, mucous production and protect against inflammation in the gut it was important to study the physiological function of the gut in pAs-mice.

3.4. pAs-exposed mice showed increase in gut permeability and decrease in tight junction (TJ)

3.4.1. Protein, Occludin

To assess the potential shifts in the gut physiological function, if any, the gut barrier function, junctional protein expression and histology of gut in pAs-mice and control-mice were studied. The gut barrier function as studied by FITC dextran permeability showed 3.9 fold increase ($p = 0.0079$) in gut permeability in pAs-mice compared to the control-mice (Fig. 3 A). Further evaluation of tight junctional protein expression in the colon by qPCR showed 4 fold decrease ($p = 0.007$) in Occludin in pAs-mice compared to control-mice whereas, claudin 1, claudin-2, claudin-4, ZO-1, and JAM-A TJ protein expression remained unaltered (Fig. 3 B). Histological examination of the gut showed inflammatory cell infiltration in pAs-mice compared to the control-mice (Fig. 3C). The mucous secreting goblet cells also showed hyperplasia in pAs-exposed animals' gut histological sections. Recalling the gut microbial analysis and production of SCFA which depicted reduced SCFA production in pAs-mice, we sought to study if the lack of SCFA production in gut has any role on occludin expression in pAs-mice. Before that, it was essential to investigate the mechanism by which SCFA may influence the expression of occludin.

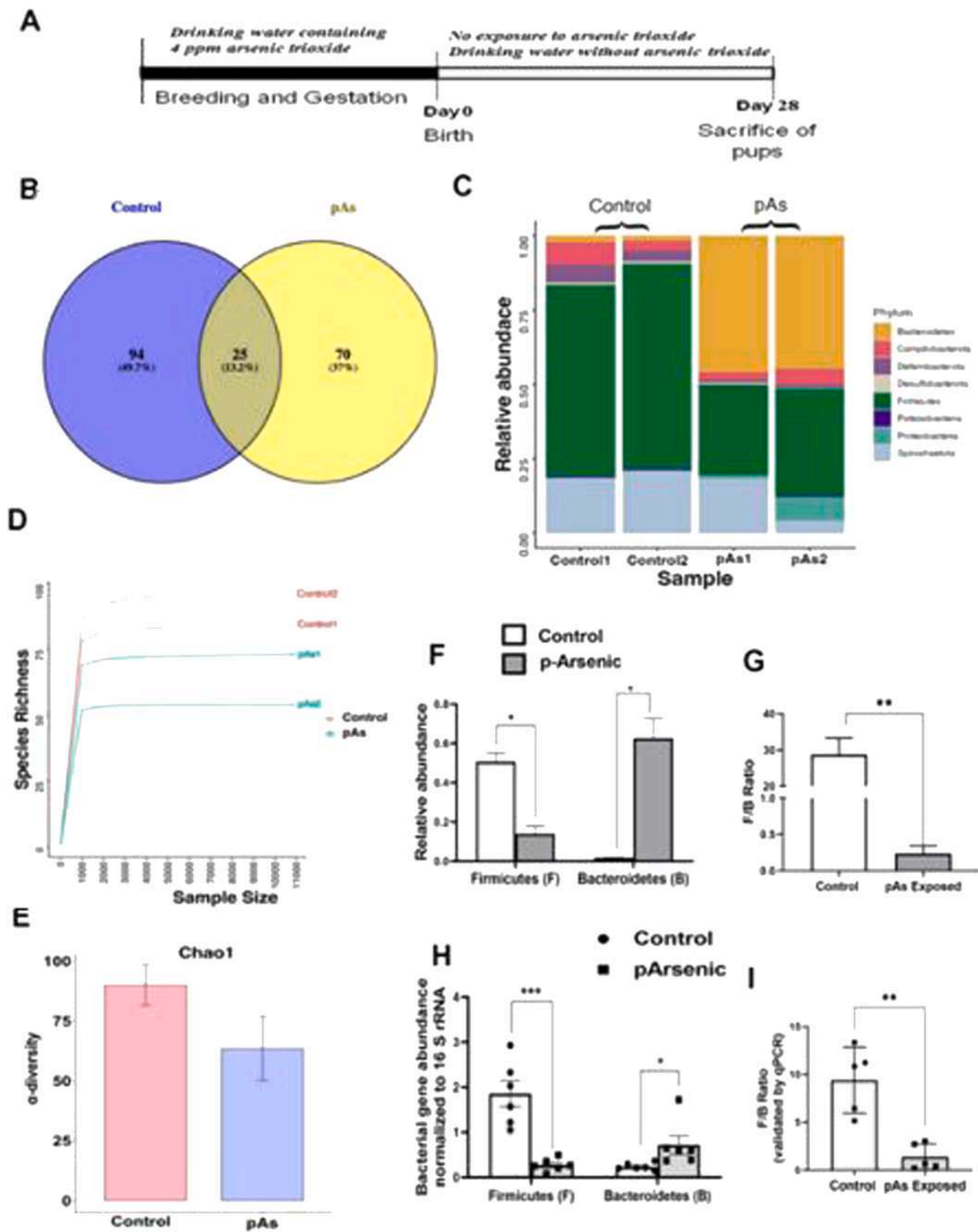
3.5. Butyrate treatment increases Occludin expression and decreases permeability in HT-29

3.5.1. Cells

HT-29 cells were treated with either butyrate or propionate or acetate with the function of concentration (0–20 mM) for 24 h. It was observed that unlike propionate and acetate, 10 mM and 20 mM butyrate treatment caused 45% and 58% increase in occludin expression respectively (Fig. S2A). These results provided initial evidence that butyrate but not propionate or acetate could increase occludin expression. For further deciphering the mechanism of regulation of occludin expression we studied miR122 expression upon butyrate treatment as it was shown previously that miR122 binds to the 3'UTR of the mRNA of Occludin, causing its degradation (Jingushi et al., 2017).

3.6. Butyrate treatment reduces miR122 expression in HT-29 cells

We monitored the status of miR122 in butyrate treated and untreated HT-29 cells by qPCR. It was observed that there was a progressive decrease in miR122 expression as a function of butyrate concentration (Fig. S2B). Notably, the expression of miR122 does not change on propionate and acetate treatment. Our result points towards the cascade of sine-qua-non events accomplished by butyrate action which is as follows: butyrate decreases miR122 which in turn increases occludin,



(caption on next page)

Fig. 1. Effect of prenatal Arsenic exposure on gut microbiome composition and diversity. Adult Balb/c mice were bred by housing two females with a male and given ad libitum access to drinking water containing 4 ppm arsenic trioxide (As). After birth of the pups, the mothers were then given ad libitum access to As-free water. When the pups reached 4weeks-of-age, their faeces were collected at random. Faeces from the age-matched pups of the dams that were never exposed to Arsenic were processed in parallel as control. The experimental plan is schematically represented (A). Venn- Diagram showing the number of microbial families' common and exclusive to control (control- mice) and prenatally As exposed mice (pAs-mice) (B) Stacked histogram showing major phylum abundant in control and pAs mice. (C). Species rarefaction curves outlining number of bacterial species in control and pAs samples (D). The Chao1 α diversity of microbial communities in control and pAs mice (E). Relative Abundance of Firmicutes and Bacteroidetes in control and pAs exposed mice (F). Firmicutes (F) to Bacteroidetes (B) ratio in control and pAs exposed mice (G) Firmicutes and Bacteroidetes abundance as measured by qPCR (H) and F/B ratio (I) Data represented as mean \pm SE. $n = 6/\text{group}$ for qPCR and $n = 2/\text{group}$ for 16 s rRNA sequencing. Values significantly different from control at * $p < 0.05$, ** $p < 0.01$ and *** $p < 0.001$.

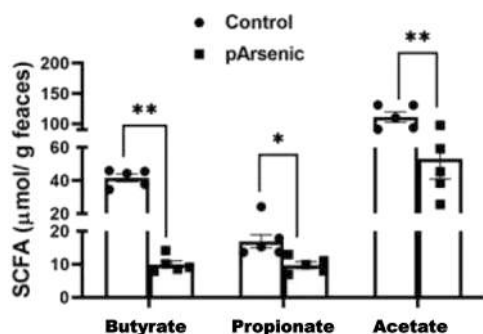


Fig. 2. Effect of prenatal arsenic exposure on concentration of faecal short chain fatty acids. Amount of faecal butyrate, acetate and propionate in control-mice and pAs-mice was determined by GC-MS. Data represented as mean \pm SE ($n = 5/\text{group}$) * $p < 0.05$ and ** $p < 0.01$.

which was further evaluated in pAs-exposed mice.

3.7. Butyrate treatment recovers gut permeability by reducing miR122 and increasing

3.7.1. Occludin expression in pAs-exposed mice

To show that decrease in gut-derived butyrate is intimately linked with decrease in barrier function in pAs mice, we supplemented butyrate orally to pAs mice and studied the reversal of barrier function. With this objective, we fed the pAs-mice from day 21–28 with 5% butyrate mixed with diet. The expression of Occludin in the gut was studied by western blot in control-mice, pAs-mice, and pAs-exposed mice fed with butyrate (pAs-butyrat-mice) (Fig. 4 A). The results showed that there was significant down regulation of occludin expression in the gut of pAs-mice which returned to normal with butyrate treatment (Fig. 4 B). Similarly, the immunohistochemical analysis showed that occludin protein expression in the gut samples of pAs-mice was 2.8 fold reduced compared to control-mice which were restored to normal in pAs-butyrat-mice (Fig. 4 C, D). The miR122 expression showed 3 fold increases in pAs-mice compared to control and after butyrate treatment the miR122 expression essentially decreased compared to pAs-mice and was equivalent to control (Fig. 4 E). As expected, there was significant increase in permeability in pAs-mice compared to control. Although in pAs-butyrat-mice the gut permeability decreased significantly compared to pAs-mice, it remains higher in respect to control-mice (Fig. 4 F). The colon histology sections revealed that butyrate restores gut health by inhibiting recruitment of inflammatory cells like neutrophils that was induced by pAs-exposure (Fig. 4 G). Furthermore infiltration of inflammatory cells and goblet cell hyperplasia were reduced in pAs-butyrat-mice.

3.8. MiR122 over-expression rescues the effect of butyrate in pAs-butyrat-mice

From the previous experiments, it was indicated that butyrate downregulates miR122 and upregulates occludin expression in colon. The level of miR122 and occludin expression in the colon of control-mice, pAs-mice and pAs-butyrat-mice were similar to the previous

experiment. MiR122 over-expression in pAs-butyrat-mice injected with miR122 expressing plasmid showed high levels of miR122 in colon indicating successful overexpression of miR122 (Fig. 5A). Corresponding analysis of occludin expression in the colon of pAs-butyrat-mice showed significant decrease with miR122-plasmid injection compared to mock-plasmid injection as studied by qPCR and western blot (Fig. 5B, C, D).

4. Discussion

The ambit of this investigation lies in answering an impending question whether *in utero* arsenic exposure can affect the gut microbiome which may alter gut physiology. Earlier reports showed that the environmentally relevant level of arsenic perturbs the normal gut microbiome in mice, decreasing abundance of *Firmicutes*, increase in *Bacteroidetes* and also changing its metabolites particularly SCFA (Chi et al., 2017). We validated this observation and showed that oral arsenic treatment causes decrease in *Firmicutes* and increase in *Bacteroidetes* in the dams. Considering the possibility of mother-offspring transmission of gut microbiome (Van Daele et al., 2019) we compared the broad microbiome composition of pAs-mice and control-mice. Overall, around 12.7% ASVs (Amplicon Sequence Variant) of normal gut bacteria was found to be lost in.

pAs-mice compared to control-mice. Arsenic is shown to prolong glycan residues of cell membrane glycoprotein of skin cancer cells (Lee et al., 2016). Glycosylation of the intestinal mucus and epithelium is quite complex and can change in response to microbial colonization (Pickard et al., 2017). This is interesting because host glycans can serve as nutrient sources or adhesion receptors for microbes (Pickard et al., 2017). Therefore it is tempting to speculate arsenic may reshape gut microbial composition in the mice by changing the extent of glycosylation pattern of the receptor proteins in the epithelial cell membrane. Diversity of a community depends on the intensity of sampling and Chao1 is measured based on species richness (number of species in the community) in the groups. Although not significant, Chao1 alpha diversity of the microbiome showed a trend of decrease in pAs-mice compared to control-mice. In some cases, microbial compositions rather than diversity seems to be the key player to determine the phenotype as it was shown earlier with the survivability of wild vertebrate population (Worsley et al., 2021).

Our further analysis of the phylum composition of gut microbiota in pAs-mice and control-mice showed a significant shift in the relative abundance of *Firmicutes* (F) and *Bacteroidetes* (B) by metagenomics analysis and also by qPCR. Surprisingly, the extent of decrease and increase of *Firmicutes* (F) and *Bacteroidetes* (B) respectively in pAs-mice compared to control-mice as determined by the two methods were not hand in hand. This discrepancy may be due to low sensitivity of qPCR compared to metagenomics (Plaire et al., 2017; Andersen et al., 2017). We report decrease in *Firmicutes* (F) and increase in *Bacteroidetes* (B) leading to consolidated decrease in F/B ratio in the gut communities of pAs-mice compared to control-mice which essentially mirrors the F/B ratio of the dams. The difference in the magnitude of the drop in F/B ratio between dams and offsprings could be attributable to the dams' vaginal microbiome and environmental factors that also.

influence the establishment of gut microbiome in neonates (Tudor et al., 2017). The decrease in F/B ratio is a major biomarker of

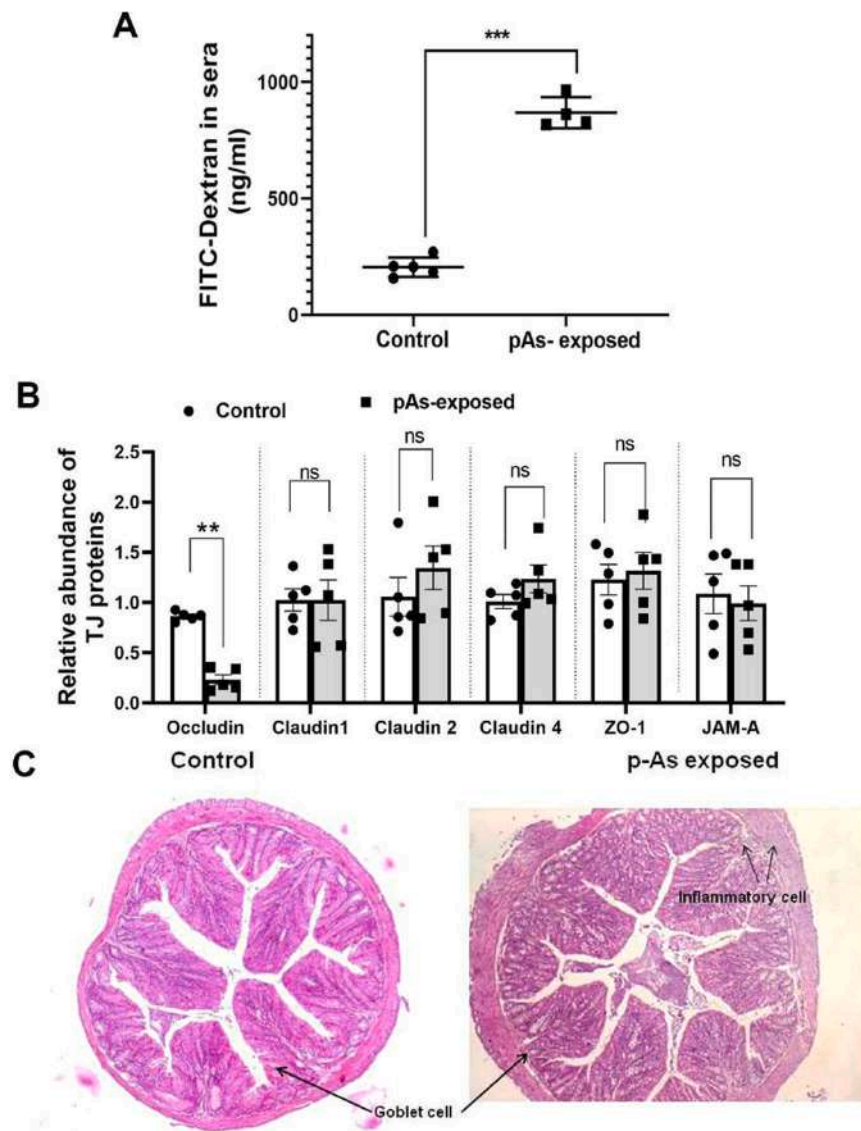


Fig. 3. Effect of prenatal Arsenic exposure on intestinal histoarchitecture and intestinal permeability. Control-mice and pAs-mice were starved for 16 h and then fed with FITC-Dextran 4000 (FD4) by oral gavage at a dose of 44 mg/100 g body weight. After 4 h the blood was collected and serum was extracted to determine the fluorescence of FD-4 in sera (A). The expression of tight junction proteins (Occludin, Claudin-1, Claudin-2, Claudin-4, ZO-1 and JAM-A) as determined by qPCR from colon tissue of Control-mice (fx1) and pAs-mice (fx2) (B). Representative micrograph of colon histology of control and pAs-mice (H&E; 10x magnification) (C). Arrows showing neutrophil infiltration. Data represented as mean \pm SE. N = 5/ group. Values significantly different from control at * $p < 0.01$ and *** $p < 0.001$. Values not significantly different from control are designated as 'ns'.

Inflammatory Bowel Disease (IBD) (Guo et al., 2021) suggesting a possibility that pAs-mice may have physiological dysfunction in the gut. The decrease in the abundance of *Firmicutes* in pAs-mice foretell the decrease in SCFA (den Besten et al., 2013). As expected, we observed significant decrease in all SCFAs including acetate, propionate and butyrate in the faeces of pAs-mice compared to control-mice. Notably, the decrease in butyrate was more pronounced than the decrease in acetate and propionate. The perturbations in the bacterial community and metabolites has overarching effect on the gut physiological functions as SCFAs particularly butyrate plays important role in multiple physiological processes in the host (Canani et al., 2011). Butyrate is an important energy source for intestinal epithelial cells (Singh et al., 1997) that maintains colonic homeostasis (Gasaly et al., 2021) and inhibits inflammation (Segain et al., 2000). The gastrointestinal epithelium forms the body's largest interface with the external environment (Groschwitz and Hogan, 2009). It effectively provides a barrier that selectively limits permeation of luminal toxins and antigens through the mucosa (Suzuki, 2013). The physical location of the intestinal epithelium, which is wedged between the luminal contents and the mucosal surface, supports the notion that a breach in the mucosal barrier causes mucosal inflammation (Ahmad et al., 2017). Studies with knockout mice with TJ proteins, develop inflammation in the gut epithelium (Ahmad et al., 2017; Lu et al., 2013) further studies support the key role of

permeability, especially in its capacity to contribute to overall mucosal barrier function in regulating mucosal immune homeostasis (Castoldi et al., 2015).

Pertinent with this idea we studied the corpus of events of gut physiological functions of mice treated *in utero* with arsenic which revealed increased permeability in gut and down regulation of tight junction protein, Occludin whereas other TJ proteins like Claudin 1, claudin-2, claudin 4, ZO-1 and JAM-A remain unaltered. Tight junctions are complex signalling centres in a continually changing milieu (Weber, 2012) serving as a permeability barrier, preventing free passage of solutes via the intercellular space. Claudins, in combination with the cytoplasmic scaffold ZO, create TJ strands and perform critical roles in epithelial barrier assembly (Furuse, 2010). In addition to claudins, TJs are home to other integral membrane proteins such as occludin, a tetraspanning membrane protein, and immunoglobulin superfamily proteins, including junctional adhesion molecules (JAMs) (Furuse, 2010). They also play an important role in the regulation of paracellular permeability. The coiled coil domain of occludin acts to organize the structural and functional elements of TJ (Nusrat et al., 2000). Paracellular permeability is, to a great extent, controlled by tight junctions, and disrupting their integrity, assembly and expression results in increased permeability (Liang and Weber, 2014). Occludin being an important component of tight junction, the decrease in its expression or

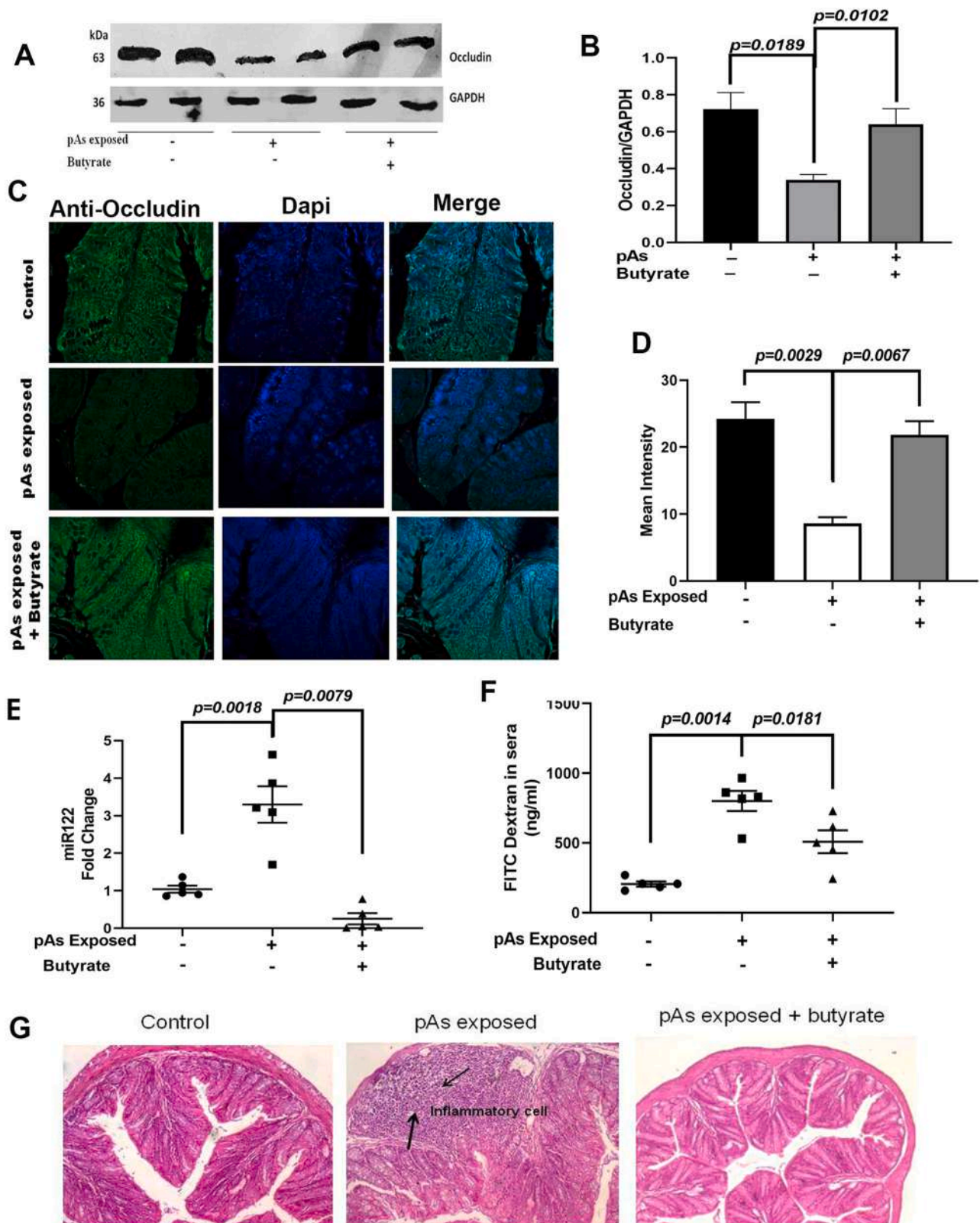


Fig. 4. Effect of oral supplementation of butyrate on colon histoarchitecture and intestinal permeability of prenatally arsenic exposed mice. Expression of Occludin as studied by Western blot (A) showing corresponding densitometry (B) and Immunofluorescence (C) showing mean intensity (D), in control-mice, pAs-mice and pAs-butyr-mice. Expression of miR-122 quantified by qPCR in control-mice, pAs-mice and pAs-butyr-mice (E). Intestinal permeability as measured by the presence of FITC-Dextran 4000 (FD4) in serum in control-mice, pAs-mice and pAs-butyr-mice (F). Representative micrographs of colon sections from control-mice, pAs-mice and pAs-butyr-mice (H&E; 20x magnification) (G). Arrows indicating neutrophil infiltration. Data represented as mean \pm SE. N = 5/ group. Values (analyzed by one way ANOVA followed by Tukey's post hoc test) significantly different from control at $p < 0.05$ and $p < 0.01$.

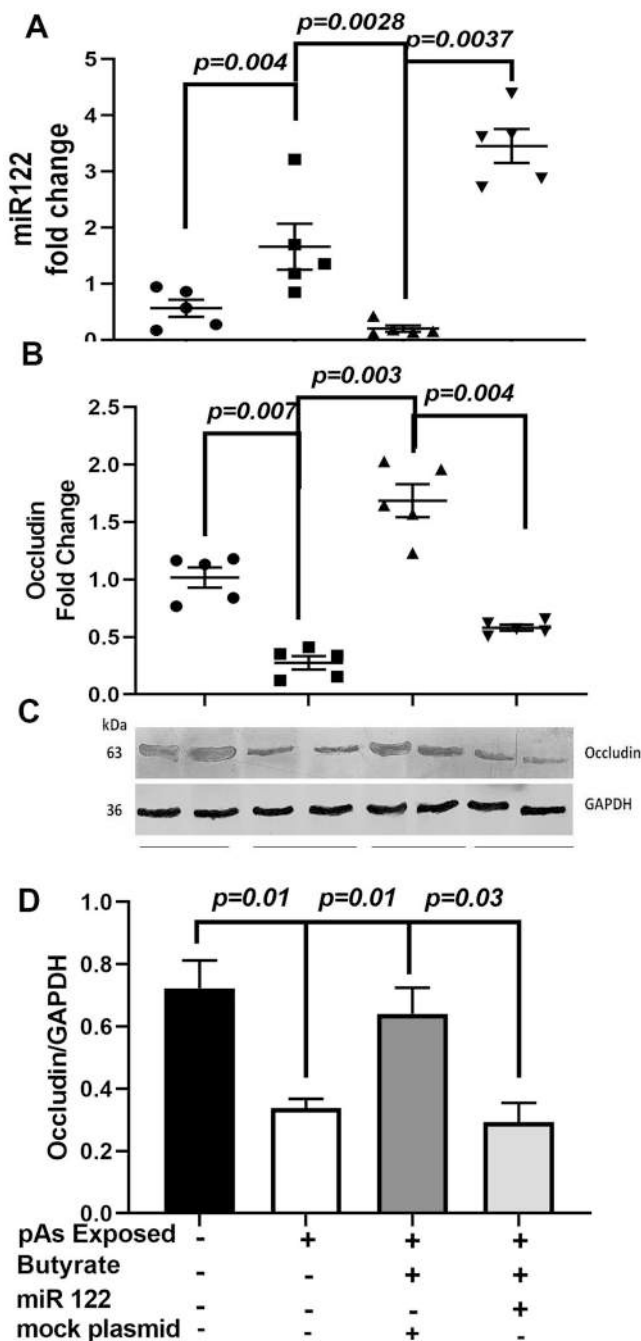


Fig. 5. Effect of overexpression of miR-122 on Occludin expression in mice colon. (A) Each butyrate treated pAs-mice were injected with either 25 μ g in 100 μ l of miR122 expressing plasmid or 25 μ g in 100 μ l of mock plasmid in tail vein. The mice were sacrificed 4 days post injection. The miR122 (A) and occludin (B) expression in colon was measured. N = 5, the data is represented as mean \pm SE. The experiment was repeated twice. Values significantly different at $p < 0.05$ and $p < 0.01$.

function leads to increase in permeability. The translocation of luminal components into the host could cause both local and systemic inflammatory pathways in the case of enhanced intestinal permeability (Mu et al., 2017). Arsenic treated Caco2 cells were shown to increase paracellular permeability by redistribution of zona occludens and reduced claudin 1 expression (Chiocchetti et al., 2019). In contrast, our study showed that prenatal arsenic exposure does not change the expression of claudin 1 and ZO-1. Possibly, as the pAs-mice were not exposed to arsenic after birth, the toxic concentration of arsenic that is required to

reduce claudin1 was not attained in the juvenile body. Recent report showed arsenic treatment impairs distinct population of intestinal stromal cells and intraepithelial and innate immune cells (Kellett et al., 2022; Medina et al., 2020). In conjunction, the histology of colon sections of pAs-mice showed infiltration of inflammatory cells and goblet cell hyperplasia. Gut barrier disruption and neutrophil infiltration are closely associated phenomena (Lin et al., 2020). The precise mechanism of goblet cell hyperplasia is unclear. A previous study showed that IL-13, the key regulator in type-2 mediated inflammation induces goblet cell hyperplasia to accelerate inflammation (Huang et al., 2020). Arsenic has been linked to IL-13 induction (Rahman et al., 2021), which could possibly lead to goblet cell hyperplasia. SCFA, particularly butyrate has been shown to strengthen barrier function and decrease intestinal permeability in several studies using cell culture models and animal models (Peng et al., 2009). Recalling the decrease of SCFA producing bacteria like members of the phylum Firmicutes and Spirochaetota and SCFA production in pAs mice we studied if SCFA has any effect on occludin expression. For deeper understanding of the effect of SCFA on occludin expression we undertook studies in colon carcinoma cell line, HT-29. The concentration of SCFA used in the treatment of HT-29 cells is effectively luminal concentration (Liu et al., 2018). Butyrate but not propionate or acetate treatment to HT-29 cells showed increase in Occludin expression. To further understand the mechanism by which butyrate regulates occludin expression we sought to study miRNA that plays a crucial role in regulating gene expression (Kaikkonen et al., 2011). It is reported that miR122, binds to the 3' UTR of Occludin mRNA causing its decay (Jingushi et al., 2017). Although miR122 abundantly found in liver, it is also reported to express in the intestinal tissue (Runtsch et al., 2014). Our study showed that butyrate decreases miR122 expression as function of its concentration. To confirm the inhibition of miR122 is specific to butyrate and not other SCFAs we showed that neither propionate nor acetate changes miR122 and Occludin expression. In another study from our group we have shown that a RNA binding protein, AUF1 plays a fulcrum point in miR122 regulation by butyrate (data not shown and the manuscript is under review).

Our findings capture transitivity of miR122 and Occludin in butyrate mediated decrease in paracellular permeability. The elegance of the interaction of these molecular players was further verified by providing butyrate orally in pAs-mice. As expected, following butyrate treatment to pAs-mice, Occludin expression in gut was increased with concomitant decrease in gut permeability. Butyrate fed pAs-mice not only restored miR122 level and occludin expression which resulted in decreased gut permeability and reduced infiltration of neutrophil in the gut. Further to understand the molecular events associated with butyrate and Occludin expression we over-expressed miR122 in butyrate treated pAs-mice resulted in appreciable recovery of Occludin expression. The limitation of our study is that it is focused only at a particular age of the post natal life. Further longitudinal studies are required to understand how microbial composition and gut functions changes with age in the post natal life if not exposed to arsenic anymore. Using technology involving CRISPR-based recording method by E coli sentinel cells to reveal transcriptional changes in intestinal and microbial physiology (Schmidt et al., 2022) will provide additional perspectives of arsenic induced changes in future.

5. Conclusion

Overall, the present study deals with an interesting connection of prenatal arsenic exposure and altered gut physiology in post natal life. We report gut microbial dysbiosis in pAs-mice leading to decrease in Firmicutes to Bacteroidetes ratio and decrease in production of SCFAs. We also document increase in gut permeability with decrease in Occludin expression which was reversed after butyrate treatment. Breach in the gut barrier function increases inflammatory gene expression in the gut of pAs-mice which was further reversed by butyrate

treatment. Employing in vitro and in vivo experiments we have shown that butyrate down regulates miR122 expression which is responsible for increase in Occludin expression leading to the decrease in permeability. By rescuing miR122 expression after butyrate treatment we further establish the sequential molecular partners- miR122 and Occludin that plays a role in butyrate mediated increase in barrier function in prenatal arsenic exposed mice.

Declaration of Competing Interest

The authors declare that they have no known competing financial interests or personal relationships that could have appeared to influence the work reported in this paper.

Data availability

Data will be made available on request.

Acknowledgement

We acknowledge the support of Director, ICMR-NICED, Kolkata for carrying out the study. We thank Dr. P. Jaisankar, Sudip Dey and Sandip Chaudhury (CSIR-IICB) for GC-MS analysis. We also thank Dr. Anjan Das for analyzing the histology. We acknowledge Prof. Syamal Roy (CSIR-IICB) for critically reviewing the manuscript. MC and OD are recipient of fellowship from the CSIR and DST respectively.

Grant support

This work was supported by ICMR-NICED.

Appendix A. Supporting information

Supplementary data associated with this article can be found in the online version at [doi:10.1016/j.toxlet.2022.11.011](https://doi.org/10.1016/j.toxlet.2022.11.011).

References

- Abdelmohsen, K., Tominaga-Yamanaka, K., Srikanth, S., Yoon, J.H., Kang, M.J., Gorospe, M., 2012. RNA-binding protein AUF1 represses Dicer expression. *Nucleic Acids Res* 40, 11531–11544.
- Ahmad, R., Sorrell, M.F., Batra, S.K., Dhawan, P., Singh, A.B., 2017. Gut permeability and mucosal inflammation: bad, good or context dependent. *Mucosal Immunol.* 10, 307–317.
- Al-Sadi, R., Khatib, K., Guo, S., Ye, D., Youssef, M., Ma, T., 2011. Occludin regulates macromolecule flux across the intestinal epithelial tight junction barrier. *Am. J. Physiol. Gastrointest. Liver Physiol.* 300, G1054–G1064.
- Andersen, S.C., Fachmann, M.S.R., Kiil, K., Moller Nielsen, E., Hoorfar, J., 2017. Gene-Based Pathogen Detection: Can We Use qPCR to Predict the Outcome of Diagnostic Metagenomics? *Genes (Basel)* 8.
- Bolyen, E., Rideout, J.R., Dillon, M.R., Bokulich, N.A., Abnet, C.C., Al-Ghalith, G.A., Alexander, H., Alm, E.J., Arumugam, M., Asnicar, F., Bai, Y., Bisanz, J.E., Bittinger, K., Brejnrod, A., Brislawn, C.J., Brown, C.T., Callahan, B.J., Caraballo-Rodriguez, A.M., Chase, J., Cope, E.K., Da Silva, R., Diener, C., Dorrestein, P.C., Douglas, G.M., Durall, D.M., Duvallet, C., Edwardson, C.F., Ernst, M., Estaki, M., Fouquier, J., Gauglitz, J.M., Gibbons, S.M., Gibson, D.L., Gonzalez, G., Gorlick, K., Guo, J., Hillmann, B., Holmes, S., Holste, H., Huttenhower, C., Huttley, G.A., Janssen, S., Jarmusch, A.K., Jiang, L., Kaehler, B.D., Kang, K.B., Keefe, C.R., Keim, P., Kelley, S.T., Knights, D., Koester, I., Kosciulek, T., Kreps, J., Langille, M.G.I., Lee, J., Ley, R., Liu, Y.X., Loftfield, E., Lozupone, C., Maher, M., Marotz, G.I., Martin, B.D., McDonald, D., McIVER, L.J., Melnik, A.V., Metcalf, J.L., Morgan, S.C., Morton, J.T., Naimey, A.T., Navas-Molina, J.A., Nothias, L.F., Orchanian, S.B., Pearson, T., Peoples, S.L., Petras, D., Preuss, M.L., Priesse, E., Rasmussen, L.B., Rivers, A., Robeson 2nd, M.S., Rosenthal, P., Segata, N., Shaffer, M., Shiffer, A., Sinha, R., Song, S.J., Spear, J.R., Swafford, A.D., Thompson, L.R., Torres, P.J., Trinh, P., Tripathi, A., Turnbaugh, P.J., Ul-Hasan, S., van der Hooft, J.J.J., Vargas, F., Vazquez-Baeza, Y., Vogtmann, E., von Hippel, M., Walters, W., Wan, Y., Wang, M., Warren, J., Weber, K.C., Williamson, C.H.D., Willis, A.D., Xu, Z.Z., Zaneveld, J.R., Zhang, Y., Zhu, Q., Knight, R., Caporaso, J.G., 2019. Reproducible, interactive, scalable and extensible microbiome data science using QIIME 2. In: *Nat Biotechnol.* 37, pp. 852–857.
- Callahan, B.J., McMurdie, P.J., Rosen, M.J., Han, A.W., Johnson, A.J., Holmes, S.P., 2016. DADA2: High-resolution sample inference from Illumina amplicon data. *Nat. Methods* 13, 581–583.
- Canani, R.B., Costanzo, M.D., Leone, L., Pedata, M., Meli, R., Calignano, A., 2011. Potential beneficial effects of butyrate in intestinal and extraintestinal diseases. *World J. Gastroenterol.* 17, 1519–1528.
- Casalino, G., Del Turco, C., Corvi, F., Rafaili, O., Bandello, F., Querques, G., 2016. Short-term retinal sensitivity and metamorphopsia changes following half-fluence photodynamic therapy in central serous chorioretinopathy. *Ophthalmic Res* 56, 23–29.
- Castoldi, A., Favero de Aguiar, C., Moraes-Vieira, P.M., Olsen Saraiva Camara, N., 2015. They must hold tight: junction proteins, microbiota and immunity in intestinal mucosa. *Curr. Protein Pept. Sci.* 16, 655–671.
- Chakraborty, M., Bhaumik, M., 2020. Prenatal arsenic exposure interferes in postnatal immunocompetence despite an absence of ongoing arsenic exposure. *J. Immunotoxicol.* 17, 135–143.
- Chen, J., Vitetta, L., 2020. The role of butyrate in attenuating pathobiont-induced hyperinflammation. *Immune Netw.* 20, e15.
- Cherry, N., Shaik, K., McDonald, C., Chowdhury, Z., 2010. Manganese, arsenic, and infant mortality in Bangladesh: an ecological analysis. *Arch. Environ. Occup. Health* 65, 148–153.
- Chi, L., Bian, X., Gao, B., Tu, P., Ru, H., Lu, K., 2017. The effects of an environmentally relevant level of arsenic on the gut microbiome and its functional metagenome. *Toxicol. Sci.* 160, 193–204.
- Chiocchetti, G.M., Velez, D., Devesa, V., 2019. Inorganic arsenic causes intestinal barrier disruption. *Metallomics* 11, 1411–1418.
- Coppola, S., Avagliano, C., Calignano, A., Berni Canani, R., 2021. The protective role of butyrate against obesity and obesity-related diseases. *Molecules* 26.
- den Besten, G., van Eunen, K., Groen, A.K., Venema, K., Reijngoud, D.J., Bakker, B.M., 2013. The role of short-chain fatty acids in the interplay between diet, gut microbiota, and host energy metabolism. *J. Lipid Res* 54, 2325–2340.
- Dong, X., Gao, Y., Chen, W., Wang, W., Gong, L., Liu, X., Luo, J., 2015. Spatiotemporal distribution of phenolamides and the genetics of natural variation of hydroxycinnamoyl spermidine in rice. *Mol. Plant* 8, 111–121.
- Dong, X., Shulzhenko, N., Lemaitre, J., Greer, R.L., Peremyslova, K., Quamruzzaman, Q., Rahman, M., Hasan, O.S., Joya, S.A., Golam, M., Christiani, D.C., Morgun, A., Kile, M.L., 2017. Arsenic exposure and intestinal microbiota in children from Sirajdikhan, Bangladesh. *PLoS One* 12, e0188487.
- Donohoe, D.R., Collins, L.B., Wali, A., Bigler, R., Sun, W., Bultman, S.J., 2012. The Warburg effect dictates the mechanism of butyrate-mediated histone acetylation and cell proliferation. *Mol. Cell* 48, 612–626.
- Endo, H., Niioka, M., Kobayashi, N., Tanaka, M., Watanabe, T., 2013. Butyrate-producing probiotics reduce nonalcoholic fatty liver disease progression in rats: new insight 667 into the probiotics for the gut-liver axis. *PLoS One* 8, e63388.
- Furuse, M., 2010. Molecular basis of the core structure of tight junctions. *Cold Spring Harb. Perspect. Biol.* 2, a002907.
- Gasaly, N., Hermoso, M.A., Gotteland, M., 2021. Butyrate and the Fine-Tuning of Colonic Homeostasis: Implication for Inflammatory Bowel Diseases. *Int J. Mol. Sci.* 22.
- Ghosh, J., Bose, M., Roy, S., Bhattacharyya, S.N., 2013. Leishmania donovani targets 673 Dicer1 to downregulate miR-122, lower serum cholesterol, and facilitate murine liver 674 infection. *Cell Host Microbe* 13, 277–288.
- Groschwitz, K.R., Hogan, S.P., 2009. Intestinal barrier function: molecular regulation and disease pathogenesis. *J. Allergy Clin. Immunol.* 124 (3–20; quiz), 21–22.
- Gumber, S., Nusrat, A., Villinger, F., 2014. Immunohistological characterization of intercellular junction proteins in rhesus macaque intestine. *Exp. Toxicol. Pathol.* 66, 437–444.
- Guo, X., Huang, C., Xu, J., Xu, H., Liu, L., Zhao, H., Wang, J., Huang, W., Peng, W., Chen, Y., Nie, Y., Zhou, Y., Zhou, Y., 2021. Gut Microbiota Is a Potential Biomarker in Inflammatory Bowel Disease. *Front Nutr.* 8, 818902.
- Guo, X., Xia, X., Tang, R., Zhou, J., Zhao, H., Wang, K., 2008. Development of a real-time PCR method for Firmicutes and Bacteroidetes in faeces and its application to quantify intestinal population of obese and lean pigs. *Lett. Appl. Microbiol* 47, 367–373.
- Hashash, J.G., Kane, S., 2015. Pregnancy and Inflammatory Bowel Disease. *Gastroenterol. Hepatol. (N. Y)* 11, 96–102.
- Hoen, A.G., Madan, J.C., Li, Z., Coker, M., Lundgren, S.N., Morrison, H.G., Palys, T., Jackson, B.P., Sogin, M.L., Cottingham, K.L., Karagas, M.R., 2018. Sex-specific associations of infants' gut microbiome with arsenic exposure in a US population. *Sci. Rep.* 8, 12627.
- Huang, Z.Q., Liu, J., Ong, H.H., Yuan, T., Zhou, X.M., Wang, J., Tan, K.S., Chow, V.T., Yang, Q.T., Shi, L., Ye, J., Wang, D.Y., 2020. Interleukin-13 Alters Tight Junction Proteins Expression Thereby Compromising Barrier Function and Dampens Rhinovirus Induced Immune Responses in Nasal Epithelium. *Front Cell Dev. Biol.* 8, 572749.
- Jingushi, K., Kashiwagi, Y., Ueda, Y., Kitae, K., Hase, H., Nakata, W., Fujita, K., Uemura, M., Nonomura, N., Tsujikawa, K., 2017. High miR-122 expression promotes malignant phenotypes in ccRCC by targeting occludin. *Int J. Oncol.* 51, 289–297.
- Kaikkonen, M.U., Lam, M.T., Glass, C.K., 2011. Non-coding RNAs as regulators of gene expression and epigenetics. *Cardiovasc Res* 90, 430–440.
- Kellett, M.P., Jariko, J.T., Darling, C.L., Ventrello, S.W., Bain, L.J., 2022. Arsenic exposure impairs intestinal stromal cells. *Toxicol. Lett.* 361, 54–63.
- Kelly, C.J., Zheng, L., Campbell, E.L., Saeedi, B., Scholz, C.C., Bayless, A.J., Wilson, K.E., Glover, L.E., Kominsky, D.J., Magnuson, A., Weir, T.L., Ehrentraut, S.F., Pickel, C., Kuhn, K.A., Lanis, J.M., Nguyen, V., Taylor, C.T., Colgan, S.P., 2015. Crosstalk between Microbiota-Derived Short-Chain Fatty Acids and Intestinal Epithelial HIF Augments Tissue Barrier Function. *Cell Host Microbe* 17, 662–671.
- Lee, C.H., Hsu, C.Y., Huang, P.Y., Chen, C.L., Lee, Y.C., Yu, H.S., 2016. Arsenite regulates prolongation of glycan residues of membrane glycoprotein: a pivotal study via wax physisorption kinetics and FTIR imaging. *Int J. Mol. Sci.* 17, 427.

- Li, H., Zhang, X., Jin, Z., Yin, T., Duan, C., Sun, J., Xiong, R., Li, Z., 2019. MiR-122 Promotes the Development of Colon Cancer by Targeting ALDOA In Vitro. *Technol. Cancer Res Treat.* 18, 1533033819871300.
- Li, M., Zhu, R., Song, X., Wang, Z., Weng, H., Liang, J., 2020. A sensitive method for the quantification of short-chain fatty acids by benzyl chloroformate derivatization combined with GC-MS. *Analyst* 145, 2692–2700.
- Liang, G.H., Weber, C.R., 2014. Molecular aspects of tight junction barrier function. *Curr. Opin. Pharm.* 19, 84–89.
- Lin, E.Y., Lai, H.J., Cheng, Y.K., Leong, K.Q., Cheng, L.C., Chou, Y.C., Peng, Y.C., Hsu, Y. H., Chiang, H.S., 2020. Neutrophil Extracellular Traps Impair Intestinal Barrier Function during Experimental Colitis. *Biomedicine* 8.
- Lin, H.V., Frassetto, A., Kowalik Jr., E.J., Nawrocki, A.R., Lu, M.M., Kosinski, J.R., Hubert, J.A., Szeto, D., Yao, X., Forrest, G., Marsh, D.J., 2012. Butyrate and propionate protect against diet-induced obesity and regulate gut hormones via free fatty acid receptor 3-independent mechanisms. *PLoS One* 7, e35240.
- Liu, H., Wang, J., He, T., Becker, S., Zhang, G., Li, D., Ma, X., 2018. Butyrate: a double-edged sword for health? *Adv. Nutr.* 9, 21–29.
- Lu, Z., Ding, L., Lu, Q., Chen, Y.H., 2013. Claudins in intestines: Distribution and functional significance in health and diseases. *Tissue Barriers* 1, e24978.
- McMurdie, P.J., Holmes, S., 2013. phyloseq: an R package for reproducible interactive analysis and graphics of microbiome census data. *PLoS One* 8, e61217.
- Medina, S., Lauer, F.T., Castillo, E.F., Bolt, A.M., Ali, A.S., Liu, K.J., Burchiel, S.W., 2020. Exposures to uranium and arsenic alter intraepithelial and innate immune cells in the 733 small intestine of male and female mice. *Toxicol. Appl. Pharm.* 403, 115155.
- Mor, A., Antonsen, S., Kahlert, J., Holsteen, V., Jorgensen, S., Holm-Pedersen, J., Sorensen, H.T., Pedersen, O., Ehrenstein, V., 2015. Prenatal exposure to systemic antibiotics and overweight and obesity in Danish schoolchildren: a prevalence study. *Int J. Obes. (Lond.)* 39, 1450–1455.
- Mu, Q., Kirby, J., Reilly, C.M., Luo, X.M., 2017. Leaky gut as a danger signal for autoimmune diseases. *Front Immunol.* 8, 598.
- Mukherjee, A., Sengupta, M.K., Hossain, M.A., Ahamed, S., Das, B., Nayak, B., Lodh, D., Rahman, M.M., Chakraborti, D., 2006. Arsenic contamination in groundwater: a global perspective with emphasis on the Asian scenario. *J. Health Popul Nutr.* 24, 142–163.
- Myers, S.L., Lobdell, D.T., Liu, Z., Xia, Y., Ren, H., Li, Y., Kwok, R.K., Mumford, J.L., Mendola, P., 2010. Maternal drinking water arsenic exposure and perinatal outcomes in inner Mongolia, China. *J. Epidemiol. Community Health* 64, 325–329.
- Nusrat, A., Chen, J.A., Foley, C.S., Liang, T.W., Tom, J., Cromwell, M., Quan, C., Mrsny, R.J., 2000. The coiled-coil domain of occludin can act to organize structural and functional elements of the epithelial tight junction. *J. Biol. Chem.* 275, 29816–29822.
- Okumura, T., Nozu, T., Ishioh, M., Igarashi, S., Kumei, S., Ohhira, M., 2021. Centrally administered butyrate improves gut barrier function, visceral sensation and septic lethality in rats. *J. Pharm. Sci.* 146, 183–191.
- Peng, L., He, Z., Chen, W., Holzman, I.R., Lin, J., 2007. Effects of butyrate on intestinal barrier function in a Caco-2 cell monolayer model of intestinal barrier. *Pedia Res* 61, 37–41.
- Peng, L., Li, Z.R., Green, R.S., Holzman, I.R., Lin, J., 2009. Butyrate enhances the intestinal barrier by facilitating tight junction assembly via activation of AMP-activated protein kinase in Caco-2 cell monolayers. *J. Nutr.* 139, 1619–1625.
- Pickard, J.M., Zeng, M.Y., Caruso, R., Nunez, G., 2017. Gut microbiota: Role in pathogen colonization, immune responses, and inflammatory disease. *Immunol. Rev.* 279, 70–89.
- Plaire, D., Puaud, S., Marsolier-Kergoat, M.C., Elalouf, J.M., 2017. Comparative analysis of the sensitivity of metagenomic sequencing and PCR to detect a bio warfare simulant (*Bacillus atrophaeus*) in soil samples. *PLoS One* 12, e0177112.
- Quast, C., Pruesse, E., Yilmaz, P., Gerken, J., Schweer, T., Yarza, P., Peplies, J., Glockner, F.O., 2013. The SILVA ribosomal RNA gene database project: improved data processing and web-based tools. *Nucleic Acids Res* 41, D590–D596.
- Rahman, A., Islam, M.S., Tony, S.R., Siddique, A.E., Mondal, V., Hosen, Z., Islam, Z., Hossain, M.I., Rahman, M., Anjum, A., Paul, S.K., Hossen, F., Sarker, M.K., Hossain, S., Salam, K.A., Haque, A., Hoque, M.A., Saud, Z.A., Xin, L., Sumi, D., Himeno, S., Hossain, K., 2021. T helper 2-driven immune dysfunction in chronic arsenic-exposed individuals and its link to the features of allergic asthma. *Toxicol. Appl. Pharm.* 420, 115532.
- Rangan, P., Choi, I., Wei, M., Navarrete, G., Guen, E., Brandhorst, S., Enyati, N., Pasia, G., Maesincee, D., Ocon, V., Abdulridha, M., Longo, V.D., 2019. Fasting-Mimicking Diet Modulates Microbiota and Promotes Intestinal Regeneration to Reduce Inflammatory Bowel Disease Pathology. *Cell Rep.* 26 (2704–2719), e2706.
- Robeson 2nd, M.S., O'Rourke, D.R., Kaehler, B.D., Ziemiński, M., Dillon, M.R., Foster, J.T., Bokulich, N.A., 2021. RESCRIPt: Reproducible sequence taxonomy reference database management. *PLoS Comput. Biol.* 17, e1009581.
- Runtsch, M.C., Round, J.L., O'Connell, R.M., 2014. MicroRNAs and the regulation of intestinal homeostasis. *Front Genet* 5, 347.
- Saitou, M., Furuse, M., Sasaki, H., Schulzke, J.D., Fromm, M., Takano, H., Noda, T., Tsukita, S., 2000. Complex phenotype of mice lacking occludin, a component of tight junction strands. *Mol. Biol. Cell* 11, 4131–4142.
- Schmidt, F., Zimmermann, J., Tanna, T., Farouni, R., Conway, T., Macpherson, A.J., Platt, R.J., 2022. Noninvasive assessment of gut function using transcriptional recording sentinel cells. *Sci.* 376, eabm6 038.
- Schulthess, J., Pandey, S., Capitani, M., Rue-Albrecht, K.C., Arnold, I., Franchini, F., Chomka, A., Iloft, N.E., Johnston, D.G.W., Pires, E., McCullagh, J., Sansom, S.N., Arancibia-Carcamo, C.V., Uhlig, H.H., Powrie, F., 2019. The Short Chain Fatty Acid Butyrate Imprints an Antimicrobial Program in Macrophages. *Immunity* 50 (432–445), e437.
- Segain, J.P., Ringeard de la Bletiere, D., Bourreille, A., Leray, V., Gervois, N., Rosales, C., Ferrier, L., Bonnet, C., Blottiere, H.M., Galmiche, J.P., 2000. Butyrate inhibits inflammatory responses through NFκB inhibition: implications for Crohn's disease. *Gut* 47, 397–403.
- Silva, J.P.B., Navegantes-Lima, K.C., Oliveira, A.L.B., Rodrigues, D.V.S., Gaspar, S.L.F., Monteiro, V.V.S., Moura, D.P., Monteiro, M.C., 2018. Protective Mechanisms of Butyrate on Inflammatory Bowel Disease. *Curr. Pharm. Des.* 24, 4154–4166.
- Singh, B., Halestrap, A.P., Paraskeva, C., 1997. Butyrate can act as a stimulator of growth or inducer of apoptosis in human colonic epithelial cell lines depending on the presence of alternative energy sources. *Carcinogenesis* 18, 1265–1270.
- Stensballe, L.G., Simonsen, J., Jensen, S.M., Bonnelykke, K., Bisgaard, H., 2013. Use of antibiotics during pregnancy increases the risk of asthma in early childhood. *J. Pediatr* 162 (832–838), e833.
- Suzuki, T., 2013. Regulation of intestinal epithelial permeability by tight junctions. *Cell Mol. Life Sci.* 70, 631–659.
- Tudor, K.I., Petracic, D., Jukic, A., Juratovac, Z., 2017. Skew deviation: case report and review of the literature. *Semin Ophthalmol.* 32, 734–737.
- Van Daele, E., Knol, J., Belzer, C., 2019. Microbial transmission from mother to child: improving infant intestinal microbiota development by identifying the obstacles. *Crit. Rev. Microbiol.* 45, 613–648.
- Weber, C.R., 2012. Dynamic properties of the tight junction barrier. *Ann. N. Y. Acad. Sci.* 1257, 77–84.
- Worsley, S.F., Davies, C.S., Mannarelli, M.E., Hutchings, M.I., Komdeur, J., Burke, T., Dugdale, H.L., Richardson, D.S., 2021. Gut microbiome composition, not alpha diversity, is associated with survival in a natural vertebrate population. *Anim. Micro* 3, 84.
- Wu, X., Yang, Y., Huang, Y., Chen, Y., Wang, T., Wu, S., Tong, L., Wang, Y., Lin, L., Hao, M., Zhong, Z.H., Zhang, F., Zhao, W., 2018. RNA-binding protein AUF1 suppresses miR-122 biogenesis by down-regulating Dicer1 in hepatocellular carcinoma. *Oncotarget* 9, 14815–14827.
- Xu, Y.H., Gao, C.L., Guo, H.L., Zhang, W.Q., Huang, W., Tang, S.S., Gan, W.J., Xu, Y., Zhou, H., Zhu, Q., 2018. Sodium butyrate supplementation ameliorates diabetic inflammation in db/db mice. *J. Endocrinol.* 238, 231–244.
- Yang, W., Xu, H.W., Lu, X.R., Xu, Q.F., Tao, M.H., Dai, Y.M., 2022. Overexpression of miR-122 Impairs Intestinal Barrier Function and Aggravates Acute Pancreatitis by Downregulating Occludin Expression. *Biochem Genet* 60, 382–394.
- Ye, D., Guo, S., Al-Sadi, R., Ma, T.Y., 2011. MicroRNA regulation of intestinal epithelial tight junction permeability. *Gastroenterology* 141, 1323–1333.
- Yip, W., Hughes, M.R., Li, Y., Cait, A., Hirst, M., Mohn, W.W., McNaghy, K.M., 2021. Butyrate shapes immune cell fate and function in allergic asthma. *Front Immunol.* 12, 628453.



Gum Odina prebiotic prevents experimental colitis in C57BL/6 mice model and its role in shaping gut microbial diversity

Debmalya Mitra^a, Sohini Sikdar^a, Mainak Chakraborty^a, Oishika Das^a, Amalesh Samanta^b, Shanta Dutta^{a,*}

^a ICMR – National Institute of Cholera and Enteric Diseases, Kolkata, India

^b Division of Microbiology & Biotechnology, Department of Pharmaceutical Technology, Jadavpur University, Kolkata, India

ARTICLE INFO

Keywords:

Prebiotics
Gum odina
Colitis
IL-10
TNF- α and iNOS

ABSTRACT

Colitis is a multifaceted disease which is a global threat in the present times. It is hypothesised that novel prebiotics like Gum Odina (GO) are emerging as preventive therapy to combat chronic gut diseases due to their ease of incorporation into diet and established health benefits. The study illustrates the efficacy of GO in preventing dextran sodium sulfate (DSS) induced colitis in C57BL/6 mice and compares the results with Inulin (IN). Mice were grouped into Control, DSS, GO, and IN. Apart from the control, mice from other groups were administered with 2% DSS orally. GO and IN were also fed to the respective groups for 28 days. The reduction in body weight, colon length, mucosal dysplasia and disease activity index were found less in GO compared to DSS. CD8⁺ T cell population were reduced in GO ($10.28 \pm 0.09\%$) when compared to DSS ($30.03 \pm 0.23\%$) and IN (15.25 ± 0.25). GO increased the release of anti-inflammatory cytokine IL-10 and reduced TNF- α , IFN- γ , IL-1 β and IL-12 along with downregulation of iNOS expression in the colon. Next-generation sequencing data revealed the stool sample of colitis patient was dominated by *Prevotella* sp. along with other pathogenic bacteria. An increase in the diversity of gut bacteria and the abundance of commensal bacteria like *Lactobacillus* sp. and *Enterococcus* sp. was observed when the stool sample of a colitis patient was cultured in the gut simulator and GO was added into the feed. Thus, GO alleviate intestinal damage and slows colitis progression.

1. Introduction

Changes in dietary patterns and fast lifestyle are interconnected to a rise in colitis cases, impacting global healthcare costs with an estimate of more than 6.8 million active cases worldwide (Piovani et al., 2019). Humans are very vulnerable to colitis as the mammalian gastrointestinal tract is continuously exposed to food-derived toxins (Solanki et al., 2013), and houses numerous bacteria (Gibson & Roberfroid, 1995). Colitis is a multifaceted disease involving a disequilibrium of immune responses that occurs in the gastrointestinal tract (Xavier & Podolsky, 2007). One of the major causes of colitis is the colonization of pathogenic bacteria leading to the alteration of commensal microflora in the intestine which contributes to disease progression by causing epithelial damage (Yi et al., 2019) and up-regulating inflammatory genes (Randhawa et al., 2014). Dextran sodium sulfate (DSS) is a chemical colitogen having the properties of an anticoagulant and is most commonly used to induce colitis in animal models (Cader & Kaser, 2013) which closely resembles human colitis (Kaplan, 2015).

Prebiotics are carbohydrates that have the ability to alter the composition of the gastrointestinal microbiota and provide health benefits (Fuller, 1991). Prebiotics exerts their effect especially on the distal parts of the colon (Chassaing et al., 2014) making them a readymade therapeutic choice for the treatment of colitis. Prebiotics selectively stimulate beneficial bacterial species (Okayasu et al., 1990) and reduce the colonization of pathogenic bacteria (Gibson et al., 2004) which can slow the overall progression of colitis. Gum Odina (GO) is obtained from the plant *Odina wodier*, which is produced at around 60 tons per year with a processing cost of USD 1.50 per kilo (app) (De, Malpani, et al., 2020). GO is an established prebiotic (Mitra et al., 2016) with cancer-prevention properties (Mitra et al., 2017). GO contains arabinose and galactose as major constituent sugars and is a type I arabinogalactan (Bhattacharyya & Rao, 1964; De, Malpani, et al., 2020; De et al., 2020, 2020). GO is being used in various pharmaceutical formulations like tablet binders (Mukherjee et al., 2006), coacervates for colon-targeted delivery systems (Roy et al., 2013) and biodegradable spongy scaffolds for healing wounds of epidermal layer (Das et al., 2021). Considering the various application and prebiotic efficacy of GO, we

* Corresponding author. Division of Microbiology, ICMR NICED, P-33, CIT Rd, Subhas Sarobar Park, Kolkata, 700010, West Bengal, India.
E-mail address: shanta1232001@gmail.com (S. Dutta).

<https://doi.org/10.1016/j.fbio.2023.102509>

Received 6 December 2022; Received in revised form 9 February 2023; Accepted 23 February 2023

Available online 24 February 2023

2212-4292/© 2023 Published by Elsevier Ltd.

List of abbreviations

ANOVA	Analysis of variance
DSS	Dextran Sodium Sulfate
ELISA	Enzyme-Linked Immuno Sorbent Assay
DAI	Disease activity index
GO	Gum Odina
IN	Inulin
MGA	Meta Gene Annotator
ORFs	Open reading frames
PBS	Phosphate buffer saline
SEM	Scanning electron microscope
SCFAs	Short-chain fatty acids
SHIME	Simulator of Human intestinal Microbial Ecosystem
SEM	Standard error of the mean
wt	Weight

Table 1

Composition of diet fed to C57BL/6 mice to conduct DSS-induced colitis model.

Composition	Amount (g per kg)
Starch	385
Sucrose ^a	250
Casein	200
Refined oil	100
Mineral mixture ^b	10
Vitamin mixture ^b	50
Choline Chloride	2
Methionine	3

^a Sucrose was replaced with GO in mice groups fed GO and IN respectively gum odina and inulin respectively.

^b Vitamin and mineral mixtures were prepared and mixed according to (Pellizzon & Ricci, 2020).

hypothesised that GO can reduce the progression of experimental colitis induced by DSS of molecular wt. ~50 k Da in C57BL/6 mice, which mimics human colitis situation (Melgar et al., 2008) and has the ability to emerge as preventive therapy. The mechanism by which GO prevents colitis progression was investigated and the obtained results were compared alongside that of Inulin (IN) as a reference. IN is the most widely marketed prebiotic which is obtained from chicory roots, beet-roots, bananas, leeks etc and contains mainly fructose, glucose, xylose and galactosamine (Qiao et al., 2022). Subsequently, the gut simulator was used for culturing the microflora of a colitis patient by collecting stool sample and richness in terms of microbial diversity attained upon the incorporation of GO was profiled using Next-generation sequencing.

2. Methodology and materials

2.1. Collection & purification of prebiotic

GO was collected from the plant *Odina wodier* which is predominantly found in tropical forests of West Bengal, India and purified using acidified ethanol which induces stable conformational changes and brings out bioactivity. The raw polysaccharide was immersed in MilliQ water and left for 12 h to achieve uniform swelling, which was followed by 6 h of stirring using a laboratory stirrer (REMI, India) at 25 °C. The solution was filtered through clean and sterile muslin cloth and centrifuged (Thermo Scientific Heraeus Biofuge Stratos Centrifuge, Osterode, Germany) at 1500 rpm for 15 min. The collected supernatant was mixed with equal parts of acidified ethanol to generate a precipitate of white colour, the collected precipitate was further washed using ethanol and

dry ether (1:1) and lyophilized for 5 days to remove traces of organic solvents. The purified GO was powdered and used to conduct experiments (De, Malpani, et al., 2020).

2.2. Animals

Twenty-four C57BL/6 male mice of 6 weeks of age were collected from the animal house of ICMR – National Institute of Cholera & Enteric Diseases, Kolkata, India with a 12-12 h light/dark cycle (Mitra et al., 2017). A temperature and relative humidity of 25 °C and 50% respectively were maintained throughout the experimental period. The animals were fed with a standard rodent diet (Pellizzon, 2016) detailed in Table 1 along with ad libitum access to water. All the experiments were performed in accordance with the institutional animal ethics committee (No. PRO/162/March 2019–March 2022), abiding by institutional guidelines.

2.3. Induction of DSS colitis

C57BL/6 mice were divided into four groups as described below, n = 6 in each cage.

- Control:** Rodent diet
- DSS:** Rodent diet along with 2% DSS.
- GO:** Rodent diet, along with 2% DSS and GO.
- IN:** Rodent diet, along with 2% DSS and IN.

Each experimental mouse was weighed, labelled and fed a standard diet (ICMR – NIN, India). Additionally, mice from GO and IN groups were fed with GO and IN (2.5 g/kg body wt.) as prebiotics respectively (Zhu et al., 2021). The animals in DSS, GO and IN groups were administered with 2% DSS orally via gavages (Wirtz et al., 2007). The DSS was administered for Four days followed by intervening gaps of three days and the cycle was repeated for 28 days.

2.4. Examination of physical parameters i.e. body weight (wt.), colon length, spleen wt. and disease activity index (DAI)

At the end of the experiment, the animals were starved for 6 h after which the final body wt. were measured. The animals were euthanized following the permitted laws of the institutional animal ethics committee. The colons were separated from the small intestine at the ileocecal junction, collected, and washed in PBS and lengths were measured individually (Li et al., 2012). The colons were then fragmented to conduct further experiments. Similarly, the spleens of test animals were also collected, washed and weighed to draw differences among various groups. Splenocytes and colonic fluids were collected for further analysis (Qiao et al., 2022).

DAI was prepared by adding below mentioned scores (Yeom et al., 2016). The scoring standards followed are:

- body wt. loss (0: no loss; 1: 1–5% loss; 2: 5–10% loss; 3: 10–15% loss; 4: over 15% loss)
- stool consistency (0: normal; 1: loose but shaped; 2: very loose; 3: diarrhoea).

2.5. Histological analysis of colonic tissue sections

To investigate the severity of intestinal inflammation in the different groups, small distal colon sections were first washed with phosphate buffer saline (PBS) and fixed with 10% formaldehyde solution and kept for 48 h. The tissues were dehydrated in alcohol and embedded in paraffin. Ultra-microtome was used to cut sections of 5–6 µm thickness and stained with eosin and haematoxylin dyes, which were observed under the microscope (Breynaert et al., 2013). Tissue sections were graded with respect to the below-mentioned parameters and the values

of each parameter were added together to form the final score (Okayasu et al., 1990).

(i) degree of inflammation along with damage to colonic architecture:

0: normal morphology; 1: lost goblet cells, 2: lost goblet cells in large areas; 3: lost crypts; 4: lost crypts in large areas.

(ii) infiltration of leukocyte:

0: no infiltration, 1: infiltrating crypt basis, 2: infiltrating muscularis mucosa; 3: extensively infiltrating muscularis mucosa with thickened mucosa and obvious swelling; 4: infiltrating submucosa.

2.6. Examination of surface morphology by scanning electron microscope (SEM)

Colon tissues from the distal part of test animals were collected and washed with PBS and immersed in a 4% glutaraldehyde solution. After sufficient fixation, the colon tissues were cut longitudinally to expose the lumen. The tissues were subjected to dehydration by immersing in a series of alcohol (30%, 50%, 70% and 100%), dried and mounted to carbon tapes. The dried tissues were coated with gold and observed under SEM (SEM44 Zeiss SIGMA FE-SEMs, CARL ZEISS, Germany) (Mitra et al., 2017; Paulsen et al., 2005).

2.7. Analysis of splenic population of CD4⁺ and CD8⁺ T-lymphocyte by flow cytometry

Immediately after sacrificing the mice, the spleens were collected in PBS. The spleens were mashed with a sterile pestle and were strained with a cell strainer (BD Falcon™, NJ, USA) to remove any tissue debris. The splenocytes collected were mixed with ficoll plaque plus (GE Healthcare, Illinois, USA) in a graduated tube in a 3:1 ratio, and centrifuged at 2500 g for 30 min keeping acceleration and deceleration as 1 (Thermo Fischer). Splenocytes were collected and re-suspended in FACS buffer and stained with PE-conjugated anti-mouse CD 8⁺ T Cells and FITC-conjugated mouse anti-CD4⁺ T Cells (BD Bio Science, San Diego, USA). The population of cells were analysed using FACS (BD Aria II) (Chen et al., 2019).

2.8. Quantification of pro and anti-inflammatory cytokines in colonic tissue by Enzyme Linked Immuno Sorbent Assay (ELISA)

To conduct cytokine analysis, colonic sections of animals were washed and homogenized in PBS. Homogenized samples were centrifuged at 6000 rpm (Eppendorf, 5417 R, Hamburg, Germany) for 10 min to obtain the supernatant devoid of any tissue debris²⁹. The concentration of protein for each sample was estimated using BCA Protein Assay Kit (Thermo Scientific™ Pierce™, USA)³⁰. ELISA was conducted for TNF- α , IL-10, IL-17, IL-1 β , IL-12 and IFN- γ (BD Bio Science, San Diego, USA) as per the manufacturer's instruction taking 50 μ g of proteins for each sample (Chen et al., 2019).

2.9. Analysis of gene expression of *Tnf- α* , *Ifn- γ* and *Inos* by Real-Time PCR

RNA was extracted by TRIZOL reagent (Invitrogen, Massachusetts, USA) and quantified using nanodrop (NanoDrop 8000 Spectrophotometer, Thermo Fisher Scientific, USA). 5 μ g RNA was taken for reverse transcription with specific primers. dNTPs, MuLV reverse transcriptase, and other reagents were added according to the kit manual (Ambion INC, Austin, USA) to produce cDNA for *Tnf- α* , *Ifn- γ* , *Inos*. cDNA of *Gapdh* was also prepared and taken as loading control (Chen et al., 2019) qPCR was conducted using SYBR green mix (Qiagen, Maryland, USA) as per

Table 2

Composition of the nutritional medium used in SHIME for the cultivation of stool sample collected from the colitis patient.

Composition	Amount (g l ⁻¹)
Arabinogalactan	1
Pectin	2
Xylan	1
Starch	4.2
Glucose ^a	0.4
Yeast extract	3
Peptone	1
Mucin	4
Cysteine	0.5

^a The amount of glucose was completely replaced by GO during the prebiotic phase of SHIME run.

the provided protocol.

The detailed sequence of forward and reverse primers used was listed below.

Gapdh: 5'ACCCAGAAGACTGTGGATGG3'
3'CACATTGGGGTAGGAACAC5'
Tnf- α : 5'CATCTTCTCAAAATTCGAGTGACAA3'
3'TGGGAGTAGACAAGGTACAACCC5'
Ifn- γ : 5'TCAAGTGGCATAGATGTGGAAGAA3'
3'TGGCTCTGCAGGATTTTCATG5'
Inos: 5'CAGCTGGGCTGTACAAACCT3'
3'CATTGGAAGTGAAGCGTTTCG5'

2.10. Culturing of gut microflora using Simulator of Human intestinal Microbial Ecosystem (SHIME)

SHIME is an *in vitro* gut model mimicking the human gastrointestinal tract and physiological conditions. The nutritional medium used in SHIME is detailed in Table 2. The start-up and adaptation period was carried out for 2 weeks and the bacteria used for inoculation was from a faecal sample of a colitis male patient which was collected from ID & BG hospital as a specimen abiding Institutional Ethics Committee of ICMR NICE, Kolkata vide Ref no.: (A-1/2015-IEC). The test period was conducted for 2 weeks, during this time samples were collected from the 3rd, 4th and 5th compartments of SHIME (Mitra et al. 2017). Collected samples were used for microbial profiling. A similar SHIME run was done during the prebiotic phase with the same stool sample where sucrose was substituted with GO.

2.11. Analysis of Gut microbiota

DNA was extracted with Qiagen's power fecal pro kit using Qiacube from the fractions collected from the SHIME run during Colitis and treatment phase. The DNA yield was checked using Qiaexpert. The DNA yield for colitis and GO run was found to be 153.01 ng/ μ l and 174.76 ng/ μ l respectively. The samples were processed on Illumina Novaseq 6000 which gave a paired-end read of 150 \times 2 bp and the samples were processed by downstream analysis. The de novo assembly of the adapter trimmed fastq files is carried out using MetaSPAdes (v 3.10.1). The contigs obtained from the assembly were used as input to MetaGeneAnnotator (MGA) for the prediction of open reading frames (ORFs). The predicted ORFs are searched against the non-redundant (NCBI-nr) database using DIAMOND (v0.7.9.58). The alignment file along with the filtered ORFs was used as input to the functional annotation using MEGAN6 (MetaGenome Analyzer) software. Further Fastq quality checks and base quality score distribution were carried out. Denovo metagenome assembly was carried out for the sample by assembling contigs from the reads using MetaSPAdes program. Further contigs were linked by the assembly algorithm to create scaffolds. Assembly was performed with default Kmer sizes 21, 33, and 55 using the de-bruijn

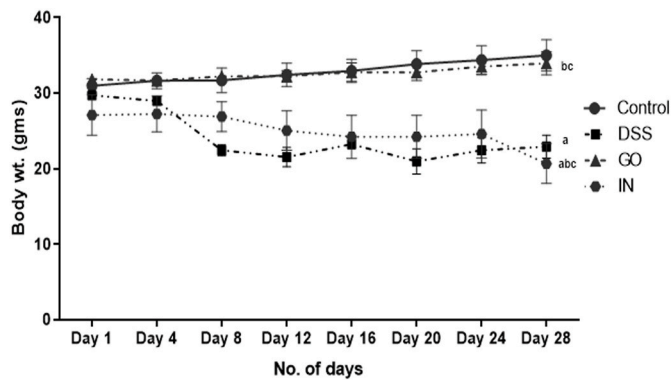


Fig. 1. GO administration halts DSS-induced reduction in body wt. of C57BL/6 mice. The variation in the body wt. of C57BL/6 mice during the development and experimental period of the colitis model. Results are expressed as mean \pm standard error means ($n = 6$). Obtained values were analysed using one-way ANOVA followed by Tukey's multiple comparison test. $p \leq 0.05$ were considered statistically significant. ^a $p \leq 0.05$ compared to Control, ^b $p \leq 0.05$ compared to DSS, ^c $p \leq 0.05$ compared to GO. ANOVA, Analysis of variance; DSS, Dextran sodium sulfate; GO, Gum Odina; IN, Inulin; Wt., Weight.

graph method. PERL and Python code was used to parse the fastq files for the downstream analysis. As a result of de novo assembly, contigs in FASTA format were generated for all samples. The contigs obtained from the assembly are used as input to MetaGeneAnnotator (MGA) for the prediction of open reading frames (ORFs). The gene-finding program MGA was used to identify the coding regions and distinguish them from noncoding DNA. The ORF obtained from the samples was queried to DIAMOND BLASTX program with an optimum e-value of $1e-5$. The gene functions of all the ORF from DIAMOND BLASTX output were parsed using an in-house PERL script. The rarefaction curve was generated by comparing the species abundance between the samples based on the

number of leaves in the taxonomy and the number of sequences that occurred. The curve was made for all taxa including Bacteria, Archaea, Eukaryote, unclassified and other sequences (Sankarasubramanian et al., 2020).

2.12. Statistical analysis

Experiments were conducted in triplicate and data are expressed as mean \pm standard error of the mean (SEM), one-way analysis of variance (ANOVA) was conducted followed by Tukey's multiple comparison tests using Graph Pad Prism 6 software (Graph Pad Software Inc., San Diego, CA, USA) and difference with $P < 0.05$ was considered significant (Mitra et al., 2017).

3. Results

3.1. Examination of physical parameters i.e. body wt., colon length, spleen wt. and DAI

The body wt. of the test animals was measured for 28 days and represented in Fig. 1, the scores of stool consistency were represented in Supplementary Table 1. After the fourth day of DSS administration, a significant ($P \leq 0.0001$) fall in the body wt. by 6.38% was observed in DSS group (DAI: 2) compared to the control group, whereas no notable changes in the body wt. were observed in GO (DAI: 0) and IN (DAI: 0) groups in the first week. Further, there was a gradual fall in body wt. by 25.49% (DAI: 6) and 12.65% (DAI: 4) from day 8 which extended until the end of the experiment to 34.71% (DAI: 7) and 24.31% (DAI: 4) for DSS and IN groups respectively when compared to control group. A slight increase in the body wt. of GO group by 6.76% (DAI: 1) was observed at the end of the 28 days compared to the DSS group. The changes in colon length of experimental animals of test groups are represented in Fig. 2 (a) and pictures of the colon are represented in Fig. 2 (c) Control, (d) DSS, (e) GO, and (f) IN respectively. In the control

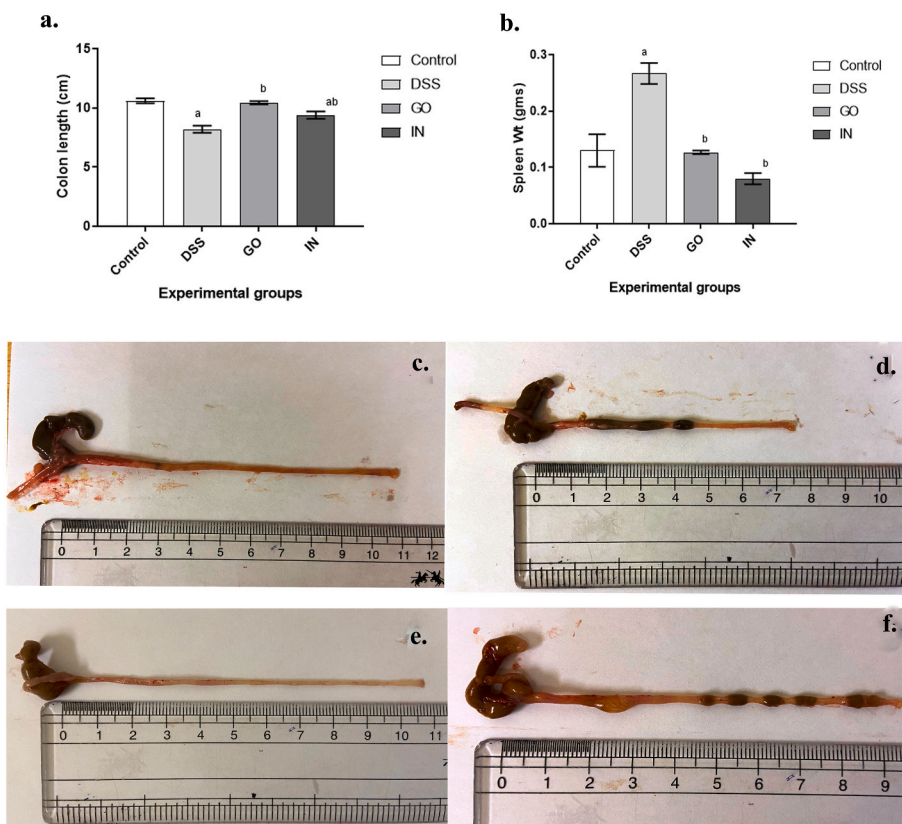


Fig. 2. GO inhibits DSS-induced shortening of colon length and splenomegaly in mice. The colon length and spleen wt. of C57BL/6 mice of different experimental groups (a) colon length (cm) (Control > DSS < IN < GO), (b) spleen wt. (gm) (DSS > Control > GO > IN). (c) picture of the colon from the control group, (d) picture of the colon from the DSS group, (e) picture of the colon from the GO group (f) picture of colon collected from the IN group. Results are expressed as mean \pm standard error means ($n = 6$). Obtained values were analysed using one-way ANOVA followed by Tukey's multiple comparison test. $p \leq 0.05$ were considered statistically significant. ^a $p \leq 0.05$ compared to Control, ^b $p \leq 0.05$ compared to DSS, ^c $p \leq 0.05$ compared to GO. ANOVA, Analysis of variance; DSS, Dextran sodium sulfate; GO, Gum Odina; IN, Inulin; Wt., Weight.

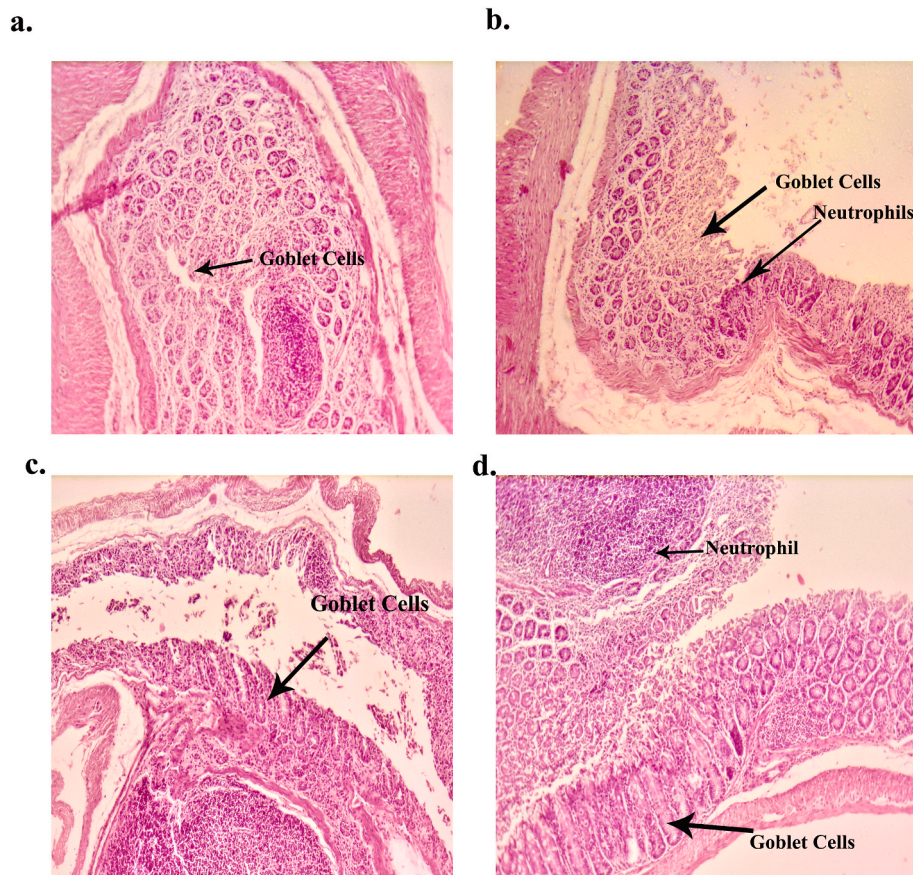


Fig. 3. GO reduces DSS-induced colonic damage at the cellular level of C57BL/6 mice. Haematoxylin and eosin stained cross-sections of colons at $20\times$ magnification (a) Control, (b) DSS, (c) GO, (d) IN. (Damage score: DSS $-7.75 \pm 0.5 > \text{IN} - 6.4 \pm 0.5 > \text{GO} - 6 \pm 0.81$). DSS, Dextran sodium sulfate; GO, Gum Odina; IN, Inulin.

group, the colon length was found to be 10.60 ± 0.36 cm which got significantly ($P \leq 0.0005$) reduced by 22.64% in DSS when compared to the control, the colon length of animals in the GO & IN group was found to be significantly ($P \leq 0.05$) larger by 21.22% (10.23 ± 0.29 cm) and 11.82% (09.33 ± 0.49 cm) respectively with respect to DSS group. The changes in the spleen weight have been represented in Fig. 2(b), the spleen wt. in the control group was found to be 0.13 ± 0.05 gms, which got significantly increased ($P \leq 0.005$) to 0.21 ± 0.03 gms in the DSS with respect to control group, whereas the spleen weight of GO and IN groups were found to be 0.13 ± 0.01 gms ($P \leq 0.0005$) and 0.08 ± 0.05 gms ($P \leq 0.0005$) respectively.

3.2. Histological analysis of colonic tissue sections

The change in cellular morphology of the colon to investigate colon injury and inflammation was done by histopathological studies and are detailed in Fig. 3 (a) Control, (b) DSS, (c) GO and (d) IN respectively. The animals from the control group had intact mucosa, tubular crypts of Lieberkuhn and goblet cells. On the contrary, severe mucosal dysplasia along with loss of integrity of crypts followed by bursting of cells and visible cell flaccidity near sub-mucosa layer in the DSS group was observed with a significant ($P \leq 0.0001$) damage score of 7.75 ± 0.5 to that of the control group. Alteration in sub-mucosa layers was also observed in the DSS group. In the GO group, the extent of dysplasia was significantly ($P \leq 0.001$) less by 22.58% with a damage score of 6 ± 0.81 compared to DSS. The crypts did not lose their orientation but a slight loss of the granular pattern of intestinal crypts was observed. Thus in IN group, we can see that the alteration in colonic structure was less, the mucosa and sub-mucosa layer were almost intact but the cells in this layer became flaccid and neutrophil infiltration in the mucosa and

submucosa layer was observed. The damage score in IN group was found to be 6.4 ± 0.5 which is significantly ($P \leq 0.0001$) less by 17.41% compared to DSS and 6.25% ($P \leq 0.01$) more than GO respectively.

3.3. Examination of surface morphology by SEM

Fig. 4 (a) depicts the colon surface of the control group which had intact intestinal crypts and goblet cells. The changes in the surface morphology when the mice groups were administered DSS and treated with prebiotics were visualized by SEM. In the DSS group, Fig. 4 (b) there was a complete loss of colonic structure and architecture with a massive loss of goblet cells, contrary to the control group. In GO, Fig. 4 (c) though we can visualize mucosal dysplasia, swollen crypts and the delineated boundary between the lesion area and the normal mucosa, the loss of goblet cells along with flat lesions was less when compared with that of the DSS group. Formation of the elevated lesion was also less in both GO and IN groups compared to DSS but the presence of flat lesions and swelling of goblet cells along with epithelial abnormalities was seen in IN group.

3.4. Analysis of splenic population of CD4^+ and CD8^+ T-lymphocyte by flow cytometry

From the flow cytometry data, we can observe that the population of CD8^+ and CD4^+ T cell in the control group was $8.9 \pm 0.13\%$ and $12.0 \pm 0.08\%$ respectively represented in Fig. 5 (a, e) which significantly ($P \leq 0.05$) increased to $30.03 \pm 0.23\%$ and $15.46 \pm 0.12\%$ respectively in DSS group as depicted in Fig. 5 (b, e). Further in GO and IN groups, it is seen that the population of CD8^+ T cells was significantly ($P \leq 0.05$) reduced to $10.28 \pm 0.09\%$ and $15.25 \pm 0.25\%$ respectively and a

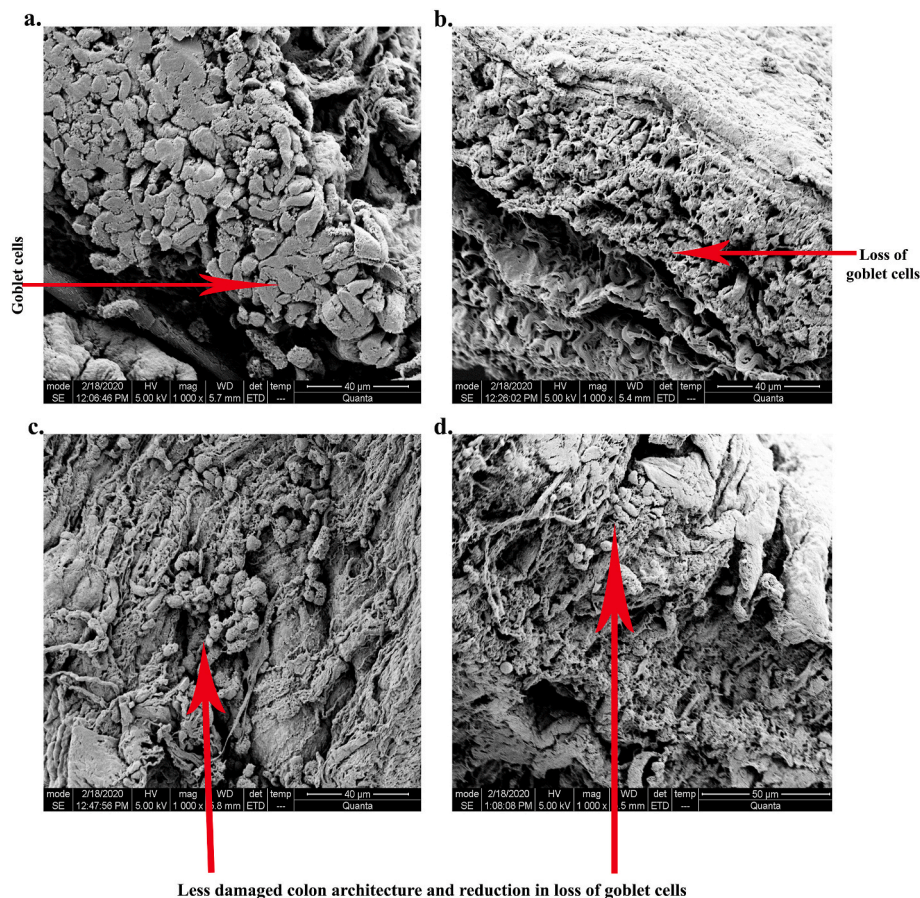


Fig. 4. Scanning electron microscopic images of colons of C57BL/6 mice depicting the changes in the surface morphology. GO reduces the loss of intestinal crypts and improves colonic integrity in C57BL/6 mice. (a) Control, (b) DSS, (c) GO, (d) IN. DSS, Dextran sodium sulfate; GO, Gum Odina; IN, Inulin.

significant ($P \leq 0.05$) increase in the number of $CD4^+$ T cells to $20.39 \pm 0.07\%$ and $25.53 \pm 0.14\%$ was seen with respect to DSS which is represented in Fig. 5 (c, e) and Fig. 5 (d, e) for GO and IN respectively.

3.5. Quantification of pro and anti-inflammatory cytokines in colonic tissue by ELISA

Cytokines were estimated and represented in Fig. 6. The levels of TNF- α , IFN- γ , IL-12, IL-17, and IL-1 β in the colonic fluids of DSS significantly increased ($P \leq 0.005$) by 68.08%, 83.01%, 32.53%, 54.03% and 45.40% respectively with respect to that of the control group. Whereas the levels of the TNF- α , IFN- γ , IL-1 β and IL-12 in the GO group got significantly reduced ($P \leq 0.005$) by 52.38%, 89.14%, 34.04% and 32.13% respectively with respect to DSS group. The levels of TNF- α , IFN- γ , and IL-1 β in IN were found to be significantly ($P \leq 0.005$) reduced by 59.14%, 74.85% and 45.29% respectively to that of the DSS group. Minute reduction in the level of IL-17 was observed in GO and IN groups and no notable change in the level of IL-12 was seen in IN group. The level of IL-10 in the colonic fluids of the control group was found to be 27.50 ± 2.09 pg/mg and in the DSS group, the level was found to be 30.09 ± 9.17 pg/mg which got significantly ($P \leq 0.01$) increased by 64.70% in GO with respect to DSS group. However, the IL-10 level in the IN group was further significantly higher by 62.19% ($P \leq 0.0001$) than that of the GO group.

3.6. Analysis of gene expression of *Tnf- α* , *Ifn- γ* and *Inos* by Real-Time PCR

Levels of *Tnf- α* , *Ifn- γ* and *Inos* expression in the colonic tissues were represented in Fig. 7. The expression of *Tnf- α* and *Ifn- γ* in the control

group were 8.11 ± 0.03 and 1.40 ± 0.38 respectively which got significantly elevated to 275.14 ± 8.09 ($P \leq 0.0005$) and 15.58 ± 2.55 ($P \leq 0.0004$) respectively in DSS group compared to control group. However a sharp fall in the expression of *Tnf- α* levels by 92.13% ($P \leq 0.0005$) and 81.46% ($P \leq 0.0005$) was seen in the GO and IN groups respectively when compared to the DSS group. The expression levels of *Ifn- γ* in GO and IN groups were 11.16 ± 0.84 and 14.36 ± 2.34 which is less than that of the DSS group but significantly higher by 87.40% ($P \leq 0.004$) and 90.25% ($P \leq 0.0004$) respectively with respect to control group. The expression levels of *Inos* in the control group was found to be 1.13 ± 0.70 which significantly increased by 93.10% ($P \leq 0.0001$) in the DSS i.e., 15.58 ± 2.55 when compared to the control group. In GO & IN groups the *Inos* levels were significantly reduced by 53.56% ($P \leq 0.0001$) and 89.74% ($P \leq 0.0001$) with respect to the DSS group.

3.7. Analysis of Gut microbiota

The Next generation sequencing data in Fig. 8, revealed that *Prevotella* sp. was predominant at the genus levels accounting for 76.28% of gut flora of the colitis patient which got reduced to 1.85% after incorporating GO in SHIME feed for 14 days. Commensals like *Lactobacillus* sp., and *Enterococcus* sp. initially possessed 9.61% and 1.76% respectively which got increased to 11.53% and 23.07% respectively representing the maximum fraction of gut flora after GO administration. However, the percentage of *Bacillus* sp. was reduced from 3.68% to 2.56% after the addition of GO. The percentage of *Klebsiella* sp. in the gut flora of the colitis patient's stool sample was found to be 3.68% which accounted for 5.12% after the addition of GO in the SHIME feed. There was no change in the composition of *Enterobacter* sp. in the colitis patient's stool sample after the addition of GO. The microflora diversified

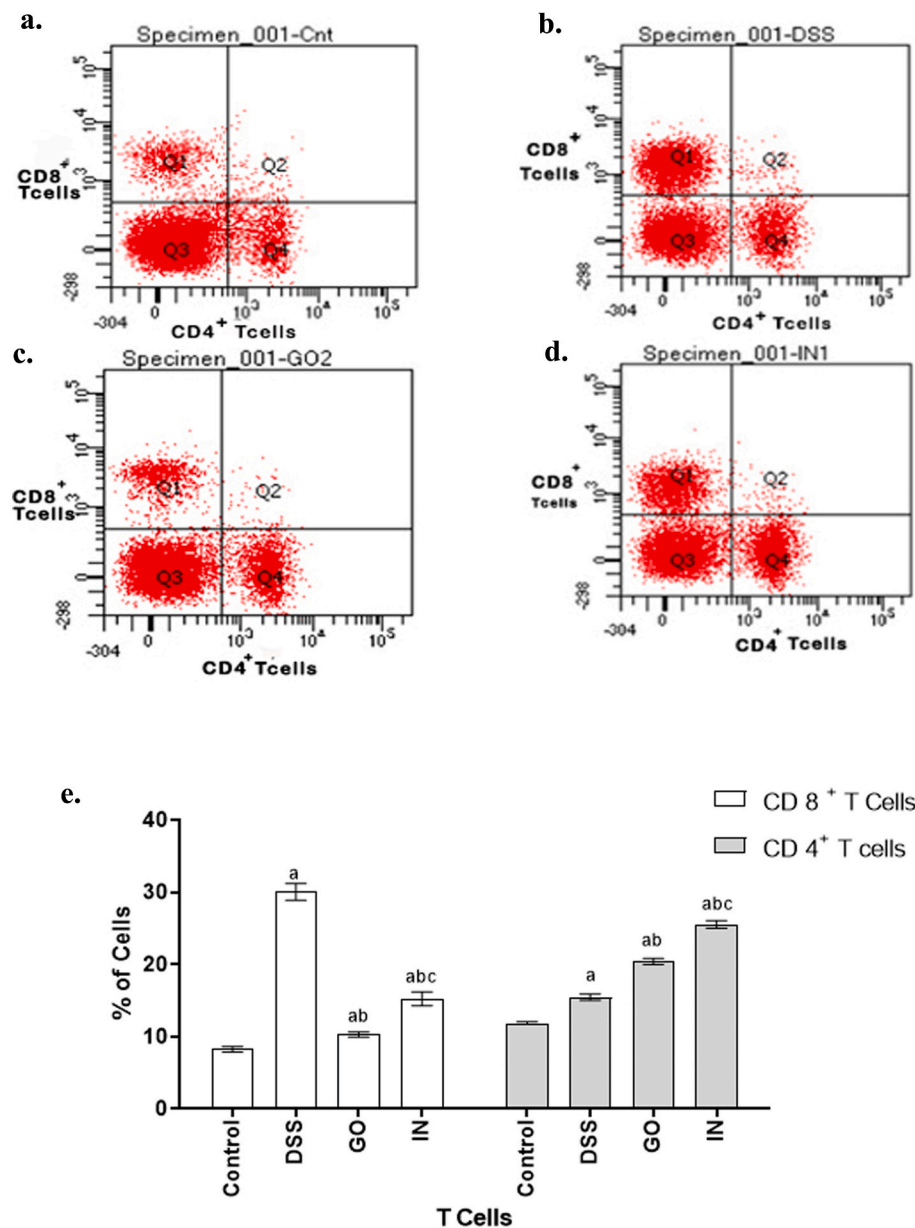


Fig. 5. GO reduces the population of CD8⁺ T cells and increases CD4⁺ T cells. Population of CD8⁺ T cells and CD4⁺ T cells in the spleen of C57BL/6 mice (a) Control, (b) DSS, (c) GO, (d) IN (e) graphical representation of CD8⁺ and CD4⁺ T cells. (CD8⁺ T cells - DSS > IN > GO > Control and CD4⁺ T cells - IN > GO > DSS > Control). Results are expressed as mean \pm standard error means (n = 6). Obtained values were analysed using one-way ANOVA followed by Tukey's multiple comparison test. ^a $p \leq 0.05$ compared to Control, ^b $p \leq 0.05$ compared to DSS, ^c $p \leq 0.05$ compared to GO. ANOVA, Analysis of variance; DSS, Dextran sodium sulfate; GO, Gum Odina; IN, Inulin.

with *Burkholderia* sp., *Achromobacter* sp., *Stenophomonas* sp., *Aeromonas* sp. along with *Delftia* sp., *Elizabethkingia* sp., *Merozyma* sp. and *Methylobacterium* sp. in the GO treated stool sample in SHIME which was previously absent in the stool of colitis patient.

4. Discussion

The present study illustrates the application of GO in the prevention of experimental colitis induced by DSS in C57BL/6 mice. 2% DSS was used in the study which is less than most previously reported studies, where the concentration used for developing colitis was 3%–5% (Naito et al., 2006; Winkler et al., 2007). DSS was administered directly via oral gavage and not mixed in drinking water like most of the studies minimising the need of constant monitoring of mice and reducing the wastage of DSS solution. Intervening gaps of three days after four days of DSS administration allowed us to run the experiments for 28 days mimicking a chronic colitis situation. Moreover, an increase in microbial diversity was also observed when sucrose was replaced by GO during the processing of the stool sample of the colitis patient in SHIME. The results

obtained from the preclinical study and human gut simulator also fabricate a platform for future clinical trials of GO on chronic non-communicable diseases.

The visible parameters of DSS-induced colitis in the animal model like reduction in body weight, shortening of colon length and increase in spleen wt. i.e. splenomegaly (Miles et al., 2017) were reversed upon prophylactic administration of GO and IN till the 7th day. From the 7th day, the body weight and colon length of animals from the GO group did not decrease and GO exhibited better results than IN. Histological changes observed in the DSS group were mainly due to damage in goblet cells, depletion of mucin (Laroui et al., 2012) and widening of the gap at the base of the crypt leading to epithelial erosion and formation of ulcer (Okayasu et al., 1990). Ulceration in the mucosa layer was accompanied by erythema and loss of granularity depicting the presence of active inflammation (Cader & Kaser, 2013). Splenomegaly was not seen in both of the prebiotic groups depicting their anti-inflammatory properties. GO is pseudoplastic (De, Malpani, et al., 2020) and fibrous in nature having the ability to absorb dietary precarious substances within the gut and limit the progression of gut damage by bulking feces (Mitra et al., 2016).

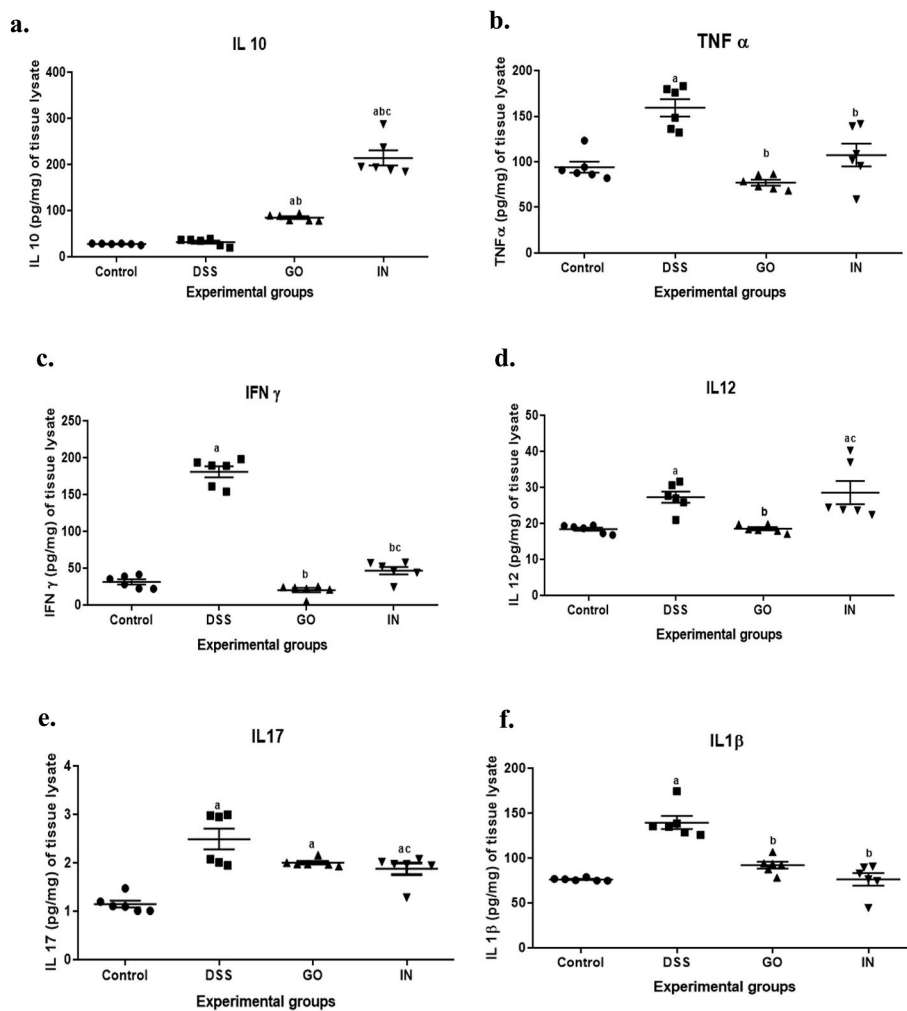


Fig. 6. Detection of proinflammatory and anti-inflammatory cytokine levels by ELISA in the colonic fluids of C57BL/6 mice of different experimental groups i.e. Control, DSS, GO, IN. GO reduced proinflammatory cytokines and increased IL-10 levels. (a) IL-10 (Control \leq DSS $<$ GO $<$ IN), (b) TNF- α (Control $<$ DSS $>$ IN $>$ GO), (c) IFN- γ (Control $<$ DSS $>$ IN $>$ GO), (d) IL-12 (Control $<$ DSS $>$ IN $>$ GO), (e) IL-17 (Control $<$ DSS $>$ GO \geq IN) and (f) IL-1 β (Control $<$ DSS $>$ GO $>$ IN). Results are expressed as mean \pm standard error means ($n = 6$). Obtained values were analysed using one-way ANOVA followed by Tuckey's multiple comparison test. $p \leq 0.05$ were considered statistically significant. ^a $p \leq 0.05$ compared to Control, ^b $p \leq 0.05$ compared to DSS, ^c $p \leq 0.05$ compared to GO. ANOVA, Analysis of variance; DSS, Dextran sodium sulfate; GO, Gum Odina; IN, Inulin.

The dysplasia was confined to the mucosa and submucosa layers in the GO group, which extended to the muscularis externa in the DSS group. The damage in the colonic cells was also less in IN group however the cells remained swollen accompanied by leukocyte infiltration. SEM studies enlighten the loss of granular pattern of intestinal crypts (Naito et al., 2006) which were also less in both GO and IN groups whereas the DSS group had extensive damage in the surface of the colonic structure along with loss of integrity. Considering these attributes, GO had a better edge over IN to limit disease progression. GO contains serine in trace amounts possessing wound healing activity (De, Malpani, et al., 2020) and upon fermentation in the gut, it liberates short-chain fatty acids (SCFAs) mainly butyric acid and lactic acid followed by acetic acid and propionic acid (Mitra et al., 2017) which enhances the epithelial barrier by regulating tight junctional integrity (Andoh et al., 1999; Naito et al., 2006). Butyric acid is considered the major energy source for colonocytes and helps the colonic cells to regenerate their structure thus attenuating damage associated with colitis which is observed in our study (Venkatraman et al., 2000). Being a soluble dietary fiber, IN also liberates adequate SCFAs but its spherical and smooth surface (Qiao et al., 2022) makes it inefficient in absorbing toxins generated from food digestion and feces bulking.

Innate immunity plays a major role in the progression of colitis as it is a heterogeneous state of intestinal inflammation (Kalužna et al., 2022). Cytotoxic CD8⁺ T cells play an early role in the development of gut ulcers and lesions (Boschetti et al., 2016) and have the ability to deviate the regulation of CD4⁺ T cells (Chen et al., 2019). The imbalance between subpopulations of CD4⁺ T cells is the leading cause of abrupt

inflammatory responses (Hegazy et al., 2017) in colitis resulting in the increase in spleen weight in the DSS group due to the accumulation of splenocytes resulting from active inflammation. The cytokine levels of IL-12 were higher in the DSS group than in the control group. Increased levels of IL-12 deviated the differentiation of CD4⁺ T cells into Th1 cells (Vacaflores et al., 2016) as a result the levels of proinflammatory cytokines like TNF- α , IFN- γ , IL-1 β and IL-17 also increased in the DSS group. The increase in the population of CD4⁺ T cells in the DSS group might be due to colonic damage and associated inflammation. Though the population of CD8⁺ T cells subsided in GO and IN groups exhibiting a reduction in gut inflammation, the population of CD4⁺ T cells further increased by 24.17% and 39.44% respectively with that of the DSS group. As there was a reduction in the cytokine levels of TNF- α , IFN- γ , IL-1 β and an increase in IL-10 levels in both GO and IN groups it can be interpreted that prebiotics turned the CD4⁺ T cells differentiation into Th2 cells promoting anti-inflammatory functions. However, a detailed study was necessary to fully understand the fact. There was no drastic reduction in IL-17 levels with respect to the DSS group which could be also linked to neutrophilic migration to the inflammation site as seen in the histopathology analysis. The mRNA expression of *Tnf- α* , *Ifn- γ* became higher in the DSS group but suppressed in GO and IN groups and can be directly related to changes in cytokine levels of TNF- α , IFN- γ which also decreased in the respective group. Colonic damage incurred by DSS-induced colitis also disrupts the balance between oxidant and antioxidant status resulting in oxidative (Osman et al., 2006) stress causing an increase in mRNA expression of *Inos*. GO possesses antioxidant properties due to the presence of uronic acids and hydroxyl groups

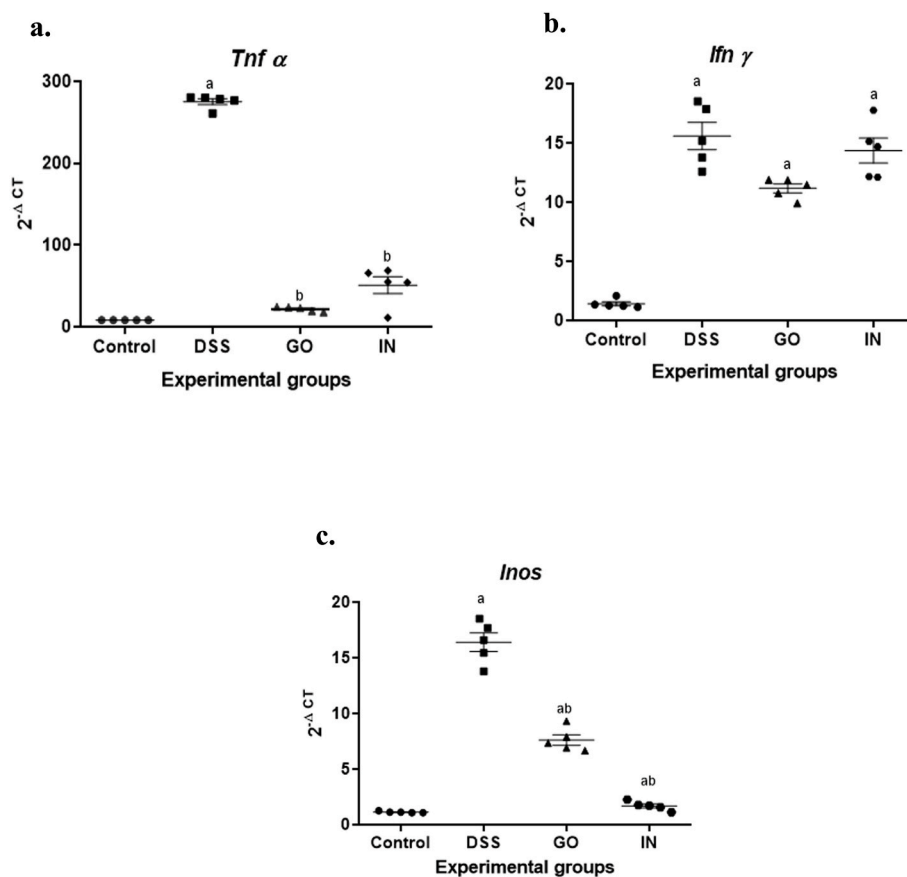


Fig. 7. GO reduces expression of *Tnf-α*, *Ifn-γ* and *Inos*. mRNA expression of (a) *Tnf-α* (Control<DSS>IN > GO) (b) *Ifn-γ* (Control<DSS>GO > IN) and (c) *Inos* (Control<DSS>GO > IN) by Real-Time PCR in colonic tissue of C57BL/6 mice of different experimental groups i.e. Control, DSS, GO, IN. Results are expressed as mean \pm standard error means ($n = 6$). Obtained values were analysed using one-way ANOVA followed by Tuckey's multiple comparison test. $p \leq 0.05$ values were considered statistically significant. ^a $p \leq 0.05$ compared to Control, ^b $p \leq 0.05$ compared to DSS, ^c $p \leq 0.05$ compared to GO.

(De, Malpani, et al., 2020) in its structure, which reduces ROS and LPO levels and increases the production of antioxidants like GSH, GST, SOD, CAT (Mitra et al., 2017) in the gut resulting in low *Inos* expression (Fig. 7 c) diluting the extent of oxidative damage caused by DSS. The mRNA expression of *Inos* in the IN group was further low by 36.18% when compared to the GO group. The IL-10 levels and mRNA expression of *Inos* exhibited that IN had slightly better anti-inflammatory activity than GO. Though IN is an extensively used prebiotic and has been reported to have health benefits in several studies (Changchien et al., 2021; Pool-Zobel et al., 2002) it is mainly composed of fructose and glucose, which can be easily utilized by both commensal and pathogenic bacteria in the gut environment. Thus, GO becomes a better choice of prebiotic as a prophylactic treatment of colitis or related diseased state combining feces bulking, anti-inflammatory, antioxidant and gut-modulating factors (Mitra et al., 2017). GO on the other hand has less processing cost than IN and does not impart any taste (De, Malpani, et al., 2020).

Additionally, we also investigated the correlation between the gut microflora from feces of colitis patient before and after the incorporation of GO into the diet using SHIME. The gut microflora of colitis patient had low microbial diversity and was mostly dominated by *Prevotella* sp. followed by *Lactobacillus* sp., *Bacillus* sp. and pathogenic bacteria like *Enterococcus* sp. *Enterobacter* sp. and *Klebsiella* sp. The gut microbiome analysis revealed an increase in the diversity of bacterial species and a reduction in the percentage of pathogenic bacteria upon the addition of GO prebiotics in the experimental phase of the gut simulator. The change in the gut flora can be mainly due to SCFAs liberated from GO further limiting the growth of disease-causing pathogenic bacteria by acting as a selective antimicrobial agent enhancing the growth of commensal bacteria in the gut (Parada Venegas et al., 2019).

5. Conclusion

The study revealed that repeated cycles of DSS administration induce shortening of colon length and splenomegaly in C57BL/6 mice, disrupt the cellular integrity, increases the expression of pro-inflammatory cytokines and *Inos* in colon, which is prevented when prebiotic like GO is introduced in the diet of mice. GO also increases gut microbial diversity. Thus, the anti-inflammatory effects of GO to combat colitis were elucidated, allowing the availability of new prebiotic i.e. arabinogalactan and extending the choice of bioactive compounds in food and pharmaceutical industries which are presently dominated by fructooligosaccharides and galactooligosaccharides.

Authors contribution

Debmalya Mitra: Conceptualization, Methodology, Investigation, Writing-Original Draft, Funding acquisition, Formal Analysis.: **Sohini Sikdar:** Methodology, Investigation, Writing-Original Draft, Investigation, Writing-Review and Editing, Formal Analysis.: **Mainak Chakraborty:** Investigation, Formal Analysis, Writing-Review and Editing.: **Oishika Das:** Investigation.: **Amalesh Samanta:** Investigation, Writing-Review and Editing, Resources.: **Shanta Dutta:** Conceptualization, Resources, Methodology, Writing-Review and Editing, Supervision, Project administration.

Declaration of competing interest

The authors confirm that they have no conflict of interest to the work described in this manuscript.

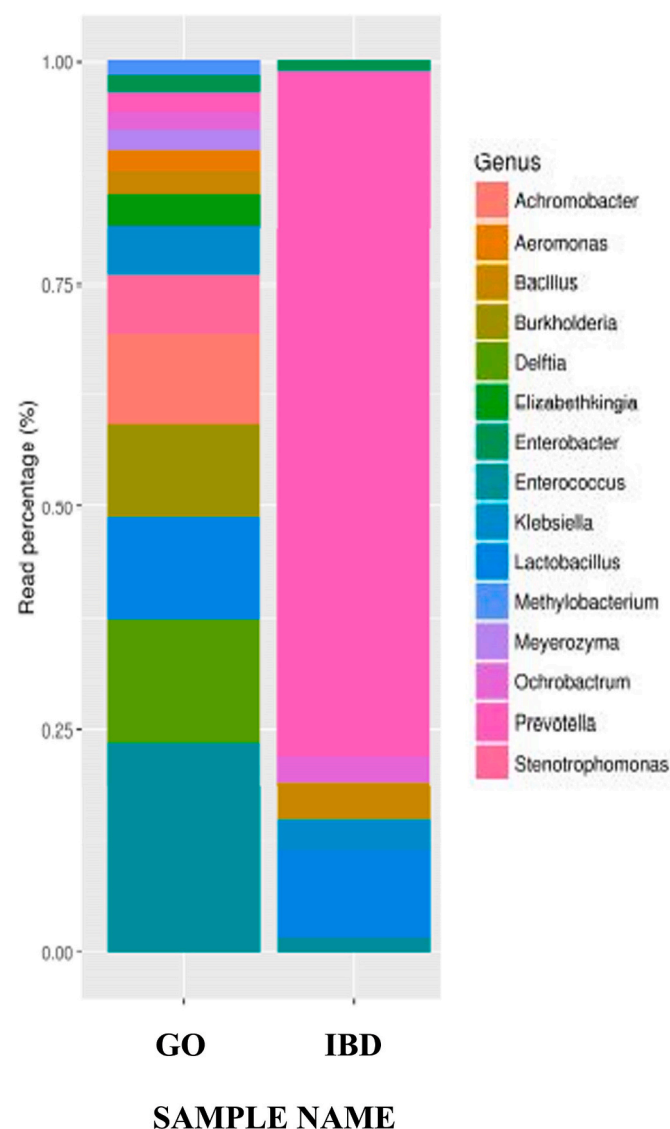


Fig. 8. Comparison of microbial communities at genus levels before and after the addition of GO in SHIME. GO increased microbial diversity in the stool sample of colitis patient. GO, Gum Odina; SHIME, Simulator of the human intestinal microbial ecosystem.

Data availability

Data will be made available on request.

Acknowledgement

The authors would like to thank ID and BG hospital for providing technical assistance in identifying and collecting a stool sample from a colitis patient. The authors are also thankful to Arpita Sarbajna and Dr Arnab De for providing technical help on scanning electron microscopy and identification of *Odina wodier* tree respectively. The study was funded by the Indian Council of Medical Research, ICMR - Post Doctoral Fellowship Scheme vide ref no.(3/1/3/PDF-19 HRD) for conducting research experiments. However, no financial support was obtained for the article's preparation and processing, i.e. publication charges required if any.

Appendix A. Supplementary data

Supplementary data to this article can be found online at <https://doi.org/10.1016/j.fbio.2023.102509>.

[org/10.1016/j.fbio.2023.102509](https://doi.org/10.1016/j.fbio.2023.102509).

References

- Andoh, A., Bamba, T., & Sasaki, M. (1999). Physiological and anti-inflammatory roles of dietary fiber and butyrate in intestinal functions. *Journal of Parenteral and Enteral Nutrition*, 23, S70–S73.
- Bhattacharyya, A. K., & Rao, C. V. N. (1964). Gum jeol: The structure of the degraded gum derived from it. *Canadian Journal of Chemistry*, 42(1), 107–112.
- Boschetti, G., Nancey, S., Moussata, D., Cotte, E., Francois, Y., Flourie, B., & Kaiserlian, D. (2016). Enrichment of circulating and mucosal cytotoxic CD8+ T cells is associated with postoperative endoscopic recurrence in patients with Crohn's disease. *Journal of Crohn's and Colitis*, 10(3), 338–345.
- Breyneart, C., Dresselaers, T., Perrier, C., Arijis, I., Cremer, J., Van Lommel, L., Van Steen, K., Ferrante, M., Schuit, F., Vermeire, S., & Van Assche, G. (2013). Unique gene expression and MR T2 relaxometry patterns define chronic murine dextran sodium sulphate colitis as a model for connective tissue changes in human Crohn's disease. *PLoS One*, 8(7), Article e68876.
- Cader, M. Z., & Kaser, A. (2013). Recent advances in inflammatory bowel disease: Mucosal immune cells in intestinal inflammation. *Gut*, 62(11), 1653–1664.
- Changchien, C. H., Wang, C. H., & Chen, H. L. (2021). Konjac glucomannan polysaccharide and inulin oligosaccharide ameliorate dextran sodium sulfate-induced colitis and alterations in fecal microbiota and short-chain fatty acids in C57BL/6J mice. *Biomedicine*, 11(3), 23.
- Chassaing, B., Aitken, J. D., Malleshappa, M., & Vijay-Kumar, M. (2014). Dextran sulfate sodium (DSS)-induced colitis in mice. *Current Protocols in Immunology*, 104(1), 15–25.
- Chen, Y. F., Zheng, J. J., Qu, C., Xiao, Y., Li, F. F., Jin, Q. X., Li, H. H., Meng, F. P., Jin, G. H., & Jin, D. (2019). Inonotus obliquus polysaccharide ameliorates dextran sulphate sodium induced colitis involving modulation of Th1/Th2 and Th17/Treg balance. *Artificial Cells, Nanomedicine, and Biotechnology*, 47(1), 757–766.
- Das, S., De, A., Das, B., Mukherjee, B., & Samanta, A. (2021). Development of gum odina-gelatin based antimicrobial loaded biodegradable spongy scaffold: A promising wound care tool. *Journal of Applied Polymer Science*, 138(12), Article 50057.
- De, A., Das, B., Mitra, D., Sen, A. K., & Samanta, A. (2020). Exploration of an arabinogalactan isolated from *Odina wodier* Roxb.: Physicochemical, compositional characterisations and functional attributes. *Polymers for Advanced Technologies*, 31(8), 1814–1826.
- De, A., Malpani, D., Das, B., Mitra, D., & Samanta, A. (2020). Characterization of an arabinogalactan isolated from gum exudate of *Odina wodier* Roxb.: Rheology, AFM, Raman and CD spectroscopy. *Carbohydrate Polymers*, 250, Article 116950.
- Fuller, R. (1991). Probiotics in human medicine. *Gut*, 32(4), 439.
- Gibson, G., Probert, H., Loo, J., Rastall, R., & Roberfroid, M. (2004). Dietary modulation of the human colonic microbiota: updating the concept of prebiotics. *Nutrition Research Review*, 17, 259–275.
- Gibson, G. R., & Roberfroid, M. B. (1995). Dietary modulation of the human colonic microbiota: Introducing the concept of prebiotics. *Journal of Nutrition*, 125(6), 1401–1412.
- Hegazy, A. N., West, N. R., Stubbington, M. J., Wendt, E., Suijker, K. I., Datsi, A., This, S., Danne, C., Campion, S., Duncan, S. H., & Owens, B. M. (2017). Circulating and tissue-resident CD4+ T cells with reactivity to intestinal microbiota are abundant in healthy individuals and function is altered during inflammation. *Gastroenterology*, 153(5), 1320–1337.
- Li, W. A. R., Sakamoto, K., & Leifer, C. A. (2012). TLR9 is important for protection against intestinal damage and for intestinal repair. *Scientific Reports*, 2(1), 1–9.
- Kałużna, A., Olczyk, P., & Komosińska-Vaske, K. (2022). The role of innate and adaptive immune cells in the pathogenesis and development of the inflammatory response in ulcerative colitis. *Journal of Clinical Medicine*, 11(2), 400.
- Kaplan, G. G. (2015). The global burden of IBD: From 2015 to 2025. *Nature Reviews Gastroenterology & Hepatology*, 12(12), 720–727.
- Laroui, H., Ingersoll, S. A., Liu, H. C., Baker, M. T., Ayyadurai, S., Charania, M. A., Laroui, F., Yan, Y., Sitaraman, S. V., & Merlin, D. (2012). Dextran sodium sulfate (DSS) induces colitis in mice by forming nano-lipocomplexes with medium-chain-length fatty acids in the colon. *PLoS One*, 7(3), Article e32084.
- Melgar, S., Karlsson, L., Rehnström, E., Karlsson, A., Utkovic, H., Jansson, L., & Michaëlsson, E. (2008). Validation of murine dextran sulfate sodium-induced colitis using four therapeutic agents for human inflammatory bowel disease. *International Immunopharmacology*, 8(6), 836–844.
- Miles, J. P., Zou, J., Kumar, M. V., Pellizzon, M., Ulman, E., Ricci, M., Gewirtz, A. T., & Chassaing, B. (2017). Supplementation of low-and high-fat diets with fermentable fiber exacerbates severity of DSS-induced acute colitis. *Inflammatory Bowel Diseases*, 23(7), 1133–1143.
- Mitra, D., Basu, A., Das, B., Jena, A. K., De, A., Das, M., Bhattacharya, S., & Samanta, A. (2017). Gum odina: An emerging gut modulating approach in colorectal cancer prevention. *RSC Advances*, 7(46), 29129–29142.
- Mitra, D., Jena, A. K., De, A., Das, M., Das, B., & Samanta, A. (2016). Prebiotic potential of gum odina and its impact on gut ecology: In vitro and in vivo assessments. *Food & Function*, 7(7), 3064–3072.
- Mukherjee, B., Samanta, A., & Dinda, S. C. (2006). Gum odina-a new tablet binder. *Trends in Applied Sciences Research*, 1, 309–316.
- Naito, Y., Takagi, T., Katada, K., Uchiyama, K., Kuroda, M., Kokura, S., Ichikawa, H., Watabe, J., Yoshida, N., Okanoue, T., & Yoshikawa, T. (2006). Partially hydrolyzed guar gum down-regulates colonic inflammatory response in dextran sulfate sodium-induced colitis in mice. *The Journal of Nutritional Biochemistry*, 17(6), 402–409.

- Okayasu, I., Hatakeyama, S., Yamada, M., Ohkusa, T., Inagaki, Y., & Nakaya, R. (1990). A novel method in the induction of reliable experimental acute and chronic ulcerative colitis in mice. *Gastroenterology*, 98(3), 694–702.
- Osman, N., Adawi, D., Molin, G., Ahrne, S., Berggren, A., & Jeppsson, B. (2006). Bifidobacterium infantis strains with and without a combination of Oligofructose and Inulin (OFI) attenuate inflammation in DSS-induced colitis in rats. *BMC Gastroenterology*, 6(1), 1–10.
- Parada Venegas, D., De la Fuente, M. K., Landskron, G., González, M. J., Quera, R., Dijkstra, G., Harmsen, H. J., Faber, K. N., & Hermoso, M. A. (2019). Short chain fatty acids (SCFAs)-mediated gut epithelial and immune regulation and its relevance for inflammatory bowel diseases. *Frontiers in Immunology*, 277.
- Paulsen, J. E., Namork, E., & Alexander, J. (2005). Scanning electron microscopy of colonic lesions in 1, 2-dimethylhydrazine-treated rats. *Anticancer Research*, 25(6B), 3883–3888.
- Pellizzon, M. (2016). Choice of laboratory animal diet influences intestinal health. *Lab Animal*, 45, 238–239.
- Pellizzon, M., & Ricci, M. (2020). Choice of laboratory rodent diet may confound data interpretation and reproducibility. *Current Developments in Nutrition*, 4(4), Article nzaa031.
- Piovani, D., Danese, S., Peyrin-Biroulet, L., & Bonovas, S. (2019). Inflammatory bowel disease: Estimates from the global burden of disease 2017 study. *Alimentary Pharmacology & Therapeutics*, 1–10, 00.
- Pool-Zobel, B., Van Loo, J., Rowland, I., & Roberfroid, M. B. (2002). Experimental evidences on the potential of prebiotic fructans to reduce the risk of colon cancer. *British Journal of Nutrition*, 87(S2), S273–S281.
- Qiao, H., Zhao, T., Yin, J., Zhang, Y., Ran, H., Chen, S., Wu, Z., Zhang, R., Wang, X., Gan, L., & Wang, J. (2022). Structural characteristics of inulin and microcrystalline cellulose and their effect on ameliorating colitis and altering colonic microbiota in dextran sodium sulfate-induced colitic mice. *ACS Omega*, 7(13), 10921–10932.
- Randhawa, P., Singh, K., Singh, N., & Singh Jaggi, A. (2014). A Review on Chemical-Induced Inflammatory Bowel Disease Models in Rodents. *The Korean Journal of Physiology & Pharmacology*, 18, 279–288.
- Roy, P. S., Samanta, A., Mukherjee, M., Roy, B., & Mukherjee, A. (2013). Designing novel pH-induced chitosan–gum odina complex coacervates for colon targeting. *Industrial & Engineering Chemistry Research*, 52(45), 15728–15745.
- Sankarasubramanian, J., Ahmad, R., Avuthu, N., Singh, A. B., & Guda, C. (2020). Gut microbiota and metabolic specificity in ulcerative colitis and Crohn's disease. *Frontiers of Medicine*, 7, Article 606298.
- Solanki, H. K., Pawar, D. D., Shah, D. A., Prajapati, V. D., Jani, G. K., Mulla, A. M., & Thakar, P. M. (2013). Development of microencapsulation delivery system for long-term preservation of probiotics as biotherapeutics agent. *BioMed Research International*, Article 620719, 2013;2013.
- Vacaflones, A., Chapman, N. M., Harty, J. T., Richer, M. J., & Houtman, J. C. (2016). Exposure of human CD4 T cells to IL-12 results in enhanced TCR-induced cytokine production, altered TCR signaling, and increased oxidative metabolism. *PLoS One*, 11(6), Article e0157175.
- Venkatraman, A., Ramakrishna, B. S., Pulimood, A. B., Patra, S., & Murthy, S. (2000). Increased permeability in dextran sulphate colitis in rats: Time course of development and effect of butyrate. *Scandinavian Journal of Gastroenterology*, 35(10), 1053–1059.
- Winkler, J., Butler, R., & Symonds, E. (2007). Fructo-oligosaccharide reduces inflammation in a dextran sodium sulphate mouse model of colitis. *Digestive Diseases and Sciences*, 52(1), 52–58.
- Wirtz, S., Neufert, C., Weigmann, B., & Neurath, M. F. (2007). Chemically induced mouse models of intestinal inflammation. *Nature Protocols*, 2(3), 541–546.
- Xavier, R. J., & Podolsky, D. K. (2007). Unravelling the pathogenesis of inflammatory bowel disease. *Nature*, 448(7152), 427–434.
- Yeom, Y., Kim, B., Kim, S., & Kim, Y. (2016). Sasa quelpaertensis leaf extract regulates microbial dysbiosis by modulating the composition and diversity of the microbiota in dextran sulfate sodium-induced colitis mice. *BMC Complementary and Alternative Medicine*, 16, 481–496.
- Yi, Q., Wang, J., Song, Y., Guo, Z., Lei, S., Yang, X., Li, L., Gao, C., & Zhou, Z. (2019). Ascl2 facilitates IL-10 production in Th17 cells to restrain their pathogenicity in inflammatory bowel disease. *Biochemical and Biophysical Research Communications*, 510(3), 435–441.
- Zhu, L., Gao, M., Li, H., Deng, Z., Zhang, B., & Yawei, F. (2021). Effects of soluble dietary fiber from sweet potato dregs on the structures of intestinal flora in mice. *Food Bioscience*, 40, Article 100880.